



27th ELGRA BIENNIAL SYMPOSIUM & GENERAL ASSEMBLY

SEPTEMBER 06th - 10th, 2022
Lisbon, Portugal

BOOK OF ABSTRACTS



27th
ELGRA BIENNIAL SYMPOSIUM
& GENERAL ASSEMBLY



SEPTEMBER 06th - 10th, 2022
Lisbon, Portugal

CONFERENCE CHAIR

Ricard González-Cinca

*Universitat Politècnica de Catalunya-BarcelonaTech
Castelldefels (Barcelona), Spain*

CONFERENCE CO-CHAIR

Christian Lockowandt

*Swedish Space Corporation
Stockholm, Sweden*

SCIENTIFIC COMMITTEE:

Philip Carvil

*Science and Technology Facilities Council (STFC)
Cheshire, UK*

Eric Falcon

*University of Paris
Paris, France*

Elisa Raffaella Ferre

*Birbeck University of London
London, UK*

Anna García-Sabaté

*New York University Abu Dhabi
Saadiyat Island, United Arab Emirates*

Thorben Könemann

*ZARM
Bremen, Germany*





27th
ELGRA BIENNIAL SYMPOSIUM
& GENERAL ASSEMBLY

TUESDAY - September 06th

TIME	SESSION	ROOM
09.00 20.00	Registration	
09.00 13.00	ELGRA Management Committee	Graça <i>(By invitation)</i>
17.00 18.30	Opening	Oriente
18.30 19.30	Poster session	Maravilla+Lapa
19.30 20.30	WELCOME RECEPTION	Sky bar

SEPTEMBER 06th - 10th, 2022
Lisbon, Portugal



WEDNESDAY - September 07th

			Physical Sciences 1 (Room Campolide + Olivais)
TIME	SESSION	ABSTRACT	TITLE
08.30 08.45	Diffusion in non-metallic mixtures	21	Instability caused by interplay of Soret and cross-diffusion in ternary mixture
08.45 09.00		22	Nonlinearities in shadowgraphy experiments on non-equilibrium fluctuations - in preparation of the GIANT FLUCTUATIONS microgravity project
09.00 09.15		46	Soret coefficients of a ternary C60-THN-Tol mixture: results from DCMIX4 experiments
09.15 09.30		70	Automatic structure function analysis using artificial intelligence
09.30 09.45		91	Two-wavelength Shadowgraphy
09.45 10.00		98	Dynamics of Non-Equilibrium Fluctuations Close to the Onset of Rayleigh-Bénard Convection



27th ELGRA BIENNIAL SYMPOSIUM & GENERAL ASSEMBLY

WEDNESDAY - September 07th

Physical Sciences 1 (Room Campolide + Olivais)

TIME	SESSION	ABSTRACT	TITLE
10.30 11.00	COFFEE BREAK		
11.00 11.15	Marangoni convection	7	Controlling the dynamics of a free surface via thermocapillary flows
11.15 11.30		8	Thermocapillary flows and phase change in rectangular containers in microgravity
11.30 11.45		10	Dependence oscillatory dynamics on gas flow temperature in liquid bridges
11.45 12.00		14	Three dimensional effects during the melting of phase change materials with thermocapillary flow in microgravity
12.00 12.15		23	Comparative experimental-numerical analysis of PCM: n-hexadecane, n-octadecane and n-eicosane
12.15 12.30		32	The Effect of Marangoni Convection on Heat Transfer in Phase Change Materials Experiment
12.30 12.45		57	Vapour cloud of an evaporating sessile droplet in microgravity

SEPTEMBER 06th - 10th, 2022
Lisbon, Portugal



WEDNESDAY - September 07th

Physical Sciences 1 (Room Campolide + Olivais)

TIME	SESSION	ABSTRACT	TITLE
13.00 14.15	LUNCH		
14.15 14.30	Thermophysical properties	1	Dielectrophoretic induced convection in a sounding rocket flight
14.30 14.45		56	Thermal diffusion experiments in CO ₂ -1-hexanol mixtures at different gravity levels – Design and data overview of a parabolic flight campaign
14.45 15.00		82	Containerless measurements of thermophysical properties on board the ISS using the electromagnetic levitator ISS-EML
15.00 15.15		83	Thermophysical properties of bulk metallic glasses measured on board the ISS using the electromagnetic levitator ISS-EML
15.15 15.30		122	Thermophysical properties of liquid Ti-Al-Cr-Nb alloys: theory vs experiments
16.00 20.15	SOCIAL ACTIVITY		



27th ELGRA BIENNIAL SYMPOSIUM & GENERAL ASSEMBLY

WEDNESDAY - September 07th

			Physical Sciences 2 (Room Castelo + Chiado)
TIME	SESSION	ABSTRACT	TITLE
08.30 08.45	Multiphase flows	29	Pool boiling heat transfer in microgravity with microstructured surfaces and electric field: preliminary results of parabolic flight campaign
08.45 09.00		104	Boil-off management in microgravity
09.00 09.15		102	Volume measurement of liquid propellants by means of acoustic fields
09.15 09.30		110	An integrated acoustic technology for application in propellant tanks
09.30 09.45		109	Electronics cooling by means of acoustic waves in microgravity
09.45 10.00		28	Capillary rise in Divergent U-Tube during parabolic flight
10.00 10.15		99	Non-Isothermal sloshing for space applications: from a ground-based experimental characterisation to microgravity conditions
10.15 10.30		101	About water droplet populations in microgravity conditions

SEPTEMBER 06th - 10th, 2022
Lisbon, Portugal



WEDNESDAY - September 07th

Physical Sciences 2 (Room Castelo + Chiado)

TIME	SESSION	ABSTRACT	TITLE
10.30 11.00	COFFEE BREAK		
11.00 11.15	Other fluids	33	Interaction of Faraday waves on alternating multi-layer fluid systems in microgravity
11.15 11.30		86	Anomalous Behaviour of Temperature Non-Equilibrium Fluctuations across pure CO ₂ Widom Line
11.30 11.45		43	AtmoFlow – Investigating large scale convection in planetary atmospheres
11.45 12.00		73	Thermoelectric convection in rectangular cavities in microgravity conditions
12.00 12.15		45	AID – Efficient Data Processing with Neuronal Networks for Microgravity
12.15 12.30		76	Heat transfer induced by thermoelectric convection in a cylindrical annulus in microgravity
12.30 12.45		80	Film-wise condensation of pure vapour on CNT-coated curvilinear fin in microgravity
12.45 13.00		119	Evaporating sessile droplet on a sounding rocket: analysis by vapour interferometry and simulation



27th ELGRA BIENNIAL SYMPOSIUM & GENERAL ASSEMBLY

WEDNESDAY - September 07th

Physical Sciences 2 (Room Castelo + Chiado)

TIME	SESSION	ABSTRACT	TITLE
13.00 14.15	LUNCH		
14.15 14.30	Emulsions	44	Preliminary Results on Emulsion Destabilisation from the ISS PASTA Experiment
14.30 14.45	Granular media	9	Osmosis in a bi-disperse compartmentalized granular material in low-gravity environment
14.45 15.00		20	Particle dynamics at the onset of the granular gas-liquid transition
15.00 15.15		41	Slow Impacts on Regolith Surfaces in Low Gravity – First Experiments on the new GTB-Pro Platform
15.15 15.30		51	Granular gas mixtures: Experiments and machine learning-aided analysis
16.00 20.15	SOCIAL ACTIVITY		

SEPTEMBER 06th - 10th, 2022
Lisbon, Portugal



WEDNESDAY - September 07th

			Life Sciences (Room Alfama + Alcantara)
TIME	SESSION	ABSTRACT	TITLE
08.30 08.45	ISGP	4	Cardiovascular deconditioning and impact of artificial gravity during 60-day head-down bed rest – Insights from 4D flow cardiac MRI
08.45 09.00		6	Effect of 3-day exposure to dry immersion on veno-arteriolar reflex
09.00 09.15		15	5 days of simulated microgravity induce skeletal muscle structural and microenvironment changes leading to global muscle deconditioning
09.15 09.30		39	Spaceflight Associated Neuro-ocular Syndrome During Long Duration Spaceflight
09.30 09.45		52	Change in circulating collagen type II biomarkers (CTX-II, C1,2C, C2C) in response to 21-days of Head-Down-Tilt Bed Rest (HDT-BR) and countermeasures.
09.45 10.00		61	Daily aerobic and resistance exercise on ISS does not correlate with measured change in peak VO2



27th ELGRA BIENNIAL SYMPOSIUM & GENERAL ASSEMBLY

WEDNESDAY - September 07th

Life Sciences (Room Alfama + Alcantàra)

TIME	SESSION	ABSTRACT	TITLE
10.30 11.00	COFFEE BREAK		
11.00 11.15	Cardio and vestibular systems	24	Ocular counter-roll is less affected in experienced compared to novice space crew after long-duration spaceflight
11.15 11.30		36	Numerical Simulation and Analysis of Human Cardiovascular Behavior During Subjection to Suborbital Spaceflight
11.30 11.45		63	The impact of long-duration spaceflight on the horizontal Vestibulo-Ocular Reflex (hVOR)
11.45 12.00		69	Effects of Altered Gravity on Human Behaviour
12.00 12.15		103	Expression of locomotor synergies under various gravitational constraints
12.15 12.30	Immune system	48	The acute gravitational stress of parabolic flight affects red blood cell aggregation and functionality of circulating immune cells
12.30 12.45		68	High Content microscopy and super-resolution microscopy profiling to unravel the role of the actin cytoskeleton in T cell activation in microgravity

SEPTEMBER 06th - 10th, 2022
Lisbon, Portugal



WEDNESDAY - September 07th

Life Sciences (Room Alfama + Alcantâra)

TIME	SESSION	ABSTRACT	TITLE
13.00 14.15	LUNCH		
14.15 14.30	Other Life Sciences topics	13	The effect of hypergravity on burn wounds in Hirudo
14.30 14.45		95	A Glimpse into Spaceflight Induced Bone Loss Over 18-Months
14.45 15.00		66	Astropharmacy – Healthcare for Earth, the Moon, Mars and beyond
15.00 15.15		67	Brain structural and functional responses to long-duration spaceflight

16.00 20.15	SOCIAL ACTIVITY		
----------------	------------------------	--	--



27th ELGRA BIENNIAL SYMPOSIUM & GENERAL ASSEMBLY

THURSDAY - September 08th

TIME	SESSION	ABSTRACT	TITLE	ROOM
09.00 10.30	ELGRA Medal		Floris Wuyts: Brains in Space	Oriente
			Nicolas Vandewalle: Handling granular materials in space	
10.30 11.00	COFFEE BREAK			
11.00 12.45	ELGRA-ASGSR	124	Plants grow in lunar regolith collected in the Apollo 11, 12 and 17 missions	Oriente
		121	Flight Experiments on Propellant Control in Conformal Propellant Tanks	
12.45 14.00	LUNCH			
14.00 15.00	ISGP		Alexander Chouker: Stress, Hibernation and the Way to Mars	Oriente
15.00 16.00	SELGRA Assembly			
16.00 18.00	ELGRA General Assembly			
19.30 00.00	GALA DINNER			

SEPTEMBER 06th - 10th, 2022
Lisbon, Portugal



FRIDAY - September 09th

			Physical Sciences (Room Campolide + Olivais)
TIME	SESSION	ABSTRACT	TITLE
09.00 09.15	Materials Science and Processing	58	Thin Liquid Film Coating and Drying under Microgravity Conditions: How parabolic flights showed the necessity of sounding rocket experiments
09.15 09.30		50	PEDOT:PSS electrodes in view of low-cost biocompatible cellulose-assisted biosensors
09.45 10.00		40	Microstructural transitions during solidification of transparent alloy NPG-DC investigated onboard the ISS using the TRANSPARENT facility
10.00 10.15		117	Gold nanoparticles synthesized by laser ablation using a random positioning machine
10.15 10.30		123	Manufacturing "in situ" of regolith simulants: Design of composites by liquid assisted processes
10.30 11.00	COFFEE BREAK		
11.00 11.15	Biophysics	3	Echographic surveillance of 14 volunteer after 40 days in confinement in a Deep cavern (Deep time experiment 2021)
11.15 11.30		38	Simulating the spaceflight environment: Combined effect of simulated microgravity, ionizing radiation, and psychological stress on in vitro wound healing
11.30 11.45		54	Microgravity experiments on Red Blood Cell aggregation dynamics in flow



27th ELGRA BIENNIAL SYMPOSIUM & GENERAL ASSEMBLY

FRIDAY - September 09th

			Physical Sciences (Room Campolide + Olivais)
TIME	SESSION	ABSTRACT	TITLE
11.45 12.00		88	Different Spaceflight-Associated Changes in the Perivascular Spaces of Astronauts and Cosmonauts
12.00 12.15		115	Study of the influence of microgravity on brain derived spheroids in acoustic levitation

12.45 14.00	FAREWELL LUNCH		
----------------	-----------------------	--	--

SEPTEMBER 06th - 10th, 2022
Lisbon, Portugal



FRIDAY - September 09th

			Life Sciences (Room Castelo + Chiado)
TIME	SESSION	ABSTRACT	TITLE
09.15 09.30	Personalized medicine	37	Human Reproduction in Space. Late Results
09.30 09.45		53	Hair follicles for non-invasive health monitoring on-site on the ISS Space Station and hair follicles derived retinal organoids for off-site biomedical research
09.45 10.00	Cell biology	5	Analyzing Calcium Signaling by CaMPARI2 during Parabolic Flights
10.00 10.15		19	Multianalyte profiling of Scaffold driven Human Mesenchymal Stem Cell Constructs in Microgravity
10.15 10.30		34	Hypergravity Attenuates Reactivity in Primary Murine Astrocytes
10.30 11.00	COFFEE BREAK		
11.00 11.15	Space Omics	16	Next steps for Space Omics research development in Europe: recommendations from an ESA Topical Team
11.15 11.30		18	Muscle atrophy phenotype gene expression during spaceflight is linked to metabolic stress crosstalk between the liver and the muscle
11.30 11.45		59	Proteomic and Functional Analysis of Acute Galactic Cosmic Radiation Exposure in the Kidney



27th ELGRA BIENNIAL SYMPOSIUM & GENERAL ASSEMBLY

FRIDAY - September 09th

			Life Sciences (Room Castelo + Chiado)
TIME	SESSION	ABSTRACT	TITLE
11.45 12.00	Space Omics	60	The impact of microgravity on kidney function during spaceflight

12.45 14.00	FAREWELL LUNCH		
----------------	-----------------------	--	--

SEPTEMBER 06th - 10th, 2022
Lisbon, Portugal



FRIDAY - September 09th

			Technology/Platforms/Education (Room Alfama + Alcantara)
TIME	SESSION	ABSTRACT	TITLE
09.15 09.30	Platforms and Education	65	The GraviTower Bremen Prototype – disruptive technology for a new age of earth based microgravity and more
09.45 10.00		81	Shared payload platform for small-sized microgravity experiments
10.00 10.15		89	The upcoming SubOrbital Express 3 and 4 Missions for Microgravity Research
10.15 10.30	Education	113	From on-site to online ESA/ELGRA Gravity-Related Research Summer School
10.30 11.00	COFFEE BREAK		
11.00 11.15	Technology developments	30	Yuri enables and develops novel biomedical applications using microgravity on the ISS and beyond
11.15 11.30		74	Efficient and Stable Hydrogen and Oxygen Production in Microgravity
11.30 11.45		92	A new experimental set-up for aerosol stability investigations in microgravity conditions
11.45 12.00		94	A Novel Attitude Control System Combining Reaction Wheels and Transformable Spacecraft Capabilities: Design, Prototyping and Testing at the 77th ESA Parabolic Flight Campaign



27th ELGRA BIENNIAL SYMPOSIUM & GENERAL ASSEMBLY

FRIDAY - September 09th

			Technology/Platforms/Education (Room Alfama + Alcantara)
TIME	SESSION	ABSTRACT	TITLE
12.00 12.15	Technology developments	90	Reduced Gravity Missions from zero to hyper g for Life Science and Process Evaluation

12.45 14.00	FAREWELL LUNCH		
----------------	-----------------------	--	--

INDEX

Abstract No.	Page No.
PLENARY TALKS	
Flight Experiments on Propellant Control in Conformal Propellant Tanks Plants grow in lunar regolith collected in the Apollo 11, 12 and 17 missions.....	27
Plants grow in lunar regolith collected in the Apollo 11, 12 and 17 missions	29
Handling granular materials in space	31
Brains in Space	32
Stress, Hibernation and the Way to Mars	34
ORALS	
O1. Dielectrophoretic induced convection in a sounding rocket flight.....	37
O3. Echographic surveillance of 14 volunteer after 40 days in confinement in a Deep cavern (Deep time experiment 2021).....	38
O4. Cardiovascular deconditioning and impact of artificial gravity during 60-day head-down bed rest – Insights from 4D flow cardiac MRI	39
O5. Analyzing Calcium Signaling by CaMPARI2 during Parabolic Flights	40
O6. Effect of 3-day exposure to dry immersion on veno-arteriolar reflex.....	42
O7. Controlling the dynamics of a free surface via thermocapillary flows.....	43
O8. Thermocapillary flows and phase change in rectangular containers in microgravity	45
O9. Osmosis in a bi-disperse compartmentalized granular material in low-gravity environment.....	47
O10. Dependence oscillatory dynamics on gas flow temperature in liquid bridges.....	49
O13. The effect of hypergravity on burn wounds in Hirudo	51
O14. Three dimensional effects during the melting of phase change materials with thermocapillary flow in microgravity.....	52
O15. 5 days of simulated microgravity induce skeletal muscle structural and microenvironment changes leading to global muscle deconditioning.....	54
O16. Next steps for Space Omics research development in Europe: recommendations from an ESA Topical Team.....	56
O18. Muscle atrophy phenotype gene expression during spaceflight is linked to metabolic stress crosstalk between the liver and the muscle	58
O19. Multianalyte profiling of Scaffold driven Human Mesenchymal Stem Cell Constructs in Microgravity	60
O20. Particle dynamics at the onset of the granular gas-liquid transition	62
O21. Instability caused by interplay of Soret and cross-diffusion in ternary mixture.....	64
O22. Nonlinearities in shadowgraphy experiments on non-equilibrium fluctuations - in preparation of the GIANT FLUCTUATIONS microgravity project	66
O23. Comparative experimental-numerical analysis of PCM: n-hexadecane, n-octadecane and n-eicosane ..	68
O24. Ocular counter-roll is less affected in experienced compared to novice space crew after long-duration spaceflight	70
O28. Capillary rise in Divergent U-Tube during parabolic flight	72
O29. Pool boiling heat transfer in microgravity with microstructured surfaces and electric field: preliminary results of parabolic flight campaign	74
O30. yuri enables and develops novel biomedical applications using microgravity on the ISS and beyond ..	76
O32. The Effect of Marangoni Convection on Heat Transfer in Phase Change Materials Experiment.....	77
O33. Interaction of Faraday waves on alternating multi-layer fluid systems in microgravity	79
O34. Hypergravity Attenuates Reactivity in Primary Murine Astrocytes.....	81
O36. Numerical Simulation and Analysis of Human Cardiovascular Behavior During Subjection to Suborbital Spaceflight	82
O37. Human Reproduction in Space. Late Results	84

O38.	Simulating the spaceflight environment: Combined effect of simulated microgravity, ionizing radiation, and psychological stress on in vitro wound healing.....	86
O39.	Spaceflight Associated Neuro-ocular Syndrome During Long Duration Spaceflight.....	87
O40.	Microstructural transitions during solidification of transparent alloy NPG-DC investigated onboard the ISS using the TRANSPARENT facility.....	89
O41.	Slow Impacts on Regolith Surfaces in Low Gravity – First Experiments on the new GTB-Pro Platform	91
O43.	AtmoFlow – Investigating large scale convection in planetary atmospheres.....	92
O44.	Preliminary Results on Emulsion Destabilisation from the ISS PASTA Experiment.....	94
O45.	AID – Efficient Data Processing with Neuronal Networks for Microgravity.....	96
O46.	Soret coefficients of a ternary C60-THN-Tol mixture: results from DCMIX4 experiments.....	98
O48.	The acute gravitational stress of parabolic flight affects red blood cell aggregation and functionality of circulating immune cells.....	100
O50.	PEDOT:PSS electrodes in view of low-cost biocompatible cellulose-assisted biosensors.....	102
O51.	Granular gas mixtures: Experiments and machine learning-aided analysis.....	104
O52.	Change in circulating collagen type II biomarkers (CTX-II, C1,2C, C2C) in response to 21-days of Head-Down-Tilt Bed Rest (HDT-BR) and countermeasures.....	105
O53.	Hair follicles for non-invasive health monitoring on-site on the ISS Space Station and hair follicles derived retinal organoids for off-site biomedical research.....	107
O54.	Microgravity experiments on Red Blood Cell aggregation dynamics in flow.....	108
O55.	Nature-Inspired, Multi-Functional Surfaces for Sustainable Life Support in Extreme Environments on Earth and in Space.....	110
O56.	Thermal diffusion experiments in CO ₂ -1-hexanol mixtures at different gravity levels – Design and data overview of a parabolic flight campaign.....	112
O57.	Vapour cloud of an evaporating sessile droplet in microgravity.....	114
O58.	Thin Liquid Film Coating and Drying under Microgravity Conditions: How parabolic flights showed the necessity of sounding rocket experiments.....	116
O59.	Proteomic and Functional Analysis of Acute Galactic Cosmic Radiation Exposure in the Kidney.....	117
O60.	The impact of microgravity on kidney function during spaceflight.....	118
O61.	Daily aerobic and resistance exercise on ISS does not correlate with measured change in peak VO ₂	119
O63.	The impact of long-duration spaceflight on the horizontal Vestibulo-Ocular Reflex (hVOR).....	121
O65.	The GraviTower Bremen Prototype – disruptive technology for a new age of earth based microgravity and more.....	123
O66.	Astropharmacy – Healthcare for Earth, the Moon, Mars and beyond.....	124
O67.	Brain structural and functional responses to long-duration spaceflight.....	126
O68.	LateralHigh Content microscopy and super-resolution microscopy profiling to unravel the role of the actin cytoskeleton in T cell activation in microgravity.....	128
O69.	Effects of Altered Gravity on Human Behaviour.....	129
O70.	Automatic structure function analysis using artificial intelligence.....	131
O73.	Thermoelectric convection in rectangular cavities in microgravity conditions.....	133
O74.	Efficient and Stable Hydrogen and Oxygen Production in Microgravity.....	134
O75.	Blue Abyss to Enable Gravity-Related Research and Training.....	135
O76.	Heat transfer induced by thermoelectric convection in a cylindrical annulus in microgravity.....	136
O80.	Film-wise condensation of pure vapour on CNT-coated curvilinear fin in microgravity.....	137
O81.	Shared payload platform for small-sized microgravity experiments.....	139
O82.	Containerless measurements of thermophysical properties on board the ISS using the electromagnetic levitator ISS-EML.....	140
O83.	Thermophysical properties of bulk metallic glasses measured on board the ISS using the electromagnetic levitator ISS-EML.....	142
O86.	Anomalous Behaviour of Temperature Non-Equilibrium Fluctuations across pure CO ₂ Widom Line ..	144
O88.	Different Spaceflight-Associated Changes in the Perivascular Spaces of Astronauts and Cosmonauts	146
O89.	The upcoming SubOrbital Express 3 and 4 Missions for Microgravity Research.....	148

O90.	Reduced Gravity Missions from zero to hyper g for Life Science and Process Evaluation	149
O91.	Two-wavelength Shadowgraphy	150
O92.	A new experimental set-up for aerosol stability investigations in microgravity conditions	152
O94.	A Novel Attitude Control System Combining Reaction Wheels and Transformable Spacecraft Capabilities: Design, Prototyping and Testing at the 77th ESA Parabolic Flight Campaign	154
O95.	A Glimpse into Spaceflight Induced Bone Loss Over 18-Months.....	156
O98.	Dynamics of Non-Equilibrium Fluctuations Close to the Onset of Rayleigh-Bénard Convection.....	158
O99.	Non-Isothermal sloshing for space applications: from a ground-based experimental characterisation to microgravity conditions.....	160
O101.	About water droplet populations in microgravity conditions	162
O102.	Volume measurement of liquid propellants by means of acoustic fields	164
O103.	Expression of locomotor synergies under various gravitational constraints.....	166
O104.	Boil-off management in microgravity	168
O109.	Electronics cooling by means of acoustic waves in microgravity	170
O110.	An integrated acoustic technology for application in propellant tanks.....	172
O113.	From on-site to online ESA/ELGRA Gravity-Related Research Summer School	174
O115.	Study of the influence of microgravity on brain derived spheroids in acoustic levitation	176
O117.	Gold nanoparticles synthesized by laser ablation using a random positioning machine.....	178
O119.	Evaporating sessile droplet on a sounding rocket: analysis by vapour interferometry and simulation	179
O122.	Thermophysical properties of liquid Ti-Al-Cr-Nb alloys: theory vs experiments.....	181
O123.	Manufacturing “in situ” of regolith simulants: Design of composites by liquid assisted processes.....	182

POSTERS

P11.	N-octadecane melting process in a rectangular cell under reboosting maneuvers conditions	185
P12.	ESA’s Scientific Research Program on Sounding Rockets: past and present.....	187
P25.	Thermodiffusion coefficients in Polystyrene-Toluene mixtures: DCMIX 4	188
P26.	Analysis of the thermogravitational effect by a 3-Laser Optical Digital Mach-Zehnder Interferometer	190
P27.	Temperature dependent measurements of the diffusion and Soret-coefficient in a binary polystyrene/toluene mixture by means of a transient holographic grating technique	192
P31.	Molecular diffusion, Thermodiffusion and Soret coefficients of fullerene C60 in aromatic solvents	194
P35.	Astrocyte Reactivity is Reduced by Exposure to Hypergravity.....	196
P42.	Adaptation to full weight-bearing following disuse: the impact of biological sex on musculoskeletal health.....	198
P47.	Measuring Neuronal Activity Live under Micro- and Hypergravity.....	199
P49.	Combined action of simulated microgravity and radiation on the transcriptome of Arabidopsis thaliana seedlings.....	201
P62.	Self-organized criticality assessed on Holter heart rate variability during spaceflight simulation by dry immersion.....	203
P71.	Ready, Steady, Go! Altered Gravity Influences Responses to Environmental Stimuli	205
P72.	Intracranial Effects of Artificial Gravity on Head Down Tilt Bedrest.....	206
P78.	Altered gravity disrupts spatial navigation	207
P85.	Localization of the ER-bodies in root cells of Arabidopsis thaliana under clinorotation.....	209
P87.	Effects of sustained hypergravity on growth and reproduction in earthworms: A pilot study.....	211
P93.	Diffusion and thermodiffusion of polymers in mixed solvents.....	213
P97.	A New Microgravity Modular Research Platform for Education	215
P105.	Diffusing Wave Spectroscopy investigations of emulsions in microgravity.....	217
P106.	FLUMIAS - high-resolution live-cell fluorescence microscopy and identifying gravity sensitive thresholds on-board the ISS.....	219

P111.	Individual susceptibility to altered gravitational environment: behavioural indicators and possible countermeasures.....	221
P112.	Behavioural indicator of susceptibility in mice exposed to simulated microgravity.....	222
P116.	A wearable-based system to reduce space motion sickness by multi-sensory pre-habituatio	223
P118.	NeuronGrav: characterizing neuronal responses in altered gravity via glider-based parabolic flights ..	225
P125.	21 day Dry Immersion Bed Exposure drives CD3+ T Cell Transcriptional Landscape Towards A Proliferative Phenotype	226
P126.	Stable and unstable component separation in Soret experiments with TEG-water mixture	227
P127.	Immune cells respond to proton irradiation in a dose- and sex-dependent manner.....	229

27th
ELGRA BIENNIAL SYMPOSIUM
& GENERAL ASSEMBLY

PLENARY TALKS



PLENARY TALK

Flight Experiments on Propellant Control in Conformal Propellant Tanks

S. Collicott¹

¹Purdue University School of Aeronautics and Astronautics, West Lafayette, USA, collicott@purdue.edu

Introduction

SmallSats, cube-sats, micro-sats, and nano-sats, that is, the new generation of miniaturized satellites can have unique liquid propellant management constraints. The smaller volume of the SmallSat “bus” is now driving design towards conformal propellant tanks which optimize the use of volume inside a small sat. If one scales down lengths in a satellite, the tank wall thickness can not be scaled down much from large satellites as it’s already a small number. So small-sat tanks are largely stronger than needed and thus need not be the axisymmetric minimum-weight pressure vessels found in traditional large satellites. Maneuvering, swarming, collaborative, and adaptive SmallSats and systems of SmallSats are all in development, bringing novel new demands on propellant management in orbit. NASA’s Technology Roadmap, lists, for example, “Optimization of the thruster and propulsion system to meet SmallSat mission-specific requirements” as a technology challenge in two specific topics.

At the small length scales of SmallSats, the traditional spherical and similar axisymmetric geometries for minimum-weight pressure vessels are not required and innovative volume-efficient conformal tanks are legitimate design options. The interiors of the novel new tanks require passive control of liquid propellants as in traditional large satellites and this passive control is performed with surface tension propellant management devices (PMDs). PMDs generally use sheet metal vanes(Jaekle, 1991), traps (or sumps)(Jaekle, 1995), sponges(Jaekle, 1993), galleries(Jaekle, 1997), and screens(Hartwig et al., 2015) designed to maintain liquid at the tank outlet, deliver gas-free propellant to thrusters, and control the location of the mass center of the liquid for superior attitude control and efficient use of propellants.

Research reported here addresses this spaceflight technology needs through multiple parabolic flights of numerous representative geometries anticipated for conformal propellant tanks. Cubes, cylinders, rectangular parallelepipeds, conformal L-shaped volumes, and similar are typical of the expected new generation of volume-efficient small-sat tanks which require proof of operations in weightlessness.

Experiment

Tank models were constructed both as volumes machined out of transparent cast acrylic and as 3D-printed structures. The printed tanks required chemical and mechanical surface finishing by hand to become as smooth and transparent as needed for this work. Many tank shapes were examined, Fig. 1 illustrates the first batch of 3D-printed tanks shapes.

PMD vanes were designed as an adaptation of a traditional interplanetary spacecraft design(Tegart, 1997). With no specific set of mission accelerations, flow rates, etc., to constrain PMD design, these PMDs are simply illustrations of PMD example function in these new tank shapes.

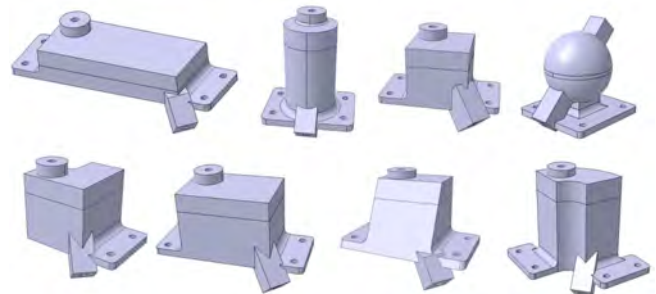


Figure 1: Initial conformal tank shapes that were tested, volume typically 15 to 20ml. Top row, left to right: credit card, cylinder, cube, sphere (a control case). Lower row, left to right: L, rectangle, trapezoid, quarter arc. Drain of each tank is the lower square projection at one bottom corner of each tank.

Weightless flight testing was in parabolic aircraft flight with the Zero-G company in the USA. Example images are presented below, where the red liquid is silicone oil with zero contact angle and the blue liquid is propylene glycol with larger, approximately 60 degree, contact angle. Figures 2 to 4 present example stills for the flight videos.



Figure 2. Low-fill fraction results for trapezoidal tanks, left column, and cube tanks, right column. Sloped face of the trapezoids faces away from the camera in this view. Drain of each tank is in the corner at the bottom, left, and into the page.

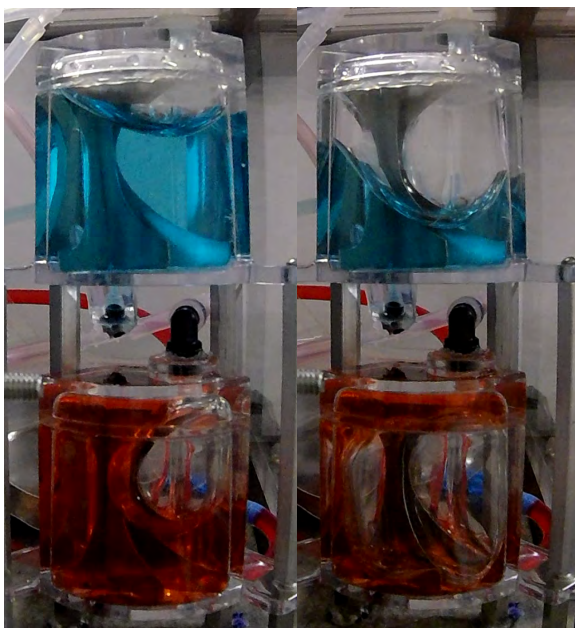


Figure 3. Example quarter-arc tanks, viewed through the large radius side, showing results in zero-g. Left column is high fill fraction, right column in low fill fraction. Drain of each tank is in the corner at the bottom, left, and into the page.

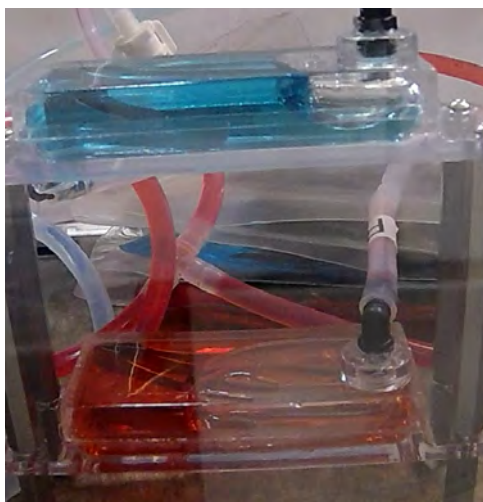


Figure 4. The credit card tanks. The silicone oil (red liquid) shows superior control of liquid by the vanes, as seen by the longer rather than thicker bubble. Drain of each tank is in the corner at the bottom, left, and into the page.

Modeling

The *Surface Evolver* code is used to begin zero-g modeling of these tanks. Example results of tanks without PMD are shown in Figure 5. In all three cases, the fillets in the corners are smallest radius at the drain of the tank as an example to investigate how tapered fillets, which are simple to 3D print, might help with draining. Note that the cube and rectangle tanks show trapped liquid (at the vertex at the top of the images) and the “credit card” will trap liquid with further draining. This illustrates the need for new PMD design approaches for these new tank shapes. Modeling of such shapes requires more labor hours than the simpler, traditional axisymmetric shapes do.

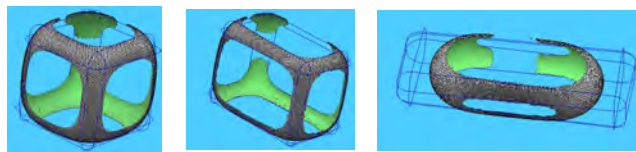


Figure 5. Three example conformal tanks with tapered fillets at fill fractions near depletion. Left to right: cube, rectangle, and a flat “credit card” tank.

Conclusions

Propellant management in the era of conformal propellant tanks brings new PMD design challenges. Weightless flight testing to date gives optimism that these challenges are manageable. The interior corners of the tank provide built-in opportunities for controlling liquid with a well-designed PMD and yet also provide regions to trap liquid disconnected from the outlet near the end of mission. It is also found that the modeling of the propellant positioning requires greater time than for traditional axisymmetric tanks. Early inclusion of liquid management in spacecraft design considerations should reduce complex analysis and problem-solving later in the design.

Acknowledgements

The author thanks the NASA Flight Opportunities Program for support through grants 80NSSC18K1287 and 80NSSC20K1811. Purdue graduate students Emily Beckman, Praveen Srikanth, and Robert Beggs contributed greatly to program success. Undergraduate students in the 22nd to 26th years of the author’s “Zero-gravity Flight Experiment” class participated in the program as a design-build-test engineering education experience.

References

- D. Jaekle, Jr., “Propellant management device conceptual design and analysis – Vanes”, *27th Joint Propulsion Conference*, (1991), 10.2514/6.1991-2172.
- D. Jaekle, Jr., “Propellant management device conceptual design and analysis - Traps and troughs”, *31st Joint Propulsion Conf. and Exhibit*, (1995), 10.2514/6.1995-2531.
- D. Jaekle, Jr., “Propellant management device conceptual design and analysis – Sponges”, *9th Joint Propulsion Conference and Exhibit*, (1993), 10.2514/6.1993-1970.
- D. Jaekle, Jr., “Propellant management device conceptual design and analysis – Galleries”, *33rd Joint Propulsion Conference and Exhibit*, (1997), 10.2514/6.1997-2811.
- J. Hartwig, and J. McQuillen, “Screen Channel Liquid-Acquisition-Device Bubble Point Tests in Liquid Methane,” *Journal of Thermophysics and Heat Transfer*, Vol.29: 364-375, (2015) 10.2514/1.T4078.
- J. Tegart, A vane-type propellant management device. *33rd AIAA/ASME/SAE/ASEE Joint Propulsion Conference*, Seattle, WA. AIAA-97-3028. (1997)

PLENARY TALK

Plants grow in lunar regolith collected in the Apollo 11, 12 and 17 missions

A-L. Paul¹, S. Elardo², R.J. Ferl³

¹University of Florida, Gainesville FL, USA, alp@ufl.edu, ²University of Florida, Gainesville FL, USA, selardo@ufl.edu, ³University of Florida, Gainesville FL, USA, robferl@ufl.edu,

Introduction

For the first time, we demonstrated that plants can use lunar regolith as the sole matrix for growth, enabling options for cultivation systems within lunar stations. Using samples from Apollo 11, 12 and 17 lunar sites, we show that the terrestrial plant *Arabidopsis thaliana* germinates and grows in diverse lunar regoliths. Compared to JSC-1A controls, plants mount site-specific stress responses that are reflected in growth morphology and in the patterns of gene expression (Paul et al., 2022).

There is a clear imperative that humans will return to the moon (Neal, 2016). Characterizing biological reactions to lunar regolith is critical to enabling safe, productive and sustainable exploration of the Moon, as well as forming the foundation of future biological science on the Moon. As developmentally complex eukaryotes, plants are fundamentally sound test subjects for biological responses to lunar regolith. In addition, plants have long been envisioned as potential life support components in future lunar bases (Wheeler, 2010; Hossner et al., 1991; Salisbury 1991; Ming et al., 1994). The ability to utilize in situ resources extends capabilities in support of humans in extraterrestrial environments.

Plants played a role in the initial characterization of the biosafety of lunar materials within the Lunar Receiving Laboratory (Walkinshaw and Johnson 1971). Walkinshaw determined that the Apollo samples had no overt pathogenic effects when presented to plant tissues. Yet even during those Apollo era studies, plants were only placed “in contact” with lunar materials and lunar regolith was never used as a major substrate for plant growth (reviewed in Ferl and Paul, 2010).

The goal of this study was to grow *Arabidopsis* directly in lunar regolith to answer the question “Can plants grow in ‘soil’ derived from the in situ utilization of lunar regolith?”.

Approaches

The lunar Allocation Analysis Review Board / AARB (formerly CAPTEM), through the Apollo Sample Curator at Johnson Space Center (Ryan Ziegler), provided 4 x 1g samples of regolith from Apollo 11 (10084), 12 (12070) and 17 (70051). These regoliths, along with the NASA lunar simulant JSC-1A, were used as the substrate for plant growth (full details see Paul et al., 2022).

Plants grew in 900mg of material; four replicates from each site, alongside 16, 900mg replicates of JSC-1A simulant. Replicates were arranged in four, 48-well plates, and each plate held a representative of each Apollo site. Each 12.5 mm x 15mm deep well held a plug of wicking rockwool topped with a 0.45um nylon filter, then 900mg regolith. Each well had a drilled hole to facilitate watering from below with a 0.125X MS nutrient solution (Figure 1).

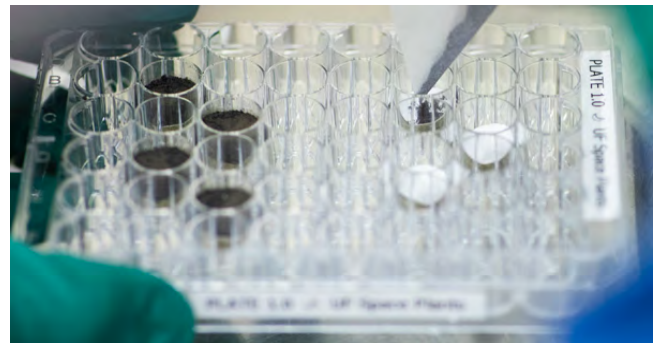


Figure 1: Transferring lunar regolith into the prepared wells of the growth plate. The four filled wells on the left contain the JSC-1A simulant control. The three wells on the right are being filled with Apollo 11, Apollo 12 and Apollo 17 regoliths (top to bottom).

Results

All of the seeds germinated, whether in the JSC-1A simulant or in lunar regolith. After about a week, differences in morphology and growth rates between controls and regolith, and among lunar sites, began to emerge, and there were marked differences by time of harvest at Day 20 (Figure 2).

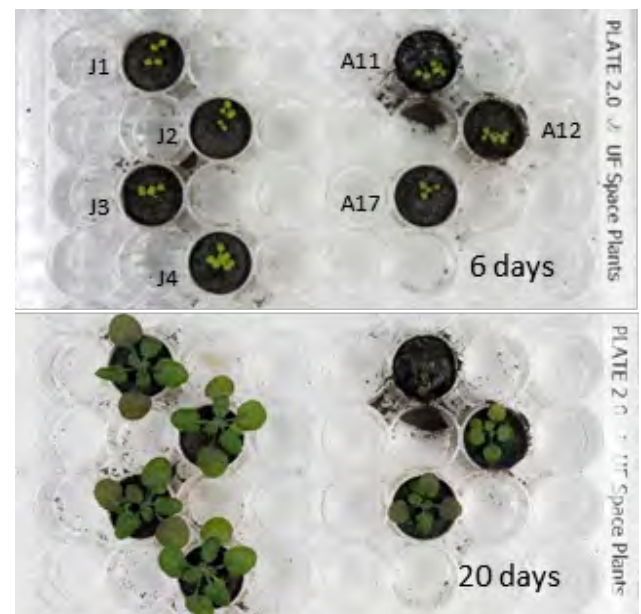


Figure 2: Development in regolith compared to JSC-1A simulant at Day 6 and Day 20 in a representative plate (Plate 2).

Data were collected to evaluate the impact of the three sources of regolith on plant growth, development and patterns of gene expression compared to the JSC-1A controls. In all cases, plants grown in lunar regolith were smaller than the controls, but plants grown in Apollo 11 regolith were typically smaller, and sometimes severely

stunted compared to plants grown in Apollo 12 and Apollo 17 regolith. The transcriptomes of the lunar regolith-grown plants showed similarity with Arabidopsis transcriptomes of plants grown under environmental stress, and genes associated with Reactive Oxygen Species (ROS) signalling (e.g. Williams et al., 2016), salt stress (e.g. Ma et al., 2006), and metal stress (e.g. Song et al., 2017) were among the most abundant differentially expressed genes in comparison to the JSC-1A controls (Figure 3).

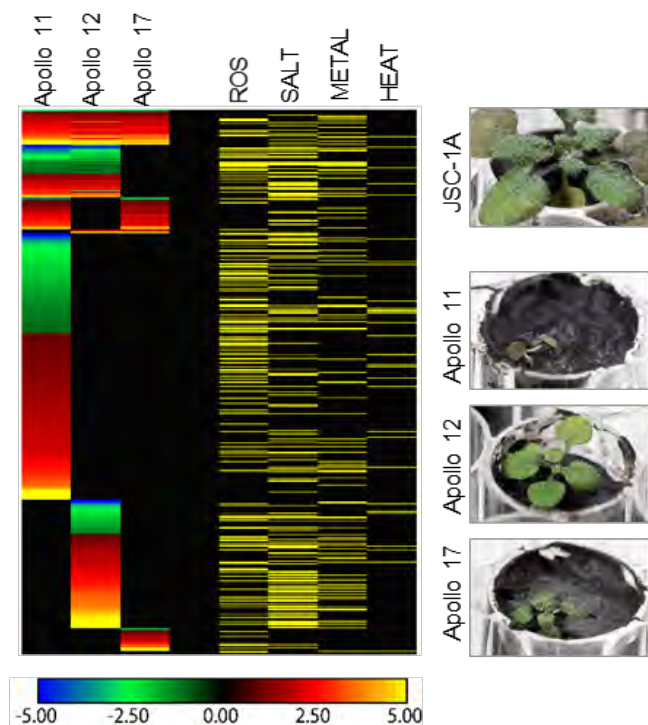


Figure 3: Transcriptome (RNAseq) analyses of plants grown in lunar regolith. A comparison of plants grouped by Apollo site after growth in lunar regolith for 20 days to those grown in JSC1A simulant. Analyses were conducted with three (Apollo 11) to four (Apollo 12, 17) replicate plants from each site. Genes associated with ROS, salt, metal and heat responses are indicated by yellow rows. The values of the heat-map colors shown in the bar below figure; fold-change presented as Log₂ (a value of 1 = 2-fold). Representative photographs of 20 day old plants to the right of the heat-map were taken just prior to being harvested for analyses.

Conclusions

These data demonstrated that terrestrial plants are capable of growth in lunar regolith as the primary support matrix. Soils derived from lunar regolith could therefore be used for plant production and experiments on the Moon. However, these data also demonstrated that lunar regolith was not a benign growth substrate. Plants broadly interpreted lunar soils as highly ionic and as eliciting oxidative stress, which is consonant with the prediction that the cosmic ray and solar wind damage to surface regolith would leave it very reactive to biological systems. Although examples of poorly developing plants were represented in each of Apollo site sources, overall, the plants grown in Apollo 11 regolith struggled the most and displayed the greatest number of differentially expressed genes. These data suggest that more mature regolith (the extent of time exposed to the surface – e.g. Morris et al, 1976; Labotka et al.1980) provides a poorer substrate for plant growth than immature regolith. Thus,

although this study demonstrates that plants can use lunar regolith as a primary substrate, further characterization and optimization would be required before regolith can be considered a routine in situ resource, particularly in locations where the regolith is highly mature.

Acknowledgements

We thank the members of the UF Space Plants Lab, particularly Jordan Callahan, Natasha Haveman and Brandon Califar for their support. We thank the NASA AARB (formerly CAPTEM) and the NASA Johnson Space Center Curation staff for allocation of the Apollo samples for this work. We also thank UF-Research and UF-IFAS Communications, particularly Tyler L. Jones for his plant photography. And finally, the UF ICBR Gene Expression Core (RRID:SCR_019145), NextGen Sequencing Core (RRID:SCR_019152), Bioinformatics (RRID:SCR_019120) core, for their services. Funding for this work included National Aeronautics and Space Administration grants NNX14AT24G (A-LP, RJF), University of Florida Office of Research - Retuned IDC (A-LP, RJF) and National Aeronautics and Space Administration grant 80NSSC19K0752 (SME).

The full description of the study can be found in Paul et al. 2022 (<https://www.nature.com/articles/s42003-022-03334-8>)

References

- Paul, A.-L., Elardo, S.M. & Ferl, R. Plants grown in Apollo lunar regolith present stress-associated transcriptomes that inform prospects for lunar exploration. *Nature Commun Biol* 5, 382, (2022)
- Neal, C. R. A return to the moon is crucial. *Scientific American*. 315, 8 (2016).
- Wheeler, R.M. Plants for human life support in space: From Myers to Mars, *Grav. and Space Biology* 23, 25-35 (2010)
- Hossner, L.R., Ming, D.W., Henninger, D.L. Allen, E.R. Lunar outpost agriculture *Endeavour* 15, 79 (1991)
- Salisbury, F.B. Lunar farming: achieving maximum yield for the exploration of space *HortScience* 26, 827 (1991)
- Walkinshaw, C. H. & Johnson, P. H. Analysis of vegetable seedlings grown in contact with Apollo 14 Lunar surface fines. *Hortscience* 6, 532-535 (1971).
- Ferl, R. J. & Paul, A.-L. Lunar plant biology--a review of the Apollo era. *Astrobiology* 10, 261-274, (2010).
- Ming, D.W. & Henninger, D.L. Use of lunar regolith as a substrate for plant growth. *Adv Space Res* 14, 435 (1994)
- Willems, P. et al. ROS Wheel: refining ROS transcriptional footprints in Arabidopsis. *Plant Physiol* (2016).
- Ma, S., Gong, Q. & Bohnert, H. J. Dissecting salt stress pathways. *J Exp Bot* 57, 1097-1107, (2006).
- Song, J. et al. cadmium stress-responsive gene AtFC1 confers plant tolerance to cadmium toxicity. *BMC Plant Biol* 17, 187, (2017).
- Labotka, T. C., et al. The lunar regolith - Comparative petrology of the Apollo sites. *Proceedings of the Lunar and Planetary Science Conference*, 11th 2, 1285-1305 (1980).
- Morris, R. V. Surface exposure indices of lunar soils - A comparative FMR study. *Proceedings of the Lunar and Planetary Science Conference*, 7th, 315-335 (1976).

PLENARY TALK

Handling granular materials in space

N. Vandewalle¹

¹GRASP, Institut de Physique B5a, Sart Tilman, B4000 Liège, Belgium, nvandewalle@uliege.be

Keynote Talk

Being a paradigmatic system of Soft Matter Physics, granular materials are composed of many solid particles with no interaction except dissipative collisions and friction. This particular class of materials may exhibit solid, fluid, or gaseous behaviors depending on the way they are manipulated. Although nearly 80% of the products used in industry are powders and grains, many fundamental questions concerning their rheology and their dynamics are still unsolved.

Granular materials are encountered in space exploration : regolith on asteroid surfaces, powder propellants of rockets, or planetary rings dynamics. They are also considered for space exploitation such as asteroid mining. Therefore, space missions will face major challenges concerning the handling of granular materials in low-gravity environments. For example, it is not obvious how to perform a simple operation like sieving in space, whereas several month efforts failed to free NASA's Mars Exploration Rover Spirit from a Martian sand trap in 2010. Therefore, it is of primary interest to better understand the flow and the dynamics of granular media in low-gravity conditions.

In this talk, I will emphasize the physical phenomena behind granular systems in space (see Figure 1). From various microgravity experiments and from models, it is possible to design methods to process granulates and powdered materials in space. In particular, I will focus on the SpaceGrains project (Aumaître et al 2018) which aims to gather various experiments from dilute to denser systems. I will make some comparisons and analogies with existing methods/physics on Earth and microgravity experiments, in order to give an overview of the differences and similitudes.

During this talk, pictures and movies about those phenomena will be shared to enjoy the beauty as well as the complexity of physics.

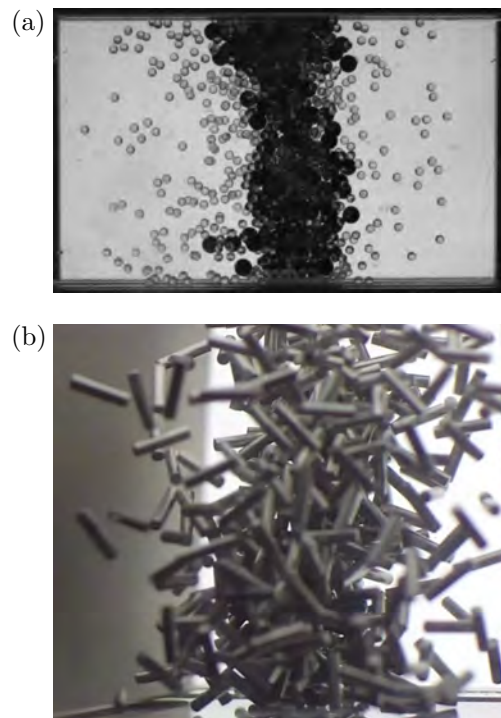


Figure 1: (a) Picture of a mixture of small and large beads in microgravity showing phase separation. (b) Picture of a granular gas made of rod-like particles.

Acknowledgements

VIP-Gran-PF instrument was built by DTM Technologies (Modena, Italy). This work was funded by European Space Agency Topical Team SpaceGrains No. 4000103461. We thank the support of Novespace during ESA Parabolic Flight Campaigns.

Reference

S. Aumaître, R. P. Behringer, A. Cazaubiel, E. Clément, J. Crassous, D. J. Durian, E. Falcon, S. Fauve, D. Fischer, A. Garcimartín, Y. Garrabos, M. Hou, X. Jia, C. Lecoutre, S. Luding, D. Mazza, M. Noirhomme, E. Opsomer, F. Palencia, T. Pöschel, J. Schockmel, M. Schröter, M. Sperl, R. Stannarius, N. Vandewalle, and P. Yu, *An instrument for studying granular media in low-gravity environment*, Rev. Sci. Instrum., 89, 075103 (2018).

PLENARY TALK

Brains in Space

Floris L. Wuyts

Lab for Equilibrium Investigations and Aerospace, University of Antwerp, Belgium

Introduction

Background

We have currently passed more than 60 years of human spaceflight, during which research on the effects of spaceflight on the human body has continuously been conducted. Yet, what happens to the brain during a space mission has long been an uncharted domain. In 2009, the ESA BRAIN-DTI project was conceived, which was the first prospective study to investigate brain structural and functional changes after spaceflight using magnetic resonance imaging (MRI).

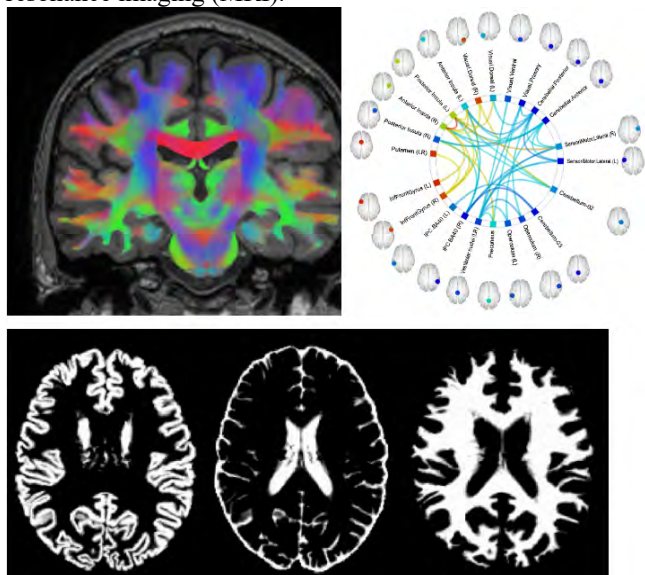


Figure 1. Different MRI techniques provide various outputs relating to biological information of the imaged brain. We can measure nerve fibre orientation (top left; colour codes refer to the direction of the nerve fibres, with green representing front to back, red left to right, and blue top to bottom), functional connectivity (top right), and volumes of MRI images segmented into grey matter (bottom left), cerebrospinal fluid (bottom centre), and white matter (bottom right).

Study design

During this ongoing study, we study Roscosmos cosmonauts and European Space Agency (ESA) astronauts (we will use the term astronauts for the remainder of the text, referring to both cosmonauts and astronauts), who endeavour on missions to the International Space Station (ISS). Typically, these missions last six months. We have the astronauts scanned using MRI before their mission, as shortly as possible after return from the ISS, and a third time approximately 8 months after return. Currently, 35 astronauts have enrolled in our study.

Main findings

The first analysis conducted based on the BRAIN-DTI project involved a case study for which we used functional MRI [1].

Specifically, we measure brain function across the whole brain while the astronauts imagine performing a motor task, in our case playing tennis, and subsequently, imagine navigating through their home. This paradigm allows us to visualize which brain regions are active during this task, and therefore we can investigate whether the brain's activity in performing these tasks changes after spaceflight.

We observed that the supplementary motor cortex was more active during the motor imagery task after spaceflight compared to before, which is interpreted as a motor region needing to work harder to perform this task. We saw also that connectivity changed in a region that is a main hub for vestibular information, as well as in the motor cortex. Vestibular information relates to the sensory input that is generated by head movements and which is highly dependent on the force of gravity. Overall, this study shows altered brain function and functional connectivity in motor and vestibular brain regions after spaceflight, which very well fits the hypothesis that motor strategies and vestibular information are required to adapt in a weightless environment.

The next study we performed related to the anatomical MRI images that we acquire in each subject, which allows us to study brain volumetric changes [2]. While this technique to study volume changes is often used to detect local areas of adaptation, our analysis generated a very different result, which was highly unanticipated. We saw volume changes of the brain grey matter (GM) and cerebrospinal fluid (CSF) across a high portion of the brain after spaceflight, rather than local volume changes. Specifically, we find GM volume decreases and CSF volume increases in the bottom half of the brain, while we see CSF volume decreases at the top surface of the brain. Additionally, we observed CSF volume increases in the brain ventricles, indicating ventricular dilation. All these findings point toward a redistribution of CSF within the skull and suggest that the CSF flow might be hampered in microgravity. The changes in GM volume point to a shape change, and not a GM volume decreases. Finally, when we look at the follow-up data obtained a half-year after the astronauts' return to Earth, we find that these brain shifts were not fully resolved yet. CSF and GM volume differences were still detectable a half-year after return from the ISS.

Because of the ventricular CSF volume increase observed after spaceflight, we subsequently performed a study quantifying the ventricular dilation [3]. We found that the lateral and third ventricles significantly increased, by 13% and 10% respectively, after spaceflight compared to before. The fourth ventricular CSF volume did not significantly increase. Again, our follow-up data revealed remaining significant differences in lateral and third ventricular CSF volume as compared to pre-flight, though the effect sizes were not as large. These findings indicate that the normalization back to baseline levels is a slow process, which is still ongoing a half-year after the ISS mission.

Our next study concerned analysis on diffusion MRI data, which is a specific type of MRI that allows us to gain information on brain microstructure and volume or macrostructure [4]. This analysis rendered similar information on brain and CSF shifts with one important addition. While our previous volumetric analysis only rendered information on volumetric changes, the current study was able to disentangle between changes where the amount of tissue is preserved (referred to here as density), and those where the net amount of tissue changes (referred to here as mass). Our results showed GM density increases at the top of the brain, and GM density decreases in the lower half of the brain. Such changes are purely due to shape changes, where GM density increases reflect a crowding of the GM (i.e. the brain gyri become more compact) and GM density decreases reflect a spreading out of the GM (i.e. the brain gyri are pushed away from each other). This is a relevant finding as it gives evidence of our previous hypothesis that the GM volume changes are not due to volume loss, but merely a redistribution or a shape change. Importantly, we did not find decreases in GM or white matter (WM) mass, meaning that we don't find evidence of atrophy in the brain. On the other hand, we did see GM and WM mass increases, which means the net amount of tissue increased. We found such changes in three major motor areas of the brain, including the primary motor cortex, the basal ganglia, and the cerebellum. These findings give strong evidence for adaptive changes in the brain, known as neuroplasticity, specifically in the motor system. As for the case study, it is expected that astronauts need to adapt their motor strategies in weightlessness, as they are optimized to function in an environment with a constant 1G gravity level. Concerning the follow-up, we again found that some of the changes were not fully resolved by the follow-up measurement, while others were. Together, we now have from different analyses results that indicate an incomplete but ongoing normalization process at a half-year after the ISS mission.

A subsequent diffusion MRI study aimed to evaluate microstructural changes at the level of fibre tracts [5]. Diffusion MRI is a suitable modality to define local fibre orientations based on the data, a technique known as tractography. In this study, we compared tractograms, which is a term for the assembly of all connections in the brain, across different time points. The results of this analysis then display those fibre tracts where there are differences in time. Specifically, we compared pre-to post-flight, pre-flight to follow-up, and post-flight to follow-up. We observed changes in various tracts, including the corpus callosum, corticospinal and corticostriatal tracts after spaceflight compared to before. Between pre-flight and follow-up, we still observe many differences in the tractograms, again highlighting the incomplete reversal of structural changes resulting from spaceflight. While this technique cannot disentangle between physiological effects such as neuroplasticity and physical effects such as brain shifts, our results can be explained by either effect. However, we can reason that the changes in corticospinal and corticostriatal tracts likely reflect neuroplasticity, because we previously found evidence of neuroplasticity in the motor areas that are connected by these tracts (i.e. we previously found neuroplasticity in the motor cortex and basal ganglia. We now see a change in the

corticostriatal tract, which connects the motor cortex with the basal ganglia). On the other hand, because we know that the ventricles enlarge after spaceflight and the corpus callosum borders on of the ventricular walls, we could reason that the changes in the corpus callosum are due to a shape change induced by the ventricular expansion. This study overall provided many confirmatory results from previous studies, though for the first time presents such effects at the level of brain fibre connections.

Overall relevance and future perspectives

The BRAIN-DTI project is the first prospective study to look at brain structural and functional changes after spaceflight and to include a follow-up measurement a half-year after the astronauts' return from the ISS. With no previous knowledge on such changes, we provided first insights into the different brain changes occurring after a space mission. Our studies mapped out various volumetric changes in the brain, indicating that the brain moves upward within the skull and the CSF around the brain is redistributed and its flow likely hampered. Our analyses further clarified that the GM volume changes do not represent a change in the net amount of GM, but rather represent a shape change. We also provide compelling evidence that these shifts are partially detectable a half-year after the space mission. An association between the CSF and GM shape changes with the spaceflight-associated neuro-ocular syndrome (SANS) has been hypothesized. SANS is characterized by ocular structural changes and impairment of visual acuity, which can have strong operational consequences. Some of the ocular structural changes that characterize SANS pertain to the area just behind the eye globe, which is a continuous compartment with the CSF space where we see the volume changes. Pursuing a more accurate characterization of this association could strongly benefit mitigating SANS and its negative consequences. Our most recent study shows a distinct difference between the perivascular spaces (PVS) of NASA crew members compared to Roscosmos cosmonauts [6]. After spaceflight, the PVS is increased with more than 30% in the NASA group compared to only 14% in Roscosmos crew. This could be explained by the use of different countermeasures on board such as ARED. Further research is needed to elaborate further on this.

References

1. Demertzi A et al. Cortical reorganization in an astronaut's brain after long-duration spaceflight. *Brain Struct Funct.* 2016
2. Van Ombergen A et al. Brain Tissue-Volume Changes in Cosmonauts. *N Engl J Med.* 2018
3. Van Ombergen A et al. Brain ventricular volume changes induced by long-duration spaceflight. *Proc Natl Acad Sci.* 2019
4. Jillings S et al. Macro- and microstructural changes in cosmonauts' brains after long-duration spaceflight. *Sci Adv.* 2020.
5. Doroshin A et al. Brain Connectometry Changes in Space Travelers After Long-Duration Spaceflight. *Front Neural Circuits.* 2022
6. Barisano et al. The effect of prolonged Spaceflight on Cerebrospinal Fluid and Perivascular Spaces of Astronauts and Cosmonauts. *Proc Natl Acad Sci.* 2022.

Acknowledgement: Steven Jillings and the BRAIN-DTI team

PLENARY TALK

Stress, Hibernation and the Way to Mars

Alexander Choukér (ISGP Plenary)

Laboratory of Translational Research, Hospital of the University of Munich, Munich, Germany, achouker@med.uni-muenchen.de,
on behalf of the involved researchers, students, administrators and the ESA TT

Introduction

Crewed space missions to Mars and beyond will impose extreme stresses of physical and psychological nature on the space travelers subjected to the space exposome. The individual effects on the organs can vary and be leading to health risks and adding mission critical risks. In addition to the psychological strain, logistical and technical challenges for life support and transportation for such long mission can increase the costs and mission realization as well. Here principles of nature to adjust to extreme environments by torpor/hibernation are considered and shall be taken into consideration for long-duration crewed missions. The key element of torpor/hibernation is the reduction of the organism metabolism, the metabolic rate, to hereby limit food intake, oxygen supply and hence reducing payloads. The widespread occurrence of this mechanism to reduce metabolism in the kingdom of animals feeds also the idea of human torpor and its beneficial applications in medicine and space exploration. As a consequence of activities of the European Space Agency's Topical Team on Hibernation and Torpor, ESA has performed a MiCRA (Mission Concept and Requirements Assessment) study on the system-level impact of human hibernation. Based on this and parallel emerging scientific projects a tentative road map to human hibernation has been discussed. Because of the yet unknown risks of such condition in humans, further significant research is needed and new advanced technical conditions to be developed in parallel. If this transition from science fiction to science increases its pace and an induction and maintenance of torpor in non-hibernating mammals and then in humans will be achieved, this will open new, game-changing opportunities for crewed space travel as well as in medicine on Earth.

Conclusions

Travel to outer space and leaving the Earth's exposome imposes extreme stresses to the human body. New insights into the biology of torpor can lead to facilitate long-duration missions to outer space and reducing the payload of a crewed spacecraft, respectively. This talk gives an overview on these ongoing activities.

Acknowledgements

The authors are grateful for the support from the European Space Agency (ESA) and the SciSpaceE programme. We thank L. Summerer from the ESA Advanced Concepts Team for the strong support of this topic. The professionalism and enthusiasm of the interdisciplinary CDF team under the leadership of R. Biesbroek. The study was initiated by the ESA Topical Team "Hibernation and Torpor" as chaired by G. Heldmaier and J. Bereiter-Hahn, and supported by the ESA Contract No. 4000117771/16. Financial support for the presenter AC comes from the German Federal Ministry of Economics and Energy / Ministry of Economic Affairs and Climate Action (BMWi/BMWK handled by DLR).

References

1. Choukér A, Ngo-Anh TJ, Biesbroek R, Heldmaier G, Heppener M, Bereiter-Hahn J. *Neurosci Biobehav Rev.* 2021
2. Pavez Loriè E, Baatout S, Choukér A, Buchheim JI, Baselet B, Dello Russo C, Wotring V, Monici M, Morbidelli L, Gagliardi D, Stingl JC, Surdo L, Yip VLM. *Front Bioeng Biotechnol.* 2021
3. Chouker A, Bereiter-Hahn J, Singer D, Heldmaier G. *Pflugers Arch.* 2019

27th
ELGRA BIENNIAL SYMPOSIUM
& GENERAL ASSEMBLY

ORALS



ORAL 1

Dielectrophoretic induced convection in a sounding rocket flight

¹M. Meier, ¹A. Meyer, ¹V. Motuz, ¹Y. Sliavin, ¹T.R. Bista, ¹M. Strangfeld, ¹P. Szabo, ¹C. Egbers

¹Brandenburg University of Technology, Cottbus, Germany, meierm@b-tu.de

Introduction

We investigate a special type of convection called thermo-electrohydrodynamic (TEHD) convection. Dielectric fluids exhibit a different type of convection compared to natural free convection, by which a non-isothermal fluid is not only driven by density changes, but also by a dielectrophoretic force due to permittivity variations, when an alternating electric field is present.

Experiments

As buoyancy is able to induce free convection in a vertical or horizontal aligned cylindrical annulus by the thermal expansion of the working fluid, we study convection induced by the temperature-dependant electrical permittivity of a dielectric fluid experimentally. To observe the evolving convective flow fields, Particle Image Velocimetry (PIV) and shadowgraph recordings were utilised. Beside laboratory investigations, we performed 12 parabolic flight campaigns (PFC) (Meier et al. 2018; Meier et al. 2018, Szabo et al. 2021) in the last 10 years.

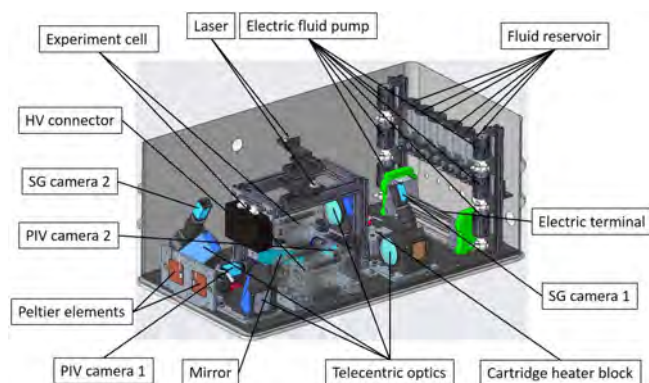


Figure 1: Sketch of the parabolic flight experiment set-up

The parabolic flight campaigns with the ZERO-G-airplane of NOVESPACE deliver a short duration of the microgravity phases - about 20s at gravity levels of about 0.1 to 17.7 m/s² ($\sim 10^{-2}g$ to $\sim 1.8g$). This is too short to obtain a fully established stable flow in a large range of our experimental parameter field. Therefore, over the last 5 years, we prepared a sounding rocket flight experiment, which shall be conducted in October 2022 as part of the TEXUS 57 campaign. These TEXUS-(Technologische Experimente unter Schwerelosigkeit) flights have a much larger μg -phase -about 6min- as PFC's with an airplane. Results of ground experiments will be presented.

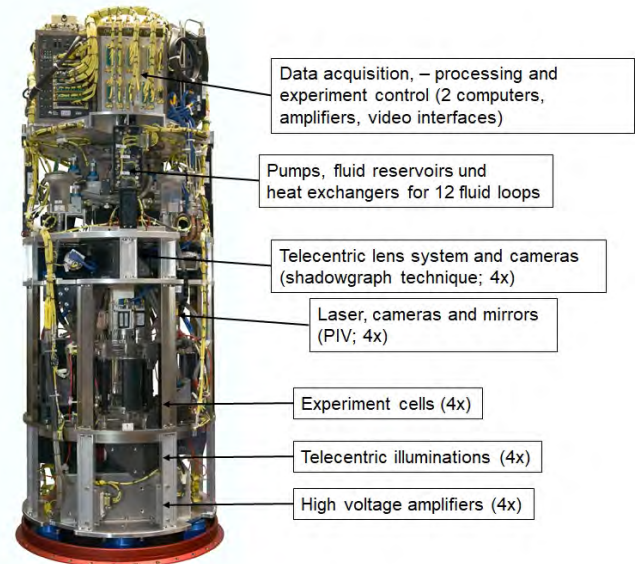


Figure 2: Final set-up of the TEKUS-module TEM06-42

Acknowledgements

The projects "Thermoelektrische Konvektion unter Schwerelosigkeit (TEKUS)" and "Dielektrophoretisch induzierte Konvektion (DEPIK)" were/ are supported by the german federal ministry of economics via the space agency of the German Aerospace Center DLR under grant no. 50WM1944 and 50WM2244. We acknowledge the support of the Airbus DS – TEXUS team, the Centre Nationale d'Études Spatiales (CNES), Novespace S.A. in Bordeaux and our technical staff at Brandenburg University of Technology.

References

- Meier, M., Jongmanns, M., Meyer, A., Seelig, T., Egbers, C., Mutabazi, I.: Flow pattern and heat transfer in a cylindrical annulus under 1g and low-g conditions: Experiments, *Microgravity Sci. Technol.* 30, 699-712 (2018)
- Meier, M., Jongmanns, M., Meyer, A., Seelig, T., Egbers, C., Mutabazi, I.: Enhanced heat transfer in a cylindrical annulus under 1g and low-g conditions, 69th International Astronautical Congress (IAC), Bremen, Germany, 1-5 October (2018)
- Schütte, A.: TEXUS/ MAXUS Sounding Rocket Program, 69th International Astronautical Congress, 1.-5. Oct., Bremen (IAC- 18.A2.5.5x45013) (2018)
- Szabo, P. S. B., Meier, M., Meyer, A., Barry, E. B., Mutabazi, I., Egbers, C.: PIV and Shadowgraph measurements of thermo-electrohydrodynamic convection in a horizontal aligned thermally heated annulus at different gravity conditions, *Experimental Thermal and Fluid Sc.* 129, 110470 (2021)

ORAL 3

Echographic surveillance of 14 volunteer after 40 days in confinement in a Deep cavern (Deep time experiment 2021).

Philippe ARBEILLE ¹ (PHD-MD), Kathryn ZUJ ¹ (PHD), Stephane BESNARD ² (MD-PHD), Benoit MAUVIEUX ² (PHD), Richard HUGHSON ³ (PHD). Christian CLOT ⁴ (PHD).

¹ UMPS-CERCOM (Unit Med Physiol Spatiale) Faculte de Medicine Universite de Tours – France

² Dept Explorations Neurologiques et ORL, CHU Caen - France

³ Schlegel-University of Waterloo Research Institute for Aging - Waterloo, Canada

⁴ Dept Adaptation comportementale et fonctionnel aux changements. Human Adaptation Institute. Paris. France.

Corresponding author:

Philippe Arbeille Prof Biophysics – MD Clinical ultrasound.

UMPS-CERCOM. University School of Medicine of Tours – France.

e-mail: arbeille@med.univ-tours.fr

Abstract :

Background : Modification of organs and vessels were discovered incidentally by echography, subjects during Spaceflights, Head down tilt, and Confinement. During Deep time experiment, 14 volunteers stayed confined 40 days inside a cavern, our hypothesis was that as during other ground and space confinements some organs will show abnormal adaptation. The objective was to assess a serie of superficial and deep organs and vessels, 1 week before and the first day after the confinement by echography.

Method: 12 different organs were investigated using a Sonoscanner echograph similar to the one used onboard ISS, and using the same tele-operated procedure as onboard the ISS due to Covid restriction.

Results: *Superficial targets*: the Carotid (diameter, bifurcation, intima media thickness, distensibility, structure/content), Jugular vein (volume, content), Femoral (diameter, intima media thickness), the Achille tendon (size, content) and the cervical vertebra distance were not affected by the confinement. The Carotid and Femoral hemodynamics (Vascular resistance, flow volume) did not change. *Deep targets*: the Portal vein (size), main bile duct (size), Pancreas head (size, structure), Aorta (diameter, wall), lumbar vertebra (distance), and kidney (size, contour, content) were not significantly changed by the confinement.

Conclusion: The no-change in superficial and deep organs/vessels was associated to a no-change in the main biological parameters. These findings were in contradiction with previous confinement studies but in the present case the lack of physiological changes suggests a potential protective effect of reduced environmental stress (huge habitat, several participants) and sustained physical activity which is deserving of further investigation.

(248 words).

Keyword: Echography, confinement, cavern, deep time.

ORAL 4

Cardiovascular deconditioning and impact of artificial gravity during 60-day head-down bed rest – Insights from 4D flow cardiac MRI

Jeremy Rabineau^{1,2*}, Margot Issertine¹, Fabian Hoffmann³, Darius Gerlach³, Enrico G. Caiani⁴, Benoit Haut², Philippe van de Borne¹, Jens Tank³, Pierre-François Migeotte¹

¹LPHYS, Département de Cardiologie, Université libre de Bruxelles, Brussels, Belgium

²TIPs, École Polytechnique de Bruxelles, Université libre de Bruxelles, Brussels, Belgium

³Institute of Aerospace Medicine, German Aerospace Center (DLR), Cologne, Germany

⁴Electronic, Information and Biomedical Engineering Department, Politecnico di Milano, Milan, Italy

*** Correspondence:**

Corresponding Author

Jeremy.rabineau@ulb.be

Keywords: bed rest, microgravity, artificial gravity, cardiac MRI, 4D flow, cardiovascular deconditioning, wall shear stress, pulse wave velocity.

Abstract (349 words)

Microgravity has deleterious effects on the cardiovascular system caused, among others, by a headward fluid shift and hypokinesia. We evaluated the parameters of blood flow and vascular stiffness obtained by 4D flow cardiac MRI to quantify the cardiovascular deconditioning during 60 days of simulated microgravity in head-down tilt (HDT) bed rest. We also tested the hypothesis that daily exposure to 30 minutes of artificial gravity (1 g) would mitigate these adaptations.

24 healthy subjects (8 women) took part in this HDT study. They were evenly distributed in three groups: continuous artificial gravity, intermittent artificial gravity, or control. 4D flow cardiac MRI was acquired in horizontal position before (-9 days), during (5, 21, and 56 days), and after (+4 days) the HDT period. We evaluated flow and vascular parameters in the aorta.

No group or group \times time differences were observed. At the end of the HDT phase, we reported a decrease in the amount of stroke volume allocated to the lower body (-30% [-35%; -22%]) and the upper body (-20% [-30%; +11%]), but in different proportions, reflected by an increased share of blood flow towards the upper body (40% [33%; 43%] versus 34% [29%; 40]). The aortic pulse wave velocity increased (+16% [+9%; +25%]), and so did other markers of arterial stiffness (*CAVI*, *CAVI₀*). In parallel, the time-averaged wall shear stress decreased -11% [-4%; -17%] and the relative residence time increased (+11% [+4%; +21%]). Most of these parameters tended to or returned to baseline after 4 days of recovery.

The effects of the artificial gravity countermeasure were not visible. We recommend increasing the load factor, the time of exposure, or combining it with physical exercise. The changes in blood flow confirmed the different adaptations occurring in the upper and lower body, with a larger share of blood volume dedicated to the upper body during (simulated) microgravity. The aorta appeared stiffer during the HDT phase, however all the changes remained subclinical and probably the sole consequence of reversible functional changes in a context of reduced blood flow. No permanent cardiovascular adaptations following 60 days of HDT bed rest were observed.

ORAL 5

Analyzing Calcium Signaling by CaMPARI2 during Parabolic Flights

S. Wuest¹, A. Hammer², G. Cerretti¹, D. Ricciardi², D. Schiffmann¹, S. Maranda¹, R. Kummer¹, C. Zumbühl¹, K. Rattenbacher-Kiser¹, S. von Arx¹, S. Ammann¹, F. Strobl², R. Berkane², A. Stolz², E. Stelzer², E. Schleiff², M. Egli¹ and M. Böhmer²

¹Lucerne University of Applied Sciences and Arts, School of Engineering and Architecture, Horw, Switzerland, simon.wueest@hslu.ch

²Johann Wolfgang Goethe University, Frankfurt am Main, Germany, boehmer@bio.uni-frankfurt.de

Introduction

Calcium is an essential secondary messenger in many cellular processes, including diseases and adaptation to environmental stimuli, such as gravitational load (Wuest et al. 2018). Mapping and quantifying calcium signaling with a high spatiotemporal resolution is a key challenge. Moreover, on microgravity platforms, experiment time, volume and weight are limited, allowing only a small number of replicates. Furthermore, experiment hardware is exposed to changes in gravity levels, causing experimental artifacts unless appropriately controlled (Wuest et al. 2022). In this project we introduced a new experimental setup based on the fluorescent calcium reporter CaMPARI2, onboard LED arrays and subsequent microscopic analysis on the ground (Hammer et al. 2022).

CaMPARI and Flight Hardware

CaMPARI (calcium-modulated photoactivatable ratiometric integrator) is an engineered protein, which irreversibly converts from green to red emission when illuminated with near UV light at 405 nm in the presence of calcium

(Moeyaert et al. 2018). We seeded transfected cells in 96-well plates prior a parabolic flight and irradiated the samples with near UV light at predefined time points during the flight, using a newly developed hardware (Figure 1). The hardware featured a LED array that allowed irradiating each well individually. A special challenge was the thermal management, as mammalian cells are temperature sensitive. For safety reasons, the experiment could not be powered during take-off and landing which prohibits active heating during this period. In addition, the LEDs produced excessive heat, which had to be conducted away from the samples reliably. This problem could be solved by a combination of electrical heating elements, thermal insulation and a thermal buffer containing a paraffin wax with a melting point at ca. 36 °C. This stabilized the temperature two-fold: First, during the unpowered condition, it slowed down cooling in combination with an insulation. Second, it also absorbed the excessive heat generated during illumination. After the flight, the 96-well plates were removed from the flight hardware and subsequently imaged in the lab on site.

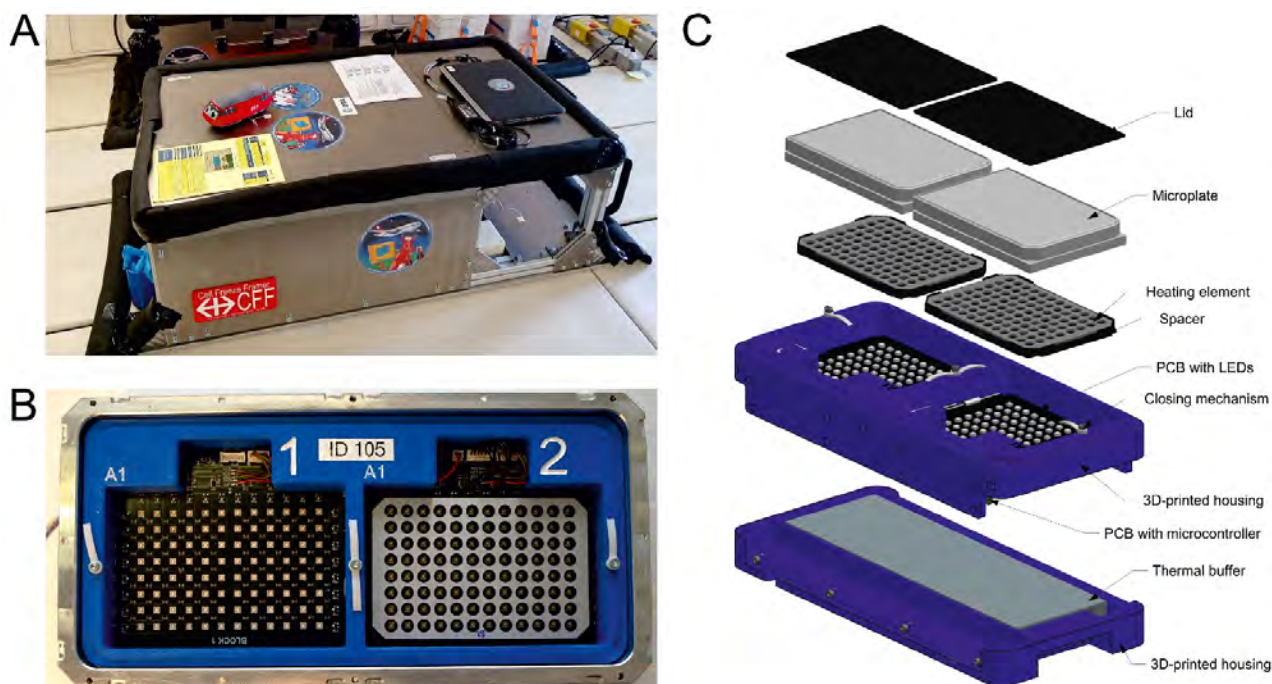


Figure 1: Parabolic flight hardware. (A) Flight rack mounted inside Novespace's aircraft. (B) Top view on the hardware units, showing the empty payload bays for the two 96-well plates. The spacer with the heating element was removed in the left bay, exposing the LED array. (C) Explosion view of the hardware, highlighting the most relevant elements. Published in (Hammer et al. 2022).

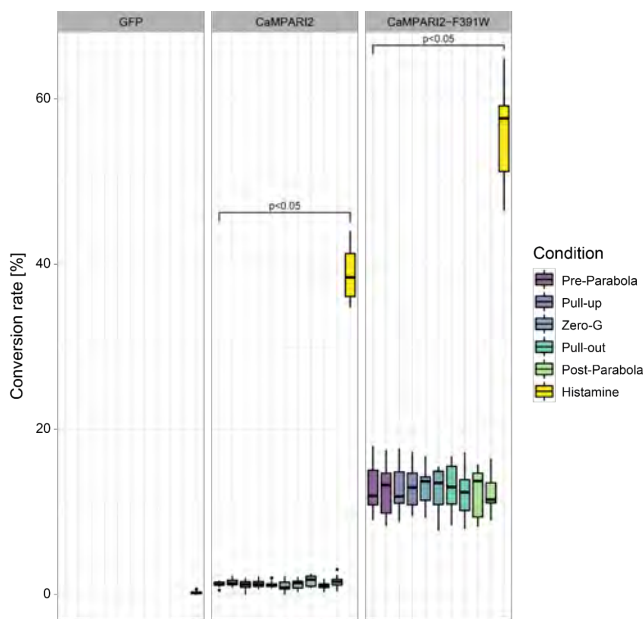


Figure 2: Conversion rates of human chondrocyte cells expressing CaMPARI2 or CaM-PARI2-F391W. The two constructs have different calcium sensitivity. The cells were illuminated during the indicated flight phase for conversion. The cells expressing GFP (negative control) were illuminated directly before a parabola. For each parabola and CaMPARI2-construct, eight wells per 96-well plate were treated with 100 μ M histamine and subsequently illuminated (positive control). Published in (Hammer et al. 2022).

Conclusions

Due to the separation of photoconversion in-flight and microscopy on ground, our novel approach allows accurate, higher throughput calcium recordings on microgravity platforms, such as parabolic flights. The excellent performance of CaMPARI2 was demonstrated with human chondrocytes during the 75th ESA parabolic flight campaign. CaMPARI2 revealed a strong calcium response triggered by

histamine in articular chondrocytes. However, calcium was not affected by the alternating gravitational load of a parabolic flight (Figure 2). (Hammer et al. 2022)

Acknowledgements

We thank Sartorius for providing the IncuCyte S3 and personnel and their support in analyzing the data. We thank the European Space Agency (ESA) and Novespace (Bordeaux, France) for the organization and support during the parabolic flight campaign. We gratefully acknowledge the financial support through PRODEX (ESA), and the Swiss Space Office (SSO), as well as through the German Space Agency (DLR).

References

- Hammer, A., Cerretti, G., Ricciardi, D.A., Schiffmann, D., Maranda, S., Kummer, R., Zumbuhl, C., Rattenbacher-Kiser, K.F., von Arx, S., Ammann, S., Strobl, F., Berkane, R., Stolz, A., Stelzer, E.H.K., Egli, M., Schleiff, E., Wuest, S.L., Bohmer, M.: Retrograde Analysis of Calcium Signaling by CaMPARI2 Shows Cytosolic Calcium in Chondrocytes Is Unaffected by Parabolic Flights. *Biomedicines* **10**(1) (2022). doi:10.3390/biomedicines10010138
- Moeyaert, B., Holt, G., Madangopal, R., Perez-Alvarez, A., Fearey, B.C., Trojanowski, N.F., Ledderose, J., Zolnik, T.A., Das, A., Patel, D., Brown, T.A., Sachdev, R.N.S., Eickholt, B.J., Larkum, M.E., Turrigiano, G.G., Dana, H., Gee, C.E., Oertner, T.G., Hope, B.T., Schreiter, E.R.: Improved methods for marking active neuron populations. *Nat Commun* **9**(1), 4440 (2018). doi:10.1038/s41467-018-06935-2
- Wuest, S.L., Cerretti, G., Wadsworth, J.L., Follonier, C., Rattenbacher-Kiser, K.F., Bradley, T., Egli, M., Ille, F.: Cytosolic calcium and membrane potential in articular chondrocytes during parabolic flight. *Acta astronautica* **193**, 287-302 (2022). doi:https://doi.org/10.1016/j.actaastro.2022.01.016
- Wuest, S.L., Gantenbein, B., Ille, F., Egli, M.: Electrophysiological experiments in microgravity: lessons learned and future challenges. *NPJ microgravity* **4**, 7 (2018). doi:10.1038/s41526-018-0042-3

ORAL 6

Effect of 3-day exposure to dry immersion on veno-arteriolar reflex

Adrien Robin¹, Nastassia Navasiolava¹, Irina Larina², Ludmila Pastushkova²,
Elena Tomilovskaya², Marc-Antoine Custaud¹

¹Univ Angers, CHU Angers, CRC, INSERM, CNRS, MITOVASC, Equipe CarMe, SFR ICAT, F-49000 Angers, France; adrien.robin08@gmail.com; ²RF SSC – Institute of Biomedical Problems, Russian Academy of Sciences, Moscow, Russia

Introduction

Veno-arteriolar vasoconstriction reflex (VAR), a local reflex activated by acute venous congestion leading to localized vasoconstriction, is important to maintain upright position. VAR impairment could contribute to microgravity-induced orthostatic intolerance. VAR state following actual or modeled microgravity remains unclear. Thus, Gabrielsen and Norsk (2007) observed an unchanged VAR after 4-6.5 months of actual microgravity, while 20 and 14-day HDBR led to increased (Gabrielsen et al. 1999), or attenuated (Wilson et al. 2003) VAR. We previously demonstrated increase in upright calf skin vascular resistance following 7-day dry immersion (DI), while cardiovascular autonomic control was not modified, suggesting increased VAR (Navasiolava et al. 2011). However the direct effect of DI on VAR was not measured. We aimed to evaluate DI effect on VAR.

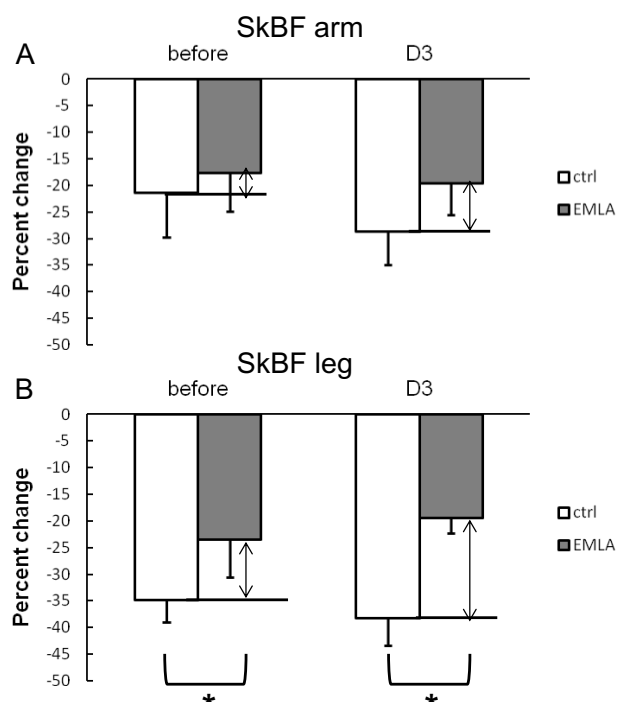


Figure 1: Percent change in skin blood flow in forearm (A) and calf (B) during cuff inflation to 40mmHg at the EMLA-treated sites and control sites. n=14 subjects. Values are mean ± SEM; *p<0.05 vs. Ctrl; arrows reflect magnitude of VAR as a difference in vasoconstriction to cuff inflation between Control and EMLA sites.

Methods

14 healthy men were studied before and at day 3 of non-strict DI (with allowed 15-min daily raise for hygiene). Skin blood flow (SkBF), accessed supine via laser-Doppler flowmetry was measured at two forearm and two calf sites:

EMLA sites with previous application of eutectic mixture of local anesthetics to block neurally-mediated skin vasoconstriction, and Control sites. “EMLA” laser-Doppler flow probes were placed at the outer surface of the leg/forearm, and “control” probes - at the inner surface. Venous congestion was induced by 40-mmHg cuff inflation for 3 min at thigh and brachial level. Skin vasoconstriction was quantified as percent change from baseline in response to cuff inflation (%ΔSkBF). This vasoconstriction occurred at Control sites due to the activation of both VAR and myogenic tone, whereas at EMLA sites neurally-mediated VAR was blocked. VAR magnitude was estimated as difference in vasoconstriction to cuff inflation between Control and EMLA sites.

Results

Resting SkBF was unmodified by DI at calf level (9.4±1.2AU - before- vs. 8.2±1.2AU - at D3, ns) while decreased at forearm (27.1±4.7AU - before- vs. 16.9±2.9AU - at D3; p<0.05). Leg skin vasoconstricted more than arm skin in response to cuff inflation (Fig. 1). Increase in VAR magnitude following DI (arm: -4±11% - before- vs. -9±9% - at D3, leg: -11±5% - before- vs. -19±5% - at D3) didn't reach statistical significance.

Discussion

Results suggest that venoarteriolar response at leg and arm skin level is not attenuated by non-strict DI. It seems that VAR does not need sustained daily orthostatic stimulation to maintain efficiency. Preserved VAR might compensate insufficient vasoconstriction of other vascular beds following exposure to microgravity.

References

- A. Gabrielsen, P. Norsk, Effect of spaceflight on the subcutaneous venoarteriolar reflex in the human lower leg. *J Appl Physiol* 103, 959–962 (2007)
- A. Gabrielsen, Y. Suzuki, P. Norsk, Preservation of veno-arteriolar reflex in the skin following 20 days of head down bed rest in humans. *J Gravit Physiol* 6, 103–104 (1999)
- T.E. Wilson, M. Shibasaki, J. Cui, B.D. Levine, C.G. Crandall, Effects of 14 days of head-down tilt bed rest on cutaneous vasoconstrictor responses in humans. *J Appl Physiol* 94, 2113–2118 (2003)
- N. Navasiolava, V. de Germain, T. Levrard, et al, Skin vascular resistance in the standing position increases significantly after 7 days of dry immersion. *Autonomic neuroscience: basic & clinical* 160, 64–68 (2011)

ORAL 7

Controlling the dynamics of a free surface via thermocapillary flows

P. Salgado Sánchez¹, D. Gligor¹, U. Martínez¹, J. Porter¹, J.M. Ezquerro¹, J. Fernández¹, F. Gavalda², X. Ruiz²

¹E-USOC, Center for Computational Simulation, Universidad Politécnica de Madrid, Madrid, Spain, pablo.salgado@upm.es

²Facultat de Química, Universitat Rovira i Virgili, Tarragona, Spain

Introduction

Since the early period of space exploration, the behavior of fluids in microgravity conditions has been a subject of interest in the scientific community. Microgravity can significantly affect fluid behavior, particularly in the context of mass and heat transport. The lack of a (strong) gravitational force allows these processes to be controlled by surface tension or pressure changes, and thermal diffusion (conduction), respectively. Although mass transport is of prominent interest for fluid management purposes (Porter et al. 2021), thermal phenomena have also received much attention. Thermocapillary flow, for instance, is a well-studied phenomenon due to its relevance for many technological applications like combustion or crystal growth. Recently, a new line of research has looked at the potential of thermocapillary flows to enhance heat transport during the melting and solidification of phase change materials in microgravity (Salgado Sánchez et al. 2020). Similarly, vibrational forcing has been used to increase the heat transfer rate in nonisothermal systems. If a free surface is present, vibrations can induce a variety of complex phenomena involving different interfacial modes like surface waves, frozen waves, and vibroequilibria (Salgado Sánchez et al. 2019).

Here, we investigate the dynamics of a free surface with a moving contact line in the presence of thermocapillary flows (Gligor et al. 2022). Due to the relevance for space applications and sloshing, we focus on steady response and on low-frequency dynamics. Below, we summarize the basic mathematical formulation used to describe the problem. Then, the response of the interface to both steady and oscillatory thermal forcing are described. Finally, a potential microgravity application to mitigate sloshing is proposed and assessed.

Mathematical formulation

We consider an open (2D) rectangular container filled with liquid that is subjected to a temperature gradient ΔT between its lateral boundaries; temperatures $T_0 \pm \Delta T/2$ are applied antisymmetrically at opposite walls with respect to the reference temperature T_0 , driving thermocapillary flow.

The flow is assumed to be laminar and incompressible so that the conservation of mass, momentum and energy are described by the Navier-Stokes equations. We apply either steady or oscillatory ΔT and analyze the subsequent response.

We allow vertical motion of the contact points, while preserving a fixed contact angle β . In Fig. 1, a sketch of the

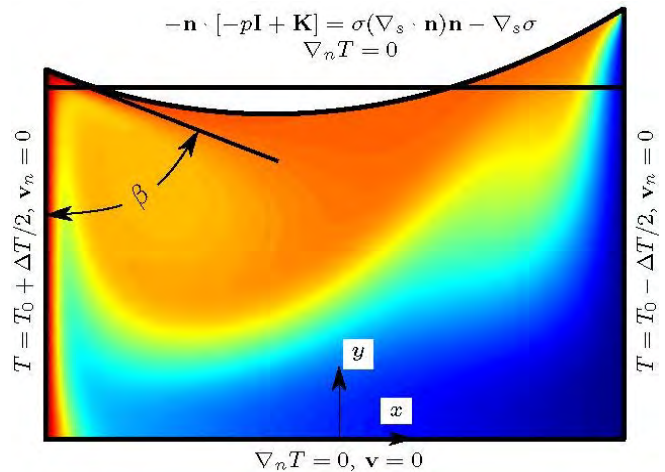


Figure 1: Sketch of the system considered.

system is shown, including the thermal field and interface deformation when subjected to steady ΔT . The set of boundary conditions are indicated.

Results below are calculated for $L = 30$ mm and $H = 15$ mm with fluid properties similar to those of silicone oils. The influence of viscosity is analyzed by varying its value between 2.5 and 100 cSt. For further details, refer to Gligor et al. (2022a,b).

Steady dynamics: asymmetry

The applied ΔT modifies the unforced symmetric solution, since the thermocapillary effect, which draws fluid from warmer to cooler regions, breaks the left-right reflection symmetry. To characterize this deformation, we use the position of the contact points and measure the asymmetry A as depicted in the inset of Fig. 2.

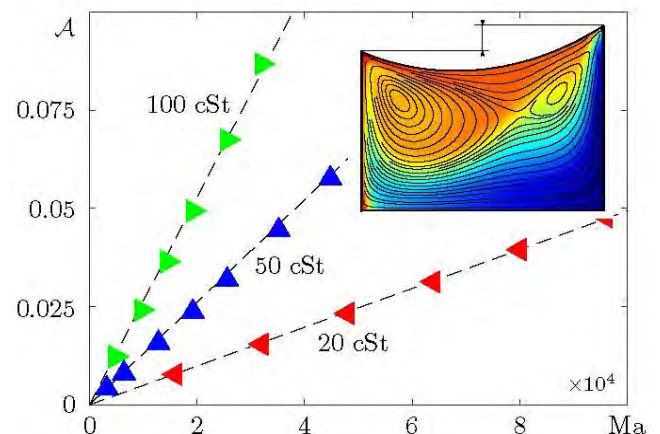


Figure 2: Asymmetry for 20 (red), 50 (blue) and 100 cSt (green).

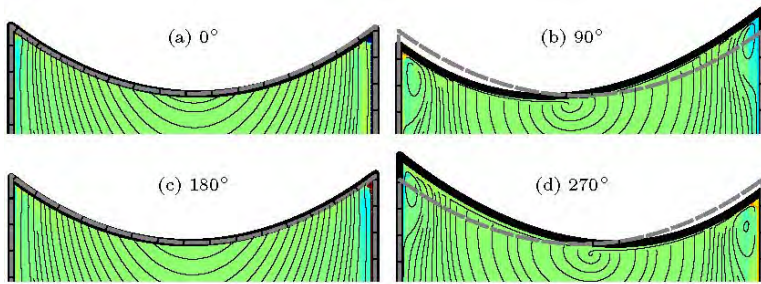


Figure 3: Snapshots showing the temperature field and streamlines over one thermal excitation cycle at the first sloshing frequency. Each panel shows equally spaced phases of the cycle, with the initial reference phase corresponding to a symmetric free surface solution (shown with a dashed line).

The results show that A depends linearly on the applied Marangoni number Ma (or equivalently, on ΔT).

Besides this, the transient dynamics from an isothermal initial condition at T_0 reveals that the motion of the contact points is significantly faster than the settling of the flow, and is characterized by damped low-frequency oscillations with a frequency equal to that of the first sloshing mode. We analyze these low-frequency oscillations next.

Oscillatory dynamics

Periodic thermal excitation is applied with amplitude ΔT and frequency ω .

This periodic excitation induces a harmonic response of the free surface, as seen in Fig. 3. Starting from an initial symmetric solution, we observe that the cycle begins with the heating (cooling) of the left (right) wall. The thermocapillary effect induces a rightward tangential velocity at the free surface, which leads to the downward (upward) motion of the left (right) contact point. The subsequent cooling (heating) of the left (right) wall, in between 90° and 270° phases, inverts the thermal gradient and the velocity at the free surface. The left (right) contact point then moves up (down). At a certain point during this process, the surface configuration becomes symmetric again and, after this, the velocity at the interface decreases and switches its sign, which initiates another cycle.

The fact that one can deliberately drive sloshing using thermal modulations suggests that one may also make use of them to counteract sloshing and other effects of microgravity perturbations; real examples include reboosting or docking maneuvers on the International Space Station (ISS).

Feed-back control and applications

For this purpose, we consider a standard PID controller that produces a control signal $\Delta T(t)$ to reduce sloshing and push the system toward the “desired” symmetric state with $A = 0$.

We test this strategy using a realistic microgravity situation during an ISS reboosting maneuver; reproduced from the data collected by OSSRAW sensor. The surface response, characterized by the motion of the left contact point, that results from this perturbation is illustrated in Fig. 4 with a grey curve. Note that the dynamics is dominated by resonant sloshing oscillations.

The proposed PID controller is implemented using only a derivative gain; see Gligor et al. (2022b) for further details.

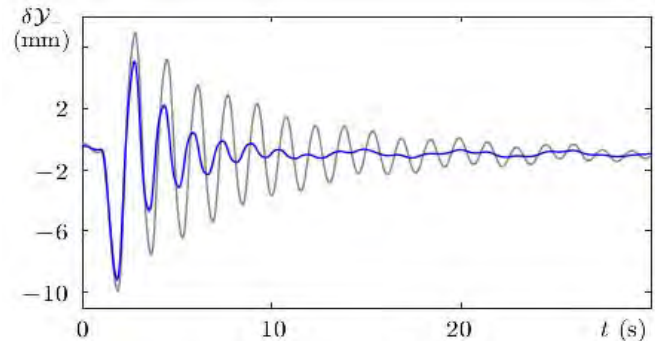


Figure 4: Control of sloshing driven by an ISS reboosting maneuver.

In Fig. 4, the controlled motion of the contact point is shown by a blue curve. The effectiveness of the proposed strategy is evident in the more rapid damping of the sloshing oscillation.

Conclusions

The response of a free surface to steady and oscillatory thermal excitation has been analyzed, suggesting the potential of using thermal forcing as a fluid control strategy in microgravity. This idea is tested to mitigate the sloshing driven by a reboosting maneuver aboard the ISS.

Acknowledgements

This work was supported by the Ministerio de Ciencia e Innovación under Project No. PID2020-115086GB-C31.

References

- J. Porter et al. A review of fluid instabilities and control strategies with applications in microgravity, *Math. Model. Nat. Phenom.* **16**, 24 (2021).
- P. Salgado Sánchez et al. Thermocapillary effects during the melting of phase change materials in microgravity: heat transport enhancement, *Int. J. Heat Mass Transf.* **163**, 120478 (2020).
- P. Salgado Sánchez et al. Interfacial phenomena in immiscible liquids subjected to vibrations in microgravity, *J. Fluid Mech.* **865**, 850-883 (2019).
- D. Gligor et al. Thermocapillary-driven dynamics of free surface in microgravity: response to steady and oscillatory thermal excitation, *Phys. Fluids* **34**, 042116 (2022a)
- D. Gligor et al. Thermocapillary-driven dynamics of free surface in microgravity: control of sloshing, submitted to *Phys. Fluids*, under review (2022b).

ORAL 8

Thermocapillary flows and phase change in rectangular containers in microgravity

P. Salgado Sánchez, J. Porter, J. M. Ezquerro, Ú. Martínez, I. Tíao, A. Laverón-Simavilla

E-USOC, Center for Computational Simulation, Universidad Politécnica de Madrid, Madrid, Spain, pablo.salgado@upm.es

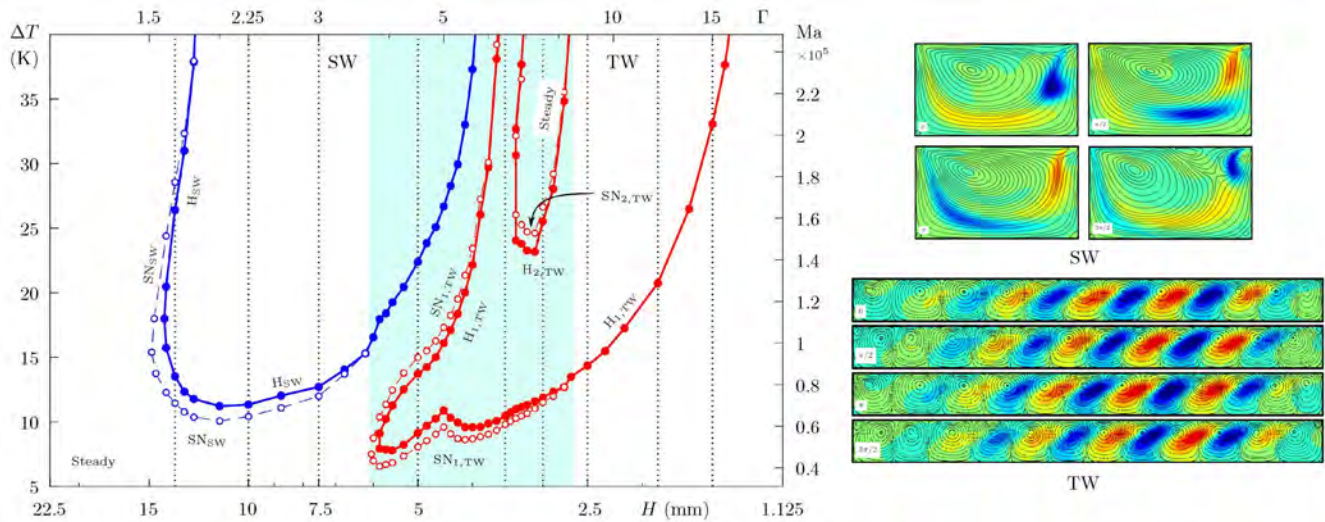


Figure 1: (left) Stability map in terms of H and ΔT (Γ and Ma on opposing axes) showing the critical boundaries for oscillatory thermocapillary flow in two regimes: standing wave (SW, blue) and traveling wave (TW, red). The Hopf (H) and saddle-node (SN) bifurcations are located by solid and dashed curves, respectively, with circular markers denoting the simulations. (right) Temperature deviation and velocity fields of the SW and TW modes over one oscillation cycle.

Introduction

Thermocapillary flows have attracted sustained interest from scientists and engineers due to their relevance in a wide variety of technological processes. However, only few theoretical studies have considered the coupling between thermocapillary flows and the *dynamic boundary condition* generated by the moving solid/liquid (S/L) front during melting or solidification. The first systematic attempt was the recent work of Salgado Sánchez et al. (2021), where the nature of the flows that appear in the liquid phase during melting was analyzed from a pattern formation perspective. Both steady and oscillatory modes, either having the appearance of traveling waves (TWs) or (approximately) standing waves (SWs), were found.

Here, we provide a detailed analysis of pattern selection in rectangular containers of liquid n-octadecane in microgravity, motivated by recent research (Ezquerro et al. 2019) and the future ISS experiment MarPCM (Laverón 2021). These experiments aim to investigate the potential of thermal Marangoni convection to increase the heat transfer rate of phase change materials with a free surface (Salgado Sánchez et al. 2020). The present results are part of the effort to predict and explain the dynamics that are expected to be observed experimentally. For further details, the reader is referred to the work of Salgado Sánchez et al. (2022).

Pattern selection: stability and bifurcations

The stability map of Fig. 1 (left) summarizes the three thermocapillary flow regimes in terms of the container

height H and applied thermal gradient ΔT (equivalently, the dimensionless aspect ratio Γ and Marangoni number Ma). The critical boundaries separate steady flows and two modes of oscillatory convection: the SW mode (blue curves) and the TW mode (red curves). Both SWs and TWs appear via a primary Hopf bifurcation that can be either supercritical or subcritical. In the latter case, this Hopf bifurcation is accompanied by a secondary saddle-node bifurcation. The Hopf and saddle-node bifurcations are labeled and indicated by solid and dashed curves, respectively.

The characteristics and driving mechanism of the SW is analogous to that described by Peltier and Biringen (1993), which relies on an interaction between the sensitivity of the thermocapillary surface to the cooling effect provided by the cold perturbations emanating from the cold boundary. Snapshots of the temperature deviation and instantaneous velocity fields over one oscillation cycle are illustrated on the right-upper panels of Fig. 1.

The TW mode, on the other hand, is analogous to that described by Smith and Davis (1983). This mode is characterized by the cyclic creation of vortices near the cold wall that detach and move toward the hot wall. The motion of these traveling waves can be seen by comparing the snapshots of the right-lower panels of Fig. 1, from which the leftward movement of the warm/cool perturbations separating traveling vortices is evident.

Now, we apply these results to analyze the melting process in microgravity.

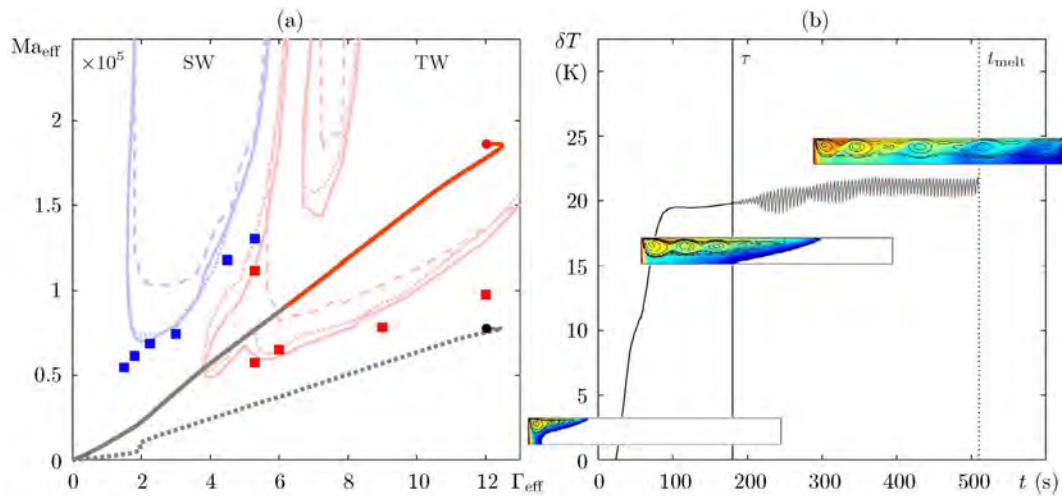


Figure 2: (a) Melting paths in effective parameters (Γ_{eff} , Ma_{eff}) for two choices of Ma in a large container of $\Gamma = 12$. The nature of the thermocapillary flow is indicated by color: steady (grey) and TW (red). (b) Temperature δT during the “oscillatory” melting, with vertical lines marking the appearance of oscillatory flow and the completion of melting (at τ , τ_{melt}).

Phase change dynamics in microgravity

During melting, the S/L front constitutes a dynamic boundary condition for the liquid phase. The time-changing shape of front generally reflects two distinct regions: one dominated by conduction, and one dominated by the thermocapillary effect near the free surface. In this latter region, the S/L front changes both its characteristic length and depth as time passes. Time-dependent effective values of Γ and Ma can be thus defined and used to characterize it.

As an example of application, Fig. 2 shows the paths traced by two meltings in large containers of $\Gamma = 12$ in the space of effective parameters (Γ_{eff} , Ma_{eff}), one representative of steady thermocapillary flow and other displaying oscillatory behavior. The nature of the observed flow is indicated by the color: steady (grey) and TW (red). The temperature deviation δT of the “oscillatory” case is included in panel (b), with vertical lines marking the appearance of oscillatory flow and the completion of melting (labeled as τ and τ_{melt} , respectively). The insets show the temperature and velocity at selected times during melting. Note that the initiation of the TW mode coincides well with the cross of the stability boundary.

Conclusions

A numerical investigation of pattern selection for thermocapillary flow in rectangular containers in microgravity was presented. The flow was analysed for liquid n-octadecane due to its relevance to current microgravity research. Bifurcation sets were organized in terms of H (Γ) and ΔT (Ma) in a stability map showing regions of steady solutions, SWs and TWs.

These results were later used to explain the dynamics observed during melting in microgravity, by defining an effective aspect ratio Γ_{eff} and Marangoni number Ma_{eff} to characterize the time-changing liquid domain. Good agreement is found between the transitions observed during melting and those located in the pure liquid case.

Acknowledgements

This work was supported by the Ministerio de Ciencia e Innovación under Project No. PID2020-115086GB-C31, and by the Spanish Users Support and Operations Centre (E-USOC), Center for Computational Simulation (CCS).

References

- P. Salgado Sánchez et al., Thermocapillary effects during the melting of phase change materials in microgravity: steady and oscillatory flow regimes, *J. Fluid Mech.* **908**, A28 (2021).
- J. M. Ezquerro et al., Experimental evidence of thermocapillarity in phase change materials in microgravity: measuring the effect of Marangoni convection in solid/liquid phase transitions, *Int. Comm. Heat Mass Transf.* **113**, 104529 (2020).
- A. Laverón, ESR document: Effect of Marangoni Convection on Heat Transfer in Phase Change Materials, issue 1, revision 1 (2021).
- P. Salgado Sánchez et al., Thermocapillary effects during the melting of phase change materials in microgravity: heat transport enhancement, *Int. J. Heat Mass Transf.* **163**, 120478 (2020).
- P. Salgado Sánchez et al., Pattern selection for thermocapillary flow in rectangular containers in microgravity, *Phys. Rev. Fluids* **7**, 053502 (2022).
- L. J. Peltier and S. Biringen, Time-dependent thermocapillary convection in a rectangular cavity: numerical results for a moderate Prandtl number fluid, *J. Fluid Mech.* **257**, 339 (1993).
- M. K. Smith and S. H. Davis, Instabilities of dynamic thermocapillary liquid layers. Part 1. Convection Instabilities, *J. Fluid Mech.* **132**, 19 (1983).

ORAL 9

Osmosis in a bi-disperse compartmentalized granular material in low-gravity environment

M. Noirhomme¹, E. Opsomer¹, E. Falcon² and N. Vandewalle¹

¹GRASP, CESAM Research Unit, Institut de Physique, University of Liège, Liège, Belgium, mnoirhomme@uliege.be,

²Université Paris Cité, CNRS, MSC Laboratory, UMR 7057, F-75013 Paris, France

Introduction

Granular gases have the particularity of being composed of dissipative particles, that is to say, which lose kinetic energy when they collide. This intrinsic property can be highlighted with the help of low gravity. Indeed, by removing gravity, a set of grains which have each received an initial kinetic energy will naturally "cool down", and the total kinetic energy will decay following Haff's law (Haff 1983), and this, whatever the shape of the particles (Maaß et al. 2008, Grasselli et al. 2009, Harth et al. 2018, Yu et al. 2020).

To keep a diluted set of grains in a gaseous state, it is essential to provide them some energy. Generally, the whole system is vibrated in order to provide the energy in a mechanical way. In this way, the total energy of the system can be kept constant and the system can reach an out-of-equilibrium steady state.

Mainly depending on the filling conditions, a granular gas state, or a phase separation between a dense aggregate (called "cluster") bathing in a less dense granular gas can be observed (Falcon et al. 1999, Opsomer et al. 2012). Using the VIP-Gran instrument, specially designed to study granular media in a low-gravity environment (Aumaître et al. 2018), the onset of the gas-cluster transition has been studied (Noirhomme et al. 2018).

Note that the mechanism for nucleation of the denser phase has recently been identified as arising from minimization of the power dissipated in the system (Noirhomme et al. 2021). On the other hand, mixing several sizes of beads, always under microgravity conditions, can also give rise to convection or segregation phenomena (Opsomer et al. 2017).

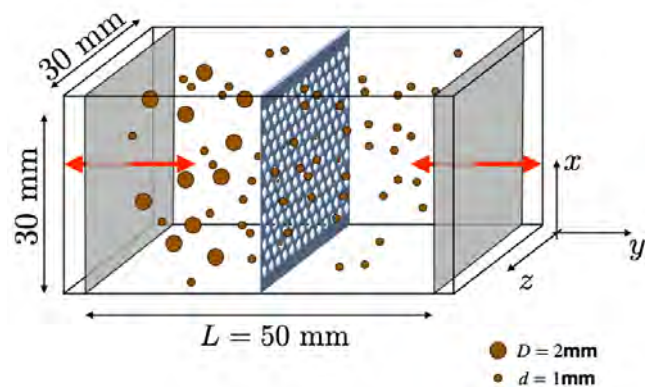


Figure 1: Sketch of the VIP-Gran 3D cell for the study of granular gases in microgravity conditions. In order to create a granular osmosis, a binary mixture of small and large spheres are placed in the cell with a wall permeable only to small grains. The large particles are all located on the left side of the wall. Vibrating pistons are displayed in red.

Experiments and simulations

Here, using the VIP-Gran instrument, we study the possibility of creating granular "osmosis" using a binary mixture of bronze spherical beads (a "solute" and a "solvent" made up of large and small particles, respectively) and a mobile wall pierced with holes whose the diameter avoids the solute to pass through it. The diameters of the particles are $D=2\text{mm}$ for the large ones and $d=1\text{mm}$ for the small ones, while the diameter of the holes is $d_h=1.2\text{mm}$. Figure 1 gives an overview of the experiment. We place 50 large particles on the left of the wall and N_s small ones on the right, with $N_s=[100; 800; 1000]$. We performed experiments during the Parabolic Flight Campaign 67 (PFC 67) of the European Space Agency (ESA), in the frame of the SpaceGrains project (SpaceGrains2022) and reproduced the experiment numerically.

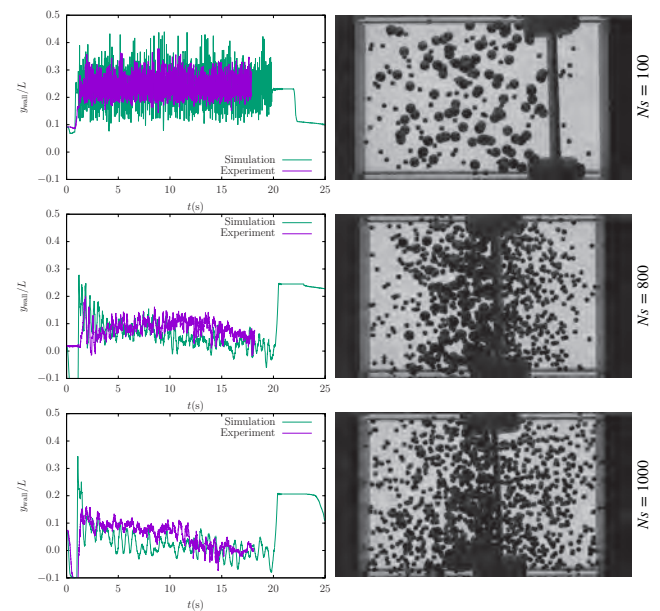


Figure 2: Left: time evolution of the normalized position of the wall y_{wall}/L measured during the parabolic flight campaign 67 (purple) and in the numerical simulations reproducing the latter (green). Right: snapshots of the corresponding experiments. The simulations take into account the g-jitter remaining in the aircraft as well as the friction of the mobile wall on the glass walls of the cell. 20s is the duration of the low-gravity phase.

Results

The first results obtained show that the position of the mobile wall, as well as the number of particles to the right of the latter, depends directly on the filling conditions of the

particles preferentially move on the side of the large ones, exactly as would be the case in a classic osmosis experiment (Marbach 2019). This being so, one could believe that it is a volume effect since the large particles exert pressure on the wall, pushing it close to the right piston. In order to remove this possible volume effect, we carried out a numerical study in which the semi-permeable wall is attached to the center of the cell. Surprisingly, the result is identical to that obtained for the mobile wall: granular osmosis, i.e. a greater number of small particles in the compartment where the large ones are, can be created under certain conditions.

Finally, the average volume occupied by each small grain remains preserved when the volumes of the left and right compartments and the numbers of particles in them are different depending on whether the wall is fixed or mobile. This volume per particle is modeled thanks to the theory of minimization of the power dissipated in the system.

Conclusions

In this work, we studied experimentally and numerically the possibility of creating a granular osmosis in low gravity thanks to the VIP-Gran instrument in which we have placed a binary mixture of particles as well as a wall permeable only to small particles. We discovered with surprise that the mobile character or not of the semipermeable wall was not relevant for the phenomenon of granular osmosis. The key parameter is the available volume per small particle minimizing the power dissipated in the system.

Acknowledgements

VIP-Gran-PF instrument was built by DTM Technologies (Modena, Italy). This work was funded by European Space Agency Topical Team SpaceGrains No. 4000103461. We thank the support of Novespace during ESA Parabolic Flight Campaigns. We also thank Y. Garrabos, F. Palencia, C. Lecoutre, S. Pillitteri and D. Fischer for operating the VIP-Gran instrument during the parabolic flights. M. Noirhomme thanks the Belgian Federal Science Policy Office (BELSPO) for the provision of financial support in the framework of the PRODEX Programme of the European Space Agency (ESA) under contract number 4000103267.

References

P. K. Haff, Grain flow as a fluid-mechanical phenomenon, *J. Fluid Mech.*, 134, 401 (1983)

C. C. Maaß, N. Isert, G. Maret, and C. M. Aegerter, Experimental investigation of the freely cooling granular gas, *Phys. Rev. Lett.*, 100, 248001 (2008)

Velocity-dependent restitution coefficient and granular cooling in microgravity, *EPL*, 86, 60007 (2009)

K. Harth, T. Trittel, S. Wegner, and R. Stannarius, Free cooling of a granular gas of rodlike particles in microgravity, *Phys. Rev. Lett.*, 120, 214301 (2018)

P. Yu, M. Schröter, and M. Sperl, Velocity Distribution of a Homogeneously Cooling Granular Gas, *Phys. Rev. Lett.*, 124, 208007 (2020)

E. Falcon, R. Wunenburger, P. Evesque, S. Fauve, C. Chabot, Y. Garrabos, and D. Beysens, Cluster formation in a granular medium fluidized by vibrations in low gravity, *Phys. Rev. Lett.*, 83, 440 (1999)

E. Opsomer, F. Ludewig and N. Vandewalle, Dynamical clustering in driven granular gas, *EPL*, 99, 40001 (2012)

S. Aumaître, R. P. Behringer, A. Cazaubiel, E. Clément, J. Crassous, D. J. Durian, E. Falcon, S. Fauve, D. Fischer, A. Garcimartín, Y. Garrabos, M. Hou, X. Jia, C. Lecoutre, S. Luding, D. Mazza, M. Noirhomme, E. Opsomer, F. Palencia, T. Pöschel, J. Schockmel, M. Schröter, M. Sperl, R. Stannarius, N. Vandewalle, and P. Yu, An instrument for studying granular media in low-gravity environment, *Rev. Sci. Instrum.*, 89, 075103 (2018)

M. Noirhomme, A. Cazaubiel, A. Darras, E. Falcon, D. Fischer, Y. Garrabos, C. Lecoutre-Chabot, S. Merminod, E. Opsomer, F. Palencia, J. Schockmel, R. Stannarius, and N. Vandewalle, Threshold of gas-like to clustering transition in driven granular media in low-gravity environment, *EPL*, 123, 14003 (2018)

M. Noirhomme, A. Cazaubiel, E. Falcon, D. Fischer, Y. Garrabos, C. Lecoutre-Chabot, S. Mawet, E. Opsomer, F. Palencia, S. Pillitteri, and N. Vandewalle, Particle Dynamics at the Onset of the Granular Gas-Liquid Transition, *Phys. Rev. Lett.*, 126, 128002 (2021)

E. Opsomer, M. Noirhomme, N. Vandewalle, S. Merminod, and E. Falcon, Segregation and pattern formation in dilute granular media under microgravity conditions, *npj Microgravity*, 3, 1 (2017)

SpaceGrains2022, European Space Agency's SpaceGrains project, <https://www.spacegrains.org/>

S. Marbach, and L. Bocquet, Osmosis, from molecular insights to large-scale applications, *Chem. Soc. Rev.*, 48, 3102 (2019)

ORAL 10

Dependence oscillatory dynamics on gas flow temperature in liquid bridges

Y. Gaponenko¹, A. Mialdun², V. Yasnou³, V. Shevtsova^{4,5}

- ¹Microgravity Research Center, Université Libre de Bruxelles, Brussels,Belgium, Yuri.Gaponenko@ulb.be,
- ²Microgravity Research Center, Université Libre de Bruxelles, Brussels,Belgium, Aliaksandr.Mialdun@ulb.be,
- ³Microgravity Research Center, Université Libre de Bruxelles, Brussels,Belgium, Viktar.Yasnou@ulb.be,
- ⁴IKERBASQUE, Basque Foundation for Science, Bilbao, Spain, x.vshevtsova@mondragon.edu
- ⁵Mondragon University, Loramendi 4, 20500 Mondragon, Spain

Introduction

The topic of our study is the influence of gas temperature on the dynamics of flow in a liquid bridge induced by thermocapillary (Marangoni) force. The gas flows parallel a liquid/gas interface. The aim of this investigation is concerned to the space experiment JEREMI (Japanese European Space Research Experiment on Marangoni Instabilities) which is devoted to the study of the threshold of hydrothermal instabilities in two-phase systems in cylindrical geometry.

In the present study two-phase flows induced by Marangoni convection on a free surface and buoyancy due to Earth’s gravity are analyzed in presence of weak evaporation through the interface. A high Prandl number liquid, Pr = 14, n-decane and air have been used as experimental fluids. We consider the system when gas flow is directed from the cold side of the liquid bridge (see Fig.1). The internal core consists of solid rods at the bottom and top, while the central part is a relatively short liquid zone filled with viscous liquid and kept in its position by surface tension. Depending on the gas temperature, the gas flow rate and the temperature difference between the rods (ΔT), various flow regimes were identified including 3D oscillatory ones. The problem is solved numerically in 3D geometry, which corresponds to a liquid bridge axially placed into an outer cylinder with solid walls. The experimental results of this problem were recently published, (Yasnou et al. 2018).

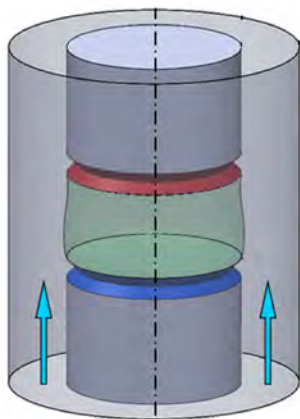


Figure 1: Geometry of the problem.

Results

Our previous results (Shevtsova et al. 2013) have demonstrated the influence of shear-stress impact of a gas

flow moving along the interface, but now the emphasis is on the influence of gas temperature on the instability in the liquid bridge via heat transfer. Depending on the gas flow temperature and temperature difference between rods ΔT , a wide variety of flow patterns is observed which correspond to different modes of an oscillatory flow. In addition, a stability window of steady flow has been found to exist in the map of dynamical states in terms of gas temperature and applied thermal stress ΔT .

In Fig. 2 an example of the numerical simulations results are show for the temperature difference between rods $\Delta T = 10^\circ \text{C}$, gas flow velocity $U_{\text{gas}} = 0.5 \text{ m/s}$ and gas flow temperature $T_{\text{gas}} = 22.5^\circ \text{C}$. Left side of the figure illustrates a snapshot with isosurface of mean temperature $T_{\text{mean}} = 25^\circ \text{C}$ in the liquid phase embedded in a gas temperature field. The phase trajectories at this gas temperature resolve the nonlinear dynamics (Fig.2, right side). It confirms that the dominant azimuthal with $m = 1$ but also it shows the strong presence of the mode $m = 2$. This flow regime corresponds to settings on hydro thermal wave map when a stability window is observed with small increasing of gas flow temperature.

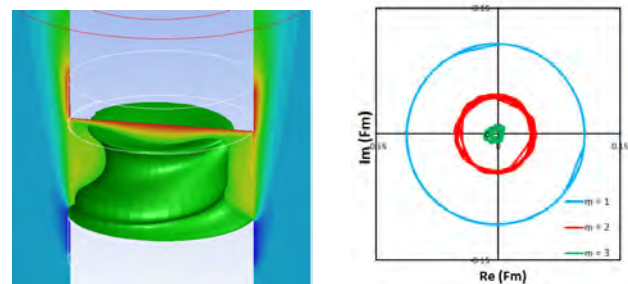


Figure 2: Temperature field and trajectories of dynamic system for different modes in case of $T_{\text{gas}} = 22.5^\circ \text{C}$.

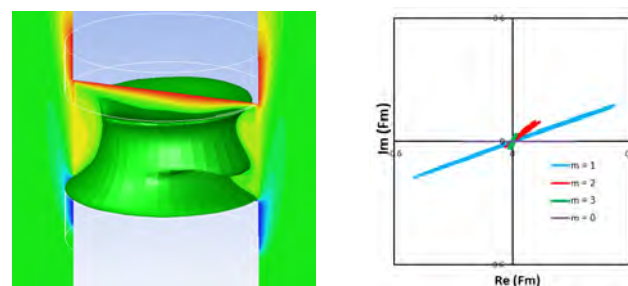


Figure 3: Temperature field and trajectories of dynamic system for different modes in case of $T_{\text{gas}} = 25^\circ \text{C}$.

The similar set of the numerical results is shown in Fig. 3, with flow structure beyond the stability window, for the increased gas flow temperature $T_{\text{gas}} = 25^\circ \text{C}$ while other parameters are the same. This small variation of T_{gas} leads to change in the dominant mode of oscillatory regime from $m = 2$ to $m = 1$ and also travelling wave become standing.

An intensive numerical study was performed in a large range of gas flow temperatures and temperature differences in order to clarify the experimental results (Y. Gaponenko et al. 2021).

Conclusions

Based on the consistency of the experimental and numerical results, it is shown that a liquid bridge system above critical temperature can be stabilized by the varying gas temperature. The identification of the stability window within the JEREMI experiment will not be the only benefit of the study. It will bring other additional values to the experiment. Notably, throughout the study, we have developed an original methodology for analysis of hydrothermal waves, which will be highly useful for analysis of the forthcoming JEREMI experiment.

Acknowledgements

The work of was supported by the PRODEX programme of the Belgian Federal Science Policy Office.

The work of V.S. was supported by MMASINT (KK-2022/00047) and IT1505-22 (Research Group Program) of the Basque Government and PID2020-115086GB-C33 financed by (MICINN/FEDER) of the Spanish Government.

References

- V. Yasnou, Yu. Gaponenko, etc, Influence of a coaxial gas flow on the evolution of oscillatory states in a liquid bridge, *Int. J. of Heat and Mass Transfer*, 123, 747 – 759 (2018)
- V. Shevtsova, Yu. Gaponenko, etc, Thermocapillary flow regimes and instability caused by a gas stream along the interface, *J. Fluid Mech.*, 714, 644 – 670 (2013)
- Y. Gaponenko, V. Yasnou, etc, Hydrothermal waves in a liquid bridge subjected to a gas stream along the interface, *J. Fluid Mech.*, 908, A34, (2021)

ORAL 13

The effect of hypergravity on burn wounds in *Hirudo*

Sharon van Rijthoven^{1,3} and Jack J.W.A. van Loon^{2,3}

¹Delft University of Technology

²Department of Oral and Maxillofacial Surgery/Pathology, Amsterdam Movement Sciences & Amsterdam Bone Center (ABC), Amsterdam UMC location Vrije Universiteit Amsterdam & Academic Center for Dentistry Amsterdam (ACTA), Gustav Mahlerlaan 3004, 1081 LA, Amsterdam, The Netherlands.

³European Space Agency (ESA), European Space Research and Technology Centre (ESTEC), TEC-MMG, Keplerlaan 1, 2201 AZ Noordwijk, The Netherlands.

Tissue repairs in microgravity at a reduced capacity compared to the 1g environment. However, it is unclear what effect hypergravity has on wound recovery. There is especially little *in vivo* research on complex wounds like burn injury in hypergravity. Therefore, exploratory research is required to monitor differences in burn wound recovery at various gravity levels. This pilot study presents the identification of those characteristics in the leech (*Hirudo Verbana*) that have similar wound recovery as vertebrates. The leeches received a thermal burn at different burn depths and were observed after exposure to 1g, 5g and 10g in the Large Diameter Centrifuge at ESA ESTEC for up to two weeks. Hypergravity seems to accelerate the recovery of the orientation of the epithelial cells while simultaneously displaying deeper burn wounds under the same conditions. Furthermore, it appears that the repair tissue in 1g forms external to the surface of the skin, while in hypergravity it assembles mainly within the tissue. Recommendations for further research include using a larger sample set to statistically validate the identified characteristics.

ORAL 14

Three-dimensional effects during the melting of phase-change materials with thermocapillary flow in microgravity

B. Šeta¹, P. Salgado Sánchez², J. Massons³, Jna. Gavalda³, J. Porter², M.M. Bou-Ali⁴, X. Ruiz³, V. Shevtsova^{4,5}

¹Department of Mechanical Engineering, Technical University of Denmark. Kogens Lyngby, Denmark.

²E-USOC, Center for Computational Simulations, E.T.S. de Ingeniería Aeronáutica y del Espacio, Universidad Politécnica Madrid. Madrid, Spain

³Departament de Química Física i Inorgànica, Facultat de Ciències Químiques, Universitat Rovira i Virgili. Tarragona, Spain

⁴Mechanical and Manufacturing Department, Mondragon Unibertsitatea. Mondragón, Spain.

⁵IKERBASQUE, Basque Foundation for Science. Bilbao, Spain

berse@mek.dtu.dk, pablo.salgado@upm.es, jaume.massons@urv.cat, finn.gavalda@urv.cat, jeff.porter@upm.es, mbouali@mondragon.edu, josepxavier.ruiz@urv.cat, x.vshevtsova@mondragon.edu

Introduction

Organic phase-change materials (PCMs), such as paraffin waxes, have large latent heats and conveniently low melting points within the range of typical spacecraft working temperatures. Unfortunately, their low thermal conductivity can lead to slow rates of energy exchange during melting/solidification cycles, which inhibits performance and usability for thermal control in space applications. To mitigate this problem without increasing the mass or volume of the system, the potential of thermocapillary convection as a simple passive thermal heat transfer mechanism in space environments has recently been considered.

Aside from this important technological application, the behaviour of thermocapillary flow during melting is an interesting and fundamental problem in fluid mechanics. A detailed two-dimensional (2D) analyses of steady and oscillatory dynamical regimes and their dependence on the melting process in shallow rectangular cavities has recently been reported (Salgado Sánchez et al., 2021).

The present work complements this analysis by including the crosswise horizontal dynamics, revealing a richness that cannot be observed in simplified 2D approaches. We consider the fully three-dimensional (3D) thermocapillary flows appearing during the melting of high Prandtl number materials in thin containers and analyze them in terms of bulk flow and pattern formation properties.

Methodology

A rectangular parallelepipedic box of $22.5 \times 25 \times 1.875$ mm³ is utilized to computationally investigate three-dimensional flow effects. Additionally, a two-dimensional rectangular box of length (L) 22.5 mm and height (H) 1.875 mm, which has an Aspect Ratio, AR (L/H) of 12, is used for comparison with 2D results. N-octadecane is selected as the PCM due to the availability in the literature (see, e.g., Salgado Sánchez et al., 2021) of reliable measurements of its thermophysical properties.

In both the 2D and 3D simulations the PCM is initially solid and undergoes a controlled phase transition to liquid driven by the application of constant temperature differences of 20, 30 and 40 K at the two opposing lateral walls. The remaining solid boundaries are assumed to be adiabatic, as in the standard treatment of the problem with lateral heating. No-slip fluid velocity conditions are imposed at all solid walls. The upper free surface permits thermocapillary flow directed from the hot to the cold wall.

All simulations are carried out within an OpenFOAM environment using the enthalpy-porosity method (see, for instance, Šeta et al. 2021 and 2022). This approach allows us

to manage the phase change interfaces without the need to track them specifically throughout the process. These non-sharp interfaces (called mushy regions) are modeled as a porous medium whose porosity is quantified by a scalar specifying the local liquid volume fraction. The latent heat generated by the phase change process is considered in this method as a source term in the energy equation.

Rectangular cells of 0.2×0.05 mm² each, orthogonally located, are used to cover the entire 2D computational domain. Orthogonal parallelepipedic cells of $0.2 \times 0.05 \times 0.6$ mm³ are used in the 3D calculations. These meshes were selected after convergence tests that required reasonable convergence of the curves for the evolution of the global liquid fraction while, at the same time, recognized the need for a good compromise between sufficient accuracy and feasible computational time.

Frequency analysis of the results is based on thermal signals obtained from the corresponding simulations at 2 Hz. The Fast Fourier transform (FFT) is calculated using a Hanning window of 2048 points, which gives a frequency resolution on the order of 1 mHz. Records of 30 s, delayed by one second between them, are systematically considered to obtain the evolution of the frequency associated with the maximum Power Spectral Density (PSD) value in each record. These frequency values are referred to below as the main frequencies.

Finally, the equivalent 2D and 3D problems with pure liquid n-octadecane, subjected to the same thermal conditions as in the case of PCM melting but without the phase change, are computationally investigated for the sake of comparison.

Results

Figure 1 shows the temporal evolution of the liquid fraction for different 2D and 3D runs.

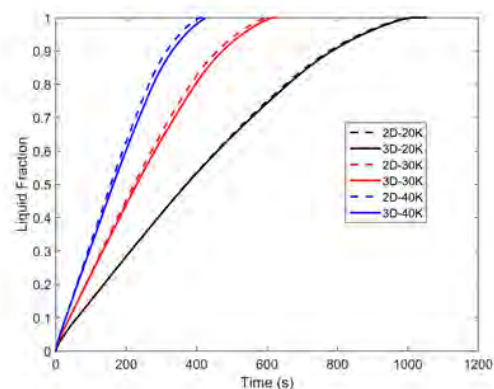


Figure 1: Evolution of the liquid fraction for different conditions

Marangoni numbers. For $\Delta T = 30$ K, for example, the reduction is approximately 40 % relative to the value for 20 K and, if $\Delta T = 40$ K, it is about 60 %. The 2D simulations of melting finish slightly sooner than the 3D ones, but this difference decreases with decreasing temperature difference (approximately 4.5 %, 2.7 % and 0.8 %, respectively, for the three ΔT values). The melting rate is similar in both 2D and 3D cases. Initially, it is very high due to the presence of Marangony convection melting the free surface; it slows down as this convection disappears.

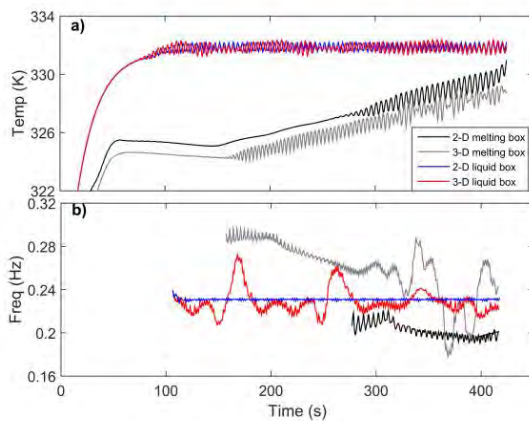


Figure 2: a) Temperature evolution at $x = 2.25$ mm and $y = 1.75$ mm in the central plane (3-D cases) for melting and liquid 2D and 3D simulations with $\Delta T = 40$ K. b) Time evolution of the main frequencies during the oscillatory regime.

Figure 2.a) shows the evolution of the temperature at $x = 2.25$ mm and $y = 1.75$ mm in the central plane (3-D case) for $\Delta T = 40$ K. The black and gray curves correspond to 2D and 3D simulations, respectively. The blue and red curves correspond to 2D and 3D simulations of pure liquid. The temperature is selected to represent the dynamics since it is a convenient magnitude for experimentalists. Note that the oscillatory regime in the 2D melting case begins later than in the 3D simulation and shows more regular behavior. This regularity is associated with the absence of transverse oscillations, which act as a complicating mechanism for the supercritical flow regime. In the purely liquid 2D and 3D problems, the onset of oscillations is nearly simultaneous although, as before, there is greater complexity in the signal from the 3D case because of transverse oscillations.

Figure 2.b) shows the evolution of the main frequencies for the same signals. Note that in the pure liquid cases (blue and red curves) there is remarkable stability of the frequency with the 2D simulation but clear fluctuations around the mean value for the 3D simulation. In the cases of 2D and 3D melting, the frequencies of oscillatory flow are different, both from the corresponding liquid case and from each other. This discrepancy is likely due to the lower percentage of liquid volume present at the onset of the oscillatory regime in the 3D case (46% compared to 83% for $\Delta T = 40$ K). Moreover, in the 3D case, two different regimes can be detected. The first one lasts for about 300 s (liquid volume, 85%) while the frequency decreases slowly and monotonically. In the second regime, the main frequency continues to decrease, on average, but also oscillates because of the coupling between vertical and transverse hydrothermal waves. We further note that the

Hz) matches quite well with the one reported in the literature (Salgado Sánchez et al. 2021).

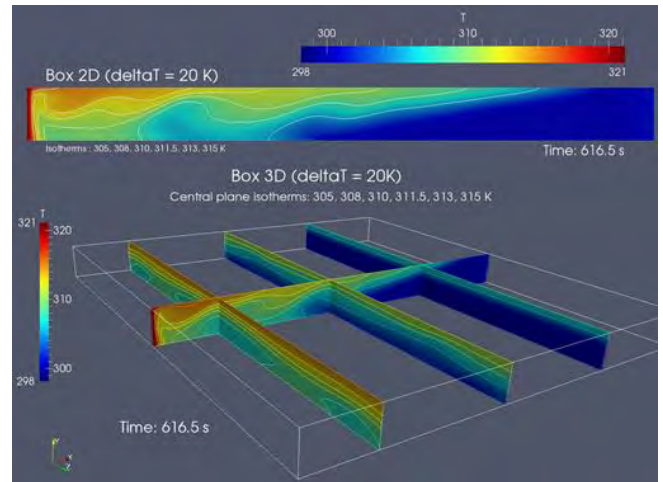


Figure 3: Snapshots of the thermal fields during melting for 2D and 3D simulations ($AR=12$, $\Delta T=20K$). The blue colored region corresponds to the solid phase.

A snapshot of the thermal field for $\Delta T = 20$ K at 616.5 s, which corresponds to a liquid fraction of approximately 0.76, is presented in Figure 3. Note that the temperature distribution in the central plane of the 3D case matches well with the 2D case.

Conclusions

A detailed numerical investigation of three-dimensional thermocapillary flows during the melting of high Prandtl phase-change materials in microgravity is presented here for large Aspect Ratio containers. It is clear that the horizontal dynamics, which are not considered in the 2D results, can play an important role in the behaviour of the system, leading, for one thing, to increased modulations. This is revealed both in the earlier onset of the supercritical regime and in the richer spectral characteristics of the flow.

Acknowledgements

The present work has been supported by grants PID2020-115086GB-C31, PID2020-115086GB-C32 and PID2020-115086GB-C33 (MCIU/FEDER) and 2021PFR-URV-74 (Rovira i Virgili University).

References

- P. Salgado Sánchez, J.M. Ezquerro, J. Fernandez, J. Rodriguez; *Thermocapillary effects during the melting of phase-change materials in microgravity: steady and oscillatory regimes*. J. Fluid Mech., 908, A20-1, 2021.
- B. Šeta, D. Dubert, J. Massons, Jna. Gavalda, M.M. Bou-Ali, X. Ruiz; *Effect of Marangoni induced instabilities on a melting bridge under microgravity conditions*. Int. J. Heat Mass Transf., 179, 121665, 2021.
- B. Šeta, D. Dubert, M. Prats, J. Jna. Gavalda, J. Massons, M.M. Bou-Ali, X. Ruiz, V. Shevtsova; *Transitions between nonlinear regimes in melting and liquid bridges in microgravity*. Int. J. Heat Mass Transf., 193, 122984, 2022.

ORAL 15

5 days of simulated microgravity induce skeletal muscle structural and microenvironment changes leading to global muscle deconditioning

Corentin Guilhot¹, Théo Fovet¹, Manon Dargegen¹, Thomas Brioché¹, Bernard Jasmin²,
Angèle Chopard¹, Guillaume Py¹

¹University of Montpellier, DMEM, INRAE, Montpellier, France

²University of Ottawa, Ontario, Canada

MEDES, Rangueil Hospital, CNES, Toulouse, France

Background

The will of space agencies to explore planets such as Mars require long term space flight for astronauts. The lack of microgravity during these flights involves extreme conditions to human musculoskeletal system. During these flights hypokinesia and hypoactivity lead to severe skeletal muscle deconditioning (MD). This situation is characterized by a loss of muscle mass and strength, increased fatigability and accumulation of ectopic adipocytes between muscle fibers called Inter muscular adipose tissue (IMATs). Only few studies have documented today the kinetic of IMAT accumulation during space flights or in ground-based models of microgravity. The parallel events such as muscle fibers size alteration, reduce strength production and IMATs accumulation leads to major muscle dysfunction, highlighting both global muscle structure, metabolism and muscle fibers microenvironment modifications. The precise underlying mechanisms of their origin, development and the possible link between them are still poorly understood.

We hypothesized that severe hypodynamia triggers both fibers and muscle microenvironment (extracellular matrix) changes that disrupt the dialog between atrophying myocytes and resident muscle stem cells, particularly the fibro-adipogenic progenitors (FAPs).

This local degradation could further trigger a shift toward harmful factors which leads to muscle resident stem cells changes impairing the muscle plasticity and capacity to ensure its function. Therefore, there is a need to decipher the precise mechanisms in order to design efficient countermeasures to prevent MD during space flight.

Methods

This study took place in the space clinic (MEDES, Toulouse) and use the Dry Immersion (DI) model, known to generate rapid and severe MD similar to space flight, caused by drastic hypoactivity without mechanical stress during a short period, i.e. 5 days. DI protocol involved 18 healthy men randomly assigned in two groups (Ctrl=9; age=33,8 ± 4, Thigh Cuff=9; age=33,4 ± 7) strictly layered in supine position and immersed in thermo-neutral water bath. Vastus lateralis biopsies were obtained before/after 5 days of immersion for each subject. Transverse serial cross sections were used to determine both cross sectional area, Pax7⁺ and PDGFRα⁺ population by immunohistochemistry. ECM density was quantified using red Sirius staining. Protein content and gene expression were respectively assessed by Western blotting and qPCR.

Results

Muscle thigh mass and cross-sectional area were significantly decreased after immersion (-2,4% and -18%, $p < 0,05$ respectively). This was associated with an increase in protein degradation levels and lower protein synthesis (+32% and -28% respectively, $p < 0,05$). Parallel to muscle fibers, ECM density was decreased after 5 days of immersion (2,5% vs 1,5% Pre-DI vs Post-DI). Moreover, the major components of ECM such as collagen I, IV and fibronectin were decreased after immersion ($p < 0,05$) indicating a degradation in ECM structure.

Concomitantly, several markers of development, accumulation and maturation of adipocytes were significantly up-regulated after 5 days of DI. Protein levels of C/EBP α , C/EBP β and PPAR γ were increased, indicating an early and later adipogenic process commitment. Perilipin and fatty acid binding protein 4, key markers of mature adipocytes were also significantly up-regulated (+34%, +29% respectively $p < 0,05$). IMATs progenitors i.e. FAPs, positive for PDGFR α surface marker, were increased after 5 days of DI (+69%, $p < 0,05$). We also showed that myogenic muscle stem cells positive for PAX7 markers were significantly decreased after immersion (-29%, $p < 0,05$)

Finally, our results also indicated development of harmful signals in muscle fiber microenvironment with a decrease in IGF1, VEGF ($p < 0,01$) and an increase in myostatin and FGF2 ($p < 0,01$) genes expressions. Degradation of muscle environment quality, seems to impact resident muscle stem cells behavior/fate.

Conclusions

We showed that the concomitant early activation of atrophic process, muscle ectopic adipogenesis and microenvironment degradation lead to a decrease in muscle function resulting in a loss of muscle strength after immersion ($p < 0,05$). This study reveals that MD appears not only at a structural level but only 5 days of DI were also sufficient to alter microenvironment signaling and resident stem cells behavior/fates. In the MD context this crosstalk seems to be rapidly altered leading to muscle loss of function. Further studies are needed to fully characterize the crosstalk between muscle fibers, resident stem cells and muscle ECM.

ORAL 16

Next steps for Space Omics research development in Europe: recommendations from an ESA Topical Team

Raúl Herranz¹ on behalf of the ESA funded Space Omics Topical Team

(*Space Omics Topical Team*: Joseph Borg², Thomas Cahill³, Henry Cope⁴, Eugénie Carnero-Díaz⁵, Colleen S. Deane^{6,7}, Timothy Etheridge⁶, Gary Hardiman³, Natalie Leys⁸, Pedro Madrigal⁹, Aránzazu Manzano¹, Felice Mastroleo⁸, F. Javier Medina¹, Manuel A. Fernandez-Rojo¹⁰, Keith Siew¹¹, Stephen B. Walsh¹¹, Silvio Weging¹², Daniela Bezdán¹³, Stefania Giacomello¹⁴, Willian A. da Silveira¹⁵, Nathaniel J. Szewczyk^{4,16}, Raúl Herranz¹)

¹ Centro de Investigaciones Biológicas “Margarita Salas” (CSIC), Ramiro de Maeztu 9, E-28040 Madrid, SPAIN, r.herranz@csic.es,

² Department of Applied Biomedical Science, Faculty of Health Sciences, University of Malta, Msida, MALTA,

³ Faculty of Medicine, Health and Life Sciences, School of Biological Sciences, Institute for Global Food Security, Queen's University Belfast, Belfast, BT7 1NN, UK, ⁴ School of Medicine, University of Nottingham, DE22 3DT, UK,

⁵ Institut Systématique, Evolution, Biodiversité (ISYEB), Muséum National d'Histoire Naturelle, Sorbonne Université, Paris, FRANCE,

⁶ Department of Sport and Health Science, College of Life and Environmental Sciences, University of Exeter, Exeter, EX1 2LU, UK,

⁷ Living Systems Institute, University of Exeter, Stocker Road, Exeter, EX4 4QD, UK,

⁸ Microbiology Unit, Belgian Nuclear Research Centre, SCK CEN, Mol, 2400, BELGIUM,

⁹ European Molecular Biology Laboratory, European Bioinformatics Institute EMBL-EBI, Wellcome Genome Campus, Hinxton, UK,

¹⁰ Hepatic Regenerative Medicine Lab, Madrid Institute for Advanced Studies in Food, Madrid, 28049, SPAIN,

¹¹ University College London, London, NW3 2PF, UK, ¹² University of Halle, Halle (Saale), 06108, GERMANY,

¹³ Institute of Medical Genetics & Applied Genomics, University of Tübingen, 72076, GERMANY, Daniela.Bezdan@med.uni-tuebingen.de,

¹⁴ Science for Life Laboratory, KTH Royal Institute of Technology, Stockholm, SE-17165, SWEDEN, stefania.giacomello@scilifelab.se

¹⁵ Department of Biological Sciences, School of Health, Science and Wellbeing, Staffordshire University, Stoke-on-Trent, UK

willian.dasilveira@staffs.ac.uk, ¹⁶ Ohio Musculoskeletal and Neurological Institute and Department of Biomedical Sciences, Heritage College of Osteopathic Medicine, Ohio University, Athens, OH43147, USA, szewczyk@ohio.edu

Introduction

The European life science community in space research has been always limited in numbers but fully devoted to microgravity research leading the international scenario in particular organisms. In the last fifteen years, the financial crisis, together with the emergence of private partners for NASA, made ESA related researchers vulnerable to the lack of manned mission launch capabilities. This has particularly affected the Space Omics research in which ESA funded activities have been reduced. European PIs have been forced to partner up with international colleagues to keep the pace in their research goals, in some cases with outstanding results.

Our Space Omics Topical Team was created as an offshoot of a successful NASA initiative called Genelab (Ray et al., 2019). Genelab is a repository for Omics data and as part of their activities they supported the creation of Analysis Working Groups (AWG's). On the Genelab AWG symposium in 2018 we realized there was a considerable number of members based in Europe, at the second symposium in 2019 they organized bilateral talks between each other as they thought could be simpler to make some actions on that side of the Atlantic Ocean. A core set of members was selected to contain a person of contact for any of the four GeneLab AWG with a geographical and gender balance approach. This core started the elaboration of the proposal and gather the rest of European members from GeneLab AWGs in a first step. Later we integrated our efforts with those of the International Standards for Space Omics Processing (ISSOP), a consortium of scientists who develop, share, and encourage sample processing standardization and metadata normalization of spaceflight “omics” experiments.



Figure 1: Key members in the Space Omics Topical Team funded by ESA (grant/contract 4000131202/20/NL/PG/pt “Space Omics: Towards an integrated ESA/NASA –omics database for spaceflight and ground facilities experiments”). From left to right, Dr. Raúl Herranz, Dr. Willian da Silveira, Dr. Daniela Bezdán, Dr. Stefania Giacomello and Prof. Nathaniel Szewczyk. You can visit our website <https://issop.space/space-omics-topical-team/> to get the full list of members of the Topical Team including their contact information, full affiliations and expertise as Space Biologists or Bioinformaticians in order to contact for information about the international networks membership or research collaborations.

Omics research in Europe

The combined efforts of NASA GeneLab AWGs (Overbey et al., 2021), ESA funded Space Omics TT (Madrigal et al., 2020) and ISSOP (Rutter et al., 2020) in the last couple of years produced two dozens of publications published in The Biology of Spaceflight collection in Cell Press journals in 2020, and now the particular contribution from Europe is represented in a continuation collection (European Space Omics collection) to be release in September 2022. The first publication of this collection (available on line early this year) (Deane et al., 2022), already detected a number of caveats in the different funding scheme/s inside the EU. This impacts the productivity of each country regarding the space omics research field. To alleviate this, national and ESA programmes supporting flight operations and science exploration need to provide a predictable and sustainable funding landscape. This would help promoting collaboration among eligible countries in addition to international collaborations.

Opportunities in Europe

Space research careers at the university level should be encouraged in Europe. Several master courses have been hosted by ESA or ELGRA in the last years. However, the low number of students (usually very young) involved and the lack of a clear path for those students to pursue a career in the field reduces the impact they could have. A network of European space research laboratories to promote student exchanges, from bachelor to post-doc level, will allow interested new researchers, particularly junior researchers, to retain the best in the field.

Another big problem for junior researchers is the timing of space research. To get a permanent position in laboratories in Europe, there is a requirement of recent top-level track record that can only be obtained after a project is performed in full. Spaceflight experiments require several years (sometimes decades) to be completed from the first concept to the analysis of the results. Also, the lack of reproducibility and relative value of ground based simulation facilities made difficult for the researchers to obtain clear and unquestionable results. Choosing the space research path is choosing a hard one. Therefore, most of the junior researchers usually change their research topics to research fields in which high impact factor articles can be obtained at a faster pace.

The European research community should use existing capacities to boost Space Omics research, maintaining our collaboration with NASA GeneLab via ISSOP, or similar international endeavors, but building our own capabilities in ESA states members. At the same time is important to work in international research announcements to maximize the results of large, reference experiments required to be performed in key model systems. ESA elaborated strategic roadmaps for the future, but the continuous redefinition of those working plans, without any call of opportunities for scientists to follow, does not allow concrete actions. At the contrary, NASA is promoting TIDES, including a continuum support to the space research community including spaceflight opportunities, funding for laboratory activities and even data processing support via GeneLab.

These, and others recommendations from the Space Omics Topical Team funded by ESA, will be disclosed together with the release of a Cell Press Article Collection enabled by the European contribution to the Space Omics research field. Our final goal is to elaborate a white chapter that could be used to improve our research capabilities in Europe to keep the pace in the context of international collaboration, now that Omics and Bioinformatics were added as part of the ESA strategy on the “Roadmaps for Future Research” as a consequence of our Topical Team efforts.

Acknowledgements

This Topical Team activities are developed from 2020 by funding from the contract 4000131202/20/NL/PG/pt “Space Omics: Towards an integrated ESA/NASA –omics database for spaceflight and ground facilities experiments” awarded to RH, which was the main funding source for this work. Individual authors also acknowledge support from their national grants.

References

- C. Deane, Space Omics Topical Team, W. da Silveira and R. Herranz, Space omics research in Europe: Contributions, geographical distribution and ESA member state funding schemes. *iScience* 25, 103920 (2022).
- P. Madrigal, Gabel, A., Villacampa, A., Manzano, A., Deane, C.S., Bezdán, D., Carnero-Díaz, E., Medina, F.J., Hardiman, G., Grosse, I., Szewczyk, N., Weging, S., Giacomello, S., Harridge, S., Morris-Paterson, T., Cahill, T., Silveira, W.a.D., and Herranz, R.. Revamping Space-omics in Europe. *Cell Systems*, doi:10.1016/j.cels.2020.1010.1006 (2020)
- E. Overbey, Saravia-Butler, A.M., Zhang, Z., Rathi, K.S., Fogle, H., Da Silveira, W.A., Barker, R.J., Bass, J.J., Beheshti, A., Berrios, D.C., Blaber, E.A., Cekanaviciute, E., Costa, H.A., Davin, L.B., Fisch, K.M., Gebre, S.G., Geniza, M., Gilbert, R., Gilroy, S., Hardiman, G., Herranz, R., Kidane, Y.H., Kruse, C.P.S., Lee, M.D., Liefeld, T., Lewis, N.G., McDonald, J.T., Meller, R., Mishra, T., Perera, I.Y., Ray, S., Reinsch, S.S., Rosenthal, S.B., Strong, M., Szewczyk, N.J., Tahimic, C.G.T., Taylor, D.M., Vandenbrink, J.P., Villacampa, A., Weging, S., Wolverton, C., Wyatt, S.E., Zea, L., Costes, S.V., and Galazka, J.M., NASA GeneLab RNA-seq consensus pipeline: standardized processing of short-read RNA-seq data. *iScience* 24, 102361 (2021)
- S. Ray, Gebre, S., Fogle, H., Berrios, D.C., Tran, P.B., Galazka, J.M., and Costes, S.V.. GeneLab: Omics database for spaceflight experiments. *Bioinformatics* 35, 1753-1759 (2019)
- L. Rutter, Barker, R., Bezdán, D., Cope, H., Costes, S.V., Degoricija, L., Fisch, K.M., Gabitto, M.I., Gebre, S., Giacomello, S., Gilroy, S., Green, S.J., Mason, C.E., Reinsch, S.S., Szewczyk, N.J., Taylor, D.M., Galazka, J.M., Herranz, R., and Muratani, M. A New Era for Space Life Science: International Standards for Space Omics Processing (ISSOP). *Patterns*, doi: 10.1016/j.patter.2020.100148 (2020)

ORAL 18

Muscle atrophy phenotype gene expression during spaceflight is linked to metabolic stress crosstalk between the liver and the muscle.

Geraldine Vitry^{1,2}, Rebecca Finch², Gavin Mcstay², Afshin Behesti³,
Tricia Larose^{1,4}, Virginia Wotring^{1,5*}, Willian Abraham da Silveira^{1,2*}

¹ International Space University, 67400 Illkirch-Graffenstaden, France. ² Staffordshire University, Department of Biological Sciences, School of Health, Science and Wellbeing, Staffordshire University, Science Centre, Leek Road, Stoke-on-Trent, ST4 2DF, U.K. ³ KBR, Space Biosciences Division, NASA Ames Research Center, Moffett Field, CA 94035, USA; Stanley Center for Psychiatric Research, Broad Institute of MIT and Harvard, Cambridge, MA 02142, USA. ⁴ Department of Community Medicine and Global Health, Institute of Health and Society, University of Oslo, Oslo, Norway. ⁵ Center for Space Medicine, Baylor College of Medicine, Houston, TX 77030 USA *Both Authors contributed equally. Corresponding author: virginia.wotring@isunet.edu, willian.dasilveira@staffs.ac.uk.

Introduction

Human expansion in space is hampered by physiological risks of spaceflight. The muscle and the liver are among the most affected tissues during spaceflights and their relationships in response to space exposure have never been studied. We compared the transcriptome response of liver and quadriceps from mice on NASA Rodent Research 1, after 37 days exposure to spaceflight using GeneSet Enrichment Analysis, Over Representation Analysis, and Sparse Partial Least Square-Differential Analysis. We found that lipid metabolism is the most affected biological process between the two organs. A specific gene cluster expression pattern in the liver strongly correlated with a glucose sparing and an energy saving response affecting high energy demand process gene expression such as DNA repair, autophagy, and translation in the muscle.

Highlights

- Lipid metabolic process genes are the most affected between the muscle and the liver in mice during spaceflight
- Glucose metabolism pathways genes are the most significantly differentially expressed genes in the quadriceps in mice during spaceflight
- Altered glucose metabolism, DNA repair, autophagy, and translation gene expression in the quadriceps are linked to altered liver lipid metabolic processes genes expression
- Muscle atrophy phenotype gene expression correlates with a specific liver lipid metabolic gene cluster expression.

Conclusions

Together our results strongly suggest that a liver-muscle metabolic crosstalk promotes protein decrease and muscle atrophy during spaceflight, in which dietary changes represent a possible countermeasure.

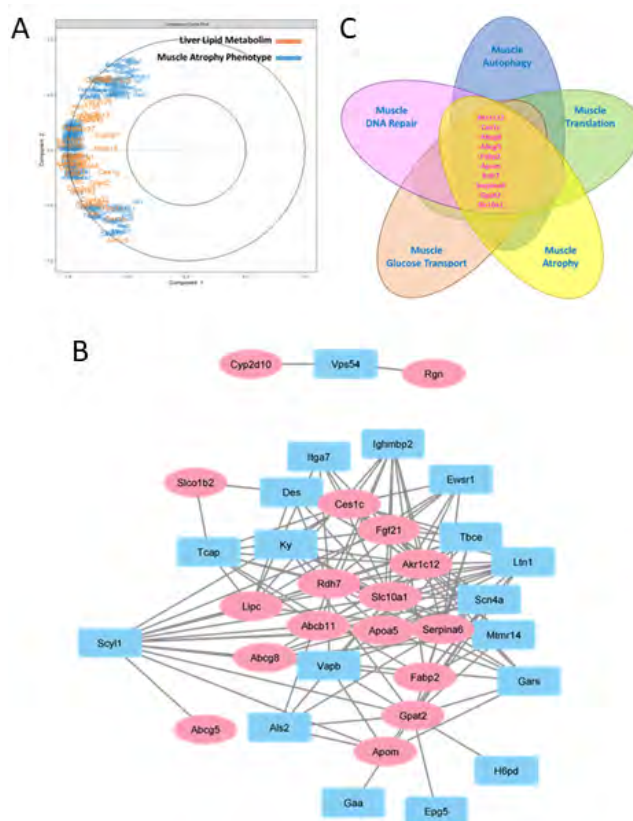


Figure 1: Caption. Figure 5. Liver lipid metabolism gene expression correlates with muscle atrophy phenotype, and DNA repair, autophagy, and translation genes decreased expression. A) Correlation circle plot between muscle Atrophy phenotype and liver Lipid Metabolism process gene expression from sPLS-DA of mice quadriceps and liver transcriptomes during spaceflight. B) Correlation network between muscle Atrophy phenotype and liver Lipid Metabolism process gene expression from sPLS-DA of mice quadriceps and liver transcriptomes during spaceflight. C) Venn diagram of strongest correlating liver Lipid Metabolism process genes in common between muscle Atrophy phenotype, Autophagy, DNA Repair, Translation, and Glucose Transport process genes. sPLS-DA: sparse Partial Least Square- Differential Analysis

Acknowledgements

W.A.d.S. acknowledge this work was partially funded by the ESA grant/contract 4000131202/20/NL/PG/pt “Space Omics: Toward an integrated ESA/NASA –omics database for spaceflight and ground facilities experiments”. V. W. . acknowledges this work was partially funded by the ESA grant/contract 4000134990/21/UK/AL.

References

Afshinnekoo, E., Scott, R.T., MacKay, M.J., Pariset, E., Cekanaviciute, E., Barker, R., Gilroy, S., Hassane, D., Smith, S.M., Zwart, S.R., Nelman-Gonzalez, M., Crucian, B.E., Ponomarev, S.A., Orlov, O.I., Shiba, D., Muratani, M., Yamamoto, M., Richards, S.E., Vaishampayan, P.A., Meydan, C., Foox, J., Myrrhe, J., Istasse, E., Singh, N., Venkateswaran, K., Keune, J.A., Ray, H.E., Basner, M., Miller, J., Vitaterna, M.H., Taylor, D.M., Wallace, D., Rubins, K., Bailey, S.M., Grabham, P., Costes, S. V., Mason, C.E. and Beheshti, A., 2020. Fundamental Biological Features of Spaceflight: Advancing the Field to Enable Deep-Space Exploration. *Cell*, 183(5), pp.1162–1184.

Beheshti, A., Chakravarty, K., Fogle, H., Fazelinia, H., Silveira, W.A. d., Boyko, V., Polo, S.H.L., Saravia-Butler, A.M., Hardiman, G., Taylor, D., Galazka, J.M. and Costes, S. V., 2019. Multi-omics analysis of multiple missions to space reveal a theme of lipid dysregulation in mouse liver. *Scientific Reports*, 9(1), pp.1–13.

da Silveira, W.A., Fazelinia, H., Rosenthal, S.B., Laiakis, E.C., Kim, M.S., Meydan, C., Kidane, Y., Rathi, K.S., Smith, S.M., Stear, B., Ying, Y., Zhang, Y., Foox, J., Zanello, S., Crucian, B., Wang, D., Nugent, A., Costa, H.A., Zwart, S.R., Schrepfer, S., Elworth, R.A.A.L.L., Sapoval, N., Treangen, T., MacKay, M., Gokhale, N.S., Horner, S.M., Singh, L.N., Wallace, D.C., Willey, J.S., Schisler, J.C., Meller, R., McDonald, J.T., Fisch, K.M., Hardiman, G., Taylor, D., Mason, C.E., Costes, S. V. and Beheshti, A., 2020. Comprehensive Multi-omics Analysis Reveals Mitochondrial Stress as a Central Biological Hub for Spaceflight Impact. *Cell*, [online] 183(5), pp.1185-1201.e20.

Durufié, H., Selmani, M., Ranocha, P., Jamet, E., Dunand, C. and Déjean, S., 2021. A powerful framework for an integrative study with heterogeneous omics data: From univariate statistics to multi-block analysis. *Briefings in Bioinformatics*, 22(3), pp.1–13.

Fitts, R.H., Riley, D.R. and Widrick, J.J., 2000. Physiology of a Microgravity Environment Invited Review: Microgravity and skeletal muscle. *Journal of Applied Physiology*, 89(2), pp.823–839.

ORAL 19

Multianalyte profiling of Scaffold driven Human Mesenchymal Stem Cell Constructs in Microgravity

A. Vivek Mann¹, B. Daniela Grimm², C. Janne Reseland³, D. Alamelu Sundaresan¹

¹Texas Southern University, Houston, USA, Vivek.Mann@tsu.edu, ²University of Magdeburg, Germany, dgg@biomed.au.dk, ³University of Oslo, Oslo, Norway, j.e.reseland@odont.uio.no, ⁴Texas Southern University, Houston, USA, Alamelu.Sundaresan@tsu.edu

Introduction

Contemporary technological advances in tissue engineering applied to medicine and regenerative medicine have a vast untapped potential for future space and terrestrial medical applications. Human cells form three-dimensional tissue constructs (e.g. cartilage, blood vessel intima constructs and others) when exposed to modeled microgravity (m- μ g). Here we have discussed different modeled microgravity models using cells alone and cells plus scaffolds to make 3D bone constructs. Human Mesenchymal stem cells grown on scaffolds [Tannic acid (TA) and P2] were exposed to a Random Positioning Machine (RPM—a model of m- μ g) which induced a significantly altered release of the cytokines and bone biomarkers like tumor necrosis factor 1 alpha (TNF-1 α), interleukin 6 (IL-6) Leptin, osteocalcin (OC), sclerostin (SOST) and osteoprotegerin (OPG). We further investigated the secretion of the cytokines involved in bone formation from HMSC cell line grown on alginate scaffolds treated and non-treated with tannic acid and adiponectin. We investigated the release of cytokines involved in the regulation of a wide spectrum of biological processes, including cell proliferation, differentiation, apoptosis, lipid metabolism and coagulation.

Introduction :

In the current study we investigated Human Mesenchymal Stem Cell (HMSC) cell lines, either exposed to modeled microgravity models (Rotary Cell Culture Systems-RCCS, Random Positioning Machine-RPM) or cultivated cells under 1 g conditions for different time points (21 days for RCCS experiment and 14 days for HMSC scaffold experiment). The purpose of this study was to scrutinize bone cell constructs along with bone cell plus scaffold constructs as acceptable biomaterials to assist bone formation, with possible implementation in bone tissue engineering and testing of particulate matter formulations of xenobiotics or implant materials.

Materials and Methods :

Cell Culture

The cell culture model used was represented by a human foetal osteoblast cell line, hFOB 1.19 (Catalogue number CRL-11372; American Type Culture Collection, Manassas, VA, USA), which is a conditionally immortalized clonal cell line [18]. hFOB 1.19 is immortalized with a gene encoding for a temperature-sensitive mutant of the SV40 large T antigen (tsA58). We cultured hFOB 1.19 in osteogenic medium (OM), α -MEM (Minimum Essential Medium) supplemented with 10% FBS, 50 μ g/ml of P-S and the osteogenic mixture containing 100nM dexamethasone, 5mM β -glycerophosphate disodium and 50mg/ml ascorbic acid (Sigma-Aldrich, S. Louis, MO, USA) to induce osteogenesis. Treatment lasted up to 21 days and the medium was changed

every 3 days. The cells were seeded in HARV's under the standard conditions of 37 C and 5% CO₂, as previously described [Mann et al 2019]. Cells in the third to fifth passage were used in the subsequent experiments. The experiment ended with the fixation of cells assigned to s-g or controls, as described earlier.

Microscopy

Phase contrast microscopy was performed before and after the RCCs experiments, to ensure viability and determine the morphological changes of the cells. Pictures were taken using a Canon EOS 550D camera (Canon GmbH, Krefeld, Germany) through a Leica DM IL LED inverted microscope (Leica Microsystems, Wetzlar, Germany).

Measurement of Secreted Bone Biomarkers

Multi-analyte profiling of the protein levels in the cell culture medium of primary human osteoblasts was performed on the Luminex 200 system (Luminex, Austin, TX, USA), using xMAP technology. Acquired fluorescence data were analysed by the xPONENT 3.1 software (Luminex). The effects of RPM on the secretion of bone markers in the culture medium was measured using the Milliplex Human Bone Panel (HBNMAG-51K, MILLIPORE Corporation, Billerica, MA, USA). The assay included analysis of the following secreted biomarkers; leptin, tumour necrosis factor alpha (TNF- α), osteoprotegerin (OPG), osteocalcin (OC), sclerostin (SOST) and interleukin-6 (IL-6). Multi-analyte profiling of the protein levels of these factors in the cell culture medium was performed using the Luminex 200 system (Luminex, Austin, TX, USA), using xMAP technology. Acquired fluorescence data were analysed by applying the Luminex xPONENT version 3.1.871 or MILLIPLEX™ Analyst version 5.1 software (Luminex).

Statistical Analysis

All statistical analyses were performed using the SPSS 24.0 software (SPSS, Inc., Chicago, IL, USA). Data are presented as the mean SD. Due to the number of samples per group, an estimation of the data distribution characteristics was not feasible. We, therefore, employed the assumption-less, non-parametric Mann-Whitney-U test to assess the differences between the experimental groups. $p < 0.05$ was considered statistically significant.

Results :

Tissue constructs of various sizes were generated in the absence of any foreign, exogenous scaffolding material using disposable 10 ml high-aspect-ratio vessels (HARV1/2) in an RCCS. We noticed formation of 3D bone constructs in both HARV1/2. Bone tissue consists of a cellular network where the osteocytes serve as sensory cells responsible for mechanotransduction, while osteoblasts and osteoclasts are

the effector cells [32]. The compressive or tensile loading mechanisms can be used in bone tissue engineering to mechanically stimulate 3D scaffold constructs seeded with osteoprogenitor cells to produce bone matrix before implantation. The prerequisite for this is to use bioreactors to impart the different mechanical forces, which mimic the mechanical stimuli that occur in vivo.

Tumor necrosis factor alpha ((TNF- α) inhibits the differentiation of osteoblast precursor cells to osteoblasts and it also acts as an inflammatory cytokine in several skeletal diseases. In our study, there was reduced secretion of TNF- α in Random positioning machine in Tannic acid + Adiponectin treated scaffold (RPM TA+P2) samples as compared to control TA+P2 samples.

Figure 1: Phase Contrast Microscopy of Treated vs Non-Treated Scaffolds.

Phase contrast microscopy of treated and nontreated alginate scaffolds after 6 days. Figure 1A shows non-treated scaffold. Figure 1B shows scaffold treat with tannic acid. Figure 1C shows scaffolds treated with tannic acid and adiponectin(P2). The scaffolds with HMSC cells were then exposed to RPM for 14 days.

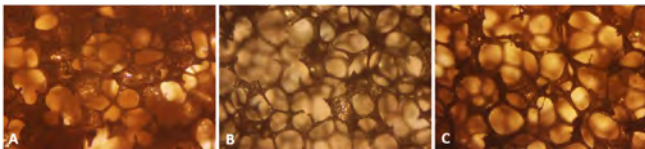


Figure 1: A Scaffold 6 days 1 g non treated; B Scaffold 6 days 1 g tannic acid treatment; C Scaffold 6 days 1 tannic acid + P2 (adiponectin) treated.

Conclusions

We found that multianalyte profiling of HMSC construct supernatants with TA and P2 scaffolds revealed a milieu of balanced bone growth cytokines indicating the promotion of bone tissue formation and organization. Significantly, inflammatory cytokine secretion such as that of TNF alpha was reduced with scaffolds loaded with TA and adiponectin which is anti-inflammatory bone regulatory factor. Detailed results are presented in this study.

Normally, interleukin 6 is known as a classical mediator of acute inflammation and reduces bone formation. IL-6 secretion was decreased in the supernatant of osteoblasts exposed for 14 days RPM TA+P2 samples as compared to control TA+P2 samples. Leptin plays a major role in neuroendocrine regulation and bone metabolism. Leptin secretion remained almost the same in RPM TA+P2 samples as compared to control TA+P2 samples but increased in RPM TA samples as compared to control TA samples

Acknowledgements

We wish to thank the Mickey Leland Study abroad scholarship from TSU for student travel funding.

References

V.Mann et al. Changes in Human Foetal Osteoblasts Exposed to the Random Positioning Machine and Bone Construct Tissue Engineering. *International journal of molecular sciences*, 20(6)., (2019)

ORAL 20

Particle dynamics at the onset of the granular gas-liquid transition

N. Vandewalle¹, E. Falcon², D. Fischer³, Y. Garrabos⁴,
C. Lecoutre-Chabot⁴, M. Noirhomme¹, E. Opsomer¹, F. Palencia⁴

¹ University of Liège, GRASP, CESAM Unit, B-4000 Liège, Belgium

² Université Paris Cité, CNRS, MSC Laboratory, UMR 7057, F-75013 Paris, France

³ Institute of Physics, Otto von Guericke University, D-39106 Magdeburg, Germany

⁴ CNRS, Université de Bordeaux, Bordeaux INP, ICMCB, UMR 5026, F-33600 Pessac, France

Introduction

Granular gases are composed by a large amount of mobile solid particles. Unlike molecular gases, they are characterized by inelastic collisions leading to an ongoing loss of kinetic energy over time. In order to avoid such cooling of the system, mechanical energy should be injected in the granular gas.

From dilute systems, increasing the number of particles also leads to the spontaneous formation of denser regions coexisting with the granular gas (Noirhomme et al 2018). This gas-liquid transition is known to depend on the collision rate in the system. Although this phenomenon has already been studied at the scale of the entire system, local clustering is still poorly investigated. The granular gas-liquid transition itself is smooth and many fundamental questions remain open. Among others, the particle dynamics (in the gas phase) near the transition is still unclear.

In the present work, we propose investigations of the gas-like to clustering transition in driven granular media thanks to the tracking of a few large tracer particles in a 2D gas made of semi-transparent tiny particles. We show that the velocity distributions of these tracers show peculiar features when the density of the system is increased above some threshold value. The latter is shown to coincide with the emergence of local clusters, that is a liquid-like phase coexisting with the granular gas.

Experiments

Our studies were thus realized using the VIP-Gran instrument (Aumaître et al 2018) that was developed in the frame of the SpaceGrains project of the European Space Agency (ESA). Experiments took place during the 66th and 69th ESA parabolic flight campaigns. Given our need to achieve particle tracking, granular media is enclosed in a quasi-2D cell composed of four transparent walls and two moving plates that can inject kinetic energy into the system. Pistons move sinusoidally in phase opposition with fixed amplitude $A=4$ mm and frequency $f=15$ Hz.

As seen in Figure 1, we placed a few large particles ($N_t=1$ and $N_t=3$) as tracers in order to follow the particle trajectories when the number of small particles N_s is increased. The gas-liquid transition takes place close to $N_s=200$. There, the trajectories are deeply modified from quasi linear segments to random paths. Some caging effect is seen and this is due to the granular droplet forming around large particles.

In order to confirm the transition with a second method, we also determined the local density of the particles in subcells covering the images. The statistical distribution of the values obtained in all subcells, as presented in Figure 2(a), shows two peaks when N_s is high enough, i.e. when the transition occurs. Average peak positions μ determining the probable local densities in subcells are drawn in Figure 2(b). This plot shows that, at low N_s values, μ keeps a linear single trend as expected for a homogeneous gas phase. However, at higher N_s values, a bifurcation is observed with two branches being gas and droplet densities respectively.

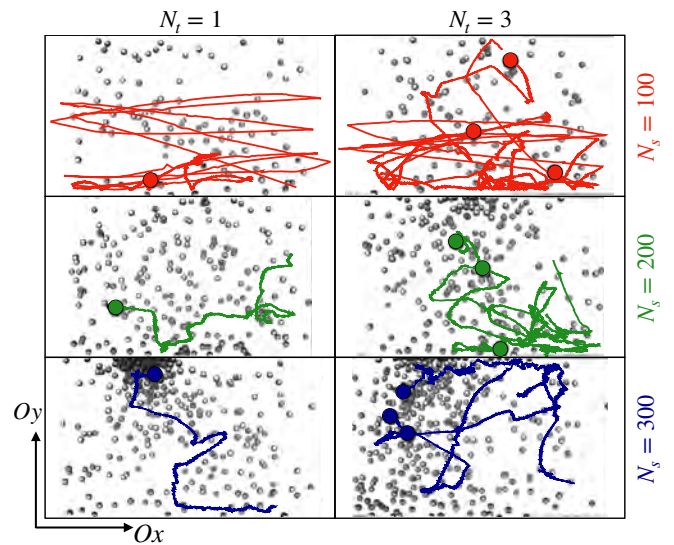


Figure 1: Trajectories of N_t tracers being large particles placed in a gas of small solid particles. When the density of the gas remains low, the trajectories are quasi linear trajectories in between moving pistons. Increasing the number N_s of small beads leads to the formation of liquid droplets in which the large particles are trapped. Trajectories become more randomized.

Model

A model (Noirhomme et al 2021) has been elaborated taking into account the dissipative nature of the particle collisions and the injection of kinetic energy from the opposite pistons. This model fits the data (red curves in Figure 2(b)) within error bars. It suggests that the transition is a subcritical pitchfork bifurcation. The signature of this kind of bifurcation is a critical point being highly sensitive to the initial conditions and the history of the system. This may explain why parabolic flight experiments were quite difficult to analyze till now.

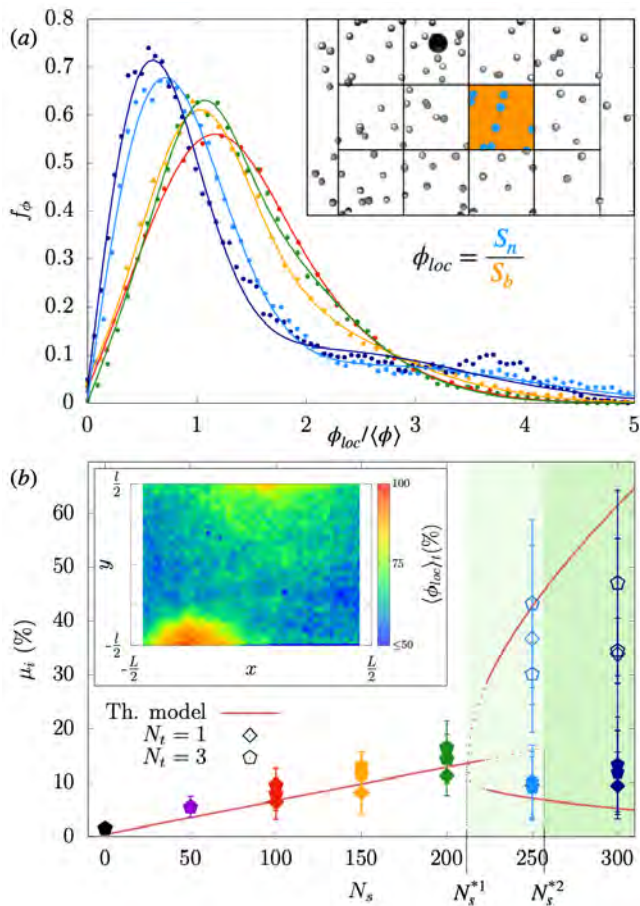


Figure 2: (a) Statistical distribution of particle density in many subcells. The color code corresponds to different N_s values. The distribution shows two peaks for high N_s values. (b) The position of the peaks for each set of data is shown using the same color code. Inset shows the density map of the VIPGRAN cell in false colors evidencing clusters (granular liquid droplets) along the side walls.

Conclusions

Parabolic flight experiments using the VIP-GRAN instrument have evidenced a gas-liquid transition in granular systems. From data analysis and from model developments, this transition appears to belong to a class of subcritical pitchfork bifurcation, showing high sensibility to experimental conditions. This may change the way future experiments will be conducted onboard ISS.

Acknowledgements

VIP-Gran-PF instrument was built by DTM Technologies (Modena, Italy). This work was funded by European Space Agency Topical Team SpaceGrains No. 4000103461. We thank the support of Novespace during ESA Parabolic Flight Campaigns. MN thanks the Belgian Federal Science Policy Office (BELSPO) for the financial support in the framework of the PRODEX Programme of the European Space Agency (ESA) under contract number 4000103267.

References

S. Aumaître, R. P. Behringer, A. Cazaubiel, E. Clément, J. Crassous, D. J. Durian, E. Falcon, S. Fauve, D. Fischer, A. Garcimartín, Y. Garrabos, M. Hou, X. Jia, C. Lecoutre, S. Luding, D. Mazza, M. Noirhomme, E. Opsomer, F. Palencia, T. Pöschel, J. Schockmel, M. Schröter, M. Sperl, R. Stannarius, N. Vandewalle, and P. Yu, *An instrument for studying granular media in low-gravity environment*, Rev. Sci. Instrum., 89, 075103 (2018).

M. Noirhomme, A. Cazaubiel, A. Darras, E. Falcon, D. Fischer, Y. Garrabos, C. Lecoutre-Chabot, S. Merminod, E. Opsomer, F. Palencia, J. Schockmel, R. Stannarius, and N. Vandewalle, *Threshold of gas-like to clustering transition in driven granular media in low-gravity environment*, EPL, 123, 14003, (2018)

M. Noirhomme, A. Cazaubiel, E. Falcon, D. Fischer, Y. Garrabos, C. Lecoutre-Chabot, S. Mawet, E. Opsomer, F. Palencia, S. Pillitteri, and N. Vandewalle, *Particle Dynamics at the Onset of the Granular Gas-Liquid Transition*, Phys. Rev. Lett., 126, 128002, (2021)

ORAL 21

Instability caused by interplay of Soret and cross-diffusion in ternary mixture

V. Shevtsova^{1,2}, B. Seta³, A. Errarte¹, M. Bou-Ali¹,

¹Mechanical and Manufacturing Department, Mondragon Unibertsitatea, Mondragón, Spain.

²Ikerbasque, Basque Foundation for Science, Bilbao, Spain

³Dept. Civil and Mechanical Engineering, Technical University of Denmark.

berse@mek.dtu.dk | aerrarte@mondragon.edu | mbouali@mondrago.edu | x.vshevtsova@mondragon.edu

Introduction

The Soret effect describes the transport of constituent species in multicomponent mixtures that occurs due to a temperature gradient. This cross-coupling effect of heat and mass transfer were successfully investigated in binary liquid mixtures, while experiments with ternary mixtures are rare as they impose significant difficulties.

Here, the main attention is paid to the appearance of instability in a ternary mixture placed in a thermogravitational column. In the thermogravitational column technique, a liquid is placed between two vertical walls with different temperatures. The horizontal temperature gradient generates the horizontal concentration gradient due to the Soret effect, which is accompanied by vertical convective flow driven by buoyancy (E. Lapeira, et al., 2018). For the successful operation of the column, the stability of vertical convective flow, which drives the separation, is required. There are several theoretical studies related to the stability of ternary mixtures in an infinite vertical layer (e.g., Ryzhkov&Shevtsova, 2009).

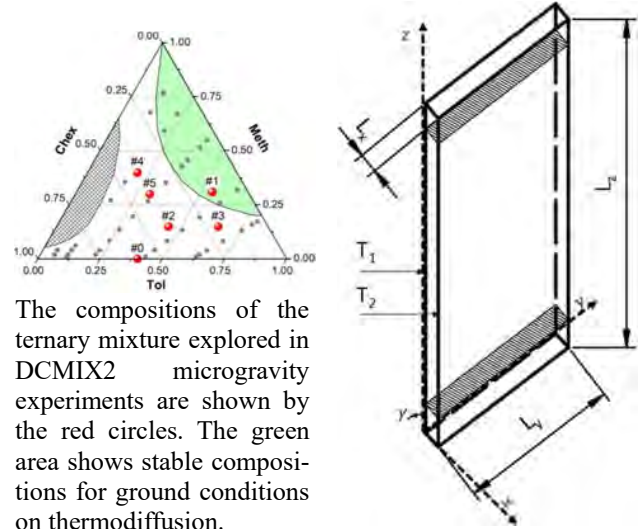
The relative importance of contributions from concentration of individual component *i* and a temperature field to the density gradient is specified by the separation ratio ψ_i . To describe the stability of ternary and higher mixtures, the net separation ratio Ψ , which is the sum of individual contributions, is introduced $\Psi = \psi_1 + \psi_2$

Still, the role of cross-diffusion is somehow elusive, and there have been no experiments or relevant non-linear simulations on this subject. The latter is due to the lack of thermodiffusion coefficients, since they can be measured reliably only in a stable system. This problem was solved by measuring thermodiffusion coefficients under microgravity conditions of the ISS in the toluene (T)-methanol (M)-cyclohexane (Ch) (Mialdun et al., 2018), see the red points at Fig.1 on the the Gibbs triangle. The values of diffusion coefficients in ternary mixtures depend on the order of the components as well as on the frame of reference for which the diffusive fluxes are written. We adopted a hydrodynamic approach to the numbering of components, which corresponds to a decreasing order of density: T(1), M (2) and Ch (3).

Laboratory experiments with T(62%)-M (31%)-Ch(7%) reveal an oscillatory behavior of the system. This finding motivated non-linear simulations.

Methodology

Sketch of the geometry and dimensions of the thermogravitational column, correlated with the laboratory setup are given in Fig. 1 (right). The lateral walls are maintained at constant but different temperatures T_1 and T_2 ,



The compositions of the ternary mixture explored in DCMIX2 microgravity experiments are shown by the red circles. The green area shows stable compositions for ground conditions on thermodiffusion.

Figure 1: (left) Here focus on the point #1: 0.62(T)-0.31(M)-0.07 (Ch) in mass fractions; (right) The geometry of thermogravitational column. The cavity has a height of $L_z=30\text{mm}$ and a gap width of $L_x=0.51\text{ mm}$, and $L_y=3\text{ mm}$.

Table 1: The mass diffusion coefficients D [m^2/s], the Soret coefficients S_{Ti} [K^{-1}], the thermodiffusion coefficients D_{Ti} [$\text{m}^2/(\text{s} \cdot \text{K})$], separation ratios ψ_i , and the net separation ratio Ψ of the) mixture (in mass fractions).

$D_{11}/10^{-9}$	$D_{12}/10^{-9}\text{s}$	$D_{21}/10^{-9}$	$D_{22}/10^{-9}$
2.244	1.337	-0.226	0.551
$S_{T1}/10^{-3}$	$S_{T2}/10^{-3}$	$D_{T1}/10^{-13}$	$D_{T2}/10^{-13}$
0.387	-1.145	-6.624	-7.184
ψ_1	ψ_2	Ψ	
0.0467	-0.0473	-0.0006	

providing $\Delta T = T_1 - T_2$. As a result, there is a horizontal thermal gradient in the fluid mixture. It is supposed that there is no vertical temperature gradient. The horizontal temperature gradient induces horizontal gradients of composition due to the Soret effect and also results in convective flow driven by the buoyancy force. All walls are impermeable, no-slip boundaries, and the vertical walls are maintained at constant but different temperatures. The fluid is considered incompressible and the flow Newtonian. Three-dimensional time dependent governing equations in the Boussinesq approximation in the geometry shown in Fig.1 were solved using the open-source package OpenFOAM.

An intriguing point of the considered mixture is that the sign of the D_{T1}' is opposite to the sign of the Soret coefficients S_{T1}' , see Table 1. To the best of our knowledge, no other mixture have been reported where S_{T1}' and D_{T1}' have different signs. It occurs due to large cross-diffusion D_{12} and different signs of S_{T1} and S_{T2} . In a binary system, the signs of the Soret and thermodiffusion coefficient coincide.

Results

Figure 2a shows the time evolution of the two independent components during the Soret separation: toluene (black) and methanol (red). The separation of component is recorded at the upper part of the column, $z=0.8L_z$, thus a positive sign of $(w_i - w_{i0})$ indicates the accumulation of a heavier component at the top. At the earliest times, accumulation of toluene is negative (back curve) since $S_{T1} > 0$. As soon as flow develops, convective mixing drive toluene to the upper part since $D_{T1} < 0$. Methanol accumulates in the upper part from the very beginning, because S_{T2}' , $D_{T2}' < 0$. It takes about 1800 s to reach critical mass before instability sets in.

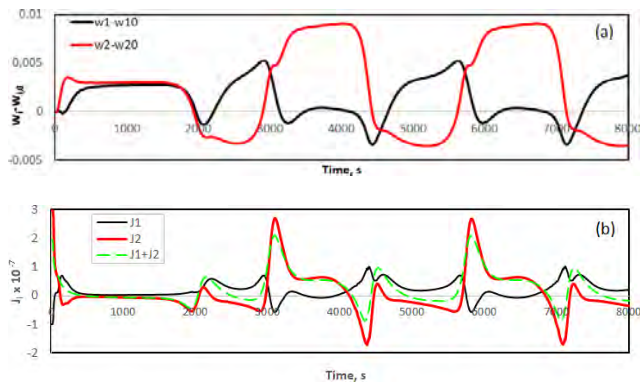


Figure 2: (a) The time evolution of the two independent components during the Soret separation: toluene (black) and methanol (red). (b) The total flux of the components and their sum (green curve). The records of $(w_i - w_{i0})$, where w_{i0} initial concentration, are taken near the middle at the column $x = 0.255\text{mm}$; close to the back wall $y=2.5\text{mm}$ and at the height $z=24\text{mm}$.

The computer simulations reveal oscillatory behavior of the system, which supports the experimental observations. The time evolution of the components in Fig.2a demonstrates that they follow the different topology. Methanol (red curve) exhibits almost sinusoidal oscillations while toluene (which has opposite signs for Soret and thermodiffusion) presents much more complex oscillations.

The net fluxes of the toluene and methanol are presented in Fig.2b and they have an opposite signs. This sign difference appears as the results of large cross-diffusion D_{12} . The scale of the figure indicates that mostly methanol plays a leading role in mass transport and can be the cause of instability. However, there are some times when the net flux is equal to zero or even J_1 prevailed by J_2 , see the green dashed curve showing $J_1 + J_2$. Thus, their interplay leads to the emerging of an oscillatory behavior. It also leads to the competition of various modes of instability.

Figure 3 presents the Fourier spectrum for both components. Although the fundamental frequency is the same, the amplitude and dominant harmonics are very different, which explains the intricate behavior of the concentration signals in Fig. 2a.

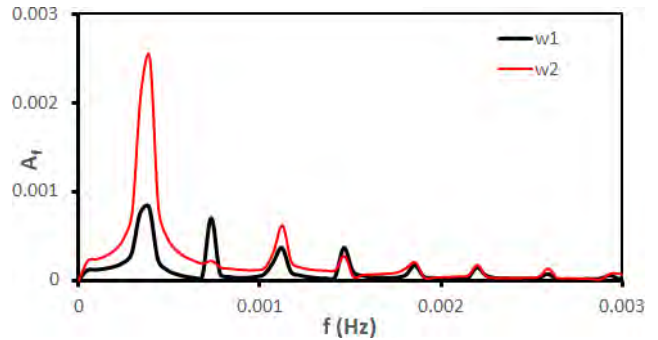


Figure 3: Fourier spectrum for toluene and methanol

Conclusions

A detailed investigation of an oscillatory instability is presented here for a ternary mixture with a large cross-diffusion. The novel instability is driven by unusual property of the mixture, when the Soret and thermodiffusion coefficients have different signs. The numerical results favorably support the experimental observations.

Acknowledgements

The authors acknowledge the support by KK-2021/00082 (micro4IoT), PRE_2021_0_0234, IT1505-22 (Research Group Program) of the Basque Government and PID2020-115086GB-C33 financed by MCIN/AEI of the Spanish Government, and 2022-CIEN-000052-01 (HOZTIKOR) of The Gipuzkoa Provincial Council.

References

- E. Lapeira, A. Mialdun, V. Yasnou, P. Aristimuno, V. Shevtsova, and M. Bou-Ali, Digital interferometry applied to thermogravitational technique., *Microgravity Sci.Tech.* **30**, 635 (2018).
- I. I. Ryzhkov and V. M. Shevtsova, Convective stability of multicomponent fluids in the thermogravitational column, *Phys. Rev. E* **79**, 026308 (2009).
- A. Mialdun, I. Ryzhkov, O. Khlybov, T. Lyubimova, and V. Shevtsova, Measurement of Soret coefficients in a ternary mixture of toluene-methanol-cyclohexane in convection-free environment, *J. Chem. Phys.* **148**, 044506 (2018).

ORAL 22

**Nonlinearities in shadowgraphy experiments on non-equilibrium fluctuations –
in preparation of the GIANT FLUCTUATIONS microgravity project**

W. Köhler¹, D. Zapf¹, J. Kantelhardt¹

¹Physikalisches Institut, Universität Bayreuth, Bayreuth, Germany, werner.koehler@uni-bayreuth.de

Introduction

Pure liquids and liquid mixtures subjected to a temperature or a concentration gradient exhibit giant non-equilibrium fluctuations (NEFs) of their associated thermodynamic variables. The amplitudes of these fluctuations diverge for small wavevectors proportional to q^{-4} , but the full divergence can only be observed under microgravity conditions. Under the influence of gravity, the amplitudes level off below a characteristic roll-off wavevector (Vailati et al. 1996). The ESA projects GIANT FLUCTUATIONS and TechNES and the associated DLR project BTGIANT aim at the investigation of NEFs in complex multicomponent systems under microgravity conditions aboard the ISS. The focus of these projects is on the investigation of non-ideal systems that can not easily be described by existing linear theories (Ortiz de Zárate et al. 2006). In our work we have performed preparatory ground based shadowgraphy experiments with large gradients that give rise to pronounced nonlinearities and complicate the determination of transport coefficients (Zapf et al. 2022).

Experiment

Experiments were performed by means of the shadowgraphy technique with a setup that shares several aspects with the one that will be employed for the space experiments. At its core is a Soret cell with sapphire windows, which allows to establish a temperature gradient parallel to the optical axis, which in turn is oriented parallel to gravity. The interfering primary and scattered beams are detected with a camera at a distance of $Z=20.87$ cm (Zapf et al. 2020). The sample is a solution of polystyrene ($M_w=17.9$ kg/mol, $M_w/M_n=1.03$, Polymer Standards Service GmbH) in toluene with a polymer mass fraction $c_0=0.01$ g/g.

Results and discussion

The Soret effect is used to create a temperature together with a superimposed concentration gradient:

$$\nabla c = -S_T c(1 - c)\nabla T \quad (1)$$

Thus, both thermal and solutal NEFs are observed simultaneously. From a time series of recorded images the structure function in q -space is calculated, from which the static amplitudes, the characteristic thermal and solutal time constants τ_T and τ_c and the two roll-off wave vectors q_{ro}^T and q_{ro}^c are extracted. The thermal diffusivity and the Fickian diffusion coefficient can be calculated from the two time constants and the Soret coefficient from the ration of the two roll-off wavevectors (Zapf et al. 2020, 2022).

The temperature gradient is the prerequisite for non-equilibrium. Strong gradients promise better signals, but how strong is too strong? In our contribution we go beyond the usual linear models and address the nonlinearities that result from strong gradients for a number of reasons, such as the temperature and concentration dependence of thermophysical parameters or, most important, the intrinsic nonlinearity of the stationary diffusion equation (1).

In (Zapf et al. 2022) we have addressed the temperature and concentration dependence of the following thermophysical parameters of the polystyrene/toluene system: the Soret, diffusion and thermodiffusion coefficient, the thermal diffusivity, the thermal conductivity, the density, the thermal and solutal expansion coefficients, and the dynamic and kinematic viscosities.

The measured shadowgraphy signal is simulated as a linear superposition of the contributions from thin parallel layers of the fluid, each characterized by its particular temperature and concentration and the appropriate set of thermophysical parameters. Fig. 1 shows the time dependent structure functions computed for the individual layers and the averaged observable signal. The fast mode corresponds to the thermal and the slow one to the solutal NEFs. Note that the amplitude of the former ones increases whereas the amplitude of the latter ones decreases with increasing temperature difference.

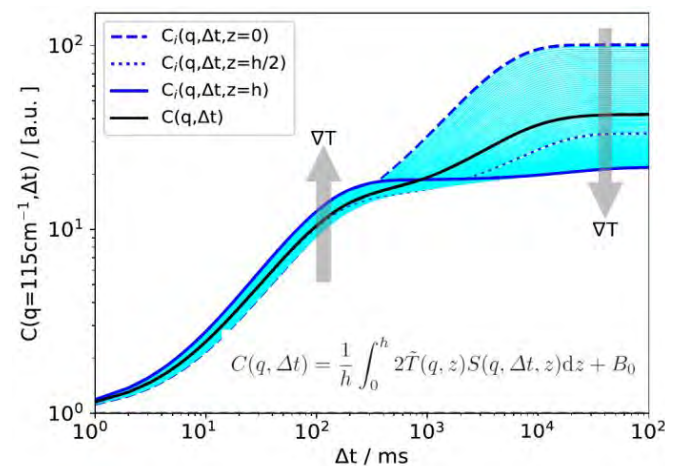


Figure 1: simulated structure functions for the individual fluid layers. The dotted line corresponds to the midplane and the black solid line to the experimentally observable averaged structure function. From (Zapf et al. 2022).

The averaged structure function is the only one that is observable in an experiment. Both the simulated structure function and the actual experiment are evaluated in the same nonlinearity-unaware way.

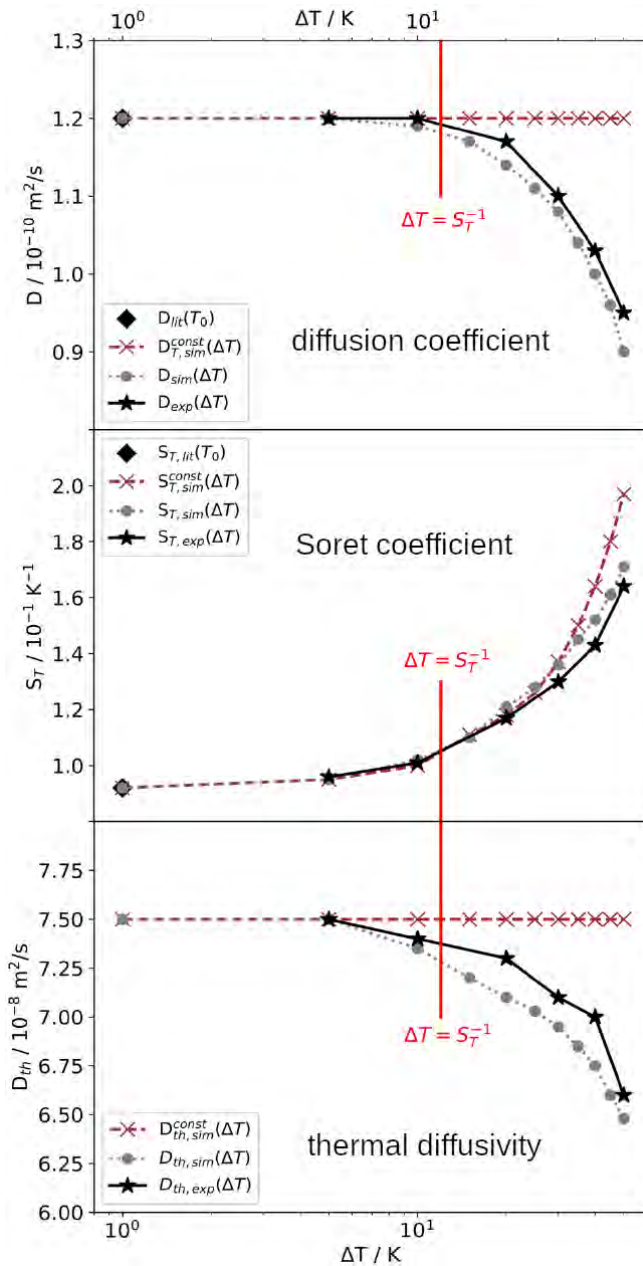


Figure 2: Transport coefficients as extracted from the measured and simulated shadowgraphy signals. The curves labeled with “const” contain the nonlinearity of the diffusion equation but constant values of all thermophysical parameters. From (Zapf et al. 2022).

Fig. 2 shows the diffusion coefficient D , the Soret coefficient S_T and the thermal diffusivity D_{th} as obtained from the simulation and from the experiment. As can be seen, and this is a major result of our work, deviations due to nonlinear effects become important for temperature differences that exceed the inverse of the Soret coefficient, S_T^{-1} .

The agreement between the experiment and the full simulation, taking all temperature and concentration dependencies and the nonlinear diffusion equation into account, is convincing. For an unknown system, which has not already fully been characterized in the literature, the situation might turn out to be even more complicated. For the case shown, the check of the criterion $\Delta T < 1/S_T$ is on the safe side, since the deviation in Fig. 2 is towards an overestimation of the Soret coefficient. But such a benign behaviour is not guaranteed. Even for PS/toluene it can lead to a detrimental underestimation in certain molar mass and concentration regimes.

Conclusions

As shown by both experiments and simulations, the transport coefficients determined from NEFs in shadowgraphy experiments agree with their true values only for sufficiently small temperature differences. A good measure for the maximum allowed difference is provided by the inverse of the Soret coefficient. The observed nonlinearity stems both from the temperature and concentration dependencies of all involved thermophysical parameters and from the inherent nonlinearity of the extended diffusion equation. It could be shown that the measured signal can be described as a superposition of contributions from thin parallel layers, each with its own temperature and concentration. Some corrections are to be expected for very small q -values, for which the assumption of fully decoupled fluctuations will eventually break down.

Acknowledgements

This work was supported by the ESA project GIANT FLUCTUATIONS, the ESA-MAP project TechNES (Grant 4000128933/19/NL/PG), and by Deutsches Zentrum für Luft- und Raumfahrt (DLR), Grant 50WM2147 (BTGIANTII).

References

- J. M. Ortiz de Zarate, J. V. Sengers, Hydrodynamic fluctuations in Fluids and Fluid Mixtures, Elsevier, Amsterdam 2006
- A. Vailati, M. Giglio, q Divergence of Nonequilibrium Fluctuations and Its Gravity-Induced Frustration in a Temperature Stressed Liquid Mixture, *Phys. Rev. Lett.* 77, 1484 (1996).
- D. Zapf, W. Köhler, Thermal and solutal non-equilibrium fluctuations in a polymer solution, *J. Chem. Phys.* 153, 224902 (2020)
- D. Zapf, J. Kantelhardt, W. Köhler, Nonlinearities in shadowgraphy experiments on non-equilibrium fluctuations in polymer solutions, *Eur. Phys. J. E* 45, 40 (2022)

ORAL 23

Comparative experimental-numerical analysis of PCM: n-hexadecane, n-octadecane and n-eicosane

A. Sanjuan¹, B. Šeta², F. Gavaldà³, X. Ruiz³, V. Shevtsova^{1,4} and M. Mounir Bou-Ali¹

¹Mechanical and Manufacturing Department, Mondragon University, Mondragon, Spain, mbouali@mondragon.edu

²Department of Mechanical Engineering, Technical University of Denmark, Kongens Lyngby, Denmark, berin.seta@gmail.com

³ Department of Physical and Inorganic Chemistry, Universitat Rovira i Virgili, Tarragona, Spain, josepxavier.ruiz@urv.cat

⁴IKERBASQUE, Basque Foundation for Science, Bilbao, Spain. x.vshevtsova@mondragon.edu

Introduction

As part of the preliminary work about the effect of Marangoni convection in PCM materials in space [1], the present work reports the values of different thermophysical properties such as density, thermal expansion coefficient, dynamic-kinematic viscosity, thermal conductivity, thermal diffusivity, specific heat, melting-solidification temperatures and surface tension of three paraffin waxes, n-hexadecane -C₁₆H₃₄, C₁₆-, n-octadecane -C₁₈H₃₈, C₁₈- and n-eicosane -C₂₀H₄₂, C₂₀. They were accurately measured at atmospheric pressure and in a wide range of temperatures. The resulting set of quantitative values was further used to properly feed numerical simulations aiming to realistic assesment of the importance played by the thermocapillary convection as a suitable enhancer of heat transfer in space environments.

Experimental methodology and results

The density of liquid samples was measured as a function of temperature using an Anton Paar DMA 5000 M densimeter (see Figure 1.a).

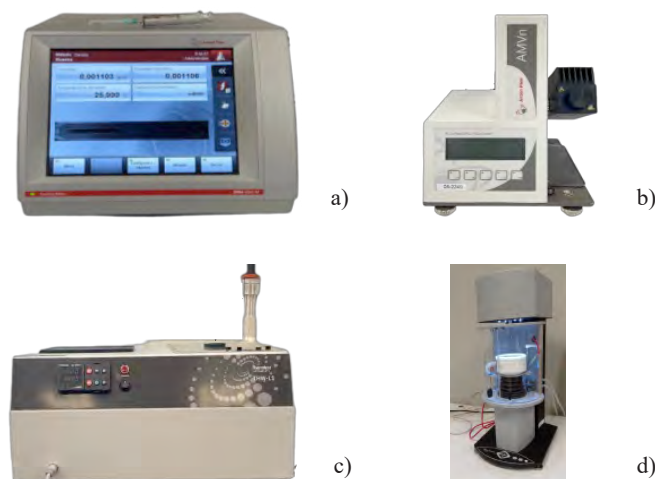


Figure 1: Equipment used for thermophysical properties determination: Anton Paar DMA 5000 densimeter a), Anton Paar AMVn microviscosimeter b), THW-L1 Thermtest instrument c) and Sigma 701 Force Tensiometer d).

The thermal expansion coefficient (α) was determined using Eqn. (1) where ρ is the density of the fluid at working temperature (T). For example, to calculate α for a temperature of 298.16 K, the density was determined from 297.16 K to 299.16 K. (increase of 0.5 K) (see Figure 2).

$$\alpha = -\frac{1}{\rho} \frac{\partial \rho}{\partial T} \quad (1)$$

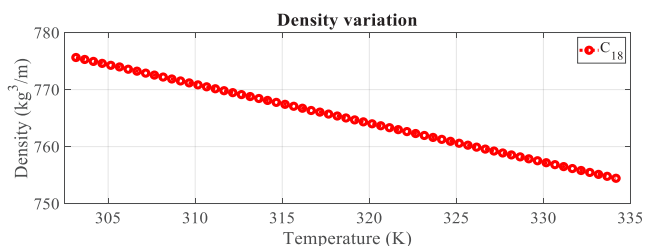


Figure 2: Variation of the density of the C₁₈ in a range of 303 K to 334 K (increase of 0.5 K).

The Anton Paar AMVn microviscosimeter Figure 1 b) was used to determine the dynamic viscosity of the liquid samples. Based on the previously determined density, the variation of the kinematic viscosity of the three waxes was, for the first time, reported in the literature. Figure 3 shows, as an example, the results corresponding to the C₁₈ case. These values show that the kinematic viscosity of the samples appreciably decreases with increasing the temperature. The same behavior was observed for the three components

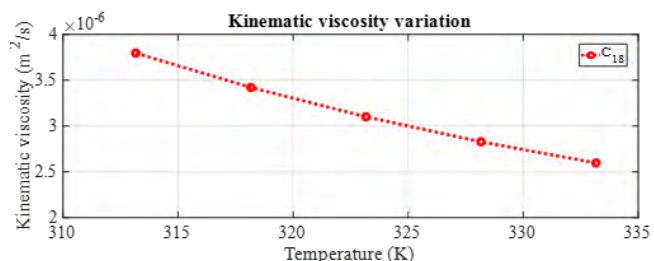


Figure 3: Kinematic viscosity variation of the C₁₈ as a function of temperature.

The THW-L1 Thermtest instrument, Figure 1.c), was used to measure the thermal conductivity (κ) and thermal diffusivity (χ) and thus calculate the specific heat (C_p) using the following relationship:

$$\frac{\kappa}{\chi} = \rho C_p \quad (2)$$

These properties were measured in the liquid, solid and transition states. The same equipment was used to determine melting and solidification temperatures. Figure 4 shows the variation of the thermal conductivity of the n-octadecane as a function of the temperature. The thermal conductivity in the solid phase is higher and the experimental results in both the liquid and solid states are in accordance with the ones reported in the literature [3]. Mention also that the experimental results presented here show a more detailed analysis around the transition state.

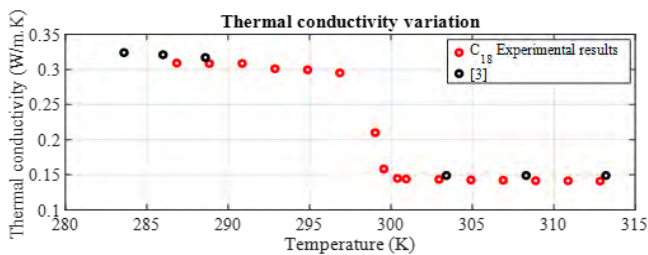


Figure 4: Thermal conductivity variation of C₁₈ sample as a function of temperature.

Finally, the surface tension of the three paraffin waxes was determined using the Sigma 701 Force Tensiometer (Biolin Scientific) Figure 1 d). This property was measured by using two different methods: Du Noüy ring and Wilhelmy plate. In Figure 5, as an example, the surface tension variation of C₁₈ component is shown as a function of temperature.

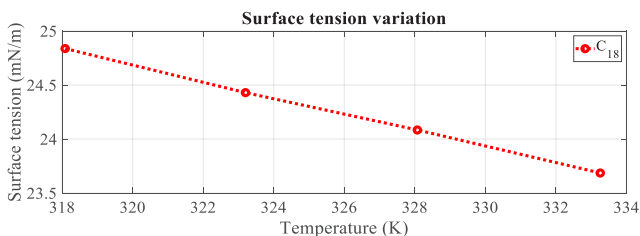


Figure 5: Surface tension variation of the C₁₈ as a function of temperature.

It should be finally remarked that all properties were experimentally measured at least three times to verify that the results obtained were reliable.

Numerical methodology and results

The computational 2D approach use a phase-change model based on the enthalpy-porosity formulation of the Navier Stokes and energy equations (see more details in Šeta et al. 2021). The dimensions of the simulated cell were 22.5×15 mm². After creating a temperature difference between the two lateral walls, the solid system begins to melt. The thermocapillary flow localized in the upper free surface enhances the melting process. Except the above-mentioned lateral walls, the rest were adiabatic. Thermophysical values obtained experimentally here were used as data inputs in all cases investigated.

Figure 6 shows, as an example, the numerical results of the liquid fraction evolution for two different paraffins, C₁₈ and C₂₀. If the thermal difference is low, this evolution is practically the same, while increasing this difference the melting time is reduced for the n-octadecane. This fact could be explained by the different surface tension coefficients and viscosities of both waxes.

A snapshot of the streamfunctions together with the solid-liquid interfaces (gray and magenta lines) at 8000s is presented in Figure 7 for C₁₈ and C₂₀. Notice the two common vortical structures originated by the thermocapillary convection acting in the free surface. Both structures are not steady; a complex oscillatory mode is detected in both liquids.

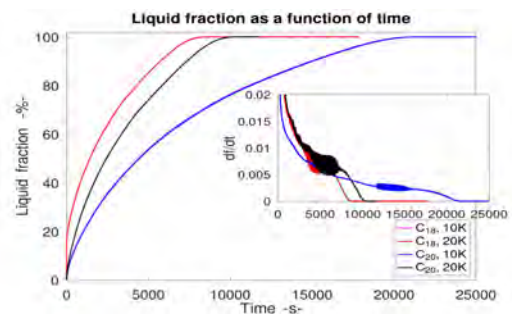


Figure 6: C₁₈ and C₂₀ liquid fraction evolution for ΔT=10 and 20K.

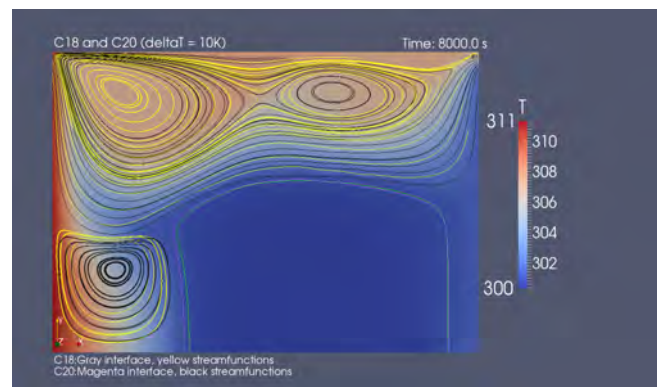


Figure 7: Snapshot of the different flow characteristics during the melting process

Conclusions

Thermophysical properties of the three paraffin waxes C₁₆H₃₄, C₁₈H₃₈ and C₂₀H₄₂ were comprehensively characterized as a function of temperature. The present experimental results are in favorable agreement with the available literature data. The numerical results suggested that the value of the surface tension coefficient is closely related with the magnitude of the thermocapillary convection established in the viscous flow and, so, with the convective enhancing of heat transfer in space environments.

Acknowledgements

The present work has been supported by grants PID2020-115086GB-C32, PID2020-115086GB-C33 (MCIU/FEDER), 2021PFR-URV-74 (Rovira i Virgili University), IT1505-22 (Research Group Program), KK-2022/00047 (MMASINT) of the Basque Government, and 2022-CIEN-000052-01 (HOZTIKOR) of The Gipuzkoa Provincial Council.

References

- [1] ESA-HRE-ESR-Marangoni in PCM “Effect of Marangoni Convection on Heat Transfer in Phase Change Materials”
- [2] B. Šeta, D. Dubert, J. Massons, Jna. Gavaldà, M.M. Bou-Ali, X. Ruiz; Effect of Marangoni induced instabilities on a melting bridge under microgravity conditions. *Int. J. Heat Mass Transf.*, 179, 121665, 2021.
- [3] C. Véléz, M. Khayet, J.M. Ortiz de Zárate; Temperature-dependent thermal properties of solid/liquid phase change even-numbered n-alkanes: n-Hexadecane, n-octadecane and n-eicosane. *Appl. Energy*, 143, 383–394, 2015 (<https://doi.org/10.1016/j.apenergy.2015.01.054>).

ORAL 24

Ocular counter-roll is less affected in experienced compared to novice space crew after long-duration spaceflight

C. Schoenmaekers¹, C. De Laet¹, L. Kornilova², D. Glukhikh², S. Moore³, H. MacDougall⁴, I. Naumov², E. Fransens⁵, L. Wille¹, S. Jillings¹, F. L. Wuyts¹

¹ Lab for Equilibrium Investigations and Aerospace (LEIA), University of Antwerp, Wilrijk, Belgium, catho.schoenmaekers@uantwerpen.be, ² Institute for Biomedical Problems, Moscow, Russia, ³ Central Queensland University, School of Engineering and Technology, Queensland, Australia, ⁴ University of Sydney, School of Physiology, Sydney, New South Wales, Australia, ⁵ University of Antwerp, StatUA Center for Statistics, Wilrijk, Belgium

Introduction

The vestibular organ: a multisensory system

Humans highly depend on the vestibular system, located bilaterally in the inner ear, for movement coordination and to ensure gaze stabilization and balance (Angelaki, et al. 2008). The vestibular organs consist of the semicircular canals (SCCs) that are stimulated by angular accelerations, and the otoliths that detect the vector sum of linear accelerations, gravito-inertial acceleration (GIA) vector, acting upon the head. The otoliths are the primary gravitational sensors by registering linear accelerations, e.g., gravity, and lateral tilts of the head. Otoliths transmit their information to the brain to determine the spatial vertical, essential for controlling our posture and eye movements. An important otolith-mediated ocular reflex is the ocular counter-roll (OCR) that is generated when the head is laterally tilted, e.g., during centrifugation. The OCR tends to rotate the eyes in the opposite direction to the roll tilt and towards the GIA (Moore, et al. 2001). As a result, you will still be able to maintain postural stability and gaze stabilization when making sharp turns during locomotion.

Effect of prolonged spaceflight

Cosmonauts who are in the International Space Station (ISS), orbiting around Earth, are subjected to microgravity (< 10⁻⁶g). The lack of gravitational input will cause a deconditioning of the otoliths by decreasing the gain (ratio of eye torsion over head tilt) of otolith-mediated reflexes (Hallgren, et al. 2016). Also, the assessment of the real vertical will be impaired with a loss of otolith input to the brain (Kornilova, et al. 2007). Deconditioning of otolith-mediated reflexes following microgravity exposure has been proposed as one of the multiple causing factors of the locomotor, postural, and gaze control problems experienced by returning astronauts. These symptoms are generally maintained until the otoliths are re-adapted to Earth's gravitational level (Hallgren, et al. 2016).

The aim of this study was to examine the effect of prolonged spaceflight on the OCR in 44 cosmonaut experiments, extending the results from our prior study (Hallgren, et al. 2016). Considering the increasing number, longer duration, and more distant destinations of future planned space missions, it is necessary to know to what extent the otoliths are affected.

Material and methods

Timeline and subjects

The Visual and Vestibular Investigation System (VVIS), located in the Gagarin Cosmonaut Training Centre in Star City near Moscow (Russia), was used to induce the OCR. We investigated 27 cosmonauts, who participated in 44 experiments, 31 conducted for experienced flyers (N=16 second, N=8 third, N=4 fourth, and N=3 fifth-time flyers), the other 13 experiments were conducted for first-time flyers (N=13 first-time). The cosmonauts were tested before and

after their 6-month space mission in the ISS. Pre-flight experiments consisted of 2 baseline recordings (*baseline data collection* (BDC)), the post-flight experiments consisted of 2 to 3 recordings. The first post-flight measurement was taken 1 to 3 days after their return to Earth (R+1/3), the second 4 to 7 days (R+4/7) and the third 8 to 12 days after their return (R+8/12). The experiment protocol was designed in accordance with the 1964 Declaration of Helsinki and was accepted by the Human Research Multilateral Review Board (HRMRB) and European Space Agency (ESA). Cosmonauts gave their voluntary written informed consent prior to their participation.

Visual and Vestibular Investigation System (VVIS)

The cosmonauts were securely fastened, with a restriction of head movements, and seated upright on the 0.5m off-axis rotation chair. The room was darkened to avoid fixation or visual motion feedback during centrifugation. A visual display, in front of the cosmonaut's face, was used to project visual targets during parts of the experiment. Binocular 3D video-oculography with infrared video goggles was used to enable continuous recordings of dynamic changes in ocular torsion.

At standstill, the calibration of the video goggles and a baseline recording were performed. After a 30°/s² acceleration phase, the cosmonaut was subjected to constant angular velocity of 254°/s resulting in an outward centripetal A_c and upward gravitational acceleration A_g of respectively 1g, for 5 minutes in a counterclockwise (CCW) direction, and subsequently 5 minutes in a clockwise (CW) direction. The cosmonaut faced the direction of motion, right ear out during CCW and left ear out during CW rotation. The vector sum of A_g and A_c , GIA, was perceived as the 'spatial vertical' and exerted a shear force on the otolith system, causing a virtual 45° perceived roll-tilt during rotation, inducing an OCR towards the GIA (away from the tilt).

OCR measurement

The OCR measurements were taken before, during, and after centrifugation. The first and fourth measurements were taken during standstill, where an OCR of 0° was observed as expected. The second OCR measurement was taken 40 seconds after the steady-state phase, the third OCR measurement 40 seconds before the deceleration phase. During centrifugation, an OCR of on average 5°-7° (Collewyn, et al. 1985) was to be expected because of GIA stimulating the otoliths. Each OCR measurement was recorded for 20 seconds, while the cosmonaut observed a fixation dot on the visual display. The OCR was calculated as the difference of the average eye torsion over these 20 second recordings, consisting of 600-1000 frames, between rotation and standstill. The obtained OCR video files were analyzed in a visual programming language (custom made by H.M. in

LabVIEW - National Instruments -11500 N Mopac Expwy. Austin, TX, USA) to measure the OCR in degrees.

Statistical analysis

The OCR measurements were statistically analyzed in JMP® (version Pro 16. SAS Institute Inc, Cary, NC, 1989-2001), with $p < 0.05$ as significance threshold, using linear mixed models. We first tested our main variables as fixed effects and then systematically tested all interaction terms. The variables included were *Timepoint* (BDC1, BDC2, R+1/3, R+4/7, and R+8/12), *Days After Return* (1 to 12 days), and *Flight* (first-time vs experienced flyers). The significance threshold used for selecting the fixed effect was set at $p = 0.001$. Non-significant terms were removed until all combinations were tested and only the significant ones remained. In all models, *Cosmonaut* was entered as random intercept, and *Cosmonaut*Flight* and *Cosmonaut*Flight*Timepoint* as random slope terms according to their Likelihood ratio tests ($p < 0.0001$). The residuals of all models were checked for normality and homoskedasticity.

Results

We evaluated the OCR measured across different time points and different experience levels of the cosmonauts. We showed an effect of time and previous spaceflight experience on the OCR ($p < 0.001$) (Figure 1). There was also a significant interaction effect of time and previous flight ($p < 0.001$). A post-hoc Dunnett's correction showed that BDC2 did not differ from BDC1, whereas the OCR significantly decreased early postflight (R+1/3 and R+4/7). At R+8/12, OCR was back to preflight level.

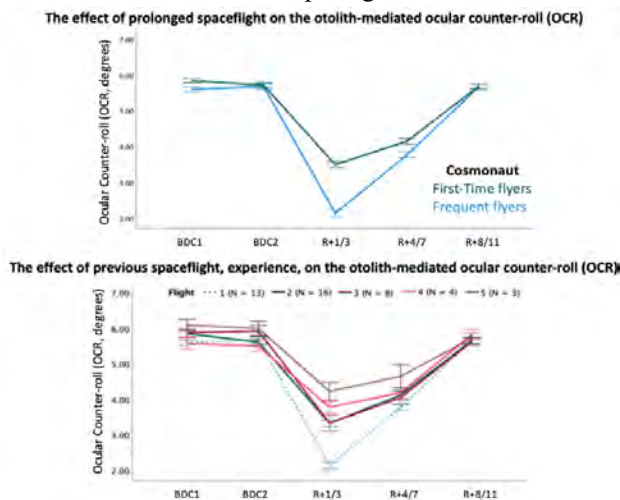


Figure 1 The effect of experience on the otolith-mediated ocular counter-roll (OCR), error bar: ± 1 SE

Conclusion

The main findings of this study were that (i) the OCR is decreased early post-flight compared to pre-flight, (ii) the OCR returns to baseline levels as measured on average 9 days after the space mission, and (iii) the OCR change over time is dependent on previous experience in space.

The decrease in OCR measured at R+1/3 reflects a deconditioning of the reflex because of a prolonged reduction in gravitational input in the ISS. It has long been established that the vestibular system is affected during space travel and that this causes various symptoms and functional changes during the first weeks in space, as well as the first weeks back on Earth. Specifically, postural control, locomotion, and gaze

stabilization are affected during this time frame, which can be attributed to the vestibular system still being adapted to the condition of microgravity (Arrott, et al. 1986, Dai, et al. 1994, Kenyon, et al. 1986, Seidler, et al. 2015). The decrease in OCR therefore strongly points to such an adaptation. Further establishing the association between OCR changes and functional changes will be essential for future missions to the Moon and Mars, where multiple gravitational level transitions will be made, forcing the vestibular system to adapt multiple times (Yates, et al. 2000, Collewijn, et al. 1985).

Concerning the re-adaptation of the OCR when back on Earth, we found that the measurements taken on average 9 days post-flight did not significantly differ from pre-flight values. While this time frame has a reasonable correspondence with the time window in which cosmonauts present with gait, posture, and locomotion issues, we were not able to prospectively investigate such an association.

Lastly, we found that cosmonauts who flew in space before showed a smaller post-flight decrease in OCR compared to first-time flyers. This is a novel finding, as often sample sizes are not large enough in both groups. These data indicate that the otoliths of first-time flyers are more affected than in experienced flyers. We hypothesize that previous time spent in microgravity triggers learning behavior at the level of the neural reflex circuits, providing a resistance against OCR deconditioning.

Acknowledgements

We would like to thank all participating cosmonauts and crewmembers. This study was funded by Belgian Science Policy (Prodex), ESA-AO-2004-093. CS is a Research Fellow of the Research Foundation Flanders (FWO Vlaanderen, Belgium).

References

- D. E., Angelaki, et al. Vestibular system: the many facets of a multimodal sense. *Annu Rev Neurosci*, 31, 125-50, 2008
- S. T., Moore, et al. Ocular counterrolling induced by centrifugation during orbital spaceflight. *Exp Brain Res*, 137, 323-35, 2001
- E., Hallgren, et al. Decreased otolith-mediated vestibular response in 25 astronauts induced by long-duration spaceflight. *J Neurophysiol*, 115, 3045-51, 2016
- A.P., Arrott, et al. M.I.T./Canadian vestibular experiments on the Spacelab-1 mission: 6. Vestibular reactions to lateral acceleration following ten days of weightlessness. *Exp Brain Res*, 64, 347-57, 1986
- L. N., Kornilova, et al. Static and dynamic vestibulo-cervico-ocular responses after prolonged exposure to microgravity. *J Vestib Res*, 17, 217-26, 2007
- M., Dai, et al. Effects of spaceflight on ocular counterrolling and the spatial orientation of the vestibular system. *Exp Brain Res*, 102, 45-56, 1994
- R. V., Kenyon, et al. M.I.T./Canadian vestibular experiments on the Spacelab-1 mission: 5. Postural responses following exposure to weightlessness. *Exp Brain Res*, 64, 335-46, 1986
- B. J., Yates, et al. Responses of vestibular nucleus neurons to tilt following chronic bilateral removal of vestibular inputs. *Exp Brain Res*, 130, 151-8, 2000
- R. D., Seidler, et al. Individual predictors of sensorimotor adaptability. *Front Syst Neurosci*, 9, 100, 2015
- H., Collewijn, et al. Human ocular counterroll: assessment of static and dynamic properties from electromagnetic scleral coil recordings. *Exp Brain Res*, 59, 185-96, 1985

Capillary rise in Divergent U-Tube during parabolic flight

D. Fiorini^{1,2}, L. Carbonnelle², A. Simonini², J. Steelant^{3,4}, D. Seveno¹, M. A. Mendez²

¹KU Leuven, Department of Materials Engineering, Leuven, Belgium, domenico.fiorini@vki.ac.be,

²von Karman Institute for Fluid Dynamics, Bruxelles, Belgium,

³KU Leuven, Department of Mechanical Engineering, Leuven, Belgium,

⁴ESTEC-ESA, Noordwijk, The Netherlands, Belgium,

Introduction

In capillary-dominated conditions, the motion of liquids along walls is controlled by the pressure jump due to the interface curvature at the contact line. This curvature depends on the forces acting at the interface and the *contact angle* formed with the solid surfaces.

The ability to predict the evolution of a liquid interface near walls is essential in developing propellant management devices (PMD) for space applications (D. E. Jaekle, 1997; Hartwig, 2017; Levine et al., 2015; White & Troian, 2018). Moreover, capillary forces play a major role in the dynamics of cryogenic propellants in partially filled tanks (Kulev et al., 2014; Kulev & Dreyer, 2010; Schmitt & Dreyer, 2015).

The development of engineering models for these applications requires experimental data on the capillary behaviour of cryogenic propellants, characterized by low surface tension, near-zero contact angles, and large interface accelerations. In the CASE (Contact Angle Sloshing Experiment) project, we analyze the behaviour of low surface tension fluids in a microgravity environment. The experiments were carried out at the 78th ESA parabolic flight. The investigated test case consists of a modified capillary rise experiment where we analyze the behaviour of different fluids at largely different Weber numbers.

Experiment

We designed a novel capillary rise experiment using a u-shaped transparent tube with a diverging diameter (DUT) as illustrated in Figure 1. The DUT is partially filled with liquid, producing a gas-liquid interface on the two sides, and sealed to avoid contamination with the environment. In microgravity conditions, surface tension becomes the leading force and sets the liquid into motion. The interface on both sides of the tube becomes spherical, with curvature inversely proportional to the tube's radius. As a result, the capillary pressure at the interface triggers the capillary rise on the side with the smallest tube.

In this work we consider two fluids, namely dipropylene glycol (DPG) and HFE7200. The DPG is a mineral oil extensively used in the literature of the capillary rise problem, while the HFE7200 is a synthetic liquid in close similarity to cryogenic propellants in terms of wetting characteristics. The experimental rack allows for testing both fluids simultaneously (see Figure 1 on the right). Four high-resolution cameras were used to visualize each side of the DUTs. The acquired images were processed to track the interface position and shape in time. We fit the interface shape $h(r, t)$ with theoretical interface model, and we compare the rise of the average meniscus height $\bar{h}(t)$ with a 1D model for the capillary rise.

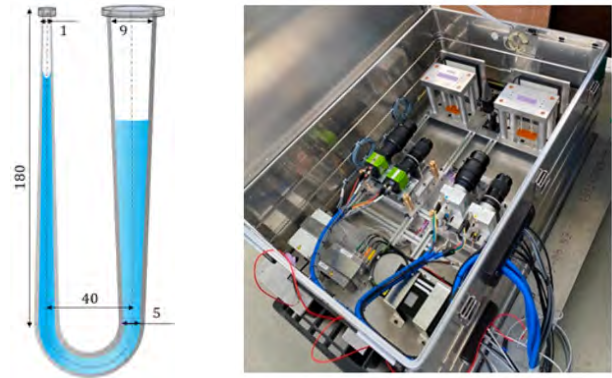


Figure 1: On the left, DUT artist design concept, all dimensions are in millimeters. On the right experimental rack, four cameras are visible. Each couple of cameras observes one DUT.

Theory

The motion of the spatially averaged liquid interface $\bar{h}(t)$ in the DUT is modelled with a 1D model inspired by the Lucas-Washburn-Rideal (LWR) equation (Wu et al., 2017). We adapt the LWR equation to account for the diverging shape of the channel and for the interface pressure drop. The model reads:

$$mA = -F_g(H) - F_\mu(V, H) - F_\sigma(V, H) \quad \text{Equation 1}$$

Where H , V , A represent respectively the position, velocity, and acceleration of the center of mass of the liquid column, m is the mass of the liquid, F_g is the gravitational force, F_μ is the viscous force and F_σ is the capillary force. In microgravity conditions, F_σ is approximated as:

$$\frac{F_\sigma(V, H)}{m} \approx \sigma \left(\frac{\cos \theta_A(V_A)}{R(H_A)} - \frac{\cos \theta_B(V_B)}{R(H_B)} \right) \quad \text{Equation 2}$$

Where H_x , V_x and $\theta_x(V_x)$, with $x = A, B$, represent the position, velocity, and contact angle of the interface on each side of the tube. $R(H_x)$ is the DUT radius at each interface, considering that this assume a spherical shape. The dynamic contact angle is modelled by means of Tanner law (Tanner, 1979). A more accurate description considering non-spherical interface is given by quasi-static gravity-based interface model (Fiorini et al., 2022).

Preliminary results and discussion

In this work, we compare the capillary rise of DPG and HFE7200. Figure 2 illustrates the average interface evolution for an experiment with DPG, together with the prediction of the 1D model using two different interface models and the measured acceleration. This figure shows that the model predicts a faster capillary rise if a spherical interface is assumed, while better agreement with the experimental data

of slope at $t \approx 24$ s occurs together with the transition of the interface from a wet to dry surface as visible from the experiment (see snapshots in Figure 2) but neglected by the 1-D model. The Weber number remains below 0.001 for all the duration of the experiment.

Figure 3 shows the same data for an experiment with HFE7200. The Weber number of the interface rises to 0.4 at $t \approx 20$ s and the interface rises outside the field of view of the camera. The experiments with HFE7200 show higher sensitivity to the gravity level compared to those with the DPG and display interface oscillation before a sudden rise. The result of the 1D model show good agreement until $t \approx 13$ s but over-predicts the interface velocity and the meniscus height between $t \approx 14 - 17$ s, that is during the last phase of the microgravity phase. After $t \approx 17$ s, the model seemingly recovers the experimental rising velocity.

Conclusions

In this work, we designed and performed a novel capillary rise experiment in a parabolic flight. We extend the Washburn 1D model for the capillary rise to describe the interface motion in the DUT. In the case of DPG, a simplified quasi-static interface model proved capable of predicting the interface dynamics while more sophisticated modeling of the liquid interface is required in the case of HFE7200. In the extended version of this work, we compare the evolution of the interface shape during the experiment with the theoretical shape yielded by the 1-D model for the capillary rise. We assess the validity of contact angle models against the measured dynamic contact angles and discuss its role on the capillary rise as well as the role of liquid films deposited along the walls.

Acknowledgements

D. Fiorini is supported by Fonds Wetenschappelijk Onderzoek (FWO), Project number 1S96120N. This work was supported by the ESA and BELSPO via the Prodex program and by the ESA-GSTP “Physical and Numerical Modeling of cryogenic sloshing for Space applications” (Contract No. 4000129315/19/NL/MG). The authors thank the Navespace for organizing the flights, Michelle Bavier and Pedro Marques for the help provided during the experimental campaign and Jean Baptiste Gourier for the advice in the experiment design.

References

D. E. Jaekle, J. (1997). AIAA-97-2811 Propellant Management Device Conceptual Design and Analysis: Galleries D. E. Jaekle, Jr. PMD Technology Andover, MA 33rd AIAA / ASME / SAE / ASEE Joint Propulsion Conference & Exhibit. Joint Propulsion Conference & Exhibit.

Fiorini, D., Alfonso, M., Simonini, A., Steelant, J., & David, S. (2022). Effect of inertia on the dynamic contact angle in oscillating menisci. Submitted to Journal of Colloid and Interface Science, 1–15.

Hartwig, J. W. (2017). Propellant management devices for low-gravity fluid management: Past, present, and future 824.

Kulev, N., Basting, S., Bänsch, E., & Dreyer, M. (2014). Interface reorientation of cryogenic liquids under non-isothermal boundary conditions. *Cryogenics*, 62, 48–59.

Kulev, N., & Dreyer, M. (2010). Drop tower experiments on non-isothermal reorientation of cryogenic liquids. *Microgravity Science and Technology*, 22(4), 463–474.

Levine, D., Wise, B., Schulman, R., Gutierrez, H., Kirk, D., Turlesque, N., Tam, W., Bhatia, M., & Jaekle, D. (2015). Surface tension and contact angle analysis with design of propellant measurement apparatus. *Journal of Propulsion and Power*, 31(1), 429–443.

Schmitt, S., & Dreyer, M. E. (2015). Free surface oscillations of liquid hydrogen in microgravity conditions. *Cryogenics*, 72(P1), 22–35.

Tanner, L. H. (1979). The spreading of silicone oil drops on horizontal surfaces. *Journal of Physics D: Applied Physics*, 12(9), 1473.

White, N. C., & Troian, S. M. (2018). Why Capillary Flows in Slender Triangular Grooves Are So Stable Against Disturbances. *ArXiv*, 1–18.

Wu, P., Nikolov, A. D., & Wasan, D. T. (2017). Capillary Rise: Validity of the Dynamic Contact Angle Models. *Langmuir*, 33(32), 7862–7872.

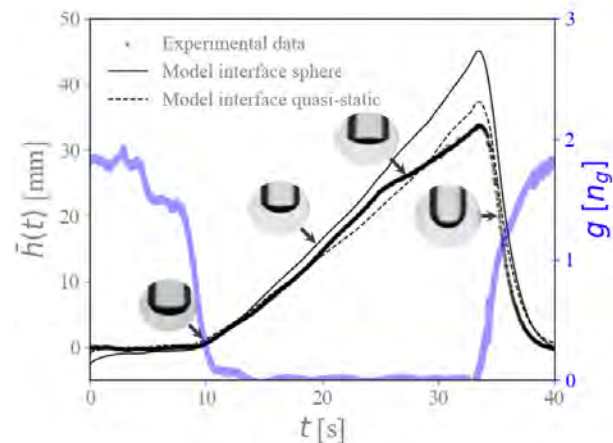


Figure 2: Capillary rise of DPG against time. The circular markers represent the experimental data and the solid line the 1D model simulation. On the right axis the gravity level is shown (blue curve).

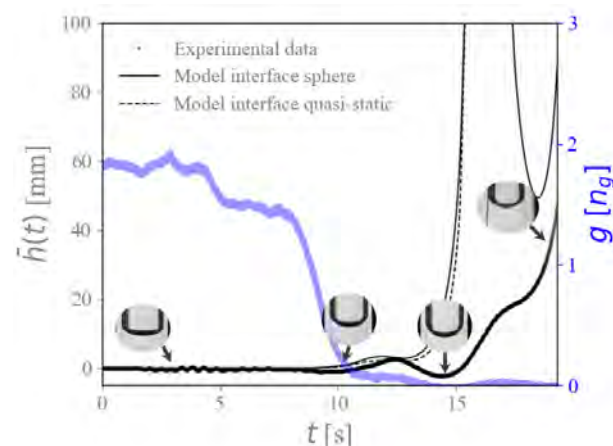


Figure 3: Same as Figure 2 but for HFE7200. The interface rise after $t \approx 20$ s is missing due to limited size of the field of view.

ORAL 29

Pool boiling heat transfer in microgravity with microstructured surfaces and electric field: preliminary results of parabolic flight campaign

A. I. Garivalis¹, B. Liu², L. Bernardini¹, B. Marangolo¹, J. Wei², P. Di Marco¹

¹DESTEC, University of Pisa, Largo Lucio Lazzarino 1, Pisa, 56122, Italy, alekos.garivalis@ing.unipi.it

²School of Chemical Engineering and Technology, Xi'an Jiantong University, No.28, Xianning West Road, Xi'an, Shaanxi, 710049, PR China

Introduction

Pool boiling heat transfer is one of the most effective ways to remove heat available nowadays – excluding forced convection. Buoyancy force, driven by gravity, is recognized as one of the external actions that contribute most to the bubble detachment and vapor removal from the wall region. Thus, in microgravity conditions, the boiling process changes. As described by Straub (2001), primary mechanisms of boiling occurs at the microscale level close to the heated surface and are weakly dependent on gravity, while secondary mechanisms include the bubble removal and are driven by gravity. Recently, efforts were done with engineered surfaces, and the use of micropillars showed enhancement in heat transfer coefficients and Critical Heat Flux – Chu et al. (2012). Even if the role of the engineered surfaces on the enhancement is still debated, it is expected to be independent on gravity, as relies on capillary forces. One aim of this study is to verify this experimentally; the second aim is to use an electric field to introduce an external action capable to remove vapor from the boiling region, in behalf of gravity force. The experiments conducted during parabolic flights will clarify the role of the structures and electric field in boiling enhancement with potential applications for space devices.

Experimental apparatus

The experimental apparatus allows to perform pool boiling experiments during parabolic flights. It consists of a test cell with a volume of 2.3 litres, filled with FC-72 (saturation temperature at 1 bar is 56.6 °C). The pressure and temperature of the liquid can be adjusted by means of dedicated subsystems. More details on the complete systems have been given by Liu et al. (2022). The test section consists of a 1 cm x 1 cm silicon chip which is electrically heated and the boiling process occurs on its top (see Figure 1). Microstructures are etched on the surface exposed to the fluid. They consist of square pillars with the dimensions tested by Liu et al. (2022). They are named PF5060, PF3060, PF50120; the smooth surface is tested as well (SS). The test section is sealed into a support made of insulating material (insulating glue and polycarbonate). The heat provided by the DC power supply (ELC ALR3206D) through the two copper wires soldered at the chip sides is transferred almost entirely to the liquid: heat losses less than 5% have been estimated. The heat flux is calculated by measuring the voltage and current through the heater and dividing by its surface; a T-type thermocouple is glued below the heater in the middle and provides the temperature of the silicon - as the Biot number is small, a small difference of temperature occurs in the silicon. To generate the electric field in the boiling region, a stainless

steel grid is placed at 6 mm from the surface; a steel plate covers the surface to ensure grounding. A DC voltage of 15 kV was applied between the grid and the ground.

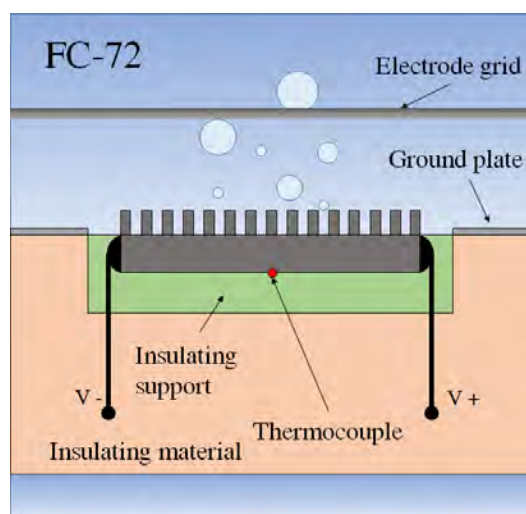


Figure 1: Experimental apparatus.

Results and discussion

A part of the boiling curves obtained during the parabolic flight is shown in Figure 2. Tests on the smooth surface (SS) were performed as comparison; the boiling curves with and without the electric field were obtained.

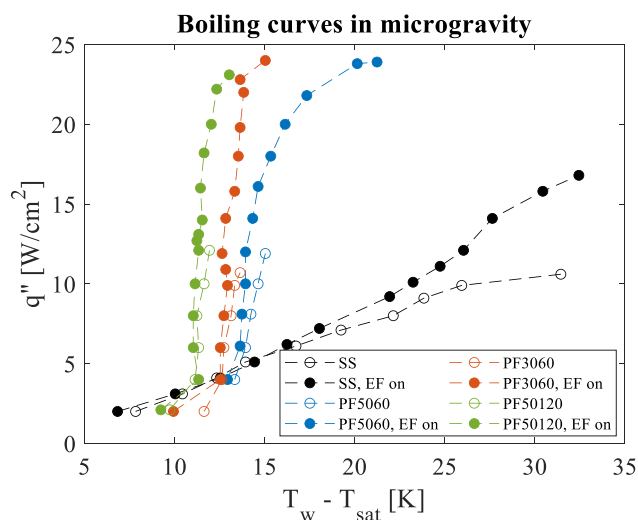


Figure 2: Comparison of the boiling curves obtained in microgravity for various surfaces with and without electric field (pressure 2 bar, subcooling 5 K).

The presence of the microstructures produces an earlier onset of boiling with respect to the smooth surface case;

moreover, the superheat is lower and the heat transfer coefficients higher. Concerning the Critical Heat Flux, the surfaces considered in this study showed little enhancement in microgravity. A previous study performed by Garivalis et al. (2021) on another parabolic flight with similar microstructures – but with smaller pillars – showed a better enhancement due to microstructures only. However, the presence of an electric field allows to increase considerably the Critical Heat Flux. Values are close to Earth’s ones, as visible in Figure 3, where the curves of a microstructured surface are compared with the boiling curves obtained on ground. The boiling curves of Figure 3, with the exception of the Critical Heat Flux, are overlapped, showing that the heat transfer coefficient is weakly affected by gravity and electric field.

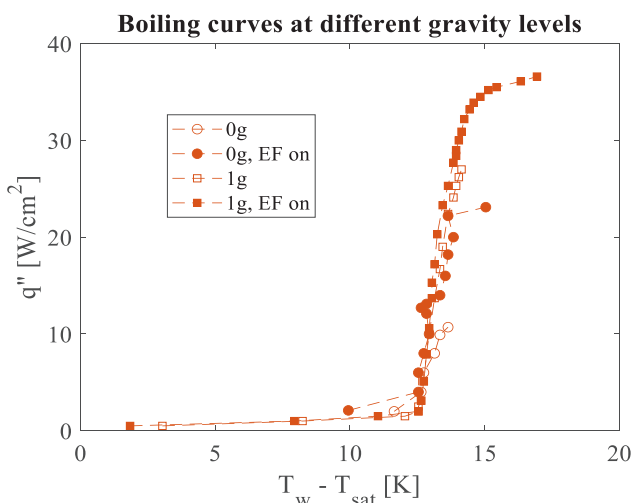


Figure 3: Comparison of the boiling curves of PF3060 at ground and in microgravity with and without electric field (pressure 1 bar, subcooling 5 K).

In microgravity phase, bubbles pattern changes dramatically: a big vapor bubble covers all the heater – see Figure 4a – and periodically detached due to inertia forces or the vibrations of the aircraft that are never completely canceled. At the Critical Heat Flux, the vapor bubble remains attached and the temperature rises abruptly. On the other hand, in the presence of the electric field, bubbles are removed by the electric forces all the time. When the Critical Heat Flux is reached, the transition to film boiling regime is evident – example in Figure 4b. The Taylor-Helmoltz instability pattern is observed.

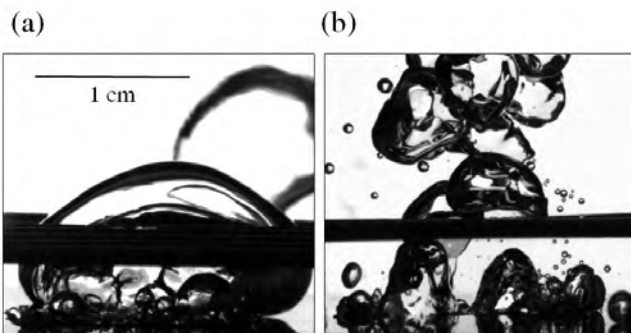


Figure 4: Examples of the bubbles patterns at the Critical Heat Fluxes in the absence of electric field (a) and in the presence of the electric field (b).

Conclusions

During ESA Parabolic Flight Campaigns 73 and 78, the effects of a range of microstructured surfaces, a DC electric field and the combination of the two on the boiling curve were studied. In this preliminary analysis, only a part of the data has been considered, as the complete results will be presented in the near future. The main outcome of the experimental campaign is the following:

- The heat transfer coefficient (for a given heat flux) is weakly affected by the gravity level or electric field for all the studied conditions (smooth and microstructured surfaces).
- The Critical Heat Flux is enhanced significantly by the microstructures on ground; however, it has been observed that the enhancement in microgravity conditions is lower.
- The electric field in microgravity it contributes to the vapor removal and restores the Critical Heat Flux Values obtained at Earth’s gravity.
- Microstructured surfaces in microgravity showed better performances in the presence of the electric field. In microgravity, the combination of the vapor removal capability of the electric force and the mechanisms promoted by the capillary forces allows to obtain boiling performances comparable to the ones on ground environments.
- It has been observed that the Critical Heat flux dynamics in microgravity is significantly different in the presence or absence of the electric field. While a large coalesced bubble covering all the heated surface is the typical condition in lack of buoyancy, the addition of an electric field impairs the bubble coalescence, improving liquid renewal towards the surface.

Acknowledgements

This work is supported by the Joint ESA-CMSA Project (TGMTYY00-RW-05-1.00), ESA (European Space Agency) under the MAP-MANBO project (AO-2004-111), Second batch of scientific experiment proposals aboard China Space Station (TGMTYY00-JY-53-1.00), and the National Natural Science Foundation of China (No.51636006).

References

- K. H. Chu, R. Enright, E. N. Wang, Structured surfaces for enhanced pool boiling heat transfer. *Applied Physics Letters*, 100(24), 241603, (2012)
- A. I. Garivalis, G. Manfredini, G. Saccone, P. Di Marco, A. Kossolapov, M. Bucci, Critical heat flux enhancement in microgravity conditions coupling microstructured surfaces and electrostatic field. *npj Microgravity*, 7(1), 1-7, (2021)
- B. Liu, A. I. Garivalis, Z. Cao, Y. Zhang, J. Wei, P. Di Marco, Effects of electric field on pool boiling heat transfer over microstructured surfaces under different liquid subcoolings. *International Journal of Heat and Mass Transfer*, 183, 122154, (2022)
- J. Straub, Boiling heat transfer and bubble dynamics in microgravity. *Advances in Heat Transfer*, 35, 57-172, (2001)

ORAL 30

yuri enables and develops novel biomedical applications using microgravity on the ISS and beyond

D.Bezdan¹, J.Pietch¹, M.Birlem¹, C.Bruderrek¹, M.Kugel¹

¹yuri GmbH, Meckenbeuren, Germany, Daniela.Bezdan@yurigravity.com

Introduction

yuri is a German space company with offices and laboratories in Luxembourg and the US. We develop new technological solutions at the intersection of aerospace engineering and life sciences with the mission to advance biomedical and biotechnological applications in the unique environment of space. With our experience of launching experiments into space (11 successful ISS payloads to date), we are transforming into one of the first space-biomedicine companies that broadly supports fully automated biomedical experiments and biotechnological manufacturing on the ISS and low Earth orbit systems. Our reusable, flight- proven hardware enables customers to reduce the cost and time needed to perform biomedical experiments in microgravity on suborbital flights, on the ISS, and in microgravity simulators such as the 2D clinostat and the Random Positioning Machine (RPM) on earth.

We have previously collaborated with various institutions on performing experiments on the ISS concerning the effect of microgravity on 1) the immune response, 2) gene expression in humans and mice, 3) thyroid cancer cells spheroid growth, 4) behavior of oligodendrocyte cells (precursors of central nervous system cells), 5) stability of therapeutic monoclonal antibodies to improve shelf-life, 6) metabolic activity of methane-producing bacteria and archaea, 7) neurobehavioral changes in *Drosophila melanogaster*, and 8) plant growth in space.

We are excited that yuri's next biomedical experiment will launch in August 2022 to the ISS. We will monitor the growth of spheroids in microgravity and test a highly anticipated solution for a safe return of bio-products such as spheroids and organoids to earth.

Conclusions

Here we present innovative solutions for biomedical experiments in microgravity, suitable for yuri's novel technological platforms RPM, ScienceShell, and ScienceTaxi. As astronaut time on the ISS is precious and costly, our hardware portfolio facilitates boxing, full automation, and monitoring of biomedical experiments in modular and reusable ScienceShells, which are customizable for utilization of cell cultures and iPSC, fluidic chips, lab-on-a-chip, or organoid-on-a-chip methods in applications such as drug development and testing, bioengineering, and crystal growth. ScienceShells are extendable with various analytical tools such as a microscope, fluorescence imaging, backscattering and various sensors (e.g., O₂/pH), and a camera, among other customizable tools. Our simple clip-in- place design allows compatible facilities (Biopack, Simplex, Kubik, ScienceTaxi (former Biobox, SIMBOX), NanoRacks Frame-3, STaARS-1 EF) to interface with experiments mechanically and electrically. ScienceTaxi enables access to microgravity experiments in low Earth orbit for researchers and companies independent of the International Space Station. It is a mid-deck-locker size incubator that fits any platform (e.g., Dream Chaser, Dragon) and hosts 36 yuri ScienceShells. It facilitates full automation, precise experiment control, and real-time data

ORAL 32

The Effect of Marangoni Convection on Heat Transfer in Phase Change Materials Experiment

J. Porter¹, A. Laverón-Simavilla¹, M.M. Bou-Ali², X. Ruiz³, F. Gavaldá³, D. Dubert³, J.M. Ezquerro¹, J. Fernández¹, L. García-Fernández⁴, D. Gligor¹, J. Gomez¹, V. Lapuerta¹, U. Martinez¹, J. Massons³, J. Rodriguez¹, P. Salgado Sánchez¹, A. Sanjuan², B. Seta⁵, V. Shevtsova^{2,6}, I. Tino¹

¹E-USOC, Center for Computational Simulation, Universidad Politécnica de Madrid, Madrid, Spain, jeff.porter@upm.es

²Mechanical and Manufacturing Department, Mondragon University, Mondragon, Spain, mbouali@mondragon.edu

³Facultat de Química, Universitat Rovira i Virgili, Tarragona, Spain, josepxavier.ruiz@urv.cat

⁴Dpto. EMFTEL, Facultad de Ciencias Físicas, Universidad Complutense Madrid, Madrid, Spain, loreto.garcia@ucm.es

⁵Department of Mechanical Engineering, Technical University of Denmark, Kongens Lyngby, Denmark, berin.seta@gmail.com

⁶IKERBASQUE, Basque Foundation for Science, Bilbao, Spain, x.vshevtsova@mondragon.edu

Introduction

There is a critical need for energy storage systems like those based on Phase Change Materials (PCMs) that can control temperatures, reduce waste and improve efficiency, including in space technology where PCM devices have a history of applications going back to the Apollo 15 Lunar Rover Vehicle, Skylab SL-1, and the Venera 8-10 missions. Organic PCMs, typified by alkanes and fatty acids, are an appealing choice of material because they are non-reactive and stable, with regular melting/freezing cycles. However, they can be hampered in many applications by their low thermal conductivity, which reduces responsiveness and requires long charge and discharge cycles. Various strategies for improving the performance of organic PCMs by augmenting heat transport have been proposed. Active systems may incorporate coolant loops and pumps as in the NASA Phase Change Material Heat Exchanger Project. Higher heat transfer rates can be achieved in passive systems simply by placing the PCM in contact with more conductive materials or by increasing the effective thermal diffusivity of the PCM through the addition of dispersed nanoparticles.

We describe the *Effect of Marangoni Convection on Heat Transfer in Phase Change Materials* (MarPCM) experiment, which is to be implemented on the International Space Station (ISS) and is the result of a collaboration between the Universidad Politécnica de Madrid, Mondragon Unibertsitatea and Universitat Rovira I Virgili.

Objectives

The main objective of this project is to prepare and execute a series of microgravity experiments on board the ISS that will evaluate the effectiveness of thermocapillary convection and complementary strategies, like nanoparticles, for improving PCM devices. Experiments on ground, simulations and theoretical work are also crucial to predicting, understanding, and interpreting the microgravity experiment results. Extensive parameter studies using two-dimensional and three-dimensional models will be conducted.

The specific objectives of the MarPCM project are:

- Quantify the effect of thermal Marangoni convection on the heat transfer rate.
- Determine the dependence on temperature gradient (applied temperature difference) of the contribution from thermal Marangoni convection.
- Compare the effectiveness of thermal Marangoni convection in cuboidal geometry (with one rectangular

free surface) and in cylindrical geometry (a liquid bridge configuration when melted).

- Compare the heat transport efficiency of a pure PCM (n-octadecane) with a Nano-Enhanced PCM material.
- Investigate the effect of different dynamical regimes on heat transfer and PCM performance, particularly the transition from steady to oscillatory convection.
- Investigate the effect of mechanical vibrations with and without thermal Marangoni convection.
- Evaluate the robustness of the proposed design and any practical difficulties associated with maintaining a free surface, and PCM performance in general, over a series of melting/freezing cycles.

Experiment Concept

The basic set-up of the experiment relies on the application of fixed temperatures to opposite ends of a PCM sample in order to establish a controlled melting/solidification process. The resulting phase change will be observed by means of optical cameras. The set-up is illustrated in Figure 1.

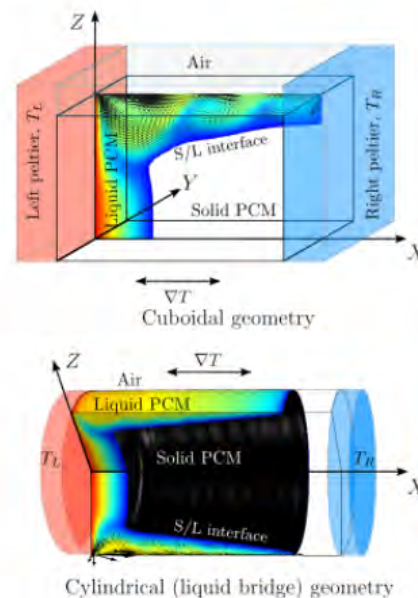


Figure 1: Illustration of MarPCM experiment concept

Both cuboidal and cylindrical geometries will be considered. With the exception of a closed reference cell, in which melting is driven purely by conduction, the containers are designed to passively maintain a PCM/gas interface. A quantitative comparison of the performance of different PCM cells will be made by comparing the evolution of the

solid/liquid interface (equivalently, the liquid volume) over time. The recorded images will be complemented by thermal measurements at key positions along the cell, which will help distinguish different dynamical regimes according to the measured time dependence, and provide a secondary (independent) diagnostic measurement of the phase change

Preliminary results

A key preliminary result for this project was the successful proof-of-concept microgravity experiment, “Thermocapillary Effects in Phase Change Materials in Microgravity” (TEPiM) that was conducted during the 65th ESA Parabolic Flight Campaign where it was found that the presence of a single free surface approximately doubled the heat transferred during the short microgravity period (Ezquerro et al. 2019, 2020) with the PCM n-octadecane. This was the first microgravity experiment to investigate the performance of PCMs in the presence of thermocapillary convection and confirmed the positive effect of thermocapillary convection on heat transport predicted by numerical simulations (Madruga et al. 2017).

Other preliminary results include a comparison of the TEPiM experiment with simulations (Salgado Sánchez et al. 2020), an investigation of dynamical modes encountered during melting and their effect on heat transport (Salgado Sánchez et al. 2020, 2021, 2022), melting with combined gravitational and thermocapillary convection (Borshchak Kachalov et al. 2021), PCM melting in a liquid bridge configuration in microgravity (Varas et al. 2021; Seta et al. 2021, 2022), analysis of the effect of surface heat exchange (Martínez et al. 2021), and a study of the coupling between thermocapillary flows and sloshing (Gligor et al. 2022).

Conclusions

The MarPCM project will evaluate new and promising strategies for improving the performance of PCM devices in space applications. These strategies take advantage of the inherent temperature gradient that is present during normal PCM use to promote Marangoni convection and thereby increase heat transfer and reduce lag. They do not appreciably increase mass or volume or require additional energy sources. Temperature and energy management are pressing problems on Earth as well as in space, and PCM devices are expected to be an important part of the effort to improve efficiency and reduce waste heat across a range of applications from food storage, to air conditioning, to solar panels. The results of this project may lead to simpler and cheaper PCM-based solutions.

Acknowledgements

This work is supported by ESA and the Ministerio de Ciencia e Innovación through projects PID2020-115086GB-C31, PID2020-115086GB-C32, and PID2020-115086GB-C33.

References

J.M. Ezquerro, A. Bello, P. Salgado Sánchez, A. Laverón-Simavilla and V. Lapuerta, The Thermocapillary Effects in Phase Change Materials in microgravity: design, preparation and execution of a parabolic flight experiment, *Acta Astron.* **162**, 185–196, 2019.

J.M. Ezquerro, P. Salgado Sánchez, A. Bello, J. Rodríguez, V. Lapuerta and A. Laverón-Simavilla. Experimental evidence of thermocapillarity in Phase Change Materials in microgravity: Measuring the effect of Marangoni convection in solid/liquid phase transitions, *Int. Commun. Heat Mass Transf.* **113**, 104529, 2020.

S. Madruga and C. Mendoza, Enhancement of heat transfer rate on phase change materials with thermocapillary flows, *Eur. Phys. J. Spec. Top.* **226**, 1169–1176, 2017.

P. Salgado Sánchez, J.M. Ezquerro, J. Porter, J. Fernández and I. Tíno, Effect of thermocapillary convection on the melting of phase change materials in microgravity: Experiments and simulations, *Int. J. Heat Mass Transf.* **154**, 119717, 2020.

P. Salgado Sánchez, J.M. Ezquerro, J. Fernández and J. Rodríguez, Thermocapillary effects during the melting of phase-change materials in microgravity: heat transport enhancement, *Int. J. Heat Mass Transf.* **163**, 120478, 2020.

P. Salgado Sánchez, J.M. Ezquerro, J. Fernández, and J. Rodríguez, Thermocapillary effects during the melting of phase-change materials in microgravity: steady and oscillatory flow regimes, *J. Fluid Mech.* **908**, A20, 2021.

P. Salgado Sánchez, J. Porter, J.M. Ezquerro, I. Tíno and A. Laverón-Simavilla, Pattern selection for thermocapillary flow in rectangular containers in microgravity, *Phys. Rev. Fluids* **7**, 053502, 2022.

A. Borshchak Kachalov, P. Salgado Sánchez, J. Porter and J.M. Ezquerro, The combined effect of natural and thermocapillary convection on the melting of phase change materials in rectangular containers, *Int. J. Heat Mass Transf.* **168**, 120864, 2021.

R. Varas, P. Salgado Sánchez, J. Porter, J.M. Ezquerro and V. Lapuerta, Thermocapillary effects during the melting in microgravity of phase change materials with a liquid bridge geometry, *Int. J. Heat Mass Transf.* **178**, 121586, 2021.

B. Seta, D. Dubert, J. Massons, Jna. Gavalda, M.M. Bou-Ali and X. Ruiz, Effect of Marangoni induced instabilities on a melting bridge under microgravity conditions, *Int. J. Heat Mass Transf.* **179**, 121665, 2021.

B. Seta, D. Dubert, M. Prats, Jna. Gavalda, J. Massons, M.M. Bou-Ali, X. Ruiz and V. Shevtsova, Transitions between nonlinear regimes in melting and liquid bridges in microgravity, *Int. J. Heat Mass Transf.* **193**, 122984, 2022.

B. Seta, D. Dubert, J. Massons, P. Salgado Sánchez, J. Porter, Jna. Gavalda, M.M. Bou-Ali and X. Ruiz, On the Impact of Body Forces in Low Prandtl Number Liquid Bridges, *Lecture Notes in Networks and Systems* **142**. Springer, Cham., 217–227, 2021.

N. Martínez, P. Salgado Sánchez, J. Porter and J. M. Ezquerro, Effect of surface heat exchange on phase change materials melting with thermocapillary flow in microgravity, *Phys. Fluids* **33**, 083611, 2021.

D. Gligor, P. Salgado Sánchez, J. Porter and I. Tíno, Thermocapillary-driven dynamics of a free surface in microgravity: Response to steady and oscillatory thermal excitation, *Phys. Fluids* **34**, 042116, 2022.

ORAL 33

Interaction of Faraday waves on alternating multi-layer fluid systems in microgravity

J. Porter¹, I. Torres¹, P. Salgado Sánchez¹, E. Labrador¹, V. Shevtsova^{2,3}

¹E-USOC, Center for Computational Simulation, Universidad Politécnica de Madrid, Madrid, Spain, jeff.porter@upm.es

²Mechanical and Manufacturing Department, Mondragon University, Mondragon, Spain, x.vshevtsova@mondragon.edu

³IKERBASQUE, Basque Foundation for Science, Bilbao, Spain

Introduction

When gravity is not present as a restoring force, fluid behaviour can be dramatically different, sometimes involving large-scale movement of the center of mass in response to relatively small forces. The frozen wave instability, for example, results from the oscillatory shear stress that can be induced by vibrating a two-layer fluid system parallel to the interface. On Earth, this periodic acceleration generates quasi-stationary small-amplitude sinusoidal interfacial waves that, with increasing forcing, grow smoothly into nonlinear trochoid-like waves. Without gravity to limit the upward movement of the heavier (lower) fluid, however, this instability is (nearly) degenerate (Gligor et al. 2020) and rapidly leads to large columnar structures of alternating lighter and heavier fluids. These structures have been observed in a number of microgravity experiments (Gandikota et al. 2014, Gaponenko et al. 2015, Shevtsova et al. 2016, Salgado Sánchez et al. 2019, Lyubimova et al. 2019). Furthermore, since the final column interfaces are oriented perpendicular to the vibrational forcing, they support Faraday waves at sufficient forcing amplitude — these have also been observed in microgravity experiments (Shevtsova et al. 2016, Salgado Sánchez et al. 2019, Lyubimova et al. 2019).

Here, we consider the interaction of Faraday waves on such an alternating columnar structure, extending the work of Labrador et al. (2021) to more than two interfaces (three columns) without an assumption of periodicity or, indeed, any other imposed relationship between the wave amplitudes on each interface. This allows a description of more complex dynamical behaviour including multiple-Hopf (torus) bifurcations and Hopf-pitchfork interactions. The modulated solutions are confirmed using direct numerical simulations, as are some of the predicted secondary transitions like the saddle-node heteroclinic bifurcation that destroys the modulated states and replaces them by constant amplitude waves.

Amplitude equations

We consider a regular series of $n + 1$ vertical columns that alternately contain one of two fluids of distinct densities. Under the typical simplifying assumptions of irrotational flow, small amplitude and low viscosity, the behaviour of the interfaces can be described by series of coupled damped Mathieu equations. Each of the n interfaces is coupled to its nearest neighbor(s) via the flow within the separating column. A separation of timescales procedure, followed by convenient rescaling, reduces these Mathieu equations to a series of n complex amplitude equations that evolve on the slow time scale:

$$\begin{aligned}\dot{A}_1 &= -(\gamma + i\nu)A_1 + iF\bar{A}_1 + i\mu A_2 \\ \dot{A}_2 &= -(\gamma + i\nu)A_2 - iF\bar{A}_2 + i\mu A_1 + i\beta A_3 \\ \dot{A}_3 &= -(\gamma + i\nu)A_3 + iF\bar{A}_3 + i\beta A_2 + i\mu A_4 \\ \dot{A}_4 &= -(\gamma + i\nu)A_4 - iF\bar{A}_4 + i\mu A_3 + i\beta A_5 \\ &\vdots\end{aligned}$$

The terms on the right hand side of these equations capture linear damping, detuning, parametric forcing and nearest neighbor linear coupling, respectively, and the parameters that appear depend on the fluid properties (density, viscosity, interfacial tension), the forcing frequency and amplitude, the column width, and the perturbation wavenumber.

Results

The steady columnar state ($A_n = 0$ for all n) loses stability when $F^2 = \gamma^2 + \nu^2$ and the nature of this bifurcation depends on whether n is even or odd. If n is even, the instability is a multiple-Hopf (torus) bifurcation with $n/2$ distinct frequencies. If n is odd, the instability is a single-pitchfork/multiple-Hopf (torus) bifurcation with $(n - 1)/2$ distinct frequencies. The pitchfork bifurcation occurs in a subspace where interfaces are alternately quiescent and excited. The Faraday waves in that subspace are isolated from each other and do not interact, although they must be of different amplitude in order that their effect on the intervening quiescent interface cancels out. Such steady solutions are almost certainly unstable in the full nonlinear system and have not been found in numerical simulations. The observed stable solution is modulated and multi-frequency (for $n > 3$).

Numerical simulations

Figure 1 shows a comparison of the predicted threshold (thin blue curve) with the transitions observed by simulating the Navier-Stokes equations in COMSOL Multiphysics for a two-interface system. The predictions of Kumar and Tuckerman (1994) and that for infinitely high columns (i.e., ignoring detuning) are also included for reference. The theory underestimates the threshold, particularly for low frequencies. This is consistent with the comparison between theory and experiment of Salgado Sánchez et al. (2019) and is likely due to damping at the boundaries and finite-depth effects not captured by the form of the linear damping term in the amplitude equations.

The addition of nonlinear terms allows secondary bifurcations to be predicted as in Salgado Sánchez et al. (2016). Of particular importance are the saddle-node of periodic orbits for negative detuning (red dashed curves) and the saddle-node heteroclinic (black dashed curve) that

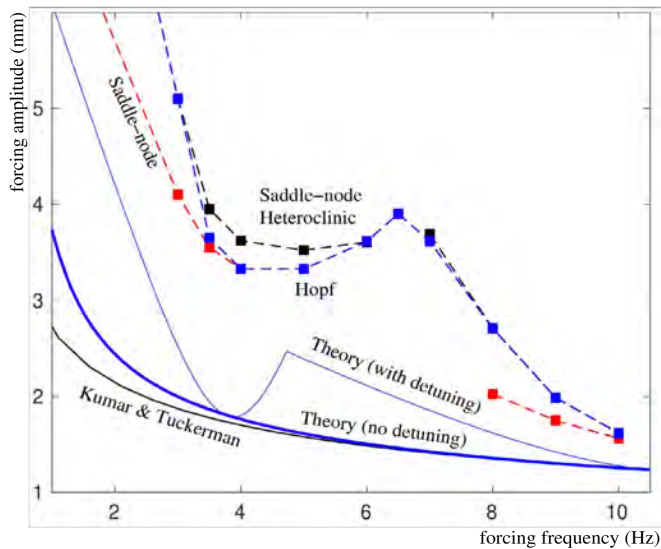


Figure 1: Comparison of theory with simulations of the Navier-Stokes equations using COMSOL Multiphysics.

destroys the modulated solution through collision with a steady state; this is signaled by the divergence of the modulation period, which is clearly observed in the simulations.

Simulations with larger numbers of columns are more time consuming and lead to more complex dynamics that have not yet been studied in detail. We have confirmed, however, the presence of a two-frequency (torus) solution in the case of four interfaces, consistent with the prediction of the linearized amplitude equations.

Conclusions

The fact that applied vibrations often lead to columnar structures in microgravity provides an interesting opportunity to study the interaction of Faraday waves, which can subsequently form on the interfaces between these columns. These wave fields interact (weakly, if the columns are thick) and are forced out-of-phase with their neighbors due to the alternating sign of the density difference. The primary instability is a multiple-Hopf (torus) bifurcation that interacts with a pitchfork bifurcation if n is odd. A modulated solution results from the interaction between interfaces and persists over an appreciable range of forcing values only if the interaction is not too small. A saddle-node heteroclinic bifurcation is the mechanism that replaces these modulated solutions by one with steady wave amplitudes (at least, in the two-interface system). This global bifurcation, along with the primary Hopf instability and a secondary saddle-node in the subcritical region, are confirmed via direct numerical simulations.

Acknowledgements

This work is supported by the Ministerio de Ciencia e Innovación under project PID2020-115086GB-C31 and by the Spanish User Support and Operations Centre (E-USOC), Center for Computational Simulation (CCS).

References

- D. Gligor, P. Salgado Sánchez, J. Porter and V. Shevtsova, Influence of gravity on the frozen wave instability in immiscible liquids, *Phys. Rev. Fluids* **5**, 084001, 2020.
- G. Gandikota, D. Chatain, S. Amiroudine, T. Lyubimova and D. Beysens, Frozen-wave instability in near-critical hydrogen subjected to horizontal vibration under various gravity levels, *Phys. Rev. E* **89**, 012309, 2014.
- V. Shevtsova, Y.A. Gaponenko, V. Yasnou, A. Mialdun and A. Nepomnyashchy, Two-scale wave patterns on a periodically excited miscible liquid-liquid interface, *J. Fluid Mech.* **795**, 409–422, 2016.
- T. Lyubimova, A. Ivantsov, Y. Garrabos, C. Lecoutre, G. Gandikota and D. Beysens, Band instability in near-critical fluids subjected to vibration under weightlessness, *Phys. Rev. E* **95**, 013105, 2017.
- P. Salgado Sánchez, V. Yasnou, Y. Gaponenko, A. Mialdun, J. Porter and V. Shevtsova, Interfacial phenomena in immiscible liquids subjected to vibrations in microgravity, *J. Fluid Mech.* **865**, 850–883, 2019.
- T. Lyubimova, A. Ivantsov, Y. Garrabos, C. Lecoutre and D. Beysens, Faraday waves on band pattern under zero gravity conditions, *Phys. Rev. Fluids* **4**, 064001, 2019.
- E. Labrador, P. Salgado Sánchez, J. Porter and V. Shevtsova, Secondary Faraday waves in microgravity, *J. Phys. Conf. Ser.* **2090**, 012088, 2021.
- K. Kumar and L. Tuckerman, Parametric instability of the interface between two fluids, *J. Fluid Mech.* **279**, 49–68, 1994.
- P. Salgado Sánchez, J. Porter, I. Tíno and A. Laverón-Simavilla, Dynamics of weakly coupled parametrically forced oscillators, *Phys. Rev. E* **94**, 022216, 2016.

ORAL 34

Hypergravity Attenuates Reactivity in Primary Murine Astrocytes

Yannick Lichterfeld¹, Laura Kalinski¹, Sarah Schunk¹, Theresa Schmakeit¹, Sebastian Feles¹, Timo Frett², Harald Herrmann³, Ruth Hemmersbach¹ and Christian Liemersdorf¹

¹ German Aerospace Center, Institute of Aerospace Medicine, Department of Gravitational Biology, Cologne, Germany; yannick.lichterfeld@dlr.de; laura.kalinski@dlr.de; sarah.schunk@dlr.de; theresa.schmakeit@dlr.de; sebastian.feles@dlr.de; ruth.hemmersbach@dlr.de, ² German Aerospace Center, Institute of Aerospace Medicine, Department of Muscle and Bone Metabolism, Cologne, Germany; timo.frett@dlr.de. ³ University of Erlangen, Institute of Neuropathology, harald.herrmann-lerdon@uk-erlangen.de

Introduction

Neuronal activity is the key modulator of nearly every aspect of behavior, affecting cognition, learning and memory as well as motion. Alterations or even disruptions of the transmission of synaptic signals are the main cause of many neurological disorders. Lesions to nervous tissues are associated with phenotypic changes mediated by astrocytes becoming reactive. Reactive astrocytes form the basis of astrogliosis and glial scar formation. Astrocyte reactivity is often targeted to inhibit axon dystrophy and thus promote neuronal regeneration. Here, we use increased gravitational (mechanical) loading induced by hypergravity to identify a potential method to modify key features of astrocyte reactivity. We exposed primary murine astrocytes as a model system closely resembling the reactivity phenotype in vivo on custom-built centrifuges for cultivation as well as for livecell imaging under hypergravity conditions in a physiological range (2g and 10g). This resulted in significant changes to astrocyte morphology, behavior and reactivity phenotypes, with the ultimate goal being to enhance neuronal regeneration for novel therapeutic approaches.

Morphological features and dynamics related to glial scarring are influenced by hypergravity

We revealed cell spreading rates to be strongly diminished under 2g hypergravity exposure, with the initial spreading after seeding of the cells being 45% lower than under normal gravity. Long-term hypergravity exposure in an incubator centrifuge over two or more days led to a consistent 20% decrease in cell spreading under 2g.

Employing astrocyte wound-healing assays, we could show that the migration velocity of astrocytes can be decreased by hypergravity exposure. Livecell microscopy under hypergravity enabled the identification of an up to 35% lower cell migration velocity as compared to 1g. Stopping and starting of the centrifuge while imaging resulted in the observation of until now unknown adaptation and re-adaptation phases to hypergravity in astrocytes, with their migration velocity lagging behind the actually perceived gravity phase.

In contrast to the changes in morphology and migration, proliferation and apoptosis rates were not affected by 2g hypergravity exposure over several days.

Livecell actin fluorescence microscopy under hypergravity supplemented by STED imaging revealed changes in actin filament and microtubule dynamics

Livecell imaging of LifeAct-GFP astrocytes under 1g and 2g

revealed changes in actin-related cellular structures under hypergravity. STED microscopy of cells fixed after hypergravity exposure confounded these findings, adding changes in the microtubule networks of the hypergravity exposed cells.

Hypergravity attenuated reactivity induction in primary murine astrocytes.

Exposure of primary murine astrocytes to hypergravity did not only influence cell morphology, behavior and cytoskeletal dynamics. By immunostaining of reactivity related proteins, we could show, that astrocyte reactivity induction was attenuated under hypergravity conditions. Our findings revealed a novel role of gravitational loading conditions on neuronal cell behavior. We plan on further investigating the underlying mechanisms of these changes, to identify the key pathways and induce these via pharmacological means, in order to treat patients suffering from the adverse effects of glial scarring.

ORAL 36

Numerical Simulation and Analysis of Human Cardiovascular Behavior During Subjection to Suborbital Spaceflight

A. Franz¹, R. Tsvetkova², L. Karliczek¹, P. Maldonado¹, A. Genzel³

¹Julius-Maximilians-Universität, Würzburg, Germany, anemone.franz@gmx.de, louiskarliczek@me.com,
felipe.maldonado@stud-mail.uni-wuerzburg.de

²Ludwig-Maximilians-Universität, Munich, Germany, Raya.Tsvetkova@campus.lmu.de

³Bundeswehr University Munich, Germany, Munich, alexander.genzel@outlook.de

The project was performed by the interdisciplinary student team “CAVARESS” for the Student Aerospace Challenge 2019/2020 hosted by the Astronaute Club Européen and its industrial and institutional partners (ArianeGroup, Dassault Aviation, the European Space Agency and Musée de l’Air et de l’Espace) and was awarded the “ESA Grand Prix”.

Introduction

Over the past years, we have observed rapid technological advancements in the space industry, making the commercialization of suborbital spaceflight possible. The extreme environment a space tourist encounters has to this date, been mostly reserved for astronauts or jet aircraft pilots, who usually show an exceptional level of physical fitness and have undergone an intensive training process.

Commercial spaceflight participants will not only lack the extensive training but will also show a broader range of ages and include people with limited physical fitness and a variety of preexisting medical conditions. Therefore, it is crucial to investigate the physiological effects and resulting potential health risks before opening space tourism to a broader audience.

A suborbital flight, which consists of the succession of phases of ascension, microgravity and finally re-entry and landing, poses a considerable physiological challenge for the human body. The cardiovascular system is especially impacted by hydrostatic gradients. In an effort to maintain steady end perfusion of body tissues, a complex system serves to compensate for dynamic changes caused by the reorientation of the body relative to the gravity vector and other physiological perturbations (Barratt et al. 2008).

The “Push-Pull Effect” is one of the many physiological phenomena observed during a suborbital flight. It describes a reduced tolerance for +Gz accelerations immediately after having been subjected to 0G or -Gz forces (Blue et al. 2014). This effect can result in serious incapacitation of the passenger, including loss of sight or consciousness. It is, therefore, crucial to understand the risk of the Push-Pull effect occurring during a suborbital flight so that precautions can be taken accordingly.

With this objective, we developed simulation software and the medical validation process to create a basis for a passenger selection and risk estimation tool.

The hemodynamic model

The hemodynamic model was created to calculate the arterial pressure based on the pump power of the heart, to output the quasi-static heart rate-blood pressure curve and to calculate the distribution of hydrostatic pressure resulting from gravity for variable acceleration and body positions. We used a hemodynamic model which is based on the differential equations of one-dimensional transient flow in elastic curves. This model approximates the cardiovascular system through an analogous electric circuit consisting of components with linear characteristics. Therefore, we could achieve an algebraization of the time axis without its discretization. This approach delivers quick results. While it slightly compromises precision at first, this can be compensated with the original nonlinear differential equations since their solutions rapidly converge, given the optimized initial conditions. The arterial system was quantified with anatomically correct geometry and elasticity of blood vessels. Windkessel terminals were used to represent the venous and peripheral systems. The heart itself was modelled as an ideal electric current source, representing a rigid pressure-volume-flow curve. The model could deliver real-time cardiovascular prognosis during flight, for example, if a medical emergency occurred.

Results

The simulated data, as illustrated in **Figure 1**, reveal that hypergravity induced heart rate changes lie under 100 bpm

and thus do not exceed the adaptations observed under terrestrial conditions. Furthermore, **Figure 2** shows that under these circumstances, the cardiovascular system would still be able to sustain the minimal cerebral perfusion (60 mmHg or 8 kPa) required to avoid loss of consciousness during maximal expected hypergravity (5G) exposure.

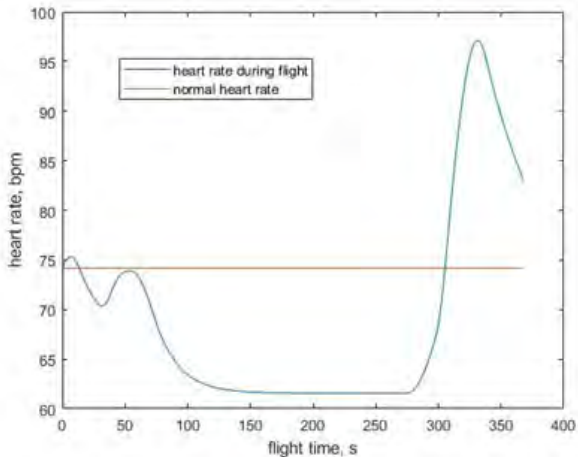


Figure 1: Change of heart rate [bpm] as a function of flight time [s].

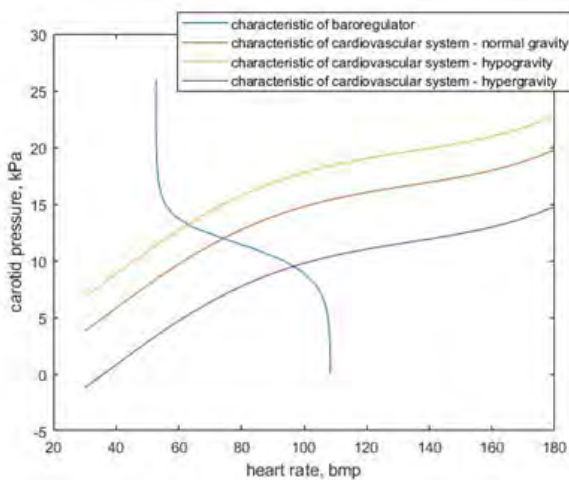


Figure 2: Change of carotid artery pressure [kPa] as a function of heart rate [bpm].

Conclusion

The data provided by our model suggest that the cardiovascular adaptations during suborbital spaceflight are greater in hypergravity than in hypogravity, yet do not exceed those experienced on earth. Passengers with certain mild cardiovascular impairments may be allowed to fly, provided that their individual condition does not hold a relevant risk of decompensation. This must be thoroughly evaluated beforehand. For this purpose, adapted centrifuge runs might prove an invaluable diagnostic tool. Through simulating exposure to varying G forces, selected according to the acceleration profile of the vehicle, the space flight participant's physical resilience and psychological endurance can be estimated.

Acknowledgements

We want to thank Professor Santiago Urquiza of the Universidad Nacional de Mar del Plata for his indispensable help with developing the computational simulation and Professor Kai Schuh of the Julius-Maximilians-Universität Würzburg for his academic guidance.

References

- MR Barratt, SL Pool, editors, Principles of Clinical Medicine for Space Flight, Springer-Verlag (2008)
- RS Blue, JM Pattarini, DP Reyes, RA Mulcahy, A Garbino, CH Mathers, et al. Tolerance of centrifuge-simulated suborbital spaceflight by medical condition. *Aviat Space Environ Med* (2014)

Human Reproduction in Space. Late results.

A. Perez-Poch¹, M. Boada², M. Ballester², M. Tresanchez²

¹Universitat Politècnica de Catalunya, Barcelona, Spain, antoni.perez-poch@upc.edu,

²Dexeus Dona, Institut Universitari Dexeus, Barcelona, Spain, monboa@dexeus.com

Introduction

The question of whether human reproduction is possible in Space has become a focus of interest in recent years after plans have been announced to establish permanent human basements on the Moon or even Mars. However, little is known on the likelihood of human reproduction in space. Some factors are potential limitants, among them psychological factors, radiation and microgravity.

The effects of changes in gravity on human reproduction are not well understood in detail and the possible involvement of human, fresh or cryopreserved gametes and embryos should be investigated in depth. This experiment reported herein tries to elucidate whether microgravity significantly affects the human sperm performance when compared to that observed on ground. The UPC Universitat Politècnica de Catalunya – BarcelonaTech is a pioneer and a university of reference in conducting experiments in microgravity, and in particular on parabolic flights in a single-engine aircraft. DEXEUS is a leading Institution in Obstetrics, Gynecology and Reproduction and a pioneer in the application of Human Assisted Reproduction Techniques and Cryobiology.

Materials and Methods

Parabolic flights have been conducted for a long time as a way of performing short-time duration experiments and technical demonstrations. Aircraft parabolic flights provide up to 23 seconds of reduced gravity and are used for conducting short investigations in Physical and Life Sciences.

Our research group has been pioneer in conducting research experiments with single-engine aerobatic aircraft. We herein report on a research conducted in Sabadell Airport (Barcelona, Spain) with a single-engine aerobatic aircraft such as the Mudry CAP10B, achieving up to 8.5 seconds of reduced gravity (A.Perez-Poch et al., 2016) per parabola.

A parabola is a trajectory followed by an airplane resulting in a limited time of exposure to microgravity inside the aircraft cockpit. The containers with the experiment are loosely attached inside the cockpit so that no vibrations produce g-jitter in the payload.

A total of fifteen normozoospermic sperm samples from healthy voluntary donors were produced in the early morning before the flight. All donor received information about the study and signed an informed consent form ad hoc for the research. Fresh samples were divided in two fractions (microgravity vs ground conditions), which took place less than two hours after being produced. Two specific containers that maintain temperature stable at 37° were used during all the experiment. The one carrying the sperm samples was located in the aircraft cockpit, with no manual operation during the parabolas. It was located on board the aircraft, strongly

attached to the co-pilot seat in front of the aircraft cockpit, whereas samples of the control group were on hold on ground in the other container of the same characteristics in order to compare the differences.

The flight operations lasted less than one hour, in VFR (Visual flight conditions). After each flight, evaluation of sperm concentration and motility using a computerized semen motility analyser as well as vitality (eosin-nigrosin staining) were performed in the Dexeus laboratory in Sabadell nearby the airport with a short time lapse between aircraft landing and analysis.

The procedure is similar to that also conducted in parabolic flight previously reported by our research group in 2019. In this experiment (M. Boada et al., 2020) we first analyzed microgravity effects on frozen human sperm samples with liquid nitrogen, with no significant effects found in mobility, neither in concentration nor in their vitality on the thawed sperm exposed to different gravitational conditions.

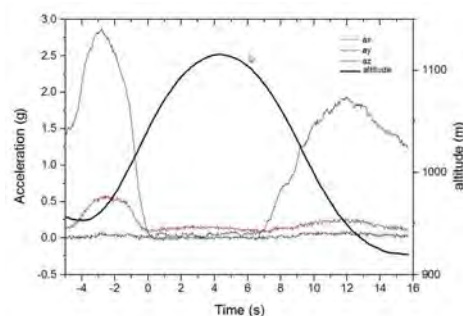


Figure 1: Typical flight profile of an average parabola performed during the research campaigns.

Results

Comparing mean values between the study group of fresh human sperm samples which underwent microgravity exposure (μ G); and the control group held on ground (1G) significant statistical differences were found in some of the parameters analyzed ($p < 0.05$).

We observed no statistically significant difference in terms of total sperm concentration between fresh samples exposed to microgravity (μ g) and fresh samples maintained on earth conditions (1g) ($81,7 \pm 112,1$ vs $79,7 \pm 89,8$ M/ml). However, computer analyses showed significant alterations in motility. A statistically significant difference was observed in the total motile sperm concentrations ($23,7 \pm 15,3$ M/ml vs $31,5 \pm 25,1$ M/ml), in the sperm concentration of grade a ($8,7 \pm 6,5$ vs $11,7 \pm 9,9$ M/ml) and in the percentage of spermatozoa with progressive motility ($30 \pm 12,9$ vs $36 \pm 14,3$ %). Moreover, analyses also showed differences in motility patterns,

Curvilinear Velocity (VCL) was statistically different ($45,7 \pm 12,8$ vs $47,7 \pm 13,3$ $\mu\text{m/s}$).

Discussion

These findings indicate that sperm motility and vitality were statistically significantly decreased under microgravity exposure under study conditions. More cases must be analyzed to confirm the results, but what is hypothesized is that the effects of exposure to microgravity could be even more significant if the exposure time is increased. Furthermore, in the first study carried out by our research team, we showed that frozen human sperm samples did not suffer any significant effect under microgravity exposure and motility was preserved, so we suggested that they could be used to create a sperm bank in space for future human reproductive clinical applications. With the present study we show that fresh samples that are not protected by cryoprotectants are vulnerable to microgravity and that the effects caused by microgravity, that probable are time-dependent, are likely to compromise the usability of the samples in assisted reproductive techniques (ART), after longer exposures.

This study has limitations. Aerobatic parabolic flights offer a limited time of microgravity (5-8 seconds) while larger aircraft provide between 20-25 seconds of microgravity thanks to a more powerful engine. Another limitation to take in consideration is that short periods (1-3 seconds) of hypergravity preceding and following microgravity which cannot be avoided. However, it is less likely that accelerations put sperm motility or vitality in jeopardy when compared to the microgravity period effects.

This research was considered not feasible in a Random Position Machine (RPM), as the continuous random rotation of the cellulae will significantly affect its motility, so it cannot be considered a model of simulated microgravity for this particular topic. Drop Towers may be considered, but the size of the cylinder containing the sample makes it unpractical to hold. Parabolic flights in larger aircraft may provide further validation for this hypothesis, as they are capable of exposing the payload to up to 23 seconds of microgravity with residual acceleration in the range of 0.01 g.

Experimentation at the International Space Station would be the best option for further studies as it offers a continuous, permanent exposure to microgravity. It is publicly known that NASA is conducting the experiment Micro-11 with human sperm samples on the International Space Station, since April 2018. In an abstract published online on their communication presented at the ASGSR Conference in 2019, it was reported (Tash et al. 2019) that microgravity effects had been observed at the ISS on bovine and humane sperm samples. These results would be compatible with our initial findings reported herein.

Conclusions

These initial results suggest that microgravity significantly decreases sperm motility and vitality of fresh samples which could have an important impact on the future human reproduction outside the earth.

The lack of significant differences obtained when comparing motility of vitality of frozen sperm samples under microgravity conditions suggested the possibility of using sperm banks in space but differences observed in fresh sperm samples should make us reflect before considering reproduction in space

Human reproduction in Space is also dependant on other important factors such as radiation as well as psychological and physiological issues. Further studies are needed to fully assess and understand the impact of microgravity on human reproduction systems functionality.

Acknowledgements

The authors would like to thank the pilot of the aircraft Daniel V. Gonzalez and the Barcelona-Sabadell Aviation Club for the logistic support and the resources provided as well as Ignacio Rodríguez and Sandra García for the statistical analysis. We are also grateful to the informed volunteers who produced the experimental samples.

This work was approved by the Review Board of the Institut Dexeus and was performed under the auspices of “Càtedra d’Investigació en Obstetrícia i Ginecologia” of the Department of Obstetrics, Gynecology and Reproduction, Institut Universitari Dexeus-Universitat Autònoma de Barcelona.

References

- A. Perez-Poch, D. V. Gonzalez, D. Lopez, Hypogravity research and educational parabolic flight activities conducted in Barcelona: a new hub of innovation in Europe, *Microgravity Sci. Technol*; 28, 603-609 (2016).
- M. Boada, A. Perez-Poch, M. Ballester, S. García, D. V. Gonzalez, P. Barri, A. Veiga, Microgravity effects on frozen human sperm samples, *Journal of Assisted Reproduction and Genetics*, vol. 37, 6, 2249–2257 (2020)
- J.S. Tash, A.J. Feustel, S. Aunon-Chancellor, E. Yarns, S. Shane Piper, L. Ngo, E. Laundry, V. Mittal, N.S. Chanliongco, M. Julo, L. Stodieck, L. Zea, S. Doraisingam, F. Karouia, G. Blanco, Micro-11: Microgravity significantly alters human and bovine sperm functions on the ISS. Abstract in the Proceedings of the American Society for Gravitational and Space Research Annual Meeting (2019), Denver, Colorado. Available online: www.asgsrc.org. (Accessed on 2022).

ORAL 38

Simulating the spaceflight environment: Combined effect of simulated microgravity, ionizing radiation, and psychological stress on *in vitro* wound healing.

W. E. Radstake^{1,2}, K. Gautam¹, S. Miranda^{1,2}, E. Rehnberg^{1,2}, R. Vermeesen¹, K. Tabury¹, B. Baselet¹, & S. Baatout^{1,2}

¹Radiobiology Unit, Belgian Nuclear Research Centre SCK CEN, Mol, Belgium, eline.radstake@sckcen.be, kiran.gautam@sckcen.be, sfdsmira@sckcen.be, emil.rehnberg@sckcen.be, randy.vermeesen@sckcen.be, kevin.tabury@sckcen.be, sarah.baatout@sckcen.be, ²Faculty of Bioscience Engineering, Department of Biotechnology, Ghent University, Belgium.

Introduction

In space, long-term exposure to microgravity, ionizing radiation and higher levels of psychological stress increase health risks for astronauts. Skin problems including rashes, itches and delayed wound healing are frequently reported during long-term spaceflight [1]–[3]. How the complex spaceflight environment induces these defects is still not fully understood. Cellular responses as result of exposure to spaceflight stressors can be investigated using *in vitro* simulation models. However, exposure to the single spaceflight stressors ionizing radiation, simulated microgravity or psychological stress fail to grasp the complete picture of the hazardous space environment and may underestimate possible synergistic interaction effects. This project aims to investigate the complex interaction of different spaceflight stressors on skin integrity and how they affect wound healing.

Methodology

In vitro simulation models were developed in which primary human dermal fibroblasts have been exposed to a combination of ionizing radiation, simulated microgravity and psychological stress. Different radiation qualities were used including exposure to X-rays, protons, carbon ions and iron ions at doses of 0.1, 0.5, and 1 Gy. For the simulation of microgravity, cells were placed on a random positioning machine (Fig. 1). Finally, to simulate chronic exposure to high psychological stress levels, hydrocortisone at concentration of 1 μ M was added to the cell culture media. Fibroblast function related to the different stages of wound healing were investigated, including the inflammatory, proliferation and remodelling phase. Fibroblast expression of pro-inflammatory

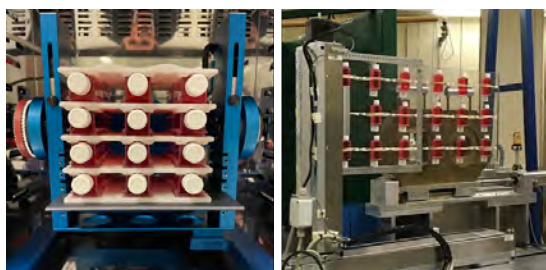


Figure 1: Experimental set-up. Left: placement of cell culture vessels on Random Positioning Machine (RPM). Right: placement of samples during proton irradiation.

cytokines and growth factors (IL6, IL-1RA, PDGF- α , TGF- β) were quantified with Multiplex immune- and ELISA assays. Furthermore, migration capacity of fibroblasts after exposure was investigated through means of an *in vitro*

scratch wound assay as well as remodelling of F-actin cytoskeleton and focal adhesion molecules using immunocytochemistry analysis. Finally, investigation into expression of extra cellular matrix proteins of collagen type I & III and fibronectin, relevant for skin remodelling after injury, were performed through means of western blot.

Results

Preliminary results show a decreased expression of PDGF- α in fibroblasts exposed to hydrocortisone. Furthermore, fibroblasts exposed to hydrocortisone showed a delayed migration 24 hours after irradiation. In addition, 24 hours of simulated microgravity significantly delayed fibroblasts migration capability as well. During the remodelling phase of wound healing, hydrocortisone and simulated microgravity further reduced the expression of pro-collagen type III in fibroblasts.

Conclusions

Using a unique set-up, we were able to expose human dermal fibroblasts to a combination of simulated spaceflight stressors and investigate their wound healing capacity after exposure to different types of ionizing radiation, simulated microgravity and psychological stress. The collection of results is currently still ongoing. With the presented set-up we aim to provide more insights into the possible interaction effects of exposure to combined simulated spaceflight stressors.

Acknowledgements

Eline Radstake is the recipient of an SCK CEN/UGent PhD grant. This work is supported by ESA/BELSPO/Prodex IMPULSE-2 contract (PEA 4000109861).

Proton and carbon irradiation performed at PARTEC facility in Groningen, the Netherlands. Financed through ESA-IBER programme.

Iron irradiation performed at GSI in Darmstadt, Germany. Financed through ESA-IBER programme.

References

- [1] B. Crucian, A. Babiak-Vazquez, S. Johnston, D. L. Pierson, C. M. Ott, and C. Sams, "Incidence of clinical symptoms during long-duration orbital spaceflight," *Int. J. Gen. Med.*, vol. 9, pp. 383–391, 2016.
- [2] C. Dunn, M. Boyd, and I. Orengo, "Dermatologic manifestations in spaceflight: A review," *Dermatol. Online J.*, vol. 24, no. 11, 2018.
- [3] I. B. Gontcharov *et al.*, "In-flight medical incidents in the NASA-Mir program," *Aviat. Sp. Environ. Med.*, vol. 76, no. 7 I, pp. 692–696, 2005.

ORAL 39

Spaceflight Associated Neuro-ocular Syndrome During Long Duration Spaceflight

B.R. Macias¹, C.R. Ferguson³, S.S. Laurie²

¹NASA Johnson Space Center, Houston, TX USA, brandon.r.macias@nasa.gov, ²KBR, Houston, TX USA, ³Aegis Aerospace, Houston, TX USA

Introduction

Spaceflight-associated neuro-ocular syndrome (SANS) affects ~69% of astronauts completing ~6-month long missions to the International Space Station (ISS) as determined by one or more findings: optic disc edema (ODE), hyperopic shifts, globe flattening, and/or choroidal folds. The lack of gravity and associated hydrostatic pressure gradient results in a headward fluid shift that affects intracranial and ocular fluid compartments and may contribute to the ocular and brain changes reported in astronauts after return from a weightless environment. The headward fluid shift associated with weightlessness may result in a sustained increase in intracranial pressure (ICP), but direct measures of ICP have not been collected during long-duration spaceflight. Observations of elevated ICP in astronauts with signs of ODE have been recorded after spaceflight, but preflight measures are not available for comparison (Mader et al. 2011). Further, during brief exposure to weightlessness in parabolic flight, ICP was similar or less than that observed in the supine posture (Lawley et al. 2017). Here we summarize our currently available data describing the spaceflight induced alteration in ocular and brain morphology and associated fluid shifts.

Methods

Twenty-three ISS astronauts participated in testing before, during, and up to 180 days after spaceflight (R+180). Before and after tests assessed non-invasive ICP and eye structure (optical coherence tomography [OCT], and magnetic resonance imaging [MRI]). Early and late (flight days [FD] 45 ± 7 and 150 ± 30) flight evaluations included nICP and OCT. We used two techniques to quantify nICP: cerebral and cochlear fluid pressure (CCFP) and otoacoustic emissions (OAE). Optic nerve head (ONH) morphology was quantified using OCT. Globe volume at the optic nerve head and lateral ventricular volume were quantified using MRI.

Results

Weightlessness induced a cephalad fluid shift during spaceflight as evidenced by an increase in internal jugular vein cross-sectional area from 9.8 mm² (95% CI, -1.2 to 20.7 mm²) upright preflight to 70.3 mm² (95% CI, 59.3 – 81.2 mm²; P < 0.001) and intraocular pressure from 14.4 mmHg (95% CI, 13.5 – 15.2 mmHg) upright preflight to 15.6 (95% CI, 14.9 – 16.4 mmHg; P < 0.001) by flight day (FD) 45 (Marshall-Goebel et al. 2019 and Greenwald et al. 2021). Minimum rim width (MRW) and total retinal thickness (TRT250) within 250 μm of Bruch's membrane (BM) opening increased from before flight by FD45 and was maximally increased on FD 150 (MRW: 50 μm; 95% CI, 37

– 62 μm; P < 0.001; TRT250: 38 μm; 95% CI, 26 – 51 μm; P < 0.001). MRW recovered to before flight values approximately 45 days after landing. In addition, in a subset of this crew cohort there was a decrease in optic nerve head cup volume (.038 mm³; 95% CI, .030 – .046 mm³; P < 0.001). Mild optic disc edema developed after 319 days of spaceflight in one crew member and choroidal folds and optic disc edema progressively developed in another crewmember during a one-year mission in low Earth orbit aboard the ISS (Macias et al. 2021). Within the broader astronaut cohort, mean ocular globe volume at the optic nerve was decreased by 9.88 mm³ (95% CI, 4.56 – 15.19 mm³; P < 0.001) on the first day of assessment after spaceflight (R[return]+ 1 day); 9.00 mm³ (95% CI, 3.73 – 14.27 mm³; P = 0.001) by R + 30 days; 6.53 mm³ (95% CI, 1.24 – 11.83 mm³; P < 0.05) by R + 90 days; 4.45 mm³ (95% CI, -0.96 to 9.86 mm³; P = 0.12) by R + 180 days; and 7.21 mm³ (95% CI, 1.82 – 12.60 mm³; P < 0.01) by R + 360 days (Sater et al. 2021). On FD 45, two measures of nICP were lower than supine preflight (CCFP: mean difference -98.5 -nl; 95% CI, -190.8 to -6.1 -nl; P = 0.037; OAE: -19.7 degrees, 95% CI, -10.4 to -29.1 degrees; P < 0.001), but not different from upright preflight. Compared to a preflight intracranial lateral ventricle volume of 19.6 mL, lateral ventricular volume increased by 2.2 mL (11.2%; P < 0.01) immediately after flight (R+1) and remained elevated through R+180 (P < 0.01) (Kramer et al. 2020).

Discussion

ODE developed in ~69% astronauts during 6-month spaceflight missions as quantified by OCT (Δ TRT250 > 19.4 μm) (Laurie et al. 2019) and persisted through R+180 in some crewmembers (Macias et al. 2020). There is some evidence that longer mission durations are associated with additional ocular structural changes. These data highlight variability in the magnitude of spaceflight induced SANS findings. Initial findings suggest that anatomical morphology may be one contributing factor to the magnitude of change of ODE. Inflight nICP results suggest that ICP during spaceflight is not elevated above values observed on Earth in the seated to supine posture. However, the typical daily fluctuations that occur terrestrially due to posture change may not occur during weightlessness due to the lack of hydrostatic pressure gradients. Chronic mild ICP levels may alter intracranial compliance sufficiently to alter ocular and brain structure, as evidenced by spaceflight induced brain ventricular volume expansion. Future studies should invasively measure CSF hydrodynamics before and after flight. Mechanical fluid shift countermeasures are currently being evaluated in the strict head down tilt bed rest analog.

References

T.H. Mader, C.R. Gibson, A.F. Pass, et al., Optic disc edema, globe flattening, choroidal folds, and hyperopic shifts observed in astronauts after long-duration space flight, *Ophthalmology*, 118, 2058-2069, (2011)

J.S. Lawley, L.G. Petersen, E.J. Howden, et al., Effect of gravity and microgravity on intracranial pressure, *J Physiol (Lond)*, 595, 2115-2127, (2017)

S.S. Laurie, S.M.C. Lee, B.R. Macias, N.B. Patel, C. Stern, M. Young, M.B. Stenger, Optic Disc Edema and Choroidal Engorgement in Astronauts during Spaceflight and Individuals Exposed to Bed Rest, *JAMA Ophthalmology*, 138(2), 165-172, (2019)

K. Marshall-Goebel, S. Laurie, I. Alferova, et al., Assessment of Jugular Venous Blood Flow Stasis and Thrombosis During Spaceflight, *JAMA Network*, 2(11), (2019)

S.H. Greenwald, B.R. Macias, S.M.C. Lee, et al., Intraocular pressure and choroidal thickness respond differently to lower body negative pressure during spaceflight, *J Appl Physiol*, 131(1), 613-620, (2021)

B.R. Macias, N.B. Patel, C.R. Gibson, et al., Association of Long-Duration Spaceflight With Anterior and Posterior Ocular Structure Changes in Astronauts and Their Recovery, *JAMA Ophthalmology*, 138(5), 553-559, (2020)

B.R. Macias, C.R. Ferguson, N.B. Patel, et al., Changes in the Optic Nerve Head and Choroid Over 1 Year of Spaceflight, *JAMA Ophthalmology*, 139(6), 663-667, (2021)

S.H. Sater, A.M. Sass, J.J. Rohr, et al., Automated MRI-based quantification of posterior ocular globe flattening and recovery after long-duration spaceflight, *Eye (Lond)*, 35(7), 1869-1878, (2021)

L.A. Kramer, K.M. Hasan, M.B. Stenger, et al., Intracranial Effects of Microgravity: A Prospective Longitudinal MRI Study, *Radiology*, 295(3), 640-648, (2020)

ORAL 40

Microstructural transitions during solidification of transparent alloy NPG-DC investigated onboard the ISS using the TRANSPARENT facility

L. Sturz¹, G. Zimmermann², C. Pickmann³

^{1,2,3}Access e.V. Materials&Processes, Aachen, Germany

¹L.Sturz@access-technology.de, ²G.Zimmermann@access-technology.de, ³C.Pickmann@access-technology.de

Introduction

A fundamental topic of interest and area of research in materials science is the link between (i) processing/experimental parameters, (ii) microstructure development and transitions in a solidifying material and (iii) related final material properties. From the numerous experimental methods and processes to solidify materials from the molten state we apply directional solidification in a Bridgman-type furnace, in which cooling-rate and temperature gradient at the solid-liquid interface can be generally chosen independently. Furthermore, here we focus on transparent organic mixtures with microstructures similar like those appearing in metallic alloys. The optical transparency allows for direct microscopical observation of the developing microstructures as a function of experimental and alloy parameters. Finally, many solidification and related phenomena occurring under gravity conditions, i.e. sedimentation or floatation of particles and fluid convection, can be largely suppressed under conditions of reduced gravity. With this, a separation of involved phenomena into alloy-, process- and gravity-dependent parameters is obtained.

The European space agency ESA with support of national space agencies developed a facility "TRANSPARENT" together with Qinetiq-Space/B, dedicated to investigate fundamental materials science in transparent analogue systems. The facility is operative since several years in the glovebox MSGB in the destiny module aboard the ISS, while a copy is located at the european user support center E-USOC in

Madrid. Within the framework of the ESA programme CETSOL (columnar - to equiaxed transition in solidification processes) involving many international and industrial partners, one research path is directed towards analysing the transition between two dendritic microstructural regimes in transparent alloys. This columnar to equiaxed transition (CET) is very common in numerous material systems and processing routes and is in general an unwanted effect because the final materials properties can change as well.

Experimental

Three different mixtures of the material NPG-DC (Neopentylglycol-(d)Camphor) with 20.0, 30.0 and 37.5 wt.-% DC have been prepared to investigate the composition effect on the CET. The materials have been purified, degassed, and filled into dedicated cartridges with the materials volume having a square cross-section (6x6 mm) and about 100 mm length. The cartridges include a volume compensation mechanism and can be moved along the direction of largest dimension (x) in between a clamping system to apply temperature fields to the cartridge. The clamp system consists of two clamp-pairs, and all four clamps can be regulated individually. For the CET-type of experiments the clamps are supposed to create a mainly one-dimensional, nearly linear temperature field along the x-axis by setting a "hot" and a "cold" temperature to the two pairs, which have a fixed distance of $\Delta x=7$ mm

Optical observation is performed perpendicular to movement and main solidification direction by light

transmission bright field microscopy in a Field of View of about 5x6 mm covering most of the “adiabatic” zone between the clamps. Additionally, a scanning mode of the microscope optic in the depth of the cartridge will allow for 3D-investigation of the dendritic structures.

The CET is known to be a function of at least composition, thermal gradient and pulling velocity of the cartridge. In the ISS experiments named CETSOL-1, a large set of combinations of thermal gradient and pulling velocity are applied to each cartridge.

Results

Fig. 1 shows one example of the CET in NPG-20.0wt.-%DC with a temperature difference of 35°C between hot and cold clamps and different pulling velocities. Since the experiment series are ongoing at the time of abstract submission, we can only provide preliminary results of the related phenomena. Such a result will be the determination of stability regimes for columnar and equiaxed growth as a function of the solidification parameters. Also, first information about the 3-dimensional growth of dendrites in purely diffusive conditions are expected.

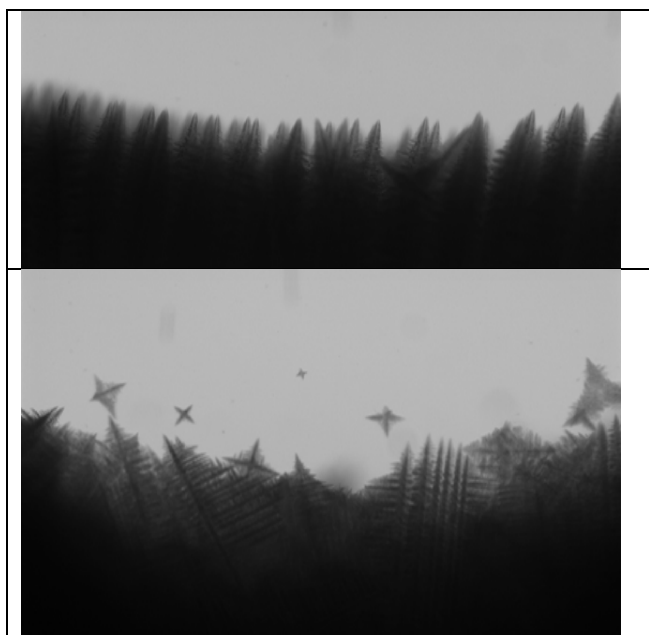


Fig. 1: Columnar dendritic growth (top) and transition to equiaxed dendritic growth – the CET (bottom). Image width is about 5 mm. Velocities have been increased from about 20 to about 50 $\mu\text{m/s}$.

Acknowledgements

We gratefully acknowledge support of the german space agency DLR (grant 50WM2043), european space agency ESA and the European user support center E-USOC in Madrid.

ORAL 41

Slow Impacts on Regolith Surfaces in Low Gravity – First Experiments on the new GTB-Pro Platform

K. Joeris, M. Keulen, J. E. Kollmer

Universität Duisburg-Essen, Duisburg, Germany, jonathan.kollmer@uni-due.de

Introduction

Rubble pile asteroids such as Itokawa, Ryugu, and Bennu are covered by regolith of various sizes. On some asteroids, for example on Itokawa, the regolith is not distributed evenly but large boulders congregate in some areas whereas other are dominated by finer material [Fujiwara2006]. Several mechanisms have been proposed to explain this size sorting. One of these mechanisms is the so-called ballistic sorting effect (BSE) [Shinbrot 2017]. The BSE depends on impacting particles rebounding more elastically from large targets (boulders) than when hitting a bed of fine grains. This mechanism of applies a) to the primary impactor hitting an asteroid surface and b) to secondary impacts from material ejected by the primary impact. In order to fully understand the effectiveness of BSE on asteroids – and to quantify how strongly it contributes to observed size sorting effects - it is therefore important to measure the elasticity of impacts and quantify the mass- and velocity distribution of ejecta generated by impacts into asteroid surfaces. In the context of BSE impacts with low velocities are the most interesting because their kinetic energy is small enough so that they will generate ejecta that is slower than the escape velocity of the asteroid and therefore has a chance to generate secondary impacts. Another effect is that cohesive forces between regolith particles on the surface can be on the same magnitude as gravity for mm sized particles and therefore the granular mechanics of the impact will be quite different than expected.

Experiment

To conduct realistic experiments under asteroid conditions we use the ERICA (Experiments on Rebounding Impacts and Charging on Asteroids) platform [Joeris 2021] under the microgravity provided by the ZARM Bremen drop tower and the new GTB-Pro, also at ZARM. To provide a low but directed gravity level, i.e. asteroid gravity, ERICA consists of a vacuum chamber that contains the sample material which is mounted to a linear stage that - once the whole setup is in microgravity - provides a linear acceleration to simulate asteroid-level gravity. Using the linear stage eliminates any Coriolis forces a centrifuge would create. Due to the long microgravity time of 9.2 s in the drop tower and 2.5 s in the GTB-Pro these experiments are able to focus on ultra low velocity impacts in the cm/s range, complementing earlier experiments by Brisset et al. [Brisset 2020]. In the sample chamber we place granular beds (regolith analog) of various sizes and a launcher mechanism that impacts a basaltic projectile at the simulated asteroid surface. Using a stereo pair of cameras, as well as a high speed camera we then record the ejecta plume created by the impact. From the resulting image data we extract ejecta velocities using particle tracking (for larger ejecta particles) and digital image correlation (for

smaller ejecta). In case the impactor rebounds from the surface we also record its trajectory to extract its coefficient of restitution.



Figure 1: Ejecta Plume generated by impacting a basaltic projectile ($v = 65 \text{ cm/s}$) in a bed of $0\text{-}300 \mu\text{m}$ sized particles at a gravity level of $2 \cdot 10^{-4} \text{ m/s}^2$

Conclusions

We have successfully built a platform to generate realistic asteroid conditions in a laboratory setting. We employ this platform to conduct impact experiments at the ZARM Bremen droptower and the new GTB-Pro facilities.

Acknowledgements

We acknowledge funding by the German aerospace agency DLR via the Federal Ministry of Economics and Climate under Grant Number 50WM1943.

References

- A. Fujiwara, J. Kawaguchi, D.K. Yeomans, M. Abe, T. Mukai, T. Okada, J. Saito, H. Yano, M. Yoshikawa, D.J. Scheeres et al., Science 312,1330 (2006)
- T. Shinbrot, T. Sabuwala, T. Siu, M.V. Lazo, P. Chakraborty, Phys. Rev. Lett.118 (2017)
- K. Joeris, L. Schönau, L. Schmidt, M. Keulen, V. De-sai, P. Born, J. Kollmer, EPJ Web of Conferences 249, 13003 (2021)
- J. Brisset, C. Cox, S. Anderson, J. Hatchitt, A. Madison, M. Mendonca, A. Partida, D. Remie, Astron. Astrophys (2020)

ORAL 43

AtmoFlow – Investigating large scale convection in planetary atmospheres

P.S.B. Szabo¹, Y. Gaillard¹, P. Haun, R. Carter², A. Adrian³, Y. Sliavin¹, F. Zaussinger¹, C. Egbers¹

¹Dep. Aerodyn. and Fluid Mech., Brandenburg Univ. of Tech., Cottbus-Senftenberg, Germany

²Institute of Photonics and Quantum Sciences, Heriot-Watt University, Edinburgh, United Kingdom

³Airbus Defence and Space GmbH, Immenstaad
 Peter.Szabo@b-tu.de

Introduction

Convection in planetary interiors or atmospheres is still of great interest in geophysical and meteorological sciences. However, understanding the origin of planetary waves and large-scale flows is still not yet fully understood. Up till now scientists are investigating such large-scale flows in experimentally miniaturised models majorly in spherical gaps or annuli that are differentially heated at their shells. While planetary convection is driven by terrestrial gravity, where gravity points towards the centre of the planet, one has to establish a vector potential in an experiment model in the same direction. This of course is challenging as in an Earth based laboratory gravity points towards the ground creating natural convection if the system is heated. Experiments are therefore limited to reproduce an atmosphere such as baroclinic wave tanks that are capable to provide an insight into mid-latitude cell formation of a planet’s atmosphere. However, poleward or equatorial flows are not well captured. A potential solution is to induced an artificial gravity-like field realized by electric or magnetic forces (Szabo et al. 2018a, 2018b, 2021a, 2021b). While terrestrial gravity has a large influence on magnetic or electrical induced convection, such experiments have to be placed in a microgravity environment. This enables to explore spherical shell convection with a central force field that are similar to planetary fluid flow in a simplified experiment model. The basic approach enables scientist to identify and understand the local formation of global planetary waves that contribute towards the large-scale thermal transport in atmospheres and planetary interiors. Based on a previous experiment named GeoFlow, designed to investigate planetary interiors which served on the International Space Station (ISS) from 2008 to 2016, a new spherical shell experiment is designed to investigate planetary atmospheres (Futterer 2013, Zaussinger et al. 2020). While the same working principle is used by a temperature and electric potential difference between the spherical shells an atmosphere of a planet may be realised in a miniaturised model. How this done is given in a brief description of the experiment in the following section.

Spherical shell experiment

The spherical shell experiment is designed to mimic a planetary atmosphere by implementing realistic thermal boundary layers as seen in Figure 1 (a) and (b), respectively. The complexity of planetary atmospheres is reduced to a simplified approach by defining three fixed regions, one the equatorial region where solar radiation is large, the polar regions where solar radiation is small implemented as heat sinks and the mid-latitudes regions between equator and each pole defined as moderate regions with heat sinks at the

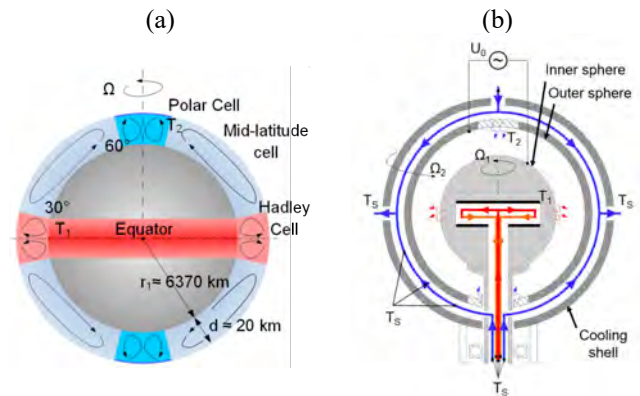


Figure 1: Simplified planetary atmosphere as found e.g. on Earth in (a). The right panel (b) shows a vertical cut through the AtmoFlow experiment. The blue and red lines indicate the flow of the cooling and heating loops, respectively. The inner and outer shell are able to rotate by Ω_1 and Ω_2 , respectively by independent rotating drives and turntables.

upper atmosphere. A working fluid, 3M Novec 7200, is confined between both shells and used to investigate convective fluid flow within the spherical gap. Planetary rotation is added by simply placing the system on a turntable. In addition, to solid body rotation the inner sphere is mounted on a second rotating drive to impose differential rotation. With the working fluid being sensitive to temperature and electric potential, one can induce an electric buoyancy that is similar to terrestrial gravity and thus impose an artificial gravity field. Adjusting the rotation speed and the magnitude of the electric potential leads to different planetary systems which can be investigated. The physical experiment is seen in Figure 2 where a transparent spherical outer shell is cooled by a thermostat water bath and the inner shell is heated at the equatorial plane. The flow is captured by a Wollaston Shearing Interferometer that is capable to detect small variation in the fluid’s refractive index which is proportional to the fluid’s temperature (Erdogdu et al. 2021).

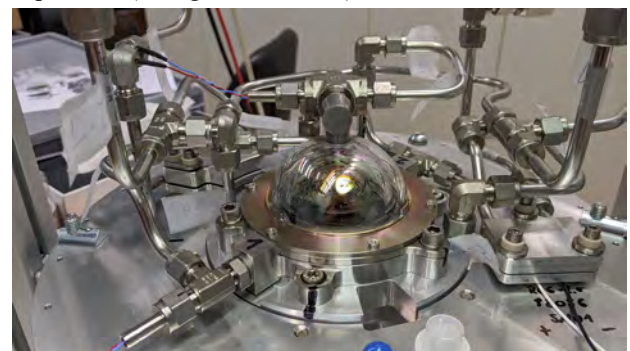


Figure 2: Image of the physical built spherical shell experiment.

Experiment program

The experiment program is designed to investigate unresolved atmospheric processes that focus up on the large-scale and small-scale nature of planetary waves. With the parametrisation of voltage and temperature the formation of such waves and convective cell formation will be studied to explain their fundamental origin. Results may also contribute to models in terms of climate change and meteorology which may be used to study the relation between external forcing and climate variability. This is in fact implemented in the model by volumetric heating of the fluid which serves as an analogy to global warming in atmospheres. In addition, the boundary temperatures of the experiment can be adjusted by the thermostat water baths to induce time periodic heating and/or cooling that can be utilised to study warming or cooling periods and their influence on global cell formation which may refer to a comparison of climate change over a certain period of time.

Expected experimental outcomes and computational investigation

The experimental results will serve as a benchmark for the accompanied numerical investigations that are capable to decouple the flow structures such as volumetric heating, boundary heating and combined heating with rotation. Linear stability analysis is used to complement the numerical simulations which provides a robust frame of reference with respect to the basic flow and the onset of TEHD convection to investigate wave development and bifurcations (Travnikov et al. 2021). Figure 3 shows an example of the iso-surface of the temperature and velocity profile which indicates convective transport from the equatorial region to poleward regions while the spherical shell is rotating. This convective development is similar to a simplified planetary atmosphere and shows the base state before adjusting more complex structural convective development like on planet Earth.

Conclusion

The AtmoFlow project is designed to model planetary atmospheres in a miniaturised model. These investigations are complemented by numerical simulations that serve to understand the fundamental origin of planetary wave development and large-scale heat transfer from equatorial regions to polar regions of different planetary systems. In addition to the geophysical and atmospheric application of spherical shell convection, TEHD convection is investigated as a counterpart to evaluate the potential technical application to increase heat transfer and their life time by effective and efficient cooling (Szabo et al. 2021b). This is mainly achieved by electric and magnetic fields where TEHD convection is one of the promising candidates alongside magnetohydrodynamics or ferrohydrodynamics. To transport heat TEHD convection may also be utilised for an active control of heat transfer such as TEHD pumps and nozzles even in the absence of terrestrial gravity to move heat away from critical parts without any moving parts.

Acknowledgements

The project AtmoFlow is supported by the BMWi via the German Space Administration of the Deutsches Zentrum für Luft und Raumfahrt (DLR) with grant no. 50WP1709, 50WP1809 and 50WM2141.

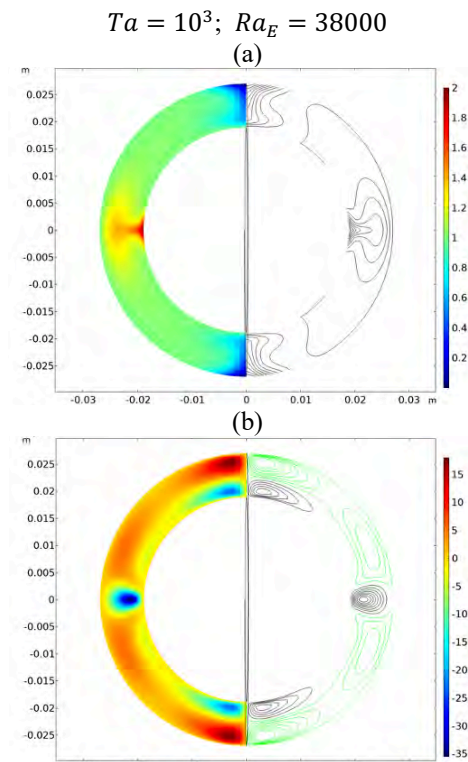


Figure 3: Numerical simulation of wave development in the AtmoFlow parameter space. Iso-surface and contour plot of temperature and velocity in (a) and (b), respectively.

References

- A.O. Erdogdu, P.S.B. Szabo, R. Carter, M.E. Gevrek, P. Haun, F. Zaussinger, B. Schulze, M. Meier, C. Egbers, Verwendung der Wollaston-Scherinterferometrie zur Untersuchung des Brechungsindexgradienten in einem differentiell beheizten Ringspalt, *Experimentelle Strömungsmechanik*, (2021)
- B. Futterer, A. Krebs, A. C. Plesa, F. Zaussinger, R. Hollerbach, D. Breuer, C. Egbers, Sheet-like and plume-like thermal flow in a spherical convection experiment performed under microgravity, *Journal of fluid mechanics* 735, 647-683 (2013)
- P.S.B. Szabo, M. Beković, W.-G. Früh, Infrared thermography of wall temperature distribution caused by convection of magnetic fluid, *Int. Journal of Thermal Sciences* 134, 129-139 (2018a)
- P.S.B. Szabo, W.-G. Früh, Using magnetic fluids to model convection of planetary or stellar interiors in laboratory scale, *PAMM* 18 (1), 1-2, (2018b)
- P.S.B. Szabo, W.-G. Früh, Thermomagnetic convection in a differentially heated rotating annulus with central force field." *PAMM* 21 (1), 1-2, (2021a)
- P.S.B Szabo, A. Meyer, M. Meier, V. Motuz, Y. Sliavin, C. Egbers, Simultaneous PIV and shadowgraph measurements of thermo-electrohydrodynamic convection in a differentially heated annulus, *Technisches Messen*, (2022)
- P.S.B Szabo, M. Meier, A. Meyer, E. Barry, V. Motuz, I. Mutabazi, C. Egbers, PIV and shadowgraph measurements of thermo-electrohydrodynamic convection in a horizontal aligned differentially heated annulus at different gravity conditions, *Experimental Thermal and Fluid Science* 129, 110470, (2021b)
- V. Travnikov, C. Egbers, Numerical investigation of atmosphere like flows in a spherical geometry, *Physical Review E* 104, (2021)
- F. Zaussinger, P. Haun, P.S.B. Szabo, V. Travnikov, M. Al Kawwas, C. Egbers, Rotating Spherical Gap Convection in the GeoFlow International Space Station (ISS) Experiment, *Phys. Rev. Fluids* 5, 063502, (2020)

ORAL 44

Preliminary Results on Emulsion Destabilisation from the ISS PASTA Experiment

L. Liggieri¹, L. Cristofolini^{1,2}, D. Orsi², V. Lorusso², M. Vaccari², F. Ravera¹, E. Santini¹, T. Karapantsios³,
M. Kostoglou³, A. Chondrou³, R. Miller⁴, E. Schneck⁴, M. Antoni⁵, J. Ferri⁶, R. McMillin⁶

¹CNR-ICMATE Genova, Italy, libero.liggieri@ge.icmate.cnr.it, ²DMPCS Univ. of Parma, Italy, luigi.cristofolini@unipr.it,

³Aristotle Univ., Thessaloniki, Greece, karapant@chem.auth.gr, ⁴Dept. Physics TU Darmstadt, Germany, miller@fkp.tu-darmstadt.de,

⁵MADIREL Aix-Marseille Univ., France, m.antoni@univ-amu.fr, ⁶Virginia Commonwealth Univ., Richmond, USA, jkferri@vcu.edu

Introduction

The PASTA experiment for the study of emulsion stabilisation/destabilisation started on board the ISS on February 2022 with a planned duration of 4 months.

Ordinary emulsions are mixtures of immiscible liquids in the form of dispersions of droplets, with sizes between tenths to tens of micron. These emulsions are intrinsically unstable and tends to separate into the constituent liquids. Emulsifying agents, containing surfactants that adsorbs at the droplet interface, are typically utilised to stabilise them. These agents, in particular hinder the basic processes responsible for the destabilisation, such as the droplet coalescence and Ostwald ripening, slowing down as much as possible the ongoing separation of the liquids. The PASTA experiment aims thus in particular at the investigation of the above elementary processes, in relation to the role (Liggieri et al., 2021) played by the physicochemical properties of the droplet interfaces, such as equilibrium interfacial tension and interfacial dilational viscoelasticity, which are induced and tuned by the presence of surfactants.

Microgravity conditions offer a unique opportunities for the investigation of the features of these elementary processes decoupled from droplet creaming, useful to push forward their comprehension and modelling, supporting the development of new concepts and sustainable and green methodologies in emulsion technology. Emulsion are in fact widespread in nature, products and technologies in many fields, such as foods, pharmaceuticals, cosmetics, paints, environment, oil and fuels, chemical processes, new materials, just to mention a few. The PASTA experiment is in fact conceived as part of the ESA MAP project "Emulsion Dynamics and Droplet Interfaces-EDDI", seeing the participation of a large academic and industrial partnership.

Experiment details

The current PASTA experiment involves 15 emulsion samples stabilised by non-ionic surfactants. Oil is a medium chain triglycerides (MCT, OIO-Germany) purified vegetable oil, interesting for applications in food, cosmetic and pharmaceuticals industry. The surfactant are non-ionic polyoxyethylenated alcohols (C12EO21 and C10EO5, Nikkol-Japan). The oil/water volume concentration in the emulsion samples ranges between 20:80 and 50:50. Surfactant concentrations varies over two decades, in a range providing from poor to good stabilisation on ground tests.

The experiments are performed in the ESA facility Soft Matter Dynamics (SMD) (Born et al., 2021) of the Columbus Fluid Science Laboratory.

The facility, allows for the study of dynamic and structural features of disperse media (foams, granular matter, emulsions) based on the Diffusing Wave Spectroscopy (DWS). The latter is a powerful optical technique based on the principles of the analysis of the intensity backscattered and transmitted of laser light diffusing in a multiphase disperse system. Details on the technique and on its application are available elsewhere (Hohler et al., 2014; Orsi et al, 2019; Salerni et al., 2019; Lorusso et al.,2021). In the PASTA experiments, the single samples are contained in individual cells, housed in a carousel. After bringing them in a processing area of the facility, the single samples are emulsified and then investigated at scheduled times from emulsification utilising the available DWS diagnostics, in order to characterise the structural and dynamic features of the emulsion as its destabilisation proceed during the first hundreds hours.

Preliminary results

On the considered timescale and for the investigated surfactants, we expect the evolution of these emulsions to be mostly driven by the process of droplet coalescence.

The DWS results from the PASTA experiment are mainly based on the following two types of acquisitions and analysis.

a) The temporal analysis of the intensity of backscattered and transmitted laser light in the sample, using self-correlation concepts. Such analysis provides relaxation times for the correlation functions which can be linked to the internal dynamics of the structure of the emulsion. In general terms, the backscattering signal is related to the size of scattering objects (the droplets), while the transmission signal is more related to the number of these objects. An example of the results from this type of analysis for one of the PASTA experiment is given in figure 1, where, the characteristic (1/e) relaxation times of the calculated correlation functions for the measured transmitted and backscattered intensities are plotted versus the age of the emulsion. According to a preliminary qualitative interpretation these signals correspond to a system where the number of droplets decreases under the effect of coalescence, while their size remain constant. That calls for an evolution of the emulsion structure, where large droplets are quickly growing their size by coalescence during the first hours (about 300 min). At larger emulsion age, the plateau in the backscattering relaxation time indicates that further coalescence between large droplets become rare. In fact, while the average droplet size, dominated by the large drops does not change, the number of droplets continue decreasing, as indicated by the increasing transmission relaxation time.

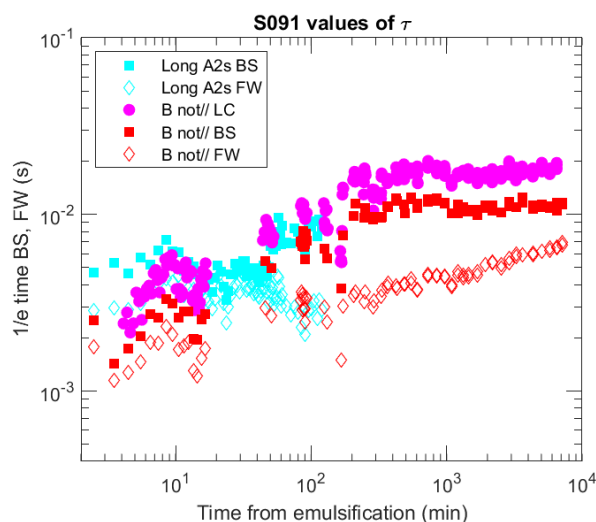


Figure 1: $1/e$ relaxation time of the backscattering (filled squares) and transmission (empty diamonds) correlation functions, as a function of the time from emulsification for the PASTA sample 09-1: oil/water ratio 20:80; surfactant (C12EO21) concentration 1×10^{-5} M in water. Circles indicate the backscattering relaxation times obtained from the Line Camera data (see text).

This is compatible with a situation where large droplets coalesce with small droplets, which in fact provides negligible increase of their size.

b) Time-resolved DWS analysis is applied to the backscattered light acquired by the Line Camera integrated in the facility. Such analysis allows in particular to study the features of transients in emulsion structure.

As an example, figure 2 reports the frequency of the transients during the early stage of the aging in microgravity of one of the PASTA emulsion sample, elaborated from the acquired Line Camera data. In the case of the studied emulsions we expect such frequency to be related to the occurrence of coalescence events. As shown by the figure, such frequency is generally decreasing with the progress of the emulsion aging.

Abrupt acceleration of such process are evidenced by the presence of spikes. The deeper analysis of the features of these spikes will allow for the identification of avalanche phenomena such as bursts of coalescence events.

Conclusions

The preliminary analysis of the DWS data from the PASTA experiment provides already a qualitative and quantitative insight on the phenomena associated with the aging of emulsions in conditions that are not reproducible on ground. More solid conclusions will stem from the analysis of these data based on ad-hoc models for the DWS that are being developed.

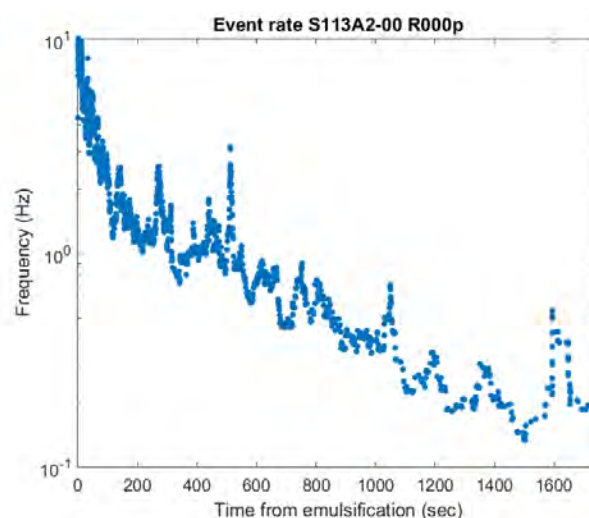


Figure 2: Frequency of the transients from the elaboration of the SMD line Camera data, for the early stage of the aging of the emulsion sample PASTA sample 11-3: oil/water ratio 50:50; surfactant (C12EO21) concentration 1×10^{-5} M in water.

Acknowledgements

ESA MAP Project "Emulsion Dynamics and Droplet Interface" (contract ESA 4000128643/19) and the other related industrial and academic partners contributing to the project development: Nikkol Chemical-Japan, Loufakis Chemistry-Greece, Unilever R&D Colworth-UK, 4Gene-Germany, Sinterface Technology-Germany, Arcofluid-France, Future Cooking Lab-Italy, St. Petersburg State University-Russia, Tokyo University of Science-Japan, Chiba Institute of Science-Japan.

References

- F. Ravera. et al., Emulsification and emulsion stability: the role of the interfacial properties, Advances in Colloid and Interface Sci, 288, 102344, (2021)*
- P. Born et al., Soft Matter Dynamics: A versatile microgravity platform to study dynamics in soft matter, Review of Scientific Instruments, 92, 12450, (2021).*
- R. Hohler et al., Multiple light scattering as a probe of foams and emulsions, Current Opinion in Colloid and Interface Science, 19, 242, (2014).*
- D. Orsi, et al., Diffusing wave spectroscopy for investigating emulsions: I. Instrumental aspects, Colloids Surfaces A Physicochem. Eng. Asp. 580 , 123574, (2019).*
- F. Salerni, et al. Diffusing wave spectroscopy for investigating emulsions: II. Characterization of a paradigmatic oil-in-water emulsion, Colloids Surfaces A Physicochem. Eng. Asp. 580, 123724, (2019).*
- V. Lorusso et al., Diffusing Wave Spectroscopy beyond average values, Advances in Colloid and Interface Science 288, 102341, (2021).*

ORAL 45

AID – Efficient Data Processing with Neuronal Networks for Microgravity

J. Auth¹, L. Schwarz², F. Zaussinger³

¹²³HS-Mittweida, Mittweida, Germany,

¹jan.auth@hs-mittweida.de, ²lschwar4@hs-mittweida.de, ³florian.zaussinger@hs-mittweida.de

Introduction

The performance of microgravity experiments, in contrast to ground-based experiments, is often restricted in measurement technology, which is a compromise between construction, weight, available experiment time and analyzability of measurements. The situation is further complicated, because the experiment-free time is mostly reserved for downloading or saving the data to local storage drives. During this time the experiment is in idle in order to check the measurement data for analyzability. This asynchronous analysis of the data brings the considerable disadvantage that technical problems or incorrect parameter selection are detected very late. A correction is then usually associated with considerable effort.

Hence, it is desirable to evaluate microgravity experiments in an early stage to determine the success or failure of the same, to influence the experiment to make it a success. To evaluate the experiment independent to crew, there is a need to ‘simulate’ an expert, which special ability is to decide which information is important and which is not to evaluate the experiment. In contrast to traditional programming the machine learning approach is suitable to implement expert knowledge without reasoning. And it has been shown that especially convolutional neuronal networks (CNNs) outperform human classification in various fields.

The AID (Artificial Intelligence Demonstrator) project aims to increase the efficiency of data processing in microgravity experiments. The measurement data is automatically analyzed for critical characteristics such as consistency, error and scientific interestingness. The main goal of the project is a universally applicable artificial intelligence (AI) for real-time analysis of the measurement data. In order to be able to use AID also in analog questions, resource-saving single-board computers are to be used as target hardware, such as Raspberry Pi or equivalent micro devices.

AID is going to be qualified on two experiments. The current schedule foresees, that the AI will be trained primarily on the ICAPS and Laplace experiments. Both experiments produce terabytes of data which makes it unfeasible to analyze the quality of results in real time.

ICAPS

The aim of ICAPS (Interactions in Cosmic and Atmospheric Particle Systems) and the LAPLACE experiment is to investigate experimentally the beginnings of planet formation, i.e., the growth of particles from micrometers to several millimeters. For this purpose, the development of a free-floating particle cloud and the agglomeration of the particles over timescales of minutes are investigated in a thin gas (approx. 50 mbar). A thermophoretic particle trap (Cloud-Manipulation-System, CMS) was developed which allows the cloud to be held in the center against diffusion and external residual accelerations. The cloud is observed by

two overview cameras (Overview Observation System, OOS) arranged orthogonally to each other with a connected high-speed camera and a Long-Distance-Mikroskop (LDM) in order to observe particle structures at the monomer level.

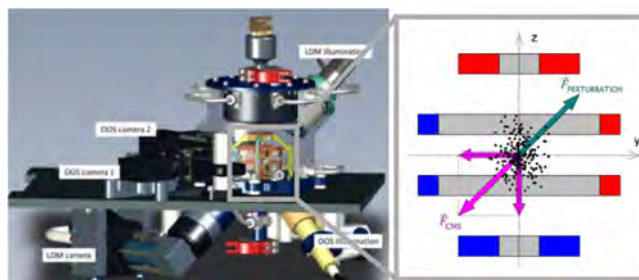


Figure 1: ICAPS experimental setup with CMS (right) and location of particle cloud (right).

The recordings of the OOS images are sent in their entirety to the ground station. However, the LDM images (see Fig. 2) exceed the transfer capacity, so AIM shall be applied to them where a CNN analyzes the images in nearly real time. The aim of AID is to detect the most scientifically interesting and affordable regions (dust particles) for later investigation. The available hardware is a compact, rugged x86 type board-level embedded Computer (Blackbird Embedded Processing Unit). Hence, large networks cannot be used here. Currently, AID is trained on ICAPS data. The application on LAPLACE is planned in January 2023.

AID within ICAPS

An (interpretable) AI will decide whether images or image areas of the LDM images are scientifically relevant or not. Fig. 2 (left) shows the original image and Fig. 2 (right) the post-processed and analyzed image after classification.

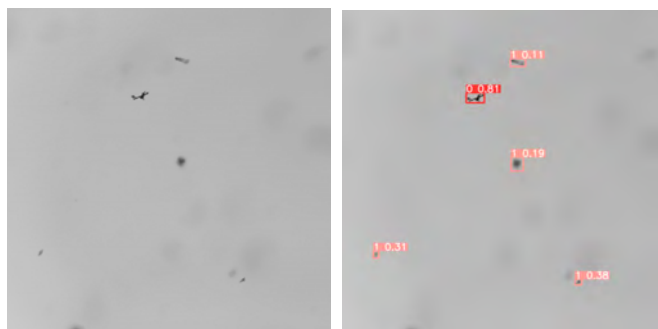


Figure 2: Recognition of particles by AID. Representative LDM image (left) with corresponding inference (right)

The images of less scientific relevance will be stored locally and after completion of the whole experimental campaign they will be sent to ground station.

In 347 images of the TEXUS-56 flight, 366 scientifically usable and 226 non-usable particles were labeled by a human expert. These data serve as training basis of the AI. The sharpness (x-axis) and the particle size (y-axis) are used for classification (see Fig. 3). The line separates particles of good and less quality. Examples of such particles are given in the corners of the figures.

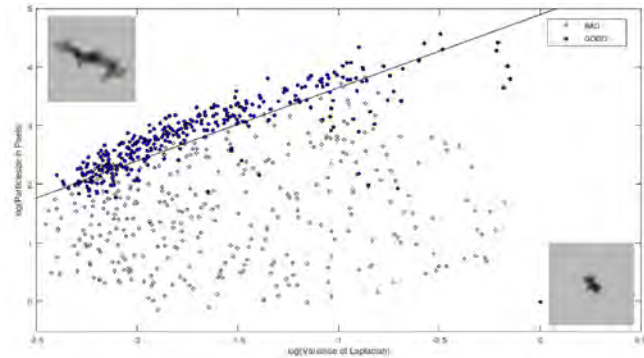


Figure 3: 2D feature space for separation of particles.

The goal of the AID project is to develop a universal AI demonstrator that can be quickly adapted to analog challenges. The approach is summarized as module structure in Fig. 4.

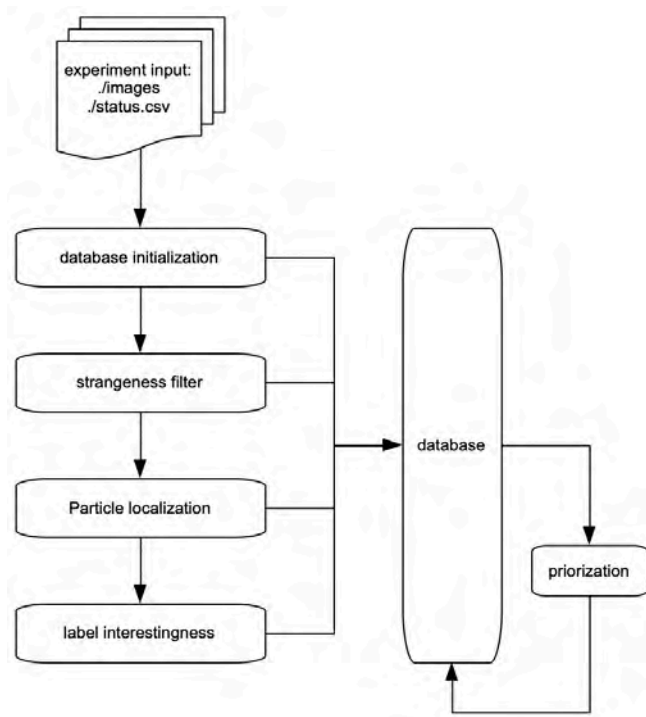


Figure 4: AID strategy

The AID receives images and a status-file with the information which sub-experiment corresponds to which image ID. This data is stored in a database and as the process progresses, the following information is added:

- strangeness number
- particle coordinates of interesting particles
- scaled features (sharpness, size of the particle, complexity, ...)

Based on this information, a prioritization is made according to a linear combination of the individual parameters.

Advantage of this linear combination is the easy comprehensibility and the possibility of the manual adjustment of weighting factors. The strangeness filter is realized via classical histogram-based image processing, so that it is possible to influence manually via parameter adjustments. The localization of potentially interesting particles and their classification will be realized with a commonly used Convolutional-Neuronal-Network (CNN) namely with YOLO v5. Preliminary results can be seen in Figure 2 (right). The first number corresponding to a box is dedicated to the class. 1 for not scientific interesting and 0 for scientific interesting. The second number corresponds to the probability how serious the network is for the classification to the group. AID is adaptable to all hard-to-access experiments where, on the one hand, training data sets exist and, on the other hand, robustness is required.

Conclusions

AID is a universal machine learning toolbox which is designed to analyze and to support micro gravity experiments with algorithms runnable on small devices such as Raspberry Pi. In the first stage AID is applied on ICAPS data where dust particles are recognized automatically. In future, AID will be applied on LAPLACE data, but also on the AtmoFlow experiment (BTU Cottbus-Senftenberg).

Acknowledgements

We thank all those involved in Project ICAPS and Laplace led by Prof. Blum (in particular Ingo von Borstel, Noah Molinski, Ben Schubert and Adrian Pöppelwerth) for their patience in transferring their knowledge to the AID and their encouragement and constant constructive cooperation. We thank DLR (DLR FKZ 50WM2163) for funding this research.

References

- J. Blum, Interactions in Cosmic and Atmospheric Particle Systems (ICAPS) - Examples of the Research Programme, ESA SP-454, 747-753, (2001)*
- F. Zaussinger et al., Recognition and tracking of convective flow patterns using Wollaston shearing interferometry. Advances in Space Research, 60(6):1327 – 1344, 2017.*
- J. Blum et al., Growth and Form of Planetary Seedlings: Results from a Microgravity Aggregation Experiment, Phys. Rev. Lett. 85, 2426-2429, (2000)*
- M. Krause and J. Blum, Growth and Form of Planetary Seedlings: Results from a Sounding Rocket Microgravity Aggregation Experiment, Phys. Rev. Lett. 93, 021103 (2004)*

ORAL 46

Soret coefficients of a ternary C₆₀-THN-Tol mixture: results from DCMIX4 experiments

A. Errarte¹, M. Schraml², W. Köhler², A. Mialdun³, V. Shevtsova^{1,4}, M. Mounir Bou-Ali¹

¹Mondragon Unibertsitatea Goi Eskola Politeknikoa, Arrasate-Mondragon, Spain
aerrarte@mondragon.edu | mbouali@mondrago.edu

²Universität Bayreuth Physikalischen Institut. Bayreuth, Germany
marcel.schraml@gmx.com | werner.koehler@uni-bayreuth.de

³Microgravity Research Centre, Université libre de Bruxelles, Brussels, Belgium
aliaksndr.Mialdun@ulb.be

⁴Ikerbasque, Basque Foundation for Science, Bilbao, Spain
x.vshevtsova@mondrago.edu

Introduction

Studies on non-isothermal mass transport phenomena are of high complexity since tiny disturbances of thermal nature can easily destroy the measurements. This is the reason why several years ago, the European Space Agency, together with Roscosmos, and several international laboratories formed the DCMIX (Diffusion Coefficient Measurements in ternary mIXtures) project, where the phenomenon of thermodiffusion in micro-gravity conditions has been studied.

In the framework of the fourth DCMIX mission, the Soret effect on a fullerene C₆₀-based ternary mixture has been investigated on the International Space Station by means of the Selectable Optical Diagnostics Instrument (SODI) [1].

Soret and effective diffusion coefficients by different data processing methods are reported for the mixture C₆₀-THN-Tol ternary mixture on a mass fraction of 0.0007-0.60-0.3993 at four different temperatures, 20°C, 25°C, 30°C and 35°C.

Facility and Measurement principle

SODI, which is on-orbit since 2009 and has been successfully used in all prior DCMIX campaigns, is a two-laser Mach-Zehnder interferometer (Figure 1).

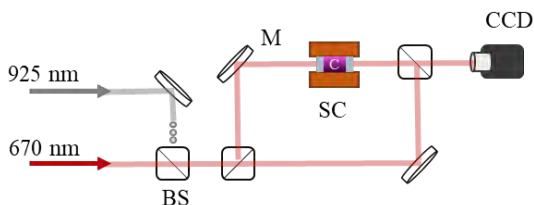


Figure 1: Sketch of SODI Mach-Zehnder Interferometer.

The interferometer simultaneously acquires data from the two wavelengths (670 nm MR and 935 nm MN lasers) and can sequentially access five cells with ternary mixtures. The experiments consist of two steps. First, the sample is homogenized, and second, almost instantaneously, a thermal gradient is applied. The temperature difference induces component separation, which allows determining the Soret coefficients of the mixtures.

Soret coefficients can be assessed by different processing methods, which may turn into different different coefficients. Both full path and differences method described in [2] has

been used to determine the Soret and effective diffusion coefficients and results have been compared to those determined by the novel Optical Beam Deflection based data processing method reported in [3].

Results

Figure 2 shows representative images regarding the processing method described in [2], the raw interferogram, the normalized refractive index map, the refractive index difference between the top and the bottom side of the Soret cell in function of time and the fitting of the full height of the cell for different time stamps.

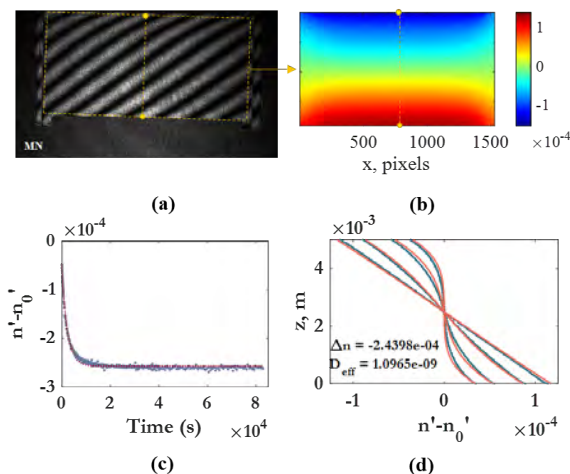


Figure 2: Interferogram processing steps based on [2], (a) raw interferogram, (b) RI map, (c) RI differences fitting and (d) full RI profile fitting in the centerline.

Conclusions

We present evaluation of the results of the C₆₀-THN-Tol mixture analysed in DCMIX-4 campaign performed on-board the ISS. We also discuss different data processing methods in order to address their effect on the transport coefficients. The analysis of these data once again demonstrates the importance of performing non-isothermal thermodiffusion experiments on-board the ISS.

As also observed for other ternary systems, the precise knowledge of the contrast factor matrix turns out to be the most critical step during the evaluation of ternary data. This sensitivity leads to very asymmetrically stretched error ellipsoids for the Soret coefficients in the 2d-space of the independent concentration variables. The high quality of the experiments and evaluation procedures is documented by the close aggregation around the long axis of this ellipsoid with a very good localization in the direction of one of the two diffusion eigenvectors. Due to the poor condition of the contrast factor matrix, a comparable localization in the direction of the second eigenvector is not possible without additional a priori assumptions.

Acknowledgements

M.S. and W.K. acknowledge the support by Deutsches Zentrum für Luft- und Raumfahrt (DLR) (Grants 50WM1544 and 50WM1850). A.E and M.BA acknowledge the support by KK-2021/00082 (micro4IoT), PRE_2021_0_0234, IT1505-22 (Research Group Program) from the Basque government, 2022-CIEN-000052-01 (HOZTIKOR) of the Gipuzkoa Provincial Council and PID2020-115086GB-C33 financed by MCIN/AEI of the Spanish Government.

References

- [1] A. Mialdun et al., Preliminary analysis of Diffusion Coefficient Measurements in ternary mixtures 4 (DCMIX4) experiment on board the International Space Station, *Eur. Phys. J. E*, 42, 1-9, (2019).
- [2] A. Mialdun, J.C. Legros, V. Yasnou, V. Sechenyh, and V. Shevtsova, Contribution to the benchmark for ternary mixtures: Measurement of the Soret, diffusion and thermodiffusion coefficients in the ternary mixture THN/IBB/nC12 with 0.8/0.1/0.1 mass fractions in ground and orbital laboratories, *Eur. Phys. J. E*, 38, 27, (2015).
- [3] D. Sommermann, T. Triller and W. Köhler, A robust data evaluation method for the DCMIX microgravity experiments, *Microgravity Sci. Tec.* 31, 465, (2019)

ORAL 48

The acute gravitational stress of parabolic flight affects red blood cell aggregation and functionality of circulating immune cells

A.Perez-Poch¹, J. Petriz², R. Salvia², L. G.Rico², M. D. Ward⁴, J. A. Bradford⁴, A. Gorgori³, G.Viscor³

¹Universitat Politècnica de Catalunya, Barcelona, Spain, antoni.perez-poch@upc.edu, ²Germans Trias i Pujol Research Institute, Barcelona, Spain, jpetriz@igtp.cat, ³Universitat de Barcelona, Barcelona, Spain, abrilgo2008@gmail.com, gviscor@ub.edu.

⁴Thermo Fisher Scientific, Eugene, Oregon, USA.

Introduction

Space exposure is the sum of biological, microbial, physical, and psychological stressors that influence crew members' physiological deconditioning in space. One of the biological systems that suffers a physiological deconditioning is the immune system. Briefly, this function is carried through circulating immune cells (neutrophils, monocytes, and lymphocytes) and organs (thymus, bone marrow, spleen, lymph node, and mucosa-associated lymphoid tissue).

The aim of this work was to assess if there are any relevant changes in the immune cells after a parabolic flight with a specific and unique profile. We hypothesize that the acute stress response caused by the intermittent exposure to hyper and microgravity could cause a change in the circulating leucocyte function and immunophenotype because of potential activation or de-regulation of some cell subtypes.

Materials and methods

Blood collection

Blood samples were obtained from 6 healthy human volunteers. From each sample, two aliquots were drawn; one stayed on ground whereas the other one was carried on a parabolic flight, being exposed to different gravitational loads. Both aliquots were maintained at equal temperature.

Parabolic flight

A parabolic flight campaign took place in Sabadell Airport (Barcelona, Spain) in March 2022 with 15 parabolas. This parabolic flight allowed for up to 8.5 seconds of microgravity per parabola, using a Mudry CAP10B aerobatic aircraft operated by Barcelona-Sabadell Aviation Club. This platform has successfully proven in the last decade to perform optimal parabolas with an average of 0.01g residual acceleration for both education and research purposes (Perez-Poch et al., 2016). Brief periods of hypergravity up to 3.2g preceded and followed each microgravity period. The samples were loosely attached to the cockpit avoiding vibrations or g-jitter, and the corresponding control samples were left on ground. Both samples were analysed in the Functional Cytomics Laboratory (IGTP) in the vicinities of the airport less than 2 hours after the flight.

Flow cytometry

Data were collected on an Attune™ NxT™ Flow Cytometer (Thermo Fisher), equipped with 4 lasers (405nm-violet, 488nm-blue, 561nm-yellow and 637nm-red), 14 fluorescent detectors and acoustic-assisted hydrodynamic focusing. Samples were prepared within 4-24h after parabolic flight for the assessment of red blood cells scattering, phagocytosis and oxidative burst, and for the analysis and quantification of T/B/NK-cells, according to the following protocols:

Red blood cells scattering: Briefly, 2µl blood were diluted in 1ml Hanks' Balanced Salts Solution (HBSS, Biowest). Diluted blood was acquired immediately and after a 15 minute-incubation at 37°C by flow cytometry for red blood cell scattering assessment following a protocol described by Rico et al. (2018).

Phagocytosis and oxidative burst: Samples were prepared following a minimal perturbation protocol (Rico et al. 2021). 50µl blood diluted in 1ml HBSS were incubated with 10µl Hoechst 33342 (1mg/ml), 2µl Dihydrorhodamine 123 (0.01mg/ml) and 10µl pHrodo™ (1mg/ml) (Thermo Fisher). For stimulation, 1µl PMA (1mg/ml) was added. Non-stimulated control samples were prepared with 1µl DMSO. Samples were incubated for 30 minutes at 37°C before flow cytometry analysis.

Immunophenotyping of TBNK cells: 100 µl blood were incubated with FITC-CD3, APC-CD4, Pacific Blue-CD8, Pacific Orange-CD16, AF700-CD19 and PE-CD56 (Sysmex). After incubation, samples were fixed and lysed with CyLyse™ (Sysmex) following manufacturer's instructions.

Data analysis: Data was analyzed using FlowJo™ v.10. For statistical analysis, GraphPad™ Prism v.9 was used.

Results

Red cell aggregation. Single cell analysis of erythrocytes was performed using flow cytometry. Single cell counts were as follows: median = 108951 cells, ranging from 83355 to 124822 cells (Group A) and median = 120506 cells ranging from 96252 to 140555 cells (Group B).

Oxidative burst. Single cell analysis of monocytes and neutrophils provided the following rhodamine 123 mean fluorescence intensity values: median = 36348 a.u. (arbitrary units), ranging from 23841 to 50336 a.u. (Group A) and

median = 32520 a.u. ranging from 22005 to 47900 a.u. (Group B).

Phagocytosis. Single cell analysis of phagocytes provided the following pHrodo mean fluorescence intensity values: median = 19902 a.u., ranging from 14850 to 25167 a.u. (Group A) and median = 22816 a.u. ranging from 18642 to 28794 a.u. (Group B).

Immunophenotyping. Peripheral blood obtained from 6 healthy donors was used for TBNK immunophenotyping. Flow cytometric results were analyzed using FlowJo™ v.10 in association with tSNE displays. CD3, CD4, CD8, CD19, CD56 and CD16 marker expression was studied before and after parabolic flight. Then, FCS files were concatenated and subjected to tSNE dimensionality reduction. CD19⁺ B cells, CD4⁺ T cells and CD8⁺ T cells, CD4⁺CD56⁺ NKTs, CD56⁺CD16^{dim} NKs, and CD56^{dim}CD16⁺ NKs subsets were clearly identified. After dimensionality reduction, no differences were observed when comparing the two different conditions.

Discussion

We have applied two specific methods aimed at potential metabolic changes in leukocyte function, including oxidative burst and phagocytosis. In addition we have assessed the TBNK immunophenotyping, and all the experiments involved the use of acoustic focused flow cytometry. To do this, we compared two different groups of healthy subjects in the setting of a blind trial. Even non-significant results were obtained, our results show a different tendency when comparing the two groups. Regarding erythrocyte cell counting, we observed an increase in Group B when compared with Group A. Previous studies (Marijke et al., 2017) have shown the effects of microgravity on red cell aggregation, with impact in important differences of aggregated cells formed in space and on the ground. Based on the observed differences between two groups, we elucidated that the Group A was composed by the set of samples subjected to brief periods of hypergravity and microgravity when compared with blood control samples that were left on ground (Group B), showing less aggregated cells. Interestingly, oxidative burst measurements were increased in Group A, whereas phagocytosis was decreased in the same group. It has been described that the oxidative burst reaction depends on gravity, responding rapidly to gravity changes in just few seconds (Adrian et al. 2013). On the contrary, phagocytosis was also altered, suggesting that hypergravity and microgravity also modify phagocytic function in humans. Interestingly, we did not observe any significant change in cell counting and TBNK cell subsets, indicating that more prolonged dependence of time exposure to changes in gravity should be needed.

Conclusions

Taken together, our results suggest that short exposure to gravity variations may result in functional cellular changes

that can be detected using flow cytometry. Cell immunophenotyping was unaffected, indicating that time exposure to gravity changes above a relevant threshold can promote further alterations. More studies will be needed to elucidate how gravity changes may alter cell immunophenotyping and function, with promise that these preliminary experiments provide valuable information after short exposure conditions.

Acknowledgements

The authors would like to thank Daniel V. González, pilot of the aircraft, and the Barcelona-Sabadell Aviation Club for the logistic support to operate this parabolic flight. We are also grateful to the informed volunteers who produced the experimental samples. This study was partially supported by Thermo Fisher Scientific. We thank the CERCA Programme/Generalitat de Catalunya and the Germans Trias i Pujol Research Foundation for institutional support and also acknowledge financial support from the Obra Social la Caixa.

Ethics Statement

This study was conducted according to the principles expressed in the Declaration of Helsinki. All participants had voluntarily given their written informed consent for this study.

References

- A. Perez-Poch, D. V. Gonzalez, D. Lopez, Hypogravity research and educational parabolic flight activities conducted in Barcelona: a new hub of innovation in Europe, *Microgravity Sci. Technol*; 28, 603-609 (2016).
- LG. Rico, J. Juncà, MD. MD. Ward, JA. Bradford, J. Bardina, J. Petriz. Acoustophoretic Orientation of Red Blood Cells for Diagnosis of Red Cell Health and Pathology, 8(1):15705, *Scientific Reports* (2018).
- LG. Rico, R. Salvia, MD. Ward, JA. Bradford, J. Petriz. Flow-cytometry-based protocols for human blood/marrow immunophenotyping with minimal sample perturbation, *STAR Protocols*, 2(4):100883 (2021).
- G. Marijke, A. Vera, V. Tobias, B. Wilhelm, S. Stefan. Erythrocyte deformability and aggregation responses to intermittent and continuous artificial gravity exposure. *Life Sci Space Res (Amst)*. Feb;12:61-66 (2017).
- A. Adrian, K. Schoppmann, J. Sromicki, S. Brungs, M. von der Wiesche, B. Hock, W. Kolanus, R. Hemmersbach, O. Ullrich. The oxidative burst reaction in mammalian cells depends on gravity. *Cell Commun Signal*. Dec 20;11:98 (2013).

ORAL 50

PEDOT:PSS electrodes in view of low-cost biocompatible cellulose-assisted biosensors

H. Machrafi^{1,2}, F. Iermano¹, C.S Iorio¹

¹Physical Chemistry Group, Université libre de Bruxelles, Brussels, Belgium, hatim.machrafi@ulb.be, fabio.iermano@ulb.be, carlo.iorio@ulb.be, ²GIGA-In Silico Medicine, Université de Liège, Liège, Belgium, h.machrafi@uliege.be

Introduction

The technological development of the last years has led to the birth of a new type of industry called “Industry 4.0”. This term includes, amongst others, the Internet of Things (IoT), which is the extension of internet connectivity into physical devices and everyday objects. The Internet of Medical Things (IoMT) is an IoT application for medical and health-related purposes, data collection and analysis for research, and monitoring. Developments in plastic and electronics fabrication methods have enabled ultra-low-cost IoMT sensors (Da Costa et al. 2018). The increasing necessity for small electronics and wireless technologies in energetic devices, such as batteries or superconductors and in medical devices, such as sensors, drug delivery systems, calls for new materials, devices and preparation methods. Such devices are not only important for space-related low-energy supply or medical monitoring, but also for on-ground biosensing applications. In this work, the possibility of using a PEDOT:PSS hydrogel film as a cathode for a biocompatible cellulose-assisted biosensing device has been explored. The effect of film formulation and preparation method on the electrical conductivity is investigated, i.e. adding a cross-linker and different solvent additives on one side and adding an ionic liquid with and without a metal salt on the other side, for two film thicknesses. The chemical composition of the electrode is studied as a function of the used formulation as well as after being used as cathode in the biosensing device. Several characterizing methods are used to investigate the electrical performance of the electrode as well its chemical stability and capability to serve in a biosensing device.

Sensor assembly

Figs. 1(a) and 1(b) present a scheme for the used sensor assembly. A particular geometry (Fig. 1(a)) with a groove for the sensor elements and holes to allow assembly was designed and produced with a 3D printer. The grooves designed have a thickness of 0.4 mm, which ensure good adhesion of the various components once assembled, allow the necessary passage of air and provides for terminals that can be connected to the measuring instruments. The doped PEDOT:PSS electrode serves as the cathode, while a 0.25 mm thick zinc (Zn) foil (Sigma-Aldrich) serves as an anode. The doped PEDOT:PSS electrode are prepared by drying a thin film solution of the order of 1 mm of its solution, obtaining a dried film of 20 μm. One of the reasons is that in such thin films of solution buoyancy is negligible with respect to surface-tension-induced convection, prevalent at microgravity. As such, we can mimic on ground the preparation of PEDOT:PSS films at microgravity conditions. A dry cellulose filter paper, with pore sizes from 20 to 25 μm, separates the electrodes. As graphene has a high conductivity,

its addition to the separator appeared to be beneficial and improve ionic charge transfer. To prepare the graphene-coated separator, the chromatographic paper was immersed in a dispersion of 2 mg/mL graphene, purchased from Cambridge University, and left to dry out for 6 hours. To ensure a good connection, an 80 μm thick gold foil was glued directly to the PLA supports and pressed, respectively, on both sides of the electrodes. A square hole was cut in the PEDOT:PSS electrode and in the PLA support at its side, leaving the filter paper exposed. Finally, all these components were stacked together and then everything was held with Teflon screws. After the assembly of the sensor, it was connected to a SourceMeter measuring instrument, a certain known amount of PBS (Phosphate Buffered Saline buffer) is added on the exposed filter paper, triggering a current response and the discharge test was started and the current was measured.

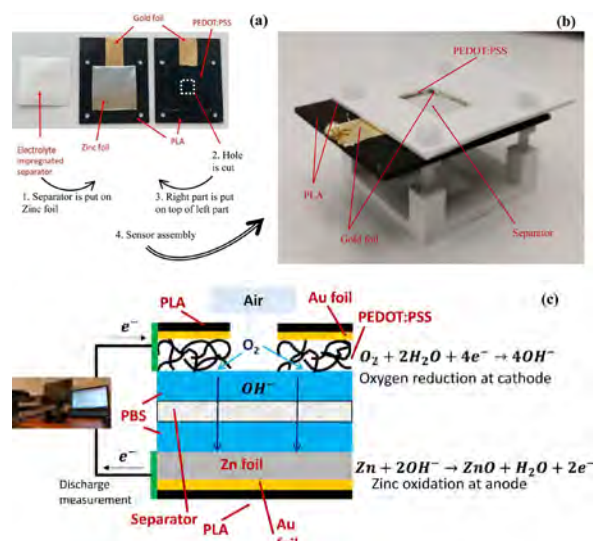


Figure 1: (a) Sensor assembly, (b) assembled biosensor, (c) schematic representation of the chemical reactions during electrolyte measurement by the biosensor.

Fig. 1(c) shows the assembled sensor with the chemical process taking place during the sensing. When the separator is dry, the electric circuit is not closed, and nothing happens. As soon as the PBS is added on the separator it wets the space between the respective electrodes and the separator. This will make the PEDOT:PSS hydrogel swell, creating micro/nanopores for oxygen to diffuse through and enabling the oxygen reduction reaction. As such, the electric circuit is now closed, and a redox reaction starts to occur. The oxygen from the air is reduced at the PEDOT:PSS cathode, releasing hydroxyl ions that diffuse through the electrolyte towards the zinc anode where it oxidizes zinc to zinc oxide (Gu et al. 2017). The measured current's value will change as the concentration of electrolytes in the PBS changes.

Electric properties and chemical stability

Table 1 shows the electric properties (sheet resistance R_s , electric resistivity ρ and electric conductivity σ), measured by the four-point method, of the PEDOT:PSS electrode for two thicknesses and as a function of ionic-liquid doping.

Table 1: Obtained values for electric properties of the PEDOT:PSS electrodes

Film thickness	IL [wt%]	R_s [Ω]	ρ [$\mu\Omega\text{m}$]	σ [kS/m]
140 μm	0	21.9	$3.07 \cdot 10^3$	0.33 ± 0.01
	15	1.05	147	6.8 ± 0.1
	30	0.72	101	9.9 ± 0.1
	45	0.99	139	7.2 ± 0.1
	60	0.54	75.6	13 ± 0.1
20 μm	0	-	-	-
	15	4.00	80	13 ± 3
	30	1.52	30.4	33 ± 6
	45	1.85	37	27 ± 4
	60	1.63	32.6	31 ± 5

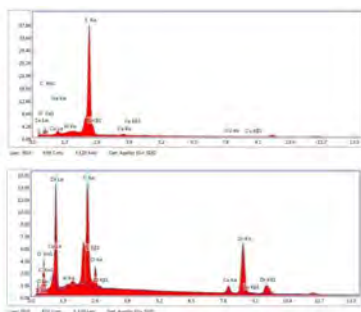


Figure 2: EDS spectra of the PEDOT:PSS spectra (upper) before using the sensing device and (lower) after complete discharge.

The electric conductivity of the pure PEDOT:PSS film agrees well with that measured in the literature (Hakansson et al. 2017). The ionic liquid had a clear enhancing influence on the electric conductivity, with a higher conductivity for the thinner film. Fig. 2 shows EDS images of the PEDOT:PSS after discharge, comparing it to the one before. Some traces of K, Cu and Cl are observed in Fig. 2. The K and Cl traces may come from the PBS, indicating some adsorption of KCl salt on the PEDOT:PSS. Fig. 2 clearly shows that, comparing the EDS spectra before the use of the PEDOT:PSS electrode and after its use, the oxygen and zinc content in the latter are substantially increased. This again shows that ZnO has been deposited on the PEDOT:PSS electrode, suggesting that the predominant reactions are indeed those between atmospheric oxygen and zinc as illustrated in Fig. 1(c), where PEDOT:PSS mainly serves as an electrode and, in aqueous medium, as a catalyst for the oxygen reduction reaction. Change in the chemical structure of the PEDOT:PSS has not been significantly observed in this work and is also confirmed by cyclic voltammetry tests. This could possibly indicate several reuses of the PEDOT:PSS electrode for the sensing device.

Towards biosensing properties

Fig. 3 shows the current response as a function of the absorption of a variable quantity of deposited electrolyte of up to 20 μL . It shows an increase of the current response as the quantity of electrolyte is added. Varying only 5 μL , there is an

evident variation of the current of almost 0.3 mA, which can easily be evaluated with common instruments. This result shows it would be possible to predict the current values for each quantity of liquid that is absorbed and associating it with a very simple system, which would generate a true sensor capable of constantly monitoring the healing process of a wound. A calibration procedure added, this would be a promising biosensor prototype.

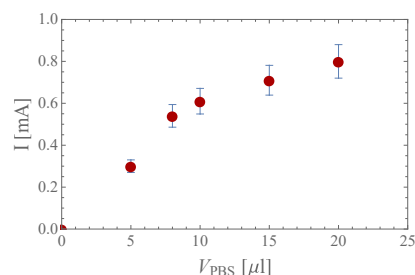


Figure 3: Current response generated by the deposition of different quantities of PBS.

Conclusions

The electrode based on the ionic liquid showed a considerable increase in electrical performance, although the mechanical stability was not easy to maintain. The thin film showed a higher electrical conductivity. EDS and cyclic voltammetry tests showed a chemical stability of the electrode. Concentrations of the order of μL were measured without difficulty and the cathode seemed to be chemically stable and therefore reusable, opening future applications in reusable low-cost wearable biosensors and with some adaptations also corresponding wearable batteries. The analysis shows that most probably this device is indeed functioning correctly and demonstrates, although further development is necessary, the possible application as a long-term monitoring sensing device. Due to the scale of the films during the preparation procedure, we are dealing with convection conditions that are prevalent at microgravity conditions. As such, these types of devices would be possible to fabricate in space. The presented fabrication process makes it easier to predict the quality of the PEDOT:PSS electrodes that would be prepared in microgravity.

Acknowledgements

This research has received funding from the European Union H2020 Programme under Grant agreement number 785219: Graphene Flagship. G. Wallaert, V. Gallo, I. Bobinac and P. Dongo are thanked for their contributions in the experiments.

References

- C.A. da Costa, C.F. Pasluosta, B. Eskofier, D. Bandeira da Silva, R. da Rosa Righi, Internet of Health Things: Toward Intelligent Vital Signs Monitoring in Hospital Wards, *Artificial Intelligence in Medicine*, 89, 61-69, (2018).
- P. Gu, M. Zheng, Q. Zhao, X. Xiao, H. Xue, H. Pang, Rechargeable zinc-air batteries: a promising way to green energy, *J. Mater. Chem. A* 5(17), 7651-7666, (2017).
- A. Hakansson, S. Han, S. Wang, J. Lu, S. Braun, M. Fahlman, M. Berggren, X. Crispin, S. Fabiano, Effect of (3-Glycidyloxypropyl) trimethoxysilane (GOPS) on the electrical properties of PEDOT:PSS films, *J. Polymer Sci. B: Polymer Physics*, 55, 814-820, (2017).

ORAL 51

Granular gas mixtures: Experiments and machine learning-aided analysis

D. Puzyrev¹, K. Harth^{1,2}, T. Trittel¹ and R. Stannarius¹

¹Institute of Physics, Otto von Guericke University, 39112 Magdeburg, Germany

²Department of Engineering, Brandenburg University of Applied Sciences, 14770 Brandenburg an der Havel, Germany
e-mail: dmitry.puzyrev@ovgu.de

Granular gases are dilute ensembles of granular matter which exhibit fascinating dynamical behavior far from equilibrium, e. g. unusual granular cooling properties, violation of energy equipartition, or clustering. Within these ensembles, the macroscopic particles propagate freely in space and interact by dissipative collisions. So far, most studies have been theoretical or numerical, and only few experiments were performed, mainly in two dimensions (2D). Falcon et al. showed dynamical clustering in a pioneering sounding rocket experiment [1], but no analysis on the grain scale level was possible. Currently, an instrument is being prepared for the experiments at the International Space Station [2].

The experimental realization of excited (permanent energy input) or cooling regimes (stop of external energy input after excitation) of granular gases in particular requires microgravity of high quality, e. g. on suborbital rocket flights or in drop towers [3]. Another important issue is the trackability of particles in large ensembles in 3D. In gases of rod-like particles, the mean free path is substantially reduced as compared to gases of spherical grains of identical volume fraction [4]. In addition to that, elongated grains allow the straightforward analysis of rotational degrees of freedom.

The experimental study of 3D granular gas mixtures is a particularly unexplored topic. The energy transfer between the mixture components and individual DOFs can strongly influence the dynamics inside the gas. We have performed a set of experiments focusing on granular cooling of the mixture of rods with two different aspect ratios [see Fig. 1]. The fulfillment of Haff's equation [5] describing the energy decay in such system is of particular interest. The experiments were done on the ZARM Drop Tower in Bremen. Preliminary experimental data analysis suggests different cooling rates, as well as different energy partition between the rotational and translational degrees of freedom for two mixture components. We have also performed DEM simulations of the rod mixtures in order to support the experimental findings and provide some insight on the cooling process.

One particular problem in the data analysis is the reliable detection and tracking of the rods in 3D, especially at volume fractions beyond the very dilute limit, which are desirable in granular gas mixture experiments in order to provide efficient energy transfer between the mixture components. At the ELGRA 2019 Symposium, we presented the first version of Machine Learning-aided software for the 3D tracking of positions and orientations of elongated particles in the ensemble, based on two-perspective video data analysis [6]. Since then, the software was significantly improved, including collection of a comprehensive dataset with 2000 annotated images (> 200,000 particle instances) from different experiments with various volume fractions, as well as experiments with mixtures. Additionally, a custom GUI

was developed for the efficient correction of results of ML-aided detection. The software can be extended to other 3D and 2D particle tracking problems.

Acknowledgements

The authors gratefully acknowledge funding by the German Aerospace Center DLR, Projects EQUIPAGE (50WM1842) and EVA (50WM2048). We are thankful to ZARM for the help with the microgravity experiments.



Figure 1: Granular gas mixture of rod-like particles with two different aspect ratios, image from the drop tower microgravity experiment (one of the views). The container dimensions are 11.2x8x8 cm.

References

- [1] É. Falcon et al., Cluster Formation in a Granular Medium Fluidized by Vibrations in Low Gravity, *Phys. Rev. Lett.*, 83, 440-443 (1999)
- [2] M. Noirhomme et al., Threshold of gas-like to clustering transition in driven granular media in low-gravity environment, *EPL*, 123, 14003 (2018)
- [3] K. Harth, T. Trittel, K. May, S. Wegner and R. Stannarius, Three-dimensional (3D) experimental realization and observation of a granular gas in microgravity, *Advances in Space Research*, 55, 1901 – 1912 (2015)
- [4] K. Harth, T. Trittel, S. Wegner, and R. Stannarius, Free cooling of a granular gas of rodlike particles in microgravity, *Phys. Rev. Lett.*, 120, 214301 (2018); K. Harth, U. Kornek, T. Trittel, U. Strachauer, S. Höme, K. Will, and R. Stannarius, Granular Gases of Rod-Shaped Grains in Microgravity, *Phys. Rev. Lett.*, 110, 144102 (2013)
- [5] P. K. Haff, Grain flow as a fluid-mechanical phenomenon *Journal of Fluid Mechanics*, 134, 401-430 (1983)
- [6] D. Puzyrev, K. Harth, T. Trittel, R. Stannarius, Machine Learning for 3D Particle Tracking in Granular Gases, *Microgravity Sci. & Technol.*, 32, 897–906 (2020)

ORAL 52

Change in circulating collagen type II biomarkers (CTX-II, C1,2C, C2C) in response to 21-days of Head-Down-Tilt Bed Rest (HDT-BR) and countermeasures.

Elie-Tino Godonou^{1,2}, Nadja Djalal^{1,2}, Maren Dreiner³, Anne Mündermann⁴, Frank Zaucke⁵, Martina Heer⁶, Georg Schett¹, Anja Niehoff^{3,7} and Anna-Maria Liphardt^{1,2}

¹Dep. of Internal Medicine 3 – Rheumatology & Immunology, Universitätsklinikum Erlangen & Friedrich-Alexander-Universität (FAU) Erlangen-Nürnberg, Erlangen, Germany ²Deutsches Zentrum für Immuntherapie (DZI), Universitätsklinikum Erlangen & FAU Erlangen-Nürnberg, Erlangen, Germany ³Inst. of Biomechanics & Orthopaedics, German Sport University Cologne, Köln, Germany ⁴Dep. of Orthopaedics and Traumatology, University Hospital Basel, Basel Switzerland ⁵Research Unit for Osteoarthritis, Dep. of Orthopaedics (Friedrichsheim), University Hospital Frankfurt, Goethe University, Frankfurt/Main, Germany ⁶Dep. of Nutrition and Food Science, Nutritional Physiology, University of Bonn, Bonn, Germany, ⁷Cologne Center for Musculoskeletal Biomechanics (CCMB), Medical Faculty, University of Cologne, Köln, Germany.

Introduction

Mechanical stress and physical activity are an important regulator of articular cartilage metabolism (Musumeci et al. 2016; Hernández-Hermoso et al. 2021). Immobilization can change tissue morphology and characteristics (Musumeci et al. 2016; Vincent et al. 2019), and HDT-BR offers an unloading model that allows to examine these effects using soluble biomarkers of cartilage metabolism (Liphardt et al. 2018). The aim of this study was to observe serum concentrations of carboxy-terminal cleavage neoepitope (C1,2C), type II collagen (CII)-related neoepitope (C2C), and urinary concentration of crosslinked C-telopeptide (uCTX-II) in response to prolonged HDT-BR and to investigate how possible changes are affected by resistive vibration exercise (RVE) alone or in combination with a protein enhanced diet (NeX) and study duration.

Methods

The ESA-funded “Medium duration nutrition and vibration exercise” (MNX) -study was conducted in a cross-over design with three campaigns (1, 2 & 3) of 34 days each: seven days of basic data collection (BDC-7 – BDC-1), 21 days of HDT + intervention (HDT1 – HDT21) and six days of recovery (R+1 – R+6). Study campaigns were separated by a wash out period of four months. Resistive vibration exercise (RVE) (Blotner et al. 2007), nutrition + RVE (NeX) and a control (CON) condition were the applied interventions. Twelve healthy male subjects (age 34.2 ± 8.3 years; BMI 22.4 ± 1.7

kg/m²) participated in the study. Blood was collected at BDC-3 to -1, HDT2, HDT3, HDT5, HDT7, HDT14 and HDT21, and at R1 and R6 of the recovery (R) period. Urine samples were collected as 2nd void morning urine (BDC-3, BDC-2, BDC-1, HDT2, HDT3, HDT5, HDT7, HDT14, HDT21, R+1, R+6) and 24-hours (24H) urine collection (BDC-4, BDC-3, HDT3, HDT4, HDT11, HDT14, HDT20, HDT21, R+3, R+4). Serum (s) concentrations of C2C and C1,2C and urinary (u) CTX-II concentrations in 2nd void and 24H were measured using Enzyme-linked immunosorbent assays (C2C & C1,2C - ELISA, IBEX Technologies Inc., Montreal, Canada; (CTXII) Urine CartiLaps® EIA, Immunodiagnostic Systems Limited). Linear Mixed-Effects Models were used to detect significant changes in the biomarkers.

Results

At BDC-3 of C1, the means of uCTX-II (2nd Void and 24H), sC2C, and sC1,2C, were 212.3±48.1 (ng/mmol Cr), 205.9±62.1 (ng/mmol Cr), 95.2±23.8 ng/mL, and 0.43±0.17 ng/mL, respectively. There was a significant main effect of HDT-BR/time points (p<0.001) on CTX-II urinary concentration in both 2nd void and 24H urines. The main effect of intervention was not significant on uCTX-II 2nd void, but statistically significant on uCTX-II 24H (p=0.0121) concentration with a decrease of 12.4% when the intervention was NeX, compared to CON. For both uCTX-II markers, the highest increase in concentration did appear at HDT21, and was of 82.8% for uCTX-II 2nd void (p<0.001) and 77.8% for

uCTX-II 24H ($p < 0.001$). The main effect of time points ($p = 0.0011$) and intervention ($p = 0.0121$) was also statistically significant for sC1,2C. During HDT-BR, sC1,2C has slightly increased, with the highest value at HDT3 (12.3%, $p = 0.004$). When the intervention was NeX, sC1,2C was 0.03 ng/ml higher ($p = 0.010$) compared to CON. sC2C at each time point of HDT-BR (HDT2 to HDT21) was significantly higher ($p < 0.001$) compared to baseline, with the highest increase of 24.2% at HDT7 ($p < 0.001$). sC2C still increases significantly from R1 to R6 (11.1%, $p = 0.003$). However, no countermeasure effect was detected for sC2C during HDT-BR.

The main effect of campaign is statistically significant ($p < 0.001$) for sC2C, sC1,2C, and uCTX-II 2nd Void & 24H ($p = 0.005$). A significant decrease of sC2C is noted over campaigns, with the highest decrease of 9.1% ($p < 0.001$) at Campaign 3, compared to campaign 1. Similar decrease was noted for sC1,2C, with the highest decrease of 27.9% at campaign 3. sC2C was not statistically different between campaign 2 and 3, while there was a significant difference of sC1,2C between campaign 2 and 3. A significant carry-over effect of campaign was noted for sC1,2C (BDC-2 to -1, R-1 to -6 of campaign 2 and BDC-1 of campaign 3) and sC2C (R6 of campaign 2 and 3). No carry-over effect was detected for uCTX-II 2nd Void and 24H.

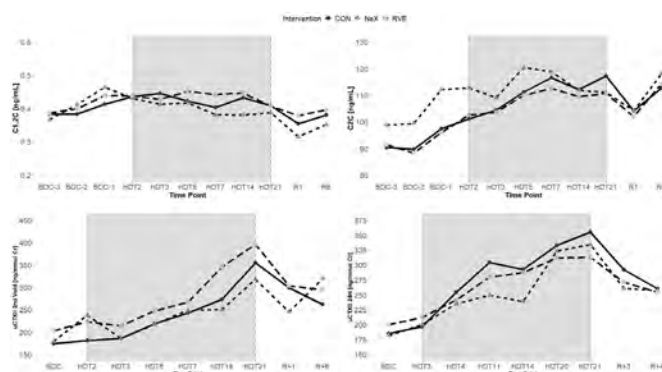


Figure 1: Mean concentrations of sC1,2C (top row left), sC2C, (top row right), uCTX-II 2nd void (bottom row left), and uCTX-II 24H (bottom row right) pre-, during- and post 21 days of HDT bed rest for the CON, NeX and RVE interventions.

Conclusion

21-days of HDT-BR caused substantial changes of cartilage biomarker concentrations reflecting collagen type II degradation during bed rest induced unloading in healthy male individuals. The marker concentrations did not regain their baseline values within a week after the end of the bed rest periods. Furthermore, concentrations of the two biomarkers sC1,2C and uCTX-II (24H) were affected by the NeX countermeasure. The significant effect at certain time points of campaign for some of the markers may indicate a carry-over effect, reflecting a persistent effect of the previous campaign (s) (HDT-BR) or intervention (s) on collagen type II biomarker concentrations.

Acknowledgements: This study was funded by the European Space Agency and the German Federal Ministry of Economic Affairs and Climate Action with the German Aerospace Center (Grant # 50WB0913, 50WB1217, 50WB1719, 50WB2021, 50WB2022).

References

Blotner D, Püttmann B, Salanova M, et al. Skeletal muscle deconditioning, nitric oxide (NO) biomarker, and exercise countermeasure-five years of bed rest studies. *J Gravitational Physiol*, 13, 49–58, (2007).

Hernández-Hermoso, J. A., Nescolarde, L., Roca, et al., Marathon Running Increases Synthesis and Decreases Catabolism of Joint Cartilage Type II Collagen Accompanied by High-Energy Demands and an Inflammatory Reaction. *Frontiers in physiology*, 12, 722718, (2021).

Liphardt AM, Mundermann A, Andriacchi TP, et al., Sensitivity of serum concentration of cartilage biomarkers to 21-days of bed rest, *J Orthop Res*, 36, 1465-71, (2018).

Musumeci G, The Effect of Mechanical Loading on Articular Cartilage, *Journal of Functional Morphology and Kinesiology*, 1,154-161, (2016).

Vincent, T. L., Wann, A., Mechanoadaptation: articular cartilage through thick and thin, *The Journal of physiology*, 597, 1271–1281, (2019).

ORAL 53

Hair follicles for non-invasive health monitoring on-site on the ISS Space Station and hair follicles derived retinal organoids for off-site biomedical research.

D.Bezdan^{1,2,4}, K. Achberger³, A. Bernal-Vergara³, V. Cora, S.Liebau³, S.Ossowski¹

¹Institute of Medical Genetics and Applied Genomics, University of Tübingen, Tübingen, Germany, ² NGS Competence Center Tübingen (NCCT), University of Tübingen, Tübingen, German, ³ Institute of Neuroanatomy & Developmental Biology (INDB), Eberhard Karls University Tübingen, Österbergstrasse 3, 72074, Tübingen, Germany, ⁴ Yuri GmbH, Germany

Introduction

Microgravity environments have significant advantages for biotechnology engineering and great risks for human space exploration. Here we like to present a novel technology to monitor astronaut health and provide new opportunities in space biotechnology engineering. In this novel non-invasive technology, we use hair roots of plucked hair to isolate cells as source material for health monitoring and production of organoids for biotechnology assignments like drug screening.

Hair roots provide several cell sources (keratinocytes of the outer root sheath, fibroblasts, and hair root cells) and are extremely easy and non-invasively harvested from every individual by plucking hair from various body parts with a focus on scalp and beard. Furthermore, hair roots can easily be subjected to cryopreservation or direct RNA extraction in a very space-saving manner preserving the excellent opportunity for long-term health studies.

Furthermore, harvesting those cells in microgravity conditions like the absence of sedimentation, hydrostatic pressure, tangential stress by the weight of fluids and shear forces will enhance the formation of natural 3D cell agglomeration. Those unique in vivo conditions lead to a new strategy for tissue engineering of multicellular cancer spheroids, organoids, artificial vessel constructs, and a variety of tissues for new opportunities for drug screening and biomarker discovery.

Conclusions

In summary, we suggest that hair keratinocytes are one of the most suitable cell reservoirs for long-termed and close-meshed investigations in space and could contribute to the understanding of the effect of microgravity on the human body and additional would be a great start for biotechnology engineering on the ISS space station, Moon or Mars.

ORAL 54

Microgravity experiments on Red Blood Cell aggregation dynamics in flow

T. Podgorski^{1,2}, F. Yaya², S. Losserand², V. Audemar², G. Coupier², C. Minetti³

¹Université Grenoble Alpes, CNRS, Grenoble-INP, Laboratoire Rhéologie et Procédés (LRP), F-38000 Grenoble, France, thomas.podgorski@univ-grenoble-alpes.fr, ²Université Grenoble Alpes, CNRS, Laboratoire Interdisciplinaire de Physique (LIPhy), F-38000 Grenoble, France, ³Université Libre de Bruxelles (ULB), Brussels, Belgium, christophe.minetti@ulb.be,

Introduction

Blood plasma proteins, especially fibrinogen, are responsible for a reversible aggregation of red blood cells (RBCs) which is known to increase blood viscosity. In spaceflight, this viscosity increase in stagnant or low shear regions promoted by microgravity together with haematological changes may favor coagulation and thrombi. For instance, a recent study on ISS crew members has shown that stagnant or retrograde flow in the jugular vein frequently occurs and may be associated with the development of occlusive thrombi during spaceflight (Marshall-Goebel et al. 2019). This suggests that microgravity may induce an enhanced coagulation state and possibly hypercoagulability in which aggregation could be a first step in the route towards coagulation and thrombus development.

The size, shape and structure of these aggregates, which determine blood rheology, are governed by a balance between hydrodynamic forces and aggregation forces that may significantly vary in conditions affecting blood composition and properties such as long-term space flight. A central issue for the understanding and modeling of blood aggregation and rheology is the description of the distribution of aggregate sizes and the rates of aggregation and disaggregation of red blood cells.

We studied this phenomenon during CNES parabolic flight campaigns (VP131, 139 and 145, 2017-2019) to eliminate the effects of sedimentation. In these experiments, a suspension of red blood cells suspended in a buffer containing a controlled concentration of aggregation-promoter (Dextran) was subjected to simple shear flow in order to analyze the size distribution of aggregates as a function of hydrodynamic and physico-chemical parameters. The collected data will improve the understanding and modeling of blood rheology. In parallel, microfluidic experiments make it possible to study aggregation in more complex flow geometries, that are representative of the microcirculation.

Results

The experimental setup consists in a shear flow chamber that was developed by the Swedish Space Corporation for previous BIOMICS experiments in MASER 11 and 12 (Podgorski et al. 2011) integrated in a Digital Holographic Microscope that was developed at ULB for parabolic flight experiments (Grandchamp et al. 2013, Podgorski et al. 2020) and allows to monitor the dynamics and shape of cells in a flow as well as the 3D-structure of the suspension (Minetti et al. 2014).

The data obtained by holographic microscopy were processed in order to extract the phase volume of the detected objects in

the suspension. By taking into account the refractive indices of the different media (suspending solution and hemoglobin solution contained in the red blood cells), the physical volume of objects can be recovered with very good precision. The histograms of the volume of objects in the suspension then clearly show peaks corresponding to the average volume of a red blood cell (80-100 μm^3) and its multiples corresponding to aggregates of 2, 3, 4 cells etc... (Fig. 1).

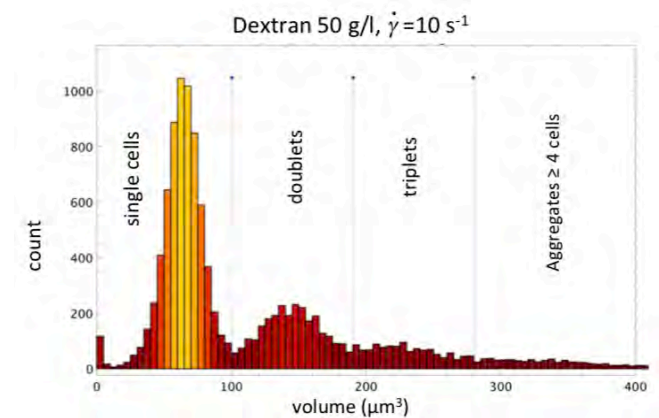


Figure 1: Sample distribution of aggregate sizes at the end of a parabola (shear rate 10 s^{-1} , dextran concentration 50 g/l)

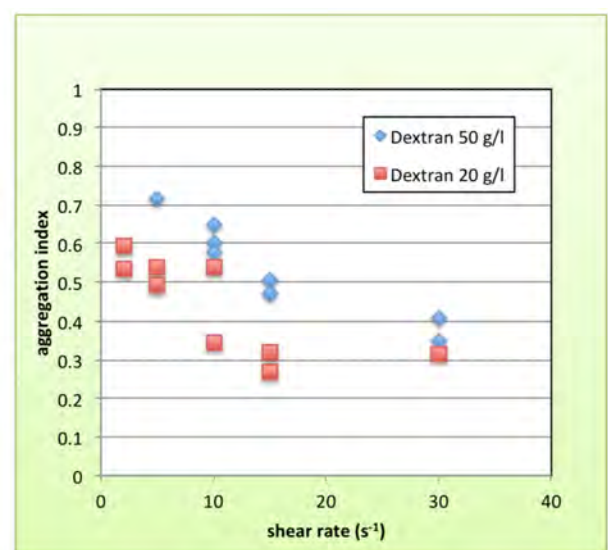


Figure 2: Aggregation index (number of aggregated RBCs / total number of RBCs) vs shear rate.

The analysis of these distributions at the end of each parabola (20s of shear) makes it possible to estimate the degree of blood aggregation in a stationary state where the events of

dissociation-aggregation under the effect of shear are balanced. The results show on the one hand that the quantity of aggregates is directly linked to the interaction energy via the Dextran concentration, in coherence with independent measurements of this energy by AFM or optical tweezers, and on the other hand that the average size of the aggregates decreases significantly with the shear rate: they are essentially made up of doublets at the highest shear rates studied. An aggregation index defined as the instantaneous fraction of red blood cells involved in aggregates (Fig. 2) will allow comparison with theoretical models of aggregation under flow and should be related to the evolution of the effective viscosity of blood. Remarkably, at shear rates higher than 10 s⁻¹, the aggregation index remains high although in this range the bulk rheology of blood does not show any significant difference between cases where aggregation is present or not.

Perspectives

Further analysis of parabolic flight data and additional experiments will allow the results to be extended to a wider range of Dextran concentrations (interaction energy). As the aggregation rate is still high at the highest shear rates studied, we are planning an additional experiment to firstly analyze the phenomenon at high shear rates, and secondly to carry out the experiment under conditions closer to the physiological conditions (composition of the suspending fluid closer to real plasma) as well as by varying the stiffness of the cells in a controlled manner to mimic certain pathologies.

In order to progress in the understanding of the mechanisms of RBC aggregation in flow and the modeling of blood rheology, and following a successful first set of parabolic flight experiments, we are also planning to investigate these phenomena in a future sounding rocket experiment. We will be able to set up kinetic equations for the aggregation and disaggregation rates of RBCs in shear flow and characterize the gel-like fractal structure of RBC aggregate networks at low shear rates. This will improve blood rheological models.

A better understanding of the rheological changes associated to RBC aggregation as well as their possible promotion of thrombus should help develop targeted countermeasures to prevent cardiovascular dysfunction in space as well as on Earth.

Acknowledgements

The authors would like to thank the Centre National d'Etudes Spatiales (CNES) and the European Space Agency (ESA) for financial support and access to microgravity campaigns (CNES parabolic flight campaigns VP131, 139 and 145) and SSC for the development of the shear flow chamber. Valuable technical assistance from Patrice Ballet is acknowledged.

References

- X. Grandchamp, G. Coupier, A. Srivastav, C. Minetti and T. Podgorski, Lift and down-gradient shear-induced diffusion in red blood cell suspensions, *Phys. Rev. Lett.* 110 (10), 108101 (2013)
- K. Marshall-Goebel et al. (2019), Assessment of Jugular Venous Blood Flow Stasis and Thrombosis During Spaceflight, *JAMA Netw Open.*, 2(11):e1915011 (2019)
- C. Minetti, T. Podgorski, G. Coupier and F. Dubois, Fully automated digital holographic processing for monitoring the dynamics of a vesicle suspension under shear flow *Biomed. Opt. Express* 5, 1554-1568 (2014)
- T. Podgorski, N. Callens, C. Minetti, G. Coupier, F. Dubois and C. Misbah, Dynamics of vesicle suspensions in shear flow between walls, *Microgravity Sci. Tech.* 23, 263–270 (2011)
- T. Podgorski, G. Coupier and C. Minetti, Red Blood Cell Dynamics : The Contribution of Microgravity in the BIOMICS project, in *Preparation of Space Experiments*, Ed. V. Pletser, Intech Open, London (2020). DOI: 10.5772/intechopen.93471

Nature-Inspired, Multi-Functional Surfaces for Sustainable Life-Support in Extreme Environments on Earth and in Space

M. Schmidt^{1,2}, R. Moeller², M. Cruz¹, M. Coppens¹

¹ Centre for Nature Inspired Engineering (CNIE), Department of Chemical Engineering, University College London (UCL), London, UK,

² Aerospace Microbiology Research Group, Institute of Aerospace Medicine, Radiation Biology, German Aerospace Center (DLR e.V.),
m.schmidt.17@ucl.ac.uk, ralf.moeller@dlr.de, m.cruz@ucl.ac.uk, m.coppens@ucl.ac.uk

Introduction

Access to fresh water is one of the necessities for life. Many people on Earth, especially in extreme environments, still lack reliable access to fresh water. Also, under even extremere conditions, for future space missions to Moon and Mars, water recycling capabilities are crucial (A. Guterres 2021). Currently, the environmental control and life-support system (ECLSS) on the International Space Station (ISS) is, among other things, responsible for the absorption of water from cabin air, which is treated, stored, and re-used. However, efficiency could be improved, as only 70-93% of water is currently reclaimable, and costly resupply from Earth is required (M. Jernigan *et al.* 2018).

Additionally, the integrity of surfaces and materials is at risk in locally moist areas, as organisms such as bacteria and fungi start to disperse and proliferate at high humidity levels. This threatens the health of astronauts with a weakened immune system, limited treatability, and no chance for immediate return to Earth (J. Rosenzweig *et al.* 2010). Therefore, novel approaches need to be investigated for sustainable support of life in extreme environments on Earth and in space (G. Bornemann, *et al.* 2015).

Nature-Inspired-Multi-Functional Surfaces

We developed nature-inspired, multi-functional surfaces (NIMFS) to absorb excess moisture produced by astronauts' indoors activities and transport it passively for use in ECLSS. Inspired by the microstructures of tree capillaries, cicada wings, and moth eyes (Coppens. 2021), the NIMFS consist of various artificially designed hollow microstructures, fabricated by a high-resolution additive manufacturing technique using two-photon polymerisation.

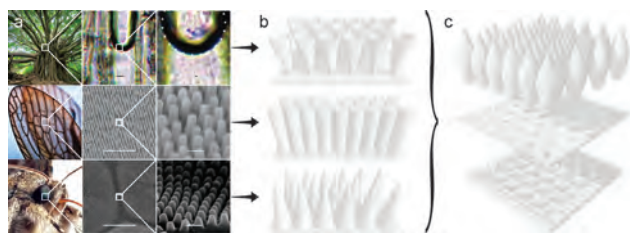


Figure 1: Nature-Inspired, Multi-Functional Surfaces (NIMFS). (a) Inspiration from tree capillaries, cicada wings, and moth eyes leads to (b) microstructured concept, (c) design, and fabrication of the artificial surface. Scale bars 5 and 1 μm , respectively.

Water Absorption via NIMFS

Informed by calculations of different capillary widths, spacing, and angles, ground-based water experiments were conducted, demonstrating a high surface tension and a significantly increased contact angle over the flat material. Further, liquid intake into the NIMFS was observed, which could be explained by capillary action pulling water droplets in.

Under microgravity, an increase in liquid intake can be anticipated. To assess this concept, we participated in the 35th DLR parabolic flight campaign, for which the ground-based experimental set-up was converted into a double-contained water-tight flight rack. The payload of the rack consisted of an experimental, analytical, and safety system. For documentation, two cameras, a humidity and temperature logging sensor, and a phone for real-time data communication were integrated. Currently, the results of the liquid intake are being analysed.



Figure 2: Experimentation on the NIMFS. (a) High surface tension, increased contact angle and water intake was noticeable during ground-based experiments and (b, c) an increase in liquid intake can be anticipated during microgravity experiments at the 35th DLR Parabolic Flight Campaign.

In addition, the NIMFS are presently being assessed in ground-based and spaceflight experiments on the ISS for their long-term microbial contamination and surface ageing, due to long-term environmental conditions, such as airflow, humidity, white light, and ionising radiation.

Conclusions

Our results aim to achieve an improved understanding of health and life comfort of astronauts and the use of passive processes, especially under extreme environmental conditions, such as microgravity and isolation analogs. This could lead to the reduction of energy consumption for freshwater conservation in Earth and space applications.

We gratefully acknowledge the support from EPSRC via DTP (EP/R512400/1) and project no. 1926173, as well as “Frontier Engineering” (K038656/1) and “Frontier Engineering: Progression” (EP/S03305X/1) awards.

Additionally, we thank all institutions involved who supported the project, especially the DLR, the European Space Agency (ESA), the Karlsruhe Institute of Technology (KIT), and P+ Studio.

References

A. Guterres, The Sustainable Development Goals Report 2021, *United Nations Publ. issued by Dep. Econ. Soc. Aff.*, pp. 1–64 (2021).

G. Bornemann, K. Waßer, T. Tonata, R. Moeller, M. Bohmeier, J. Hauslage, Natural microbial populations in a water-based biowaste management system for space life support, *Life Sci. Sp. Res.*, vol. 7, pp. 39–52 (2015).

J. Rosenzweig, O. Abogunde, K. Thomas, A. Lawal, Y. Nguyen, A. Sodipe, O. Jejelowo. Spaceflight and modelled microgravity effects on microbial growth and virulence. *Appl. Microbiol. Biotechnol.* 85, 885-891 (2010).

M. Jernigan, R. Gatens, J. Joshi, J. Perry, The Next Steps for Environmental Control and Life Support Systems Development for Deep Space Exploration, *48th Int. Conf. Environ. Syst.* 1-8 (2018).

M.-O. Coppens, Nature-Inspired Chemical Engineering for Process Intensification, *Annu. Rev. Chem. Biomol. Eng.*, vol. 12, no. 1, pp. 187–215 (2021).

Thermal diffusion experiments in CO₂-1-hexanol mixtures at different gravity levels – Design and data overview of a parabolic flight campaign

P. Fruton^{1,*}, E. Lisoir¹, F. Croccolo¹, C. Giraudet¹

¹Universite de Pau et des Pays de l'Adour, E2S UPPA, CNRS, TotalEnergies, LFCR UMR5150, Anglet (France)
*paul.fruton@univ-pau.fr

Introduction

When we impose a thermal gradient to a binary fluid mixture, a concentration gradient is induced by the Soret effect. In non-associative systems, as the one consisting in carbon dioxide and 1-hexanol, the Soret coefficient is negative and can lead to the formation of hydrodynamic instabilities in the form of convective rolls. Before convection sets-in, non-equilibrium fluctuations (NEFs) spontaneously emerge in the presence of a density gradient and can be amplified by the presence of gravity, thus generating convection (Giavazzi and Vailati 2009). The shadowgraph method allows to visualize and analyze both NEFs and convective patterns (Croccolo and Brogioli 2011). The signal rising from convection, however, overwhelms the one from NEFs. Thus, studying this process under reduced gravity conditions allows a deeper understanding of the behaviour of NEFs in conditions close to the onset of convection.

In this work, we present the set-up developed for a parabolic-flight campaign. Then, we describe the analysis method and the results obtained during thermodiffusion experiments on both normal and different gravity levels. The selected mixture is made of 1-hexanol and CO₂ at different molar concentrations. Positive and negative temperature gradients are applied to the system to study both stable and unstable conditions. The influence of gravity levels (terrestrial, hyper-, and reduced-gravity) on convection is investigated.

Materials and Method

The sample under study is prepared in a vapour-liquid-equilibrium (VLE) vessel by mixing CO₂ at a given pressure with 1-hexanol. We shake the vessel to quickly reach a VLE with a given concentration of CO₂ in the 1-hexanol phase, as determined by the thermodynamic conditions of temperature and pressure.

Thereafter, the liquid phase of the mixture is transferred to a sample cell that mainly consists in a stainless-steel annulus sandwiched between two thermally-controlled sapphire windows. A thermal gradient is settled by two Peltier elements featuring a 13 mm diameter hole to provide optical access. The cell is placed in a shadowgraph apparatus that consists in a collimated beam provided by a superluminescent diode (SLD) passing through the sample cell towards a high-speed sCMOS camera. The latter can record intensity maps of 2048x2048 pixels at a maximum frequency of 100 Hz, thus providing information about the variations of the refractive index and, thus, of the density inside the cell.

During an experiment, we first apply a thermal gradient, and, once the macroscopic thermal equilibrium is reached, we record a series of images at a constant time delay.

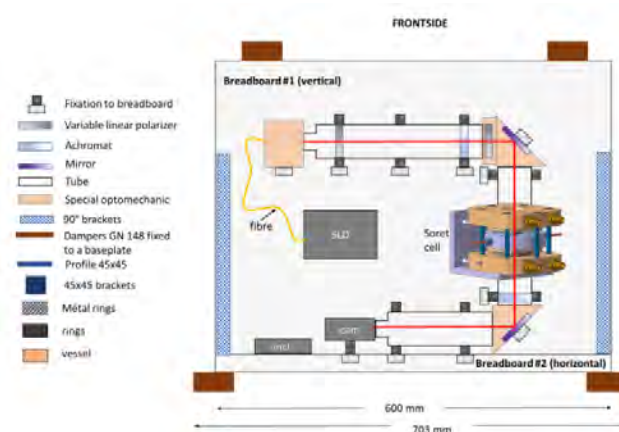


Figure 1: Illustration of the experimental set-up: two breadboards mounted at 90° with the vertical one hosting most of the elements of the setup (SLD, camera, achromats, mirrors, polarizers, optomechanic items, tubing, cell, inclinometer).

The NEFs are studied using a dynamic differential algorithm (DDA) that computes the spatial Fourier transform of image differences for each pair of images (Croccolo et al. 2012). Thus, we obtain the structure functions (SFs) containing information on the static and dynamic behaviour of the process. When the thermal gradient is destabilizing, the convective rolls can emerge inside the bulk and prevent us from analysing the NEFs. In these cases, we focus on the temporal evolution of the contrast of the patterns, quantified by the computation of the variance of the images.

Ground-based results

Preliminary investigations have been performed to define the boundaries of parabolic-flight experiments. It was found that the strength of convective rolls increases with increasing CO₂ concentration and pressure.

When x_{CO_2} is smaller than about 10%, no convective rolls could be observed independently of the distance from the bubble pressure. Nonetheless, NEFs feature a very limited optical contrast, so that smaller concentrations were discarded. For $x_{CO_2} = 40\%$, we rapidly observed convection for pressures in the range 6 - 24 MPa, thermal gradients of 15 and 18 K and a mean temperature of 303 or 313 K. We observed convective rolls that are more contrasted at high pressures and vanish at low pressure. They hide the NEFs and prevent their analysis. Looking at the Fourier transform, we observe the existence of a preferential direction.

Those results suggest that at these temperatures, the Soret coefficient increases with decreasing x_{CO_2} and approaching first-order fluid-phase transition.

Results during parabola

During the parabolic flight campaign, we investigated two molar fractions, $x_{CO_2} = 26$ and 56 %. We applied both positive and negative thermal gradients in the range -6 to 6 K (the negative sign means heating from below). At the largest molar fraction, we observed convection for every thermodynamic condition during the terrestrial gravity phase. The contrast of the patterns increases during the hyper-gravity period, while it decreases in micro-gravity (Fig.4).

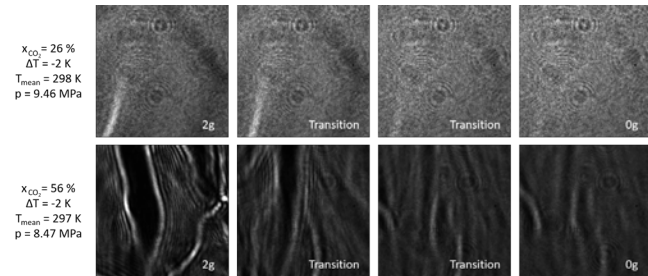


Figure 2: Shadowgraph images of two experiments for a temperature difference $\Delta T = -2$ K and two molar fractions of $x_{CO_2} = 26$ (top) and 56 % (bottom).

Some experiments do not show anymore convection during the reduced-gravity phase; see figure 2. This provides us periods to study the NEFs. Unfortunately, the SFs computed with the DDA do not provide appropriate data. Indeed, the vibrations of the plane and the g-jitters induce large perturbations of the thermally stratified layers inside the sample. This is especially amplified during the transition from hypergravity to micro-gravity.

Despite this, we are still able to provide quantitative results from the analysis of the image variance. The variance of the raw images (*var2*) provides information on the presence of local variation of the contrast, i.e. convective patterns. The variance of the difference of successive images (*var1*) provides information on the movement of the patterns.

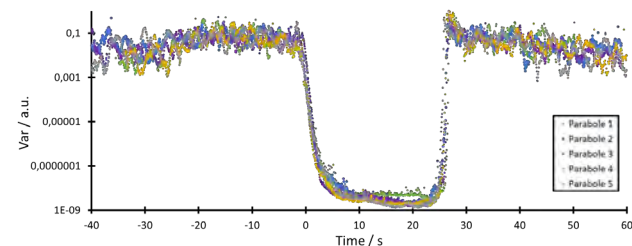


Figure 3: Temporal evolution of the variance (*var1*) for the 5 parabolas of one series ($\Delta T = -2$ K, $x_{CO_2} = 56$ %).

In figure 3, we first notice that we obtained an excellent repeatability between different parabolas at the same thermodynamic conditions, despite non-negligible variations in the vertical acceleration.

Second, we observe that the convective patterns are stabilized during the reduced gravity phase, which is illustrated with the decrease of *var1* in figure 4. In the same period, we observed that the patterns are losing contrast and tend to vanish diffusively, which is demonstrated by the decrease of *var2* in figure 4. From this, we are able to link the characteristic time decay of *var2* with the thermal diffusivity of the mixture.

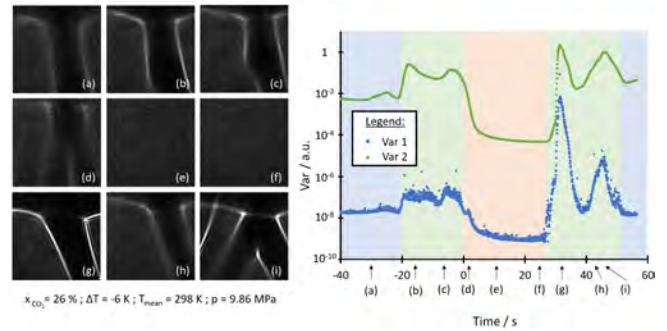


Figure 4: (left) Sample images during a parabola. (right) Temporal evolution of the variance of the difference of the image with the previous one (*var1*) and the variance of raw images (*var2*) over an entire parabola. The blue area corresponds to the terrestrial gravity phase, the green one to the hyper gravity phases, and the orange one to the reduced gravity phase.

Conclusions

We developed an experimental set-up to study the establishment of convection in a mixture of CO_2 and 1-hexanol stressed by a thermal gradient. We could highlight the effects of the gravity levels, from 1.8g close to microgravity conditions, on the intensity of convection. This can vary depending on the molar fraction of the mixture and on the applied thermal gradient. During reduced gravity phases, we observed that the convective patterns are vanishing diffusively. The analysis of the transitory allowed us to measure the value of the thermal diffusivity that is in good agreement with literature.

However, we were not able to study the NEFs because of the strength of g-jitters and vibrations of the plane. They lead to a lost of the autocorrelation plane of the NEFs. In further campaigns, we would need to develop a better vibration removal apparatus, or perform the experiments in other microgravity facilities, like e.g. sounding rockets or satellites.

Acknowledgements

We would like to thank the CNES for their financial support to this campaign, Novespace and especially A. Jacquemet for her support during the preparation phase.

References

- J. Oh, J. M. Ortiz de Zárate, J. V. Sengers, G. Ahlers, Dynamic of fluctuations in a fluid below the onset of Rayleigh-Bénard convection, *Physical Review E* **69**, 021106, (2004)
- F. Croccolo, C. Giraudet, H. Bataller, R. Cerbino, A. Vailati, Shadowgraph analysis of non-equilibrium fluctuations for measuring transport properties in micro-gravity in the GRADFLEX experiments, *Microgravity Sci. Technol.*, 28:647-475, (2016)
- C Croccolo, D. Brogioli, Quantitative Fourier analysis of shlieren masks: the transition from shadowgraph to schlieren, *Applied Optics*, vol. 50, No. 20, 3419-3427, (2001)
- F. Croccolo, H. Bataller, F. Scheffold, A light scattering study of non-equilibrium fluctuations in liquid mixtures to measure the Soret and mass diffusion coefficient, *The Journal of Chemical Physics*, 137, 234202, (2012)
- F. Giavazzi, A. Vailati, Scaling of the spatial power spectrum of excitations at the onset of solutal convection in a nanofluid far from equilibrium, *Physical Review E* **80**, 015303(R), (2009)

ORAL 57

Vapour cloud of an evaporating sessile droplet in microgravity

Parimalanathan Senthil Kumar¹, Adam Chafai¹, Hatim Machrafi², Alexey Rednikov¹, Pierre Colinet¹

¹TIPs Laboratory, Université libre de Bruxelles, Brussels, Belgium, sparimal@ulb.ac.be,

²Université de Liège, Liège, Belgium, H.Machrafi@uliege.be

Introduction

Being in the era of evolutionary space expeditions, it is essential to test and study the behaviour of various physical systems in the microgravity environment. Moreover, these systems' operation and integration characteristics depend on our knowledge of fundamental science. One such venture of the European Space Agency (ESA) is to study the evaporation behaviour of liquid sessile droplets in microgravity. The experimental host module called the DRop Evaporation (DRE) will be installed and tested in the ISS soon. One of the primary objectives of this module is to use vapour interferometry to investigate the vapour cloud surrounding a liquid drop in microgravity conditions.

In relation to this objective, a dedicated experimental test rig has been designed and developed in the Transfers, Interfaces and Processes (TIPs) Laboratory, ULB. The rig has been successfully tested during the recent parabolic flight campaign (March 2022) organized by ESA at Novespace, Bordeaux. One of the objectives of this test campaign is to investigate the effect of Marangoni flow inside the droplet on the vapour cloud captured by interferometry. In this paper, some of the results will be presented.

Experimental setup

The experimental setup consists of two parts, the experimental rig and the control rack with touch screen monitors, interface hardware systems, advanced CPUs and gas canisters. HFE-7100 has been used as the working fluid in all the cases following ESA's choice for space experiments as it is non-flammable and electrically insulating. A Mach Zehnder's interferometry (shown in Fig. 1) has been employed to capture the vapour distribution around an evaporating droplet injected on a unique substrate made of silicon coated with platinum. There are two circular grooves (diameter of 4 mm and 8 mm) etched onto the substrate surface to keep the drop pinned during the experiments. In all the cases presented here the droplet is pinned to the inner groove of 4 mm.

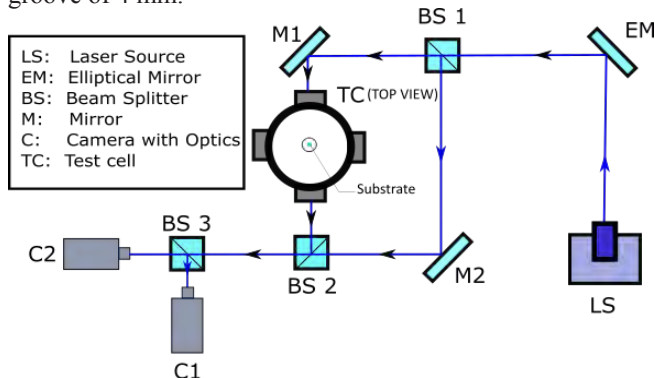


Figure 1: Mach Zehnder's interferometry with the test cell

All the optics, test cell, electronic devices and instruments are mounted on a custom made breadboard. A stable and reliable laser source (Cobolt Samba 532 nm laser) has been used to obtain high-quality interferometric images through two camera optics. The interferometric images are post-processed for the phase-wrapped images of the vapour cloud using an in-house code. These phase-wrapped images allow us to qualitatively analyse the vapour cloud distribution without the need for any complex calibration experiments. The entire setup is enclosed inside a zarges box. All the controls have been automated and can be executed by pressing a digital button.

Effect of g-jitter and Marangoni flow on the vapour cloud distribution

In the present paper, the vapour cloud is represented by the shape of the phase-wrapped fringes close to the vapour source. The main reason for considering such phase-wrapped images is that converting unwrapped images to concentration plots requires the need for complex inverse Abel transformation and knowledge of the phase field beyond the present field of view. Unfortunately, these boundary conditions are not known in most of our experiments. So, the phase-wrapped images more or less represent the pseudo-isoc-concentration lines. The other advantage is that significant variations in the fringes can be observed even for a slight change in external conditions.

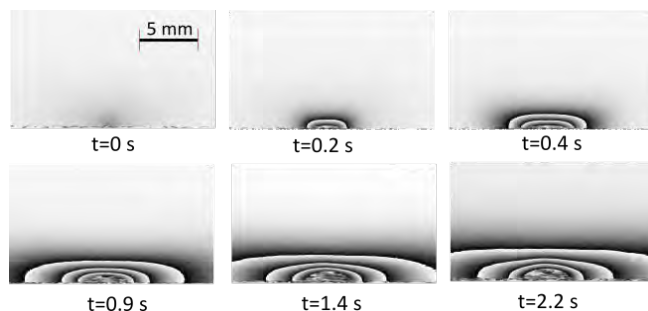


Figure 2: Vapour cloud distribution surrounding a droplet evaporating in normal gravity

A set of phase-wrapped images for a sessile droplet evaporating in normal gravity conditions is presented in Fig. 2. The time $t = 0$ s represents the start of injection. The vapour cloud is flattened by the presence of gravity and remains close to the droplet surface. The droplet continues to evaporate after injection. The evaporation rate of the drop can be estimated through volume reduction calculated from the extracted droplet background images. The analysis is much more involved in microgravity conditions.

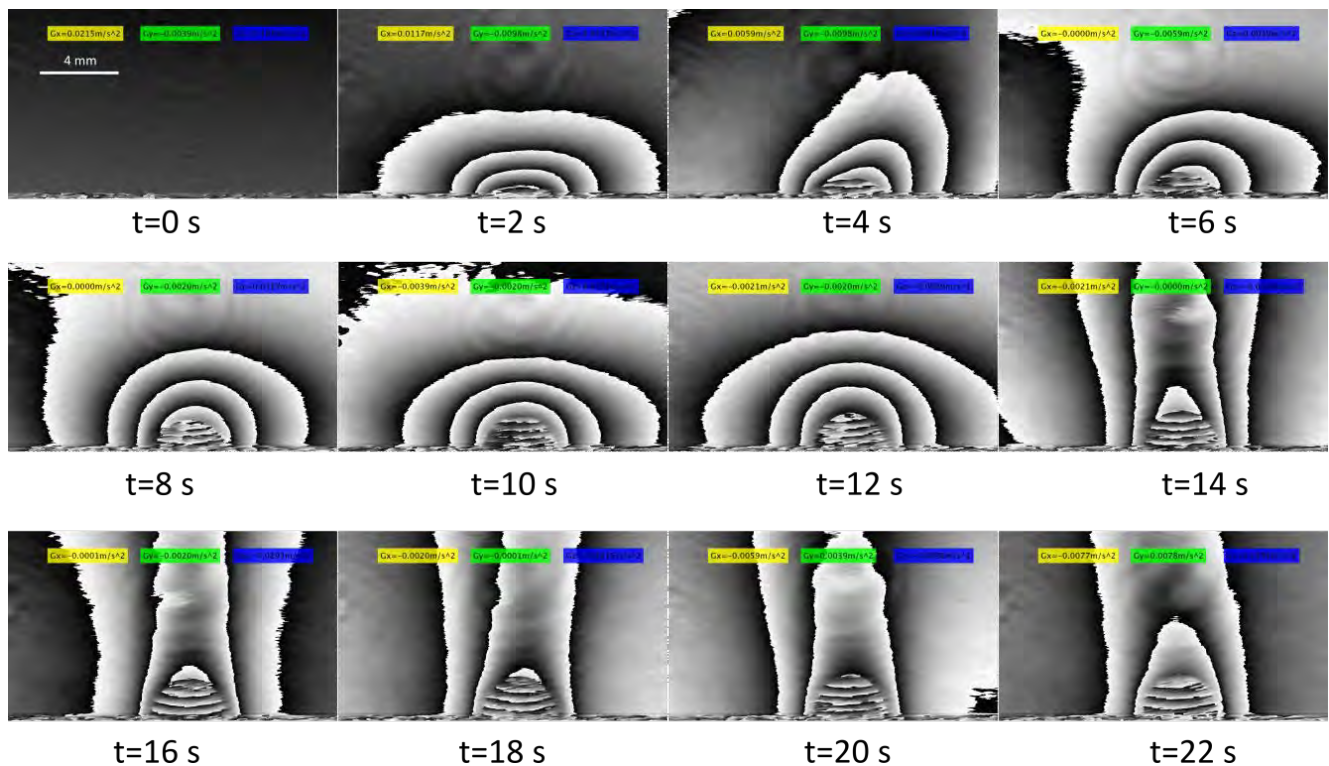


Figure 3: Vapour cloud distribution surrounding a droplet evaporating in microgravity: influenced by g-jitter and Marangoni flow.

Unfortunately, the total time span and the gravity values during the parabolic flight manoeuvres depend on the flight altitude, meteorological conditions, and sometimes even the pilots' experience and timings. Hence the exact injection timings are complicated to program and execute. Nevertheless, one such successful droplet injection at the right timing during the start of microgravity is presented in Fig. 3. The droplet initially spreads over the surface until the contact line pins to the inner 4 mm groove. Then the droplet continues to grow in volume ideally forming a hemispherical cup surrounded by the vapour cloud. The vapour cloud has a strong influence from g-jitters and the dominating Marangoni flow inside the droplet. The impact is very significant during the later stages of the microgravity phase. The vapour clouds, being initially of a hemispherical shape, rise after $t = 12$ s. Although there is interference from g-jitters, this plume is also the consequence of Marangoni convection in the droplet. Further, there is always an anomaly concerning the droplet volume in microgravity conditions. However, the main task here is to investigate and clearly distinguish between the influence of g-jitters and the Marangoni flow on the vapour cloud shape. Since some computation studies could shed some light on this issue, preliminary simulations have already been planned and being executed.

Conclusions

The effect of microgravity on the vapour cloud is investigated using interferometry. The vapour cloud is flattened by gravity in normal gravity, affecting the evaporation rate. However, in microgravity conditions, the vapour plume initially forms a hemispherical shape. Later, the combined effect of g-jitters and the Marangoni flow influences the shape of the vapour cloud.

Acknowledgements

The authors are grateful for the support and funding from ESA and BELSPO PRODEX (Evaporation and Heat Transfer) and the Fonds de la Recherche Scientifique-F.N.R.S.

References

- [1] Dehaeck S., Colinet P., Vapour cloud dynamics induced by evaporation, arXiv 1010.3258, 2010, Download the publication (from <http://arxiv.org/abs/1010.3258>).
- [2] Dehaeck S., Rednikov A. and Colinet P., Vapor-based interferometric measurement of local evaporation rate and interfacial temperature of evaporating droplets, *Langmuir* 30, pp 2002-2008 (2014).

Thin Liquid Film Coating and Drying under Microgravity Conditions: How parabolic flights showed the necessity of sounding rocket experiments

Jan van Stam¹, Leif Ericsson², Ishita Jalan³

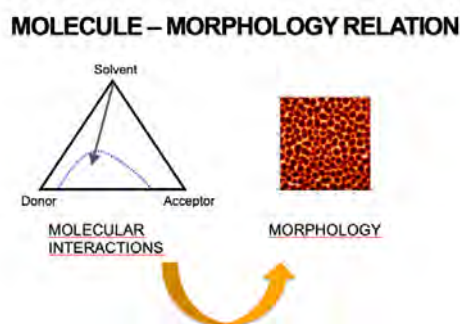
¹Department of Engineering and Chemical Sciences, Karlstad University, Sweden, Jan.van.Stam@kau.se

²Department of Engineering and Physics, Karlstad University, Sweden, Leif.Ericsson@kau.se

³Department of Engineering and Chemical Sciences, Karlstad University, Sweden, Ishita.Jalan@kau.se

Telephone to all authors: +46-54-700 1000

Preferred session: A10. Material science and processing



In 2018, we participated in our first parabolic flight campaign, the 70th ESA PFC. For the first time, we performed wet chemistry deposition on a solid substrate, with subsequential evaporation of the solvent, under microgravity conditions. This year, we got the opportunity to further develop our microgravity experiments during the 78th ESA PFC. One result that was clear already during the campaign, is that 20-25 seconds of microgravity is not long enough if one wants to ensure that the solvent is completely evaporated, and the blend film dry and arrested, under microgravity conditions. This is the basis for our upcoming sounding rocket experiments, *Liquid film coating and drying under microgravity conditions in systems relevant for organic solar cells. Exploration of the blend film morphology caused by a partial phase separation* (LiFiCo).

The LiFiCo project aims at, on the one hand, a better fundamental understanding and a better control of the molecular interactions yielding the structures found in the molecular blend thin films making up the active layer of an organic solar cell, and, on the other hand, developing a new coating method for solution-borne organic optoelectronics by a stationary substrate and a mobile solution. The evaporation of the solvent causes a fast-developing concentration gradient, eventually leading to an evolving phase separation. Due to the fast solvent evaporation, the phase separation process is arrested before it reaches completion. For the blend films formed under such a process, the partial phase separation will result in a specific film structure, known as the film morphology. It is of both fundamental and applied interest to be able to control and manipulate the film morphology.

In the case of an organic solar cell, the solution contains donor, acceptor, and sometimes additional molecules, and the active layer morphology is shown to be decisive for the solar cell performance. It is known that the kinetics of phase separation is slowed down under microgravity conditions. Hence, this provides a possibility to study the early stage of the phase

separation in more detail, due to a more extended timescale for this process to develop. By applying microgravity conditions in preparations during parabolic flights, we have already found differences related to the slower phase separation. To ensure that the whole drying process is performed under microgravity conditions, we need to prolong the microgravity timespan, which is achieved by performing the process during a sounding rocket experiment. In this way, we can better judge the results obtained during parabolic flights and at the same time develop the wet chemistry methods for producing the thin film active layer under microgravity conditions.

The characterisation of the blend films' morphology and its influence on the photophysical charge transfer processes will mainly be performed through atomic force microscopy combined with infrared spectroscopy and time-resolved fluorescence spectroscopy. Combining the new observations with fluid mechanics calculations, thermodynamics, and theoretical modelling of the systems' solution chemistry will yield an opportunity to find better process routes, for instance finding less environmentally and health-damaging solvents than those frequently used in research laboratories. To find these new solvents, a screening model based on solution thermodynamics, yielding the possibility to match the properties of the solvent with the solutes, will be employed. Finding more environmentally and health-friendly solvents is a necessity for manufacturing cheap and flexible solar cells on an industrial scale.

The LiFiCo project is part of a multi-disciplinary research programme, in which scientists from different fields, e.g., chemistry, materials physics, and modelling, develop projects in the field of molecular interactions under normal and microgravity conditions.

The LiFiCo project is scheduled to be part of a sounding rocket launch in October 2023.

ORAL 59

Proteomic and Functional Analysis of Acute Galactic Cosmic Radiation Exposure in the Kidney

Keith Siew¹, Stephen B. Walsh¹

¹University College London, London, United Kingdom, k.siew@ucl.ac.uk

Introduction

There is concern regarding the effect of galactic cosmic radiation (GCR) exposure on cancer risk, cardiovascular and neurological health posed by longer missions planned as part of the Deep Space Transport/Mars Missions.

However the kidney is the dose limiting organ in abdominal radiotherapy and total body irradiation. Chronic kidney dysfunction can occur with acute low linear energy transfer (LET; e.g. γ -radiation or X-rays) radiation doses as low as <0.5Gy. An astronaut on a Mars exploration mission has an estimated absorbed dose of 0.47Gy.

We hypothesise that GCR may cause acute renal failure within the timeframe and GCR dose expected for an exploratory mission to Mars, which may require renal replacement therapy and would thus be mission critical.

Method

To investigate this, snap-frozen kidneys from mice either exposed to an acute 0.5Gy dose of simulated GCR or sham control (n=10 per group) at Brookhaven National Laboratory, underwent quantitative TMT mass spectrometry proteomic analysis for markers of proximal tubule damage and pathways known to be involved in radiation nephropathy. Urine and plasma were also collected from these mice 24hrs after acute GCR exposure for biochemical and electrolyte analysis to look for early signs of renal tubular and glomerular filtration dysfunction.

Results

Network analysis of the proteome of whole homogenised kidney of GCR exposed animals showed a biologically significant (>-10%) decrease in proteins associated with mitochondrial (e.g. CYC1, COX7C) or ribosomal function, intracellular transport and cell membrane transport (e.g. SLC12A1, SLC12A3) compared to sham exposed animals. There was a >10% increase in apolipoproteins and HDL proteins (e.g. APOA4, APOA1) in GCR compared to sham exposed animals.

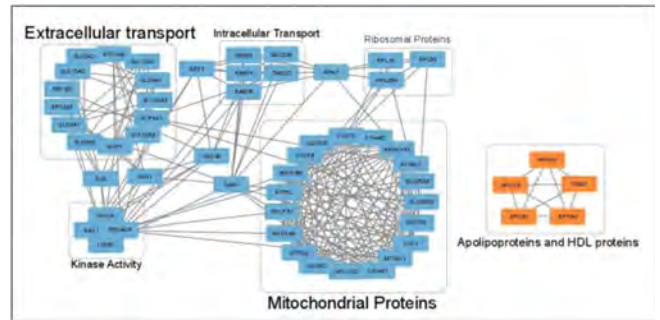


Figure 1: Network analysis of proteome of homogenised renal tissue for animals exposed to GCR compared to animals exposed to sham. Blue nodes represent proteins with decreased expression (>-10% decrease) after GCR, Orange nodes represent proteins with increased expression (>10% increase) after GCR. Only highlighted (>10 1st degree neighbours) nodes are shown.

Conclusions

GCR exposed animals had proteomic and biomarker evidence of renal damage. This requires further investigation.

Acknowledgements

This communication is supported by the ESA SpaceOmics Topical Team (4000131202/20/NL/PG/pt) grant

ORAL 60

The impact of microgravity on kidney function during spaceflight

Keith Siew¹, Stephen B. Walsh¹

¹University College London, London, United Kingdom, k.siew@ucl.ac.uk

Introduction

The impact of microgravity (MG) on deep space travellers has mainly focused on cardiovascular, musculoskeletal, neurological and ocular health. However, MG exposed astronauts have an unusually high rate of kidney stone formation which poses a mission critical risk. In fact, over 30 incidents have been reported and previous missions have almost been aborted due renal stone formation

Method

To investigate this, we studied kidneys and biofluids from mice aboard the Rodent Research-10 (RR-10) Mission that launched with SpaceX-21 to the International Space Station and spent ~30 days in MG. These were compared to ground controls (n=10 per all groups) and underwent spatial transcriptomics and miRNA analysis, quantitative proteomics/phosphoproteomics, urine/plasma electrolyte analysis and 3D imaging of immunostained optically cleared tissues for histomorphometry.

Results

Thus far, our network analysis of the data supports evidence of mitochondrial damage, extracellular matrix dysfunction and decreased glomerular filtration rate. Interestingly, there are also marked dysregulation in gene products relating to lipid metabolism, SLC membrane transporter superfamily and phosphorylation status.

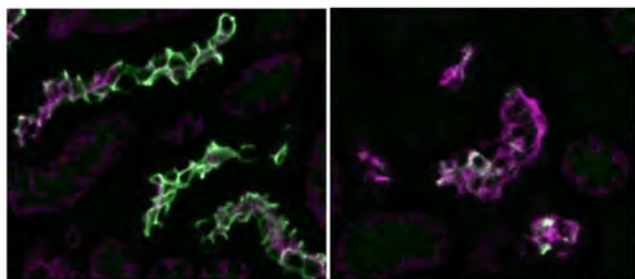


Figure 1: Immunofluorescence staining of NCC and phospho-NCC. Lightsheet microscopy of SHIELD cleared Renal tissues stained for total SLC12A3 (Magenta) and Phospho-Thr53 SLC12A3 (Green), Representative slide of distal convoluted tubule from animal under Earth's gravity [A], and from an animal exposed to microgravity aboard the International Space Station [B].

Conclusions

Our data suggest that there are detrimental changes in the abundance and activity of key transporters/channels that either directly or indirectly regulate calcium homeostasis, and that these may be primary changes in the kidney that drive renal stone formation on the backdrop of milieu of increased renal stone risk factors (e.g. bone resorption, dehydration, enhanced crystal formation in MG).

Acknowledgements

This communication is supported by the ESA SpaceOmics Topical Team (4000131202/20/NL/PG/pt) grant

TOPIC

B5. Space Omics

ORAL 61

Daily aerobic and resistance exercise on ISS does not correlate with measured change in peak VO₂

R.L. Hughson¹, D.K. Greaves², P. Arbeille²

¹Schlegel-UW Research Institute for Aging, Waterloo, Canada, hughson@uwaterloo.ca, ²Schlegel-UW Research Institute for Aging, Waterloo, Canada, dgreaves@uwaterloo.ca, CERCOM-UMPS . Faculte de Médecine Université de Tours, Tours, France, arbeille@med.univ-tours.fr.

Introduction

Astronauts normally have two exercise sessions scheduled into their workdays on ISS. A one-hour block is assigned to aerobic exercise and 90-minutes to resistive exercise. Because of scheduling constraints aerobic exercise is typically between other activities requiring the astronauts to use part of their 1-hour time to change into exercise gear, set up the exercise device and then change back to normal work clothes. A consequence of this is that astronauts perform less than 30-minutes per day of aerobic exercise (Hughson et al. 2016). There is limited information on the quantity and quality of the resistive exercise performed by astronauts and no statistical analyses have been presented for data linking daily exercise to changes in aerobic fitness as expressed by measured maximal, or peak, oxygen uptake (Peak VO₂).

Peak VO₂ decreases by ~17% early during spaceflight then recovers toward pre-flight upright values toward the end of flight before decreasing again immediately post-flight (Moore et al. 2014). There are between person differences in the degree of fitness change that might be related to total exercise countermeasures performed on ISS.

The data presented here are from astronauts participating in the Vascular Echo study. The data were collected as part of an investigation of changes in fitness of leg muscle determined by blood flow recovery following a standardized leg exercise challenge.

Methods

Nine astronauts participated in standard pre-, in-, and post-flight tests of aerobic fitness on the cycle ergometer. These data were collected by the space agencies and provided via the Life Sciences Data Archive.

Results

There was considerable between person variation in the type and intensity of exercises across the 6-month missions. Treadmill exercise was more common performed on an average of 51% of days on ISS compared to 33% of days for cycle exercise. The total minutes of aerobic exercise per day averaged 23.2 but ranged from 12 to 40 minutes/day.

Resistive exercise on the ARED device was conducted an average of 71% of days with one astronaut exercising on ARED 98% of days on ISS. The type of exercise was categorized as leg (squats, heel raises) and other (bench press, bicep, deadlift, upright rowing, etc.). The total loading in pounds lifted per kg body mass per day averaged 189 for

the legs and 194 for the other for a total of all ARED exercises of 382 pounds/kg/day. Again, there was considerable between person variation with four astronauts having a total <200 for all ARED exercises while one exceeded 900.

There was a strong relationship between quantity of aerobic and resistance exercise ($r^2=0.70$).

No relationships were found between the aerobic or resistance exercises and the change in Peak VO₂. The Peak VO₂ did not relate linearly with the time to the end of the maximum test in all astronauts (Figure 1)

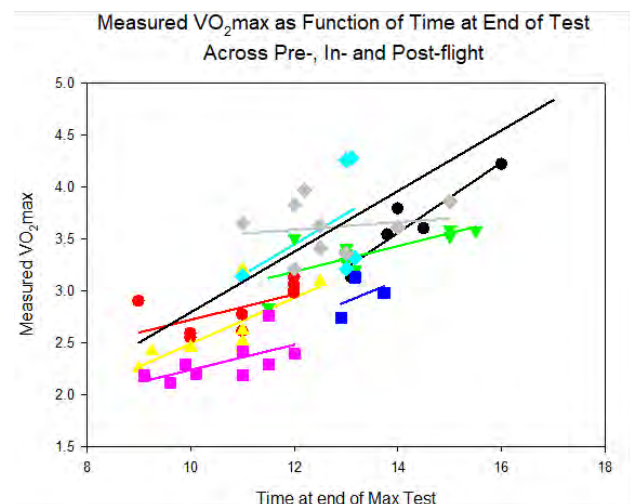


Figure 1. Measured Peak VO₂ as a function of time to the end of the maximum cycle ergometer test. The solid black line represents the predicted Peak VO₂ for the work rate corresponding to the times of the test.

Conclusions

Astronauts are individuals who will modify their daily exercise countermeasures within the guidelines provided by space agencies. While we observed large between person differences in the quantity and intensity of aerobic and resistance exercise, we did not find a correlation with the aerobic fitness index Peak VO₂. Close examination of the measured Peak VO₂ with the duration of the exercise test revealed some variation suggesting factors other than the time to exhaustion might have influenced the results.

Acknowledgements

Supported by the Canadian Space Agency and CNES

References

R.L. Hughson, A.D. Robertson, P. Arbeille, J.K. Shoemaker, J.W. Rush, K.S. Fraser, D.K. Greaves. "Increased postflight carotid artery stiffness and in-flight insulin resistance resulting from 6-mo spaceflight in male and female astronauts." *American Journal of Physiology - Heart and Circulatory Physiology* **310**(5): H628-H638, 2016.

A.D. Moore Jr., M.E. Downs, S.M.C. Lee, A.H. Feiveson, P. Knudsen, and Lori Ploutz-Snyder. "Peak exercise oxygen uptake during and following long-duration spaceflight." *Journal of Applied Physiology* **117**(3): 231-238, 2014.

ORAL 63

The impact of long-duration spaceflight on the horizontal Vestibulo-Ocular Reflex (hVOR)

Chloë De Laet¹, Ludmila Kornilova², Dmitrii Glukhikh², Catho Schoenmaekers¹, Hamish MacDougall³, Steven T. Moore⁴, Ivan Naumov², Leander Wille¹, Steven Jillings¹, Floris Wuyts¹

¹ Lab for Equilibrium Investigations and Aerospace, University of Antwerp, Belgium;

² Institute of Biomedical Problems, Moscow, Russia;

³ University of Sydney School of Psychology, Sydney, New South Wales, Australia;

⁴ School of Engineering and Technology, Central Queensland University, Rockhampton, Australia.

Introduction

The Semi-Circular Canals (SCCs) and the Otoliths are the two main organs of the vestibular system responsible for balance and gaze-stabilization. Weightlessness impacts the otolith organs, the main gravity detectors, which is evident from the decreased otolith-mediated ocular counter roll reflex observed after spaceflight (Hallgren et al., 2016). However, as the SCCs are not gravity-dependent, it is expected that a prolonged stay in microgravity would not affect the vestibulo-ocular reflex (VOR) generated by the SCCs. But little is known about the intricate interplay between the otoliths and the canals. Despite the number of studies that have tried to reveal the effect of microgravity on the SCCs through VOR measurements in the past decades, most of those studies were strongly limited by a restricted sample size and short-duration missions (Clement et al., 2019; Reschke et al., 2018). This study aims to characterize the hVOR changes before and after a long duration spaceflight (>6 months) in an unprecedentedly large cohort of 44 pre- and post-flight vestibular measurements in cosmonauts.

Material and methods

44 pre- and post-flight measurements were performed, of which 13 were from first time flyers (1F group) and 31 were from frequent flyers (FF, N=31), by exposing cosmonauts to off-axis centrifugation before and after their 6-month space mission to the ISS. This study was conducted between ISS expedition 16 (2007) and ISS expedition 61 (2020). Measurements were done approximately two months preflight, three days after landing (Early postflight R+3) and nine days after landing (Late postflight R+9). The hVOR induced by the Visual and Vestibular Investigation System (VVIS) mini centrifuge was assessed and recorded with infrared goggles during a 30-second acceleration phase until the maximum velocity of 254°/s was reached. Extraction of nystagmi and associated computations of Slow-Phase Velocity (SPV) and Time Constant (Tc) were made using a custom MatLab routine (Fig.1). The Time Constant of hVOR was then further statistically analyzed in SPSS (V.27), using a linear mixed-model with $p < 0.05$ as significance threshold.

Results

We found a significant decrease in hVOR time constant Early

postflight (R+3) and Late postflight (R+9) compared to preflight ($p < 0.001$). A partial but incomplete recovery was seen nine days after the return of the cosmonauts (Late postflight R+9) (Fig. 2).

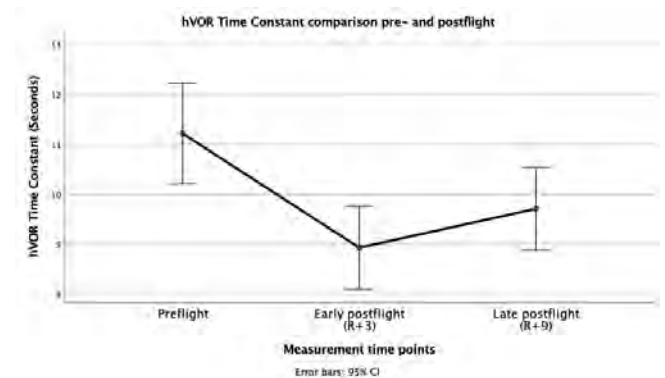


Figure 2 Comparison of the Time Constant values for hVOR preflight and respectively early and late postflight during CCW centrifugation acceleration.

Preflight are measurements acquired before launching, **Early postflight** and **Late postflight** measurements are respectively acquired 3 and 9 days after landing. The y-axis depicts the average hVOR Time Constant for these timepoints. Preflight vs Early postflight and Preflight vs Late postflight comparison were significantly different ($p < 0.001$).

Conclusions

For the first time, our large sample size allowed us to reveal a significant effect of spaceflight on the hVOR. The time constant values measured in cosmonauts are in the physiological range. These findings show an interaction between the otoliths and the canals. Our hypothesis is that the effect shown after spaceflight on both the otolith and the canals are centrally mediated rather than peripheral.

References

Clement, G., Wood, S. J., Paloski, W. H., & Reschke, M. F. Changes in gain of horizontal vestibulo-ocular reflex during spaceflight. *J Vestib Res*, 29(5), 241-251. (2019)

Hallgren, E., Kornilova, L., Fransen, E., Glukhikh, D., Moore, S. T., Clement, G., Van Ombergen, A., MacDougall, H., Naumov, I., & Wuyts, F. L. Decreased otolith-mediated vestibular response in 25 astronauts induced by long-duration spaceflight. *J Neurophysiol*, 115(6), 3045-3051. (2016)

Reschke, M. F., Wood, S. J., & Clement, G. Effect of spaceflight on the spatial orientation of the vestibulo-ocular reflex during eccentric roll rotation: A case report. *J Vestib Res*, 27(5-6), 243-249. (2018)

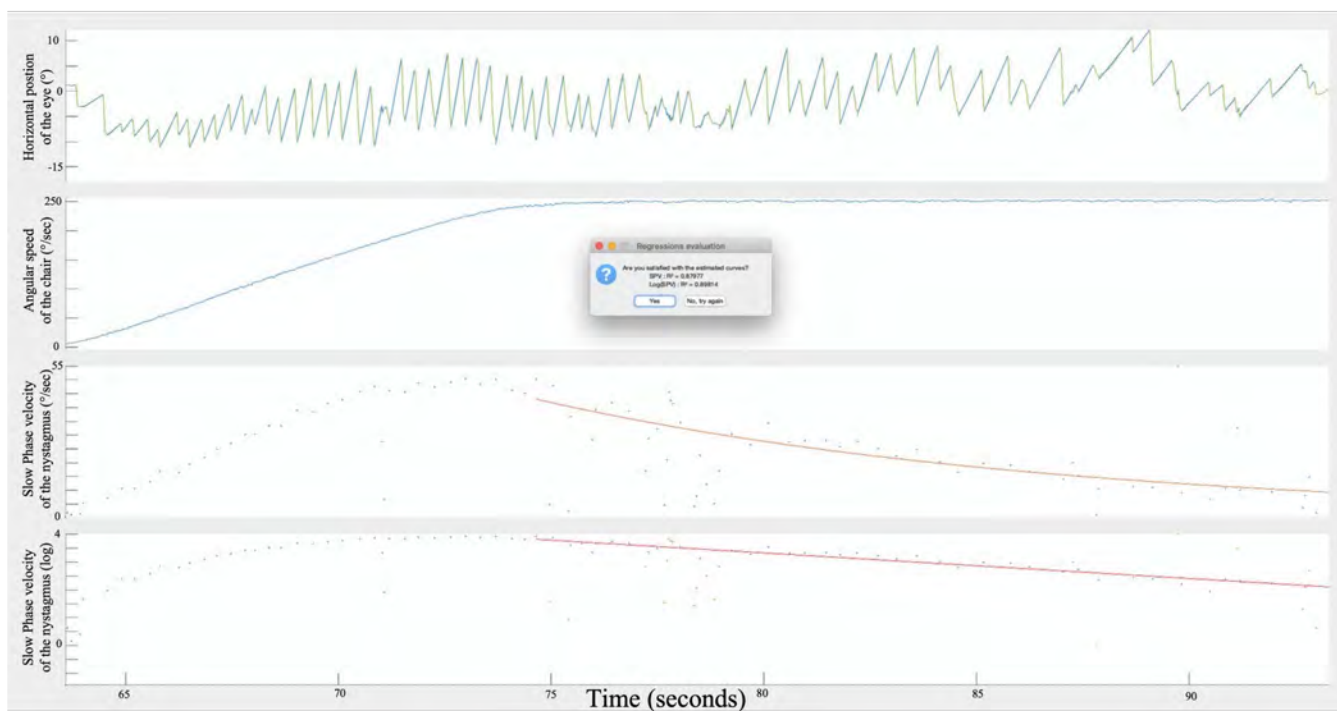


Figure 1 Processing of the horizontal position of the eye
Horizontal position of the eye in degrees in the first row, **slow phase of the nystagmus** in blue and **fast phase** in green, **Angular speed of the VVIS (ω) ($^{\circ}/s^2$)** in the second row, **Slow Phase Velocity (SPV) of the eye ($^{\circ}/s$)** in the third row and the **Log transform of the SPV** in the last row.

ORAL 65

The GraviTower Bremen Prototype – disruptive technology for a new age of earth based microgravity and more

Dr. Andreas Gierse¹, Michael Heseding², Marcel Bernauer³, Anna Becker⁴, Prof. Dr. Marc Avila⁵

¹ZARM Fab GmbH, Germany, andreas.gierse@zarm.uni-bremen.de,

²ZARM Fab GmbH, Germany, michael.heseding@zarm.uni-bremen.de,

³ZARM Fab GmbH, Germany, marcel.bernauer@zarm.uni-bremen.de,

⁴ZARM Fab GmbH, Germany, anna.becker@zarm.uni-bremen.de,

⁵ZARM Fab GmbH, Germany, marc.avila@zarm.uni-bremen.de,

Introduction

A new drop tower was put into operation in late 2021 at ZARM. This new drop tower is called GraviTower Prototype and offers 960 flights of 2.5 seconds microgravity per day (compared to up to three flights in the Bremen drop tower) and is prepared to also offer reduced gravity like moon and mars gravity.

The high repetition rate is achieved by avoiding a drop vacuum chamber as in the Bremen Drop Tower and replacing it by an actively accelerated and rail guided drag shield. An installed Power of 3.5MW of the drives allows to accelerate the drag shield together with the experiment with up to 5g (or less if required by the experiment) whereby a smooth harmonic time function was chosen for the initial acceleration to minimize structural vibrations during the microgravity or reduced gravity time. A novel Release-Caging Mechanism (RCM) developed at ZARM mechanically decouples the experiment from the drag shield already during the initial acceleration in five degrees of freedom. During microgravity time the experiment floats free inside the drag shield to achieve the highest possible microgravity quality. Just before deceleration the experiment gets softly recaged to the drag shield. Between flights full access to the experiment is possible. It takes less than ten seconds to open the doors after flight. The experiment can also be turned inside the slider to get access to every part of it without taking it out of the drag shield.

The GraviTower is 100% compatible to the existing Bremen Drop Tower. Experiments that were designed and already operated in the Bremen Drop Tower can use the GraviTower without any modifications. On the other hand, the workflow with the GraviTower and also the requirements on the experiment to make full use of this new facility differs strongly from the existing Bremen Drop Tower. The GraviTower is fully automated and can be operated by the scientists or, preferred, by the experiment. An easy to use communication between the GraviTower and the experiment allows the experiment to request supplies like electrical power, cooling/heating or any kind of media between flights and also to request and trigger the next flight. Fully automated experiments can also change the flight kinematics of the GraviTower and therewith add all possibilities of the GraviTower to their scientific parameter space.

Commissioning of the GTB-PRO was in late 2021. Lunar and Martian gravity will be made possible in a second development step very soon.

ORAL 66

Astropharmacy – Healthcare for Earth, the Moon, Mars and beyond

MJ. Green¹, T. Shivakumar¹, D. Robson¹, H. Cope¹, PM. Williams¹

¹School of Pharmacy, University of Nottingham, Nottingham, United Kingdom

Macauley.Green@nottingham.ac.uk, Tejasvi.Shivakumar@nottingham.ac.uk, Daniel.Robson@nottingham.ac.uk, Henry.Cope@nottingham.ac.uk, Phil.Williams@nottingham.ac.uk

Introduction

Founded in 2019, the Astropharmacy research group are the world's first PhD cohort to be studying the field of Astropharmacy. Based in the School of Pharmacy at the University of Nottingham, the group provides cutting edge research from a globally ranked top 10 school and participate in many educational outreach programmes. Their most recent major achievement is being selected to participate in the European Space Agency's 'Orbit Your Thesis! 3' (ESA OTY!3) programme in which they plan on testing cell-free production of pharmaceuticals onboard the International Space Station (ISS).

As technology advances and the once inaccessible reaches of space transition from science fiction to explorable within our lifetimes, the challenges facing healthcare, wellbeing and performance in space evolve. The space exposome consists of unique stressors rarely or not experienced on Earth. Some of these major factors include; microgravity, increased radiation exposure, elevated carbon dioxide levels, circadian rhythm alterations and other psychological stressors (Patel et al, 2020). Before a crew has arrived at their destination after time in space, coping with lunar/Martian dust and a quick return to work in gravity may produce additional challenges. Targeted research opportunities in space medicine are rarely available to PhD students in the UK and worldwide, despite the pressing need for breakthroughs and critical enabling technology in crew member countermeasures. Astropharmacy does not just benefit space exploration, however. Parallels between health issues experienced by astronauts and patients on Earth can be drawn and give researchers a different insight into these afflictions that may have not arisen otherwise (figure 1).

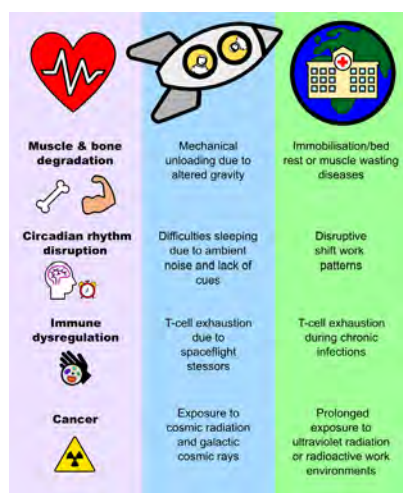


Figure 1: Select parallels between Earth and space healthcare for risks encountered during spaceflight.

The aim of this paper is to discuss and emphasise the challenges posed to astronauts as mission duration increases and novel solutions to combat these changes. We also aim to highlight how the space exposome induces health related changes similar to that of diseases/conditions on Earth and how adopting a different viewpoint may lead to breakthroughs in Earth healthcare research as well. Finally, the educational benefits of Astropharmacy will be discussed.

Benefits for space healthcare

Space travel poses a set of unique challenges. Immune deficiency has been reported as far back as the Apollo missions with astronauts reporting illness during and after the missions. Bacteria have also learned to adapt and become more biofilm-forming and develop antibiotic resistances due to said formations and an increased mutation rate (Green et al, 2021).

Future plans to send crews to the Moon or Mars, tourists into Low Earth Orbit (LEO) or beyond, will require better and more varied preparation to support them. Even the most thoroughly planned cargo of pharmaceutical supplies to Mars may not have the variety or volume of medicines to support all crew situations on a 2-3 year mission (particularly given the scale of new challenges faced). Given pharmaceuticals' reduced shelf-life in the space environment (as a consequence of radiation), this may also require impractically large amounts of up-mass and cost for reliable support in these risky missions. Additionally, the greater variation in – and potentially less stringent - medical standards for space tourists may lead to preventable accidents if not accounted for properly.

Our OYT!3 project, VITA (Visualising In-space Tx-TI Astropharmaceuticals), aims to eliminate both these problems by offering a solution of on-site, on-demand production of pharmaceuticals. We aim to achieve this by leveraging the power of transcription-translation (Tx-TI) from lyophilised bacterial cell-free lysate. The lysate and DNA (protein-coding) components are lyophilised on cellulose discs, which can simply be stacked and rehydrated to kickstart protein synthesis. By simply changing the DNA component, any protein-of-interest (*e.g.* therapeutic) can be manufactured on-site and on-demand. The OYT!3 VITA project aims to demonstrate this technology by showing real-time, in-orbit synthesis and detection of fluorescent proteins as a model, following rehydration (figure 2). Upon sample return, we plan on studying the yield, structure and integrity of synthesized product(s) and any protein-protein interactions. This educational project is giving hands-on experience from design to launch of the payload to demonstrate the experiment onboard the ISS.

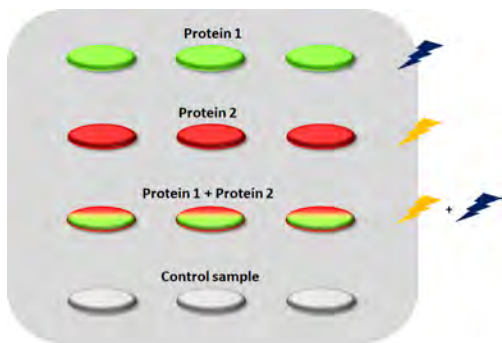


Figure 2: The biological component of VITA, showing protein production and detection on cellulose stacks.

Benefits for Earth healthcare

Health afflictions affecting astronauts in space can have parallels drawn to patients on Earth with similar afflictions. Thus, space research may motivate “outside-the-box” thinking, spin-off applications, transferrable research and access to unique laboratory conditions, leading to new avenues of research into managing or even curing these conditions in space and on Earth.

Due to microgravity, muscles and bones experience less mechanical stress which can cause muscles to atrophy and bones to lose mineral density – increasing operational and post-flight risks to crew. This musculoskeletal atrophy also leads to destruction of insulin receptors manifesting into a form of diabetes if left untreated (Tobin et al, 2002). Interestingly, bed-rest patients on Earth show pre-diabetic markers after 7 days bed rest (Mikines et al, 1989) even though they are in a normal gravity environment. Exercise-related countermeasures for both groups can have many difficulties, and pharmaceutical supplements or interventions present a complementary tool.

Astronauts returning to Earth also exhibit T-cell exhaustion on the same scale as a patient on Earth suffering from a chronic infection (Bradley et al, 2017). By overcoming this problem, not only could we increase an astronaut’s immunity during the mission, we may also be able to decrease effects of long-term infection on Earth and reduce chances of re-occurring infection by restoring/protecting T-cell function.

Educational Benefits

The Astropharmacy cohort is an interdisciplinary group of PhD students and post-doctoral researchers spanning a range of disciplines such as engineering, synthetic biology, immunology, microbiology, food sciences and many more. The University of Nottingham (UoN) also offers final year research projects and an optional module in Astropharmacy as part of the pharmacy undergraduate course.

Additionally, Astropharmacy is being taught at KS4 level in local secondary schools and colleges by team members and various other educational workshops, in collaboration with The Brilliant Club. These outreach programmes spark interest in space healthcare research at a young age and prepare young minds for an exciting career in the space sector – using bioastronautics as a well-known and interesting gateway topic.

As successful applicants of ESA’s OYT13, the Astropharmacy group along with the UoN Space Society will be launching an educational science mission to the ISS. The current team consists of three Astropharmacy members as well as several other students at UoN. As the project gathers pace, there are multiple opportunities for new extra-curricular and accredited students to get involved, including masters-level dissertation projects in engineering. By promoting this research at national and international conferences, as well as internally within the University, the team aspires to increase interest in Astropharmacy and its benefits for Earth-based and space healthcare.

Conclusions

In conclusion, Astropharmacy offers novel insights into healthcare on both Earth and beyond by tackling new healthcare issues posed by the space exposome and alternate insights into existing healthcare issues on Earth. By involving students in ESA led projects such as OYT13 and participating in community outreach through KS4 teaching and conferences, the educational aspect of Astropharmacy highlights the benefits of this research to the wider community and brings Astropharmacy to the forefront of the space-related healthcare field and shines light on its relevance to Earth-based healthcare as well.

Acknowledgements

The authors would like to acknowledge the University of Nottingham and the EPSRC for funding of their PhD projects. The authors would also like to acknowledge the European Space Agency for selection into the ‘Orbit Your Thesis!’ programme.

References

- Bradley JH, Stein R, Randolph B, Molina E, Arnold JP, Gregg RK. T cell resistance to activation by dendritic cells requires long-term culture in simulated microgravity. *Life Sci Space Res (Amst)*. 2017 Nov;15:55-61. doi: 10.1016/j.lssr.2017.08.002. Epub 2017 Aug 8. PMID: 29198314.
- Green MJ, Aylott JW, Williams P, Ghaemmaghami AM, Williams PM. Immunity in Space: Prokaryote Adaptations and Immune Response in Microgravity. *Life (Basel)*. 2021 Feb 2;11(2):112. doi: 10.3390/life11020112. PMID: 33540536; PMCID: PMC7912908.
- Mikines KJ, Dela F, Tronier B, Galbo H. Effect of 7 days of bed rest on dose-response relation between plasma glucose and insulin secretion. *Am J Physiol*. 1989 Jul;257(1 Pt 1):E43-8. doi: 10.1152/ajpendo.1989.257.1.E43. PMID: 2665517.
- Patel, Z.S., Brunstetter, T.J., Tarver, W.J. *et al*. Red risks for a journey to the red planet: The highest priority human health risks for a mission to Mars. *npj Microgravity* 6, 33 (2020). <https://doi.org/10.1038/s41526-020-00124-6>
- Tobin BW, Uchakin PN, Leeper-Woodford SK. Insulin secretion and sensitivity in space flight: diabetogenic effects. *Nutrition*. 2002 Oct;18(10):842-8. doi: 10.1016/s0899-9007(02)00940-1. PMID: 12361776.

ORAL 67

Brain structural and functional responses to long-duration spaceflight

S.Jillings¹, A.Van Ombergen¹, B.Jeurissen², E.Pechenkova³, J.Annen⁴, L.Litvinova⁵, A.Rumshiskaya⁵, I.Nosikova⁶, I.Rukavishnikov⁶, V.Sinitsyn⁷, V.Petrovichev⁵, S.Sunaert⁸, P.M.Parizel⁹, J.Sijbers², S.Laureys⁴, A.Demertzi¹⁰, P.zu Eulenburg¹¹, E.Tomilvoskaya⁶, F.L.Wuyts¹

¹Lab for Equilibrium Investigations and Aerospace - University of Antwerp, Antwerp, Belgium, steven.jillings@uantwerpen.be, ²imec-Vision Lab - University of Antwerp, Antwerp, Belgium ³Laboratory for Cognitive Research - Higher School of Economics University, Moscow, Russia ⁴Coma Science Group - University of Liège, Liège, Belgium; ⁵Centre for Treatment and Rehabilitation, Moscow, Russia ⁶State Scientific Centre of the Russian Federation - Institute for Biomedical Problems, Moscow, Russia; ⁷Department of Radiology - Lomonosov University, Moscow, Russia ⁸Department of Imaging and Pathology - KU Leuven, Leuven, Belgium; ⁹Department of Radiology - University of Western Australia, Perth, Australia; ¹⁰Physiology of Cognition - University of Liège, Liège, Belgium; ¹¹Institute for Neurology - Ludwig-Maximilian's University Munich, Munich, Germany

Introduction

In over half a century of crewed missions to space, many different effects of spaceflight on the human body have been uncovered so far. However, little focus has been directed to investigating how space stressors affect the human brain.

Methods

Through an ongoing longitudinal prospective study in Russian cosmonauts and ESA astronauts, we use magnetic resonance imaging (MRI) of various modalities to investigate brain structural and functional changes in the brains of space travelers. The combined use of multiple MRI modalities renders a large range of biological information on the brain and is suitable to detect changes related to neuroplasticity, which is the brain's ability to adapt to new exogenous and endogenous conditions. Specifically, we acquire anatomical T1-weighted (T1), diffusion MRI (dMRI), and resting-state functional MRI (rsfMRI) data in cosmonauts before their mission, as soon as possible post-flight, and again approximately seven months after the mission as a follow-up measurement. T1-weighted and diffusion MRI were used to unravel changes in macroscopic volumetric and microstructural architectural information in space crew. Resting-state functional MRI was used to study functional reorganisation of the brain after spaceflight by deriving functional connectivity measures from these data. Sample sizes differed across the various analyses performed and ranged from 10 to 15 pre- and post-flight measurements, with three missing data points for the follow-up measurement. All included space crew spent typical 6 months on the International Space Station (ISS).

Results

Contrary to our initial hypotheses, our first results revealed brain changes that appear unrelated to neuroplasticity. In summary, we find a widespread redistribution of the cerebrospinal fluid (CSF), including ventricular expansion, with secondary mechanistic effects on the grey matter (GM) tissue and white matter tracts (Van Ombergen et al. 2018; Van Ombergen et al. 2019; Jillings et al. 2020; Doroshin et al. 2022) (figure 1A). Additionally, we found evidence for neuroplasticity, according to our hypotheses. We detected net neural tissue increases in motor regions of the brain,

including primary motor cortex, basal ganglia, and cerebellum (figure 1B) (Jillings et al. 2020). Lastly, we found functional connectivity changes after spaceflight in higher-order brain regions, such as the cingulate cortex, insula, thalamus, and angular gyrus (figure 1C). Data at follow-up for most analyses indicate that early post-flight changes remain (partially) detectable seven months after the mission (Van Ombergen et al. 2018; Van Ombergen et al. 2019; Jillings et al. 2020; Doroshin et al. 2022). These findings at follow-up either indicate that the brain is slowly normalizing toward pre-flight levels, or either that some changes persist, potentially reflecting long-term learning effects.

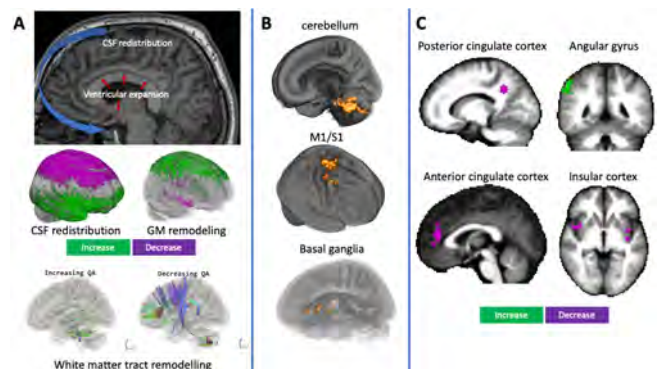


Figure 1. Overview of brain structural and functional changes following long-duration spaceflight. A) Structural changes pertaining to fluid and brain shifts and remodeling. These include CSF redistribution, ventricular expansion, GM crowding and displacement, and fibre tract reorganisation (bottom figure reused from Doroshin et al. 2022). B) Structural changes pertaining to neuroplasticity, including microarchitectural changes in primary motor cortex, basal ganglia, and cerebellum. C) Functional changes pertaining to neuroplasticity, including functional connectivity changes in higher order brain regions.

Conclusions

Before the year 2016, there was hardly any evidence on brain structural and functional changes occurring as a result of spaceflight. This study has rendered a vast increase in available information on this topic. In the future, the underlying mechanisms of the observed findings need to be understood in more detail. Ultimately, we aim to fully characterise the effects of space stressors on the brain to

mitigate the negative changes through countermeasures. Likewise, it will be important to characterise the beneficial coping mechanisms to microgravity, which can be promoted or enhanced to facilitate adaptation to the space environment. Altogether, pursuing these research studies will be crucial to ensure proper brain health for future human space travel.

Acknowledgements

This work was supported by the Belgian Science Policy (BELSPO) - Prodex.

References

Doroshin, A., Jillings, S., Jeurissen, B., Tomilovskaya, E., Pechenkova, E., Nosikova, I., Rumshiskaya, A., Litvinova, L., Rukavishnikov, I., De Laet, C., Schoenmaekers, C., Sijbers, J., Laureys, S., Petrovichev, V., Van Ombergen, A., Annen, J., Sunaert, S., Parizel, P. M., Sinitsyn, V., Zu Eulenburg, P., Osipowicz, K., Wuyts, F. L. Brain Connectometry Changes in Space Travelers After Long-Duration Spaceflight. *Frontiers in Neural Circuits*, 16, 815838. (2022).

Jillings, S., Van Ombergen, A., Tomilovskaya, E., Rumshiskaya, A., Litvinova, L., Nosikova, I., Pechenkova, E., Rukavishnikov, I., Kozlovskaya, I. B., Manko, O., Danilichev, S., Sunaert, S., Parizel, P. M., Sinitsyn, V., Petrovichev, V., Laureys, S., Zu Eulenburg, P., Sijbers, J., Wuyts, F. L., & Jeurissen, B. Macro- and microstructural changes in cosmonauts' brains after long-duration spaceflight. *Science Advances*, 6(36). <https://doi.org/10.1126/sciadv.aaz9488>. (2020).

Van Ombergen, A., Jillings, S., Jeurissen, B., Tomilovskaya, E., Rühl, R. M., Rumshiskaya, A., Nosikova, I., Litvinova, L., Annen, J., Pechenkova, E. V., Kozlovskaya, I. B., Sunaert, S., Parizel, P. M., Sinitsyn, V., Laureys, S., Sijbers, J., zu Eulenburg, P., & Wuyts, F. L. Brain Tissue–Volume Changes in Cosmonauts. *The New England Journal of Medicine*, 379(17), 1678–1680. (2018).

Van Ombergen, A., Jillings, S., Jeurissen, B., Tomilovskaya, E., Rumshiskaya, A., Litvinova, L., Nosikova, I., Pechenkova, E., Rukavishnikov, I., Manko, O., Danylichev, S., Maxine Rühl, R., Kozlovskaya, I. B., Sunaert, S., Parizel, P. M., Sinitsyn, V., Laureys, S., Sijbers, J., Eulenburg, P. zu, & Wuyts, F. L. Brain ventricular volume changes induced by long-duration spaceflight. In *Proceedings of the National Academy of Sciences* (Vol. 116, Issue 21, pp. 10531–10536). <https://doi.org/10.1073/pnas.1820354116>. (2019).

ORAL 68

High Content microscopy and super-resolution microscopy profiling to unravel the role of the actin cytoskeleton in T cell activation in microgravity

Julien Record¹, Christian Oertlin¹, Alf Vaerneus³, Edwin Langerak², Nikolai Kouznetsov¹, Sergey Ponomarev⁴, Lisa Westerberg¹

¹ Karolinska Institutet, Department of Microbiology, Tumor and Cell Biology (MTC), Solnavägen 9, 17165 Solna. Email: lisa.westerberg@ki.se

² Sioux Technologies B.V., 5633 AA Eindhoven, The Netherlands. Email : edwin.langerak@sioux.eu

³ Swedish Space Corporation, Torggatan 15, 17104 Solna, Sweden. Email: Alf.Vaerneus@sscspace.com

⁴ Institute of Bio-medical Problems of the Russian Academy of Sciences, 76a, Khoroshevskoe Shosse, Moscow, 123007, Russia. Email: dr.grey@bk.ru

Introduction

Cells of the immune system are able to quickly remodel their cytoskeleton to change shape during cell migration and cell-cell interaction. This allows immune cells to patrol our body and destroy pathogens and cancer cells [1]. At normal gravity, activation of the T cell receptor by a target cell stimulates large rearrangement of the actin cytoskeleton within minutes of activation. The structure formed is termed an immune synapse and is capable of conveying signals from the interacting cell to the T cell nucleus and induce gene expression [2]. The formation of the immune synapse aggregates the signals needed to determine the fate of the T cell and drive several T cell dependent immune processes, such as the activation of B cells and antibody production and the destruction of target cells by cytotoxic T cells[3,4].

Previous results from a dry immersion study showed that development and maturation of T cells was altered. This suggests that during space flight, T cell immunity would be compromised and result in difficulties to control viral infections and prevent development of cancer.

Our hypothesis is that microgravity affects the actin cytoskeleton which is the scaffold structure that integrate the signals during T cell activation.

To understand how microgravity alters early T cell activation, we will use the MASER sounding rocket equipped with a BIM module. Using this ESA platform, we will study cells carrying mutations in regulators of the actin cytoskeleton. We will examine the initial signalling events of T cell activation using activating surfaces that can mimic a target cell and activate T cells. Once recovered, the cells will be first imaged using a high content imaging system to assess phenotype modification on the whole population. Then, mutants affected by microgravity will be imaged using super-resolution microscopy to analyse the perturbations of the actin cytoskeleton with nanometric resolution (**Figure 1**).

Conclusions

Using a combination of advanced microscopy, we will study the early stages of the formation of the T cell immune synapse and unravel the connection between the actin cytoskeleton, T activation and microgravity

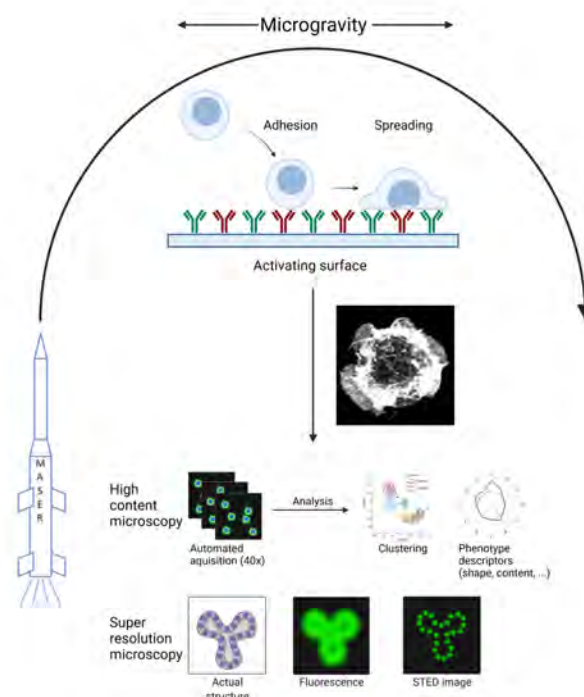


Figure 1: Experimental setup of micActin

Cells carrying mutations in the actin cytoskeleton will be sent on a MASER rocket. Once in microgravity, the cells will be activated by activating surfaces and fixed before the end of the microgravity. Once recovered, the cells will be imaged first by a high content imaging system and then by super-resolution microscopy.

References

- [1] Saeed MB, Record J, Westerberg LS. Chapter One - Two sides of the coin: Cytoskeletal regulation of immune synapses in cancer and primary immune deficiencies. *International Review of Cell and Molecular Biology*. 2020;356:1–97.
- [2] Huppa JB, Davis MM. T-cell-antigen recognition and the immunological synapse. *Nat Rev Immunol*. 2003;3(12):973–983.
- [3] He M, Saeed MB, Record J, et al. Overactive WASp in X-linked neutropenia leads to aberrant B-cell division and accelerated plasma cell generation. *Journal of Allergy and Clinical Immunology*. 2021;S0091674921012070.
- [4] Kritikou JS, Oliveira MMS, Record J, et al. Constitutive activation of WASp leads to abnormal cytotoxic cells with increased granzyme B and degranulation response to target cells. *JCI Insight*. 2021;

ORAL 69

Effects of Altered Gravity on Human Behaviour

Elisa Raffaella Ferre¹

¹ Department of Psychological Sciences, Birkbeck University of London, London, UK

Introduction

Human missions to Mars and the Moon along with commercial ventures for space travel are fast becoming a reality. As humanity prepare for a new space exploration age, understanding the impact of spaceflight on the human body and brain has never been timelier. Space is an extremely hostile environment. Astronauts face both physical and mental challenges; ionizing radiation, absence of circadian rhythm, confinement and isolation combined with prolonged exposure to non-terrestrial gravities. While the effects of non-terrestrial gravities on human bodily physiology, such as the musculoskeletal (Lang et al., 2017) and cardiovascular (Tanaka et al., 2017) systems are well-documented, relatively little is known on the impact of altered gravity on the human brain and behaviour. That is, most current scientific work on the effects of non-terrestrial gravity on cognition have largely been driven by isolated observations of behavioural alterations. As a result, no comprehensive view of the effects of both simulated and actual non-terrestrial gravity on neurocognitive functioning has been developed.

Here, we critically review key findings across the last 10 years of space research to provide a framework of cognition in zero gravity exploring findings in healthy individuals.

Cognition in Zero Gravity: Diffuse Framework vs. Cascade Framework?

Astronauts often describe dramatic alterations in sensorimotor functioning, including orientation, postural control and balance. Changes in cognitive functioning as well as in socio-affective processing have also been observed. Strikingly, no comprehensive theoretical model exists to outline the impact of non-terrestrial gravity on behaviour. Based on the anatomical and functional features of the brain areas affected by non-terrestrial gravity, we hypothesised that altered vestibular-gravitational signals might affect three main domains of neurocognitive function (Figure 1). First, a Sensorimotor Domain which includes pathways for the integration of sensory signals for orientation, perception and motor control. Second a Cognitive Domain which includes pathways for regulation of attention, executive functions, decision making and other higher cognitive functions. Finally, a Socio-Affective Domain which includes pathways for regulation of social behaviour and emotions.

We hypothesised two neurocognitive frameworks to potentially explain the effects of altered gravity on behaviour. First, a Diffuse Framework outlines an independent effect of zero gravity on the three domains (Figure 1). That is, deficits in one domain are independent to others. Independent interactions between altered vestibular-gravitational input would occur with each domain. Alternatively, a Cascade Framework takes a stepped approach whereby vestibular-

gravitational alterations firstly impact sensorimotor functioning and then cascade onto cognitive and socio-affective processing (Figure 1). According to this model, deficits in sensorimotor functioning for instance in arm reaching may lead to deficits in measures of cognitive processing such as increased reaction time and slower speed. This framework suggests a reliance of cognition and socio-affective processing on sensorimotor functioning, and potential bidirectional influences between cognition and socio-affective processing. Thus a competition for resources may take place whereby the brain is dealing with the unusual sensory information about gravity while performing cognitive and affective tasks. Specifically, the slowed movements in altered gravity environments impact the speed and accuracy of responses to cognitive tasks that often include a key response. A competition for resources may explain this delay, whereby the brain is processing not only unusual sensory information and challenging sensorimotor delays but also competing to process cognitive and affective information.

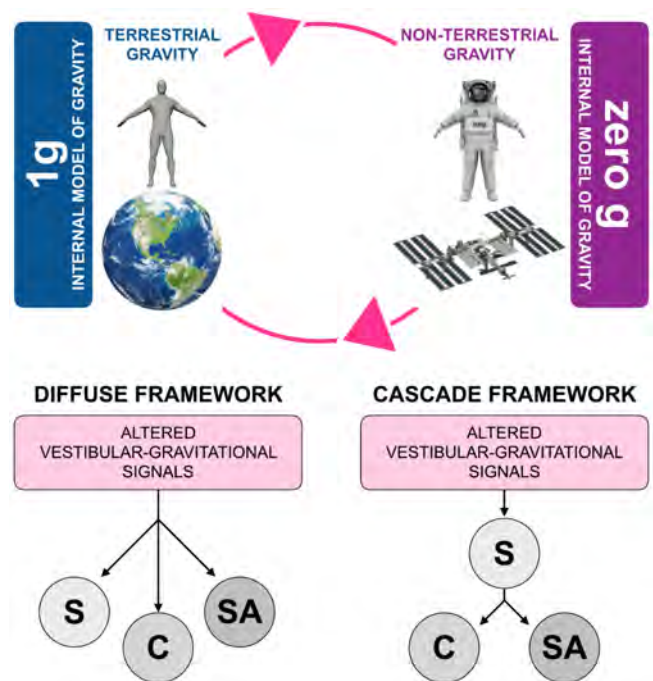


Figure 1. Effects of non-terrestrial gravity on sensorimotor functioning, cognition, and socio-affective processing.

Non-terrestrial gravity may affect three key functional domains: sensorimotor functioning (S), cognition (C) and socio-affective processing (SA). The Diffuse Framework suggests these three domains are implicated independently. The Cascade Framework suggests that sensorimotor functioning is mainly impacted by altered vestibular-gravitational signals and in turn affects cognitive and socio-affective skills.

A novel Effect Size approach

But, would it be possible to differentiate between the Diffuse Framework and the Cascade Framework? We have attempted to tackle this challenge by estimating the *effect size* on a selection of studies in the sensorimotor, cognitive and socio-affective domains to capture a representative, though clearly *not* systematic, sample. Effect sizes are quantitative measures of the magnitude of an experimental effect. They are tied to the magnitude of what has been measured in a study and is used to estimate a specific population parameter, avoiding the arbitrary logic of inferential statistics (i.e., significance testing).

We focussed on papers that have been peer-reviewed in the last ten years, that are widely cited and that used established methods to simulate non-terrestrial gravity environments. Focus was given to quantitative reports. Studies exploring social factors, culture, group conflict or team dynamics were not included. Our preliminary search identified approximately 146 articles relevant for sensorimotor domain, 91 articles for the cognitive domain and 63 for the socio-affective domain. However, for most of these studies it was not possible to compute the effect size estimates based on the reported statistical details.

Data support the Cascade Framework; the effect sizes are much higher in the sensorimotor domain compared to the cognitive and socio-affective domains highlighting an interesting neurofunctional architecture for the contribution of gravity on behaviour. Importantly, this is aligned with evidence suggesting that there is a strong interaction between vestibular and sensorimotor cues for controlling orientation, posture and motor control.

Conclusion

Having a coherent and accurate perception of the external environment is critical especially during space missions. We have reviewed the effects of non-terrestrial gravity on the human brain and behaviour across the sensorimotor, cognitive and socio-affective domains and have proposed a neurocognitive model based on the effect size of gravity effects on these key functions. The effect sizes are much higher in the sensorimotor domain compared to the cognitive and socio-affective domain, supporting a Cascade Framework. Fundamentally, our exercise highlighted the limitations of current human space research. Future studies should take a more systematic approach with a priori hypotheses driven by neurocognitive and neuroanatomical evidence and models. While the methodological challenges of creating physical zero gravity on Earth are inherently insurmountable, generating theoretically driven approaches, recruiting diverse large samples, using a range of tasks across domains and testing across multiple timepoints can help develop a coherent understanding of the effect of non-terrestrial gravity on the human body and brain. This quantified and systematic approach will not only allow us to identify how gravity constitutes foundational and fundamental signals for cognition, but also enable the development of effective training and interventions for future exciting space exploration, ultimately mitigating against risk.

Acknowledgements

This work was supported by a European Low Gravity Association Research (ELGRA) Prize to E.R.F.

References

Lang, T., van Loon, J. J. W. A., Bloomfield, S., Vico, L., Chopard, A., Rittweger, J., Kyparos, A., Blottner, D., Vuori, I., Gerzer, R., & Cavanagh, P. R. (2017). Towards human exploration of space: The THESEUS review series on muscle and bone research priorities. In *npj Microgravity* (Vol. 3, Issue 1, pp. 1–10).

Tanaka, K., Nishimura, N., & Kawai, Y. (2017). Adaptation to microgravity, deconditioning, and countermeasures. In *Journal of Physiological Sciences* (Vol. 67, Issue 2, pp. 271–281).

ORAL 70

Automatic structure function analysis using artificial intelligence

M. Chraga¹, H. Bataller¹, F. Croccolo¹

¹ LFCR UMR5150, E2S UPPA, CNRS, TotalEnergies, Universite de Pau et des Pays de l'Adour, Anglet, France
mohammed.chraga@univ-pau.fr

Introduction

Shadowgraphy is a powerful tool to characterize the structure and dynamics of simple and complex fluids. It is an efficient near-field scattering optical technique able to study density non-equilibrium fluctuations (NEFs). Fluctuations occur spontaneously in a fluid and are amplified by the presence of a gradient of, at least, one thermodynamic variable (concentration, temperature or pressure). The spatio-temporal evolution of NEFs, can be represented by the structure function of the Shadowgraph images (Croccolo et al. 2007, Croccolo et al. 2012, Schulz-DuBois and Rehberg 1981) over a wide range of wave numbers, as calculated by means of the differential dynamic algorithm (DDA) (Croccolo et al. 2007, Norouzisadeh et al. 2021). At each wave number, the structure function can be analyzed after providing a theoretical model (fitting equation) in order to extract the amplitudes and the dynamics of the fluctuations. The applicable model varies depending on the nature and conditions of the experiment, which can be a real challenge for the analysis of large amount of data. This is particularly true when different physical phenomena can dominate at different wave numbers. In this study, we take advantage of artificial intelligence (AI) to analyse the experimental structure function. We develop a program based on neural networks that predicts the best model to fit the structure function for each wave number thus allowing an automatic, fast and efficient analysis independent of the amount of data to be treated.

Structure function analysis

The basic theoretical equation of the structure function is given by (Croccolo et al. 2007):

$$SF = 2\{T(q)S(q)[1 - ISF(q, \Delta t)] + BG(q, \Delta t)\}, \quad (1)$$

where q and Δt represent the wave number and the correlation time, respectively. $T(q)$ is the optical transfer function of the shadowgraph, $S(q)$ the static power spectrum of the fluid density fluctuations and $ISF(q, \Delta t)$ is the Intermediate Scattering Function. The latter corresponds to the dynamic part of the structure function that can be modelled by a sum of exponential decays:

$$ISF(q, \Delta t) = \sum_{i=1}^n a_i \exp(-\frac{\Delta t}{\tau_i(q)}), \quad (2)$$

where n is the number of relaxation modes in the system (e.g. concentration and temperature). At small wave number, in the presence of propagating modes, a sinusoidal term needs to be included to describe the oscillations in the SF (Croccolo et al. 2019):

$$ISF(q, \Delta t) = a_1 \exp(-\frac{\Delta t}{\tau_1(q)}) + \frac{a_2}{\cos[\phi(q)]} \times \cos[\Omega(q)\Delta t + \phi(q)] \exp(-\frac{\Delta t}{\tau_2(q)}), \quad (3)$$

where Ω and ϕ depend on q and represent the oscillation frequency and phase. a_i are the relative amplitudes of the different modes such as $\sum_i a_i = 1$ and the $\tau_i(q)$ represent the decay times.

$BG(q, \Delta t)$ represents the optical background that can take different forms depending on the experimental conditions. Here, we take two possible forms, constant or quadratic:

$$BG_1(q, \Delta t) = A(q), \quad (4)$$

$$BG_2(q, \Delta t) = A(q) + B(q)\Delta t^2, \quad (5)$$

where A describes the experimental noise, while B is related to the stability of the background itself.

Therefore, depending on the investigated system and the wave number, the fitting equation of the structure function can be modelled by including different terms as described by Eq. (3), (4) or (5) for small wave numbers and by Eq. (2), (4) or (5) for large wave numbers. Additionally, it can be $n = 1$, if there is only one concentration mode (like in free diffusion experiments in binaries mixtures), or $n = 2$ if both concentration and temperature modes are present (like in thermodiffusion experiments in binaries mixtures). The optimal fit equation needs to be chosen for each wave number. Fig. 1 shows different representative shapes of the structure function depending on the model, as described above.

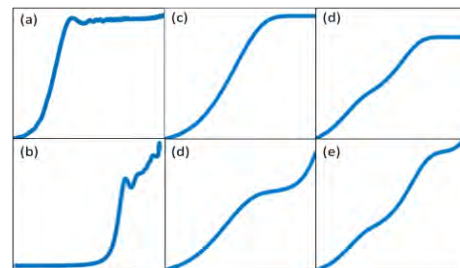


Figure 1: Different structure function shapes for constant (upper row) and quadratic BG (lower row), with oscillatory behavior (left column), one exponential (central column) and two exponentials (right column).

Automatic analysis

AI is a set of techniques that enable machines to perform tasks and solve problems automatically, after a learning procedure. Learning methods are needed to give computers the ability to perform tasks by imitating the way humans do the same. These methods include Machine Learning (ML) and Deep Learning (DL). They aim to give computers the ability to learn by themselves what calculation to perform rather than programming that calculation explicitly. ML involves developing a model using an optimization algorithm to minimize errors between the model and the data. DL is a subfield of machine learning in which, instead of developing a model, we develop a network of functions connected to each other, called artificial neural network (ANN). The deeper this network is (i.e. the more functions it contains), the better the machine is able to learn to perform complex tasks (Shinde et al. 2018). In this work, we show how we can leverage the power of the deep learning, especially convolutional neural networks (CNN) (Albawi et al. 2017) to analyze the experimental structure functions.

Our approach consists of two steps. First, we build-up the

learning data. We identify six homogeneous image classes; each class contains several images of different structure function shapes corresponding to the same fitting equation. Then, based on these image classes, the program decides what fit equation to use for new data. To do so, the experimental structure function at each wave number is smoothed using an artificial neural network, which consist of two-layer feedforward network with a sigmoid transfer function in the hidden layer and a linear transfer function in the output layer. Ten neurons are used in the hidden layer. Second, based on the homogeneous classes of the first step, the software chooses the more appropriate fit equation for new data using CNN. There are many known existing CNN models for image classification that have already learned to extract powerful and informative features from images, such as googlenet, alexnet, resnet50 and others. They have different architectures that make them adaptable for different kinds of data. In this work, we used Squeezenet (Iandola et al. 2016). It is a CNN architecture with few parameters maintaining high accuracy. Two strategies are used in Squeezenet, the first strategy is about judiciously decreasing the quantity of parameters in the CNN while attempting to preserve accuracy. The second is about maximizing accuracy on a limited budget of parameters. Smaller CNN architectures offer several advantages; in terms of the computation time, they require less commutation across servers during distributed training. Moreover, they are easier to deploy on FPGAs and other hardware with limited memory.

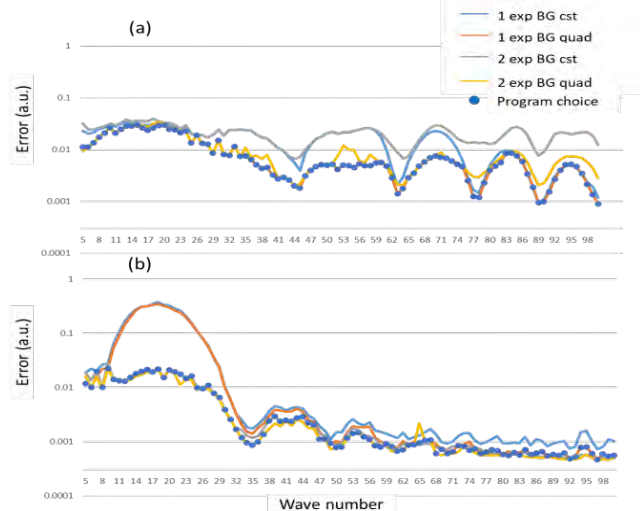


Figure 2: Error between thermodiffusion experimental data and SF model as a function of the wave number using different fit equation, one exponential with constant and quadratic background, two exponentials with constant and quadratic background, represented by the blue, orange, gray and yellow lines, respectively. The blue points represent the choice of the CNN program. (a) for TEG-water binary mixture and (b) for the PS-Toluene mixtures.

Results

Our approach shows high performance on choosing the best fit equation of the experimental structure function for each wave number. The graphs in Fig. 2 represent the error between the experimental data and the fitting equation for four fit models (one exponential with constant or quadratic background and two exponentials with constant or quadratic background) in two thermodiffusion experiments: Fig. 2a shows data from triethylene glycol (TEG)-water binary mixture and Fig. 2b from the polystyrene (PS)-toluene binary mixture. In both graphs, we used the concatenated angular

average of bi-dimensional structure functions of three series taken at 1Hz, 10Hz and 100Hz. We notice that our program predicts the best fit equation as compared to the minimum error for most of the wave numbers.

Conclusions

In this work, we show how we can take advantage of the power of artificial intelligence, especially deep learning, in the analysis of the experimental structure function. Our approach consists of two steps. “Data smoothing” allows creating homogeneous learning classes containing different structure function shapes. “Data clustering” predicts the fit equation of new experimental structure functions. The two steps are based on neural networks. High performance computing techniques using graphics processing unit (GPU) are highly recommended to obtain results in an optimal time. Once the software has selected the right model, we use an implemented Levenberg-Marquadt non-linear least square fitting routine to extract the amplitudes and the decay times of the fluctuations.

Acknowledgements

The authors express their gratitude to CNES and ESA for their support to the Giant Fluctuations project, as well as to the partners of the CO2ES Industrial Chair: E2S-UPPA, TOTAL, CNES and BRGM.

References

- F. Croccolo, D. Brogioli, A. Vailati, M. Giglio, and D. S. Cannell, “Nondiffusive decay of gradient-driven fluctuations in a free-diffusion process,” *Phys. Rev. E*, vol. 76, no. 4, p. 041112, Oct. 2007.
- F. Croccolo, H. Bataller, and F. Scheffold, “A light scattering study of non equilibrium fluctuations in liquid mixtures to measure the Soret and mass diffusion coefficient,” *J. Chem. Phys.*, vol. 137, no. 23, p. 234202, Dec. 2012.
- E. O. Schulz-DuBois and I. Rehberg, “Structure function in lieu of correlation function,” *Appl. Phys. A*, vol. 24, no. 4, pp. 323–329, Apr. 1981.
- M. Norouziadeh, M. Chruga, G. Cerchiari, and F. Croccolo, “The modern structurator: increased performance for calculating the structure function,” *Eur. Phys. J. E*, vol. 44, no. 12, p. 146, Dec. 2021.
- F. Croccolo, L. García-Fernández, H. Bataller, A. Vailati, and J. M. Ortiz de Zárate, “Propagating modes in a binary liquid mixture under thermal stress,” *Phys. Rev. E*, vol. 99, no. 1, p. 012602, Jan. 2019.
- P. P. Shinde and S. Shah, “A Review of Machine Learning and Deep Learning Applications,” in *2018 Fourth International Conference on Computing Communication Control and Automation (ICCCUBEA)*, Aug. 2018.
- S. Albawi, T. A. Mohammed, and S. Al-Zawi, “Understanding of a convolutional neural network,” in *2017 International Conference on Engineering and Technology (ICET)*, Antalya, Aug. 2017.
- F. N. Iandola, S. Han, M. W. Moskewicz, K. Ashraf, W. J. Dally, and K. Keutzer, “SqueezeNet: AlexNet-level accuracy with 50x fewer parameters and <0.5MB model size,” *ArXiv160207360 Cs*, Nov. 2016.

ORAL 73

Thermoelectric convection in rectangular cavities in microgravity conditions

¹A. Meyer, ¹M. Meier, ¹V. Motuz, ¹Y. Sliavin, ²E.B. Barry, ¹M. Strangfeld, ¹P. Szabo, ¹C. Egbers, ²I. Mutabazi

¹Brandenburg University of Technology, Cottbus, Germany, meyer@b-tu.de

²Normandie Université, Le Havre, France,

Introduction

For our latest parabolic flight campaign (CNES VP 161th, Sept./ Oct. 2021), we investigated the effect of the dielectrophoretic (DEP) force in a rectangular cavity, similar to our experiments performed during the CNES-PFC VP139 in autumn 2018. The DEP force originates from the combination of a non-homogeneity in electric field and of a stratification of permittivity, here due to a temperature variation. Under microgravity conditions, theoretical (Yoshikawa et al. 2013) and numerical investigations (Tadie Fogaing et al. 2014) showed the increase of the heat transport in the rectangular cavity due to the DEP force, as well as the important feedback effect of the perturbation electric gravity in this configuration. We aim to observe experimentally the destabilization of a dielectric fluid and to characterize this thermoelectric instability in parabolic flight conditions.

Experimental Set-up

The gap between the two TCO-coated plates has a length of 200 mm, a width of 40 mm and a depth of 5 or 10mm. The Synthetic Schlieren technique (Dalziel et al. 2000) is used to visualize the density variations. For that technique, an LED panel to which is directly placed a foil with randomly distributed black dots illuminates the gap from one side of the rectangular cavity. A camera is placed on the other side of the rectangular cavity and captures the dots displacement with respect to a reference image corresponding to the case when no temperature gradient and no high voltage are applied. The horizontal plate is heated from the top and cooled from the bottom so that there is no flow due to the previous gravity phases of the parabolic flight when the high voltage is applied. In the CNES VP 161th campaign, the chosen fluid was 1-Nonanol for its quite high relative electric permittivity of about 8.6. However the liquid we used has been found to be contaminated and its dielectric property could not be ensured. Our experience from the-PFC VP139 in 2018 indicates that only Novec 7200 fluid has shown instabilities during the microgravity phases of the CNES-PFC VP139.

Results

Figure 1 shows the Synthetic Schlieren result obtained for Novec 7200 at the end of the microgravity phase of two different parabolas. For $V_p = 1\text{kV}$, the displacement field of the pattern shows no particular divergence, indicating a homogeneous temperature field in the (x, y) plan. For $V_p = 2\text{kV}$, a disturbance of the displacement field is measured and its divergence highlights a modal structure of the perturbation with a certain wavelength of the order of twice the gap size ($d = 5\text{mm}$). The Novec 7200 fluid has then destabilized to a Rayleigh-Bénard like instability induced by the electric gravity.

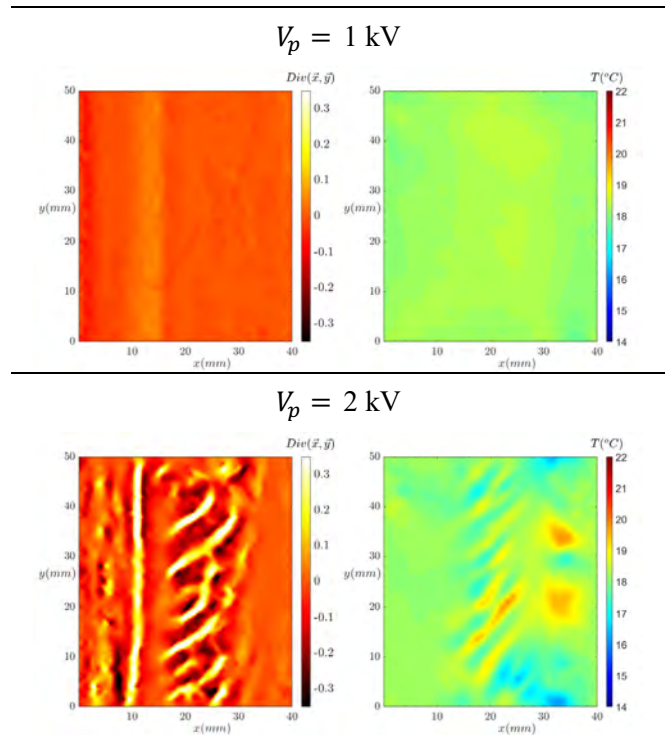


Figure 1: Divergence of the displacement field of the random pattern (left) and simulation of the temperature field resulting from the divergence of the displacement field (right) for Novec in a 5mm gap with $\Delta T = 6.5\text{K}$ at the end of the microgravity phase of two parabolas corresponding to two different kV tensions applied.

Acknowledgements

The projects ”Thermoelektrische Konvektion unter Schwerelosigkeit (TEKUS)” was supported by the german federal ministry of economics via the space agency of the German Aerospace Center DLR under grant no. 50WM1944. We acknowledge the support of the Airbus DS – TEXUS team, the Centre Nationale d’Études Spatiales (CNES), Novespace S.A. in Bordeaux and our technical staff at Brandenburg University of Technology.

References

Yoshikawa, H.N., Tadie Fogaing, M., Crumeyrolle, O., Mutabazi, I. Dielectrophoretic Rayleigh-Bénard convection under microgravity conditions. *Phys. Rev. E*, 87, 043003 (2013).
Tadie Fogaing, M., Yoshikawa, H.N., Crumeyrolle, O., Mutabazi, I. Heat transfer in the thermo-electro-hydrodynamic convection under microgravity conditions. *Eur. Phys. J. E*, 37, pp. 35-40 (2014).
Dalziel, S., Hughes, G., Sutherland, B. Whole-field density measurements by ‘synthetic schlieren’, *Exp. Fluids*, 28, pp. 322-335 (2000).

ORAL 74

Efficient and Stable Hydrogen and Oxygen Production in Microgravity

Ö. Akay¹, S. Saravanabavan², E. Sokalu², A. Romero-Calvo*³, K. Brinkert*^{1,2}

¹ ZARM - Center of Applied Space Technology and Microgravity, University of Bremen,
28359 Bremen, Germany, oemer.akay@zarm.uni-bremen.de, katharina.brinkert@zarm.uni-bremen.de

² Department of Chemistry, University of Warwick, CV4 7AL Coventry, United Kingdom, s.saravanabavan.1@warwick.ac.uk,
eniola.sokalu@warwick.ac.uk, katharina.brinkert@warwick.ac.uk

³ Daniel Guggenheim School of Aerospace Engineering, Georgia Institute of Technology, Atlanta, Georgia, 30332, USA,
alvaro.romerocalvo@colorado.edu

Introduction

The management of fluids in microgravity is hindered by the absence of buoyancy, which impacts a wide variety of space technologies including propellant management, heat transfer, and life support. The production of hydrogen and oxygen and the recycling of carbon dioxide are of particular importance for in-situ resource utilization, energy storage, and advanced habitation systems, which have been identified as critical technology development areas by NASA's STMD.

Of particular interest for this work are (photo-)electrochemical (PEC) devices as they can produce essential chemicals such as oxygen and hydrogen in two set-ups: either, by coupling the electrochemical cell to external photovoltaic cells as currently utilized on the *International Space Station* (Takada et al. 2015, Chow et al. 2019) or by direct utilization of sunlight in a monolithic device, where integrated semiconductor-electrocatalyst systems carry out the processes of light absorption, charge separation and catalysis in one system in analogy to natural photosynthesis (Young et al. 2017, Cheng et al. 2018). The latter device is particularly relevant for space applications due to present mass and volume constraints.

Here, we discuss two combined approaches to overcome phase separation challenges in (photo-)electrolyzer systems in reduced gravitational environments: using the hydrogen evolution reaction (HER) as a reference, we combine nanostructured, hydrophilic electrocatalyst surfaces for efficient gas bubble desorption (Brinkert et al. 2018, Akay et al. 2021) with magnetically-induced buoyancy (Romero-Calvo et al. 2022) to direct the produced hydrogen gas bubbles on specific trajectories away from the (photo-)electrode surface. (Photo-)current-voltage (J-V) profiles obtained in micro-gravity for 9.2 s at ZARM's drop tower in Bremen show that our systems can operate with our two-fold approach near terrestrial efficiencies. A comprehensive analysis of the magnetic environment generated by our magnetic setup accompanies experimental observations, allowing us to attribute the achieved phase separation in the PEC cells to the increased electrode wettability as well as the systematic use of diamagnetic and Lorentz forces. These results inform the design of future electrolytic cells with no moving parts.

Acknowledgements

This work was supported by the German Aerospace Center (DLR) with funds provided by the Federal Ministry for Economics Affairs and Energy (BMWi), Germany, under Grant No. DLR 50WM2150 (project LiMo). A.R.C. acknowledges the financial support offered by the Rafael del

Pino Foundation under its 2021 Excellence Fellowship. The authors thank the ZARM team around Dr. Thorben Könemann for their outstanding support of this project.

References

- (1) Takada, K. C., Ghariani, A. E., Van Keuren, S., Advancing the Oxygen Generation Assembly Design to Increase Reliability and Reduce Costs for a Future Long Duration Mission, *45th International Conference on Environmental Systems* (ICES-2015-115), Bellevue, Washington (July 2015).
- (2) Chow, R., Nelson, G. J., Perry, J. L., Electrolyzer Exergy Analysis for an Environmental Control and Life Support System, *Proceedings of the ASME International Mechanical Engineering Congress and Exposition*, vol. 6A. 2018.
- (3) Young J. L., Steiner M. A., Döscher H., France R. M., Turner J. A., Deutsch T. G., Direct solar-to-hydrogen conversion via inverted metamorphic multi-junction semiconductor architectures, *Nature Energy* 2, 17028, 2017.
- (4) Cheng W. H., Richter M. H., May M. M., Ohlmann J., Lackner D., Dimroth F., Hannappel T., Atwater H. A., Lewerenz H. J., Monolithic Photoelectrochemical Device for 19% Direct Water Splitting, *ACS Energy Letters* 3 (8), 1795-1800, 2018.
- (5) Brinkert, K., Richter, M. H., Akay, Ö., Liedtke, J., Giersig, M., Fountaine, K. T., Lewerenz, H. J. Efficient Solar Hydrogen Production in Microgravity Environment, *Nature Communications* 9, 2527, 2018.
- (6) Akay, Ö., Poon, J., Robertson, C., Abdi, F. F., Roldan-Cuenya, B., Giersig, M., Brinkert K., Releasing the Bubbles: Nanotopographical Electrocatalyst Design for Efficient Photoelectrochemical Hydrogen Production in Microgravity Environment. *Advanced Science*, 2105380, 2021.
- (7) Romero-Calvo, Á., Schaub, H., Cano-Gómez, G. Diamagnetically Enhanced Electrolysis and Phase Separation in Low Gravity, *Journal of Spacecraft and Rockets*, 59 (1), 59-72, 2022.
- (8) Romero-Calvo, Á., Akay, Ö., Schaub, H., Brinkert, K. Magnetic Phase Separation in Microgravity, *npj Microgravity*, accepted (May 2022).

ORAL 75

Blue Abyss to Enable Gravity-Related Research and Training

V. Pletser¹, M. Howard¹, S.N. Evetts¹, J. Vickers¹

¹ Blue Abyss, Pool Innovation Centre, Trevenson Road, Pool, Redruth, Cornwall TR15 3PL, UK
vladimir.pletser@blueabyss.uk, mindy.howard@blueabyss.uk, simon.evetts@blueabyss.uk, john.vickers@blueabyss.uk
Topics: C1, C2

Introduction

The number of astronauts in space will increase exponentially in the coming years as the number of commercial suborbital flights and orbital flights increase, and as human missions to the Moon and Mars become a reality. This new step in space exploration will only be possible if research and training at different gravity levels is actively pursued.

1. Blue Abyss

Blue Abyss (<http://www.blueabyss.uk>), a UK company based in Newquay, Cornwall, with expected expansion to the USA, the Arabic peninsula, and the Far-East, proposes a versatile approach for astronaut training and research at various gravity levels and in different environments.

The Blue Abyss project [1-2] is built around four main axes: (1) A versatile multi-use dive pool with several platforms from 3 to 20 m, a space research area, the Astrolab, located at a depth of 12m, and a 50 m deep shaft (see Fig.1);

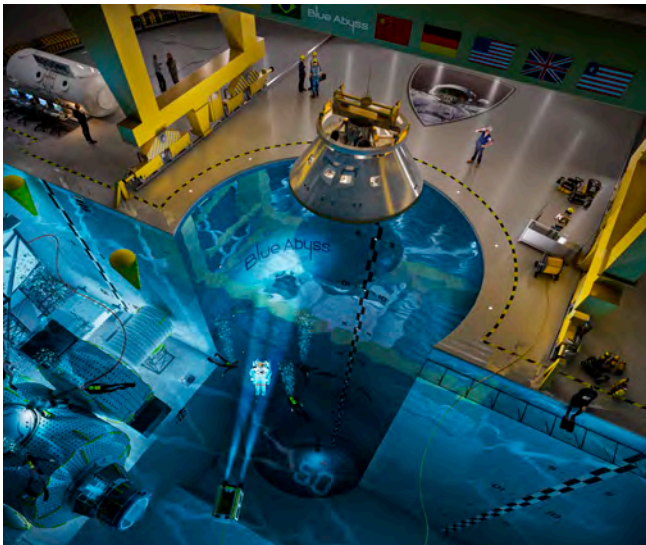


Figure 1: Artist view of the Blue Abyss pool, with the Astrolab on the lower left and 50m shaft in the middle. (Credit: CityScape).

(2) The provision of centrifuge services to refine the study of hypergravity physiological effects; (3) A parabolic flight capability to offer zero, reduced and hyper gravity for physical, biology and human physiology research; and (4) A pedagogical and outreach program offering an interactive, dynamic approach to STEM-related education for students, tomorrow's scientists.

2. Ground Infrastructure for Research

The ground infrastructure will include laboratories and classrooms; hypobaric and hyperbaric chambers; and the

Kuehneger Human Performance Centre, a unique research centre that will house specialized test and evaluation facilities. The centre will include a microgravity simulation suite with a traversable, full-body suspension system and other microgravity and hypergravity simulators that will be used for physiological studies, rehabilitation and training. Astrolab will offer a pressurized module which can accommodate crews for short and long duration missions to train at 0g, at Moon-g or at Mars-g with special buoyancy equipment. Aircraft parabolic flights with dedicated mock-ups of space vehicles, space station modules and extra-terrestrial planetary base modules will offer further capabilities for orbital research and training. Meticulous preparation using multiple parabolas will enable space mission procedures and protocols to be carefully and successfully practised to prepare for future Moon and Mars exploration missions.



Figure 2: Example of a Blue Abyss projected Airbus A330/40 aircraft (Credit: Airbus/Blue Abyss).

Conclusion

This paper will present the latest planning for these unique capabilities under development with international partners.

References

1. V. Pletser, S. Evetts, J. Vickers, and S. Parazyński "Commercial Space Flight Preparation and Extra Vehicular Activities Training: The Next Generation", *New Space, J. Space Entrepreneurship and Innovation*, 7(3), pp. 120-125, 2019.
2. V. Pletser, M. Howard, S. Evetts, and J. Vickers "Blue Abyss to train future Moon and Mars Astronauts: Enabling astronaut operations for extra-terrestrial planetary exploration and exploitation", *Space Resources Week 2021*, ESRIC, Luxembourg, 19-22 April 2021.

ORAL 76

Heat transfer induced by thermoelectric convection in a cylindrical annulus in microgravity

C. Kang¹, H.N. Yoshikawa², I. Mutabazi³

¹Jeonbuk National University, Jeonju, Republik of Korea, changwoo.kang@jbnu.ac.kr, ²Université de Nice Côte d'Azur, Nice, France, harunori.yoshikawa@unice.fr; Normandie Université, Le Havre, France, innocent.mutabazi@univ-lehavre.fr

Introduction

A dielectric liquid under the action of an alternating nonuniform electric field pertains a dielectrophoretic force. This force is due to the inhomogeneity of permittivity of the medium [1]. In case of the inhomogeneity induced by temperature gradient, the dielectrophoretic force contains a conservative term which contributes to the pressure in the fluid and a non conservative component which can generate vorticity even in a quiescent liquid and thus lead to thermal convection called thermoelectric convection [2,3]. In cylindrical and spherical configurations with a radial temperature gradient and central electric field, the dielectrophoretic force is radial and thus can be used to model the heat transfer in planets. Since few decades, there are few studies which have addressed the thermoelectric convection in spherical configurations [4,5].

Electric gravity

We investigate the conditions of development of thermoelectric convection in a dielectric liquid confined in a cylindrical annulus of radii R_1 and R_2 subject to radial temperature gradient $\Delta T/d$ and a radial electric field under microgravity conditions. The dielectric liquid is characterized by the electric permittivity $\epsilon(T)$, the density ρ , the thermal diffusivity κ , the thermal expansion coefficient α and the kinematic viscosity ν .

The dielectrophoretic buoyancy reads $\delta\rho g_e$ where $\delta\rho = \rho - \rho_{ref}$ and $g_e = \frac{e}{\alpha\rho_{ref}} \nabla \left(\frac{\epsilon_{ref} E^2}{2} \right)$ is the electric gravity which is collinear with the gradient of the electric energy stored in the cylindrical capacitor. We assume the so-called electrohydrodynamic Boussinesq approximation [2] which consists in taking the linear dependence of the density and permittivity with the temperature in the buoyancy term i.e. $\epsilon(T) = \epsilon_{ref}[1-e(T-T_{ref})]$ and $\rho(T) = \rho_{ref}[1-e(T-T_{ref})]$ with T_{ref} being the reference temperature.

Governing equations

The flow system is described by the Navier-Stokes equations together with the energy equation, the mass conservation and the Gauss equation for the charge conservation.

$$\frac{\partial \vec{u}}{\partial t} + (\vec{u} \cdot \vec{\nabla})\vec{u} = -\vec{\nabla}H + \Delta\vec{u} - \frac{L}{Pr} \vec{g}_e \theta$$

$$Pr \left[\frac{\partial \theta}{\partial t} + (\vec{u} \cdot \vec{\nabla})\theta \right] = \Delta\theta$$

$$\vec{\nabla} \cdot \vec{u} = 0, \quad \vec{\nabla} \cdot [(1 - \gamma_e \theta)\vec{\nabla}\phi] = 0.$$

where \vec{u} is the velocity field, θ is the temperature deviation from the reference temperature T_{ref} , $\vec{E} = -\vec{\nabla}\phi$ is the time-averaged of the electric field. The flow control parameters are the radius ratio $\eta = R_1/R_2$, the Prandtl number $Pr = \nu/\kappa$ and the electric Rayleigh number $L = \alpha\Delta T g_e d^3/\nu\kappa$. The boundary conditions in the time-averaged description of the electric field are given by :

$$\vec{u} = 0, \theta = 1; \phi = 1 \text{ at } r = \eta/(1-\eta)$$

$$\vec{u} = 0, \theta = 0; \phi = 0 \text{ at } r = 1/(1-\eta)$$

These equations are solved using a DNS code [3] to produce flow patterns (Fig.1-a), velocity, vorticity (Fig.1-b) and temperature distributions and thus to compute the Nusselt number and its dependence with the electric Rayleigh number. We found that the TEHD convection is efficient for heat transfer under microgravity conditions.

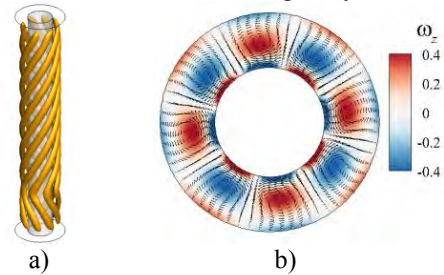


Figure 1: a) Helical convective vortices, b) axial vorticity distribution in the cross-section $z = \text{const}$.

Conclusion

Thermoelectric convection in a cylindrical annulus in microgravity appears in form of stationary helical vortices [6]. As the electric Rayleigh number L is increased, vortices become time-dependent and the heat transfer is increased.

Acknowledgements

The work has benefited from a financial support CNES and the ANR through the program ‘‘Investissements d’Avenir (Grant N°ANR-10 LABX-09-01), LABEX EMC³ and the bilateral exchange program PHC-STAR.

References

- [1] L.D. Landau and E.M. Lifshitz, *Electrodynamics of Continuous Media*, MIR (1990).
- [2] P.H. Roberts, Electrohydrodynamic convection, *Q.J. Mech. Appl. Maths*, **22**, 211-220 (1969)
- [3] C. Kang and I. Mutabazi, Dielectrophoretic buoyancy and heat transfer in a dielectric liquid in a cylindrical annular cavity, *J. Appl. Phys.* **125**, 184902 (2019)
- [4] J.E. Hart, G.A. Glatzmaier and J. Toomre, Space-laboratory and numerical simulations of thermal convection in a rotating hemispherical shell with a radial gravity, *J. Fluid Mech.* **173**, 519-544 (1986).
- [5] B. Futterer, M. Gellert, T. von Larcher and C. Egbers, Thermal convection in rotating spherical shells: an experiment and numerical approach within GEOFLOW, *Acta Astronaut.* **62**, 300-307(2008).
- [6] V. Travnikov, O. Crumeyrolle and I. Mutabazi, Numerical investigation of the heat transfer in cylindrical annulus with a dielectric fluid under microgravity, *Phys. Fluids* **27**, 054103(2015).

ORAL 80

Film-wise condensation of pure vapour on CNT-coated curvilinear fin in microgravity

E. Barakhovskaia^{1,2}, A. Glushchuk¹, C. S. Iorio¹

¹Université libre de Bruxelles, Belgium, ²Novosibirsk State University, Russia
Ella.Barakhovskaia@ulb.be, Andrey.Glushchuk@ulb.be, Carlo.Iorio@ulb.be

Introduction

There is a growing demand for high-performance condensers to improve device efficiency. One of the efficient intensification methods of vapour condensation is the finning of a condenser surface (Gregorig, 1954). The intensification is provided not only by increasing the contact area between the vapour and the cold surface but also by the local action of surface tension forces, which helps move the condensate from the finned condenser additionally to gravity force. Another method gaining popularity is the modification of heat exchange surfaces through the application of coatings (Deisenroth et al., 2018). However, most published works analyse the coatings' effect on drop-wise condensation, while a film-wise regime occurs for most used fluids. Particularly relevant for heat exchangers are carbon-based coatings (Preston et al., 2015). Additionally to unique physical properties, carbon-based coatings create particular structures like “spaghetti-like” carbon nanotubes (CNT) or graphene “flakes” (Zhang and Li, 2009).

In this work, the condensation intensification is achieved due to curvature variation along the condenser’s interface and by using the CNT-based multilayer coating. Experiments were conducted during ESA Parabolic Flight Campaign 69. The results include thermal data and accurate optical measurements of the condensate thickness distribution. The impact of a CNT-coated surface on heat transfer is analysed by comparing a mirror-like polished condenser’s surface.

Experiment

The experimental concept is shown in Fig.1. The experiments were carried out under microgravity conditions. To stabilise condensate flow, the capability of a curvilinear surface to drive liquid and a combination of a porous media and a pump, as an active condensate retraction system, were used. The condenser has a curvilinear brass body and a plastic porous media surrounding it. Condenser and porous media are placed in a tight container with pure vapour. The porous media collects and stores condensed fluid. The condenser’s axisymmetric shape choice is well suited to applying the afocal measuring technique to detect thin film thickness with high accuracy. A liquid with low surface tension provides a film-wise condensation regime.

A particular experimental set-up has been created (Barakhovskaia et al., 2021). The pressure and temperature of the vapour were maintained constant. The condenser’s temperature was lower than the vapour with the help of a thermoelectric module, which was also used to evaluate condensation heat. By controlling the walls' temperature, the condensation occurred only along the condenser's surface and nowhere else. The temperature field in the condenser’s body was measured. The afocal optical system consisted of a collimated light source and an image projection system.

During the experiment, the vapour temperature was maintained at 57-60°C, the vapour pressure was 750-890 mbar. The temperature of the inner box walls was 61±0.5°C. The condenser’s temperature was varied between 11-40°C. Methoxy-nonafluorobutane (HFE-7100) was used as a working fluid because of its latent heat value (111 kJ/kg) and low surface tension (0.00136 kN/m). The CNT-based coating applied on a brass surface has been compatible and stable with HFE-7100 for a long time.

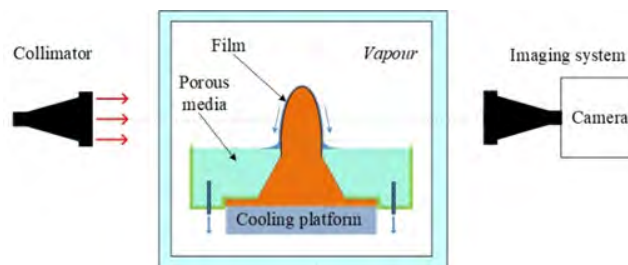


Figure 1: Concept of the experiment

Condenser’s description

The experiment was conducted on two condensers initially having the same curvilinear shape but different coatings (*Mirror* and *CNT*). The visible part of each condenser (Fin) is demonstrated in Fig.2. A porous media around the fins was made of polypropylene (average pore size 100-160 μm). INVAR reference object was installed to detect any displacements of the fin for precise optical measurements. The first fin remained uncoated and was polished to have a *Mirror-like surface*. Water solutions of single-wall carbon nanotubes (CNT) with a mass-volume concentration of 0.3% were used to coat another fin. The dip-coating method (Barakhovskaia et al., 2022) was applied to create the multilayer CNT-based coating.

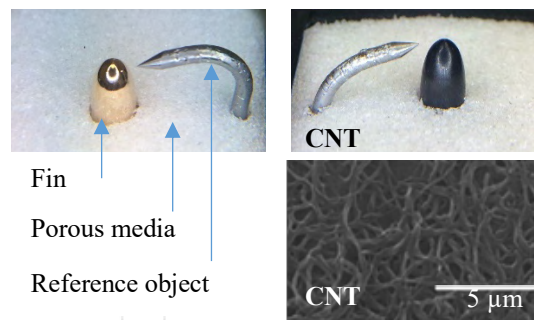


Figure 2: Fins and Scanning electron microscope image of CNT-coated surfaces

Results

The condensation capability of each fin was compared using two parameters: condensation heat and film thickness

distribution. The schematic of the fin is shown in Fig.3a, where T_1 indicates the temperature sensor's position inside the fin used for the analysis, the accuracy of the used sensor was 0.1°C.

The coating quality is essential for the heat transfer devices in terms of durability and uniformity. Adhesion tests showed that created coating is durable and robust; however, the uniform distribution was not reached (Fig.3b). The thickness along the fin surface changes significantly along the right and left sides. If a homogeneous coating is desired, the dip-coating technique should be adapted or reconsidered for curvilinear fins.

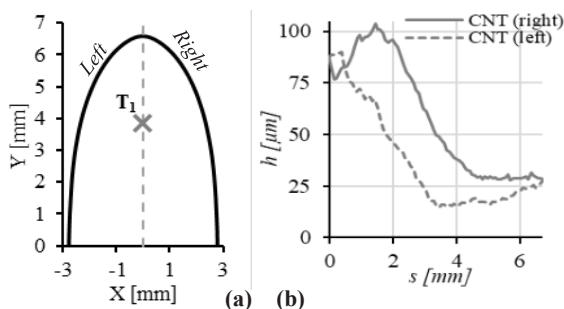


Figure 3: (a) Fin profile and position of temperature sensors; (b) CNT coating thickness distribution along the surface.

Fig.4 shows the condensation heat Q released during the condensation depending on temperature drop $\Delta T = T_{sat} - T_1$ (T_{sat} is saturation temperature). The CNT-coated surface's condensation heat showed higher up to three times when $\Delta T = 22^\circ\text{C}$.

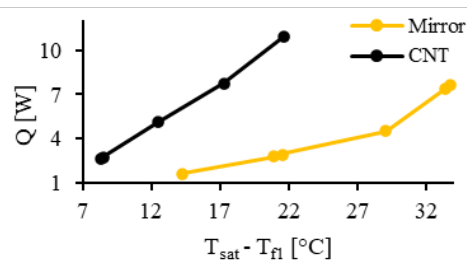


Figure 4: Condensation heat depending on ΔT

Fig.5 shows condensate distribution along the fin's surface during the microgravity period when vapour pressure and temperatures inside the fin were stable. The condensate film distribution was evaluated by comparing each point of the imaged fin contour with and without liquid. The accuracy of the method was 2 μm.

The film thickness distribution grows with the increase of temperature drop in the case of the mirror-like surface. The porous media is located at the surface arc length of 7.7 mm in Fig.5. The film's abrupt thinning can be observed due to the presence of porous media of the same material and close pore size. Interesting to note that if the difference is obvious for the uncoated mirror sample than for the CNT-coated sample, the behaviour of the film is entirely different. The film thickness did not increase as was expected. However, the condensation heat increased to 2 times at the same ΔT .

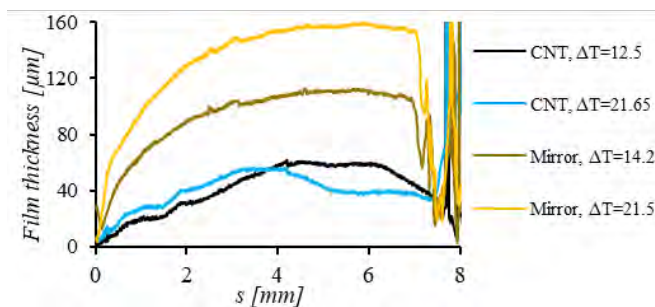


Figure 5: Film thickness distribution

Conclusion

During ESA PFC-69, experiments were conducted on film-wise vapour condensation on the curvilinear fin with the mirror-like surface and the multilayer CNT-based coated surface.

Compared with the mirror-like sample, a significant increase in condensation heat was observed on the CNT-coated surface. The condensation heat increases up to 3 times with the growth of temperature drop for the CNT-coated sample at $\Delta T = 22^\circ\text{C}$. The CNT-based coating influences condensate film distribution. Further investigation is needed to explain better the results of coating impact on the condensation process.

Acknowledgements

This work was done in the framework of Heat Transfer Prodex project under the financial support of the Belgian Federal Science Policy Office.

References

- R. Gregorig, Hautkondensation an feingewellten Oberflächen bei Berücksichtigung der Oberflächenspannungen, *Zeitschrift für angewandte Mathematik und Physik*, 5 (1), 1954
- D.C. Deisenroth, R. Moradi, A.H. Shooshtari, F. Singer, A. Bar-Cohen, M. Ohadi, Review of heat exchangers enabled by polymer and polymer composite additive manufacturing, *Heat Transf. Eng.*, 39 (19), 2018
- D. Preston, D. Mafra, N. Miljkovic, J. Kong, E. Wang, Scalable Graphene Coatings for Enhanced Condensation Heat Transfer, *Nano letters*, 15, 2015
- M. Zhang, J. Li, Carbon nanotube in different shapes, *Materials Today*, 12 (6), 2009
- E. Barakhovskaia, A. Glushchuk, P. Queeckers, C.S. Iorio, Stabilisation of condensate flow from curvilinear surfaces by means of porous for space applications, *Exp. Therm. Fluid Sci.*, 121 (2021).
- E. Barakhovskaia, L. Apicella, A. Glushchuk, C. Minetti, C.S. Iorio, A fast methodology to assess the quality of coatings on rough 3D surfaces, *Diamond and Related Materials*, 125, 2022

ORAL 81

Shared payload platform for small-sized microgravity experiments

Gunnar Florin¹, Stefan Krämer¹, Christian Lockowandt¹

¹ Swedish Space Corporation SSC, Sweden, gunnar.florin@sscspace.com, stefan.kramer@sscspace.com, christian.lockowandt@sscspace.com

Introduction

Swedish Space Corporation (SSC) provides advanced space services and access to space including rideshare service within SSC's SubOrbital Express (SIX) sounding rocket program. SIX is an extension of the heritage MASER program, which has provided successful flights since 1987.

The rideshare service is a complement to the flight implementation of the larger microgravity experiments of ESA and other customers, which constitutes the basis for the 285 kg scientific payload mission.

Shared Module for multiple small-sized experiments

With the forthcoming SubOrbital Express mission (SIX-3/M15 in 2022), SSC offers launch opportunities for small payloads within a new service, based on a shared accommodation concept. The "Shared Module" is a new payload platform, hosting multiple small-sized experiments in a joint rideshare compartment.

The main objective is to provide sub-orbital flight opportunity with 6 minutes of high-quality undisturbed microgravity environment to a broader audience than a custom-made experiment system, traditionally flown on SSC's SubOrbital Express rockets. This new service may benefit customers with small-sized, self-contained payloads, designed to fit into the Shared Module payload format.

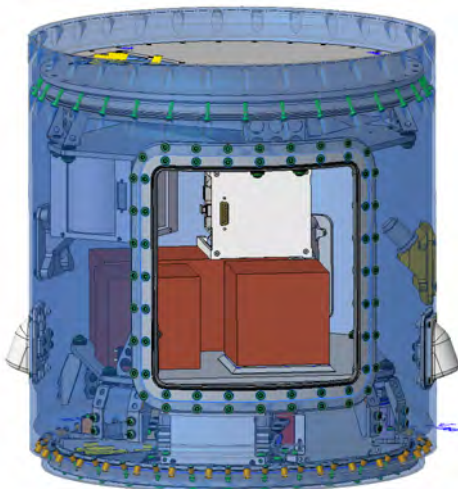


Figure 1: Shared Module populated by five U-sized payloads

Concept

The basic concept is a shared compartment, housing several small sized experiments from different customers or scientific groups, Standard interface solutions for power, communication, thermal control and mechanical implementation can be provided. The Shared Module service also includes a common resource system (e.g. power, lift-off status and telemetry) for basic flight support.

Each experiment is individually powered by the platform's support electronics and can therefore be individually switched on/off during test and launch campaign. One TM/TC communication line is available for each experiment, when integrated in the module. The communication line can be used for monitoring and control of experiment during tests on ground, and/or live stream data during flight.

The support for biological and life science experiments including late access and fast recovery is optional and supported by the Shared Module rideshare concept.

Shared Module experiments on forthcoming flight

Contracted experiments for the first Shared Module flight – in the fields of biology, radiation deflection and space qualification – on SIX-3/M15 are

- *LabOnPaper* by Universities of Lisbon and Porto, Portugal (funded by ELGRA);
- *MUSA* by Orbital Space Technology, Costa Rica;
- *RADICALS* by RMIT, Australia;
- *ADI-Alpha* by ResearchSat, Australia;
- FORTIS Watches, Switzerland

Conclusions

The SubOrbital Express rideshare service has been extended to include a dedicated system for accommodation of small-sized payloads (1-5 kg). Small 1U payloads of institutions and universities worldwide as well as commercial operators will benefit from the service.

This paper will further discuss the technical Shared Module approach and the first mission outline, focusing on the payload requirements for this typical rideshare mission.

ORAL 82

Containerless measurements of thermophysical properties on board the ISS using the electromagnetic levitator ISS-EML

M. Mohr¹, Y. Dong¹, H. Fecht¹

¹Institute of Functional Nanosystems, Ulm University, Ulm, Germany
markus.mohr@uni-ulm.de, yue.dong@uni-ulm.de, hans.fecht@uni-ulm.de

Introduction

A solid materials properties are defined by its chemistry and its crystalline structure and grains morphology. The typical manufacturing processes of metallic alloys contain a step where the molten metal alloy is solidified. This is not only the case for traditional material casting, but also for 3D-printing techniques, such as Laser Powder Bed Fusion. The generated solid materials microstructure (e.g., single-crystalline, polycrystalline, or even glassy), depends on the processing conditions, especially the cooling rate.

As a consequence, the solidification process has to be controlled closely, in order to obtain the desired microstructure. A number of computer simulations exist, which assist the design and optimization of solidification processes. These simulation models require reliable data on the thermophysical properties of the liquid and forming solid phases. As a consequence, precise measurements of these properties are necessary.

While for the solid phase, these property data can be obtained by conventional measurement equipment, precise measurements in the liquid phase have several challenges.

The relevant properties are related to the transport of heat and mass in the liquid, such as the surface tension, viscosity and mass density, specific heat capacity, and thermal conductivity.

The contact of liquid metal with a container is often the main source of measurement errors. As an example, reactions between the liquid metal and the container walls can interfere with the measurement of the heat flux during calorimetric measurements. Furthermore, the dissolution of container material into the melt will alter the composition and can considerably change the observed surface tension.

The best approach to overcome these challenges is the use of containerless processing methods, such as electromagnetic levitation (Fecht and Wunderlich, 2017). Electromagnetic levitation offers the benefit of a self-stabilizing sample positioning, as long as the sample is electrically conductive. Hence, electromagnetic levitation is the method of choice for containerless processing of metals and their alloys.

Nonetheless, the large gravitational force, that needs to be overcome on earth requires strong positional forces. These lead to strong fluid flows in the liquid sample which make the measurement of properties that require a laminar flow (e.g. viscosity) impossible. Furthermore, the sample is usually strongly deformed, which makes precise measurement of the sample temperature a challenge. The strong positioning force also considerably heats up the samples, which prevents the access of the undercooled liquid range.

In order to overcome this shortcomings, electromagnetic levitation processing can be performed on microgravity platforms, where the positional forces needed to keep the sample in place are small.

As a result, heating and positioning are de-coupled and a large temperature range in the stable and undercooled liquid range are accessible. This enables the application of a number of well-established measurement methods, in order to obtain thermophysical property data, such as the surface tension, viscosity, specific heat capacity, thermal conductivity, mass density, and electrical resistivity (Mohr and Fecht, 2021).

The ISS-EML

The Electromagnetic levitation facility ISS-EML is located in the European experiment module «Columbus» module of the International Space Station ISS. A photograph is shown in Figure 1. The device, developed by Airbus Defence and Space, was installed in the European Drawer Rack in 2014. Until now, the EML was operational in orbit for more than 6000 h. In total, over 1500 melting cycles have been performed so far, which generated about 15 TByte of data.



Figure 1: The ISS-EML in the Columbus module of the International Space Station ISS.

Conclusions

Precise data on thermophysical properties of a number of generic and industrial metallic alloys has been measured and analyzed in the last years. These encompass high-temperature alloys like Ti- and Ni-based alloys, steel and bulk metallic glasses (Fecht and Mohr, 2022). This presentation will give an overview over the measurement facility, applied methods and some highlight results.

Acknowledgements

The authors acknowledge the access to the ISS-EML, which is a joint undertaking of the European Space Agency (ESA) and the DLR Space Administration. We further acknowledge the funding from the DLR Space Administration with funds provided by the Federal Ministry for Economic Affairs and

Energy (BMW) under Grant No. 50WM2143.

References

Fecht, H. J. and Wunderlich, R. K. (2017) “Fundamentals of Liquid Processing in Low Earth Orbit: From Thermophysical Properties to Microstructure Formation in Metallic Alloys”, *JOM*, 69(8), 1261–1268.

Mohr, M., and Fecht, H.-J. (2021) “Investigating Thermophysical Properties Under Microgravity: A Review.” *Advanced Engineering Materials* 23(2), 2001223.

Fecht, H.-J., and Mohr, M., Eds. “Metallurgy in Space – Recent Results from ISS”, *The Minerals, Metals & Materials Series*, Cham: Springer (2022)

ORAL 83

Thermophysical properties of bulk metallic glasses measured on board the ISS using the electromagnetic levitator ISS-EML

Y. Dong¹, M. Mohr¹, H. Fecht¹

¹Institute of Functional Nanosystems, Ulm University, Ulm, Germany
yue.dong@uni-ulm.de, markus.mohr@uni-ulm.de, hans.fecht@uni-ulm.de

Introduction

Metallic glasses are amorphous solids with metallic atomic bonds. Because of the lack of a lattice dislocation slip system, as in crystalline alloys, metallic glasses exhibit some outstanding properties, such as high elastic strain, high hardness and high strength [1,2]. However, the glass transition process is still not fully understood. And their industrial applications are still limited. One key problem is the scarcity of accurate data of thermophysical quantities of the glass forming liquids. At high temperature, the routine container-based measurement methods are difficult to carry out. The high reactivity of liquid metals leads to reactions with containers, disturbing the precise measurement. In addition, the container walls present a source for heterogeneous nucleation, influencing the glass formation / crystallization process significantly. Thus, containerless methods for the measurement of thermophysical properties of liquid alloys are necessary [1,3].

Electromagnetic levitation (EML) is a well-developed containerless technique. However, the high electromagnetic field required to lift the sample against gravity causes excessive heating and turbulence due to induced eddy currents, resulting in large uncertainty. In order to avoid it, in this project, we applied EML measurements on board International Space Station (ISS). Under microgravity conditions, much smaller levitation forces are needed since the force of gravity no longer has to be overcome (only a weak positioning field is required). This means that heating effects, magnetic pressure, melt turbulence, and asphericity of the molten drop are significantly reduced, allowing considerably more accurate results to be obtained [1,4].

Investigated Metallic Glass Alloys

Several different glass former systems have been analyzed in this project, including Fe-, Zr-, Pd-, Pt-based alloys and Cu-Zr. Fe-based metallic glasses show excellent soft ferromagnetic properties. They have been widely used in electric transformers. Fe-based metallic glasses also have high corrosion and wear resistance, which have large application potential in additive manufacturing. In this project, the alloy Fe_{57.75}Ni_{19.25}Mo₁₀C₅B₈ was investigated, supplying the needed thermophysical property data for development of a 3D-printing process [5].

Zr-based metallic glasses have high strength and good elastic properties. Spacecraft inserts brackets and gears made by Zr-based bulk metallic glasses have been developed by NASA. However, the brittleness and toxic material (such as Be) limit their application. In this project, we studied various Be-free Zr-based alloys, such as LM105 and VIT106a. Their thermophysical properties have been obtained for process simulations using these alloys, as well as for development of new metallic glass materials [6,7].

Pd-based and Pt-based metallic glasses formers have excellent glass-forming ability with a large supercooled liquid region. Therefore, they possess good formability. In this project, thermophysical properties of Pd₄₃Ni₁₀Cu₂₇P₂₀ and Pt_{57.3}Cu_{14.6}Ni_{5.3}P_{22.8} alloys have been measured, which are important for the simulation of continuous casting processes [8,9].

A sample of the simple composition Cu₅₀Zr₅₀ was investigated, due to its reliable potential functions for MD simulations. Comparing the measured physical properties with the results derived from molecular dynamics simulations is helpful to understand the connection between atomic structure and macroscopic thermophysical properties of liquid/metallic glasses [10].

Results

The surface tension of the liquid alloys can be calculated from the surface oscillation frequency. Short heater pulses were applied during the sample cooled down process to initiate the surface oscillation [11]. The surface tension of the glass former Fe_{57.75}Ni_{19.25}Mo₁₀C₅B₈ and Pd₄₃Cu₂₇Ni₁₀P₂₀, show a boomerang-like shape with temperature. The reason could be oxygen adsorption or surface-active species of the alloy.

The surface oscillations are damped, exhibiting an exponentially decreasing amplitude. This is due to internal friction by the liquids viscosity. The time constant of the exponential decay can be used to get the liquid viscosity [12]. The temperature-dependent viscosity of a liquid gives a manifestation of the change of the liquid's kinetics during cooling, which plays an important role in glass formation.

The modulation calorimetry was applied to analyze the specific heat capacity. It is based on the modulation of the heating power and the observation of the temperature response [13]. The specific heat can be used together with other thermodynamic quantities to describe the Gibbs free energy difference between the crystalline solid and liquid phase, required for models of nucleation. A slight decrease in specific heat with increasing temperature is found in the temperature range just above the melting point of the alloys. The Fe-based metallic glass shows a higher molar heat capacity than the Zr-based metallic glasses.

Using the calorimetry method, the total hemispherical emissivity can also be obtained. No strong temperature dependence was found for all samples.

The sample coupling electronics (SCE) of the microgravity EML facility can be used to measure the electrical resistivity of samples. It can monitor the radio frequency voltages and currents and store their amplitudes and phase relationships with high resolution [14].

During the processing of LM105 in helium, an average cooling rate of about 8 K/s was achieved, which is similar to the reported critical cooling rate of it (~ 10 K/s). A cycle performed in a helium atmosphere is shown in Figure 1(a), where no recalescence is observed. This means that the sample solidified as a glass [15]. Hence, this was the first production of a metallic glass sphere in space!

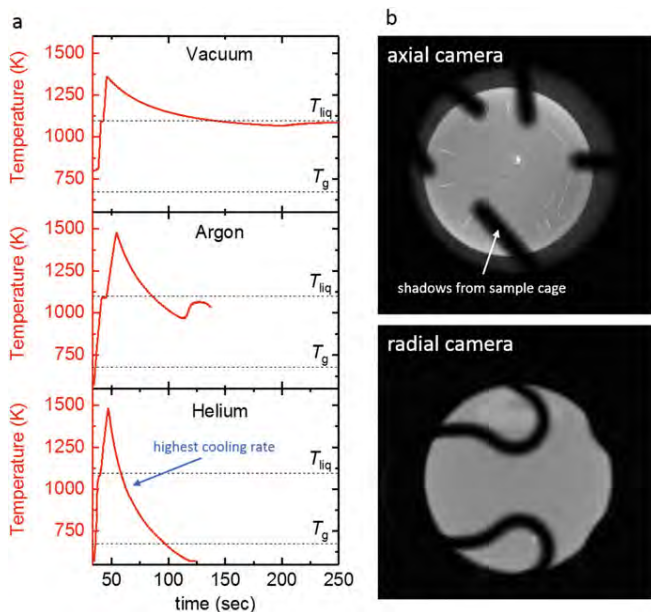


Figure 1: (a) Containerless processing cycles of LM105 in the ISS-EML under different atmospheres. (b) Camera images of the liquid sample during cooling [15].

Conclusions

Thermophysical properties of various metallic glass formers have been measured using containerless methods under microgravity condition. The obtained data gives access to the thermodynamic quantities relevant for the description of the glass formation or crystallization. The thermophysical properties in the solid and liquid phases are also important input parameters for numerical simulations of the production processes such as casting, blow moulding, injection moulding, continuous casting and 3D printing. By the successful vitrification of a 6.5 mm diameter sphere of LM105, the first metallic glass was fabricated in space.

Acknowledgements

The authors acknowledge the access to the ISS-EML, which is a joint undertaking of the European Space Agency (ESA) and the DLR Space Administration. We further acknowledge the funding from the DLR Space Administration with funds provided by the Federal Ministry for Economic Affairs and Energy (BMWi) under Grant No. 50WM2143.

- [1] H.-J. Fecht, M. Mohr, *Metallurgy in Space - Recent Results from ISS. The Minerals, Metals & Materials Series. Cham: Springer, (2022)*
- [2] W. Johnson, Bulk glass-forming metallic alloys: science and technology, *MRS bulletin*, 24, 42-56, (1999)
- [3] M. Mohr, H.-J. Fecht, Investigating Thermophysical Properties Under Microgravity: A Review, *Advanced Engineering Materials*, 23, 2001223, (2021)
- [4] W. Soellner, EML-containerless processing facility for materials science research on board the ISS, *J. Jpn. Soc. Microgravity Appl.* 27, 4 (2010)
- [5] C. Suryanarayana, A. Inoue, Iron-based bulk metallic glasses, *Int. Mater. Rev.* 58, 131–166, (2013)
- [6] A. Peker, W.L. Johnson, A highly processable metallic glass: $Zr_{41.2}Ti_{13.8}Cu_{12.5}Ni_{10.0}Be_{22.5}$, *Appl. Phys. Lett.* 63, 2342–2344, (1993)
- [7] X.H. Lin, W.L. Johnson, W.K. Rhim, Effect of oxygen impurity on crystallization of an undercooled bulk glass forming Zr-Ti-Cu-Ni-Al alloy. *Mater. Trans. JIM* 38, 473–477, (1997)
- [8] H.W. Kui, A.L. Greer, D. Turnbull, Formation of bulk metallic glass by fluxing. *Appl. Phys. Lett.* 45, 615–616, (1984)
- [9] A.J. Drehman, A.L. Greer, D. Turnbull, Bulk formation of a metallic glass: $Pd_{40}Ni_{40}P_{20}$. *Appl. Phys. Lett.* 41, 716–717 (1982)
- [10] W.H. Wang, J.J. Lewandowski, A.L. Greer, Understanding the glass-forming ability of $Cu_{50}Zr_{50}$ alloys in terms of a metastable eutectic. *J. Mater. Res.* 20, 2307–2313, (2005)
- [11] S. Sauerland, K. Eckler, I. Egry, High-precision surface tension measurements on levitated aspherical liquid nickel droplets by digital image processing, *Journal of Materials Science Letters*, 11, 330-332, (1992)
- [12] H. Lamb, On the oscillations of a viscous spheroid, *The Proceedings of the London Mathematical Society*, 13, 51, (1881)
- [13] H.J. Fecht, W.L. Johnson, A conceptual approach for noncontact calorimetry in space. *Rev. Sci. Instrum.* 62, 1299–1303, (1991)
- [14] G. Lohöfer, High-resolution inductive measurement of electrical resistivity and density of electromagnetically levitated liquid metal droplets, *Review of Scientific Instruments*, 89, 124709, (2018)
- [15] M. Mohr, R.K. Wunderlich, D.C. Hofmann, H.-J. Fecht, Thermophysical properties of liquid $Zr_{52.5}Cu_{17.9}Ni_{14.6}Al_{10}Ti_5$ – Prospects for bulk metallic glass manufacturing in space. *npj Microgravity*, 5, 24, (2019)

ORAL 86

Anomalous Behaviour of Temperature Non-Equilibrium Fluctuations across pure CO₂ Widom Line

P. Fruton, E. Lisoir, F. Croccolo, C. Giraudet*

Universite de Pau et des Pays de l'Adour, E2S UPPA, CNRS, TotalEnergies, LFCR UMR5150, Anglet (France)

*cedric.giraudet@univ-pau.fr

According to classical thermodynamics, there is no physical distinction between a gas and a liquid beyond the critical plait point of a fluid. However, recent studies have shown that there is a specific (p,T) -region, emanating from the critical plait point, where the response function of thermophysical properties is maximum (Gallo2014) and shows a critical enhancement (Giraudet2016). The (p,T) -line forming the Widom line represents the transition from a gas-like to a liquid-like behavior demarked by notable changes in the network-like structure at the molecular scale (Simeoni2010). Owing to the long-ranged nature of fluctuations (NEFs) in fluids stressed by a temperature gradient (Ortiz de Zárate2004), they can be used as a probing tool for the simultaneous determination of several thermophysical properties (Wu2020) as well as the effect of confinement (Giraudet2015) and propagating waves (Croccolo2019). Until now, it remains unclear how NEFs behave across the Widom line of a fluid out-of-equilibrium. In particular, it is worth understanding if, and under which conditions, their analysis allows the determination of a gas-like and a liquid-like phase. In the present work, we are focusing on pure CO₂ subjected to a purely conductive temperature gradient. In the following, we analyze the dynamical behavior of NEFs in presence of symmetric and assymetric density gradients at various distances from the critical plait point; see conceptual brown thin lines terminated by open circles in Figure 1.

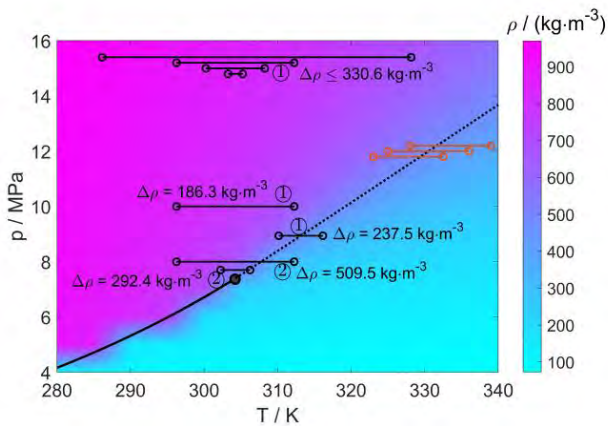


Figure 1: Density map of pure CO₂ around the gas-liquid coexistence curve (thick continuous line). The dotted line represents the critical isochore along which Widom lines merge (Fomin2015) close to the critical plait point (filled large circle: $T_c = 304.21$ K, $p_c = 7.37$ MPa, $\rho_c = 469.03$ kg·m⁻³). Thin lines terminated by open circles depict some of the temperature differences that have been investigated on a 5 mm thick layer of CO₂. The circled numbers define the number of “phases” that must be considered when the fluid is stressed by a stable temperature gradient.

The present ground-based experiments are preliminary investigations for future experiments under reduced gravity conditions on the spatiotemporal behavior of NEFs in supercritical CO₂.

The experiments were conducted on a shadowgraph apparatus equipped with a high-speed camera and a superluminescent diode operated at 670 nm. A brief description of the optical and mechanical arrangement of the setup as well as of the sample cell can be found in Ref. (Giraudet2014). All measurements were repeated several times using different acquisition frequencies to provide the highest accuracy. The refractive index structure functions (SFs) were determined using a differential dynamic analysis (Cerchiari2012) after image windowing (Giavazzi2017). In total, more than 20 temperature gradients were studied at difference distances from the critical plait point, crossing or not the Widom line, with symmetric and assymetric density gradients.

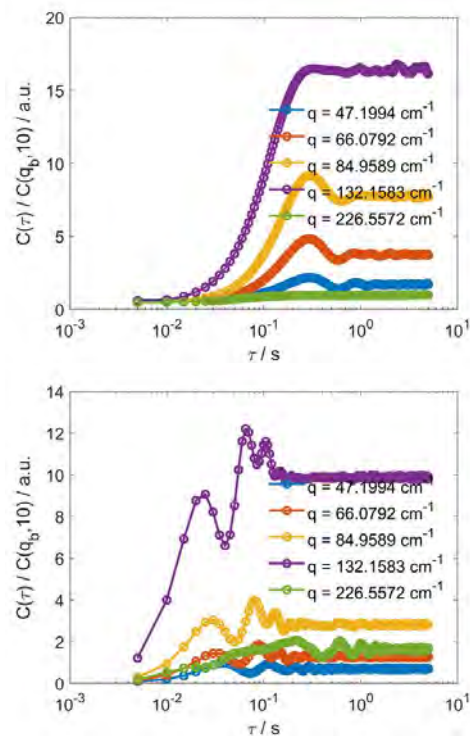


Figure 2: Autocorrelation functions of refractive index NEFs for different wavenumbers when 1 (top: $p = 15$ MPa, $T = 308.15$ K, $\Delta T = 44$ K) or 2 (bottom: $p = 7.4$ MPa, $T = 304.25$ K, $\Delta T = 4$ K) phases have to be considered.

Figure 2 shows several SFs as a function of the delay time for different wavenumbers when the density gradient is far from the critical isochore (top) and crosses the Widom region (bottom). In the upper part of Figure 2, all SFS can be described by the exponential growth of fluctuations with propagating waves for $q \leq 85$ cm⁻¹, as commonly found in liquids. Independently of the strength of the density gradient, however, when it crosses the Widom line, experimental SFs consist in the sum of two exponential functions with two corresponding propagating wave regimes; see bottom part of Figure 2. Under these circumstances, the fluid can be

assimilated to a two-phase system with distinct thermophysical properties. The lower and upper parts of the fluid have distinct thermal diffusivities and compressibilities that can be derived from the dynamics of small NEFs and from the frequency of the propagating modes for large NEFs, respectively. Besides the concept for characterization of the continuous transition between liquid-like and gas-like in supercritical fluid, we will discuss the influence of the symmetry and asymmetry of the density gradients as well as the influence of the relative distance from the critical plait point.

Besides a better understanding of non-equilibrium thermodynamics in supercritical fluids, the present results have direct implication in the long-term storage of CO₂ in saline aquifers or depleted gas reservoirs, as well as for thermal energy storage and dispatchable green electricity using sCO₂ Carnot batteries.

Acknowledgements

We acknowledge financial support from the CNES, the ESA and from the E2S UPPA Hub Newpores and the Industrial Chair CO2ES supported by the Investissements d'Avenir French programme managed by ANR (ANR16IDEX0002).

References

- P. Gallo, D. Corradini, M. Rovere, Widom line and dynamical crossovers as routes to understand supercritical water, *Nat Commun* **5**, 5806 (2014)
- C. Giraudet, L. Marlin, D. Bégué, F. Croccolo, H. Bataller, Concentration dependent refractive index of CO₂/CH₄ mixture in gaseous and supercritical state, *J Chem Phys* **144**, 134304 (2016)
- G. Simeoni, T. Bryk, F.A. Gorelli, M. Krisch, G. Ruocco, T. Scopigno, The Widom line as the crossover between liquid-like and gas-like behaviour in supercritical fluids, *Nature Phys* **6**, 503–507 (2010)
- J. M. Ortiz de Zárate, J. V. Sengers, On the physical origin of long-ranged fluctuations in fluids in thermal nonequilibrium states, *J Stat Phys* **115**, 1341-1359 (2004)
- W. Wu, J.H. Jander, M.H. Rausch, A.P. Fröba, C. Giraudet, Simultaneous determination of multiple transport properties over a wide range of temperatures and pressures from the analysis of non-equilibrium fluctuations by the shadowgraph method, *J Chem Phys* **153**, 144201 (2020)
- C. Giraudet, H. Bataller, Y. Sun, A. Donev, J.M. Ortiz de Zárate, F. Croccolo, Slowing-down of non-equilibrium fluctuations in confinement, *Europhys Lett* **111**, 60013 (2015)
- F. Croccolo, L. Garcia-Fernández, H. Bataller, A. Vailati, J.M. Ortiz de Zárate, Propagating modes in a binary liquid mixture under thermal stress, *Phys Rev E* **99**, 012602 (2019)
- Y.D. Fomin, V.N. Ryzhov, E.N. Tsiok, V.V. Brazhkin, Thermodynamic properties of supercritical carbon dioxide: Widom and Frenkel lines, *Phys Rev E* **91**, 022111 (2015)
- C. Giraudet, H. Bataller, F. Croccolo, High-pressure mass transport properties measured by dynamic near-field scattering of non-equilibrium fluctuations, *Eur Phys J E* **37**, 107 (2014)
- F. Giavazzi, P. Edera, P.J. Lu, R. Cerbino, Image windowing mitigates edge effects in differential dynamic microscopy, *Eur Phys J E* **40**, 97 (2017)
- G. Cerchiari, F. Croccolo, F. Cardinaux, F. Scheffold, Note: Quasi-real-time analysis of dynamic near field scattering data using a graphics processing unit, *Rev Sci Instrum* **83**, 106101 (2012)

ORAL 88

Different Spaceflight-Associated Changes in the Perivascular Spaces of Astronauts and Cosmonauts

G. Barisano^{1,2}, F. Sepehrband¹, I. Rukavishnikov³, I. Nosikova³, L. Litvinova⁴, V. Petrovichev⁴, E. Pechenkova⁵, J. Sijbers⁶, B. Jeurissen^{6,7}, C. De Laet⁷, C. Schoenmaekers⁷, S. Jillings⁷, H.R. Collins⁸, M. Law^{9,10}, A. Grishin¹¹, E. Tomilovskaya^{3,*}, D. Roberts^{8,*}, F.L. Wuyts^{7,*} (* Equal contributions)

¹Laboratory of Neuroimaging, Stevens Neuroimaging and Informatics Institute, University of Southern California, Los Angeles, CA. ²Neuroscience Graduate Program, University of Southern California, Los Angeles, CA. ³Institute of Biomedical Problems, Russian Academy of Sciences, Moscow, Russia, ⁴Radiology Department, City Clinical Hospital, Moscow, Russia, ⁵Laboratory for Cognitive Research, National Research University Higher School of Economics, Moscow, Russia, ⁶imec - Vision Lab, Department of Physics, University of Antwerp, Antwerp, Belgium, ⁷Lab for Equilibrium Investigations and Aerospace, University of Antwerp, Antwerp, Belgium. ⁸Department of Radiology and Radiological Science, Medical University of South Carolina, Charleston, SC. ⁹Department of Radiology, Alfred Health, Melbourne, Australia. ¹⁰Department of Neuroscience, Department of Electrical and Computer Systems Engineering, Monash University, Melbourne, Australia. ¹¹Gagarin Cosmonauts Training Center, Star City, Russia. results of brain data from 3 different space agencies.

Abstract

Very recently, it was observed that long duration spaceflight is associated with an upward shift of the brain towards the cranium, redistribution of CSF with narrowing of the subarachnoid space at the vertex, crowding of brain tissue along the superior sagittal sinus, and enlargement of the cerebral ventricles. Continued enlargement of the ventricles has been documented after spaceflight even up to one year after return to Earth in both NASA astronauts and Russian cosmonauts.

The current study focuses on perivascular spaces (PVS), a brain-wide network of perivascular channels along which a large proportion of CSF (or CSF-like fluid) circulate through the brain parenchyma, which have not yet been evaluated after spaceflight. Hereto, a comparative, joint quantitative analysis of alterations in cerebral CSF spaces across astronauts and cosmonauts, using the same analysis pipeline thereby eliminating investigators bias, has been performed for the first time in space research history.

We performed a joint analysis of MRI brain scans in 23 NASA astronauts, 13 Roscosmos cosmonauts, and 4 ESA astronauts before and after long-duration spaceflight (mean: 179.0 ± 48.3 days) on the ISS. An additional follow-up scan was performed in 4 ESA astronauts and 10 cosmonauts 7 months after return to Earth. Brain MRI data from 13 age- and education-matched male volunteers acquired with a time interval similar to the preflight-postflight and preflight-follow-up (n=8) intervals and from 7 NASA astronauts acquired before and after missions of short duration in the Space Shuttle Program were used as controls.

The NASA ISS group (n = 23, M = 25.27%, SD = 17.24) had a significantly greater percent change in PVS than the Roscosmos group (n = 13, M = 12.44%, SD = 6.27, p = .03), the NASA Shuttle group (n = 7, M = 1.31%, SD = 4.57, p < .001), and the control group (n = 13, M = 5.27%, SD = 9.12, p < .001). We hypothesize this difference may be related to on-board differences in countermeasure or exercise usage between the American and Russian programs. Additionally, PVS differences between the Russian and American crewmembers could point towards a physiological mechanism underlying spaceflight associated neuro-ocular syndrome (SANS), a condition associated with visual acuity changes and ophthalmological exam findings which is considered a serious medical risk for long-duration spaceflight. Our study is the first ever reporting on combined

References

1. Barisano G et al. The effect of prolonged spaceflight on cerebrospinal fluid and perivascular spaces of astronauts and cosmonauts. Proc Natl Acad Sci U S A, 2022.
2. Roberts DR, Albrecht MH, Collins HR, et al. Effects of Spaceflight on Astronaut Brain Structure as Indicated on MRI. N Engl J Med. 2017;377(18):1746-1753.
3. Koppelmans V, Bloomberg JJ, Mulavara AP, Seidler RD. Brain structural plasticity with spaceflight. NPJ Microgravity. 2016;2(1):2.
4. Van Ombergen A, Jillings S, Jeurissen B, et al. Brain Tissue-Volume Changes in Cosmonauts. N Engl J Med. 2018;379(17):1678-1680.
5. Iliff JJ, Wang M, Liao Y, et al. A paravascular pathway facilitates CSF flow through the brain parenchyma and the clearance of interstitial solutes, including amyloid beta. Sci Transl Med. 2012;4(147):147ra111.
6. Stegner MB, Tarver W, Brunstetter TJ, et al. Evidence Report: Risk of Spaceflight Associated Neuro-ocular Syndrome (SANS). 2017

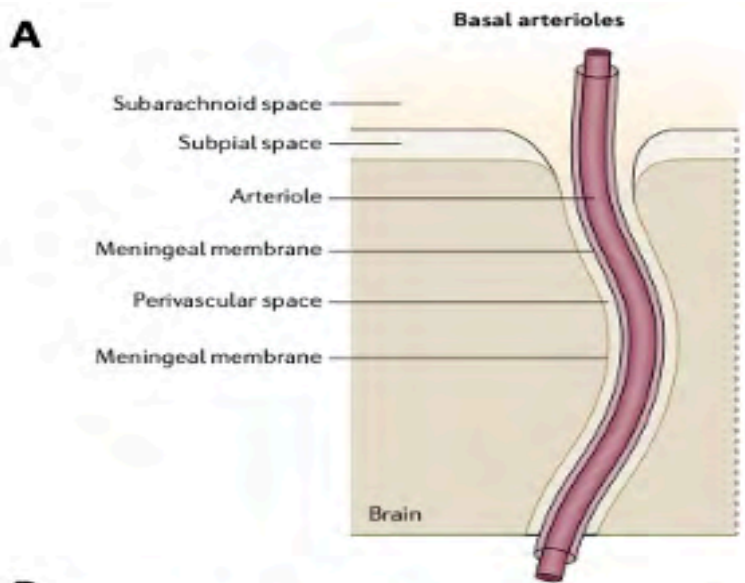


Figure 1: Illustration of arteries and their perivascular spaces with respect to the brain parenchyma and meningeal layers. Illustration adapted from Wardlaw et al. (2020), *Nature Reviews Neurology*.

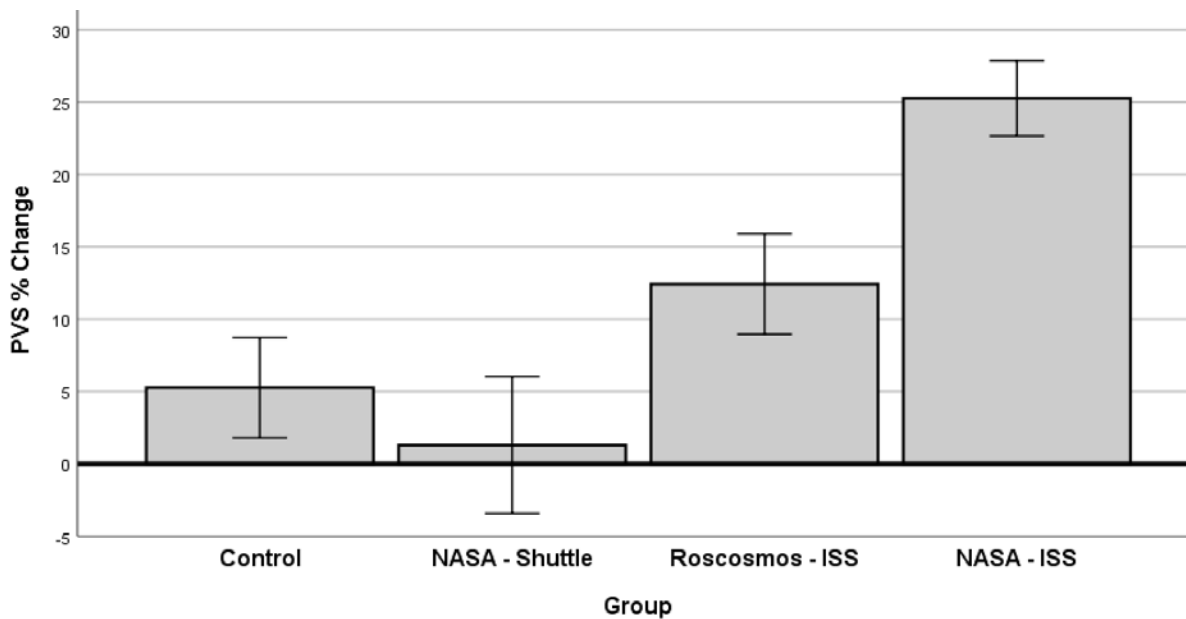


Figure 2: Percentage change in perivascular space volume from pre-flight MRI to post-flight MRI data for different groups, namely controls, NASA shuttle astronauts (short-duration spaceflight), Roscosmos ISS cosmonauts (long-duration spaceflight), and NASA ISS astronauts (long-duration spaceflight).

ORAL 89

The upcoming SubOrbital Express 3 and 4 Missions for Microgravity Research

S. Krämer¹, G. Florin¹, C. Lockowandt¹

¹SSC (Swedish Space Corporation), Sweden; stefan.kramer@sscspace.com, gunnar.florin@sscspace.com, christian.lockowandt@sscspace.com

Introduction

The upcoming years are lifting the sounding rocket ride-share concept into new spheres. Two missions within the commercial SSC - SubOrbital Express ride-share program are in the flight schedule for the next two years. With introducing the Shared Module, student teams, academia or private companies can enter the microgravity research platform in a cost-effective manner.

The upcoming mission

The SubOrbital Express 3 - M15 Mission consists of a number of major payloads as well as smaller experiments. For the first time, the rideshare concept includes a dedicated *Shared Module* enabling the access to the microgravity environment, even for smaller payloads of cubesat size or similar. For the upcoming flight, the shared module hosts experiments from all over the world: a biological experiment connected to the *MUSA* project of Costa Rica investigating on fungi spores, an active radiation shield experiment *RADICALS* by a research team of the RMIT / Australia. The *Lab on Paper* experiment by student teams from Lisbon, Porto and the USA has been selected by ELGRA for the grant covering the flight ticket on this mission.

The first passenger of the mission is *Mini-IRENE*, an atmospheric re-entry drop body experiment by CIRA / Italy with a funded flight ticket by ESA.

As known from the previous MASER Program, ESA funded experiments are filling a significant part of the ride share mission naming the evaporation experiment *ARLES-II* by the Free University of Brussels, the *CHIP* experiment of University Duisburg-Essen investigating the behaviour of charged particles in μg as well as the Swedish *NeuroBeta* experiment from Uppsala University, with focus on stem-cells and pancreatic islets. These ESA experiments are entirely development by SSC.

The launch campaign is planned for the second half of November 2022.

The next mission in planning

While the SubOrbital Express 3 mission is fully booked and undergoing the last integration and testing activities prior the launch, the fourth subsequent flight, scheduled for 2023, is currently almost filled by the ESA experiments *MicACTin* of Karolinska Institute / Stockholm, the *LiFiCo* experiment on liquid evaporation and sedimentation processes by University of Karlstad / Sweden and the *JACKS* experiment about granular cooling by University of Magdeburg. Furthermore,

the DLR funded experiment SIMONA will be hosted on this particular mission underlining the flight ticket approach.

The shared module will be available again on SubOrbital Express 4 - M16 with space for approx. 4-8 smaller μg experiments, tech demonstrations or commercial flight items.

Conclusion

SubOrbital Express provides 6 minutes of high quality microgravity and access to the atmosphere regimes up to 260 km altitude from Esrange, northern Sweden.

This paper will provide additional information on the payload configurations, the mission outlines as well as details on the experiments with their requirements on the mission.

ORAL 90

Reduced Gravity Missions from zero to hyper g for Life Science and Process Evaluation

S. Krämer¹, G. Florin¹, C. Lockowandt¹

¹SSC (Swedish Space Corporation), Sweden; stefan.kramer@sscspace.com, gunnar.florin@sscspace.com,
christian.lockowandt@sscspace.com

Introduction

Biological, and physical processes are often gravity sensitive. Plants and biological cells response on changing gravity conditions within a very short time. Chemical reactions are influenced, and mechanisms are experiencing deviating loads in absence of earth gravity.

Finding thresholds in processes and cell responses may require different gravity levels throughout a mission with a defined gradient over a longer experimenting time. Furthermore, stable gravity levels are needed e.g. for Mars and Moon exploration studies.

Reduced Gravity Platforms

Parabolic flight campaigns have been setting the baseline for the research under reduced gravity using aircrafts to provide the Moon and Mars gravity environment for the short range of 20-30 seconds.

Considering the next logical step for easily accessible platforms, this paper discusses the opportunity of using sounding rockets to provide the desired accurate reduced gravity or Moon or Mars gravity conditions the range of several minutes, undisturbed.

New concepts

Utilising the established platform for microgravity experiments with a different focus, offers a whole new field of opportunities for research activities and evaluation of technological developments, long before entering the long way to our neighbouring planets or to the asteroid belt. Cell behaviour can be studied, mechanical systems verified, and processes evaluated - close to earth and with immediate access to the results.

Conclusion

This paper guides the reader through the different options for missions on sounding rockets utilising different approaches to enable the reduced gravity environments.

SSC – Swedish Space Corporation is providing the platform within the SubOrbital Express Sounding Rocket Program on a dedicated mission or on a ride share approach with focus reduced gravity as well as Moon and Mars gravity research from Esrange / northern Sweden.

Two-wavelength Shadowgraphy

D.E. Bouyou Bouyou¹, C. Giraudet¹, H. Bataller¹, F. Croccolo¹

¹Laboratoire des Fluides Complexes et leurs Réservoirs - IPRA, UMR 5150, E2S-Univ Pau & Pays de l'Adour/CNRS/TotalEnergies, Anglet, France, fabrizio.croccolo@univ-pau.fr

Since a couple of decades, Shadowgraphy is routinely used to quantitatively investigate the statics and dynamics of non-equilibrium fluctuations (NEFs) in complex fluids (Croccolo et al. 2006a, Croccolo et al. 2012). Besides diffusive processes, NEFs allow probing the effect of gravity (Croccolo et al. 2006b), confinement (Giraudet et al. 2015) and the presence of propagating waves due to coupling of different hydrodynamic modes (Croccolo et al. 2019, García-Fernández et al. 2019) in fluids and fluid mixtures. Similar to what has been done in SODI in the frame of the DCMIX project using two-wavelength interferometry (Mialdun 2020), two-wavelength shadowgraphy can be used to resolve the fluctuating fields of the two independent concentration signals in ternary mixtures at the steady state of a thermodiffusion experiment. Nevertheless, here we will show that the same approach can provide also large benefit for the separation of refractive index fluctuations stemming from temperature and concentration NEFs in a binary liquid mixture stressed by a temperature gradient.

The main interest in using two wavelengths to separate two distinct signals in SODI was to be able to distinguish the variation of concentration of the two independent components in a ternary mixture during a thermodiffusion experiment. In fact, in a ternary mixture, the evolution in time of the two independent concentration values completely describes the mixture behaviour with respect to Fick diffusion and thermodiffusion. The system of two equations requires a 2×2 matrix for the mass diffusion coefficient, plus a 2-components vector for the Soret coefficient. The signal recorded by the SODI optical technique is related to density variations over the cell height and time. This signal is then related to the variations of the temperature and the two concentrations. If the mixture is composed of molecular components, then the two eigenvalues of the mass diffusion coefficient matrix will be rather similar. Therefore, while it is easy to distinguish the density variations stemming from temperature variations with respect to concentration variations due to the quite different temporal evolution, the two concentration signals cannot be easily separated based on their dynamics. It is therefore indispensable of taking advantage of the two colours technique to separate the different contributions within the concentration signal.

Given the fact that the concentration signal also includes, in principle, contributions from off-diagonal elements of the mass diffusion coefficient matrix that make the separation more complicated, it should be somewhat simpler to separate the signal of temperature variations from the signal of concentration variations. Then, the simplest case is that of a binary mixture, where the concentration independent term is only one.

In the special case of non-equilibrium fluctuations, the separation should be done for any wave number in the system,

with the advantage that, the related correlation function should reduce to the sum of two simple exponential decays rather than the sum of two series like in the case of SODI. In this presentation, we will describe the case of the structure function of non-equilibrium fluctuations during a thermodiffusion experiment, where a system of two equations is constituted by the two shadowgraph signals obtained from the analysis of series of images acquired at the two wavelengths of the Giant Fluctuations experiment, i.e. 405 and 675 nm. The two unknowns are given by the static power spectra of temperature and concentration NEFs in a binary mixture stressed by a stabilizing temperature difference of $\Delta T = 20$ K over a thickness of $L = 5$ mm. In this case, the static power spectra can also be separated by the differential dynamic algorithm (DDA) analysis, thanks to the fact that the dynamics are well separated at most of the analysed wave numbers due to the large Lewis number of the sample $Le = D/\nu$. Therefore, a comparison of the power spectra can be performed among the temperature and concentration ones obtained separately for the two colors by the DDA approach and the ones obtained by the two-wavelength separation.

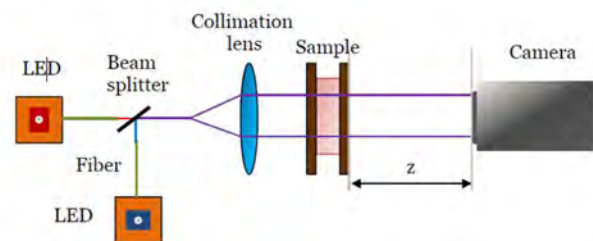


Figure 1: Schematic optical setup for a two-wavelength shadowgraph.

Acknowledgements

We acknowledge financial support from the CNES and from the E2S UPPA Hub Newpores and the Industrial Chair CO2ES supported by the Investissements d'Avenir French programme managed by ANR (ANR16IDEX0002). Work partially supported by the European Space Agency, CORAMAP TechNES Contract No. 4000128933/19/NL/PG.

References

- F. Croccolo, D. Brogioli, A. Vailati, M. Giglio and D.S. Cannell, Use of dynamic schlieren interferometry to study fluctuations during free diffusion, *Applied Optics*, 45, 2166, (2006a)
- F. Croccolo, D. Brogioli, A. Vailati, M. Giglio and D.S. Cannell, Effect of gravity on the dynamics of non equilibrium fluctuations in a free diffusion experiment, *Annals of the New York Academy of Sciences*, 1077, 365, (2006b)

of non-equilibrium fluctuations in liquid mixtures to measure the Soret and mass diffusion coefficient, *The Journal of Chemical Physics*, 137, 234202, (2012)

F. Croccolo, L. Garcia-Fernández, H. Bataller, A. Vailati and J.M. Ortiz de Zárate, Propagating modes in a binary liquid mixture under thermal stress, *Phys. Rev. E*, 99, 012602, (2019)

L. García-Fernández, P. Fruton, H. Bataller, J.M. Ortiz de Zárate, and F. Croccolo, Coupled non-equilibrium fluctuations in a polymeric ternarymixture, *Eur. Phys. J. E*, 42, 124, (2019)

C. Giraudet, H. Bataller, Y. Sun, A. Donev, J.M. Ortiz de Zárate and F. Croccolo, Slowing-down of non-equilibrium fluctuations in confinement, *Europhys. Lett.*, 111, 60013, (2015)

A. Mialdun et al., Data quality assessment of Diffusion Coefficient Measurements in ternary mIXtures 4 (DCMIX4) experiment, *Acta Astronautica*, 176, 204-215 (2020)

ORAL 92

A new experimental set-up for aerosol stability investigations in microgravity conditions

C. Graziani¹, M. Nespoulous¹, R. Denoyel¹, S. Fauve², C. Chauveau³, L. Deike⁴, M. Antoni¹

¹MADIREL Aix-Marseille University, ²LP ENS-Paris, ³ICARE University Orléans, ⁴MAE/HMEI Princeton University

Introduction

An aerosol is a complex medium, sensitive to temperature and pressure conditions, sometimes chemically active, whose continuous phase is a gas in which liquid and/or solid phases are dispersed. It is naturally subject to the influence of gravity, which determines the settling speed of the particles it contains. Aerosols have many applications in the pharmaceutical and cosmetic industries (inhalers, sprays), in metallurgy (spray drying) and in agriculture (pesticides). From an academic point of view, they are the subject of intense research activity. The description of their evolution is, for example, a major issue in climatology. This is why CNES recently supported the development of an experimental facility for the investigation of cloud micro-physics in micro gravity conditions (Figure 1). The main goal is to produce aerosols and to follow their evolution with optical tomography microscopy in controlled thermodynamic conditions.



Figure 1 : Overall view of the rack used for the parabolic flight experiments.

1. Principle of the experiments

Aerosols under consideration in this work are similar to fogs and consist of populations of droplets of few micrometers in radius (Figure 2). They are produced from water saturated air with a pneumatic circuit consisting of two chambers: a cylindrical experimentation chamber (EC, diameter 3 cm, length 6 cm) inside which droplets are generated and an expansion-compression chamber (ECC, volume about 170 cm³) acting alternatively as a gas reservoir or an expansion tank (Figure 3). EC and ECC are initially at room temperature and pressure and both contain water saturated air. A membrane pump is used to circulate the air from the ECC into the EC. Then, by means of a system of valves, a fast expansion between the EC and the ECC is achieved. This expansion leads to a temperature drop inside the EC, which results in a decrease of the equilibrium saturation vapour pressure. An excess of water vapor is created that condensates into small droplets. This protocol takes only a few seconds and has the important advantage of limiting heat transfers with the walls of the EC.

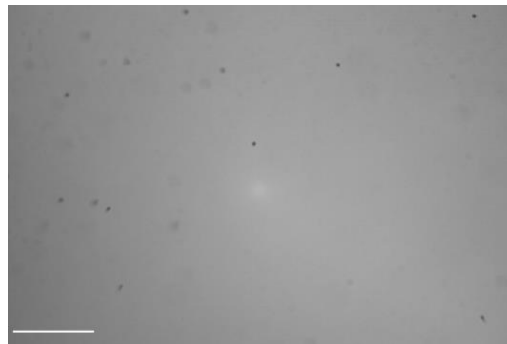


Figure 2 : Image of a population of droplets (black spots). Field of view is 1280x860 pixels. The white line at the bottom left gives the scale (here 200 μm). (Source: Image#10354 from parabola 00, 62nd parabolic flight campaign).

A temperature measurement device composed of a type K thermocouple driven by an Agilent 34972A LXI is implemented in the EC. The pressure inside the EC and the ECC are measured with two pressure sensors (KELLER PAA-33X). A hygrometric sensor is mounted inside the EC (Sensirion SEK-SHT35). It also gives the temperature which allows a redundancy of the measurements. All the above sensors are placed at selected locations in order to give measurements as close as possible to what is happening in the EC without being too intrusive.

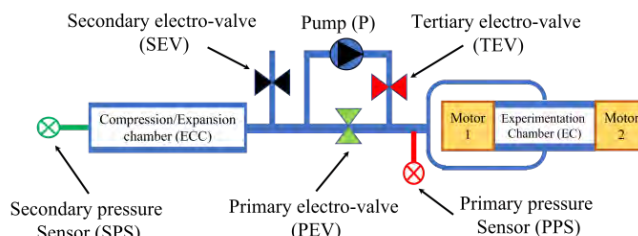


Figure 3 : Schematic view of the set up.

2. Camera and optical Tomography

Optical tomography microscopy is used to observe the droplets once formed and to track their evolution (Figure 4). This technique consists in acquiring images with a microscope with moving object plane. It has the great advantage of enabling analyses in the visible spectrum and, in the particular case of droplet populations as the ones produced here, to allow in-depth analyses since they are optically transparent. The acquisition of tomographic scanning sequences allows a 3D reconstruction and thus a precise follow-up of the evolution of droplets over time. To make the best use of this technique in the context of this study, an Optronis CP70-1HS-MC-1900 grabbing camera has been implemented. It allows a frequency acquisition up to 2000 fps in full frame that ensures coherence between all successive images.

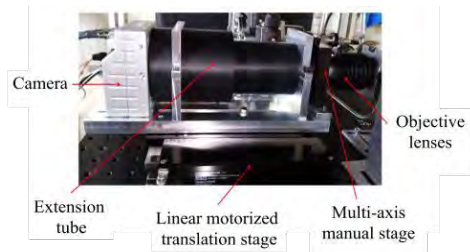


Figure 4 : View of the microscope and optical tomography system.

3. Von Karman swirling flows

The EC is equipped with two coaxial contra-rotating rotors (smooth flat disks of diameter 29 mm facing each other) that generate a von Karman swirling flow within the EC. The fluid is driven radially outward by the centrifugal force of the disks. This generates an axial flow toward the disks along their axis and a recirculation along the opposite direction along the EC lateral boundary. Therefore, a radially inward flow is generated in the mid-plane between the disks such that there is a stagnation point at center of the EC. It is expected that the liquid droplets driven by the flow of gas accumulate in the vicinity of that stagnation point, being submitted there to the shear of azimuthal velocity that is driven in the mid-plane by the counter-rotating disks. The objective is to describe the evolution of the density (actually the liquid fraction) and the mean size of the droplets in the vicinity of the stagnation point under the influence of the flow that can involve more or less turbulent fluctuations depending on the Reynolds number. Such experiments aim at helping to understand coalescence of droplets in clouds.

The stirring is achieved with two FAULHABER servomotors (Figure 3) (4221G 024EXTH) equipped with an encoder (IE3-2024) each controlled by a motion controller (MC5005 S RS) allowing regulation of the rotation frequency. Rotors are both attached to a relay magnetically driven by a motion transmitter attached to the motors allowing rotation frequencies in the range 1 to 75 Hz. The sealing is obtained by a flange which separates the relay from the EC and therefore from the outside. Magnetic neodymium segmental arc magnets provide the magnetic coupling. The main advantage of this configuration is to allow for an optimal level of sealing as no transmission shaft is required.

4. Preliminary ground tests

Experimental conditions have to be known in terms of pressure, temperature and relative humidity. Initial pressure and temperature are ambient ones while relative humidity (H) conditions range between 2.8% and 96.0%. Each experiment follows the same protocol : (i) closure of all electro valves, (ii) opening of TEV, (iii) pressure increase in the CE to a target value, (iv) closure of TEV, (v) 10 seconds delay for temperature relaxation, (vi) opening of PEV for expansion and droplet formation, (vii) image recording. The interest of this protocol is to produce almost similar temperatures and pressures in the EC before and after droplet formation and thus to avoid the thermal control of the whole set up which would be, from an instrumental point of view, highly challenging.

Figure 5 displays the resulting temperature and pressure evolution for a target pressure of 2000 mbar. Reference time ($t=0$) is set at opening of PEV (step (vi)). As expected, two jumps in both temperature and pressure obviously associated to step (iii) and (vi) show up. Temperature relaxes back to its

initial value sufficiently fast for both phases which confirms that air, within the EC, keeps close to its initial conditions despite droplet formation. In other words, forming droplets did not lead to significant heat transfers with the boundary conditions defined by the EC structure and it is therefore reasonable to assume that the further study of such droplet populations can be achieved under quasi-isothermal conditions.

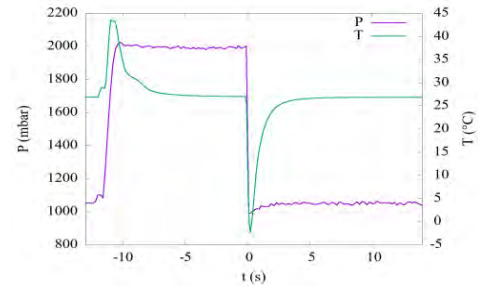


Figure 5: Evolution of pressure and temperature as a function of time inside the EC. Reference time $t=0$ is set at the opening of the PEV (step(vi)).

The typical relaxation time, t_{relax} , as a function of H is plotted in Figure 6 for 108 experiments and four target pressures (2000, 2100, 2200 and 2300 mbar). t_{relax} is defined as the time required for the system to recover 95% of the temperature drop after step (vi). The higher the relative humidity, the higher the thermal heat capacity. The increasing trend of t_{relax} as a function of H (Figure 6) is therefore consistent with thermodynamics and a straightforward consequence of the fact that equilibration time of a system increases with its thermal capacity. This set of experiments also gives fundamental information about droplet formation. Image analysis (not shown here) indicate that within the pressure range investigated here, no droplets are formed when $H < 40\%$.

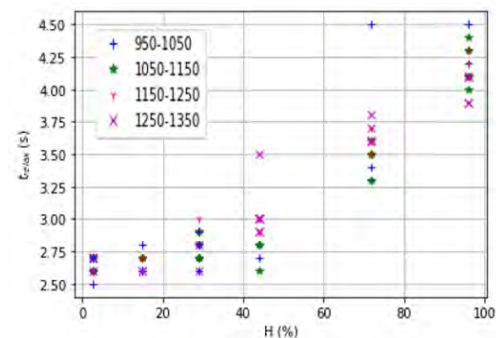


Figure 6 : Time required for temperature stabilization after expansion as a function of H. The legend indicates the pressure difference in mbar at step (iii) (compression phase). Temperature of the experiments is about 22 °C.

Conclusion

The instrumental developments carried out within the framework have demonstrated the possibility of generating droplet populations under relatively well-controlled thermodynamic conditions. The data obtained from parabolic flight campaigns recently carried out have qualified the techniques used within the framework of this project and confirmed the feasibility of relevant investigations on droplet populations in micro-gravity.

Acknowledgements

Authors gratefully thank CNES, in particular Christophe Delaroche and Laurent Arnaud, CNRS and Region Sud for financial support.

ORAL 94

A Novel Attitude Control System Combining Reaction Wheels and Transformable Spacecraft Capabilities: Design, Prototyping and Testing at the 77th ESA Parabolic Flight Campaign

I. Castro-Fernández¹ and JM. Tejada²

¹Departamento de Bioingeniería e Ingeniería Aeroespacial, Universidad Carlos III de Madrid, Leganés (28911 Madrid), Spain, ivcastro@ing.uc3m.es,

²Space Propulsion Laboratory, Department of Aeronautics, Imperial College London, London, United Kingdom jesus.munoz.tejada@imperial.ac.uk

Introduction

The Dzhanibekov (DZH) effect is a periodic 180-degree flipping motion which naturally appears in rigid bodies when spinning around their intermediate axis of inertia. In the past, it has been theoretically demonstrated that the DZH effect could benefit space missions either acting solely or in combination with current technology (P. Trivailo and H. Kojima 2016; P. Trivailo and H. Kojima 2020). In this work, we conduct microgravity research to experimentally demonstrate that the effect can be controlled, i.e., switched ON and OFF customarily, by providing the spacecraft (S/C) with transformable (namely, Inertial Morphing -IM-) capabilities. To do so, a microgravity platform is needed to replicate torque-free conditions where the effect can be triggered, and the research demonstrated. Parabolic flights have become effective platforms to carry out experiments in microgravity conditions where both scientific and technological research was carried out (V. Pletser 2016; C. Menon et al. 2005; S. Hauschild et al. 2014). With that premise, the team DZH Dynamics participated in the 77th ESA Parabolic Flight Campaign with the following objective: “Designing, developing and testing in microgravity conditions a prototype of a transformable satellite able to change its mass distribution and allow for a more energy and time efficient Attitude Control and Determination System (ADCS)”.

Design, Prototyping and Experiment Procedure

The experimental setup consisted of three main components:

- 1) Transformable Satellite (Figure 1): prototype to be tested in microgravity conditions. Transformable capabilities are achieved by means of two inner moving masses. The ADCS consists of 3 RWs in an orthogonal configuration, an Inertial Measurement Unit (IMU) and an onboard computer (STM32 microcontroller) which, in combination with the transformable properties, configures the novel ADCS system to be tested.
- 2) Release Mechanism (Figure 2 (a)): launching system that provides the prototype with the desired spinning initial conditions in microgravity conditions. It is composed of a rotating electromagnet, which can be activated (prototype attached) or deactivated (prototype released), and gives the initial rotation of the prototype. It can also be manually displaced in the longitudinal direction, coincident with the aircraft longitudinal direction to safely introduce the prototype inside the free-floating area.

- 3) Rack (Figure 2 (b)): light structure made of standard aluminium profiles where the release mechanism and the rest of the electrical elements are assembled.

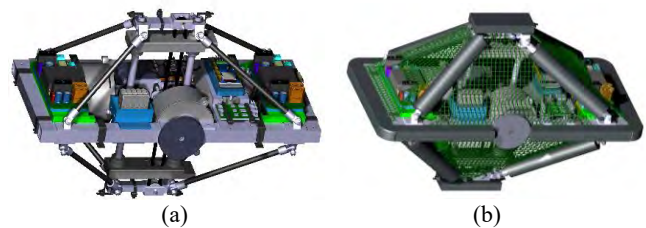


Figure 1: Satellite prototype CAD model: (a) inner structure and (b) flight configuration.

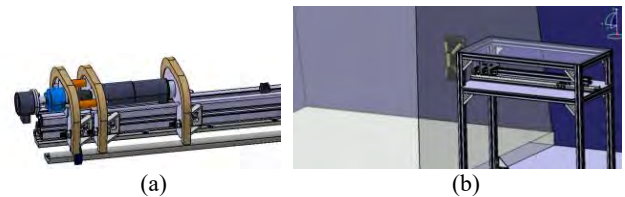


Figure 2: Release mechanism (a) and experiment rack (b).

Figure 3 shows the real experimental setup assembled in the microgravity platform (Airbus A310 AirZeroG). Besides the three main components, a net (2x2x2 m³) to limit the free-floating area and a mattress to absorb impacts of the prototype in the 1g and 2g phases were arranged.



Figure 3: Real experimental setup assembled in the Airbus A310 AirZeroG.

Experimental Results

To achieve the main objectives of the present research, 4 different types of experiments were carried out along the 90 available parabolas of the flight campaign:

- **Experiment type 1 (DZH effect demonstration):** the moving masses are fixed in the innermost position for the whole experiment, enabling the effect when the prototype is rotated around the spinning axis (it becomes the intermediate axis of inertia).
- **Experiment type 2 (DZH ON to OFF):** the moving masses initially start in the inner position and once one or two 180-degree flips have occurred, the masses move to the outer position disabling the effect.
- **Experiment type 3 (DZH OFF to ON):** the moving masses are initially out, then they move inwards to enable the DZH phenomenon.
- **Experiment type 4 (DZH + RWs):** the moving masses are fixed in the innermost position for the whole experiment. The ADCS is activated in combination with the DZH flip to achieve certain attitude maneuvers (desired Euler angles). There exists a total of 13 attitude maneuvers that were tested within type 4.

Figure 4 shows the experimental angular rates obtained in two example experiments by the IMU attached to the prototype. Figure 4 (a) presents an experiment type 1 where the prototype was accelerated from 0 to 13 rad/s (2 rev/s) during the first 5 seconds. The prototype remained attached to the release mechanism until second 10. Then, a total of 4 180-degree loops are performed (periodic change of sign of ω_x , being x the intermediate axis in this experiment type). Figure 4 (b) shows an experiment type 2 with an initial behavior similar to type 1. However, the moving masses were moved from the inner to the outer position after the first 180-degree flip of the prototype once released. Some seconds of stable rotation around the x axis (major axis after moving the masses) were achieved, demonstrating the ability of the IM system to stop the DZH effect.

Conclusions

With this microgravity research, it has been experimentally demonstrated, for the first time since the discovery of the DZH effect in 1850s, that this phenomenon can be controlled. An inertial morphing system has been integrated in a transformable satellite prototype being able to switch ON and OFF the phenomenon customarily. Moreover, the DZH effect has been combined with reaction wheels to allow for more efficient maneuvers in time and energy. This research opens the possibility of benefiting from the inertial distribution by converting the state-of-the-art spacecraft into transformable space vehicles.

Acknowledgements

We would like to thank all the entities who have collaborated to make this research possible; from our institutions (Imperial College London, Universidad Carlos III de Madrid and Technical University of Delft) to our

sponsors (Acatec Aeronautics, Maxon motors, Sensing, RS Components, UKSpace Agency). Likewise, we would like to thank all team members of DZH Dynamics for their help and significant contributions throughout the programme: Manuel Muñoz Arroyo (Acatec), José María Castillo, Jorge Alonso Rosell, Guillermo Reales, Alberto Rodríguez, Adrián García, Fran Piernas, Antonio Checa, Javier Domínguez, Andrés Rubio Doiztua (Acatec), Miguel Segovia, Carmen García, Miguel Ángel Gordo, Víctor Domínguez, Arvin Tan, Gorakula Srilochan, Samrith Patjal, Shehara Perera, Mahmoud Assaf, Enrique Alguacil, Álvaro Martínez Ocón, Sharon Rose, Harshal More and Gourav Namta.

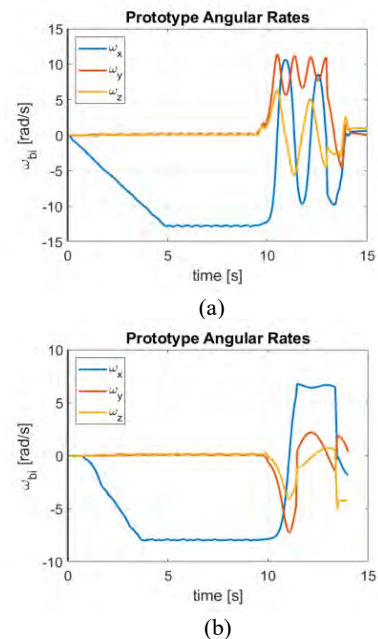


Figure 4: Prototype IMU postprocessed results for an experiment type 1 (a) and type 2 (b). The vertical axis represents the angular rates of the body frame (attached to the prototype) with respect to an inertial frame.

References

- [1] S. Hauschild, S. Tauber et al. T cell regulation in microgravity – The current knowledge from in vitro experiments conducted in space, parabolic flights and ground-based facilities, *Acta Astronautica* 104, 365-377, (2014).
- [2] C. Menon, A. Aboudan et al. Free-Flying Robot Tested on Parabolic Flights: Kinematic Control, *Journal of Guidance, Control, and Dynamics*, 28, 4, (2005).
- [3] V. Pletser, European aircraft parabolic flights for microgravity research, applications and exploration: A review, *REACH*, 1, 11-19, (2016).
- [4] P. Trivailo. and H. Kojima, “Utilisation of the “dzhanibekov’s effect” for the possible future space missions,” in *26th International Symposium on Space Flight Dynamics ISSFD* (2016).
- [5] P. Trivailo. and H. Kojima, “Enhancement of the attitude dynamics capabilities of the spinning spacecraft using inertial morphing”, *The Aeronautical Journal*, 124, 34 (2020).

ORAL 95

A Glimpse into Spaceflight Induced Bone Loss Over 18-Months

P.Fernandez¹, K.Gordienko², H.Locrelle¹, M.Linossier¹, P.Lau³, J.Rittweger³, G.Vassilieva³, L.Vico¹

¹INSERM, U1059 – SAINBIOSE, Laboratory of Osteoarticular Tissue Biology, University of Lyon, France, peter.fernandez@kcl.ac.uk, herve.locrelle@chu-st-etienne.fr, linossier@univ-st-etienne.fr, vico@univ-st-etienne.fr

²Russian Federation State Scientific Centre - Institute of Biomedical Problems of the Russian Academy of Sciences, Russia, k.vl.gordienko@gmail.com, galvassilieva@mail.ru

³Institute of Aerospace Medicine, German Aerospace Centre, Germany, patrick.lau@dlr.de, joern.rittweger@dlr.de

Introduction

Prolonged exposure to the microgravity environment is known to elevate the rate of bone resorption in astronauts. (Vico L. et al., 2017; Gabel L. et al., 2021). Despite various forms of exercise countermeasures to regulate this rate of loss, the effect on bone continues to pose a significant challenge for both the present and future of long-duration spaceflight. While international space agencies continue to work towards developing a lunar habitat and eventually the colonisation of Mars, the unresolved consequences of spaceflight physiology on bone need to be understood so that effective countermeasures can be developed. For this reason, a longitudinal study (EDOS-2) examining the change in bone geometry and bone architecture is underway with a focus on determining reversibility, the quantity of deterioration, and identifying factors associated with intra-individual responses to spaceflight.

Materials and methods

8 male participants (48.11±6.05 years) had their volumetric BMD and microarchitecture parameters measured at the non-dominant distal radius and tibia using HRpQCT imaging (Xtreme CT, SCANCO Medical). Pre-flight measurements were taken at (1 or 2 months pre-flight, or at both time points) for a baseline reference and followed up for 1.5 years after landing. Post-flight measurements were obtained at the following time points: 1 day (R+1); 14 days (R+14), 3 months (R+90); 6 months (R+180); 12 months (R+360); and 18 months (R+540).

Results and discussion

Preliminary results demonstrated a decrease in cortical volumetric BMD from baseline values in both the distal radius and tibia upon return, with more pronounced differences in the tibia (Fig. 1). In addition, these values were also below pre-flight levels even 18-months later (Fig. 1). Cortical porosity levels followed a similar trend with elevated levels upon return and no signs of recovery to pre-flight values (Fig. 2). These preliminary results are consistent with a one-year longitudinal follow-up (Vico L. et al., 2017; Gabel L. et al., 2021) and further highlight that a return to baseline levels is currently not observed even after 18-months.

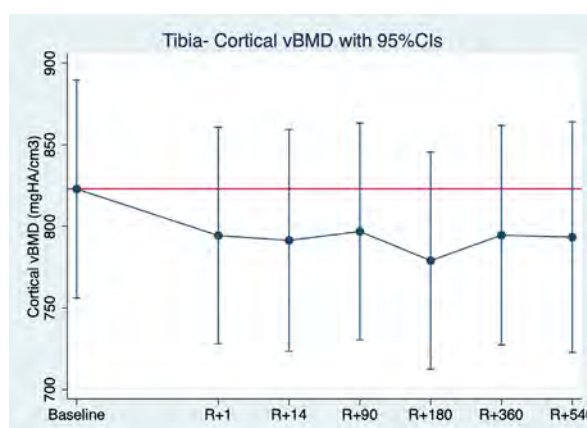


Figure 1: Cortical vBMD changes over time at the distal tibia. Red line represents the reference line to baseline values.

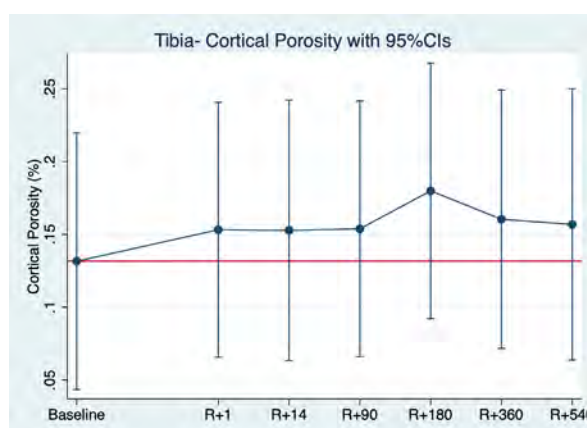


Figure 2: Cortical porosity levels over time at the distal tibia. Red line indicates the reference line to baseline values.

Conclusion

Preliminary data examining spaceflight effects on bone currently shows no signs of a return to baseline values even after 18-months.

Acknowledgements

We want to thank our partners at IMBP for their tremendous help and support. We would like to also extend our gratitude

and appreciation to all the cosmonauts that took the time to participate and continue to do so in this study.

References

L.Vico, B.Rietbergen, N.Vilayphiou, M.Linossier, H.Locrelle, M.Normand, M.Zouch, M.Gerbaix, N.Bonnet, V.Novikov, T.Thomas, G.Vassilieva, Cortical and Trabecular Bone Microstructure Did Not Recover at Weight-Bearing Skeletal Sites and Progressively Deteriorated at Non-Weight-Bearing Sites During the Year Following International Space Station Missions, Vol. 32, pp 2010–2021, 2017

L.Gabel, S.Zwart, A.Liphardt, P.Hulme, M.Heer, J.Sibonga, S.Smith, S.Boyd, Pre-flight exercise and bone metabolism predict unloading-induced bone loss due to spaceflight, Vol 56, pp 196–203, 2021

ORAL 98

Dynamics of Non-Equilibrium Fluctuations Close to the Onset of Rayleigh-Bénard Convection

C. Giraudet^{1,*}, M. Carpineti², F. Croccolo¹, A. Vailati²

¹Universite de Pau et des Pays de l'Adour, E2S UPPA, CNRS, TotalEnergies, LFCR UMR5150, Anglet (France)

²Dipartimento di Fisica « Aldo Pontremoli », Università degli Studi di Milano, Milano (Italy)

*cedric.giraudet@univ-pau.fr

In the presence of a density gradient, non-equilibrium fluctuations (NEFs) are established spontaneously over the entire volume considered and are well described by the linearized hydrodynamics (Ortiz de Zárate2004). This has been widely proven in nearly ideal cases through numerical simulations (Giraudet2015) and thermodiffusion experiments on binary fluids on Earth (Giraudet2014) and in microgravity conditions (Vailati2011; Croccolo2016). However, questions remain on the validity of this theoretical approach when the temperature and/or concentration gradients are very large (Zapf2022), or in transient processes occurring before steady state is reached.

These questions represent the heart of the ESA space project Giant Fluctuations (formerly NEUF-DIX; Vailati2020). The experimental apparatus developed in the framework of this project consists in a series of 4 bichromatic dynamic shadowgraphs, each equipped with a thermodiffusion cell; see picture of the prototype in Figure 1.



Figure 1: Picture of the bichromatic dynamic shadowgraph developed and validated during the phase C0.

The present calibration-free setup has been validated with the help of molecular and polymeric binary and ternary solutions at the steady state of thermodiffusion experiments wherein a stable temperature gradient was applied.

In addition, experiments on pure Toluene stressed by unstable temperature gradients, i.e., by heating from below, were conducted at different temperature differences below the onset of Rayleigh-Bénard convection. We have a first indication that the emergence of convective patterns can be interpreted based on temperature fluctuations, where fluctuating sub-volumes organize the fluid on a macroscopic scale.

The mean lifetimes of NEFs, whose wavenumber corresponds to the bifurcation from conduction to convection, $\tilde{\tau}_{C,b}$ show a critical enhancement approaching the onset of Rayleigh-Bénard convection, see upper part in Figure 2. Before convection sets in, the fluid undergoes a transition from a

quiescent state (Figure 2a) to a sub-critical state (Figure 2b). The latter is characterized by the coexistence of multiple local equilibrium states, which does not influence the probability density function of thermophysical properties, on average; see lower part in Figure 2.

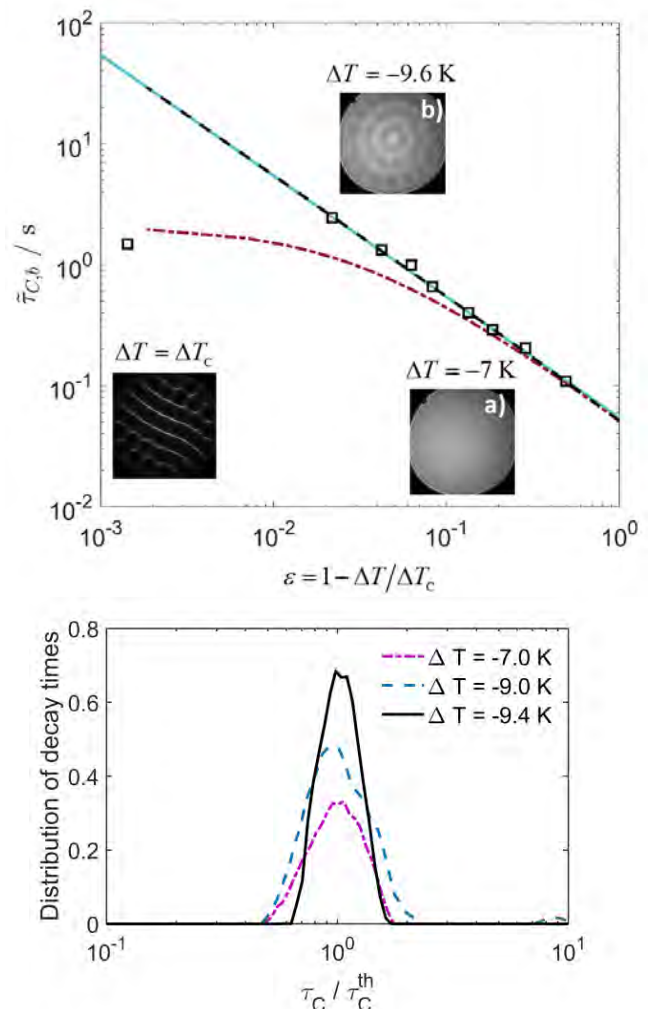


Figure 2: Top: Critical slowing-down of the mean relaxation time of nonequilibrium fluctuations whose wavenumber corresponds to that of the macroscopic convective rolls ($q_b = 31.1 \text{ cm}^{-1}$). Insets show raw images representative of the quiescent ($\Delta T \ge -9 \text{ K}$), sub-critical ($\Delta T \ge -9 \text{ K}$), and critical ($\Delta T = \Delta T_c$) states observed in our experiments. ΔT_c is the temperature difference at the onset of Rayleigh-Bénard convection. Bottom: Distribution of the mean lifetimes of fluctuations whose dissipation process is driven by diffusion ($q = 2q_b$).

All measurements, consisting in the acquisition of 10^4 images with two incident radiations, were repeated several times using different acquisition frequencies to provide sufficient accuracy. Refractive index structure functions (SFs) were

determined using a differential dynamic analysis (Cerchiari2012).

Acknowledgements

We acknowledge support from ESA through the TechNES MAP project grant n. 4000128933/19/NL/PG, and from team members of the Giant Fluctuations project. CG and FC acknowledge financial support from the CNES and from the E2S-UPPA Hub Newpores and the Industrial Chair CO2ES supported by the Investissements d'Avenir French programme managed by ANR (ANR16IDEX0002).

References

- J. M. Ortiz de Zárate, J. V. Sengers, On the physical origin of long-ranged fluctuations in fluids in thermal nonequilibrium states, *J Stat Phys* **115**, 1341-1359 (2004)
- C. Giraudet, H. Bataller, Y. Sun, A. Donev, J.M. Ortiz de Zárate, F. Croccolo, Slowing-down of non-equilibrium fluctuations in confinement, *Europhys Lett* **111**, 60013 (2015)
- D. Zapf, J. Kantelhardt, W. Köhler, Nonlinearities in shadowgraphy experiments on non-equilibrium fluctuations in polymer solutions, *Eur Phys J E* **45**, 40 (2022)
- C. Giraudet, H. Bataller, F. Croccolo, High-pressure mass transport properties measured by dynamic near-field scattering of non-equilibrium fluctuations, *Eur Phys J E* **37**, 107 (2014)
- A. Vailati, R. Cerbino, S. Mazzoni, C.J. Takacs, D.S. Cannell, M. Giglio, Fractal fronts of diffusion in microgravity, *Nat Commun* **2**, 290 (2011)
- F. Croccolo, C. Giraudet, H. Bataller, R. Cerbino, A. Vailati, Shadowgraph analysis of non-equilibrium fluctuations for measuring transport properties in microgravity in the GRADFLEX experiment, *Microgravity Sci Technol* **28**, 467–475 (2016)
- F. Giavazzi, P. Edera, P.J. Lu, R. Cerbino, Image windowing mitigates edge effects in differential dynamic microscopy, *Eur Phys J E* **40**, 97 (2017)

ORAL 99

Non-Isothermal sloshing for space applications: from a ground-based experimental characterisation to microgravity conditions

F. Monteiro^{1,2}, P. Marques^{2,3}, A. Simonini², A. Silva¹, M. A. Mendez²

¹Universidade da Beira Interior, Department of Aerospace Sciences, Covilhã, Portugal, francisco.monteiro@vki.ac.be,

²von Karman Institute for Fluid Dynamics, Bruxelles, Belgium,

³Université Libre de Bruxelles, Transfers, Interfaces & Processes (TIPs), Bruxelles, Belgium.

Introduction

Liquid cryogenic propellants are at the forefront of space propulsion due to their optimal trade-off between performance and weight (Sutton et al. 2017). As a result, investigations on the sloshing dynamics of such fuels have been carried out since the early 1960s. Sloshing, defined as the movement of the free liquid surface within a reservoir (Abramson, 1966), induces two types of undesirable effects: (a) displacement of fuel tank's centre of mass, which disturbs the stability and manoeuvrability of the spacecraft; (b) thermal mixing between the pressurised ullage and subcooled liquid, which can generate large fluctuations in the tank pressure, leading to structural instabilities and thrust oscillations in the propulsive system.

Prior to launch, the propellant tanks are pressurised according to the optimal operating conditions for the propellant feed system. If the holding time is large enough, a vertical thermal stratification develops in the liquid due to natural convection and conduction. As depicted in Figure 1a, the liquid's thermal field features a warmer region extending from the interface until a depth δ_T , and a subcooled region defined by a quasi-homogeneous condition. If dynamic perturbations (e.g., booster separation or aerodynamic forces) induce liquid sloshing, the warmer liquid in the thermal boundary layer mixes with the subcooled liquid from the bulk, lowering the temperature at the free surface. The destratification (depicted in Figure 1b) results in the cooling of the ullage gas, hence condensation and consequently a pressure drop in the tank. The magnitude of this pressure drop depends on (a) the sloshing regime, (b) the pressurisation technique, (c) the pressurant type and (d) the ullage volume (Arndt, 2012; Foreest, 2014).

The present research aims to develop a reduced-scale experiment using non-cryogenic replacement fluids to characterise the heat and mass transfer between the liquid and the gas due to sloshing-induced mixing.

The research questions we seek to answer are:

1. What is the impact of different initial non-isothermal sloshing conditions (e.g., tank pressure, ullage temperature and thermal boundary layer thickness) on the thermodynamic evolution of the system under lateral sloshing conditions?
2. What is the sloshing excitation condition's impact on the thermodynamic evolution of the system?

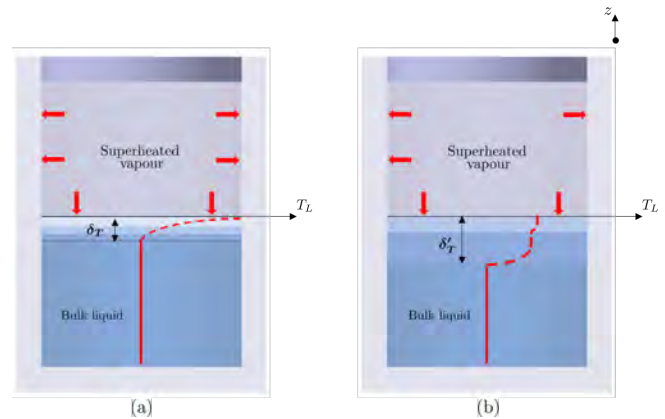


Figure 1: Schematic representation of the evolution of vertical temperature profiles and the thickness of thermal boundary layers in the liquid's uppermost region adapted from Lacapere et al. (2009): (a) thermal profile before sloshing initialisation; (b) thermal profile after sloshing induced mixing.

The developed small-scale experiment for ground-based characterisation represents the first iteration for the experimental campaign under reduced gravity conditions, which will take place next year on the 80th ESA Parabolic Flight. This presentation reports on the lessons learned and the refinements that will be considered for the campaign in microgravity.

Preliminary experimental setup

The experimental setup, represented in Figure 2, has been designed to study lateral sloshing for different non-isothermal conditions resorting to non-cryogenic fluids, such as HFE-7200 and HFE-7000. The setup comprises a quartz sloshing cell, an external reservoir, and a connecting pressure line with several valves.

The sloshing cell is a quartz rectangular cuboid, allowing non-intrusive optical measurement techniques (Simonini et al. 2021), with a radius $R_S = 40$ mm, and a total height $H_S = 120$ mm. It is instrumented with thermocouples across the ullage and liquid to analyse the thermal evolution of the system, as well as a pressure transducer mounted on the top cover to monitor pressure fluctuations. An active pressurisation system is employed by resorting to an external reservoir with heating capabilities and a total volume $V_R = 2.4$ L. A thermocouple connected to a PID controller and a pressure transducer are used to impose the desired superheated vapour conditions in this reservoir. The quartz cell is connected to this external reservoir via the pressure line shown in Figure 2.

To avoid impingement of the vapour jet on the liquid surface, the vapour is injected through a diffuser at the sloshing cell

controlled through a ball valve and a swing-check valve. A pressure regulator and transducer are also built into the line, ensuring operational safety. Both tanks have a port that allows a vacuum pump connection to ensure a single species system by extracting the air. A graded filling bottle is connected, through the same port, ensuring an accurate filling of the sloshing cell and reservoir.

The experimental setup is mounted on the SHAKESPEARE (SHaking Aparatus for Kinetic Experiments of Sloshing Projects with EArthquake Reproduction) shaking table with three sliding modules at the von Karman Institute. Here the setup will be laterally excited in the x -direction.



Figure 2: Experimental setup composed of quartz sloshing cell (clear blue), heating reservoir (grey and white), connecting pipeline (light grey) and vacuum and filling port (blue).

With the vision set in future iterations for the parabolic flight test campaign, the following high-level requirements for the experimental setup were employed to drive the design: (a) compact setup, quick to assemble and disassemble; (b) rapid initialisation, restricted to under five minutes; (c) redundant measures must be employed to meet safety constraints; (d) optical measurement techniques capability.

Expected results and facility outcomes

Initially, it is critical to perform pressurisation tests in which an initial condition for the reservoir's superheated vapour and sloshing cell ullage is fixed. Hereafter, resorting to the employed instrumentation, the objectives are the following: (a) evaluate the thermal boundary layer thickness for a pressurisation cycle; (b) quantify the heat rate transfer between the pressurant vapour, the liquid and walls; (c) evaluate the sloshing cell pressurisation time; (d) determine the number of pressurisation cycles for an initial vapour mass in the external reservoir.

Once the initialisation procedure is well understood, the non-isothermal sloshing experiments will consider different excitation amplitudes and frequencies to generate wave dynamics from the three main wave regimes: planar, chaotic and swirl waves (Miles, 1984). Temperature and pressure evolutions will be extracted, reconstructing the vertical temperature profiles, and characterising the sloshing-induced thermal mixing and the characteristic pressure drop.

Regarding the facility operational learning outcomes, the prominent question marks to be answered settle on: (a) the number of pressurisation cycles attainable for an initial reservoir condition; (b) pressure tightness across the system; (c) compatibility between the system components and

on-ground will be translated into an improved design for the parabolic flight campaign.

Conclusions

The present work aims to develop an experiment to characterise non-isothermal sloshing. The outcomes from this campaign will set an experimental database to allow future development and calibration of simplified models capable of predicting the pressure and temperature evolutions during sloshing excitations. In the extended version of this work, the experience acquainted through the operation of the designed facility will determine how to proceed further with the architecture of the next VKI (von Karman Institute) microgravity experimental campaign taking place next year on board the 80th ESA Parabolic Flight. The described experimental setup and respective test campaign is expected to occur at VKI between July and August 2022.

Acknowledgements

This work is supported by the European Space Agency (ESA) in the framework of the project number 4000129315/19/NL/MG. The authors gratefully acknowledge the financial support of the "Fonds de la Recherche Scientifique (F.R.S.-FNRS)" for the FRIA grant supporting the PhD of Mr Marques.

References

- Abramson, H. N. (1966). The dynamic behavior of liquids in moving containers, with applications to Space Vehicle Technology. Scientific and Technical Information Division, National Aeronautics and Space Administration.
- Sutton, G. P., & Biblarz, O. (2017). Rocket Propulsion Elements (9th ed.). Hoboken: J. Wiley & Sons.
- Arndt, T. (2012). Sloshing of cryogenic liquids in a cylindrical tank under normal gravity conditions. Göttingen: Cuvillier Verlag.
- Foreest, A. van. (2014). Modeling of cryogenic sloshing including heat and Mass Transfer. Göttingen: Cuvillier Verlag.
- Lacapere, Jerome & Vieille, B. & Legrand, Benjamin. (2009). Experimental and numerical results of sloshing with cryogenic fluids. EUCASS Proceedings Series. 267-278. 10.1051/eucass/200901267.
- Simonini, A., Fontanarosa, D., De Giorgi, M. G., & Vetrano, M. R. (2021). Mode characterization and damping measurement of liquid sloshing in cylindrical containers by means of reference image topography. Experimental Thermal and Fluid Science, 120, 110232.
- Miles, J. W. (1984). Resonantly forced surface waves in a circular cylinder. Journal of Fluid Mechanics, 149, 15-31. Cambridge University Press.

ORAL 101

About water droplet populations in microgravity conditions

C. Graziani¹, M. Nespoulous¹, R. Denoyel¹, S. Fauve², C. Chauveau³, L. Deike⁴, M. Antoni¹

¹MADIREL Aix-Marseille University, ²LP ENS-Paris, ³ICARE University Orléans, ⁴MAE/HMEI Princeton University

Introduction

Aerosols are divided systems in which liquid and/or solid particles evolve in a continuous gas phase. They are naturally subject to the influence of gravity, which determines the settling speed of the particles they contain. Aerosols have many applications in the pharmaceutical and cosmetic industries (inhalers, sprays), in metallurgy (spray drying) and in agriculture (pesticides). From an academic point of view, they are the subject of intense research activity. The description of their evolution is, for example, a major issue in climatology. With global warming, more water is evaporating in the air resulting in more cloud formation and a higher importance of cloud microphysics in the understanding of the climate evolution. In this context, CNES has recently supported the development of a new instrument allowing not only to produce aerosols under controlled thermodynamic conditions but also to follow their evolution in microgravity. This work presents results of parabolic flight experiments. It demonstrates the possibility of producing aerosols and to investigate their properties with optical microscopy for periods of about twenty seconds.

1. Experimental conditions and image reconstruction

Aerosols under consideration in this work are similar to fogs and consist of populations of water droplets of few micrometers in radius (Figure 1). They are produced by a fast compression/expansion of air in a small cylindrical experimental chamber (diameter 3 cm, length 6 cm) from/in a reservoir. Optical tomography microscopy in transmission mode is used to identify the droplets and to track their evolution in time. In ground conditions, such systems are getting drained very fast (about one second) which prevents investigations of their properties. Micro-gravity conditions are therefore required.

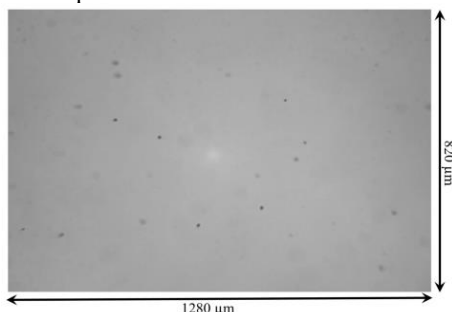


Figure 1 : Image of a population of droplets (black spots). (Ref: parabola P57, CNES, 59th parabolic flight campaign).

Parabolic flight experiments have been conducted. Experimental conditions after aerosol formation are close to ambient (1 atm, 22 °C). They demonstrated the possibility of producing droplets with a quasi-adiabatic expansion and their good observability. The continuous phase being air, fast turbulent transient regimes occur right after expansion. This makes tomographic microscopy analysis potentially

ineffective, as successive image coherence is essential. Fortunately, it turns out that the rapid flows created by the initial expansion are damped out within typically 7 seconds. Beyond this time, droplets have small amplitude movements only due to the residual acceleration of the parabolic flight conditions. Sequences of more than 13 seconds of reduced gravity during which the evolution of droplets can be investigated in scientifically relevant conditions.

The microscope travelling distance is 2 mm with travel speed up to 10 mm/s and acquisition frame rate of the camera 2000 images/s. A tomographic shot (ie. a single scan forwards or backwards) therefore lasts 0.2 s and generates 400 images. The distance between two successive images is 5 μm and the overall analyzed volume is about 2.1 mm³. One parabola accumulates typically 55 Gb data.

The identification of the droplets in the images is performed by thresholding predetermined grey levels (about ten). The quality of the images allows detection of droplets with radius down to 2 μm. Droplets being spherical, the principle is to detect the position of the center of each of them in a given image (whether focused or not) and then to construct, from the set of the centers of all the droplets and all the images of a given scanning shot, their individual optical axis. The location of a droplet on its optical axis is finally obtained by the image in which it exhibits the sharpest contrast. For this image processing technique to be functional, consecutive images must be coherent and thus droplets must evolve slowly compared to the acquisition capabilities of the image grabber. This is the case here. Figure 2 shows an example of a 3D reconstruction and illustrates the achieved level of precision.

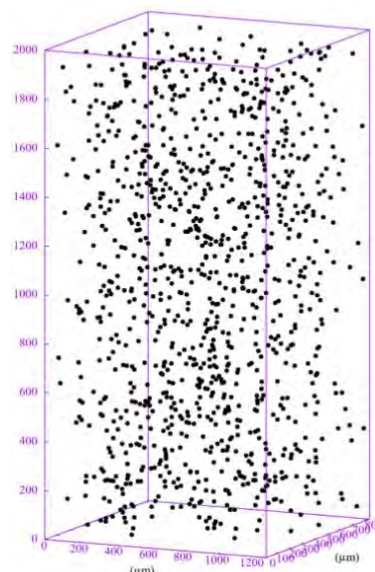


Figure 2 : 3D reconstruction of an aerosol (parabola P57, CNES 59th parabolic flight campaign, scan taken about 10 s after expansion). Droplets are black spots. Their radius is multiplied by a factor 10 for visibility. About 72 hours CPU are necessary for such a reconstruction.

2. Preliminary results

Tomographic shots are processed one by one to identify each individual droplet (Figure 2). This process is iterated to investigate the properties of the droplet populations generated for each experiment. Figure 3 shows the evolution of the number of droplets (N) in the analyzed volume (2.1 mm^3) as a function of time for four replica experiments and two values of relative humidity: $H=100\%$ and $H=70\%$. Droplets are generated by compressing the air in the experimental chamber up to 2 bar and expanding it back to atmospheric pressure. The expansion phase ($t = 0$) is operated at the very beginning of the micro-gravity phase. The gray shaded area ($t < 7 \text{ s}$) indicates the time period within which image reconstruction is not guaranteed. For longer times, water-saturated experiments ($H=100\%$) show droplets persisting for the time of the parabolas while they have all disappeared after typically 11 s when $H=70\%$.

These results, although expected, are nonetheless essential. First of all, they clearly demonstrate the possibility to measure the number of droplets over time in microgravity conditions. This is an essential condition for assessing the feasibility of aerosol investigations over longer periods. They indicate, moreover, that evaporation of the droplets in the sub-saturated regime is a fast phenomenon as it takes place in less than a fraction of second. Fundamental questions such as how quickly droplet populations evaporate as relative humidity conditions change or the precise number of droplets (e.g. liquid fraction) remaining after expansion thus become quantitatively accessible. Despite these original perspectives, Figure 3 raises practical questions that have yet to be resolved. The experiments show indeed low reproducibility, the origin of which is still not understood to this day. The droplet size distribution follows qualitatively a Maxwell-Boltzmann law (not shown). But accurate measurement of the radius of individual droplets is subject to uncertainties of more than $2 \mu\text{m}$. Further efforts in image analysis are therefore still needed.

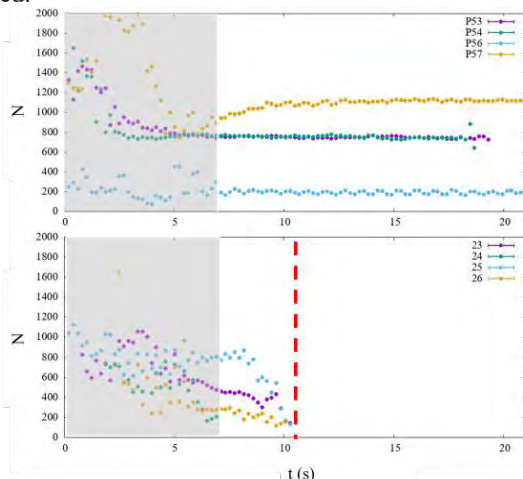


Figure 3 : Evolution of the number of droplets as a function of time. Pressure 1 bar. Top: $H=100\%$. Bottom $H=70\%$. The gray shaded area corresponds to the transient period. Vertical red dashed line indicates evaporation time. For parabolas P53 and P54 microgravity duration was shorter than expected.

Besides droplet formation and kinetics, another goal of this study is to investigate the influence of von Karman swirling flows on the evolution of droplet populations. The experimental chamber is equipped with two coaxial contra-

rotating rotors (smooth flat disks of diameter 29 mm facing each other). When rotating both of them with the same frequency (f), air is driven radially outward by the centrifugal force of the disks. This generates an axial flow toward the disks along their axis and a recirculation along the opposite direction along the EC lateral boundary. Therefore, a radially inward flow is generated in the mid-plane between the disks such that there is a stagnation point at the center of the EC. It is expected that droplets are driven by the flow of gas and accumulate in the vicinity of that stagnation point.

The experiments carried out so far are focused on the measurement of the lag time (t_{lag}) between rotor activation and droplet response. The protocol is similar to that of Figure 3 with the following additional step: after 7 seconds of an ongoing parabola, as the droplets are at rest, the rotation is started. The behaviour of $1/t_{\text{lag}}$ as a function of f is displayed in Figure 4. It increases linearly with f in the range $5 < f < 15 \text{ Hz}$. $1/t_{\text{lag}}$ extrapolates to zero for $f \sim 2 \text{ Hz}$ which is consistent with the fact that no motion is observed for the duration of the parabolas when $f < 4 \text{ Hz}$. This corresponds to a Reynolds number $Re = 2\pi f R^2/\nu$ close to 400 (where ν is the kinematic viscosity of air and $R \approx 1.45 \text{ cm}$ de rotor radius) for which it is known that the first instabilities of the von Karman swirling flow between counter-rotating disks take place. When Re is small, the flow is laminar and the motion is expected to develop on a diffusive time scale $(2R)^2/\nu \sim 60 \text{ s}$ when the rotors are set into motion. Therefore, no flow can be observed on the duration of a parabola.

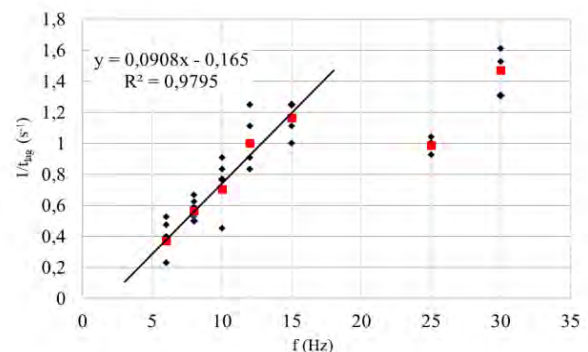


Figure 4 : t_{lag} as a function of rotation frequency f . Up to 5 replica experiments were achieved for each experiment. Squares shows the average of data points.

Conclusions

The preliminary experiments presented herein have established the possibility to describe quantitatively droplet populations in the microgravity conditions offered by parabolic flights. The flows generated by the initial expansion are shown to fade out within 7 seconds. Beyond this time, droplets are almost at rest. Optical microscopy tomography is shown to allow 3D reconstructions of such droplet populations and to follow their evolution as time runs. This work has finally shown how droplets can be set in motion when evolving in a von Karman swirling flow.

Acknowledgements

Authors gratefully thank CNES, in particular Christophe Delaroche and Laurent Arnaud, CNRS and region Provence-Alpes-Côte d'Azur for financial support. ESA - European Space Agency, within the project 'EDDI-Emulsion Dynamics and Droplet Interfaces - EDDI', ESA Contract n. 4000128643/19/NL/P.G.

Volume measurement of liquid propellants by means of acoustic fields

S. C. Abecia-Hernanz¹, N. Lainé², R. González-Cinca³

¹ Space Exploration Lab, Department of Physics, UPC-BarcelonaTech, Castelldefels (Barcelona), Spain, sara.cecilia.abecia@upc.edu, ² Centre National d'Études Spatiales (CNES), Paris, France, nicolas.laine@cnes.fr, ³ Space Exploration Lab, Department of Physics, UPC-BarcelonaTech, Castelldefels (Barcelona), Spain, ricard.gonzalez@upc.edu

Introduction

The ability to gauge liquid propellants accurately in low gravity environments is a key yet challenging aspect to successfully sustain human presence in space. A liquid contained in a tank adopts an unknown configuration in microgravity, which hinders its mass measurement since it prevents the use of conventional approaches used in ground based on the monitoring of fluid level. Some classical techniques that have been proposed to address mass measurement in low-gravity include bookkeeping, which relies on the accuracy of the thruster flow rate prediction, Pressure–Volume–Temperature (PVT), which uses the ideal gas law to estimate a propellant volume based on telemetry temperature and pressure readings, and thermal Propellant Gauging System (PGS), based on measuring the thermal capacitance of a tank containing liquid fuel and pressurant gas by measuring the thermal response of the propellant tank to heating and comparing the observed temperature rise to simulation results obtained from a tank thermal model (Yendler 2006). Nevertheless, each of these techniques suffers from a different problem: the bookkeeping technique tends to an uncontrollable accumulation of errors with time, the PVT method loses accuracy when pressure drops due to propellant drainage from the propellant tank, and thermal PGS has lower accuracies at the start of the mission, which increases with time as the tank load decreases due to temperature rise sensitivity. Two mass gauging techniques that have been developed to higher TRL are the radio frequency mass gauging (RFMG) (Zimmerli et al. 2006), and the Modal Propellant Gauging (MPG) technique (Crosby et al. 2021). Both approaches use pattern matching algorithms to compare the measured radio waves (RFMG) or acoustic (MPG) resonance frequencies with a database of the eigenfrequencies that are known for a series of liquid configurations, and the best match is used to predict the fill level of liquid.

The Spectral Mass Gauging (SMG) technique has been recently proposed as a liquid configuration-independent alternative and its feasibility has been tested and demonstrated both in ground (Delzeit et al. 2021) and microgravity conditions (Fili et al. 2021). This technique is based on a spectral invariant of the response of a partially filled tank under an acoustic actuation. In an application of SMG, sound waves are used to probe the natural modes of the system, and the mathematical properties of the modal spectral density are used to determine the liquid volume. The modal resolution generally increases with the characteristic size of the tank. Independence of the SMG on the knowledge of liquid configuration in the tank makes it an attractive technique for cryogenic propellant management.

The Spectral Mass Gauging technique

In his work in 1911, Weyl demonstrated that the high frequency asymptotics of the spectrum of the Laplacian in a three-dimensional spatial domain with Dirichlet boundary conditions depends on the domain only through its volume (Weyl 1911). Later research on the topic provided rigorously justified asymptotic expansion formulas for the large eigenvalue asymptotics in the case of various differential operators and boundary conditions as well. Applied to acoustic resonators filled with liquid, Weyl's Law can be written as:

$$N(f) = \frac{4\pi V}{3c_L^3} f^3 + \frac{\pi A_+}{4c_L^2} f^2 - \frac{\pi A_-}{4c_L^2} f^2 + o(f^2), \quad f \rightarrow \infty$$

where $N(f)$ is the liquid mode counting function up to frequency f , V is the volume of liquid in the resonator, A_+ is the area of the liquid surface adjacent to a rigid wall (Neumann boundary condition), A_- is the area of the liquid surface adjacent to a compliant wall (Dirichlet or pressure release boundary condition), and c_L is the speed of sound in the medium of the resonator, *i.e.*, the liquid. The leading order term in Eq. (1) is proportional to the liquid volume while being independent of the liquid shape (unlike the second order terms which depend on the areas that enclose the resonator). The determination of the liquid volume by means of the SMG technique requires first to identify the liquid modes in the Fourier spectrum. Next, the experimental curve of the counting function $N(f)$ is built and fitted to a third order polynomial of shape $Af^3 + Bf^2$. Finally, from the determination of the fitting coefficient A , and the speed of sound in the liquid, the volume of liquid can be computed from $V = 3Ac_L^3/4\pi$.

Experimental system

The experimental setup consists of three main subsystems: the test cell (a 300 L tank) containing distilled water at different fill-levels, a subsystem for the generation of an

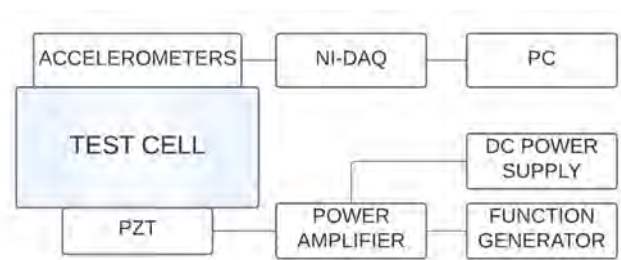


Figure 1: Block diagram of the experimental setup.

acoustic field within the test cell (function generator, power amplifier and piezoelectric transducer or PZT), and the data acquisition subsystem (accelerometers, NI-DAQ and computer). A block diagram of the setup can be seen in Figure 1.

Figure 2 shows the liquid-storage tank with dimensions (diameter x height x thickness) of Ø633 x 950 x 2 mm made of aluminium 5754.

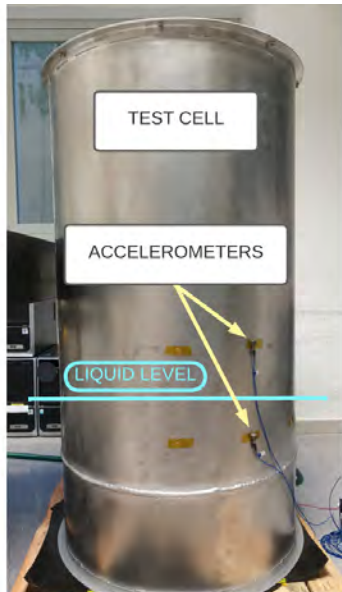


Figure 1: Partially filled tank with accelerometers attached to the wall below and above the liquid level.

The PZT that generates the acoustic wave is attached to the centre of the outer face of the bottom wall of the test cell using conductive epoxy adhesive. This actuator is fed by a sinusoidal tone-burst-like electrical signal, which generated promising results with small tanks in previous tests

Experiment procedure and analysis

The acoustic field is generated within the tank by applying a signal to the PZT and, at the same time, the response from the system is recorded by the accelerometers placed at the walls. The Fast Fourier Transform (FFT) of the time signal from the accelerometers is then computed to obtain its corresponding spectrum. Figure 3 shows an example of the FFT spectra obtained at different positions of the accelerometers. The accelerometers below the liquid level gave a higher density of peaks in the spectra for the studied cases. Likewise, it was found that the parameters of the tone-burst-like signal applied to the PZT actuator (central frequency, number of cycles and amplitude) significantly affected the envelope of the obtained spectra, thus enabling the optimization of these parameters for a better identification of the peaks present in the spectra, which correspond to the natural modes of the system. After locating the modes in the spectra that correspond to the liquid, the experimental mode counting function can be built and this curve can be fitted to the theoretical expression presented above, $N(f)$, to obtain a prediction of the volume of the liquid contained in the tank.

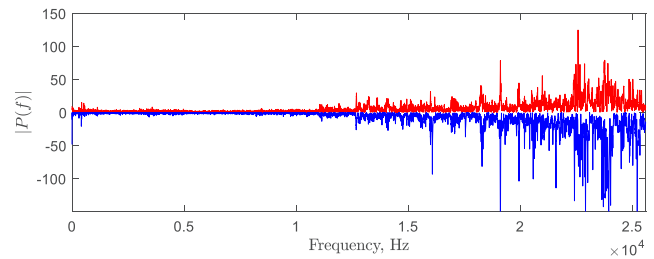


Figure 3: Frequency response to a sinusoidal tone-burst signal at a central frequency of 25 kHz, with the accelerometer placed above (red) and under (blue) the liquid level (60 L of distilled water).

Conclusions

We present an experimental setup that provides promising results for the application of the SMG technique to medium-sized tanks. The placement of the accelerometers with respect to the level of liquid is found to have the effect of measuring more spectral modes when located below the level of liquid. As next steps, we seek to study how the different parameters of the experiment can affect the prediction of the volume of liquid.

Acknowledgements

This work was financially supported by the French Space Agency (CNES) through contract 5700006207 / DLA090, and by the Agencia Estatal de Investigación (Spain) project PID2020-116413GB-I00 (MCIN / AEI / 10.13039/501100011033). We thank Michael Khasin (NASA Ames) for fruitful discussions.

References

- B. Yendler, Review of propellant gauging methods, *44th AIAA Aerospace Sciences Meeting and Exhibit* (2006).
- G. A. Zimmerli, K. R. Vaden, M. D. Herlacher, D. A. Buchanan, and N. T. Van Dresar, Radio frequency mass gauging of propellants, *NASA Technical Report TM-2007-214907* (2006).
- K. M. Crosby, N. J. Williams, R. J. Werlink, and E. A. Hurlbert, Modal Propellant Gauging: High-resolution and non-invasive gauging of both settled and unsettled liquids in reduced gravity, *Acta Astronautica*, vol. 159, p. 499-507 (2019).
- L. Delzeit, J. Feller, B. Helvensteijn, A. Kashani, M. Khasin, and V. Osipov, Spectral Mass Gauging of Liquids with Acoustic Waves, *50th International Conference on Environmental Systems* (2021).
- T. Fili, G. Quintana-Buil, and R. González-Cinca, Spectral mass gauging in terrestrial gravity and microgravity conditions. *Acta Astronautica*, vol. 194, p. 174-184 (2022).
- H. Weyl. Ueber die asymptotische verteilung der eigenwerte, *Nachr. Ges. Wiss. Gött. Math.-Phys.*, Kl. 110–117 (1911).

ORAL 103

Expression of locomotor synergies under various gravitational constraints

E. Guillaud¹, E. Doat¹, J.R. Cazalets¹

¹Aquitaine Institute for Cognitive and Integrative Neuroscience, INCIA, UMR 5287 CNRS, Université de Bordeaux, Bordeaux, France. etienne.guillaud@u-bordeaux.fr

Introduction

Gravity is often considered as the main constraint that applies to terrestrial human locomotion. The goal is to move forward, without falling, while regulating the energy cost of the movement as much as possible (Kuo et al., 2010). The result is a coordinated, cyclic, and highly reproducible muscular activity from one cycle to another and from one individual to another. However, the coordination patterns of locomotor activities without gravity constraints have never been documented, and very few studies have looked at the impact of gravity on the muscle synergies involved. We know that these rhythmic activities are coordinated by innate spinal generators (Klärner et al. 2018), which are fortunately able to adapt to the different constraints encountered in terrestrial life. But is the free expression of the spinal generators, without imposed cadence or gravitational constraint, different from that encountered on earth? Are the pedalling cadence or the muscular coordination patterns modified? Can these changes explain the physiological effects observed on astronauts (muscle loss, modification of fiber typology, ...) when they return to earth?

The objective of the experiment presented here was to identify the impact of a gravity change on the muscular coordination of the lower limbs in a pedalling task. A single group of 10 participants performed a pedalling task during CNES parabolic flights, allowing to perform successively several electromyographic recordings with repeated measurements in normogravity, hypergravity (1.75g) and microgravity (0g). Participants had to pedal on a cycloergometer, in upright position with arms at the side of the body. EMG was recorded on the right Gluteus Maximus, Rectus Femoris, Biceps Femoris, Anterior Tibialis and Medial Gastrocnemius. Self-selected cycling cadence, muscular synergies and neural frequencies discharges were analyzed.

Cadence and muscular synergies

Firstly, a major effect of gravity was observed on cadency, with a pedalling speed that decreased in micro- and that increase in hyper-gravity.

Muscle coordination during pedalling has often been described in terms of synergies, which provides a simplified view of locomotor patterns by reducing the dimensionality of motor behaviors (d'Avella et al., 2003). This type of analysis makes the hypothesis that the central nervous system generates a reduced number of rhythms, as several muscles can be activated synchronously on the same rhythm. We extracted muscle synergies using non-negative matrix factorization (Hug et al., 2010), and two synergies were sufficient to support the recorded pattern. Activation coefficient, which represents the relative contribution of the synergy to the overall muscle activity over time (e.g., during a pedal revolution), were modified by gravity. This was

illustrated in microgravity by a significant lag in the activation of the propulsive muscular group, accompanied by a decrease in activity peak. However, the muscle vector that specify the relative weight of each muscle, were only slightly modified by gravity.

Spectrum analysis of electromyogram

After a space mission, a decrease in neuromuscular action potential discharge frequencies has been shown for a force production identical to pre-mission tests, an effect similar to that of a period of bedrest (Ruegg et al. 2003) and confinement (Meigal and Fomina 2016). However, astronauts maintain significant physical activity during their mission, including on the CEVIS cycloergometer. This raises the question of a change in the typology of muscle fibers used during pedalling in microgravity, which could explain these changes despite regular training.

We analyzed the frequency contents of electromyogram during activation phases of each muscle. The gravity significantly affect the median frequency, with a decrease for certain muscles only. These results will be discussed in term of favored use of fibers type (Ia vs. II) according to gravity.

Conclusions

We present here the first observation of the unconstrained expression of locomotor coordinations, under micro and hyper-gravity. Our results showed a modulation of the synergies by the central nervous system according to the gravity context, that contrast with previous studies on muscular synergies during cycling on earth (Hug et al. 2011, Cartier et al. 2022) or during postural task in microgravity. (Holubarsch et al., 2019). These results suggest that the innate spinal generators, that coordinate the locomotor rhythmic activity, immediately adjust their pattern to the gravity constraint, whereas their free expression differ from that encountered on earth.

At the same time, a change in the type of muscle fiber used during exercise in microgravity is discussed for the different muscles, according to their anti-gravitational role on earth.

Acknowledgements

This work was supported by CNES (Centre National d'Etudes Spatiales, France) and the grant LABEX BRAIN ANR-10-LABX-43 (France).

References

- Cartier T, Vigouroux L, Viehweger E, Rao G. Subject specific muscle synergies and mechanical output during cycling with arms or legs. PeerJ. 2022 Mar 29;10:e13155.
- d'Avella A, Saltiel P, Bizzi E. Combinations of muscle synergies in the construction of a natural motor behavior. Nat Neurosci. 2003; 6(3):300-8.

Holubarsch J, Helm M, Ringhof S, Gollhofer A, Freyler K, Ritzmann R. Stumbling reactions in hypo and hyper gravity - muscle synergies are robust across different perturbations of human stance during parabolic flights. *Sci Rep*. 2019 Jul 19;9(1):10490.

Hug F, Turpin NA, Couturier A, Dorel S. Consistency of muscle synergies during pedaling across different mechanical constraints. *J Neurophysiol*. 2011; 106(1):91-103.

Hug F, Turpin NA, Guével A, Dorel S. Is interindividual variability of EMG patterns in trained cyclists related to different muscle synergies? *J Appl Physiol* (1985). 2010 Jun;108(6):1727-36.

Klamer T, Zehr EP. Sherlock Holmes and the curious case of the human locomotor CPG. *J Neurophysiol*. 2018; 120(1):53-77.

Kuo AD, Donelan JM. Dynamic principles of gait and their clinical implications. *Phys Ther*. 2010; 90(2):157-74.

Meigal A, Fomina E. Electromyographic evaluation of countermeasures during the terrestrial simulation of interplanetary spaceflight in Mars500 project. *Pathophysiology*. 2016 Mar;23(1):11-8.

Ruegg DG, Kakebeeke TH, Gabriel JP, Bennefeld M. Conduction velocity of nerve and muscle fiber action potentials after a space mission or a bed rest. *Clin Neurophysiol*. 2003 Jan;114(1):86-93.

ORAL 104

Boil-off management in microgravity

G. Quintana-Buil¹, R. González-Cinca²

¹ Space Exploration Lab, Department of Physics, UPC-BarcelonaTech, Castelldefels (Barcelona), Spain, Email: guillem.quintana@upc.edu

² Space Exploration Lab, Department of Physics UPC-BarcelonaTech, Castelldefels (Barcelona), Spain, Email: ricard.gonzalez@upc.edu

Introduction

An efficient management of cryogenic propellants (LH₂, LO_x) in a microgravity environment is required for applications such as storage, transfer, or mass gauging (Muratov et al. 2011). One of the main issues to address during long term cryogenic propellant storage is boil-off. The vapour bubbles formed at hot spots in the tank walls can generate undesired foam structures, which could be hazardous for operations in orbit. Since boil-off in propellant tanks is unavoidable with the current insulating techniques, approaches able to minimize the effects of boiling are required.

A promising method to manage boiling in propellant tanks consists in using acoustic waves for the control and removal of vapour bubbles (Quintana-Buil et al. 2018, Suñol et al. 2020, Quintana-Buil & González-Cinca 2021). This technique requires far fewer resources than other methods (e.g. pressurization and ullage motor). The acoustic approach lies on the control of bubble dynamics by means of the acoustic (Bjerknes) force exerted on the bubbles (Crum 1975, Mendéz & González-Cinca 2011).

Few studies have been carried out on the interaction between acoustics and boiling in microgravity. Sitter et al. (Sitter et al. 1998, Sitter et al. 1998) applied a 10 kHz standing wave in pool boiling of FC-72 generated by a wire. In gravity conditions, the heat transfer coefficient was found to be higher with acoustics and highest/lowest when the heater wire was in the antinode/node. Largest heat transfer enhancement was found at the inception of boiling and during film boiling. Similar observations were found in microgravity. The applied acoustic wave enhanced boiling heat transfer and increased the critical heat flux (CHF) in gravity. In microgravity, acoustics played the role of gravity to maintain nucleate boiling and increased the CHF, although not as much as in gravity conditions.

A realistic approach to study the heat transfer in the acoustics-boiling interaction to manage boil-off in propellant tanks lies in the use of a two-dimensional heating element to represent a hot spot in the tank walls. Pool boiling on flat plates in microgravity has been studied for a few decades (Colin et al. 2017). A square heater was used in (Quintana-Buil & González-Cinca 2021), where the effects of the acoustic technique on heat transfer in terrestrial gravity and microgravity were analysed.

We present an experimental analysis of the effects of acoustic actuation on the bubble dynamics in a square heater in microgravity conditions. This experiment complements the results in (Quintana-Buil & González-Cinca 2021). The

facilities of the ZARM drop tower in Bremen (Germany) were used for the experiments in microgravity.

Experimental setup

The experimental setup (Figure 1) is composed of a test cell, and subsystems for acoustic actuation, boil-off generation (heater) and data acquisition (Quintana-Buil & González-Cinca 2021). Working fluid is HFE-7100. An acoustic actuation applied to the walls of the test cell generates pressure nodes and antinodes in the liquid, which are responsible of the Bjerknes force on the bubbles generated by boil-off.

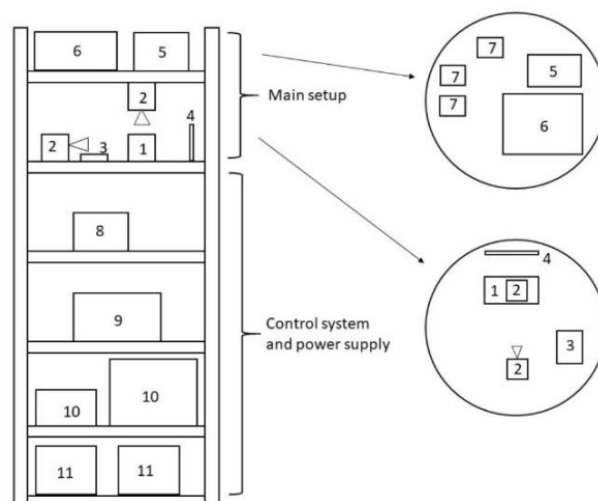


Figure 1: Experimental setup: 1) Test cell, 2) High-speed cameras, 3) KUSB, 4) LED matrix, 5) PC, 6) Power amplifier, 7) Electronics for data acquisition and heater power management, 8) High speed cameras acquisition device, 9) DC/AC converter, 10) ZARM equipment, 11) Batteries.

Bubble dynamics and heat flux enhancement

Different observations can be derived depending on the scenario of each drop. In some scenarios, the Bjerknes force is able to move bubbles away from the heater towards colder regions where they can condensate (Figure 2). In other scenarios where the acoustic actuation started before the power supply to the heater, boil-off was removed. In this case, an acoustics-induced convection could increase the heat flux from the heater towards the liquid, which in turn decreased the heater surface temperature. When the temperature of the heater became smaller than the boiling temperature of the liquid (61°C for HFE7100) boil-off did not take place.

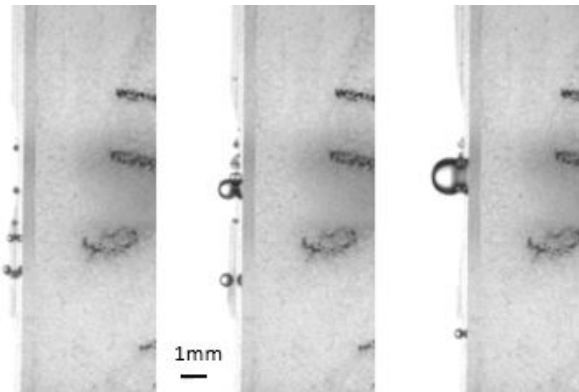


Figure 2: Bubble dynamics and condensation by means of an acoustic excitation.

Schlieren imaging was used in order to observe and analyse the heat flow when the acoustic excitation and the heater were activated in microgravity (Figure 3). Images obtained from this technique show that the application of an acoustic wave generates an induced heat flow similar to buoyancy-induced flows in terrestrial gravity conditions. Remarkably, the acoustics-induced convective flows in microgravity are independent of the direction of propagation of the generated acoustic wave, and are always perpendicular to the heater surface.

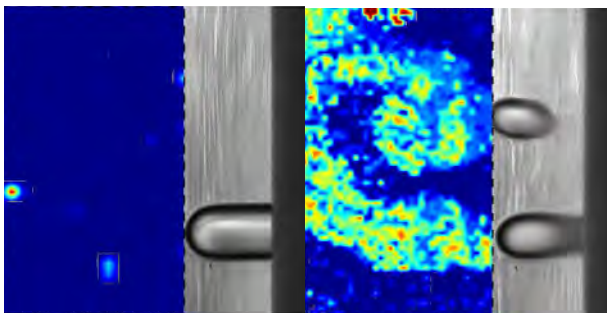


Figure 3: Left: Heat flux observed in microgravity without acoustic excitation. Right: Heat flux observed in microgravity with acoustic excitation.

Conclusions

A qualitative analysis of boil-off bubble dynamics and heat transfer enhancement under the effects of acoustic actuation in microgravity is presented. Acoustic actuation is able to detach bubbles from hot spots and move them towards colder regions where condensation can take place. Even if bubbles cannot be detached from the heater surface, they can be controlled and moved to colder regions on the heater surface (away from the nucleation spot) where they can condensate. The acoustic actuation can also avoid bubble nucleation and growth during boiling. This is explained by the capabilities of the acoustic wave to enhance heat transfer from the heater surface towards the liquid, decreasing the heater surface temperature. Furthermore, an acoustic-induced convection has been identified employing the Schlieren photography technique.

Acknowledgements

This work was financially supported by the Agencia Estatal de Investigación (Spain) project PID2020-116413GB-I00 (MCIN / AEI / 10.13039/501100011033).

References

- Muratov, C. B., Osipov, V. V. & Smelyanskiy, V. N. Issues of long-term cryogenic propellant storage in microgravity. NASA Technical Report, TM-2011-215988, (2011).
- Quintana-Buil, G., Garcia-Sabaté, A., Batlle, S., López, G., Sierra, V., Casas, O. & González-Cinca, R. A sounding rocket experiment to control boiling by means of acoustic waves. *Microgravity Sci. Technol.* 29 (5), 731-736, (2018).
- Suñol, F., Ochoa, D.A., Granados, M., González-Cinca, R. & García, J.E. Performance assessment of ultrasonic waves for bubble control in cryogenic fuel tanks. *Microgravity Sci. Technol.* 32 (5), (2020).
- Quintana-Buil, G. & González-Cinca, R. Acoustic effects on heat transfer on the ground and in microgravity conditions. *International Journal of Heat and Mass Transfer* 178, 121627, (2021).
- Crum, L.A. Bjerknes forces on bubbles in a stationary sound field. *J. Acoust. Soc. Am.* 57, 1363, (1975).
- Méndez, N. & González-Cinca, R. Numerical study of bubble dynamics with the Boundary Element Method. *J. Phys.: Conf. Ser.* 327, 012028, (2011).
- Sitter, J.S., Snyder, T.J., Chung, J.N. & Marston, P.L. Acoustic field interaction with a boiling system under terrestrial gravity and microgravity. *J. Acoust. Soc. Am.* 104, 2561-2569, (1998).
- Sitter, J.S., Snyder, T.J., Chung, J.N. & Marston, P.L. Terrestrial and microgravity pool boiling heat transfer from a wire in an acoustic field. *Int. J. Heat Mass Transfer* 41, 2143, (1998).
- Colin, C., Kannengieser, O., Bergez, W., Lebon, M., Sevilleau, J., Sagan, M. & Tanguy, S. Nucleate pool boiling in microgravity: Recent progress and future prospects. *Comptes Rendus Mécanique* 345, 21-24, (2017).

Electronics cooling by means of acoustic waves in microgravity

I. El Kraye Ziade, A. Dias Pierres, A. Drago González, M. Cachón Vigil, Y. Ferreiro Cuevas,
R. González Cinca

Space Exploration Lab, Department of Physics, Universitat Politècnica de Catalunya-BarcelonaTech, Castelldefels (Barcelona), Spain,
ioana.el.kraye.ziade@estudiantat.upc.edu, alejandro.dias@estudiantat.upc.edu, alex.drago@estudiantat.upc.edu,
manuel.cachon@estudiantat.upc.edu, yago.ferreiro.cuevas@estudiantat.upc.edu,
ricard.gonzalez@upc.edu

Introduction

Space missions are increasing in complexity and duration, so do both power and heat dissipation demands. Electronic devices are miniaturized to fit into compact spaces, whilst the processing speed and memory capacity is increasing constantly, leading to higher power consumption. As most of the electric power consumed transforms into heat, electronic components are more prone to failure due to overheating. The absence of buoyancy in microgravity results in an increase in the surface temperature of electric devices. As the performance and the failure process of electronics depend on their operational temperature range, effective cooling techniques are becoming more important.

The ability to reduce the size, weight, power consumption and cost of cooling technologies will have a major impact on thermal management systems. We propose a simple technique for electronics cooling based on previous studies carried out at the UPC Space Exploration Lab with acoustic actuation on multiphase flows. The proposed approach uses an acoustic wave to enhance the heat transfer between a heat source and the surrounding gas. We present the experimental setup designed to test the acoustic technique at the ZARM drop tower, and results obtained in numerical simulations and in tests carried out on ground.

State of the art

Most of the current cooling techniques are based on liquid cooling and phase change principles. Heat is transported away from the heated surfaces either directly, when the coolant and the electric component are in direct contact, or indirectly, when the coolant is pumped through a heat exchanger. Micro-channels and pin fins are added on the surface of chips to increase heat transfer. However, there are challenges from transforming micro-scale cooling systems to a macro-scale technology. The highest macro-scale heat transfer values can be reached by using phase change principles (Wits 2008).

There have been some experimental studies on the interaction between heat transfer and acoustics in normal gravity conditions. The heat transfer coefficient increased significantly when an acoustic wave was applied (Cooper et al. 1986). The results of convective heat transfer rates from an isolated sphere in the presence of standing acoustic waves showed a temperature difference of 42.8 K (Hyun et al. 2005). Acoustic actuation in microgravity increased the heat flux from a heater to a liquid by 8.4% compared to scenarios without actuation thanks to an acoustic-induced convection (Quintana-Buil & González-Cinca 2021). In summary, acoustic actuation is an efficient approach for heat transfer enhancement in multiphase flows in terrestrial gravity.

Therefore, an acoustic technique is expected to be feasible to induce a convective gas flow, increasing heat transfer and cooling electronics in space.

Experimental Setup

The experimental setup for the study of the acoustic technique consists of a test cell and subsystems for heat generation, acoustic wave generation and data acquisition (Figure 1).

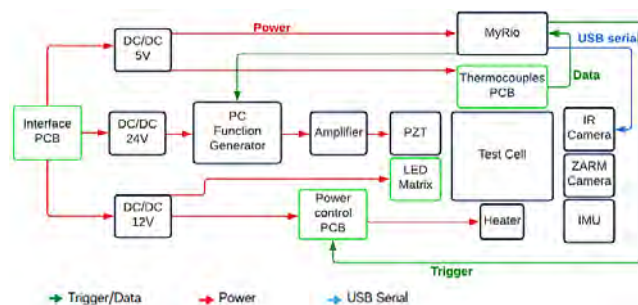


Figure 1: Block diagram of the experimental setup

The heat generation subsystem consists of a ceramic heater and a PCB designed to control the power supplied to the heater. The acoustic wave generation subsystem consists of a ceramic piezoelectric transducer (PZT), a function generator and an amplifier. The distance between the PZT and the heater is determined by the frequency of the acoustic actuation. The resonance frequency of the PZT provides a wave with the highest amplitude and, hence, is likely to generate the strongest effect on the gas flow.

Thermocouples are used in the setup to detect variations in temperature inside the heater and in its surroundings. A thermal camera is used to measure the temperature of the heater and to visualize the temperature distribution on the heater surface. Background Oriented Schlieren technique is used to depict the changes in density caused by the application of the acoustic wave (Figure 2).

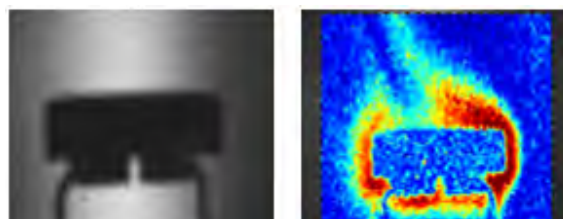


Figure 2: Left: Heater, Right: Processed image of the heater surroundings with Background Oriented Schlieren technique.

Numerical modelling

The numerical modelling and simulations performed by means of COMSOL provide valuable information to build the experimental setup. Results from simulations are used to determine the heater size and the optimal distance between the heater and the acoustic wave generator. Moreover, simulations show an increase of the Nusselt number (ratio of convective to conductive heat transfer) when acoustic actuation is applied under normal gravity conditions (Figure 3).

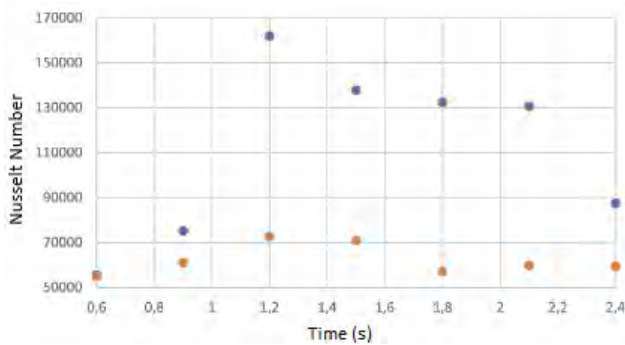


Figure 3: Nusselt number at 1cm from the heater as a function of time.

Ground tests

Different orientations between the PZT (and, thus, the generated acoustic wave) and the heater are considered. When the piezoelectric transducer is parallel to the heater, differences in the temperature measured by the thermocouples are obtained when the piezoelectric transducer is excited at its resonance frequency. When the piezoelectric transducer is perpendicular to the heater, both standing and travelling waves enhance heat transfer. Overall, standing acoustic waves seem to be more efficient for heat transfer enhancement when the piezoelectric transducer is parallel to the heater, generating a distribution of nodes and antinodes planes which are also parallel to the heater itself. Nevertheless, there is an effect in the heat transfer regardless of the orientation of the acoustic wave when traveling waves at the transducer resonance frequency are applied. Finally, it has been observed that the distance between the piezoelectric transducer and the heater is a key factor, as the effect of the acoustic field vanishes at large distances.

Conclusions

An experimental setup to study heat transfer enhancement by means of acoustic actuation in microgravity is proposed. Acoustic waves have been proven to increase heat transfer in gas in numerical simulations and in ground tests. We expect that the heat transfer enhancement will be higher when buoyancy is absent and the acoustic force is the only one present.

Acknowledgements

We thank the European Space Agency for selecting this project in the ELGRA Drop your Thesis! program and ZARM for technical support and assistance. We thank BACH RC for providing the heater.

References

- W. W. Wits, Integrated cooling concepts for printed circuit boards, University of Twente, Enschede, The Netherlands, 5-15 (2008).
- P. I. Cooper, J. C. Sheridan, and G. J. Flood, The effects of sound on forced convection over a flat plate, *International J. of Heat and Fluid Flow*, 7, 1, 61–68 (1986).
- S. Hyun, D. R. Lee, and B. G. Loh, Investigation of convective heat transfer augmentation using acoustic streaming generated by ultrasonic vibrations, *Int. J. of Heat and Mass Transfer*, 48, 3–4, 703–718 (2005).
- G. Quintana-Buil and R. González-Cinca, Acoustic effects on heat transfer on the ground and in microgravity conditions, *Int. J. of Heat and Mass Transfer*, 178, 121627 (2021).

ORAL 110

An integrated acoustic technology for application in propellant tanks

G. Quintana-Buil¹, S. Abecia¹, W.C. Mangram², M. Kashin³, F.K. Chang², R. González-Cinca¹

¹ Space Exploration Lab, UPC-BarcelonaTech, Castelldefels (Barcelona), Spain, Emails: guillem.quintana@upc.edu, sara.cecilia.abecia@upc.edu, ricard.gonzalez@upc.edu, ² Stanford University, Stanford, CA, USA, Emails: wmangram@stanford.edu, fkchang@stanford.edu, ³NASA Ames Research Center, Moffett Field, CA, USA, Email: michael.khasin@nasa.gov

Introduction

The exposure of the propellant tanks in long-term missions to the operational environment implies the need for efficient technologies to mitigate environmental effects on the propellant and the tank. Cryogenic fluid management in microgravity faces several physical challenges, such as the boil-off control and gauging of. Despite the advances in multi-layer insulation, keeping the fuel at the required cryogenic temperatures for long periods is challenging. Thus, tanks experience localized boiling due to heat leaks. Moreover, given the unknown propellant configuration in the tank in microgravity, accurate mass gauging is also a challenging task. Structural damages and eventually, the creation of hot spots in the tank structure can be localized by precise structural health monitoring (SHM).

Acoustic techniques

Approaches based on the use of acoustic actuation have been recently used for boil-off control (Quintana and González-Cinca. 2021), mass gauging (Kashin et al. 2017, Fili et al. 2022), and structural health monitoring. Experiments carried out in microgravity showed that the dynamics of bubbles generated by boil-off can be managed by means of acoustic waves. The acoustic force can detach bubbles from hot spots and move them to colder regions, where they can condensate. Moreover, acoustic actuation can enhance heat transfer in microgravity by inducing a convective flow and reducing the temperature in the hot regions. Acoustic waves can also be used to measure the amount of liquid in partially-filled tanks. This technique is based on the mathematical properties of the high-frequency spectral asymptotic of a resonator. Sensor networks based on ultrasounds have also been successfully employed in structural health monitoring of aircraft and space structures.

The acoustic approaches for boil-off control, mass gauging, and structural health monitoring have only been tested separately despite they share many features related to the common basis of using acoustic waves. We present the integration of the three techniques in an experimental setup that will be tested in a NASA-funded suborbital flight.

Experimental setup

The maturation of an integrated technology towards its intended applications is expected to progress by being fed with the maturation of the individual techniques for each

application (boil-off control, mass gauging, structural health monitoring). Each of these techniques can be matured independently from the others. For boil-off control, the next steps for maturation consist of the consideration of scenarios not analysed up until now (such as partially filled tanks, high-frequency acoustic waves, etc.) as well as experimentation with cryogenic fluids. In the case of the mass gauging technique, the next planned steps are to perform additional tests in microgravity conditions with small tanks and experimentation at cryogenic temperatures. In the case of structural health monitoring, the objective is to develop advanced real-time data-driven diagnostic methods for providing reliable and quantifiable information of the anomalies in the tank in a cryogenic environment based on a distributed sensor network during the operation.

The experimental setup is based in the payload to mature the boil-off control technology that flew in the UP Aerospace flights SL-9 and SL-11 in the framework of the NASA Flight Opportunities Program. A similar experimental setup was also used in an ESA-funded suborbital flight and, with some modifications to adapt it to the drop tower conditions, it was also used in ESA-funded campaign in the ZARM drop tower in Germany. Figs. 1 and 2 show a sketch and a block diagram, respectively, of the experimental setup to study the integrated technology. The setup consists of a test cell (tank) and subsystems for experiment control, acoustic wave generation, and data acquisition. Fig. 3 shows the actual experimental setup during the vibration tests carried before the launch. The main differences with the setups used so far are associated to the mass gauging and structural health monitoring techniques, such as the accelerometers and the mesh of transducers that will be attached to the external walls of the tank, or the ScanGenie hardware to generate acoustic waves for SHM.

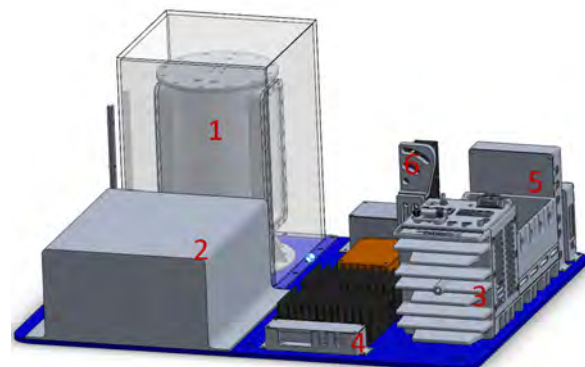


Figure 1: Experimental setup: 1) Test cell, 2) Scangenie, 3) CompactDAQ 9134, 4) DC/DC regulators, 5) Electronic boxes, 6) Camera support.

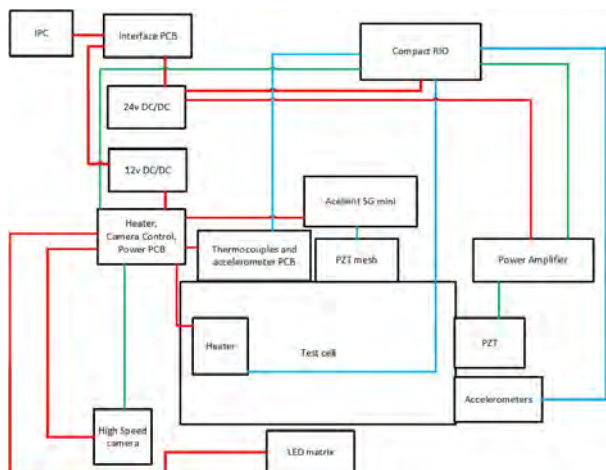


Figure 2: Experiment block diagram.

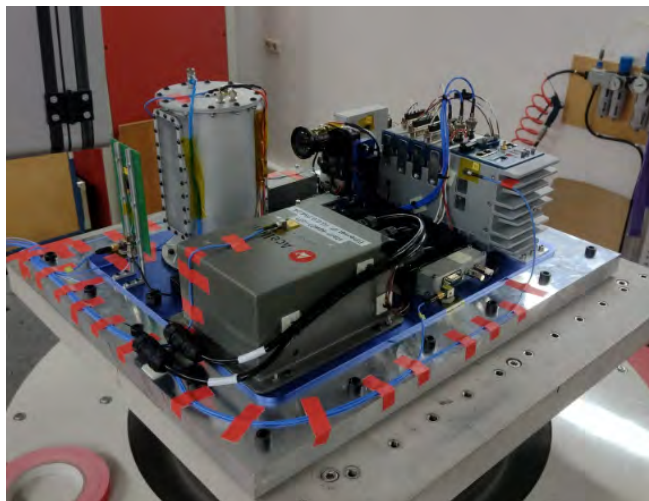


Figure 3: Experimental setup during a vibration test.

Conclusions

An integrated cryogenic fluid management, including boil-off control and mass-gauging, and structural health monitoring, is a critical technology for propellant depots, long loiter upper stages, and, generally, for deep space exploration missions. We present an integrated experimental setup to test acoustic techniques for the three applications. The main objective of our current research is to develop an integrated technology that contains all the capabilities (such as performance, low cost, etc.) of the individual ones at lower expenses (weight, cost, power, etc.) than the sum of the three separated technologies would have.

Acknowledgements

This work is financially supported by the NASA Flight Opportunities Program and the Agencia Estatal de Investigación (Spain) project PID2020-116413GB-I00 (MCIN / AEI / 10.13039/501100011033).

References

- G. Quintana-Buil, and R. González-Cinca, Acoustic effects on heat transfer on the ground and in microgravity conditions. *International Journal of Heat and Mass Transfer* 178, 121627, (2021).
- J. Feller, A. Kashani, M. Khasin, C. Muratov, V. Osipov, V. and S. Sharma, Spectral mass gauging of unsettled liquid with acoustic waves, NASA/TM-2018-219876, (2018).
- T. Fili, G. Quintana-Buil, and R. González-Cinca, Spectral mass gauging in terrestrial gravity and microgravity conditions. *Acta Astronautica*, 194, 174-184 (2022).

ORAL 113

From on-site to online ESA/ELGRA Gravity-Related Research Summer School

M. Van Walleghem¹, E.R. Ferre², P. Carvil³, N. Callens⁴

¹Redu Space Services for European Space Agency (ESA), ESEC- Galaxia, Transinne, Belgium, merel.van.walleghem@esa.int

²Department of Psychological Sciences, Birkbeck University of London, London, UK, elisa.ferre@bbk.ac.uk

³Daresbury Laboratory, Science and Technology Facilities Council, Warrington, UK, philip.carvil@stfc.ac.uk

⁴European Space Agency (ESA), ESEC- Galaxia, Transinne, Belgium, natacha.callens@esa.int

Introduction

The European Low Gravity Research Association (ELGRA, 2022) and the European Space Agency (ESA, 2022) co-organise an annual Summer School on gravity-related research every June since 2016 (N. Callens et al. 2021). The Summer School explains the fundamentals of performing research at different gravity levels and offers an overview of current research activity under microgravity and hypergravity conditions. During this educational activity, ELGRA and ESA members freely share their experience and know-how with up to 30 Bachelor and Master students, including their day-to-day work and research experience in life science, human physiology, physics and engineering. Students attend stimulating lectures and work within small groups to devise project ideas for prospective experiments. Each year the programme incorporates new elements to enhance the experience for the students based on their feedback. From 2016 to 2019 the Summer School took place at ESA Academy's Training and Learning Facility in ESA's European Space Security and Education Centre (ESEC) in Transinne (Belgium) during four and a half days. In 2020 and 2021 due to the Covid-19 pandemic the Summer School was adapted and delivered online over two weeks. 164 university students and more than 50 different experts have already participated in this Summer School. In 2022, ESA and ELGRA have decided to try a blended format including a week delivered on site and a second one online.

The Summer School concept

The main objective of the Summer School is to promote gravity-related research amongst future scientists and engineers. These young minds are introduced to the benefits of performing research at different gravity levels and offered an overview of current research under microgravity and hypergravity conditions in life sciences, physical sciences and engineering. Other related objectives are:

- transfer of knowledge and expertise
- inspire and network with the future generation
- encourage students to participate in hands-on research opportunities

• attract future scientists and engineers into the space sector. Each year, ELGRA contacts their members to offer them the opportunity to participate in the Summer School by submitting an abstract to propose a lecture. Two to three lectures in life science, human physiology, physics and engineering are selected. The selected ELGRA members join the Summer School for a minimum of one day and along with some additional ESA experts provide a background to their topic area, examples of gravity-related research and share their experience and expertise. After the selection of the 15-

20 experts and the finalisation of the programme of the Summer School, a call for student applications is launched by ESA Education Office. The Summer School is opened every year to 30 Bachelor and Master students in science or engineering disciplines from ESA Member and Associate States not yet involved in the space sector. The participating students and experts (Fig. 1) are sponsored by ESA and ELGRA to cover their travel, accommodation and meals.



Figure 1: Group picture at ESA/ELGRA Gravity-Related Research Summer School 2019 in ESEC-Galaxia (Belgium)

The Summer School programme includes lectures in the following topics:

- gravity-related research and platforms
- hands-on opportunities for university students
- introduction to project management
- gravity-related experiment development
- experiment life cycle
- life and physical sciences, human physiology and engineering at different gravity levels.

These lectures are complemented by testimonials from university students who have, with their respective student teams, designed, built, tested and performed a scientific experiment or technology demonstration in microgravity or hypergravity conditions in the frame of ESA Academy's hands-on projects (Callens et al, 2011).

Throughout the Summer School, the students are asked, in groups of four or five, to generate an idea for a future gravity-related experiment or technology demonstration, to choose a suitable gravity-related platform and propose a preliminary experimental setup and procedure.

On the final day of the Summer School, the student groups get the opportunity to present their project and are evaluated by experts from ELGRA and ESA. Upon completion of this process, the students are presented with a certificate of participation and a transcript including their evaluation. These

documents allow them to request European Credit Transfer System (ECTS) credit(s) for their participation at their respective universities.

Adaptation to online delivery

When the Covid-19 pandemic started, ESA and ELGRA decided to take the challenge of adapting the Summer School to an online format in less than three months. All the experts also adhered to the idea and in June 2020 the first online edition was delivered. The objective was to try and keep as much as possible the same opportunity and engagement for the participating students. For that the Summer School was extended to ten days to not overwhelm the students with long days of online lectures and allow additional time for Q&A sessions with the experts and work on the group project. The first half of the Summer School allowed the participants to acquire a theoretical foundation of what gravity-related research entails and the different opportunities and benefits it offers, including examples of research done in different fields and student research projects. In parallel, the student groups had to think about a topic for their group project and pitch their idea at the end of the first week and received initial feedback. The second week, the groups could further develop their experiment proposal during online group work sessions with support of ESA or ELGRA experts acting as tutors. In addition to the project management workshop, the participants also attended a systems engineering and requirements definition workshop to further help them with the design of their experiments. The Summer School concluded with the final project presentations and evaluation by the panel of tutors.

Following this successful first online edition, a second online edition was organised in 2021 (Fig. 2). The same structure of the ten days was kept with minor adjustments based on the feedback of the year before.



Figure 1: Group picture of the online ESA/ELGRA Gravity-Related Research Summer School 2021

Although the two online editions of the Summer School were a useful educational opportunity for the university students and a pleasant experience for the experts, everyone agreed that the networking and social aspect of the Summer School could not be fully replicated in an online format. However, the experts also highlighted that the distribution of the more theoretical content and group work sessions over two weeks gave the students more time to consider their ideas and experiment design and resulted in a higher quality of the final results of the group projects.

A new concept for 2022 edition

Reflecting on the feedback of the six delivered editions of the Summer School, ELGRA and ESA have decided to test a new format in 2022. The Summer School will be organised in a blended format over two weeks. During the first week the students and the experts will meet in-person at ESA Academy's Training and Learning Facility for the delivery of the lectures and workshops and start brainstorming about ideas for the group project. The week will conclude with the project pitch presentations. During the second week, the students will work from Monday to Thursday in the mornings online per group on their respective projects and have several opportunities for tutorial and Q&A sessions. On Friday, all groups will present their final projects online to each other and be evaluated by the tutors.

Conclusions

The ESA/ELGRA Gravity-Related Research Summer School aims at complementing what future scientists and engineers learn at university, inspire them and attract them into the space sector and its multiple research opportunities. It is on the one hand a unique opportunity for university students to discover and/or get an overview of the research conducted in microgravity and hypergravity, work on a group project and network with experts. On the other hand, it is an engaging way for ELGRA and ESA experts to share their knowledge with the future generation and discuss innovative ideas with them. Over the years the Summer School content, format and duration have evolved, implementing the feedback of both students and experts, to give the university students an insight into the world of gravity-related research and a head start for a possible future professional research career.

Acknowledgements

We would like to thank ESA and ELGRA experts who developed and delivered voluntary lectures during the seven editions of the Summer School and shared their knowledge and enthusiasm with participating university students.

References

- www.elgra.org
- www.esa.int/Education
- N. Callens, P. Carvil, M. Walleghem, R. González-Cinca, *ESA/ELGRA Gravity-Related Research Summer School: an Introduction to Microgravity and Hypergravity Research for University Students*, *Microgravity Science and Technology*, 33, 13 (2021).
- N. Callens, N., J. Ventura-Traveset, T.L. De Lophem, C. Lopez De Echazarreta, V. Pletser, J. Van Loon, *ESA Parabolic flights, drop tower and centrifuge opportunities for university students*, *Microgravity Science and Technology*, 23-2, 181–189 (2011).

ORAL 115

Study of the influence of microgravity on brain derived spheroids in acoustic levitation

Pierre-Ewen Lecoq¹, Chloé Dupuis, Xavier Mousset, Xavier Benoit-Gonin, Mauricios Hoyos, Jean-Michel Peyrin², Jean-Luc Aider³

¹PMMH, Paris, France, pierre-ewen.lecoq@espci.fr,

²IBPS, Paris, France, jean-michel.peyrin@sorbonne-universite.fr, ³PMMH, Paris, France, jean-luc.aider@espci.fr

In a Bulk Acoustic Wave (BAW) resonator, spherical objects, such as particles, can be maintained in an equilibrium position, between the walls of a resonant cavity. In the so-called acoustic levitation plane, the gravity is counterbalanced by the Acoustic Radiation Force (ARF) created when the resonance condition is respected ($h = \frac{1}{2}\lambda_{ac}$, with h the height of the cavity and λ_{ac} the acoustic wavelength).

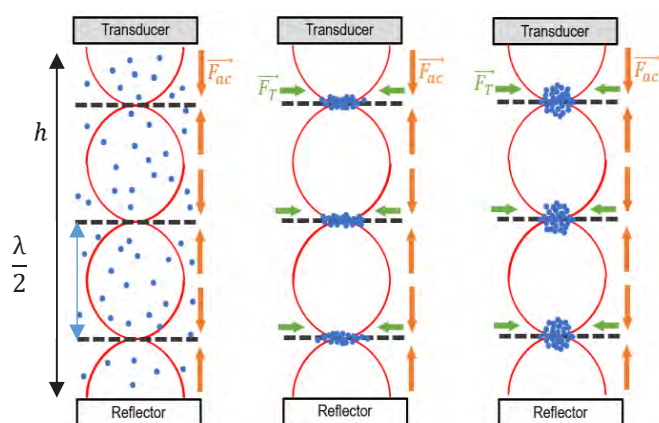


Fig. 1: Acoustic resonator applied to cells (blue points). We observe, thanks to the acoustic radiation force, the rapid formation of layers of cells in the acoustic nodes. After a few hours, the cell sheets turn spontaneously into spheroids.

The analytical expression commonly used to describe the ARF applied to a single spherical particle is obtained by assuming that the diameter d_p of the irradiated particle is very small compared to the acoustic wavelength ($d_p \ll \lambda_{ac}$). This assumption is called "Rayleigh's approximation" or "Rayleigh's limit" [1,2]. It is therefore perfectly applicable to objects of microscopic sizes ($d_p = 1$ to $20 \mu\text{m}$) and an ultrasonic frequency of the order of a few MHz (i.e. λ_{ac} of the order of a few hundred μm). In this context, particles or cells can be moved toward the acoustic levitation plane where they can form large aggregates.

We introduce a new scaffold-free approach to structure and cultivate organoids using multi-nodes

acoustic levitation. It can be used to create large aggregates of cells in a contact-less, label-free manner and with enhanced cell-cell interactions. We previously showed that human mesenchymal stem cells (hMSC) grown for 24 hours in acoustic levitation self-organized into spheroids and exhibited accelerated differentiation compared to classical 2D culture conditions [3]. These cultures also grow in a 3D environment where they can thrive, mimicking in vivo organs with more accuracy, which allows them to be used as model for organ growth or drug tests. Another advantage of acoustic levitation lies in the possibility to control and shape a dynamic mechanical force field, through ARF, around growing cell aggregates.

Moreover, this observation proves that another expression of the ARF should be derived for the case where $d_p \approx \lambda_{ac}$. In order to study more precisely the limits of this hypothesis, we carried out experiments in microgravity, during parabolic flights. In these experiments, the gravity no longer hinders the ARF and it becomes possible, even with small amplitudes ARF, to handle large and / or dense objects, which would otherwise sediment quickly in standard laboratory conditions on Earth.

A dedicated setup has been designed and built to run acoustic levitation experiments during parabolic flights. The setup should allow observation of particles or cells in acoustic levitation. A Zeiss Axiovert inverted microscope has been integrated in a Zargues box, together with a highly sensitive high-speed camera. A motorized moving plate and a stage incubator has also been integrated. All the parameters are controlled and monitored using computers and interfaces installed in a dedicated rack (Fig. 2).

Using this technology, we were able to observe the electrical activity of both 2D neuron layers and 3D neurons spheroids trapped in acoustic levitation, during the CNES parabolic flight campaign of

spring 2022. The analysis of this experiment will allow us to better understand the impact of gravity on neuronal activity in 3D as well as in 2D.

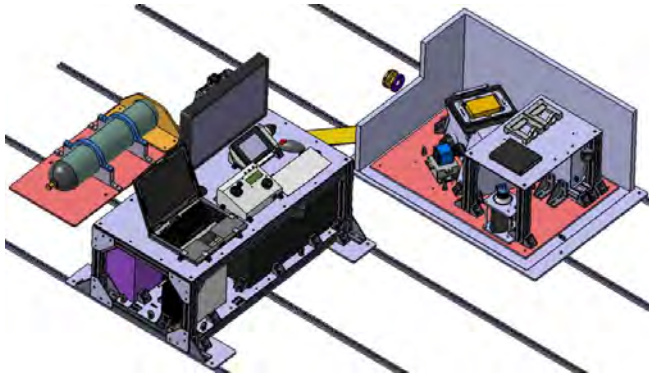


Fig. 2: Experimental setup used for the parabolic flights. On the left one can see the control rack, giving access to all parameters of the experiments. On the right, one can see a closed box in which an inverted microscope has been installed. The acoustofluidic cavity lies inside a stage incubator.

We will present in this talk the first experimental evidences showing that indeed ARF can move and levitate large objects far beyond the Rayleigh's limit. We will also show for the first-time that is indeed possible to monitor calcic activity of a neuronal spheroids in acoustic levitation. Preliminary results after this first campaign show that indeed the neuronal activity seems to be influenced by the variation of gravity, from hyper gravity (2g) to micro-gravity (0g).

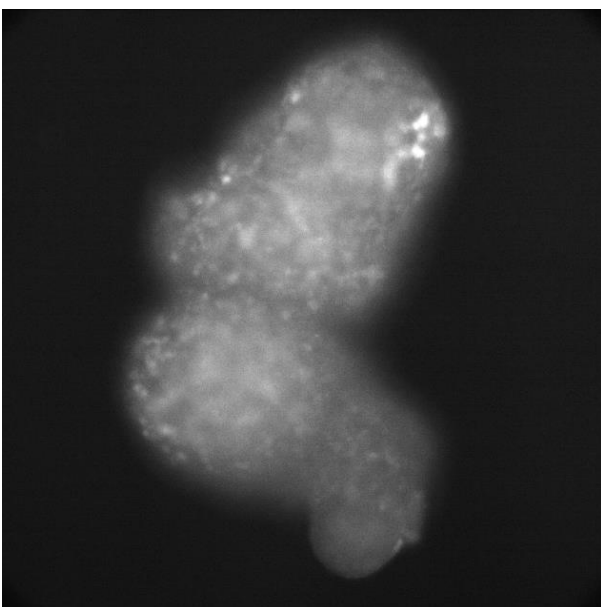


Fig. 3: Observation of two neuronal spheroids in acoustic levitation. Using fluorescence microscopy, it was possible to monitor calcic activity in the spheroids during the parabolic flights.

References

- [1] Doinikov, A. (1994). Acoustic radiation pressure on a compressible sphere in a viscous fluid. *Journal of Fluid Mechanics*, 267, 1-22.
- [2] G. T. Silva, H. Bruus (2014). Acoustic interaction forces between small particles in an ideal fluid, *Phys. Rev. E* 90, 063007.
- [3] Nathan Jeger-Madiot and al. Self-organization and culture of Mesenchymal Stromal Cell spheroids in acoustic levitation. (2020).

ORAL 117

Gold nanoparticles synthesized by laser ablation using a random positioning machine

Tânia M. Ribeiro¹, T. E. C. Magalhães¹, H. Crespo^{1,2}

¹Instituto de Física de Materiais Avançados, Nanotecnologia e Fotónica (IFIMUP), Departamento de Física e Astronomia, Faculdade de Ciências, Universidade do Porto, Rua do Campo Alegre s/n, 4169-007 Porto, Portugal

²Present Address: Blackett Laboratory, Imperial College, London SW7 2AZ, UK

Introduction

Laser ablation in liquids (LAL) (V. Amendola et al., 2013) is a top-down method for the synthesis of nanostructures. The technique stands out due to its versatility, low cost, and low environmental impact, being one of the most promising approaches toward sustainable nanotechnology. In LAL the nanomaterials are obtained by focusing an intense continuous wave or pulsed laser beam on the desired bulk target which is immersed in a liquid solution. Thanks to advances in ultrashort-pulse laser technology, the duration of the applied pulses can range from nanoseconds to a few femtoseconds. Frequently, nanomaterials are tailored according to the desired application. The specific use of nanostructures relies on their morphological (i.e. shape and dimension) and physicochemical properties (i.e. composition, structure, and colloidal stability). Therefore, the fine control and development of new synthesis strategies are continuously being reviewed. LAL can be considered a relatively recent method compared to some wet chemistry approaches, with plenty of room for investigation. Here we present the synthesis of gold nanoparticles by LAL, where the solution and the immersed bulk target are placed in a random positioning machine (RPM) providing a simulated low-gravity environment. The experimental setup and the preliminary characterization of the ablated material will be presented and discussed. Based on the results obtained, some future work will also be addressed.

Methodology

Laser ablation for nanoparticle synthesis was carried out with an ultrafast Ti:Sapphire laser amplifier (Coherent Astrella) delivering <35 fs pulses with an energy of approximately 7 mJ at a repetition rate of 1 kHz, with a central wavelength of about 800 nm. A quartz cuvette was placed in the center of a custom-built RPM where the laser beam was focused with a spot size of about 80 μm . A bulk piece of gold was used as the ablation target. The material was immersed in ultrapure water and the ablations were carried out for 180 minutes with a fluence of 2 J cm^{-2} . The motion of the RPM prevents two consecutive laser shots from striking the same point of the target, which is desirable in LAL.

Preliminary Results

The ablated gold nanoparticles (AuNPs) dispersed in water show a pale pink color and appear to be stable for a few days (i.e. no visible sedimentation). UV-visible spectrophotometer analyses showed an absorption band around 525 nm, due to

the presence of a resonant surface plasmon excitation. The value is in good agreement with the literature (J.-P. Sylvestre et al., 2005), suggesting the presence of gold nanoparticles with a spherical shape. Analysis from dynamic light scattering shows a mean hydrodynamic size of about 55 nm.

Conclusions

This work shows the potential of earth-based low-gravity platforms for the synthesis of nanomaterials. In particular, it is pioneering and of great importance for understanding the impact of gravity on the laser ablation process and consequently on the synthesized material's morphology and physicochemical properties.

Acknowledgements

The authors thank Sara Freitas and João H. Belo for providing the bulk target used in this work and Clara Pereira for the help with the dynamic light scattering analysis. Tânia M. Ribeiro acknowledges the support from the Fundação para a Ciência e a Tecnologia (FCT, Portugal) through the grant PD/BD/140872/2018.

References

- V. Amendola, M. Meneghetti, What controls the composition and the structure of nanomaterials generated by laser ablation in liquid solution?, *Phys. Chem. Chem. Phys.*, 15, 3027-3046, (2013)
- J.-P. Sylvestre, A.V. Kabashin, E. Sacher & M. Meunier, Femtosecond laser ablation of gold in water: influence of the laser-produced plasma on the nanoparticle size distribution, *Applied Physics A*, 80, 753–758, (2005)

ORAL 119

Evaporating sessile droplet on a sounding rocket: analysis by vapour interferometry and simulation

A. Rednikov¹, S. Dehaeck¹, H. Machrafi², A. Garivalis³, P. Di Marco³, P. Colinet¹

¹Université libre de Bruxelles–TIPs, Belgium, alexey.rednikov@ulb.be, ²Université de Liège, Belgium, ³University of Pisa, Italy

Introduction

The ESA Sounding Rocket Experiment ARLES (Advanced Research on Liquid Evaporation in Space) is aimed at studying sessile droplet evaporation in μg , in the absence of buoyancy, practically unavoidable on Earth. The experiment involves both droplets of pure liquids and complex droplets containing low concentration of nanoparticles. Among the fundamental questions raised are the roles of Stefan flow and Marangoni flow (accentuated in μg , where no buoyancy effects are present) on the evaporation rate, vapour cloud distribution, nanoparticle deposition patterns and self-assembly in μg , thermocapillary instabilities as well as the possible role of an electric field as a forcing factor alternative to Earth’s gravity. The launch was realized at Esrange (Sweden) in June 2019. A more detailed description of the context /literature and experimental setup and a first analysis of the results are provided by Kumar et al. 2020 and Garivalis et al. 2022. This includes measurement of the droplet volume evolution from the side view and infrared diagnostics of the droplet from the top view. The volume decreases supposedly due to the evaporation, and this is used to experimentally determine the evaporation rate. The infrared images are used, among other things, to reveal thermocapillary instabilities in the droplet as well as to detect the moment the droplet depins from a groove of a radius of 2 mm where it finds itself pinned upon the injection (Kumar et al. 2020). In the present communication, we rather focus on the findings made possible owing to vapour interferometry (Dehaeck et al. 2014) in conjunction with numerical simulation.

Experimental

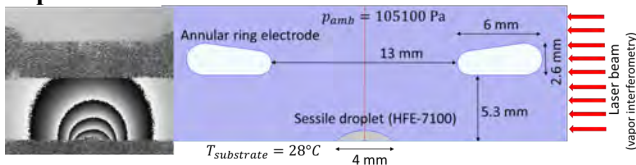


Figure 1: Schematic of the evaporation site. The left picture represents a fringe pattern typical for the diffusion regime of evaporation (roughly hemispherical fringes), when gravity, Marangoni convection, and the electric field are either absent or not essential.

Mach-Zehnder interferometry is used to visualize the vapour cloud from a sessile droplet composed of the pure HFE-7100 liquid and evaporating into pure nitrogen. Following the beam splitter, one part of the expanded laser beam passes parallelly over the substrate with the sessile droplet (Fig. 1). It is recombined with the other part in the camera (not shown), yielding an interferometric pattern. Processing the latter results in a so-called wrapped-phase image, as in Fig. 1 (left). The ‘phase’ here is actually the phase increment acquired by the beam due to the presence of the HFE-7100 vapour, relative to the pure nitrogen atmosphere. The spatial

non-uniformity of the phase reflects the one of the vapour cloud. The fringes one can observe in Fig. 1 (left) are actually lines of a constant phase (2π difference between the neighbouring fringes). Ideally, a (planar) fringe pattern permits to reconstruct the underlying axisymmetric vapour concentration field by means of the inverse Abel transform (as realized e.g. by Dehaeck et al. 2014). However, this is generally not feasible here, for the extent of the vapour cloud may well exceed the field of view (determined by the window size). Fortunately though, the ‘topology’ of the fringes is often representative of the iso-concentration lines. Therefore, the shape of the vapour cloud can well be judged by the fringe pattern.

Theoretical

The model of an evaporating sessile droplet pinned at the groove is based upon the continuity and Navier-Stokes equations in the gas and liquid phases, an advection-diffusion equation for the vapour concentration in the gas, and a convective heat transfer equation in the liquid. Heat transfer through the gas phase, estimated to be insignificant, is neglected, as well as the gas viscosity in the stress balance. Stefan flow, evaporative cooling and the resulting Marangoni (thermocapillary) stresses are taken into account. The evaporation-induced flow inside the droplet is neglected versus the Marangoni flow. A noteworthy feature of the present formulation is that the gas density is by far not constant and rather varies by the order of itself in view of large HFE-7100 molecules and a heavy vapour. This is fully taken into account in the model. Another noteworthy feature is accounting for the dielectrophoresis force in the gas within the Taylor-Melcher leaky dielectric model, due to the gradient of the dielectric permittivity induced by the vapour cloud, in the cases when the electric field is switched on (cf. the electrode in Fig. 1). Normally, as the dielectric permittivity of gases is quite close to unity, no such dielectrophoresis is expected. The gravity force can be switched off (to model the microgravity conditions) or on (to model the ground tests within the same setup).

The computations are accomplished with the help of COMSOL Multiphysics® within an axisymmetric configuration. Two kinds of computations are carried out: transient computations following the course of the experiment as close as possible, and quasi-steady benchmark computations closer to the associated standard arrangements typically considered in the literature. The former are used for a direct comparison with experiment, while the latter for the analysis of the role of various physical factors (on the evaporation rate, in particular). In most computations, the droplet shape is assumed to be a spherical cap pinned at 2 mm, which is either indeed a good approximation (especially in the absence of the electric field and gravity), or merely used for simplicity (as at the injection stage and in some cases with the electric field). Some isolated benchmark

computations are nonetheless carried out with the droplet shapes strongly deformed by the electric field. In transient computations, the evolution of the droplet volume at the injection and evaporation stages is adopted from experiment. The (direct) Abel transform is applied to the computed vapour concentration field to obtain the corresponding fringe pattern so as to make comparison with the experimental results (for which the inverse Abel transform to the concentration field is problematic as mentioned earlier).

Results and discussion

The typical fringe patterns obtained in experiments are represented by Fig. 1 (left) for a pure diffusion regime of the vapour cloud and by Fig. 2 for a regime where the vapour transfer is determined by the buoyancy force as for the heavy HFE-7100 vapour in normal gravity.

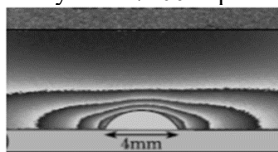


Figure 2: Typical fringe pattern in 1g on ground (heavy vapour), when the vapour cloud and the fringes are flattened by gravity.

The microgravity experiment offers a unique opportunity to see what would happen without such an overwhelming gravity action. One could foresee the existence of a Marangoni flow in the droplet due to a stronger non-compensated evaporative cooling at the apex. This is confirmed by vapour interferometry visualisation as in Fig. 3 and agrees well with simulation.

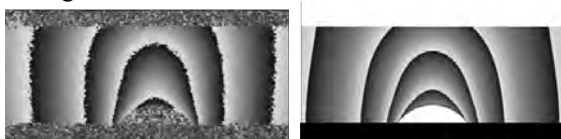


Figure 3: Typical fringe pattern in μg and with no electric field (7DP μg droplet in terms of Kumar et. al 2020): ARLES experiment (left) and simulation (right). An elongation of the fringes along the symmetry axis testifies to a Marangoni jet entrained in the gas by Marangoni convection in the droplet directed from the contact line towards the apex along the surface.

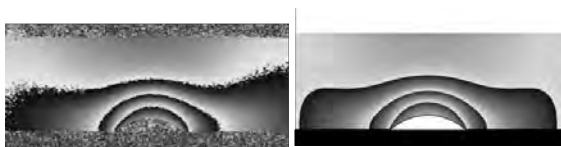


Figure 4: Typical fringe pattern in μg and in the presence of the electric field (5.7 V, 8DP μg EF droplet in terms of Kumar et. al 2020): ARLES experiment (left) and simulation (right). One observes the vapour cloud being attracted by the electrode.

Furthermore, a direct influence of the electric field on convection in the gas came as a surprise, revealed by vapour interferometry and confirmed by simulation (Fig. 4). A key factor here seems to be once again a large size of HFE-7100 molecules such that the gas dielectric permittivity is affected more than typically for gases.

Vapour interferometry in conjunction with simulation has also permitted examination of the causes of a certain malfunction in the ARLES experiment. In particular, the measured (by side-view volume evolution, Kumar et al. 2020) evaporation rates in μg turned out to be well lower than the computed ones (while there was a good agreement

in 1g tests). Namely, the measured values of 0.087 $\mu\text{L/s}$ and 0.109 $\mu\text{L/s}$ for 7DP μg and 8DP μg EF droplets against the computed values of 0.14 $\mu\text{L/s}$ and ~ 0.16 $\mu\text{L/s}$, respectively. A possible cause advanced by the Science Team during discussions was a non-ideal flashing of the evaporation cell between the runs in μg , leaving behind a considerable residual HFE-7100-humidity in the gas, which would give rise to lower evaporation rates. Such a hypothesis seemed all the more plausible given an unfortunate progressive blurring of infrared images observed in μg and also attributable to the residual HFE-7100-humidity. Nonetheless, vapour interferometry + simulation did not support such a hypothesis, for this would have resulted in a substantial phase difference reduction, which was actually not detected. Thus, another explanation, of leaking into the droplet from a very considerable ‘dead volume’ of liquid in the tube system, becomes the most plausible one.

Then how can one explain the mentioned progressive degradation of infrared images? Vapour interferometry gives a hint here too. Namely, it revealed a weird uniform phase increase throughout the μg runs, not even related to the presence of a droplet. In discussions within the Science and Engineering Teams, an accidental *water*-humidity condensation on the windows from *outside* the evaporation cell, due to a sharp temperature drop during the flight, was advanced as a plausible cause explaining both indicated drawbacks.

A new edition of the ARLES experiment, ARLES-II, is currently in preparation, where these and other shortcomings are hopefully corrected.

Acknowledgements

The present work was carried out in the framework of the European Space Agency research project AO-1999-110: EVAPORATION. We thank the ARLES Science Team: Dr. C.S. Iorio (coordinator), MRC – Université libre de Bruxelles, University of Pisa, IUSTI – Aix-Marseille University, TIPs -- Université libre de Bruxelles, Université de Liège, University of Alberta, Technical University of Darmstadt, University of Edinburgh, University of Loughborough, Trinity College Dublin, Institute of Mechanics – Chinese Academy of Sciences, and Kutateladze Institute of Thermophysics – Siberian Branch of the Russian Academy of Sciences. We are grateful to Dr. D. Mangini, Dr. B. Toth and Dr. A. Verga (ESA coordinators) and the Swedish Space Corporation (technical realization of the experiment). We are indebted to Dr. S.K. Parimalanathan for the measured value of the refractive index of the HFE-7100 vapour. We acknowledge the funding from the BELSPO PRODEX Evaporation project.

References

- S. Kumar, M. Medale, P. Di Marco and D. Brutin, Sessile volatile drop evaporation under microgravity, *npj Microgravity*, 6, 37 (2020).
- A. Garivalis, P. Di Marco, S. Dehaeck, A. Rednikov and P. Colinet, Experimental study on evaporation of droplets in microgravity and in the presence of electric field, *J. Phys.: Conf. Ser.*, 2177, 012047 (2022).
- S. Dehaeck, A. Rednikov and P. Colinet, Vapour-based interferometric measurement of local evaporation rate and interfacial temperature, *Langmuir*, 30, 2002 (2014).

ORAL 122

Thermophysical properties of liquid Ti-Al-Cr-Nb alloys: theory vs experiments

R. Novakovic¹, D. Giuranno¹, M. Mohr², H.-J. Fecht²

¹National Research Council (CNR-ICMATE), Via de Marini, 6, 16149 Genoa, Italy, rada.novakovic@ge.icmate.cnr.it, donatella.giuranno@ge.icmate.cnr.it, ²Institute of Functional Nanosystems, Ulm University, Albert-Einstein-Allee 47, 89081 Ulm, Germany, markus.mohr@uni-ulm.de, hans.fecht@uni-ulm.de

Introduction

The surface tension and viscosity of liquid Al-Ti-Cr-Nb alloys were analysed with respect to the Ti-Al system consisting of the major alloying elements and estimating the effects of the other alloy components on the two properties. In the case of the surface tension, the analysis was extended to the Al-Ti-Nb and Al-Ti-Cr ternary subsystems. The surface tension of these systems was calculated by the Compound Formation Model (CFM) and/or Quasi Chemical Approximation (QCA) for regular solution (Novakovic et al. 2012). Preliminary test of the models used to calculate the viscosity isotherm of liquid Al-Ti alloys indicated the Terzieff model as the most appropriate. Subsequently, the surface tension and viscosity experimental data of the Ti48Al48Nb2Cr2 (Wunderlich et al. 2021; Mohr et al. 2022) was compared to the model predicted values as well as with the literature data.

Section 1

The analysis of the models used for the calculations of the surface tension and viscosity of liquid Al-Ti-Cr-Nb alloys (Novakovic et al. 2012; Mohr et al. 2022)

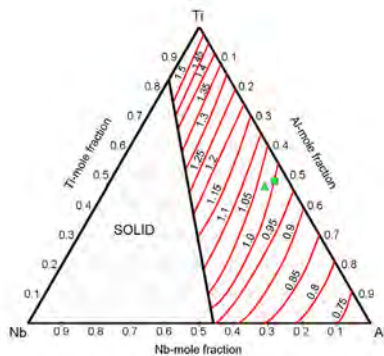


Figure 1: Iso-surface tension lines of liquid Ti-Al-Nb alloys calculated for T=1973 K. In the Gibbs triangle the square symbol indicates the compositional locations of the Ti48Al48Nb4 (in at%) that approximates the Ti48Al48Nb2Cr2 alloy.

Section 2

The surface tension and viscosity literature data (Novakovic et al. 2012; Wunderlich et al. 2021; Mohr et al. 2022) were used for a comparison with the corresponding model predicted values. Among the experimental data, there are also datasets obtained in EML (Electromagnetic Levitation) on board of the International Space Station (ISS).

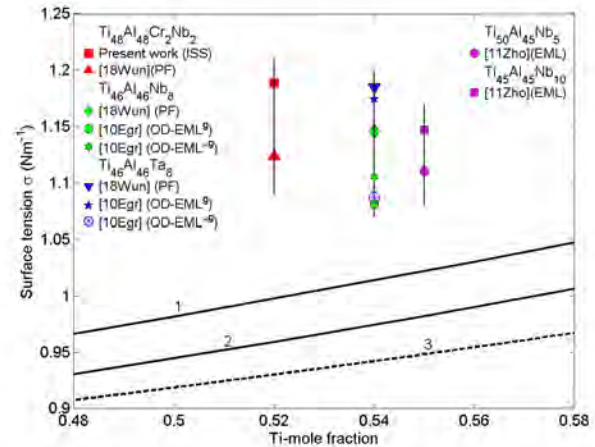


Figure 2: Surface tension isotherms (1-CFM, 2-QCA, 3-Ideal solution) of liquid Al-Ti alloys calculated for T=1973 K. Al-content (at %) in Al-Ti alloys (zoom) is comparable to those of Ti-Al based multicomponent alloys

Conclusions

In the present study, the model predicted values of the surface tension and viscosity of liquid Al-Ti, Al-Ti-Cr and Al-Ti-Nb alloys were used to evaluate the effects of minor alloying components on these properties of Al-Ti-Cr-Nb melts. The calculated thermophysical properties values are related to the lower limit of estimation and with the available experimental datasets substantiate the reliability assessment of the two properties.

Acknowledgements

This work has been performed in the framework of the ESA MAP Programme under contract no. AO-99-022 (14306/01/NL/SH).

References

- R. Novakovic et al., Surface, dynamic and structural properties of liquid Al-Ti alloys, *App. Surf. Sci.* 258(7) 3269-3275, (2012)
- R.K. Wunderlich et al., Thermophysical properties of the TiAl-2Cr-2Nb alloy in the liquid phase measured with electromagnetic levitation device on board of International Space Station, ISS-EML, *Int. J. Mater. Res.*, 112(10) 770-780, (2021)
- M. Mohr et al., *Metallurgy in Space*, Chapter 16, Thermophysical Properties of Titanium alloys, 357-375, (2022)

Manufacturing “in situ” of regolith simulants: Design of composites by liquid assisted processes

D. Giuranno¹, A. Bianchin², R. Novakovic¹

¹National Research Council (CNR-ICMATE), Via de Marini, 6, 16149 Genoa, Italy, donatella.giuranno@ge.icmate.cnr.it, rada.novakovic@ge.icmate.cnr.it, ²MBN nanomaterialia s.p.a., Via G.Bortolan 42, 31050 - Vascon di Carbonera – TV, Italy, alvise.bianchin@matres.org

Introduction

The assessment of in situ manufacturing on the Moon requires the knowledge of model materials and processes, previously investigated on the Earth approximating lunar living conditions: no atmosphere (vacuum), large variations of temperature, strong radiations, no weather and no oceans of water (N. Kalapodis et al. 2020). To produce materials with desired properties it is necessary to understand the relationships between the elements of a quadriade “composition-processing route-microstructure-properties” and based on it, to achieve tailored microstructure associated with a unique combination of properties.

The present work aims to contribute to the design and development of regolith based composites by liquid assisted processes such as infiltration (M. Caccia et al. 2019) and liquid phase sintering (R.M. German et al. 2009). Indeed, in both cases, the reinforcement of regolith by the metallic matrix can offer superior mechanical properties with respect to regolith / polymer composites or sintered layer-by-layer lunar regolith using the solar 3D printing technology on the Moon.

Section 1

The challenge is to design and produce composite materials, to assess in situ manufacturing and to identify the optimum processing conditions. To this aim, a DNA-1 regolith simulant rich in SiO₂, Al₂O₃ and Fe₂O₃ and containing small amounts of MgO and TiO₂ and two Al-rich alloys (Al-6061 and/or Al-7075) were selected.

Section 2

Design of a metal / regolite composite by the infiltration and liquid phase sintering involve wetting experiments. From thermodynamic and thermophysical properties considerations of both composites components, the choice of metallic phases is related to the formation of Fe-Al, Mg-Al and Ti-Al intermetallic compounds (IMCs) that will favour both, the reactive infiltration and liquid phase sintering resulting in reinforced microstructure. Therefore, for the investigation of both processes, preliminary wetting experiments are performed, followed by the microstructural characterisation of the interfaces between the metallic and ceramic phases.

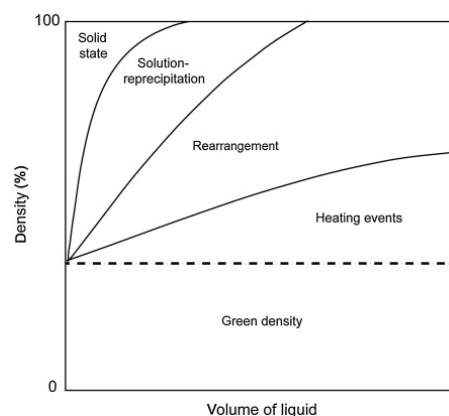


Figure 1: Phase evolution and densification during the liquid phase sintering

Conclusions

The human habitats and laboratories to be built on the Moon are related to the design and construction of pre-built laboratories by means of new materials produced by optimisation of existing processing routes. In the present study, a complex DNA-1 lunar simulant and an Al-rich alloy are used to produce composite materials by conventional processing routes such as the liquid phase sintering and infiltration. To this aim, theoretical studies, wetting experiments and microstructural characterisation of new composite materials were performed. Once the samples are produced, they will be subjected to mechanical testing (cryo, room temperature and high temperature mechanical properties) covering the specific temperatures on the Moon. A particular attention is paid to the green porosity and the relative density of regolith simulant specimens, surface and wetting properties of the liquid phase as well as operating process parameters that will determine the feasibility of fabricating new composite materials.

References

- N. Kalapodis, G. Kampas, O.-J. Ktenidou, A review towards the design of extraterrestrial structures: From regolith to human outposts. *Acta Astronautica*, 175, 540-569, (2020)
- R.M. German, P. Suri, S.J. Park, Review: liquid phase sintering, *J. Mater. Sci.*, 44, 1–39, (2009)
- M. Caccia, J. Narciso, Key parameters in the manufacture of SiC-based composite materials by reactive melt infiltration, *Materials*, 12, 2425 (pp 1-15), (2019)

27th
ELGRA BIENNIAL SYMPOSIUM
& GENERAL ASSEMBLY

POSTERS



POSTER 11

N-octadecane melting process in a rectangular cell under reboosting maneuvers conditions

D. Dubert¹, B. Šeta², M.J. Simón³, J. Massons¹, X. Ruiz¹, Jna. Gavalda¹

¹Departament de Química Física i Inorgànica, Universitat Rovira i Virgili. Tarragona, Spain.

²Department of Mechanical Engineering, Technical University of Denmark. Kogens Lyngby, Denmark.

³Departament d'Enginyeria Mecànica, Universitat Rovira i Virgili. Tarragona, Spain.

dianacristina.dubert@urv.cat, berse@mek.dtu.dk, mariajose.simon@urv.cat, jaume.masons@urv.cat, josepxavier.ruiz@urv.cat,
fina.gavalda@urv.cat

Introduction

Currently heat transport phenomena based on Phase Change Materials (PCMs) occupies an important place in the energy production and storage technologies both on Earth and in Space. Its rise is largely due to the advantages of PCM-based devices: they are cheap, sustainable systems with a simple design. The PCMs are recognized as an important tool for optimizing thermal control systems in space vehicles and in future habitats on Mars or the Moon (Collette et al 2011). It is in this context that the ESA project named “Effect of Marangoni Convection on heat transfer in Phase Change Materials (MarPCM)” will be carried out on the ISS during the next years. Its main objective focuses on the optimization of the extraction and storage of the energy within the PCM systems by using thermocapillary convection generated on a free surface. Since the purpose of the MarPCM project is to perform the phase change experiment on the International Space Station (ISS), it is of the utmost importance to know how the vibratory environment affects the experiment.

To do so, various simulations of the phase solid-liquid change (melting process) are thought to be carried out, by introducing a real acceleration signal coming from the ISS. This signal contains the period of a short reboost maneuver, since during this maneuver high levels of the acceleration on ISS can occur and may affect the melting process. In the past, it has been detected that the thermodiffusive experiments conducted on ISS (DCMIX3 campaign), were influenced by these kind of disturbances (Jurado et al. 2018). The system flow patterns were compared with those subjected to zero gravity levels. Finally, the response of the system was evaluated under higher acceleration levels in order to predict the safety margins in which the efficiency of the system is not affected.

Methodology

The PCM material picked was the n-octadecane (Prandtl number equal 52.53) due to the fact that it has the optimal properties for the melting process under microgravity conditions and successfully accomplish the ISS safety requirements. Its physical properties can be found in Šeta et al. 2021. The experimental cell has a parallelepipedic geometry with the following dimensions 15×22.5×25 mm. A rectangular cell with 15×22.5 mm was chosen for two dimensional simulations. Initially, the n-octadecane was in the solid phase, with its temperature under the melting temperature ($T_{\text{solidus}} = 298.15$ K, $T_{\text{melting}} = 301.15$ K). Once applied a ΔT ($T_{\text{hot wall}} - T_{\text{cold wall}}$) over the lateral walls a

controlled solid-liquid phase change began ($\Delta T = 30$ K in the present case). The upper wall is a free surface where appears the Marangoni convection that drives thermocapillary flow in the liquid phase. The momentum and the continuity equations for incompressible newtonian fluids describe the dynamics of the system. Concerning the energy equation, enthalpy method has been employed to model the melting process. More details about the applied method can be found in Šeta et al. 2021. In addition, the boundary conditions were considered the same as published by Salgado et al. (2021).

The OpenFOAM environment was used to solve the set of the governing equations specified earlier (see Šeta et al. 2021). The mesh convergence test was applied for different meshes. Finally, a mesh with 19800 (180×110) cells has been chosen for the simulation. This mesh was refined near the free surface and the lateral hot wall, where the gradients of the physical magnitudes are expected to intensify. In addition, this mesh offered a good compromise between spatial accuracy and the elevated computing time needed to accurately simulate the melting process. As the ISS experiment is still pending of a starting date, a recent reboost signal (24th June 2021) has been looked at as representative of the high residual acceleration levels (see Figure 1.a and 1.b).

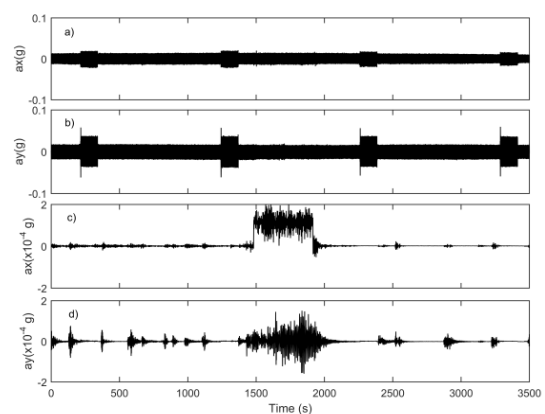


Figure 1: Raw acceleration components in the X_A and Y_A directions a) and b) and their denoised signals c) and d).

The signal was recorded by 121f03 SAMS sensor with the sampling rate of 500 Hz. In order to eliminate the frequencies higher than 1 Hz, contained in the signal, a level 9 denoised technique has been applied. More details of this technique can be found in Dubert et al. 2020. Figures 1.c and 1.d plot the denoised acceleration components, X_A and Y_A (ISS absolute

coordinates), clearly showing the reboost period location and its intensity. The reboost activity lasted about 7 minutes and achieved a mean intensity around 122 μg which produced a g-dose of $\Delta v = 0.5$ m/s. Finally, the time step needed for completing the simulations was 0.002 s that coincides with the recorded time of the signal. As can be seen in Figure 1, the onset of the reboosting manoeuvre is around 1500 s of the melting process starting point.

Results and Discussion

Figure 2 presents the temporal evolution of the liquid fraction during melting process for five different g-levels conditions: the black solid line represents the zero gravity condition, taken as background, the red and blue solid lines symbolize the introduction of the X_A reboosting acceleration component in the x and y directions, respectively (Figure 1.c). The x direction coincides with the thermal gradient orientation and the y direction is parallel to the walls in which different temperature has been applied. The red and blue dashed lines (RBX \times 1000 and RBY \times 1000) stand for the reboost signals having the same conditions as those presented earlier (RBX and RBY) though the g-dose was multiplied by 1000.

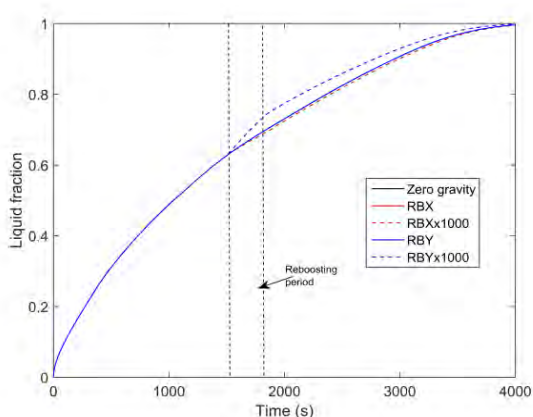


Figure 1: Evolution of the liquid fraction for the cases of g-levels of the reboosting event applied on x and y directions.

The effect of the reboosting on the melting process was detected only by introducing the enhanced g-level signal in the simulation, having a stronger influence if the reboost maneuver was done in the y direction, orthogonal to the thermal gradient applied.



Figure 3: Snapshot of the interface solid-liquid at 1800 s for different cases.

Figure 3 plots the three snapshots of the solid-liquid interface at 1800s and $\Delta T = 30\text{K}$ for the RBX \times 1000 (red line) and RBY \times 1000 (blue line) cases compared to the zero-gravity case (white line). Under these conditions, the shape of the interface was altered.

Conclusions

By adding a real reboost signal into the n-octadecane melting process simulation no significant effect has been detected in the time evolution of the liquid fraction. Although, increasing the g-doses of the reboost some alterations in the solid-liquid interface were detected compared to the zero gravity case.

The above data confirm once more that the reboost is a disturbance that has to be taken into account when planning an experiment up on ISS, though deeper data analysis needs to be considered.

Acknowledgements

The present work has been supported by grants PID2020-115086GB-C32 (MCIU/FEDER) and 2021PFR-URV-74 (Rovira i Virgili University).

References

- J.P. Collette, P. Rochus, R. Peyrou-Lauga, O. Pin, N. Nutal, M. Larnicol, J. Crahay; *Phase change Material Device for Spacecraft Thermal control*. IAC Congress, IAC-11.C2.8.1, 2011.
- D. Dubert, M. Marin-Genescà, M.J. Simón, J.M. Ezquerro, J. Massons, Jna. Gavaldà, X. Ruiz, V. Shevtsova; *On the monitoring of the vibratory environment of DCMIX4 campaign. Preliminary results*. Microgravity Science and Technology, 32(4), 615-628, 2020.
- P. Salgado Sánchez, J.M. Ezquerro, J. Fernández, J. Rodríguez; *Thermocapillary effects during the melting of phase-change materials in microgravity: steady and oscillatory regimes*. J. Fluid Mechanics, 908, A20-1, 2021.
- B. Šeta, D. Dubert, J. Massons, Jna. Gavaldà, M.M. Bou-Ali, X. Ruiz, *Effect of Marangoni induced instabilities on a melting bridge under microgravity conditions*, International Journal of Heat and Mass Transfer, 179 121665, 2021.

POSTER 12

ESA's Scientific Research Program on Sounding Rockets: past and present

A. Orr^{1,2}; L. Cacciapuoti¹; G. Correale¹; W. Sillekens¹; S. Vincent-Bonnieu¹; L. Surdo¹; A. Van Ombergen¹; P. De Gieter¹

¹European Space Agency, Noordwijk, The Netherlands; ²astrid.orr@esa.int

ESA has been using Sounding Rockets to carry out experimentation in low gravity and in the space environment since more than 50 years. ESA has carried out hundreds of individual experiments on Sounding Rocket flights. In this poster, we give an overview of ESA's scientific research program performed over the years and until now, both in Life and Physical Sciences, with the help of this unique research platform.

Thermodiffusion coefficients in Polystyrene-Toluene mixtures: DCMIX 4

A. Sanjuan¹, V. Shevtsova^{1,2} and M. Mounir Bou-Ali¹

¹Mechanical and Manufacturing Department, Mondragon University, Mondragon, Spain, mbouali@mondragon.edu

²IKERBASQUE, Basque Foundation for Science, Bilbao, Spain. x.vshevtsova@mondragon.edu

Introduction

In this work, the thermodiffusion (D_T) coefficients of the polymeric solution Polystyrene-Toluene (PS-Tol) of the Diffusion Coefficient Measurements in ternary mIXtures 4 (DCMIX 4) project [1] at atmospheric pressure and room temperature (298.16 K) in a wide range of concentrations 2-5-10-15 % (mass fraction of Polystyrene) were determined. In order to be able to measure D_T thermophysical properties of the mixtures were also measured experimentally in the Fluid Mechanics Laboratory of the University of Mondragón. The objective of this work is to confirm the results obtained so far [2], as well as to explore the performance of a new laboratory technique, by comparing with the results determined under microgravity conditions. The new technique is a thermogravitational approach based on digital optical interferometry [3].

Methodology

As for the methodology followed, first the necessary thermophysical properties (for each sample) such as density (ρ), thermal expansion coefficient (α) and kinematic viscosity (ν) were determined. These properties are introduced into Eqn. (1) [3] to calculate the thermodiffusion coefficient when the mixture reaches the stationary state. Here L_x corresponds to the gap of the column, g is the gravity force, c represents the mass fraction of the densest component (c_0 initial one) of the mixture and y is the axis in the column height direction.

$$D_T = -\frac{L_x^4}{504 \nu c_0 (1 - c_0)} \frac{\alpha g}{\rho} \frac{\partial c}{\partial y} \quad (1)$$

The Anton Paar DMA 5000 M equipment was used to measure the density of the samples. Furthermore, the same dispositve was utilized to determine the thermal expansion coefficient (α) using the following Eqn. (2) where (T) is the working temperature. For example, to calculate α at ambient temperature (298.16 K) the density was determined from 297.16 K to 299.16 K (increase of 0.5 K).

$$\alpha = -\frac{1}{\rho} \frac{\partial \rho}{\partial T} \quad (2)$$

Furthermore, the dynamic viscosity (μ) was measured using the Anton Paar AMVn microviscosimeter. Based on the previously determined densities, it was possible to determine the kinematic viscosity of the samples under study using the following Eqn. (3).

$$\nu = \frac{\mu}{\rho} \quad (3)$$

As for the experimental procedure and determination of the thermodiffusion coefficient, the thermogravitational column

technique based on digital interferometry was used [3]. The same microcolumn and optical installation were considered.

The geometry of the setup is shown in Figure 1 (a), which has the following dimensions: $L_x = 0.51$ mm (gap) and $L_y = 30$ mm (height). The column in Figure 1 (a) consists of 4 main units. First, it is the central part of the Ketron Peek together with two sapphire crystals that form the cavity where the sample is to be confined. For the sealing, two copper plates are placed. The column also consists of two aluminum elements. These are in direct contact with the copper plates and have a cavity in which the water circulates, thus generating the temperature difference in the perpendicular direction to the gravitational field. In addition, the microcolumn has an inlet-outlet for injecting the mixture and a window to pass the laser beam.

The optical configuration, see Figure 1 (b), includes three lasers of different wavelengths (473 nm, 543 nm and 633 nm). At the beginning, three pneumatic cylinders are located Figure 1 b) (A) so that the laser beams do not interfere with each other. Then the filters to clean the beam and the collimation lens for its expansion are placed Figure 1 b) (B). At the final part, the Mach-Zehnder interferometer is located Figure 1 b) (C). This splits the laser beam into two equal parts, one is the reference and the other one pass through the microcolumn window. Later, both interfere in the point of the image acquisition camera.

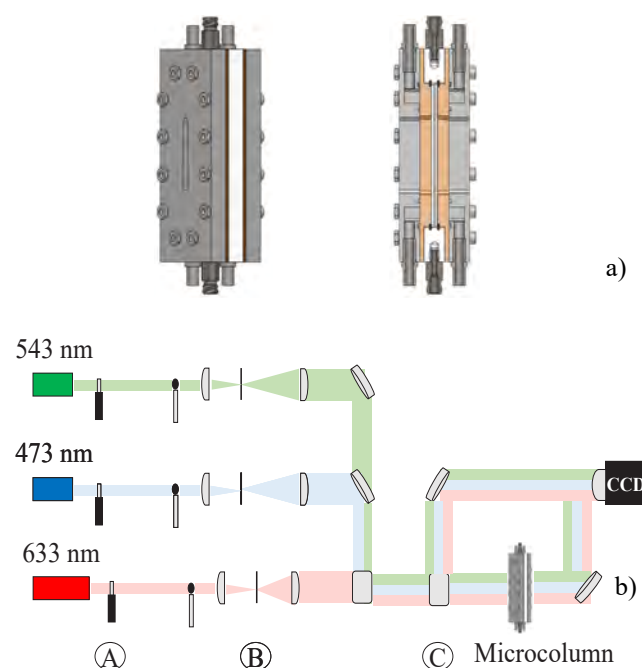


Figure 1: Experimental procedure: used thermogravitational microcolumn a) and optical installation b).

Once the interference pattern was obtained, the Matlab software was used to measure D_T . In this procedure, the first step is to obtain the phase variation of the acquired images. The phase change ($\Delta\phi$) is directly related to the refractive index variation (Δn), Eqn. (4) [3]. λ corresponds to the laser wavelength. Finally, by means of the optical contrast factors ($\partial n/\partial c$), the variation of the concentration along the thermogravitational microcolumn (Δc) is obtained by using Eqn. (5) [3]. For this work, the contrast factors presented in literature [2] were taken into account.

$$\Delta n(x, y) = \frac{\lambda}{2\pi L_x} \Delta\phi(x, y) \quad (4)$$

$$\Delta n(x, y) = \left(\frac{\partial n}{\partial c}\right)_{T_0, c_0, \lambda} \Delta c(x, y) \quad (5)$$

In this manner, and following the experimental methodology explained above, it was possible to use Eqn. (1) and determine the thermodiffusion coefficient when the mixture reaches the equilibrium.

Preliminary results

This section shows the preliminary results obtained of the studied PS-Tol sample. Figure 2 presents as an example the variation of the concentration for the polymeric mixture at a concentration of 15 % (mass fraction) for both the transient and steady state regimes applying a temperature difference of 6 K. As for the results obtained, a linear tendency of the concentration along the microcolumn $L_y = 25$ mm is observed.

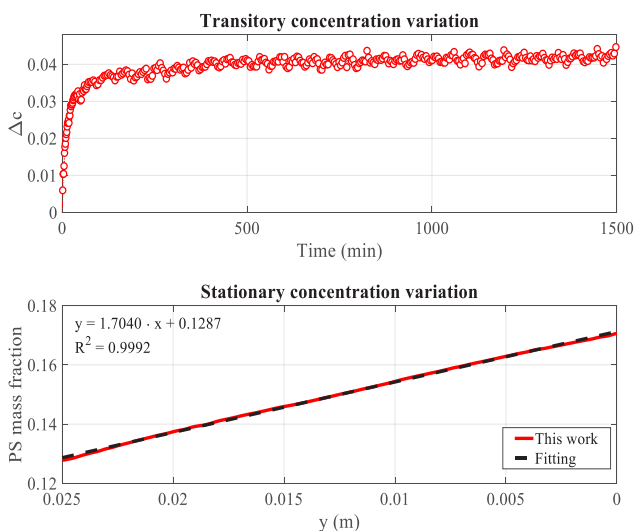


Figure 2: Variation of polystyrene concentration along the thermogravitational microcolumn: transitory (top graph) and stationary (bottom graph) mixture PS-Tol 15 %.

Furthermore Figure 3 shows the variation of the thermodiffusion coefficient as a function of the concentration (PS component) for the same polymeric solution. At the same time these results were compared with those presented in literature [2]. A similar tendency is observed between the experimental results and [2]. However, at low concentrations (2 % and 5 %) the difference between the experimental results and literature is higher and therefore the thermodiffusion coefficient will have to be redetermined for more mixtures at low PS concentrations.

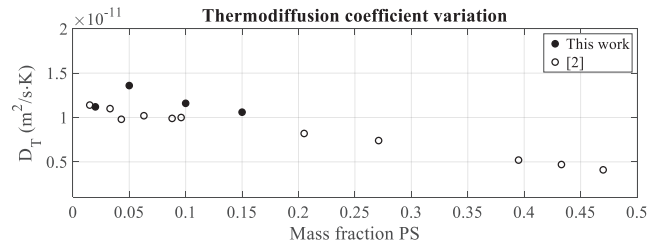


Figure 3: D_T variation as a function of concentration. Comparison between experimental and literature results.

Conclusions

The thermodiffusion coefficients of the polymeric solution of the DCMIX 4 as a function of concentration were determined. As for the preliminary results, it was noted that the thermodiffusion coefficients of this work have a similar tendency to those published in literature. However, a greater deviation was observed at low concentrations.

Acknowledgements

The present work has been supported by KK-2021/00082 (micro4IoT), IT1505-22 (Research Group Program) and PID2020-115086GB-C33 financed by MCIN/AEI of the Spanish Government.

References

- [1] Mialdun, A., Bataller, H., Bou-Ali, M. M., Braibanti, M., Crococo, F., Errarte, A., Ezquerro, J. M., Fernández, J. J., Gaponenko, Yu., García-Fernández, L., Rodríguez, J., & Shevtsova, V. (2019). Preliminary analysis of Diffusion Coefficient Measurements in ternary mixtures 4 (DCMIX4) experiment on board the International Space Station. *The European Physical Journal E*, 42(7), 87. <https://doi.org/10.1140/epje/i2019-11851-6>.
- [2] Rauch, J., & Köhler, W. (2003). Collective and thermal diffusion in dilute, semidilute, and concentrated solutions of polystyrene in toluene. *The Journal of Chemical Physics*, 119(22), 11977–11988. <https://doi.org/10.1063/1.1623745>.
- [3] Lapeira, E., Mialdun, A., Yasnou, V., Aristimuño, P., Shevtsova, V., & Bou-Ali, M. M. (2018). Digital Interferometry Applied to Thermogravitational Technique. *Microgravity Science and Technology*, 30(5), 635–641. <https://doi.org/10.1007/s12217-018-9632-7>

POSTER 26

Analysis of the thermogravitational effect by a 3-Laser Optical Digital Mach-Zehnder Interferometer

A. Errarte¹, A. Sanjuan¹, A. Mialdun², M. Alonso¹, I. Andonegui¹, V. Shevtsova^{1,3}, M. Mounir Bou-Ali¹

¹Mondragon Unibertsitatea Goi Eskola Politeknikoa, Arrasate-Mondragon, Spain

aerrarte@mondragon.edu | asanjuan@mondragon.edu | malonson@mondragon.edu | iandonegui@mondragon.edu |

x.vshevtsova@mondragon.edu | mbouali@mondragon.edu

²Microgravity Research Centre, Université libre de Bruxelles, Brussels, Belgium

aliaksndr.Mialdun@ulb.be

³IKERBASQUE, Basque Foundation for Science, Bilbao, Spain.

Introduction

For many years, thermogravitational columns have been used only for the determination of thermodiffusion coefficients by steady-state concentration separation analysis [1]. That technique determines accurately the thermodiffusion coefficients, but the working mixture volume is high and it only gives information of a single time instant per experiment. However, the transient analysis allows determining the molecular diffusion coefficients of mixtures. Performing transient analysis in extraction thermogravitational columns is a long and error-prone process, since each time interval to be measured is a new experiment.

To overcome these problems, a thermogravitational micro-column (μ TC) was developed, where ODI, Optical Digital Interferometry is used to track components separation during the thermodiffusion experiment [2]. As described in [3] the analysis of binary mixtures by optical techniques is straightforward, since a single independent concentration describes the mass transfer of the system; despite, the processing and determination of transport properties of ternary mixtures is rather complex and limited to a certain number/type of mixtures. The problem arises in the determination of the optical contrast factors matrix, values which are used to transform the refractive index values into concentration, which several times is ill conditioned. A prior analysis of the matrix condition number helps to determine the suitability of the mixture to the system to accurately measure the transport properties.

In this context, the originally designed two-laser (blue and red) Mach-Zehnder Interferometer, the optical installation in Mondragon University, has been adapted into a three-laser (green, blue and red) Mach-Zehnder interferometer. In this work, we discuss the feasibility of our system for the determination of the thermodiffusion (D_T), the molecular diffusion (D) and the Soret coefficients ($S_T = D_T/D$) by the thermogravitational technique, analysing the well-known DCMIX1 system, THN-IBB- nC_{12} . The main target is to demonstrate the capabilities and limitations of the technique for the measurement of these properties in both binary and ternary liquid mixtures from an optical point of view.

Measurement principle and the instrument

The thermogravitational technique consists of placing a mixture between two vertical walls – a cold one and a hot one

– and applying a horizontal thermal gradient. The horizontal temperature gradient applied to the mixture originates a concentration gradient. In turn, that separation induces a mass flow in the opposite direction due to molecular diffusion, which tries to homogenize the system, and the convective flow generated by the gravitational force amplifies the separation of species vertically. The main objective of the μ TC consists on determining compositional changes over the whole thermodiffusion experiment time until the mixture reaches the steady state.

The actual system consists of a three laser – blue (473.0 nm), green (543.0 nm) and red (632.8 nm) – Mach-Zehnder interferometer. ODI allows determining the concentration of a mixture by analyzing the phase variation of the interference patterns by $\Delta n(y, z) = (\lambda/2\pi L_x)\Delta\phi(y, z)$, where λ is the wavelength and L_x is the beam length through the sample.

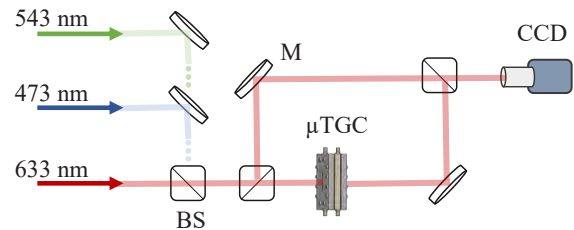


Figure 1: Sketch of the three laser Mach-Zehnder interferometer.

Fitting the temporal evolution of the refractive index changes between the top and the bottom part of the column, enables determining the vertical relaxation time (t_r) and steady-state separation (Δn_∞) of the mixture.

$$\Delta n = \Delta n_\infty \left[1 - \frac{8}{\pi^2} \sum_{k=0}^{\infty} \frac{e^{-\frac{(2k+1)^2 t}{t_r}}}{(2k+1)^2} \right]$$

With prior knowledge of the the solutal contrast factors, the refractive index change can be transformed into concentration differences.

$$\begin{pmatrix} \Delta c_1 \\ \Delta c_2 \end{pmatrix} = \begin{bmatrix} \frac{\partial n_1}{\partial c_1} & \frac{\partial n_1}{\partial c_2} \\ \frac{\partial n_2}{\partial c_1} & \frac{\partial n_2}{\partial c_2} \end{bmatrix}^{-1} \begin{pmatrix} \Delta n_1 \\ \Delta n_2 \end{pmatrix}$$

In this case, the solutal contrast factors ($\partial n_\lambda / \partial c_i$) have been measured in a multiwavelength MW Anton Paar Abbemat refractometer and the values to the exact operating wavelengths have been adjusted by Cauchy dispersion fitting. Thermodiffusion coefficients of binary and ternary mixtures have been calculated via

$$D_T = -\frac{\alpha g L_x^4}{504 \nu c_0 (1 - c_0)} \frac{\partial c}{\partial z'}$$

$$D'_{T,i} = -\frac{\alpha g L_x^4}{504 \nu} \frac{\partial c_i}{\partial z}$$

and diffusion coefficients by

$$D = \frac{(\alpha \pi \Delta T g)^2 L_x^6}{\nu^2 9! L_y^2} t_r.$$

In the case of the ternary mixtures, the quasi-binary approach have been adopted, and the effective diffusion coefficients have been calculated the same way as in binary mixtures.

Results

The 3-laser interferometer has been validated by the well-known Fontainebleau Benchmark [4] mixture THN-nC12 at an equimassic mass fraction. Figure 2 shows the analysis of the concentration of tetralin during the thermodiffusion experiment.

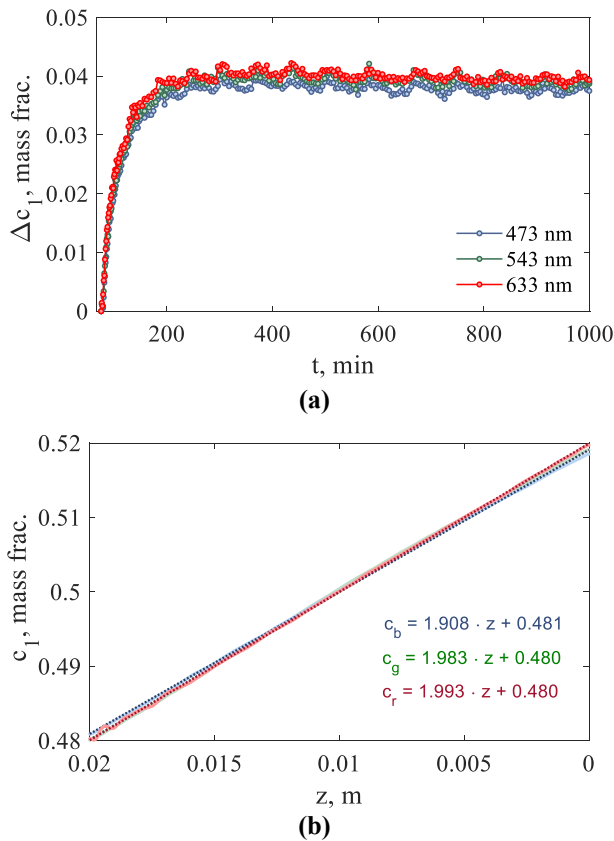


Figure 2: Green laser verification results. (a) Temporal evolution of tetralin concentration during the thermodiffusion experiment for a $\Delta T = 8$ °C and (b) steady-state concentration separation along the column height.

The variation of the concentration along the height of the column shows very good agreement during the transition, and slight difference in the steady state. Apart from being in good agreement with the blue and red lasers, the separation corresponds to the one expected in the dimensions of the μ TC based on the results of the Fontainebleau Benchmark [4].

Conclusions

The system is very robust for the analysis of binary mixtures, since results obtained by the recently installed green laser are in very good agreement with the obtained by the red and blue and the Fontainebleau Benchmark. The study of ternary mixtures is of higher complexity, since the accuracy of the technique may be impaired if the optical contrast factor matrices are ill conditioned. Even if first ternary mixture experiments showed good agreement in the mean values [5], the uncertainties of thermodiffusion values are huge. The installation of a third laser enables to combine the different wavelength pairs in order to be able to reduce the uncertainties obtained by the thermogravitational microcolumn.

Acknowledgements

The authors acknowledge the support by KK-2021/00082 (micro4IoT), PRE_2021_0_0234, IT1505-22 (Research Group Program) of the Basque Government and PID2020-115086GB-C33 financed by MCIN/AEI of the Spanish Government.

References

- [1] M. Larrañaga et al., Contribution to the benchmark for ternary mixtures: Determination of Soret coefficients by the thermogravitational and the sliding symmetric tubes techniques, *Eur. Phys. J. E*, 38, 28, (2015).
- [2] B. Šeta et al., Determining diffusion, thermodiffusion and Soret coefficients by the thermogravitational technique in binary mixtures with optical digital interferometry analysis, *Int. J. Heat Mass Transf.*, 147, 118935, (2020).
- [3] A. Mialdun and V. Shevtsova, Analysis of multi-wavelength measurements of diffusive properties via dispersion dependence of optical properties, *Appl. Opt.*, 56, 572, (2017).
- [4] J. K. Platten et al., Benchmark values for the Soret, thermal diffusion and diffusion coefficients of three binary organic liquid mixtures, *Philos. Mag.*, 83, 1965–1971, (2003).
- [5] B. Šeta et al., Steady-state Measurements of Ternary Mixtures in Thermogravitational Microcolumn Using Optical Digital Interferometry, *Microgravity Sci. Technol.*, 33, 1-11, (2021).

POSTER 27

Temperature dependent measurements of the Diffusion and Soret-coefficient in a binary polystyrene mixture measured with TDFRS

J.Kantelhardt¹, W. Köhler¹

¹Physikalisches Institut Universität Bayreuth, Bayreuth, Germany, werner.koehler@uni-bayreuth.de

Introduction

Thermodiffusion in liquids is a complicated process and therefore many experiments are performed with different goals in mind. The most important ones are the investigation of Fickian diffusion and of the Soret-effect. These are quantified, respectively, by the diffusion and by the Soret coefficient. While the first one describes isothermal interdiffusion, the second one describes the coupling of the concentration variable to an imposed temperature field. In this work we have investigated how the Soret coefficient changes in regard to different temperatures of the sample. The here investigated system, a solution of polystyrene in toluene, has in a similar concentration also been used in the binary companion cell of the DCMIX4 microgravity campaign on ternary mixtures. Furthermore, binary and ternary polystyrene solutions are candidates for the forthcoming GIANT FLUCTUATIONS project of ESA for the investigation of non-equilibrium fluctuations under microgravity conditions.

Measurement technique is the Thermal-Diffusion-Forced-Rayleigh-Scattering (TDFRS) method. It is a heterodyne procedure where the measured signal is directly correlated with the change of the refractive index. With this kind of experiment one can get the diffusion, the thermodiffusion, the Soret-coefficient and the thermal diffusivity (J. Rauch et al. 2003).

Experimental set-up

In TDFRS there are two laser beams needed, first a writing laser (532nm) and secondly a readout laser (632.8nm). The first one gets split via a beam splitter and both partial beams are brought to interference in the middle of the sample. Thereby a holographic grating is created that heats the solution with a spatial period of approximately 10 micrometers and with temperature modulation well below 0.1 mK. For this heating the liquid must be coloured with a negligible amount of an inert dye (quinizarin) that absorbs at the incident laser wavelength. The periodic temperature grating in turn leads to a superposed concentration grating in the binary sample.

Both changes of the temperature and the concentration lead to changes of the refractive index, which can be measured by Bragg-diffraction of the readout laser beam, which is at a longer wavelength and, hence, not absorbed by the dye. (W. Köhler et al. 2000)

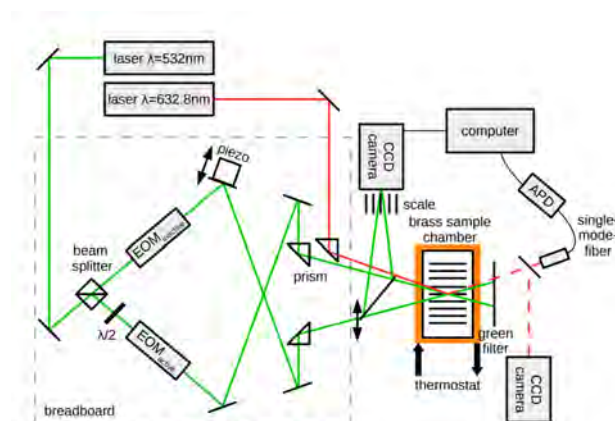


Figure 1: The TDFRS setup for temperature dependent measurements of the diffusion and Soret-coefficient in a binary liquid.

Experiment

The liquid is a binary mixture consisting of Polystyrene (PS) with a molar mass of 4840 g/mol dissolved in Toluene (Tol), which is a well-established and researched system. The weight fraction of PS is $c_{PS}=1\%$.

The measurements of the diffusion, thermodiffusion and Soret coefficient were done for a number of different temperatures (10°C, 15°C, 20°C, 22°C, 25°C, 30°C, 35°C, 40°C, 45°C, 50°C). The results of these measurements are reported and, where applicable, compared to literature data (J. Rauch et al. 2003).

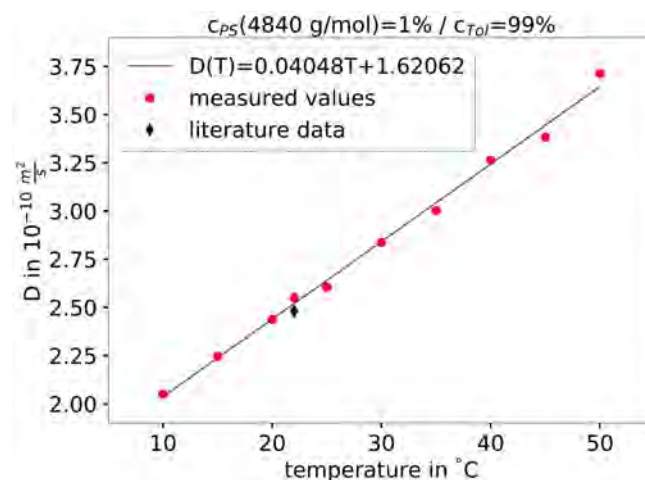


Figure 2: The diffusion-coefficient of the sample PS/Tol with $c_{PS}=1\%$. The measured values of the diffusion-coefficient are the red dots. The literature data (J. Rauch et al. 2003) is a black diamond.

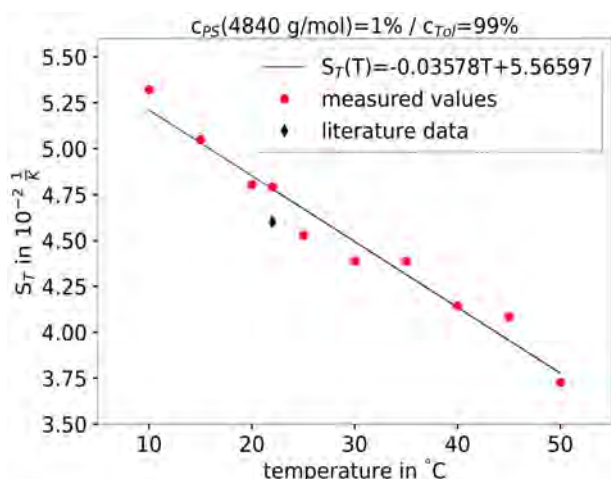


Figure 3: The Soret-coefficient of the sample PS/Tol with $c_{PS}=1\%$. The measured values of the Soret-coefficient are the red dots. The literature data (J. Rauch et al. 2003) is a black diamond.

Results

The measured data (red dots) are in good agreement with literature data (black diamonds) which were also measured with TDFRS. With increasing temperature there is a clear increase of the diffusion-coefficient, which follows a linear behavior. For the Soret-coefficient a similar result is found, albeit its value is decreasing lineary over the whole temperature range.

Another interesting parameter to look at is the hydrodynamic radius (R_h) for the different temperatures. They are calculated with the Stokes-Einstein equation $R_h=(k_B T)/(6\pi\eta D)$ (A. Einstein 1905). Here k_B is the Boltzmann-constant, T the temperature in Kelvin, D the diffusion coefficient and η the dynamic viscosity. Because our sample is a diluted solution, we can approximate its value as the dynamic viscosity of the pure solvent (D. Stadelmaier et al. 2008) with the equation from (F.J.V. Santos et al. 2006):

$$\ln(\bar{\eta}) = -5.2203 + \frac{8.964}{\bar{T}} - \frac{5.834}{\bar{T}^2} + \frac{2.089}{\bar{T}^3},$$

with the reduced variables $\bar{\eta} = \eta_0(T)/\eta_0(T_0)$ and $\bar{T} = T/T_0$, where $T_0=298.15K$ and $\eta_0(T_0)=554.2\mu Pas$. It can be seen that the hydrodynamic radius follows a constant behaviour which is shown via the black horizontal line with $R_h=1.51nm$. This result indicates that while the temperature increases the quality of the solvent stays the same.

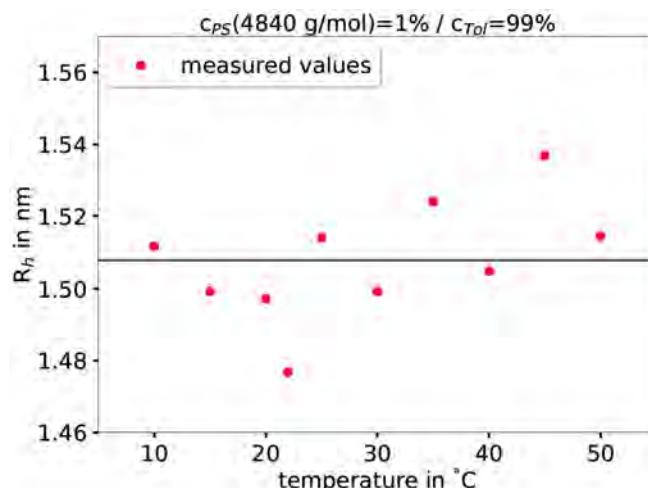


Figure 4: The hydrodynamic radius of the sample PS/Tol with $c_{PS}=1\%$. The values were calculated with the Stokes-Einstein equation.

Acknowledgements

This work was supported by the ESA project GIANT FLUCTUATIONS, the ESA-MAP project TechNES (Grant 4000128933/19/NL/PG), and by Deutsches Zentrum für Luft- und Raumfahrt (DLR), Grant 50WM2147 (BTGIANTII).

References

- W. Köhler, R. Schäfer, Polymer Analysis by Thermal-Diffusion Forced Rayleigh Scattering, *Advances in Polymer Science*, Vol. 151, (2000)
- J. Rauch, W. Köhler, Collective and thermal diffusion in dilute, semidilute, and concentrated solutions of polystyrene in toluene, *J. Chem. Phys* 119, 11977 (2003)
- D. Stadelmaier, W. Köhler, From Small Molecules to High Polymers: Investigation of the Crossover of Thermal Diffusion in Dilute Polystyrene Solutions, *Macromolecules*, 41, 16, 6205–6209, (2008)
- F.J.V. Santos, C.A. Nieto de Castro, J.H. Dymond, N.K. Dalaouti, M.J. Assael, A. Nagashima, *J. Phys. Chem. Ref. Data* 35, 1 (2006)
- A. Einstein, Über die von der molekularkinetischen Theorie der Wärme geforderte Bewegung von in ruhenden Flüssigkeiten suspendierten Teilchen, *Annalen der Physik*, Band 17, (1905)

POSTER 31

Molecular diffusion, Thermodiffusion and Soret coefficients of fullerene C₆₀ in aromatic solvents

A. Errarte¹, D. Sommermann², M. Mounir Bou-Ali¹, W. Köhler²

¹Mondragon Unibertsitatea Goi Eskola Politeknikoa, Arrasate-Mondragon, Spain

aerrarte@mondragon.edu | mbouali@mondrago.edu

²Universität Bayreuth Physikalischen Institut, Bayreuth, Germany

daniel.sommermann@uni-bayreuth.de | werner.koehler@uni-bayreuth.de

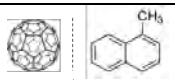
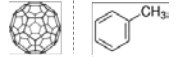
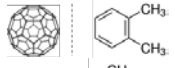
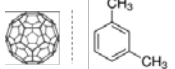
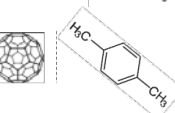
Introduction

One of the most relevant properties that influence both the ease of extraction and purification, as well as the subsequent functionalisation and use of fullerenes, is their solubility. Fullerenes are the only allotropic modifications of carbon that are soluble in organic compounds. However, their solubility is in most cases low, and this is one of the main obstacles to progress in the study of their transport properties. This work is a continuation of the study of the transport properties of fullerene, which started with the analysis of the ternary mixture C₆₀-THN-Tol within the framework of the DCMIX project [1].

Diffusion (*D*), thermodiffusion (*D_T*) and Soret (*S_T*) coefficients of C₆₀ fullerene in five organic solvents have been measured by the Optical Beam Deflection (OBD) technique. All selected solvents are aromatic solvents and contain one or two methyl groups. Although the structures of the molecules are similar, thermophysical properties are different. This is why, in this work, the effect of the number of rings in the molecular structure (Methylnaphthalene | Toluene) and the number and position of the methyl group (Toluene | oXylene | mXylene | pXylene) over the mentioned transport properties have been investigated.

We have tested several diluted fullerene concentrations (Table 1).

Table 1: Definition of the five C₆₀-aromatic mixtures: their structure and the analysed mass fractions.

Mixture	Structure	Mass fraction [C ₆₀], %
C ₆₀ -MN		0.10/0.15/0.18/0.20/0.25
C ₆₀ -Tol		0.10/0.15/0.20/0.25
C ₆₀ -oXyl		0.10/0.15/0.18/0.20/0.25
C ₆₀ -mXyl		0.10/0.15/0.18/0.20/0.25
C ₆₀ -pXyl		0.10/0.15/0.18/0.20/0.25

To analyse that same effect in liquid mixtures, all combinations of binary mixtures of aromatic solvents have been analysed at equal mass fractions. Four ternary mixtures have also been analysed, all of them composed of C₆₀ fullerene and methylnaphthalene, to which toluene or one of the xylene isomers has been added at a mass fraction of

0.0020-0.4990-0.4990. In the case of these mixtures, the two eigenvalues of the diffusion matrix have been determined. All OBD experiments have been performed at a mean temperature of 25°C.

Principle of measurement and evaluation

The OBD technique consists of determining the concentration variation induced by the Soret effect studying the deflection of a perpendicularly incident laser beam on a Soret cell. The Soret phenomenon induces a concentration gradient due to the temperature difference across the height of a cell, which in turn generates a refractive index gradient. If a laser beam passes through the cell perpendicular to the resulting refractive index gradient, it experiences a deflection Δz, which allows to determine the abovementioned transport coefficients.

The four laser OBD (4-OBD, sketch in Figure 1), has been used in this work. However, due to the absorption of fullerene in the blue (405.8 nm) and green (532.0 nm) spectrum, red (632.8 nm) and infrared (935 nm) lasers have only been used.

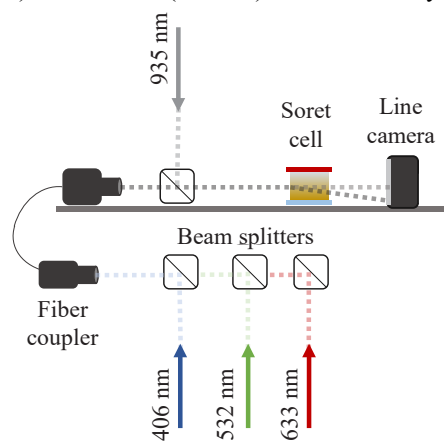


Figure 1: Scheme of the 4-OBD installation of the used for the thermodiffusion experiment.

Fitting analytical solutions to the OBD curves (Figure 2), the relaxation time τ and the value of M (ratio between the value of the amplitude at the thermal plateau and the Soret plateau) can be determined, and, thus, the molecular diffusion and Soret coefficient of a binary mixtures can be determined from $D = h^2/\tau$ and

$$S_T = \frac{M}{c_0(1-c_0)} \left(\frac{\partial n}{\partial T} \right)_{p,c} \left(\frac{\partial n}{\partial c} \right)_{p,T}^{-1}$$

respectively. Here, *h* is the cell height and *c*₀ the initial concentration. In the case of a ternary mixture, two eigenvalues of the diffusion matrix and two independent Soret coefficients are obtained. The concentration effect over the

refractive index ($\partial n/\partial c$) has been determined measuring the refractive index of different samples by the Abbemat WR and MW refractometers. The thermal contrast factor $\partial n/\partial T$ has been measured by interferometry.

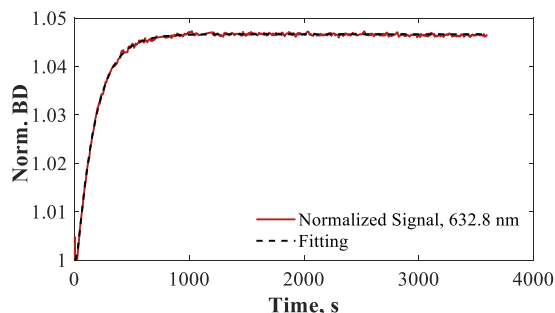


Figure 2: Normalized beam deflection for the mixture C₆₀-Tol at 0.20 % and a temperature difference of 1°C.

Once diffusion and Soret coefficients of the binary mixtures have been calculated, the thermodiffusion coefficients have been determined as $D_T = S_T \cdot D$.

Preliminary results

Molecular diffusion, thermodiffusion and Soret results of the binary mixtures C₆₀-Tol and C₆₀-pXyl are shown in Figure 3, for all the measured concentration range.

As it can be observed, both the Soret and thermodiffusion coefficients in mixtures with C₆₀ fullerene are an order of magnitude larger than in a mixture of hydrocarbons, but no such difference is observed for molecular diffusion. There is neither a clear effect of transport properties over the C₆₀ concentration. Nevertheless, even if these two molecules (used as an example) are only differentiated by an addition of a methyl group the obtained transport properties are different; in all cases, the diffusion, thermodiffusion and Soret coefficients of the Toluene are larger than the one of p-Xylene.

Conclusions

When analysing the effect of the number of solvent rings (MN | Tol), a lower diffusion and thermodiffusion coefficient is observed for methylnaphthalene, but the Soret coefficient is similar to that of toluene.

Regarding the effect of methyl groups, xylene isomers show slightly lower diffusion and thermodiffusion coefficients than toluene. The order of the value of the coefficients changes with the shape of the organic compound, depending on the position of the methyl group. That fact was again observed for binary mixtures of MN + (Tol | o-Xyl | m-Xyl | p-Xyl).

The eigenvalues of the diffusion matrix of ternary mixtures show a lower coefficient corresponding to C₆₀ and a coefficient very close to the binary mixtures MN + (Tol | o-Xyl | m-Xyl | p-Xyl), which, again, show the effect of the position of the methyl group in the molecules.

Acknowledgements

The team from Mondragon Unibersity thanks the support by KK-2021/00082 (micro4IloT), PRE_2021_0_0234 and EP_2022_1_0026 IT1505-22 (Research Group Program) from the Basque government and PID2020-115086GB-C33 financed by MCIN/AEI of the Spanish Government. The team from Bayreuth kindly acknowledges support by DFG (KO1541/13-1).

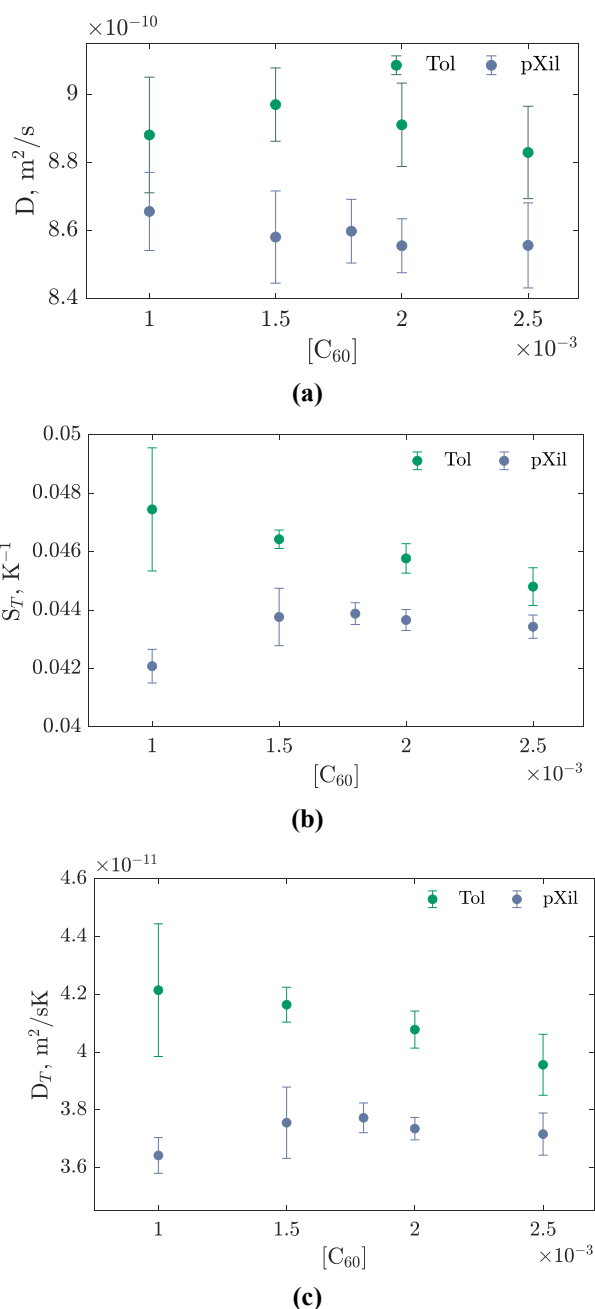


Figure 3: Variation of Diffusion (a), Soret (b) and Thermodiffusion coefficients (c) for C₆₀-Tol and C₆₀-pXyl mixtures for different C₆₀ concentrations at 25°C.

References

- [1] A. Mialdun et. al., Preliminary analysis of Diffusion Coefficient Measurements in ternary mIXtures 4 (DCMIX4) experiment on board the International Space Station, *Eur. Phys. J. E*, 42, 1-9, 2019.
- [2] M. Gebhardt, W. Köhler, What can be learned from optical two-color diffusion and thermodiffusion experiments on ternary fluid mixtures?, *J. Chem. Phys.*, 142, 084506, 2015.

POSTER 35

Astrocyte Reactivity is Reduced by Exposure to Hypergravity

Yannick Lichterfeld¹, Laura Kalinski¹, Sarah Schunk¹, Theresa Schmakeit¹, Sebastian Feles¹, Timo Frett², Harald Herrmann³, Ruth Hemmersbach¹ and Christian Liemersdorf^{1*}

¹ German Aerospace Center, Institute of Aerospace Medicine, Department of Gravitational Biology, Cologne, Germany; yannick.lichterfeld@dlr.de; laura.kalinski@dlr.de; sarah.schunk@dlr.de; theresa.schmakeit@dlr.de; sebastian.feles@dlr.de; ruth.hemmersbach@dlr.de

² German Aerospace Center, Institute of Aerospace Medicine, Department of Muscle and Bone Metabolism, Cologne, Germany; timo.frett@dlr.de

³ University of Erlangen, Institute of Neuropathology, harald.herrmann-lerdon@uk-erlangen.de

* Correspondence: christian.liemersdorf@dlr.de; Tel.: +49 176 811 09 333

Introduction

Neurodegeneration caused by various diseases and neuronal injuries is among the most central challenges society has to meet momentarily. Following neurodegeneration, neuronal regeneration and remyelination are inhibited by glial cells, i.e. majorly astrocytes that transfer into a reactive state and further mediate the formation of a glial scar.

Reactive astrocytes inhibit neuronal regeneration by migrating towards the injured area and inducing an inhibitory extracellular environment. On the one hand reactive astrocytes prevent the widespread of damaged tissue, however, they also prevent axonal regrowth and therefore the regeneration of the injured tissue, leading to long-lasting restrictions of the patients.

The aim of project NeuroSpace is thus to investigate the influence of hypergravity on primary astrocytes as a novel potential approach to reduce astrocyte reactivity and thus could further promote neuronal regeneration.

Methods

We cultivated primary murine astrocytes from C57BL/6J mouse embryos, as these cells are closely related to human astrocytes *in vivo* in neuronal tissues, can be cultured up to several months, and serve as an ideal model system for human glial cell function and astrogliosis *in vitro*.

We exposed these cells to hypergravity conditions at constant g up to several days by using the **DLR Multi Sample Incubator Centrifuge (MuSIC)** and compared key cellular characteristics to normal gravity (1g) controls. The MuSIC is a custom-built swing-out centrifuge inside a cell culture incubator, which is able to expose cultured cells to various hypergravity conditions (exposures from seconds to months if possible; 1-50g). It enables steady environmental conditions for various experimental setups. In dependency of the centrifugal force, the gondolas ensure that the gravity vector is acting perpendicular on the cell sample, erasing unwanted shear forces and side effects, e.g. caused by vibrations. The same incubator can be used to expose 1g control samples to the same environmental conditions.

To better understand and investigate cellular dynamics and migration speed of primary astrocytes under hypergravity, we employed our **Hyperscope Live-Cell Imaging Microscope** platform at DLR, a combination of two separate research platforms at the Institute of Aerospace Medicine. This novel system consists of a fully automated fluorescent live-cell imaging microscope installed on a swing-out platform on the DLR human short-arm centrifuge (SAHC). With this setup, the microscope can be operated in real time and samples can be imaged remotely during centrifugation. This novel facility enables research on the immediate and most dynamic responses to altered gravity loading live at high frame rates (up to 128 fps) and maximal resolution (40x NA1.4 oil objective) for various fluorescent channels (385 nm, 475 nm, 550 nm, 590 nm, 640 nm excitation LEDs).

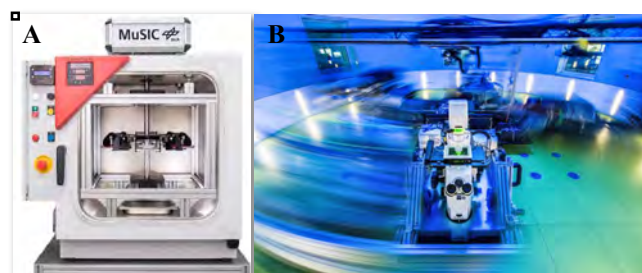


Figure 1: The Multi Sample Incubator Centrifuge (A) and the Hyperscope on the human centrifuge (B) at German Aerospace Center (DLR), Cologne, Germany

Results

We exposed primary astrocytes on our unique platforms to hypergravity in the physiologically tolerable range of 2g. We investigated several mechanisms including spreading rates, migration velocities, morphological alterations, protein expression and reactivity levels.

Following exposure to hypergravity key features of astrocyte reactivity could be detected and reactivity indicators could be attenuated.

Cell spreading is a morphological feature that requires dynamic cytoskeletal rearrangements, which are further mandatory for the initiation of cell migration. Decreasing cell

spreading capabilities could furthermore lead to diminished cell migration. For astrocytes, such a behaviour would indicate a reduced potential for astrogliosis induction, where increased astrocytic migration towards the lesion site is a well-conserved feature.

Indeed, over the course of 48 h, astrocyte cells exposed to 2g hypergravity showed a consistent area reduction of approximately 20%. Similarly, the migration speed was significantly reduced initially by approximately 35% and still by 15% over 5 days. Furthermore, live-cell imaging revealed impaired adaptation and dynamics of astrocyte migration under increased gravitational loading. Interestingly, the cells showed a recurrent “lag phase” of 1-2 h before the effects were mostly stabilized.

In addition, astrocytes altered their cellular morphology in a gravity-dependent manner, in line with decreased reactivity induction and inhibited stellation. Upon 2g hypergravity exposure, astrocytes showed a decrease in cell polarity and a less stellate cell shape was observed. Astrocytes exposed to 2g hypergravity also changed in actin filament and microtubule dynamics. During hypergravity exposure, live actin filament dynamics were visualized by expression of the LifeAct-GFP transgene derived from the respective mouse line. Actin-rich structures, such as lamellipodia retracted from mostly the cell perimeter. Super-Resolution STED imaging revealed, that the fine architecture of cytoskeletal elements was disturbed following increased gravitational loading. Actin filament retraction was concurrent with microtubule extension especially in cell perimeters with high dynamic rearrangements.

Furthermore, it was shown that hypergravity did not induce a shift to astrocyte reactivity, but rather inhibits the expression of key genes involved in astrogliosis. All investigated reactivity markers exhibited a similar reduction. The observed effects were specific to cytoskeletal rearrangements, as proliferation and apoptosis rates were not affected by increased gravitational loading.

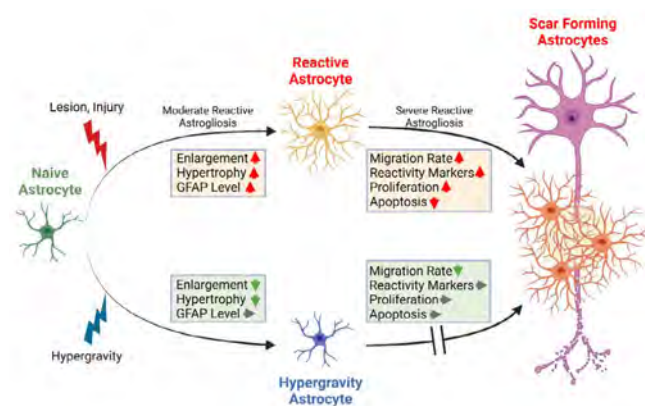


Figure 2: Schematic overview of the process of astrocyte reactivity induction and the influence of hypergravity.

Conclusions

In summary, the DLR ground-based facilities allowed us to gain insights into cellular dynamics and stimulus responses due to hypergravity that could not have been investigated before. Overall, we could show that altered gravity exposure has a direct effect on primary astrocytes and reactive astrogliosis. We revealed that hypergravity in the physiological relevant range of 2g did not induce a reactive phenotype in primary astrocytes, but was even able to inhibit several phenotypes coincidental with astrocyte reactivity. As a potential new non-invasive approach, hypergravity in particular may enhance neuronal regeneration by attenuating the otherwise inhibitory environment produced by reactive astrogliosis.

Acknowledgements

This work was funded by the German Aerospace Center (DLR) NeuroSpace project grant.

Animal welfare permits was granted by LANUV Nr. 84-02.04.2017.A319.

References

Lichterfeld, Y.; Hemmersbach, R.; Liemersdorf, C. Hypergravity Attenuates Reactivity in Primary Murine Astrocytes. *Biomedicines* 2022, submitted

POSTER 42

Adaptation to full weight-bearing following disuse: the impact of biological sex on musculoskeletal health

Mortreux M¹, Rosa-Caldwell¹ ME, ISSERTINE M¹, Sung D-M¹, Rutkove SB¹

¹ *Harvard Medical School Beth Israel Deaconess Medical Center, Boston, USA*

Introduction

In addition to musculoskeletal deconditioning during spaceflight, astronauts experience further injury during re-adaptation to Earth gravity (i.e., back pain, muscle weakness). However, the impact of biological sex on musculoskeletal health during and after disuse is not yet fully understood.

Section 1

21 adult Wistar rats (10 males and 11 females) were unloaded for 14 days to establish musculoskeletal deconditioning, and allowed to recover at full weight-bearing for 7 days. Musculoskeletal health was assessed longitudinally during the disuse and recovery periods.

Section 2

During simulated microgravity, males and females showed comparable muscle deconditioning with significant decline in grip strength ($47.3 \pm 7.3\%$ and $46.2 \pm 4.6\%$ reduction from baseline, respectively). However, after 7 days of recovery, females recovered significantly more muscle strength than males. Indeed, after recovery, males still exhibited a $16.4 \pm 5.4\%$ reduction in grip force (compared to their baseline), while females showed a significant augmentation ($+3.7 \pm 5.3\%$).

In the tibia, females had higher bone mineral density (BMD) than males ($246 \pm 5.1 \text{ mg/cm}^3$ and $342 \pm 14 \text{ mg/cm}^3$ at baseline for males and females, respectively). Throughout the experiment, trabecular BMD was significantly impacted by time and biological sex ($p < 0.0001$) while cortical BMD was not ($p = 0.167$). In males, we observed a large reduction in trabecular BMD in response to disuse ($20.41 \pm 2.5\%$ compared to baseline values), that persisted during the 7 days of reloading at full weight-bearing ($27.8 \pm 2.9\%$ reduction compared to baseline values). On the other hand, females did not experience any significant bone loss in the trabecular compartment throughout the experimental protocol.

Conclusions

Our results show that females are more resistant to skeletal deconditioning during simulated microgravity, and are able to recover significantly more muscle function than males after 7 days of reloading. These results also emphasize that males experience significant bone loss during the recovery period, which may represent a significant health risk for returning male astronauts.

Acknowledgements

This work was supported by NASA (80NSSC19K1598).

POSTER 47

Measuring Neuronal Activity Live under Micro- and Hypergravity

Maximilian Sturm*, Laura Kalinski*, Johannes Striebel, Yannick Lichterfeld, Ruth Hemmersbach, Jens Hauslage and Christian Liemersdorf

* Shared 1st author

German Aerospace Center (DLR), Institute of Aerospace Medicine, Department of Gravitational Biology, Cologne, Germany
Christian.liemersdorf@dlr.de

Introduction

Behavior and cognitive performance vary due to different environmental conditions. Astronauts experienced various forms of cognitive deficits, yet the mechanisms causing these effects remain unclear. Neurons are the fundamental building block of the human brain that relay information and process every aspect of behavior, cognition, and psychomotor functions. Alterations in signal propagation and neuronal transmissions in human brains cause a variety of disturbances, e.g. diminished cognitive performance, and fine motor control in space. Therefore, understanding the mechanisms in which altered gravity influences neuronal transmission is crucial for successful space exploration. Membrane potentials and especially action potentials (APs) can be utilized to detect the propagation of signals and neuronal activity.

Employing an experiment module suited for electrophysiological recordings in millisecond-ranges using multi-electrode arrays (MEAs), neuronal activity changes should be measured live during micro- and hypergravity conditions. The whole experiment system employs several supporting mechanisms, e.g. elaborated thermal control, to enable the functionality under varying gravitational loads.

Drop tower in Bremen, Germany as well as under hypergravity on the human centrifuge at DLR in Cologne, Germany. Importantly, neuronal cells were kept at optimal conditions of 37°C including the supply of culture medium, neglectable electromagnetic interference and vibrations. The system was exposed to hyper- and microgravity conditions and potentials could be measured for primary murine hippocampal neurons and human iPSC-derived neuronal cells. Activity data was constantly acquired with a ten-minute baseline before and after each altered gravity condition.

Experiment Module

The novel experiment module encases the MEA system in a pressure chamber to hold the surrounding pressure conditions. Utilizing the integrated heaters of the MEA system, the cells are kept at their ideal temperature. The electronics supply a PC to record the electrophysiological data of the MEA system and store it redundantly on 2 physically separate hard drives. Considering the largest allowed dimensions for different microgravity research platforms, outer dimensions were restricted to the MAPHEUS sounding rocket module size, resulting in a compact system. Intercompatibility between gravity research platforms resulted in an exchangeable design capable of being integrated within short time spans on the most relevant gravity research platforms (DLR human centrifuge, ZARM drop tower, parabolic flights and sounding rockets). For cell loading and unloading a rail system was integrated into the design for easy access to the cells where the complete experiment module can be removed improving usability and time-sensitive operations.

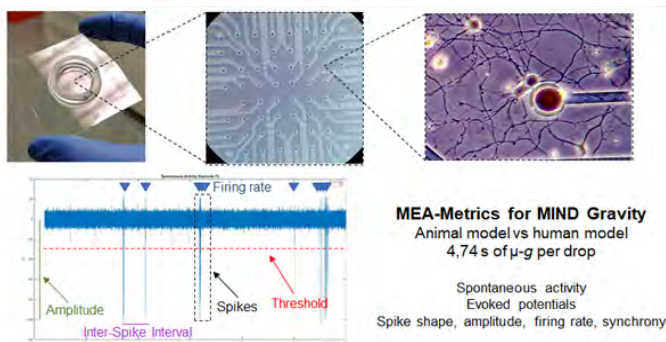


Figure 1: Multi-electrode array on the MEA glass substrate with cultivated neurons and the real-time display of electrophysiological recordings

Methods

Targeting neuronal activity changes under altered gravitational loads has been tried for decades to investigate the demanding and complex issue of disturbed cognitive and motor functions in spaceflight environments.

Traditionally, invasive methods such as patch clamping have been employed and indirect measurements via calcium-sensitive dyes to assess activity patterns in neuronal systems. We employed multi-electrode arrays (MEAs) as a novel innovative method that enables the measurement of live membrane potential changes in cultivated neurons. MEAs thus allow the observation of not only individual cells, but also whole functional neuronal network potentials.

A custom-built experiment system module was used to conduct experiments under real microgravity at the ZARM

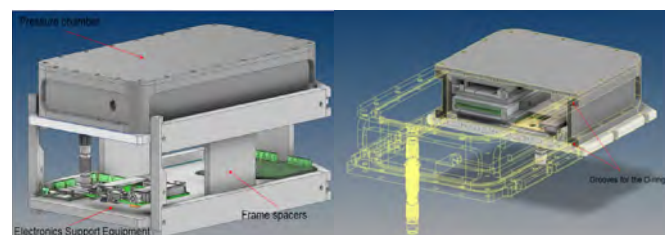


Figure 2: The design of the MEA module experiment system.

Results

In the drop tower, iPSC-derived neuronal cells were exposed to 4.7 seconds of microgravity. Activity changes could be measured, as the mean action potential frequency was significantly elevated on the whole network level. A longer-lasting effect of altered gravity, potentially from the hypergravity stimulus on impact, could be found as the cell's activity could be observed to return to baseline levels during ten minutes after the drop.

Hypergravity conditions were applied on the human centrifuge at DLR for primary neurons and iPSC-derived neurons. The cells were exposed to 2g and 4g increased gravitational load. A gravity-dependent increase in mean firing rate and bursting rate could be observed as well.

Conclusions

The experiments showed that real-time recording of neuronal activity under altered gravity conditions is possible. Differences in neuronal activity could be detected even within small time frames in the millisecond range. The microgravity conditions acting on the neuronal cells influence the activity of neuronal networks in line with previously published findings. This poses further questions regarding astronaut brain health.

Further deployment of the module is feasible in the most relevant gravity research platforms, such as the DLR human centrifuge, ZARM drop tower, sounding rockets or parabolic flights as the system proved to withstand the g loads of ca. 50g without disturbances.

Apart from neuronal cells, other electrically active cell types, such as cardiomyocytes or myotubes could be investigated similarly.

POSTER 49

Combined action of simulated microgravity and radiation on the transcriptome of *Arabidopsis thaliana* seedlings

I. Le Disquet¹, M. Valbuena², E. Carnero Diaz³

Institut de Systématique, Evolution, Biodiversité-Sorbonne Université-Muséum National d'Histoire Naturelle, Paris, France
¹isabel.le-disquet@mnhn.fr, ²miguel.valbuena@gmail.com, ³eugenie.carnero_diaz@sorbonne-universite.fr

Introduction

In the context of the space conquest of Mars, a controlled life-support system must be developed to revitalize atmosphere (liberate oxygen and fix carbon dioxide), purify water (via transpiration), and provide human fresh food. In order to better understand the plant adaptation to spaceflight environment, we investigate the response of *Arabidopsis thaliana* 6-day-old seedlings to artificial microgravity and the cosmic radiation obtained in a MarSimulator device located in the Groupe Scientifique de Biologie et de Médecine Spatiale of the University of Toulouse. In this device, microgravity ($10^{-4}G$) was simulated by a Random Positioning Machine and the radiation rate of 0.33 mSv/d was produced by a thorium nitrate source. The response of plants to a microgravity (μG) environment in the presence of radiation was characterised by a transcriptomic study. For this purpose, total RNAs were extracted from roots and leaf rosette separately and sequenced in the platform of the Institut du Cerveau et de la Moelle Epinière in Paris.

Differential expression analysis of transcripts was performed using DeSeq2 program in the Galaxy server. The ontological analysis of differentially expressed genes was done in the Gene Ontology Resources website (<http://geneontology.org/>) and finally, the Venn diagram was obtained from the Bioinformatics and Evolutionary Genomics website (<https://bioinformatics.psb.ugent.be/webtools/Venn/>). We considered that gene expression was modified when the P-value was less than 5% and the $\log_2FC < 1$ (down-regulated genes) or > 1 (up-regulated genes).

The roots seem to be better adapted to space flight conditions than the leaf rosette

The number of differentially expressed genes was determined in leaf rosettes and roots of plants exposed to either microgravity, radiation or both environmental factors (Figure 1).

The first observation is the fact that the number of upregulated genes was much higher than the number of downregulated at both microgravity and radiation environment.

The results showed that the number of differentially expressed genes in roots was lower than in leaves, indicating that roots are more resistant than leaves to the applied environmental conditions. Radiation induced a stronger transcriptional response than microgravity in both leaves and roots.

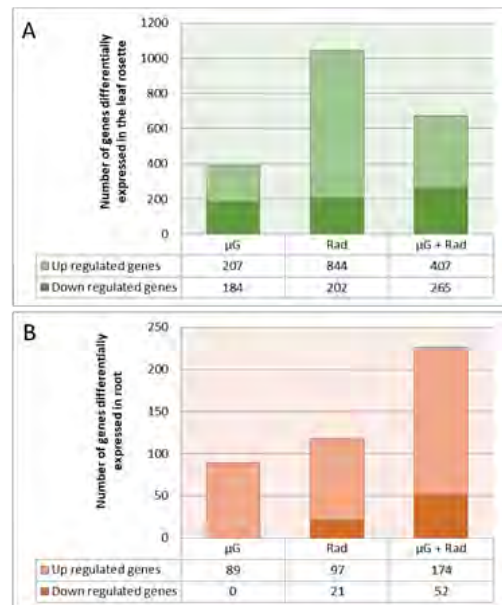


Figure 1: Number of genes whose expression varied according to the environmental factor applied. (A) Down- and up-regulated genes in the leaf rosette. (B) Down- and up-regulated genes in the roots. μG : microgravity, Rad: radiation.

These results indicate that plants are more sensitive to radiation than to microgravity. Furthermore, it appears that the response to the two factors combined is not a simple addition of the response to each environmental factor applied separately.

Specificity of plant response pathways to microgravity and radiation

To dissect the transcriptomic changes provoked by microgravity and radiation, we performed an additional set of transcriptomic comparisons between irradiated seedlings, microgravity exposed seedlings and seedlings cultivated under the effect of the two combined factors (Figure 2).

The Venn diagrams show that the majority of genes are located outside the intersection zones. This is due to the fact that each factor induces its own response pathway in the plant. On the other hand, some genes are located in the intersection zone between microgravity and radiation, indicating that part of the plant responses to these two factors follow a common pathway. The existence of these common response pathways allows plants to respond to several environmental factors with a lower energy cost than if the plants used only specific pathways.

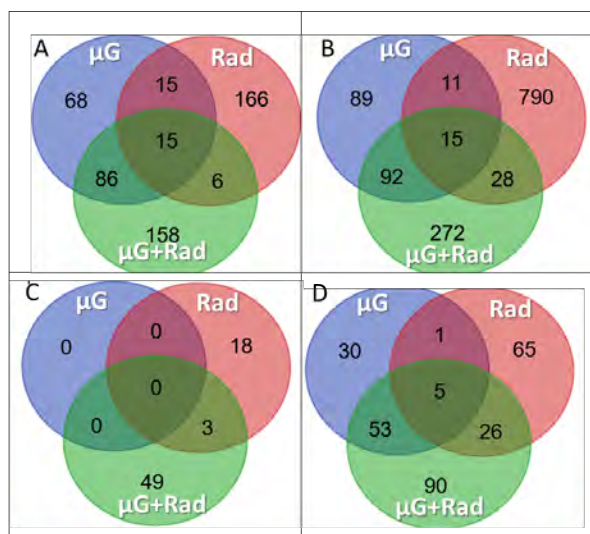


Figure 2: Venn diagrams showing global transcriptomic effects of microgravity and radiation on leaf rosette and roots. (A) down-regulated genes in leaf rosettes, (B) up-regulated genes in leaf rosettes, (C) down-regulated genes in roots and (D) up-regulated genes in roots. μ G: microgravity, Rad: radiation.

Conclusions

Microgravity and radiation induce in the plant a broad non-targeted response to the inducing factor that applies to both biotic and abiotic factors. This type of response is characteristic of a short-term reaction allowing the plant to acclimatize rapidly to changes in its environment.

It should be noted that this response can sometimes be inappropriate as for example the induction of the expression of genes involved in photosynthesis in root cells, inducing an unnecessary energy cost to the plant.

All the results obtained lead to the definition of a model (Figure 3) where the two factors, isolated or combined, are perceived as stress factors that induce oxidative stress that trigger a common cellular response. The main components of this response are hormone signaling, cell wall integrity and membrane permeability. The whole of these reactions requiring a strong energy contribution, induce a stimulation of the general metabolism of which that of the photosynthesis and the protein biosynthesis. All these modifications have consequences on the development of the plant leading to an environmental adaptation. Even if the simultaneous response to both factors is, in part, through a common pathway, the energy cost is relatively high. A longer term study would allow us to evaluate the long term consequences. Some of these results have been previously observed in real microgravity conditions alone or in combination with other factors like light (Poulet et al., 2016 ; Paul et al., 2013 and 2017 ; Villacampa et al., 2021)

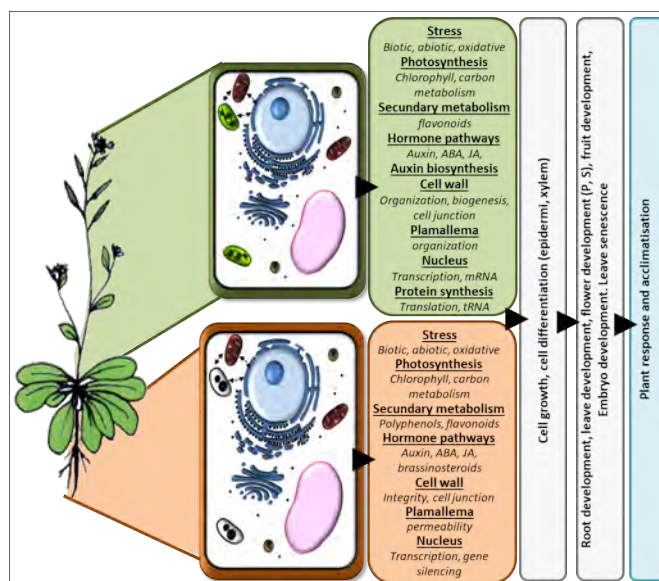


Figure 3: Model of microgravity and radiation adaptation mechanism in *Arabidopsis thaliana* leaf rosettes and roots

Acknowledgements

This work was financially supported by the French Space Agency CNES and by the ESA Space Omic Topical Team (4000131201/20/NL/PG/pt,grant)

The authors would like to thank the Artbio platform of the Institut of Biology-Paris Seine of Sorbonne University, for its assistance in the analysis of the sequences. The biological material was produced in the GSBMS platform of the University of Toulouse.

References

- A-L. Paul, R M. Wheeler, H G. Levine and R J. Ferl, Fundamental Plant Biology Enabled By The Space Shuttle *American Journal of Botany*, 100, 226-234 (2013)
- A-L. Paul, N J. Sng, A K. Zupanska, A. Krishnamurty, E R. Schultz and R J. Ferl, Genetic dissection of the Arabidopsis spaceflight transcriptome: are some responses dispensable for the physiological adaptation of pants to spaceflight? *Plos one*, 12:e0180186 (2017)
- L. Poulet, J-P. Fontaine and C-G. Dussap, Plant's response to space environment: a comprehensive review including mechanistic modelling for future space gardeners. *Botany letters*, 163,337-347 (2016)
- A. Villacampa, M Ciska, A. Manzano, JP. Vandenbrink, J Z. Kiss, R. Herranz ans F J. Medina, From spaceflight to Mars g-levels: adaptative respons of *A. thaliana* seedlings in a redused gravity environment is enhanced by red-light photostimulation, *International journal of molecular sciences*, 22-899 (2021)

POSTER 62

Self-organized criticality assessed on Holter heart rate variability during spaceflight simulation by dry immersion

J.O. Fortrat^{1,2}, A. Robin^{2,3}, N. Navasiolava^{2,3}, M.A. Custaud^{2,3}

¹Service de Médecine Vasculaire, CHU d'Angers, Angers, France, jofortrat@chu-angers.fr, ²Mitovasc UMR INSERM 1083-CNRS 6015, Université d'Angers, Angers, France ³Centre de Recherche Clinique, CHU d'Angers, Angers, France, adrien.robin08@gmail.com, Nastassia.Navasiolava@chu-angers.fr, MACustaud@chu-angers.fr

Introduction

Self-organized criticality (SOC) is a universal theory that explains the behaviour of dynamical systems including this of the cardiovascular system (Bak 1996; Fortrat & Gharib 2016; Muñoz 2018). The term criticality refers to large spontaneous sudden dynamical events that are called catastrophes. Time distribution of these catastrophes draws power laws such as Gutenberg-Richter and Zipf's laws. Self-organized criticality is more easily demonstrated on cardiovascular time series obtained during the gravitational stress of the standing position (Fortrat & Ravé 2020). This position challenges brain perfusion and increase the risk of vasovagal syncope that are the cardiovascular catastrophes (Fortrat & Gharib 2016). Spaceflight or its simulation by prolonged head-down bed-rest or dry immersion challenges the cardiovascular function leading toward cardiovascular deconditioning with increased orthostatic intolerance when back in the standing position (Robin et al. 2020). This raises the question whether simulated spaceflight influences self-organization of the cardiovascular dynamics. We hypothesized that long term dry immersion alters Zipf's law of heart rate variability on Holter recordings.

Methods

A long term spaceflight simulation was performed by a five day dry immersion on nine healthy men. Details of the experiment have been previously reported (Robin et al., 2020). Holter recordings were performed three days before and on day 1, 3, and 5 of the immersion (B3, I1, I3, and I5, respectively). Two hours of continuous heart rate were obtained for daytime and night-time for each Holter recording cumulating at least 5000 heart beats each (day, and night, respectively). Heart rate time series were manually filtered by a trained operator (JOF). Bradycardia episodes were identified and counted according to their length in number of beats as previously described and in order to draw the Zipf's plots (Fortrat, 2020). Slope of the long and short bradycardias were determined according to the initial description of bradycardia Zipf's law. Comparison of immersion periods has been performed by mean of Friedman's tests.

Results

The slope of the Zipf's distribution of the long bradycardias was systematically higher at day in comparison with night while this slope of the short bradycardias was systematically lower at day in comparison with night. There was not significant course of this slope during the dry immersion (Figure 1). Despite high coefficients of regression that were

systematically obtained, the overall shape of the Zipf's distribution seems to be curvilinear rather than an expected linear one (Figure 2)

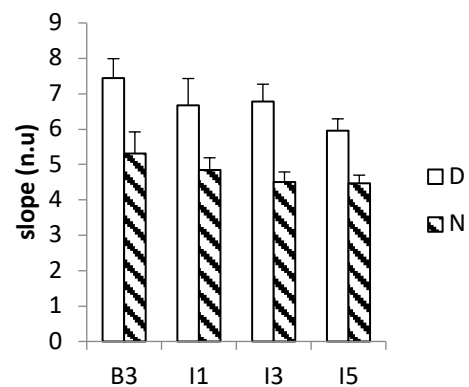


Figure 1: Slope of the Zipf's distribution of spontaneous long bradycardias during a 5 day dry immersion (B3: 3 days before the immersion; I1, I3, and I5: day 1, 3, and 5 of immersion, D and N: data on daytime and night-time, respectively). No significant changes have been observed.

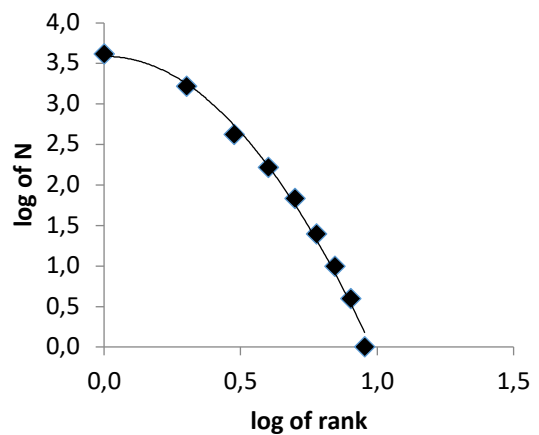


Figure 1: Zipf's distribution of spontaneous bradycardias according to their length of a healthy subject before a dry immersion. Data shown were obtained on daytime period by means of Holter. The distribution is unexpectedly curvilinear.

Discussion

Despite the gravitational influence on cardiovascular self-organized criticality previously reported, a long-term dry immersion did not influence Zipf's law of heart rate variability on Holter recordings.

Studying the self-organized criticality during a long term spaceflight simulation is based on the seducing hypothesis of

position and the criticality as shown by the vasovagal syncope. Actually, spaceflight simulation leads to increased orthostatic intolerance. Such a study is however challenging since spaceflight simulation suppresses the standing position during which self-organized criticality is more easily observed. Data length analyzed in this experiment has been dramatically increased as compared with previous experiments to try turn round this pitfall. Thanks to Holter, the data length has been increased by a factor of 10 in order to catch more spontaneous bradycardia events. This experiment failed to show any influence of simulated spaceflight on cardiovascular self-organized criticality. The difficulty to study cardiovascular self-organized criticality during simulated spaceflight could be the lack of standing position included in the data set. A Holter obtained right after the end of the spaceflight simulation that would include periods of standing positions might be more informative than one obtained at the end of the immersion period.

The length of data analyzed was a chance to accurately describe the distribution of bradycardia episodes. This distribution seems to be curvilinear and is not in accordance with a Zipf's distribution. A curvilinear distribution challenges the self-organized criticality of the time series. All the previous experiments that have dealt with HRV power laws to study self-organized criticality have been performed on quiet motionless subjects and not on Holter. We previously showed that the influence of data data collection on heart rate variability analysis including when focusing on the mathematical complexity (Fortrat et al., 1999). Question remains whether Holter recordings might mask self-organized criticality of cardiovascular dynamics.

Conclusions

Further studies should clarify the influence of Holter settings on heart rate variability self-organization in comparison to laboratory settings and should consider a recording that includes standing position during the recovery soon after the end of spaceflight simulation.

Acknowledgements

The volunteers and MEDES, supported by CNES (DAR 2018 – 4800000970).

References

- P Bak. *How Nature Works: The Science of Self-Organised Criticality*; Copernicus Press: New York, NY, USA, pp. 1–212 (1996)
- JO Fortrat, C Formet, J Frutoso, C Gharib. Even slight movements disturb analysis of cardiovascular dynamics. *Am J Physiol*, 277,H261-7 (1999)
- JO Fortrat, V de Germain, MA Custaud. Holter heart rate variability: are we measuring physical activity? *Am J Cardiol*,106:448-9 (2010)
- JO Fortrat, C Baum, C Jeanguillaume, MA Custaud. Noisy fluctuation of heart rate indicates cardiovascular system instability. *Eur J Appl Physiol*, 113:2253-61 (2013)
- JO Fortrat, C Gharib. Self-Organization of Blood Pressure Regulation: Clinical Evidence. *Front Physiol*, 7:113 (2016)

Variability Sequences. *Entropy* (Basel), 22:413 (2020)

JO Fortrat, G Ravé, Autonomic influences on Heart rate variability Self-organized criticality: Insights of Zipf's law, 11th ESGCO, pp. 1-2 (2020)

T Mora, W Bialek. Are biological systems poised at criticality? *J Stat Phys*, 144, 268–302 (2011)

MA Muñoz. Colloquium: Criticality and dynamical scaling in living systems. *Rev Mod Phys*, 90, 031001 (2018)

A Robin, A Auvinet, B Degryse, R Murphy, MP Bareille, A Beck, C Gharib, G Gauquelin-Koch, A Daviet, F Larcher, MA Custaud, N Navasiolava. DI-5-CUFFS: Venoconstrictive Thigh Cuffs Limit Body Fluid Changes but Not Orthostatic Intolerance Induced by a 5-Day Dry Immersion. *Front Physiol*, 11:383 (2020)

POSTER 71

Ready, Steady, Go!

Altered Gravity Influences Responses to Environmental Stimuli

Iqra Arshad¹ and Elisa R Ferre²

Department of Psychology, Royal Holloway University of London, London, UK

Department of Psychological Sciences, Birkbeck University of London, London, UK

Humans have evolved in a 1g gravitational environment. That is, on Earth gravity is always there, stable and unchanging. The vestibular system in the inner ear constantly monitors the magnitude and direction of gravitational acceleration. Gravity is the most persistent sensory signal in the brain, and it may play an important role in regulating behaviour. Accordingly, astronauts have reported perceptual and cognitive alterations during spaceflight. Responding to changes in the environment is crucial for survival. Using the oddball task, we investigated how people react to environmental stimuli in physical and visually altered gravity. In Experiment 1, the vestibular system was stimulated by passively tilting participants in body orientations congruent or incongruent to terrestrial gravity. No differences were found in accuracy; however participants were slower in detecting the oddball stimulus when the body was incongruent to terrestrial gravity. In Experiment 2, the oddball task was administered during Virtual Reality simulation of terrestrial and non-terrestrial gravity. Again, no differences were found in accuracy, yet responses were significantly slower in non-terrestrial gravity compared to terrestrial gravity. Taken together, our results demonstrate sub-optimal behavioural responses in both physical and visually altered gravity. Vestibular-gravitational signals may be crucial in successfully adapting to the environment.

POSTER 72

Intracranial Effects of Artificial Gravity on Head Down Tilt Bedrest

Authors:

L KRAMER¹, K Hasan², X Zhang³, B Macias⁴, K Marshall-Goebel⁵, S Laurie⁴, E Bershad⁶

Institutions:

¹UTSHC-Houston, Houston, TX, ²University of Texas Health Science Center, Houston, TX, ³Univ. Of Texas Health Science Center, Houston, TX, ⁴NASA, Houston, TX, ⁵KBR, Houston, TX, ⁶Baylor College of Medicine, Houston, TX

Purpose:

Spaceflight associated neuro-ocular syndrome (SANS) is characterized by the development of optic disc edema, posterior globe flattening, choroidal/retinal folds and hyperopic refractive errors(1), hypothesized to be due to headward fluid shift that invariably occurs in microgravity. As a countermeasure, artificial gravity (AG) through centrifugation has been proposed to reduce this headward fluid shift. As an indicator of efficacy, the goal of this study was determine if AG can prevent or reduce known changes in brain volumetry, internal carotid artery (ICA) stroke volume and cerebral spinal fluid (CSF) flow velocity that occur during simulated chronic headward fluid shift using head down tilt bed rest (HDTBR) methodology(2).

Materials and Methods:

24 volunteers (16 men, mean age = 33 years \pm 9; mean BMI = 24.3 kg/m² \pm 2.0) were recruited for a prospective study using strict six-degree HDTBR for 60 days. Short-arm centrifugation was utilized to generate AG at 0.3g. Subjects were divided equally into three groups: No AG (control; n=8), daily intermittent AG (6 x 5 min iAG; n=8), and daily continuous 30 min cAG (n=8). Phase-contrast imaging was used to quantify ICA stroke volume and peak-to-peak CSF flow velocity in the mid cerebral aqueduct. 3D-SPGR was acquired for volumetric segmentation of the brain and CSF spaces. MRI studies were performed on a dedicated 3T scanner at baseline (BDC), 14 days into HDTBR (HDTBR14), 52 days into HDTBR (HDTBR52) and 3-5 days after HDTBR (recovery, R+3/5). The data were analyzed by the mixed model, which included intervention and time (BDC, HDTBR 14, HDTBR 52, R+3/5) as the fixed effects and included subject as the random effect.

Results:

Strict six-degree HDTBR was characterized by progressive increases in combined brain and CSF volumes and progressive decreases in mean ICA stroke volume from baseline to 52 days post intervention ($P < .01$) (Figs. 1-2). Overall, mean CSF peak-to-peak flow velocity increased from baseline to 52 days post intervention ($P < .01$), reaching its maximum value at HDTBR14 (Fig. 3). Compared to baseline, only combined brain and CSF volumes did not return to baseline values in the recovery period ($P < .01$). Neither iAG nor cAG exerted any significant effects on the measured MRI brain parameters as compared to HDTBR alone ($P = NS$).

Conclusions:

Thirty minute daily exposure to either iAG or cAG appears to be insufficient in preventing or reducing the intracranial effects of chronic HDTBR and thus may not be a suitable countermeasure as currently deployed.

POSTER 78

Altered gravity disrupts spatial navigation

S. Zanchi^{1,2,3}, L.F. Cuturi², G. Sandini², M.Gori², E.R. Ferrè³

¹University of Genoa, Genoa, Italy, silvia.zanchi@iit.it, ²Italian Institute of Technology, Genoa, Italy, ³Birkbeck University of London, London, United Kingdom, elisa.ferre@bbk.ac.uk

Introduction

Perceiving gravity is crucial for balance and orientation in space. All living creatures have evolved under a constant terrestrial gravitational field of approximately 9.81 m/s^2 , known as 1 g. It has been shown that the constant presence of gravity on Earth leads the human brain to internalize the physical constraints of Earth's gravity, resulting in behaviour shaped according to it (Indovina et al. 2005; Gallagher et al. 2020). The vestibular system is a key source of sensory information about the orientation of one's own body relative to the gravitational force. In particular, the vestibular otolithic organs detect the position of our head with respect to terrestrial gravitational acceleration (Beck et al. 2020). When exploring an environment – and especially if it is a novel one – estimating the spatial relationships among objects and our own position is crucial. Although previous studies described a vestibular contribution to spatial perception (Ferrè et al. 2013) and visuo-spatial memory (Hilliard et al. 2019), the influence of altered vestibular-gravitational signals in target localisation remains unclear.

Methods and Procedure

Here we altered vestibular signalling using stochastic Galvanic Vestibular Stimulation (sGVS) and investigated its effects on the encoding of the location of visual targets in the environment. Critically, sGVS is a safe and non-invasive method to stimulate vestibular afferences and mimic vestibular alterations similar to spaceflight conditions (Fitzpatrick & Day 2004). Accordingly, sGVS induces postural instability (MacDougall et al. 2006) and locomotor dysfunction (Moore et al. 2006) simulating an altered gravity environment. A sham stimulation condition was used to control for non-specific effects.

Twenty healthy participants were administered with sGVS or sham stimulation while encoding the position of LED lights placed on the floor. The room was darkened and participants wore sunglasses to reduce the availability of environmental visual cues. Participants were instructed to focus on the

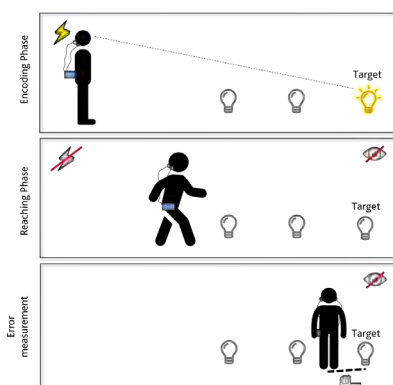


Figure 1: Experimental set-up.

location of the lights, and then localise them by walking towards the LED lights. Both accuracy and precision in localisation were measured and compared between sGVS and sham conditions.

Results

We took the distance error as a measure of accuracy and the variability (standard deviation, SD) in distance error as a measure of precision. We performed paired t-tests on both error and variability comparing sGVS and sham conditions to look for any difference. As depicted in Figure 2, both error ($t(19) = 1.78, p = .045, \text{Cohen's } d = 0.399$) and variability ($t(19) = 2.21, p = .019, \text{Cohen's } d = 0.494$) resulted to be significantly greater in sGVS condition than in sham condition, indicating less accuracy and less precision in localising and reaching the visual targets.

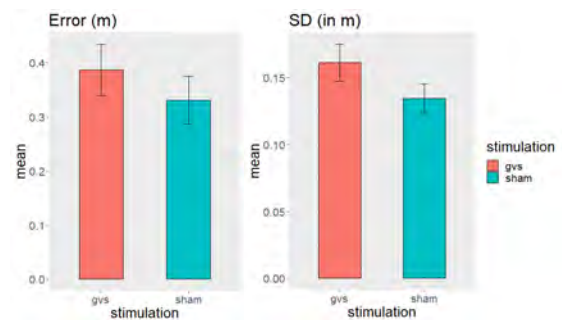


Figure 2: Error and standard deviation (SD) in sGVS (red) and sham (green) conditions.

Conclusions

Our results demonstrate a clear contribution of the vestibular system in localising visual targets in the environment, suggesting a functional interaction between vestibular and visual inputs during the encoding of spatial cues that influences the ability to reach objects in space.

These findings suggest that our ability to functionally navigate in space and interact with environmental objects is disrupted in altered gravity conditions, potentially affecting human performance during human spaceflight missions.

Acknowledgements

This work has been supported by the UK EPS, BIAL and an ELGRA Research Prize to ERF.

References

- I. Indovina, V. Maffei, G. Bosco, M. Zago, E. Macaluso, & F. Lacquaniti. Representation of visual gravitational motion in the human vestibular cortex. *Science*, 308(5720), 416-419. (2005)

- M. Gallagher, A. Torok, J. Klaas, E.R. Ferrè, Gravity prior in human behaviour: a perceptual or semantic phenomenon?, *Experimental Brain Research*, 238(9), 1957-1962. (2020)
- B. Beck, A. Saramandi, E.R. Ferrè, P. Haggard, Which way is down? Visual and tactile verticality perception in expert dancers and non-experts. *Neuropsychologia*, 146, 107546, (2020)
- E.R. Ferrè, M. Longo, F. Fiori, P. Haggard, Vestibular modulation of spatial perception. *Frontiers in human neuroscience*, 7, 660, (2013)
- D. Hilliard, S. Passow, F. Thurm, N.W. Schuck, A. Garthe, G. Kempermann, S.C. Li, Noisy galvanic vestibular stimulation modulates spatial memory in young healthy adults. *Scientific reports*, 9(1), 1-11, (2019)
- R.C. Fitzpatrick & B.L. Day, Probing the human vestibular system with galvanic stimulation. *Journal of applied physiology*, 96(6), 2301-2316, (2004)
- H.G. MacDougall, S.T. Moore, I.S. Curthoys, & F.O. Black, Modeling postural instability with Galvanic vestibular stimulation. *Experimental brain research*, 172(2), 208-220, (2006)
- S.T. Moore, H.G. MacDougall, B.T. Peters, J.J. Bloomberg, I.S. Curthoys, & H.S. Cohen, Modeling locomotor dysfunction following spaceflight with galvanic vestibular stimulation. *Experimental brain research*, 174(4), 647-659, (2006)

POSTER 85

Localization of the ER-bodies in root cells of *Arabidopsis thaliana* under clinorotation

S.M. Romanchuk, E.L. Kordyum

Institute of Botany, National Academy of Sciences of Ukraine, Kyiv, Ukraine, e-mail: cellbiol@ukr.net

Introduction

The presence of ER-bodies, which are derivatives of the granular endoplasmic reticulum (GER) and contain the highly specific component – an enzyme β -glucosidase (glucoside-glucohydrolase, EC 3.2.1.21) (Hayashi et al., 2001; Matsushima et al., 2003), is the inherent and unique feature of the Brassicaceae family. It is supposed that these bodies enhance the resistance of plant species to different adverse factors (Nakazaki et al., 2019). So, we studied the influence of simulated microgravity on the localization, shape and structure of ER-bodies in root cells of *Arabidopsis thaliana* model object by methods of light and transmission electron microscopy.

1. Material and Methods

A. thaliana (Col-0) etiolated seedlings, which grew during 3, 5 and 7 days in the stationary conditions and under horizontal clinorotation, 2 rev/min, served as the material for the study by using methods of light and electron microscopy. A root cap containing the gravisensitive central statenchyma and the root distal elongation zone (DEZ), which is the most sensitive to the influence of external factors (Blancaflor, 2002; Mancuso et al., 2005) were studied (Fig. 1).

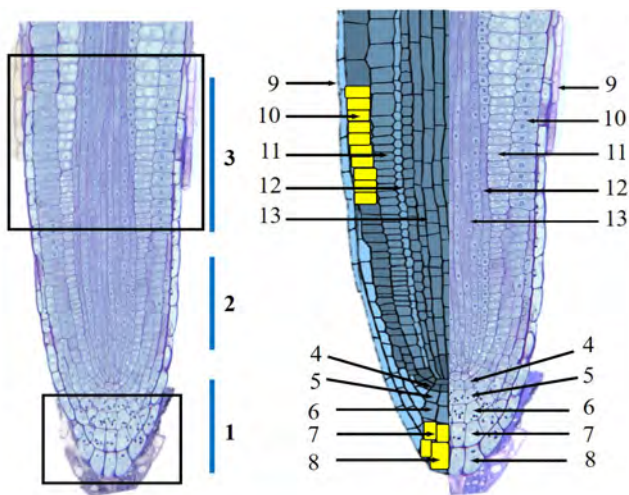


Figure 1: Scheme of the ER-bodies localization of in root cells of *A. thaliana* etiolated seedlings: 1 – root cap, 2 – meristem, 3 – distal elongation zone, 4 – meristematic cells of the root cap, 5 – differentiating statocytes, 6 – mature statocytes, 7 – statocytes transient to secretion, 8 – secretory cells, 9 – peripheral cells, 10 – epidermal cells, 11 – parenchyma cells, 12 – endodermal cells, 13 – central cylinder. Cells with ER-bodies marked in yellow (schematic image and light microscopy). Bar: 20 μ .

2. Results and Discussion

In stationary growth conditions, ER-bodies were absent in mature statocytes but 1–2 rounded bodies with the content of

medium electron density per cell section appeared in statocytes transient to secretion (Fig. 1). In the root cap secretory cells, the number of round and oval ER-bodies increased significantly (Fig. 2).

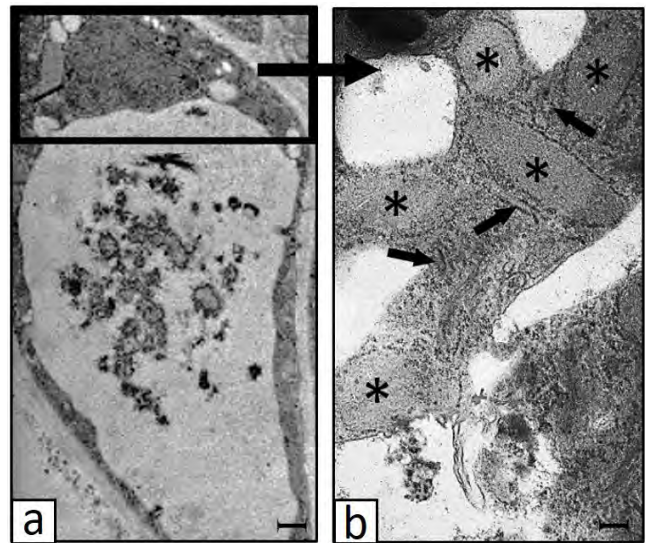


Figure 2: A root cap secretory cell of *A. thaliana* etiolated seedling (a) and its fragment (b). ER-bodies marked with asterisks. Arrows indicate GER (transmission electron microscopy). Bars: 2 μ (a), 0.5 μ (b).

In the DEZ, ER-bodies were observed only in the epidermal cells, whereas they were absent in other tissues of this root growth zone (Fig. 1). Our data are consistent with the literary ones (Matsushima et al., 2002). ER-bodies of epidermal cells are characterized by rounded, sometimes oval shape, and the content of medium electron density. The total area and a number, 8–9 per cell section, of ER-bodies remained constantly on the 7th day of seedling growth. The appearance of ER-bodies in the area of GER profiles indicated their origin from this component that was confirmed by the presence of ribosomes on the outer surface of the ER-body membrane (Fig. 3, a–c).

Although clinorotation caused disorientation of seedling growth, differentiation of root cap central statenchyma cells and cell growth in the DEZ occurred the same as in control. Only a slight decrease in the width of DEZ cells was observed (Shevchenko et al., 2007). In general, the ultrastructure of root cap cells and DEZ cells in clinorotated seedlings was similar to that in control, but there were also some differences.

Under clinorotation, amyloplasts-statoliths in root cap statocytes did not settle in the distal part of a cell, but they were located throughout the cytoplasm volume or grouped in the cell center. It means that statocytes, which are specialized graviperceptive cells, remained functionally unloaded (Kordyum, 1997). As in control, the ER-bodies

appeared in statocytes transient to secretion and they also had a rounded shape and the content of medium electron density. But a number of ER-bodies and their average area per section increased 1.5–2 times for all periods of clinorotation in comparison with control. In the DEZ epidermal cells, the GER profiles became more branched compared with those in control (Fig. 4).

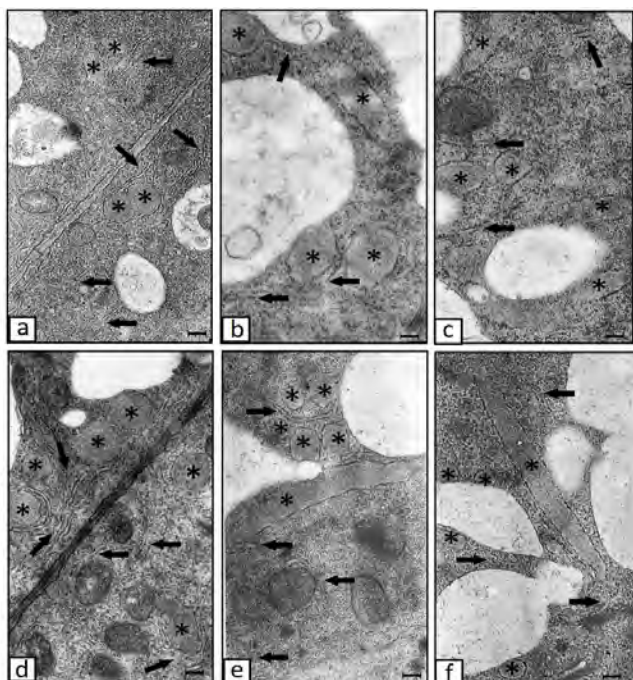


Figure 3: ER-bodies (marked with asterisks) and GER (arrows) in DEZ epidermal cells of *A. thaliana* etiolated seedlings grown during in stationary growth conditions (a–c) and under clinorotation (d–f) for 3 (a, d), 5 (b, e) and 7 (c, f) days (transmission electron microscopy). Bar: 2 μ .

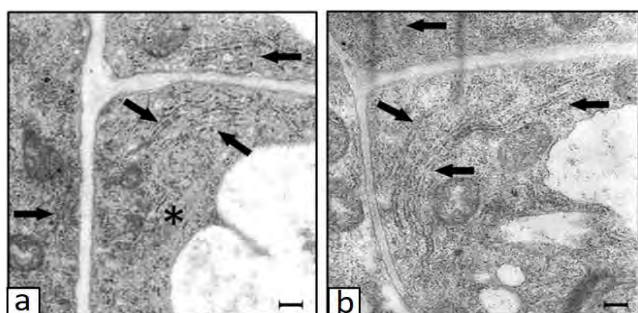


Figure 4: GER (arrows) and ER-body (marked with asterisk) in DEZ epidermal cells of *A. thaliana* etiolated seedlings in stationary growth conditions (a) and under clinorotation (b) (transmission electron microscopy). Bar: 1 μ .

Usually, ER-bodies were located in the immediate proximity to the GER profiles. Their average number and area on the cell section increased two times compared to control under all periods of clinorotation. ER-bodies population was also more heterogeneous in a shape and size under clinorotation, in particular, their shape could be rounded, oval and significantly elongated, that was especially pronounced in the DEZ epidermal cells of 7-day-old seedlings. In some elongated ER-bodies, the length exceeded the width by more than 10 times (Fig. 3, d–f).

The revealed increasing in amount and branching of GER profiles in DEZ epidermal cells under clinorotation may indicate an increase in its functional activity. Simultaneous significant increase in a number and mean area of ER-bodies, as well as their variability in a shape and size may testify the β -glucosidase enhanced accumulation in them under the influence of clinorotation.

Conclusions

It was found that presence of ER-bodies in *A. thaliana* roots is related to DEZ cells and statocytes transient to secretion and they are sensitive to simulated microgravity.

The established patterns open up new approaches to the study and understanding the mechanisms of plant adaptation at the cellular level to real microgravity in space flight. It is also important, that ER-bodies formation is a characteristic feature of the Brassicaceae family and many vegetable crops, namely *Raphanus sativus* var. *sativus*, *R. sativus* var. *radicula*, *R. sativus* subsp. *acanthiformi*, *B. oleracea*, *B. rapa* and *Lepidium sativum*, proposed for cultivation in the Bioregenerative Life Support System in long-term space missions belong to this family.

References

- A. Nakazaki, K. Yamada, T. Kunieda, R. Sugiyama, M.Y. Hirai, K. Tamura, I. Hara-Nishimura, T. Shimada, Leaf endoplasmic reticulum bodies identified in Arabidopsis rosette leaves are involved in defense against herbivory, *Plant Physiology*, 179(4), 1515–1524, (2019).
- Y. Hayashi, K. Yamada, T. Shimada, R. Matsushima, N.K. Nishizawa, M. Nishimura, I. Hara-Nishimura, A proteinase-storing body that prepares for cell death or stresses in the epidermal cells of Arabidopsis, *Plant and Cell Physiology*, 42, 894–899, (2001).
- R. Matsushima, M. Kondo, M. Nishimura, I. Hara-Nishimura, A novel ER-derived compartment, the ER body, selectively accumulates a beta-glucosidase with an ER-retention signal in Arabidopsis, *The Plant Journal*, 33(3), 493–502, (2003).
- E.B. Blancaflor, The cytoskeleton and gravitropism in higher plants, *Journal of Plant Growth Regulation*, 21, 120–136, (2002).
- S. Mancuso, A.M. Marras, V. Magnus, F. Baluska, Noninvasive and continuous recordings of auxin fluxes in intact root apex with a carbon nanotube-modified and self-referencing microelectrode, *Analytical Biochemistry*, 341, 344–351, (2005).
- R. Matsushima, Y. Hayashi, M. Kondo, T. Shimada, M. Nishimura, I. Hara-Nishimura, An endoplasmic reticulum-derived structure that is induced under stress conditions in Arabidopsis, *Plant Physiology*, 130, 1807–1814, (2002).
- G. Shevchenko, Ia. Kalinina, E.L. Kordyum, Interrelation between microtubules and microfilaments in the elongation zone of Arabidopsis root under clinorotation, *Advanced in Space Research*, 39, 1171–1175, (2007).
- E.L. Kordyum, Biology of plant cell microgravity and under clinostat, *International Review of Cytology*, 171, 1–72, (1997).

POSTER 87

Effects of sustained hypergravity on growth and reproduction in earthworms: A pilot study

C-M van der Merwe¹, M Maboeta¹, H Bouwman^{1*}

¹Research Unit: Environmental Science and Management, North-West University, Potchefstroom, South Africa, henk.bouwman@nwu.ac.za

Introduction

It is likely that humans will establish colonies on Mars and Moon (Rappaport and Szocik, 2021). For this to happen, we believe that earthworms will play a crucial role in ameliorating regolith into arable soils by composting organic waste organic matter and incorporating it into the regolith (Duri et al., 2020). To the best of our knowledge, no studies have been performed on earthworms in micro- or hypergravity.

We conducted the first experiments on the effects of hypergravity on the earthworm *Eisenia andrei*, a common compost earthworm used almost globally (Neuhauser et al., 1988). Concurrently, we ran three different gravity treatments (3 G, 5 G, and 6.5 G) to determine survival, change in biomass, and reproduction over five days. The medium we used was sieved cow manure that is able to sustain growth, wetted to an appropriate consistency, and within which the worms were originally cultured. Cow manure is a common medium to test growth and reproduction of earthworms (Mitchell, 1997.). Six earthworms were used per treatment, weighed before and after the five-day run. The medium was also searched for possible cocoons as sign of reproduction.

Results

All worms survived at all treatments. There were no significant differences in mean earthworm biomass between treatments as the beginning of the experiment, nor between treatments after five days. However, the worms did increase in biomass significantly ($p < 0.05$) at all treatments (Figures 1 and 2).

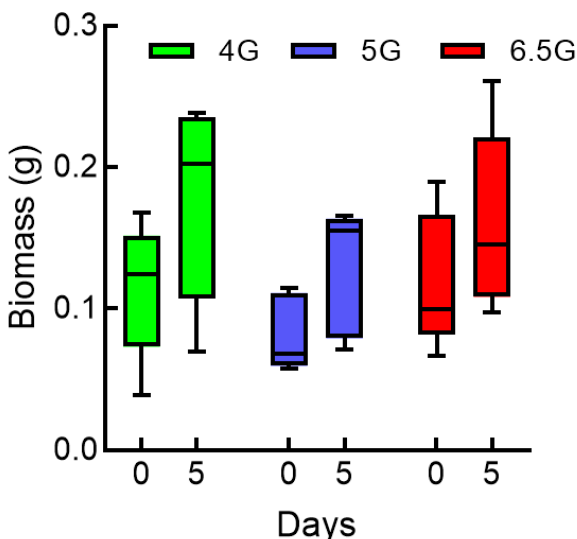


Figure 1. Significant increases in biomass of earthworms treated at 4 G, 5 G, and 6.5 G.

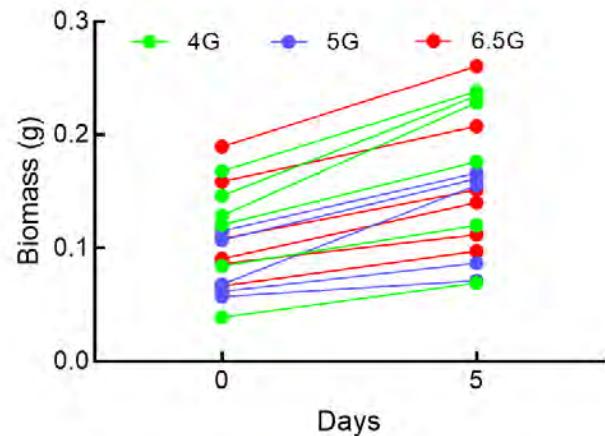


Figure 2. Individual increases in biomass for the worms in the three different hypergravity treatments were consistent for all worms.

Repeated measures two-way Anova showed no differences between treatments. This is also reflected in Figure 2 where all worms showed parallel increases in biomass. However, while Gravity and Day X Gravity were not significant sources of variation in the two-way Anova, Day, and Gravity separately were significant sources.

No cocoons were found.

Discussion

Variable changes in body mass have been reported for rats and mice under long-term hypergravity (e.g. Ronca et al., 2000; Oyama and Zeitman, 1967). However, we could not find any reports on the effects of hypergravity on biomass of soil-dwelling organisms, and very little on invertebrates in general. Effects of hypergravity on soil dwelling animals are important to know, as the weight of the overlaying medium adds to the pressure experienced by the animal, in addition to possible compaction of the underlying medium. Both factors would compress the medium and the animal and may hinder movement, and therefore affect feeding, growth, and reproduction.

Here, we have shown with this pilot study that earthworms seem to tolerate and accommodate hypergravity up to at least 6.5 G for five days with an increase in biomass, apparently able to adjust muscular performance requirements, as was the case with fruit flies (Schilder and Raynor, 2017).

However, the two-way Anova suggests that gravity plays a role. This may be deduced from Figure 1 where the relative

increase in biomass decreased with an increase in gravity. This pilot study points the way towards more experiments, with longer duration with more worms to confirm this finding, as well as to determine whether reproduction will occur as suggested by the increases in biomass across the treatment range.

The earthworm would therefore be a very good model to investigate the effects of hyper- and microgravity.

References

Duri LG et al. (2020) Mars regolith simulant ameliorated by compost as in situ cultivation substrate improves lettuce growth and nutritional aspects. *Plants* 9: <http://dx.doi.org/10.3390/plants9050628>

Mitchell, A., 1997. Production of *Eisenia fetida* and vermicompost from feed-lot cattle manure. *Soil biology and biochemistry*, 29(3-4), pp.763-766.

Neuhauser EF (1988). The potential of earthworms for managing sewage sludge. C.A. Edwards, E.F. Neuhauser (Eds.), *Earthworms in Waste and Environmental Management*, SPB Academic Publishing BV, The Hague, pp. 9-20

Oyama J and Zeitman B (1967) Tissue composition of rats exposed to chronic centrifugation. *American journal of physiology*. 213:1305-1310.

Rappaport MB & Szocik K (2021) The human factor in the settlement of the Moon. Springer Nature, Switzerland.

Ronca AE et al. (2000) Body mass, food and water intake, and activity of pregnant and lactating rat dams during 1.5-g centrifugation. *Journal of gravitational physiology* 7:131–132.

Schilder RJ and Raynor M (2021) Molecular plasticity and functional enhancements of leg muscles in response to hypergravity in the fruit fly *Drosophila melanogaster*. *Journal of experimental biology*. 220:3508.

POSTER 93

Diffusion and thermodiffusion of polymers in mixed solvents

L. García-Fernández^{1,2}, D. Sommermann³, J. Kantelhardt³, F. Croccolo¹, W. Köhler³, H. Bataller¹

¹Laboratoire des Fluides Complexes et leurs Réservoirs - IPRA, UMR 5150, E2S-Univ Pau & Pays de l'Adour/CNRS/TotalEnergies, Anglet, France, henri.bataller@univ-pau.fr

²Department of Structure of Matter, Thermal Physics and Electronics, Faculty of Physics, University Complutense of Madrid, Avda. Complutense s/n, 28040 Madrid, Spain, loreto.garcia@ucm.es

³Physikalisches Institut, Universität Bayreuth, 95440 Bayreuth, Germany, werner.koehler@uni-bayreuth.de

Introduction

Transport phenomena occur in any multicomponent fluid present in the nature and/or the industry subjected to non-equilibrium conditions. Its comprehension is of great interest for many applications. Thermodiffusion, which leads to a component separation in a mixture due to a thermal gradient, still does not have an unambiguous microscopic picture. Therefore, experimental studies, especially in convection free environment, are important. So far, most works on thermodiffusion have dealt with binary systems in general or, more recently, ternary mixtures of small molecules (Köhler et al. 2016). Binary samples with polymers in solvents have been studied over a broad range of both concentration and polymer molar mass (Rauch et al. 2003). Experiments for highly asymmetric ternary systems like a polymer in a binary solvent, were recently performed (Bataller et al. 2017, García-Fernández et al. 2019, García-Fernández et al. 2022), but remain scarce. While binary mixtures are readily characterized by one diffusion and one thermodiffusion coefficients, the number of coefficients increases to four plus two for ternaries, respectively. We are particularly interested in the question, to what extent the dynamics of the large molecule, the polymer, is coupled to the solvent-solvent dynamics, with respect to both diffusion and thermodiffusion. In this work, samples containing polystyrene (PS), toluene and cyclohexane have been analysed in our laboratories using single-color shadowgraphy (1-SG), single-color thermal diffusion forced Rayleigh scattering (1-TDFRS) and two-color optical beam deflection (2-OBD). Results obtained by two-color optical digital interferometry (2-ODI) during the convection free experiments performed onboard the ISS of the DCMIX4 campaign (Mialdun et al. 2019, Mialdun et al. 2020) are also reported.

Experimental results

The shadowgraph apparatus (1-SG) involves two main parts: a thermodiffusion cell allowing precise differential temperature control over a precise layer of a liquid mixture and the optical setup aimed at acquiring shadowgraph images of the density fluctuations within the fluid (Croccolo et al. 2019). A light beam at wavelength (675 ± 13) nm passes through the sample in the vertical direction parallel to the imposed temperature gradient. A mixture of 2% in mass fraction of PS ($M_w=4730$ g/mol) in pure toluene has been subjected to a temperature difference of 20 °C over a 5 mm-thick sample, by heating from above. Once the steady state is reached, images are recorded, from which the structure

function reveals the presence of two relaxation modes of the non-equilibrium fluctuations (NEFs). The fast one is to be attributed to the thermal NEFs, and the slow one, to concentration NEFs. The fitting of the relaxation times as a function of the wave vectors with the model obtained in the frame of the fluctuating hydrodynamics allows to obtain the thermal diffusivity and the mass diffusion of the binary mixture (PS/toluene), values in agreement with literature data (Rauch et al. 2003).

Thermal diffusion forced Rayleigh Scattering (1-TDFRS) is a heterodyne transient holographic grating technique with a characteristic diffusion length of the order of 10 μm and temperature gradients of the order of 1K/m. The laser wavelength for writing of the grating was 532 nm and the one for reading was 633 nm. A small amount of an inert dye (quinizarin) was added for optical absorption at the writing wavelength. A similar technique has been used, e.g., by Rauch et al. (Rauch et al. 2003).

Two color Optical Beam Deflection (2-OBD) utilizes an optical Soret cell, where both the temperature and the concentration gradient are sensed by deflection of a laser beam that traverses the cell along a direction perpendicular to the temperature gradient, i.e., parallel to the hot and cold walls. Three time constants can be identified in measurements on ternary mixtures. A fast one is related to the heat diffusion and the two slow ones to the two diffusion eigenvalues. The two different detection colors allow for a separation of the Soret amplitudes of the individual components (Königer et al. 2010).

The Selectable Optical Diagnostic Instrument (SODI) on board the ISS consists of a two-wavelength Mach-Zehnder interferometer (2-ODI) equipped with two lasers operating at 670 nm and 935 nm for ternary mixtures, plus a monochromatic Mach-Zehnder interferometer with one laser only, operating at 670 nm wavelength for binary mixtures. The SODI has been used in order to obtain the temperature and concentration fields inside the cells during thermodiffusion experiments. The 4th campaign of the DCMIX project (Mialdun et al. 2019, Mialdun et al. 2020) was performed from 13th December 2019 until 4th March 2019. One of the cells was filled with a ternary mixture of PS ($M_w=4730$ g/mol), toluene and cyclohexane with mass fractions of 2/39/59 %. The so-called companion cell of the project was filled with a binary mixture of 2% mass fraction of the same PS in pure toluene. Experiments at mean temperature of 20, 25, 30 and 35 °C have been performed for

a difference of temperature of 5 °C over a thickness of 5 mm. After a fast evolution of the refractive index across the cell due to the application of the thermal gradient, two opposite evolutions have been detected for the ternary at the two wavelengths. The two behaviours are associated to the mass separation in the solvent binary mixture followed by that of the polymer in the mixed solvent. These two variations of opposite directions are compatible with Soret coefficients of opposite sign, as expected for the PS/toluene/cyclohexane mixture, since toluene/cyclohexane has a negative Soret coefficient (Lapeira et al. 2017) while PS/toluene mixtures typically show positive Soret coefficient (Rauch et al. 2003, Croccolo et al. 2019). In this case, even with only one wavelength, thanks to the well distinguishable dynamics, one can determine the two eigenvalues of the diffusion matrix of the ternary mixture.

In Fig. 1 we report the smallest eigenvalue of the mass diffusion matrix of the ternary mixture of PS/toluene/cyclohexane at 25°C, as a function of the mass fraction of PS, for different toluene/cyclohexane ratios in the solvent binary mixture, and for all the experimental techniques compared in this work.

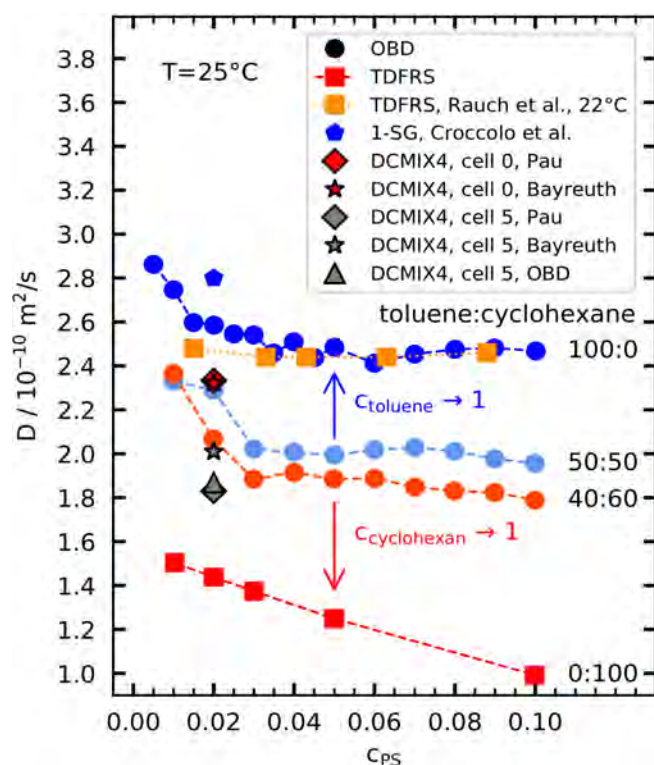


Figure 1: Smallest eigenvalue of the mass diffusion matrix of the ternary mixture of PS/toluene/cyclohexane at 25°C, as a function of the mass fraction of polystyrene and for different content of toluene in the solvent binary mixture. Literature data from (Rauch et al. 2003) and (Croccolo et al. 2019).

Conclusions

Thermodiffusion experiments on weakly concentrated mixtures of PS in a binary solvent of toluene and cyclohexane were carried out. Four experimental optical techniques of different nature were used in order to study, either the

relaxations of the thermal and concentrations modes of NEFs at the stationary state, or the evolution of the transient state of the thermal and concentrations fields across the mixture. The measured signals show three well separated modes that can be assigned to the thermal diffusivity and the two eigenvalues of the mass diffusion matrix. A first analysis supports the picture of an effective solvent whose internal dynamics is decoupled from the one of the polymer.

Acknowledgements

This work has been developed in the framework of the cooperative project DC MIX (No. AO-2009-0858/1056) of the European Space Agency. LGF, FC and HB acknowledge financial support from the Centre National d'Etudes Spatiales (CNES) and from the E2S UPPA Hub Newpores and the Industrial Chair CO2ES supported by the Investissements d'Avenir French program managed by ANR (ANR16IDEX0002).

References

- W. Köhler, K. Morozov, The Soret Effect in Liquids Mixtures – A Review, *J. Non-Equilib. Thermodyn.*, 41, 151-197 (2016)
- J. Rauch, W. Köhler, Collective and thermal diffusion in dilute, semidilute, and concentrated solutions of polystyrene in toluene, *J. Chem. Phys.*, 119, 11977 (2003)
- H. Bataller, T. Triller, B. Pur, W. Köhler, J. M. Ortiz de Zárate, F. Croccolo, Dynamic analysis of the light scattered by the non-equilibrium fluctuations of a ternary mixture of polystyrene-toluene-n-hexane, *Eur. Phys. J. E*, 40, 35 (2017)
- L. García-Fernández, H. Bataller, J.M. Ortiz de Zárate, F. Croccolo, Coupled non-equilibrium fluctuations in a polymeric ternary mixture, *Eur. Phys. J. E*, 42, 124 (2019)
- A. Mialdun, H. Bataller, M.M. Bou-Ali, M. Braibanti, F. Croccolo, A. Errarte, J.M. Ezquerro, Yu. Gaponenko, L. García-Fernández, J.J. Fernández, J. Rodríguez, V. Shevtsova, Preliminary analysis of diffusion coefficient measurements in ternary mixtures 4 (DCMIX4) experiment onboard the International Space Station, *Eur. Phys. J. E*, 42, 87 (2019)
- A. Mialdun et al., Data quality assessment of Diffusion Coefficient Measurements in ternary mixtures 4 (DCMIX4) experiment, *Acta Astronautica*, 176, 204-215 (2020)
- L. García-Fernández, H. Bataller, P. Fruton, C. Giraudet, A. Vailati, F. Croccolo, Stabilized convection in a ternary mixture with two Soret coefficients of opposite sign, *Eur. Phys. J. E*, in press
- F. Croccolo, L. García-Fernández, H. Bataller, A. Vailati, J.M. Ortiz de Zárate, Propagating modes in a binary liquid mixture under thermal stress, *Phys. Rev. E*, 99, 012602 (2019)
- E. Lapeira, M. Gebhardt, T. Triller, A. Mialdun, W. Köhler, V. Shevtsova, M.M. Bou-Ali, Transport properties of the binary mixtures of the three organic liquids toluene, methanol and cyclohexane, *J. Chem. Phys.*, 146, 094507 (2017)
- A. Königer, H. Wunderlich, W. Köhler, Measurement of diffusion and thermal diffusion in ternary fluid mixtures using a two-color optical beam deflection technique, *J. Chem. Phys.* 132, 174506 (2010)

POSTER 97

A New Microgravity Modular Research Platform for Education

Dinis Afonso Ribeiro

Escola Superior Náutica Infante D. Henrique, Paço de Arcos, Portugal, aepor@netcabo.pt

Introduction

The goal of this system is to provide a faster and cheaper way to develop experiments. Using the same basic shape, three different versions of a Microgravity "Modular Research Platform" (MRP) are presented. The general layout of the development platform is illustrated by the mock-up, originally designed to be launched once a year by a VS-30 sounding rocket from Brazil into a suborbital flight. It is similar to a payload from Swedish Space Corporation: DYLCO "Dynamic behaviour of Liquids in Corners and edges" an experiment module was launched by MAXUS 2 on November 28, 1995. It was designed in 2001 to be used on an educational project involving cooperation among the eight countries that use the Portuguese language which are physically connected by the oceans. New sub-systems to improve space aquaculture are designed using modern software tools, as an educational tool.

Initial Hardware

The basic design has eight reservoirs with liquid placed around a central cylindrical mixing area. A solenoid valve (in white on the CAD drawing) is used to inject the water into the central reservoir. Beneath it there is an illumination subsystem. Above it there is a mirror that is aligned with an imaging subsystem. The batteries and onboard computer are placed on top.

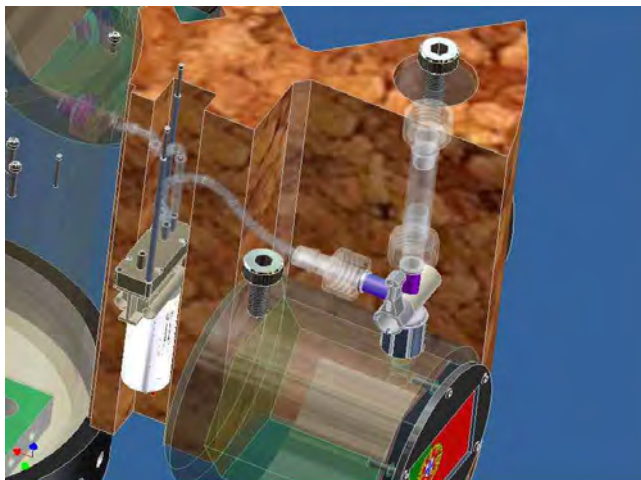


Figure 1: Stacked blades of cork for thermal insulation

As an example, experiments on microgravity regarding the effectiveness of subsystems to study fish in microgravity (water flows, filters, miniaturized water quality monitoring) that are used for life-support systems for space aquarium research projects such as the "Lunar Hatch" program from IFREMER will be presented. This program explores space aquaculture, using recirculating systems, which recycles fish waste to convert it into food. The development and

application of space aquaculture shares the same objectives with sustainable aquaculture on Earth, and thus, could indirectly participate in the preservation of our planet, including the development of advanced water sensors and bacterial filters that can be used to monitor the contamination of ballast water from merchant navy ships that sometimes carry various water-borne pathogens over long distances.



Figure 2: The MRP 1:1 scale mock-up has a 30 cm diameter

Valispace is a digital productivity tool that helps your engineering team share up to date dynamic data quickly and easily. The possibility of customizing this basic design, will be illustrated using the Valispace software in order to enable the assembly of different microgravity experiments, on different various platforms using agile engineering planning and concurrent design as tools. Configurations for drop towers, sounding rockets, and parabolic flights will be presented.

Conclusions

A new software tool is used for the redesign of microgravity payloads. Examples of space aquarium designs are presented. The focus is on the design of better filters and water quality sensors that can operate in microgravity. This approach will help students streamline their documentation requirements, allowing more complex designs to be explored faster.

Acknowledgements

I would like to thank Valispace GmbH for the use of an Educational Licence of their software

References

R. Dinis, C. Richard, Alma da Água: A Space Awareness Initiative. *Leonardo, Journal of the International Society for the Arts, Science and Technology*, MIT Press, volume 36, page 280, (2003)

P. Cyrille, Space Aquaculture: Prospects for Raising Aquatic Vertebrates in a Bioregenerative Life-Support System on a Lunar Base. *Astrobiology, a section of the journal Frontiers in Astronomy and Space Sciences*, (2021)

Supreet Kaur, Stefan Siarov, Louise Lindblad, Marco Witzmann, A PRACTICAL GUIDE TO AGILE MISSION DESIGN AND SPACECRAFT DEVELOPMENT WITH DATA-DRIVEN SYSTEMS ENGINEERING. (*Systems & Concurrent Engineering for Space Applications Conference*), (2020)

Charmaine Ng, Thai-Hoang Le, Shin Giek Goh, Liang Liang, Yiseul Kim, Joan B. Rose, Karina Gin Yew-Hoong. A Comparison of Microbial Water Quality and Diversity for Ballast and Tropical Harbor Waters, *PLoS ONE Public Library of Science*, (2015)

POSTER 105

Diffusing Wave Spectroscopy investigations of emulsions in microgravity

Valentina Lorusso¹, Davide Orsi¹, Marco Vaccari¹, Libero Liggieri², Luigi Cristofolini¹

¹ Department of Mathematical Physical and Computer Sciences, University of Parma, Italy, valentina.lorusso@unipr.

² CNR - Institute of Condensed Matter Chemistry and Technologies for Energy, Genova, Italy

Introduction

The PASTA experiment, under way since February 2022 on board the International Space Station (ISS), is included in the project ESA MAP project "Emulsion Dynamics and Droplet Interfaces-EDDI". The main aim of the project is to contribute to disentangle the role of the different mechanisms driving emulsion stability. Among them the coalescence mechanisms in low-surfactant-content emulsions stabilised by non-ionic surfactants, the droplets dynamic in its Ballistic and Brownian regime or coalescence event frequency.

The on-board analysis is mainly by DWS, complemented by a time-resolved multi-speckle analysis Linecamera applied to the backscattered light. The synergy of this two types of techniques allows us to explore not only the dynamics and structure of emulsions during the aging process, but also the characteristics of transient and intermittent events due to coalescence processes between drops.

Diffusing Wave Spectroscopy (DWS) is a powerful tool to investigate structure and dynamics in turbid samples, such as foams and emulsions. Its non-invasive character, makes it ideally suited to investigate the ageing processes of emulsions and foams with unparalleled statistics. For this reason it was chosen as one of the diagnostic tools for investigations of granular materials, foams and emulsions in microgravity in the "Soft Matter Dynamics" (SMD) instrument aboard the ISS. However, this advantage is weighted by the complexity of the analysis required to extract the relevant physical parameters from the measured intensity autocorrelation functions. Indeed, decoupling structural and dynamical information relies on the knowledge of the distribution $P(s)$ of the length, s , of the paths followed by photons before reaching the detector.

While the classical analysis for DWS is based on analytical forms for $P(s)$, which are only valid for idealized geometries, we recently showed that in realistic conditions this assumption might lead to drastically unreliable estimates for the time-dependent mean square displacement. This can lead incorrect assumptions regarding models of droplet dynamics and

limitations on the use of DWS to study the kinetics of emulsions destabilization.

The numerical determination of $P(s)$ provide a more flexible approach; by using a realistic Monte Carlo simulation random diffusion of photons propagating in the volume of the sample before reaching a detector, $P(s)$ are modelled and then used to analyse experimental correlation functions obtained in any scattering geometry, even when specialized sample cells are employed.

Optical Monte Carlo methods

We will present results from DWS experiments when $P(s)$ is obtained by Monte Carlo simulations accounting for the experimental geometry, namely shape and dimensions of the sample cell and the scattering geometries. This is applied to experiments on emulsions performed in a setup built for investigations in microgravity on the SMD facility aboard the ISS, where some of the parameters of the scattering geometry might not be directly measurable with the required accuracy.

The proposed calibration procedure of a DWS setup (Figure 1) consists in prepare a calibration standard of a stable suspension of polystyrene nanoparticles of uniform size undergoing Brownian diffusion (density-matched water phase prepared by mixing normal H₂O and D₂O). Then, this model sample is characterized using a standard and road-tested DWS laboratory setup. Analysis with a suitable set of Monte Carlo simulations of $P(s, l^*)$ yields a measurement of the mean free path of transport l^* and of the diffusion coefficient D of the nanoparticles. The measurement on the calibration sample is repeated on the specialized DWS setup to be validated, i.e. characterized by one optical/geometrical parameter, whose value is unknown.

A new set of Monte Carlo simulations of $P(s, l^*)$ is computed for the specialized DWS setup, now validated. This exercise makes the interpretations of measurements not affected by the setup parameters on which they are performed.

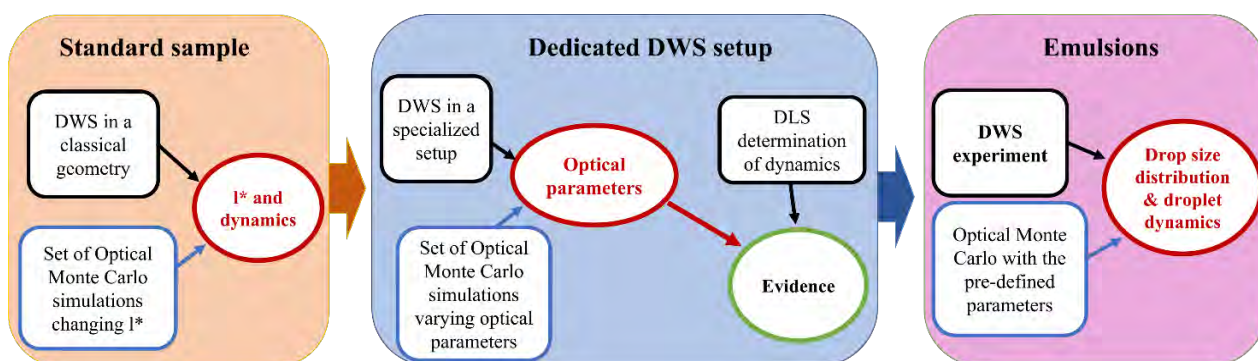


Figure 1: The proposed procedure: from left to right, by DWS experiments and a set of Optical Monte Carlo (OMC) simulations, a calibration sample is fully characterized with respect to its internal dynamics and the photon transport mean free path l^* . Then, this same sample is measured by the specialized DWS to be calibrated; by analysing the results in the light of OMC simulations, the optical parameters of this setup are determined. Finally, this is used (right panel) to investigate the emulsions of interest

Emulsions in microgravity

The emulsions subjects to investigation a dispersion of Medium Chain Triglycerides (MCT oil, Migloyl 812N, IOI OLEO, Hamburg) in water (by varying oil/water fraction), with the non-ionic surfactant C12EO21 (Nikkol, Japan) stabilizing water/oil interface (at different molar concentrations).

The simultaneous DWS analysis of the correlograms acquired for the backscattered and transmitted light, and the subsequent estimate of l^* contains information about the size and number of scattering centers. Their decay provides a hint on the type of dynamics of the system as shown in the preliminary results in the figure (figure 2 and 3) with relaxation times against the age of the emulsion, for two different surfactant limit concentrations and three different water/oil fractions used in preparation. There are clearly different trends in the temporal evolution of the sample.

At higher concentrations (figure 2) it is noted that the average free path of transport, qualitatively represented by the ratio of dynamics in forward and backscattering acquisition, remains constant at different oil-water concentrations. While the number of drops formed during emulsification and their size becomes larger to greater amounts of oil.

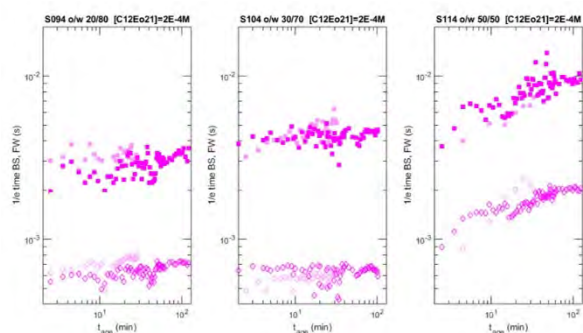


Figure 2: $1/e$ relaxation time of the backscattering (filled squares) and transmission (empty diamonds) correlation functions, as a function of the time from emulsification for the PASTA sample xx-4: oil/water ratio (20:80,30:70,50:50); surfactant (C12EO21) concentration $2 \cdot 10^{-4}$ M in water.

For lower concentrations (figure 3) l^* changes depending on the amount of oil present in the emulsions,

the drops are on average larger and smaller in number and up to show clear signs of coalescence as the oil fraction in water increases. Afterwards, the best fit of the correlation functions will give us results in a determination of l^* and τ_B, τ_S (Brownian and shear time).

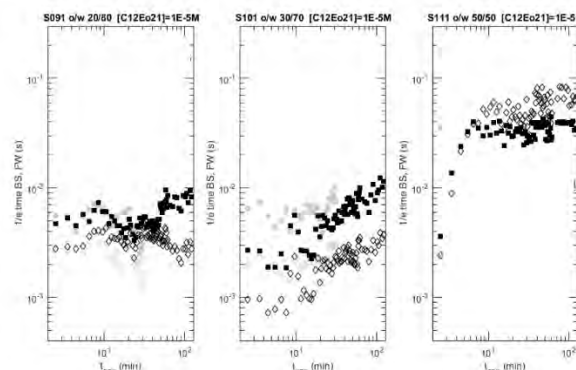


Figure 3: $1/e$ relaxation time of the backscattering (filled squares) and transmission (empty diamonds) correlation functions, as a function of the time from emulsification for the PASTA sample xx-1: oil/water ratio (20:80,30:70,50:50); surfactant (C12EO21) concentration 10^{-5} M in water.

This preliminary results by the DWS data from the PASTA experiment provide a picture of the phenomena for micro-gravity emulsions undergoing aging and will be compared with DWS experiments on the same relevant samples on ground. Finally, further conclusions will be drawn from the analysis of these data on the basis our DWS models that are under development.

References

- P. Born et al., Soft Matter Dynamics: A versatile microgravity platform to study dynamics in soft matter, Review of Scientific Instruments, 92, 12450, (2021).
- R. Hohler et al., Multiple light scattering as a probe of foams and emulsions, Current Opinion in Colloid and Interface Science, 19, 242, (2014).
- D.J. Pine, D.A. Weitz, P.M. Chaikin, E. Herbolzheimer, Diffusing wave spectroscopy, Phys. Rev. Lett. 60 (1988) 1134–1137. doi:10.1103/PhysRevLett.60.1134.
- D.J. Durian, Accuracy of diffusing-wave spectroscopy theories, Phys. Rev. E. 51 (1995) 3350–3358. doi:10.1103/PhysRevE.51.3350.
- V. Lorusso et al., Diffusing Wave Spectroscopy beyond average values, Advances in Colloid and Interface Science 288, 102341, (2021).

Acknowledgements

ESA MAP Project "Emulsion Dynamics and Droplet Interface" (contract ESA 4000128643/19)

POSTER 106

FLUMIAS - high-resolution live-cell fluorescence microscopy and identifying gravity sensitive thresholds on-board the ISS

T. Schmakeit¹, Y. Lichterfeld¹, L. Kalinski¹, M. Braun², A. Carstens², S. Daali², S. Herbert³, R. Sütterlin³, R. Hemmersbach¹, C. Liemersdorf¹

¹Institut für Luft- und Raumfahrtmedizin, Deutsches Zentrum für Luft- und Raumfahrt (DLR)
Linder Hoehe, D-51147 Köln, Germany, firstname.lastname@dlr.de, ²Organisation / Raumfahrtmanagement, Forschung unter
Weltraumbedingungen, Deutsches Zentrum für Luft- und Raumfahrt (DLR)
Königswinterer Str. 522-524, D-53227 Bonn, Germany, firstname.lastname@dlr.de, ³Airbus Deutschland

Introduction

Since the dawn of space-research it was clear that microgravity is one of the most important environmental factors affecting biological systems in space, from whole animals to human as well as plant cells. Many biological research questions can be targeted at platforms providing short-duration microgravity conditions, such as parabolic flights or sounding rockets. For many questions, prolonged time frames are necessary for e.g. cell differentiation, tissue development or gravity adaptation processes. The ISS provides constant high-quality microgravity and therefore grants an excellent research platform for gravitational science. Until now the possibility to target research goals on the cellular level for various biological systems employing high-resolution live-cell microscopy in real microgravity was missing. FLUMIAS (FLUorescence Microscopy At Space) is a newly developed research platform, which combines a structured illumination (SIM) laser microscope with a life support system for optimal environmental conditions and a centrifuge to apply variable gravitational loads onboard the ISS. The immediate impacts of gravity changes as well as adaption processes of biological systems ranging from mammalian cells to microorganisms, animals and plants can be performed fully automated from 1g to 0g.

The Concept

Investigations of cellular systems have always required spatiotemporal high-resolution imaging within living cells by various fluorescence-based techniques. A multitude of research questions need real microgravity conditions over large periods of time that can currently only be provided by the ISS. FLUMIAS/LCI makes it possible to perform fluorescent microscopy from real microgravity to 1g. FLUMIAS was designed to grant new possibilities for cell cultivation, since a novel life support system (LSS) enables medium exchange, incubation and pharmacological stimulation or live staining. With a variation of the SIM technique in a laser scanning microscope, spatial and temporal high-resolution fluorescent live-cell imaging is now possible to investigate novel questions that previously could not have been targeted. The acquired images and videos can be used to study the impact of various levels of gravity ranging from 0g to 1g on mammalian cells, microorganisms, basic plants, 3D culture systems or even whole tissue samples. Identifying gravity-sensitive signaling pathways will further enhance the development of countermeasures for health risks of manned space flight. A Science Reference Model (SRM) provides the possibility

for reference experiments with the same setup as on the ISS only lacking the centrifuge capabilities. Reference experiments need to be performed to verify all experimental parameters before a space mission will be feasible.

The DLR facilities in Cologne, Germany will provide access to the FLUMIAS SRM microscope system and additionally provide well-established platforms for gravitational research. The DLR Hyperscope on the human centrifuge at the :envihab research facility can be utilized for live-cell imaging at hypergravity conditions for increased gravitational loads of up to 4g. For simulation of microgravity, various models of clinostats can be employed for adherent or suspended cells, organoids, 3D cultures, irradiation or online-kinetics. Laboratory facilities including simulated microgravity, hypergravity and the combination with FLUMIAS/LCI thus form a research environment at DLR, which is unique in the world.

Therefore, FLUMIAS enables studies including, e.g., adaptation processes to altered gravity conditions, dynamic cytoskeletal rearrangements, visualization of Ca-fluctuations, cell development progression, as well as pharmacokinetics.

FLUMIAS/LCI Capabilities

FLUMIAS/LCI provides the ability to incubate various samples inside of specific Experiment Blocks (EBs) with automated medium exchange and a controlled temperature environment (25-40°C, 0.5°C increment). During the experiment run, perfusion of up to 4 different fluids is possible, e.g. nutrient solutions, pharmacological stimulants, or staining solutions (1x100ml, 3x5ml). The EBs can be transferred to a centrifuge that is able to accelerate the experiments in the range of 0g to 1g. The centrifuge was designed for minimal vibration and shall be capable to change from 0g to 1g within 3 seconds and from 1g to 0g within 7 seconds.

Imaging parameters include a standard FoV (Field of View) of 400µm x 350µm (using the 40x air NA 0.95 objective), with multi-dimensional acquisition modes such as tile/mosaic imaging to create overview images of regions of interest or the whole slide, time lapse acquisition with a frame rate of up to 3 fps, as well as z-stacks. The microscope supports brightfield and fluorescence illumination with 4 excitation lasers (405 nm/488 nm/561 nm/640 nm) and 10 mW power each. Each EB will have one objective installed, with an air objective in the range of 10-40x to be chosen from.

Two different types of specialized EBs are planned, a plant (EB-P) and a cell EB (EB-C). Within the EB-C, a 4-channel or 1-channel slide can be utilized. The EB-P grants a Phyto-LED with a spectrum equal to the spectrum of the cLED

part of the plant EB LSS shall be a closed fluidic loop with a volume of at least 100 ml.

Conclusions

Bringing fluorescent microscopy to the ISS grants unique opportunities that were previously impossible to gain insights on the gravity-sensitivity of cellular processes. With this microscope facility, we are now able to decipher questions that were targeted for decades in a comprehensive manner. Countermeasure development and identification of gravity-sensitive pathways and target molecules will be largely accelerated.

Acknowledgements

Organisation / Raumfahrtmanagement, Forschung unter Weltraumbedingungen, Deutsches Zentrum für Luft- und Raumfahrt (DLR) Königswinterer Str. 522-524, D-53227 Bonn, Germany, Till I.D., Am Klopferspitz 19a, D-82152 Planegg/Martinsried, Germany, info@till-id.com, Airbus

POSTER 111

Individual susceptibility to altered gravitational environment: behavioural indicators and possible countermeasures

Alessandro Stronati¹, Giorgia Macchioni¹, Arianna Racca¹, Matteo Cerri², Daniela Santucci¹

¹Center for Behavioral Sciences and Mental Health, Istituto Superiore di Sanità, Rome, Italy, alessandro.stronati@iss.it, giorgia.macchioni@iss.it, arianna.racca@iss.it, daniela.santucci@iss.it

²Department of Biomedical and NeuroMotor Sciences, Alma Mater Studiorum -University of Bologna, Bologna, Italy, matteo.cerri@unibo.it

Introduction

Individual response to stress and the study of possible new strategies to reduce negative effects of altered gravity exposure are relevant for the future of human space exploration.

Behavioural indicators of vulnerability to un-physiological gravity represent unique endpoints of complex integrated systems when facing challenging environments. Moreover, thanks to the introduction of specific methods to induce hibernation-like conditions (a state of reduced metabolic activity followed by a decrease in body temperature in non-hibernating animals), the idea of exploiting hibernation as a possible countermeasure to reduce human suffering and individual susceptibility to stress in space is becoming more realistic (Cerri et al. 2016).

To characterize behavioural indicators of susceptibility to gravitational stress, male and female C57BL6J mice were exposed to rotational induced hypergravity (2g) in a custom built centrifuge (Figure 1). Stationary controls were placed close to the centrifuge during the rotation test.



Figure 1: The centrifuge facility at the “Istituto Superiore di Sanità”, Rome, I-00161, Italy (designed and manufactured by “Isolceram”, Rocca Priora, Rome, I-00040, Italy)

Mouse behaviour was monitored before, during and after rotation, and frequency and duration of several behavioural items (*rearing, wall rearing, grooming, sniffing, digging*) assessed (Santucci et al. 2000).

Secondly, in order to exploit the hibernation-like condition as a possible countermeasure to reduce hypergravitational stress, the behavioral profile of C57BL6J mice subjected to synthetic torpor and relative controls were monitored before, during and after rotation, and frequency and duration of several behavioral items assessed. Short- and medium-term effects in spontaneous behavior and in emotional and cognitive performances were evaluated in the successive days.

In both experiments cerebral NGF and BDNF were assessed in selected area of the central nervous system to correlate behavioral changes with alterations in central levels of neurotrophins, involved in neuroplasticity phenomena.

Conclusions

Short-term changes were observed in several behavioral items, some of them probably correlated with thermoregulatory function, in subjects who undergone synthetic torpor, while subtle but specific differences were evident in their emotional profile. Data will be discussed in the framework of individually-related neurobehavioral responsiveness in the context of hypergravitational exposure and the possibility that synthetic torpor may favorably impact on it through improving neuroplasticity.

Acknowledgements

This study was supported by “MARS-PRE, marcatori biologici e funzionali per la medicina astronautica di precisione”. The authors thank Antonio Maione for technical support.

References

- M. Cerri, W. Tinganelli, M. Negrini, A. Helm, E. Scifoni, F. Tommasino, ...M Durante. Hibernation for space travel: Impact on radioprotection. *Life sciences in space research*, 11, 1-9 (2016).
- D. Santucci, G. Corazzi, N. Francia, A. Antonelli, L. Aloe, E. Alleva. Neurobehavioural effects of hypergravity conditions in the adult mouse. *Neuroreport*, 11, 3353-3356 (2000).

POSTER 112

Behavioural indicator of susceptibility in mice exposed to simulated microgravity

Arianna Racca¹, Pignataro Patrizia², Maria Grano², Daniela Santucci¹

¹Center for Behavioral Sciences and Mental Health, Istituto Superiore di Sanità, Rome, Italy, daniela.santucci@iss.it, arianna.racca@iss.it

²Department of Emergency and Organ Transplantation, University of Bari, Bari, Italy, maria.grano@uniba.it, patrizia.pignataro@uniba.it

Introduction

The initial and adaptive responses to environmental changes are manifested in animal behaviour: exploiting such response represents an opportunity to investigate coping strategies, mechanisms underlying neuroplasticity phenomena, and the individual vulnerability to stress.

Although it has been demonstrated that altered gravitational environments strongly influence the behavioral profile of the animals and several neurobiological parameters connected to synaptic plasticity (Santucci et al., 2009), very little it is known about individual coping strategies to gravitational stress.

Aim of the present study was to determine neurobehavioral indicators of vulnerability to un-physiological gravity evaluating the behavioural profile of mice subjected to the hindlimb unloading procedure (HU), i.e. removing gravitational loading from the hindlimbs by suspending the animal by its tail to explore muscle atrophy and osteoporosis caused by gravitational alterations (Milstead et al., 2004; Chowdhury et al., 2013).

C57BL6 mice were subjected tail suspension procedure from one to 4 weeks (Wronski and Morey-Holton, 1987). Their spontaneous activity was videorecorded and the behavioural repertoire evaluated before, during and after the end of the procedure. The individual ethogram has been defined, studied across the 4 weeks and compared with pre and post suspension data. Moreover, neurobiological parameters (NGF and BDNF) have been also evaluated at the end of the procedure in order to correlate behavioral changes with central levels of neurotrophins known to be involved in neuroplasticity phenomena.

Differences in the exploratory and habituation profile in HU mice were observed. In particular, impairment in the vertical movements (*rearing, wall rearing*) and a reduction in locomotory activity (*crossings*) were evidenced, in line with previous behavioural studies in mice exposed to hypergravity.

The observations of mice during the suspension procedure revealed some emerging behavioural elements and subtle changes in the typical specie-specific behaviours (Table 1). Interestingly, the study of HU ethogram shown some analogies with behavioral elements observed in on-orbit mice, confirming that gravitational fields represent a continuum as well as the biological adaptive responses to changes across the spectrum of gravity.

Table 1: ethogram of HU mice

<i>Fully extended hindlimbs</i>	the animal stretches its hindlimbs upward in order to bring its head towards the base of the cage
<i>Alternative extended hindlimbs</i>	the animal changes the position of its body or rotates its body moving unilaterally the hindlimbs in the opposite direction that guided by the head and forelimbs
<i>Runng</i>	the animal moves frantically its forelimbs and/or hindlimbs in order to find balance
<i>Forelimbs hanging</i>	the animal grabs the component of the cage with the forelimbs or the mouth
<i>Inactivity</i>	the animal is in resting position
<i>Vertical head rising</i>	the animal raises its head upward and/or forwards
<i>Vertical self grooming</i>	the animal licks any part of the body

Conclusions

An overview of the experiments set-up to investigate the individual vulnerability to gravitational environments will be reported. In particular, the ethogram of the HU mice will be compared with tboth pre and post suspension data in order to identify behavioural biomarkers for individual differences in coping with the HU paradigm.

Acknowledgements

This study was supported by “MARS-PRE, marcatori biologici e funzionali per la medicina astronautica di precisione”. The author thank Antonio Maione for technical support.

References

T.J. Wronski, E.R. Morey-Holton, Skeletal response to simulated weightlessness: a comparison of suspension techniques, *Aviation Space and Environmental Medicine*, 58, 63-8, (1987).
D. Santucci, N. Francia, V. Trincia, F. Chiarotti, L. Aloe, E. Alleva, A mouse model of neurobehavioural response to altered gravity conditions: an ontogenetical Study, *Behavioural Brain Research*, 30, 109-18, (2009).
P. Chowdhury, A. Long, G. Harris, M.E. Soulsby, M. Dobretsov, Animal model of simulated microgravity: a comparative study of hindlimb unloading via tail versus pelvic suspension, *Physiological Reports*, 1, e00012, (2013).
J.R. Milstead, S.J. Simske, T.A. Bateman, Spaceflight and hindlimb suspension disuse models in mice, *Biomedical Sciences Instrumentation*, 40, 105-10, (2004).

POSTER 116

A wearable-based system to reduce space motion sickness by multi-sensory pre-habitation

C.A. Vollette¹, C. Bockisch¹, D. Straumann¹, G. Bertolini¹

¹Vestibulo Oculomotor Lab, University Hospital Zürich, Zürich, Switzerland, dominik.straumann@usz.ch

Introduction

Motion sickness (MS) is a common disturbance occurring in healthy people exposed to specific real or illusory motion conditions. The most widely accepted hypothesis suggests a sustained conflict between expected and actual sensory inputs as the triggering factor for MS (G. Bertolini et al. 2016). As we evolved with gravity as the only reference, our brain makes use of estimated gravity direction to integrate reliable self-motion cues and discard aberrant ones. In space, any movement leads to unexpected combinations of vestibular signals. These mismatches cannot be resolved into a stable self-motion perception as the brain cannot sense gravity. Accordingly, each transition between gravity levels implies space motion sickness SMS (M. Heer et al. 2006; HJ. Ortega et al. 2020) for roughly half of trained astronauts, significantly impairing missions and safety for days. Symptoms of motion sickness include vomiting and nausea, but also higher risk of disorientation, visual illusions and sopite syndrome. The definition of effective countermeasures for MS is a major topic for both space research and terrestrial applications (from transport, to virtual and augmented reality and patients' care). Although drugs diminish symptoms (e.g. meclizine, promethazine or scopolamine), they come with unwanted side-effects (sedation, drowsiness) (M. Heer et al. 2006; AP. Weerts et al. 2014) and risks related to intolerances, adaptation and addiction. An alternative to ameliorate MS symptoms are training programs employing centrifuges, rotating chairs and even rotating rooms. These highly demanding programs were proven effective in aircraft pilots, but not in astronauts (HJ. Ortega et al. 2020). Accordingly, current pre-flight training programs account for instructions on MS management, but paradigms for adaptation or pre-adaptation of astronauts' self-orientation to weightlessness that minimize MS do not exist. The key problem in defining such program is that how self-motion perception adapts to weightlessness is not yet established. The most accredited hypothesis (DM. Merfeld et al. 2003), suggests that the brain reweights sensory inputs to optimize sensing in 0-g, without discounting the core assumption of self-orientation (i.e. "up and down exists and the desired body orientation is upright") (M. Dai et al. 2014). This may explain why nor desensitization programs nor hours of aviation experience protect astronauts from SMS (HJ. Ortega et al. 2020). Interestingly, astronauts with natural tendency to rely more on an ego-referenced frame (body z-axis or ideotropic vector - i.e. my feet are "ground", my head is "up") than on visual cues have been shown to have less SMS symptoms and a shorter adaptation time (DL. Harm et al. 1998). Pathological visual over-reliance may occur in patients after a transient vestibular insult and become chronic (Persistent postural-perceptual dizziness (PPPD) (S. Cousins et al. 2014)). These patients face disorientation and motion sickness-like symptoms when exposed to complex visual stimuli (e.g. patterned floors, supermarket aisles). A sudden exposure to weightless

represent the equivalent of a strong vestibular insult: the vestibular sensors for gravity direction abruptly stop working. As for the PPPD patients, developing visual dependence is not uncommon in astronauts. It is however a risk factor and it has been related to higher and persistent SMS (DL. Harm et al. 1998). In light of these considerations, it is advisable that any training paradigm to facilitate vestibular adaptation to 0-g not simply avoids increasing reliance on visual cues, but also aims to decrease the risk of developing it in orbit. In the last decade, combinations of vestibular stimuli with manipulation of visual cues using VR (S. Cousins et al. 2014) have been studied for vestibular patients' rehabilitation programs and MS desensitization program for lay people. Patients with an overreliance on visual cues (DM. Merfeld et al. 2003) or chronic maladapted self-motion perception (M. Dai et al. 2014) clearly benefit from these novel multisensory adaptation paradigms. Multi-sensory cues to force reweighting of sensorial integration appear overall quite successful (A. Viziano et al. 2019). Although visual dependence and maladaptation are also issues for astronaut, transfer of the know-how from these novel patient rehab in pre-flight habituation or inflight SMS management has yet to be evaluated.

The main aim is to develop a pre-rehabilitation lessening space motion sickness (SMS) by simultaneous manipulation of different sensory cues to create sensory conflict conditions that can be resolved when the subject adopts our desired reference frame. In practice, as astronauts with natural tendency to adopt an ego-referenced frame have been shown to suffer less SMS and adapt faster, the pre-rehabilitation should reinforce this reference frame against a visual-based one. A training paradigm successfully achieving this adapted state will have a double advantage: will prevent overreliance on visual cues and promote a rapid switch to this learned strategy when gravity cues are absent (i.e. in orbit).

Methods

The project is divided in three steps. The first one is to identify the optimal combination of non-vestibular stimuli (visual and haptic) that successfully manipulate the perceived "down" in a gravity-related illusion. Then we aim to create the Pre-Rehabilitation paradigm that reinforces the reliance on the ego-centric reference and avoids development of visual dependence by combining the stimuli from the previous step (visual and/orhaptic) with a real angular tilt motion stimulus to induce a lasting reduction of the reliance on gravito-inertia as a cue for tilt. Finally, we will test the efficacy and retention of adaptation as well as the reduction of motion sickness in parabolic flights (0-g analog) organized by the UZHSpaceHub. We will also evaluate the implementation with Galvanic Vestibular Stimulation in order to make the whole equipment wearable. Currently working on the first step, using a motion simulator (Stewart platform), we expose participants to a "Hilltop" illusion (i.e., lateral translations at

0.16 Hz in darkness are interpreted as tilt-while-translating). The illusion is due to uncertainty in the sensed angular motion at low frequency, which leads to uncertainty on the correctness of the estimated of gravity direction. Due to limitations in amplitude of movements of the platform, translations only were not sufficient to induce the illusion. Thus, random angular tilts (-6° to 6°) were added to the motions, expecting participants to overestimate such tilts due to the Hilltop illusion. During the basic experimental stimulus (control condition in darkness - Cond. A), we manipulate the visual information (polarity cues via VR Headset - Cond. B), the haptic feedback (pressure/vibration in down direction-Cond. C) and both (Condition D) to provide verticality cues in contrast with gravitational reference (i.e. coherent with the illusion of an angular tilt). We measure perception of gravity using a continuous joystick alignment to verticality by the participant, as well as a Subjective Visual Vertical (SVV) test.

Preliminary Data

We obtained recordings from 15 participants experiencing the hilltop illusion in order to validate a change in gravity perception. In Fig1, the participant’s bar adjustments (yellow) should show a counter tilt during the actual platform tilts (red) plus/minus the effect of the illusory tilts due to translations (blue).

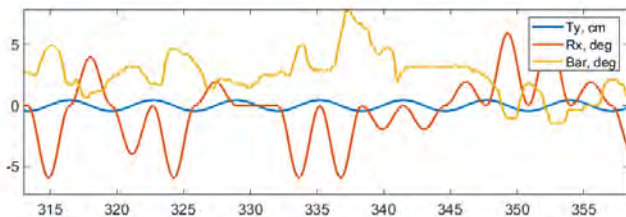


Figure 1: Fraction of one recording of three parameters on a moving platform (hexapod): in blue the oscillations of the platform (left-right translations at 0.16Hz, 0,88m amplitude on the z axis); in red the tilt angles of the platform (positive = tilt to the right, negative = tilt to the left); and in yellow the angles of the joystick controlled by the subject.

Since the number of positive and negative oscillations is high enough during a trial, their values should average to zero, and so should the values of the counter tilts if there was no effect of the translations (blue) on the subject. However, after averaging all the joystick movements (yellow) for each half translation cycle, we obtained Fig 2:

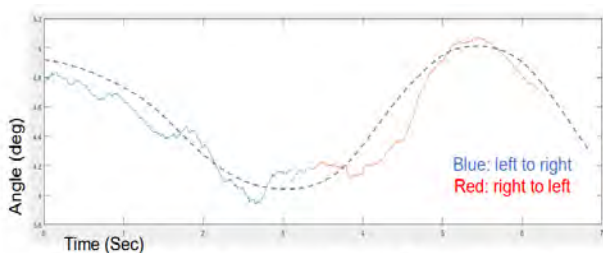


Figure 2: Average bar movement for each half translation cycle

This sinusoidal shape shows that for each maximum acceleration value of the platform (extreme left and extreme right), there was an increased modified perception of the actual tilt angle of about 0.5° (interval between max and min peak divided by two). Similar results have been observed using the SVV measures.

Conclusion

The first step of this project is to determine how and if we could change the perception of gravity using multisensory cues. As the hilltop illusion is a perceptual task, we had to make sure our protocol could creat such illusion. Now that we have a satisfying illusion protocol, we are in the process of adding visual stimuli using a virtual reality headset. Visual verticality cues (buildings, trees, mountains...) show amplified or reduced tilts in comparison to the actual angles of the platform. The bar task and SVV will reveal to what extent gravity perception could be modified.

References

1. G. Bertolini, D. Straumann, Moving in a moving world: A review on vestibular motion sickness, *Front Neurol*, 2016
2. M. Heer, WH. Paloski, Space motion sickness: Incidence, etiology, and countermeasures, *Auton Neurosci Basic Clin*, 2006
3. HJ. Ortega, DL. Harm, MF. Reschke, Space and entry motion sickness, *Principles of Clinical Medicine for Space Flight*, 2020
4. AP. Weerts, R. Vanspauwen, E. Fransen, PG. Jorens, PH. Van De Heyning, FL. Wuyts, Space motion sickness countermeasures: A pharmacological double-blind, placebo-controlled study, *Aviat Sp Environ Med*, 2014
5. DM. Merfeld, Rotation otolith tilt-translation reinterpretation (ROTTR) hypothesis: A new hypothesis to explain neurovestibular spaceflight adaptation, *IOS Press*, 2003
6. M. Dai, B. Cohen, E. Smouha, C. Cho, Readaptation of the vestibulo-ocular reflex relieves the mal de debarquement syndrome, *Front Neurol*, 2014
7. DL. Harm, DE. Parker, MF. Reschke, NC. Skinner, Relationship between selected orientation rest frame, circular vection and space motion sickness, *Brain Res Bull*, 1998
8. S. Cousins, NJ. Cutfield, D. Kaski, A. Palla, BM. Seemungal, JF. Golding, JP. Staab, AM. Bronstein, Visual dependency and dizziness after vestibular neuritis, *PLoS One*, 2014
9. A. Viziano, A. Micarelli, I. Augimeri, D. Micarelli, M. Alessandrini, Long-term effects of vestibular rehabilitation and headmounted gaming task procedure in unilateral vestibular hypofunction: a 12-month follow-up of a randomized controlled trial, *Clin Rehabil*, 2019

POSTER 118

NeuronGrav: characterizing neuronal responses in altered gravity via glider-based parabolic flights

José Figueiredo¹, Barbara M. de Sousa², Filipe Senra³, Sara Santos², Denis-Gabriel Caprace⁴, Mohammad Iranmanesh⁴, Mehdi Scoubeau⁴, Camille Gontier⁴

¹Faculty of Medicine, University of Lisbon, Portugal, jose.figueiredo@edu.ulisboa.pt, ²University of Aveiro, Portugal, {bmsousa,santossara}@ua.pt, ³University of Beira Interior, Portugal, filipesenra98@hotmail.com, ⁴LIDE Space, Louvain-la-Neuve, Belgium, {dg,mohammad,mehdi,camille}@lide.space

Abstract

Experiments in an altered gravity environment are a fundamental part of many branches of applied sciences, including biology, physiology, and space medicine. In this scope, either earth-bound weightlessness or hypergravity conditions are typically achieved by means of parabolic flights. Recently, gliders have been proposed as a practical and cost-efficient alternative to classical microgravity platforms, such as airliners and light aircraft (Caprace et al. 2020). However, their relevance and usability for biology experiments have not been demonstrated yet. Here, we present the results of the NeuronGrav (Neuronal responses in altered Gravity) experiment. Its main aim is to characterize adaptative alterations induced on human neuronal-like cells by short exposures to altered gravity. Previous studies have demonstrated modulation of neuronal plasticity, changes in neurite network, neuron morphology and viability, and induced autophagy through mitochondrial dysfunction, followed by fast recovery processes upon short periods of exposure to microgravity (Morabito et al. 2015, Pani et al. 2013, Pani et al. 2016, Khandia et al. 2019). Our main contribution is to discuss the possibility to reproduce and further characterize these observed effects during parabolic flights performed with a glider. Using a custom framework, which allows to host an incubator and several cell lines during the flight, we measure cellular viability and toxicity, cytoskeletal alterations, and quick onset biochemical alterations in response to altered gravity in neuronal-like cell cultures. Overall, we aim at validating gliders as an adequate altered gravity platform for biology and medicine experiments.

Acknowledgements

The authors acknowledge the contribution of the Study Center in Aerospace Medicine from the Faculty of Medicine of the University of Lisbon, the Institute of Biomedicine – University of Aveiro (iBiMED-UA), the COMPASS Research Group (CICECO-Aveiro Institute of Materials, UA), and the Faculty of Engineering - University of Beira Interior (FE-UBI) for the scientific and equipment support. The author also acknowledge the contribution of P. Billuart in the preparation of the flights, the collaboration with the Centre National de Vol à Voile (Saint-Hubert) through which the airframe was made available, and the collaboration with the laboratory of Prof. Nicaise (University of Namur). They also express their gratitude to the personnel of UCLouvain- iMMC for technical advising and sharing of resources.

References

- Caprace DG, Gontier C, Iranmanesh M, Scoubeau M, Pletser V. *Experimental Characterization of Weightlessness During Glider Parabolic Flights*. *Microgravity Sci Technol*. 2020.
- Morabito C, Steimberg N, Mazzoleni G, Guarnieri S, Fanò-Illic G, Mariggiò MA. *RCCS bioreactor-based modelled microgravity induces significant changes on in vitro 3D neuroglial cell cultures*. *Biomed Res Int*. 2015.
- Pani G, Samari N, Quintens R, de Saint-Georges L, Meloni MA, Baatout S, Van Oostveldt P, Benotmane MA. *Morphological and Physiological Changes in Mature In Vitro Neuronal Networks towards Exposure to Short-, Middle- or Long-Term Simulated Microgravity*. *PLoS One*. 2013.
- Pani G, Verslegers M, Quintens R, Samari N, De Saint-Georges L, Van Oostveldt P, Baatout S, Benotmane MA. *Combined Exposure to Simulated Microgravity and Acute or Chronic Radiation Reduces Neuronal Network Integrity and Survival*. *PLoS One*. 2016.
- Khandia R, Dadar M, Munjal A, Dhama K, Karthik K, Tiwari R, Yattoo MI, Iqbal HMN, Singh KP, Joshi SK, Chaicumpa W. *A comprehensive review of autophagy and its various roles in infectious, non-infectious, and lifestyle diseases: Current knowledge and prospects for disease prevention, novel drug design, and therapy*. *Cells*. 2019.

POSTER 125

21 day Dry Immersion Bed Exposure drives CD3⁺ T Cell Transcriptional Landscape Towards A Proliferative Phenotype

Christian Oertlin¹, Julien Record¹, Nikolai Kouznetsov¹, Sergey Ponomarev², Lisa Westerberg¹

¹ Karolinska Institutet, Department of Microbiology, Tumor and Cell Biology (MTC), Solnavägen 9, 17171 Solna, Sweden.

² Institute of Bio-medical Problems of the Russian Academy of Sciences, 76a, Khoroshevskoe Shosse, Moscow, 123007, Russia.

Introduction

The immune system plays a pivotal role during the defense against invading pathogens and malignancy in our bodies. Space flight has been shown to negatively affect the immune system of astronauts causing immunodeficiencies and awakening of latent viruses¹. For safe and prolonged space missions for astronauts it is paramount to better understand the effects of space flight on the immune system and how to prevent or counteract them. Due to the limited availability and high cost of space flight, ground-based analogs are a necessity to propel space life sciences forward^{2,3}. We here studied the effects of 21 day dry immersion bed exposure on CD3⁺ T cells isolated from blood of 8 volunteers. Samples were collected at 7 day intervals with 7 day pre- and post-immersion references. Bulk RNA-sequencing of CD3⁺ T cells revealed transcriptional alterations across all time points, with the most drastic changes 14 days after dry immersion exposure. Notably, these changes persisted 7 days post-immersion. Well-known T cell subset differentiation markers were down regulated, while the IL-2 and IL-7 receptors aiding proliferation were upregulated.

Conclusions

Taken together, these findings point towards that simulated weightlessness via dry immersion exposure drives CD3⁺ T cell expansion and limits differentiation.

References

1. Crucian, B. E. *et al.* Immune System Dysregulation During Spaceflight: Potential Countermeasures for Deep Space Exploration Missions. *Front Immunol* 9, 1437 (2018).
2. Pandiarajan, M. & Hargens, A. R. Ground-Based Analogs for Human Spaceflight. *Front Physiol* 11, 716 (2020).
3. Tomilovskaya, E., Shigueva, T., Sayenko, D., Rukavishnikov, I. & Kozlovskaya, I. Dry Immersion as a Ground-Based Model of Microgravity Physiological Effects. *Front Physiol* 10, 284 (2019).

POSTER 126

Stable and unstable component separation in Soret experiments with TEG-water mixture

C.I.A.V. Santos¹, A.C.F. Ribeiro¹, M.M. Bou-Ali², A. Mialdun³ and V. Shevtsova²

¹ CQC-IMS, Department of Chemistry, University of Coimbra, Coimbra, Portugal, ceciliansantos@qui.uc.pt, anaefrib@ci.uc.pt;

² Mechanical and Manufacturing Department, Mondragon University, Loramendi 4, Mondragon 20500, Spain mbouali@mondragon.edu, valentina.chevtsova@ulb.be;

³ MRC, CP165/62, Université libre de Bruxelles, 50, av. F.D. Roosevelt, Brussels 1050, Belgium, aliaksndr.mialdun@ulb.be;

Introduction

Transport phenomena occurring in many of the multicomponent mixtures present in both nature and industry are subject to non-equilibrium conditions and its comprehension is of great interest for many applications. When a liquid mixture is subject to a temperature gradient, its constituent species move, and a concentration gradient is generated. The coupling between temperature and concentration gradients is known as thermodiffusion or the Ludwig-Soret effect [1]. Soret effect is quantified by the Soret coefficient S_T , the ratio between the thermodiffusion coefficient D_T and the molecular diffusion coefficient D [2]. Several experimental methods have been developed in past years, providing accurate measurements of both molecular and thermal diffusion coefficients for binary mixtures, e.g. optical methods, since no perturbation is introduced into the diffusive process. Still, the study of thermodiffusion in complex mixtures is difficult because the sign of the Soret coefficients of the various species in the mixture could be different and it destabilizes the system. As consequence, only a limited number of thermodiffusion coefficients for binary and ternary mixtures are available and often data are not consensual.

In this work, we examined the Soret coefficient of the mixture composed of a nonpolar hydrocarbon solute triethylene glycol (TEG) and water, exploring the full concentration region of the mixture at 25 °C. Research on triethylene glycol is particularly important due to its applications as a dehydration agent in natural gas streams to prevent corrosion in pipelines.[3]. Moreover, this is a non-ideal mixture, and thus, it has a potential to demonstrate a complex dependence of the Soret coefficient on concentration, including its sign change. The instrument used for the determination of Soret coefficients is based on the optical digital interferometry (ODI) technique [4].

Experimental

A. Materials

The reagent grade triethylene glycol (purity 0.99%, CAS Number: 112-27-6) and water extra pure, deionized (CAS Number: 7732-18-5) were obtained from Acros Organics and were used as received, with no further purification. Liquid samples of ≈ 15 g were prepared in mass fraction, by weighing each component using the Sartorius 1712 analytical balance with a resolution/capacity of 0.1 mg/160 g and then remixed by a magnetic stirrer during several hours.

B. Experimental setup: Optical digital interferometry

The experimental setup for the measurement of the Soret effect used in this work was optical digital interferometry (ODI), a validated and reliable optical method very well described in literature [4-5].

Results

A. Overview of the component separation

Separation in the TEG–water mixtures was studied by moving from low to high concentration of TEG with a step of 0.1 mass fraction. The mixtures of low concentration feature stable separation, well accessible by ODI, with the maximum optical signal found at $c \approx 0.2$ mass fraction. A further increase of the TEG concentration resulted in a gradual decrease of the optical signal corresponding to steady-state separation, which was found unstable (negative) in the experiment at $c = 0.5$ mass fraction. Several experiments, made at even higher concentrations of TEG (at $c = 0.75$ and 0.98 mass fraction), confirmed the instability of the separation over all regions of high TEG concentrations, until $c = 1$. The summary plot of the observed concentration dependency of the optical separation is shown in Fig. 1.

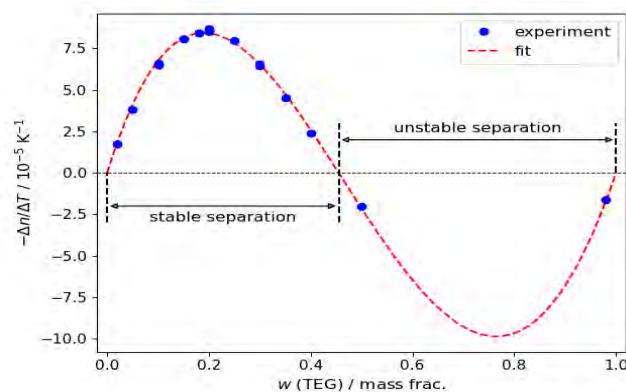


Figure 1: General trend of separation for the mixture TEG–water (dots represent the experimental data, and the dashed line is the fit).

The fitting of the results shows that an R–K polynomial of first-order (which explicitly accounts for the vanishing of the separation at the diluted limits) [6] offers a satisfactory description of the explored region and a reasonable guess about the unexplored one. The obtained fitting curve, dash line in Fig. 1, allowed to precisely locate the concentration specific to the sign change of the separation, at a 0.45 mass fraction of TEG. Until this point, the separation of

components is stable and develops normally, having the point of maximum separation at 0.2 mass fraction of TEG. Trying to determine the dependency more accurately, we added measurements at intermediate concentrations, with a smaller step of 0.05 mass fraction, in the region of stable separation. We have to draw attention that two data points in Fig. 1 belong to the region with unstable separation, while the ODI setup configuration (with a large cell height) is optimized for the measurement of mixtures with the positive Soret separation.

B. Unstable separation

When running the experiments with mixtures featuring small unstable separation (e.g., at $c = 0.50$ and 0.98 mass fraction), we made an important observation. At first, the separation, even being generally unstable, develops in accordance with the analytical solution. At later time, when enough amount of the heavier component (TEG) has accumulated at the top of the cell, the 1-D character of the developing separation breaks, and a hydrodynamic instability develops [5]. The instability should start after a certain threshold and may take either long-wave or finger-type character, with both the threshold and the character being dependent on thermophysical and transport properties of the mixture, as well as on the applied temperature difference and the cell size. The most important feature here was the duration of the step of the stable development of the separation. In the two most interesting cases, at $c = 0.5$ and 0.98 mass fraction, this duration was found as 2–3 h. The separation development in the case of $c = 0.5$ is shown in Fig. 2.

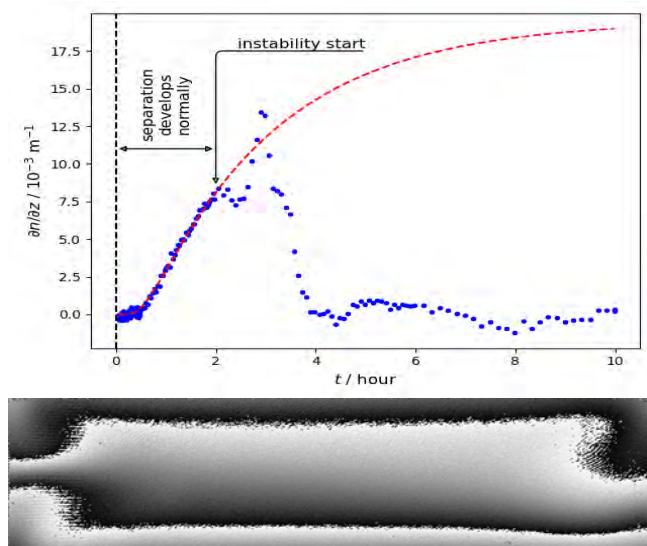


Figure 2: General trend of separation for the mixture TEG–water of $c = 0.5$ (dots are experimental data, and the dashed line is the fit). The wrapped optical phase map shown below corresponds to the beginning of instability development.

It is seen in the plot that, during the first hours, the separation develops in a perfect agreement with the 1-D analytical solution and that due to the faster image acquisition at the beginning of the experiment, this time interval is quite densely covered by interferograms.

It appeared that this amount of data is enough for fitting and extracting the separation magnitude and diffusion coefficient, despite that the separation does not reach even a half of the steady-state level. The 2-D phase map specific to the end of the short period of the stable separation development is shown

in Fig. 2, below the separation curve. There are visible traces of the developing instability in the corners of the cell, while in the liquid bulk in the center of the cell, the distribution resembles the steady one [5]. Thus, in certain cases of unstable separation, the data allow access to the transport properties in the same manner as for fully stable separation. This, however, is not always the case. For example, the experiment with the mixture of $c = 0.75$ mass fraction concentration did not allow one to apply this approach since the instability development started after 0.5 h, obstructing a further extraction of meaningful data. Nevertheless, this possibility let us adding two additional points to our results, having a reliability comparable with all other cases featuring the stable separation.

Conclusions

Soret coefficients ST were determined for the TEG–water mixture with ODI setup, showing that ST changes its sign at 0.1 mol fraction of TEG (0.45 mass fraction of TEG) and that the separation of the components at high concentration of TEG is unstable.

Acknowledgements

C.I.A.V.S. and A.C.F.R. are grateful for funding from “The Coimbra Chemistry Centre,” supported by the Fundação para a Ciência e a Tecnologia (FCT), Project No. UID/QUI/UI0313/2013 and COMPETE Program and for the funding granted by FEDER through the COMPETE Programme and FCT for the KIDIMIX Project No. POCI-01-0145-FEDER- 030271. A.M. acknowledges support from the PRODEX program of the Belgian Federal Science Policy Office. V.S. acknowledges support from micro4IoT (Grant No. KK-2019/00101) from the Basque government and M.M.B.-A. acknowledges support from Project No. PID2020-115086GB-C33 financed by MCIN/AEI of the Spanish Government.

References

- [1] C. Soret, “Sur l’état d’équilibre que prend au point de vue de sa concentration une dissolution saline primitivement homogène dont deux parties sont portées à des températures différentes.,” *Arch. Sci. Phys. Nat. Geneve*, 2(3) 48–61 (1879)
- [2] W. Köhler and K. I. Morozov, “The Soret Effect in Liquid Mixtures- A Review,” *Journal of Non-Equilibrium Thermodynamics*, 41 (3) (2016).
- [3] L. Trueba, T. Gaston, J. Brackin, J. Miller, and B.-H. You, Effective strategies to reduce triethylene glycol consumption in natural gas processing plants, *Case Stud. Chem. Environ. Eng.* 5, 100196 (2022).
- [4] A. Mialdun, V. Shevtsova, “Digital interferometry as a powerful tool to study the thermodiffusion effect”, *C. R. Mécanique.*, 339, 362 (2011).
- [5] C. I. A. V. Santos, M. C. F. Barros, A. C. F. Ribeiro, M. M. Bou-Ali, A. Mialdun, and V. Shevtsova, "Transport properties of n-ethylene glycol aqueous solutions with focus on triethylene glycol–water", *J. Chem. Phys.* 156, 214501 (2022)
- [6] O. Redlich and A. T. Kister, Algebraic Representation of Thermodynamic Properties and the Classification of Solutions, *Ind. Eng. Chem.* 40, 345 (1948).

POSTER 127

Immune cells respond to proton irradiation in a dose- and sex-dependent manner

U. Ławrynowicz^{1,2}, W. Bartosik³, N. Zawrotna³, A. Grymanowska³, J. Swatler⁴, J. Janiec⁴, D. Krzempek⁵, R. Kopec⁵, K. Piwocka⁴, J. Mieczkowski^{2,3}

¹ Department of Medical Immunology, Medical University of Gdansk, Gdansk, Poland; ² P-Medicine Laboratory, Medical University of Gdańsk, Gdańsk, Poland; ³ Genegoggle Sp. z o.o. Warsaw, Poland; ⁴ Laboratory of Cytometry, Nencki Institute of Experimental Biology, Polish Academy of Sciences, Warsaw, Poland; ⁵ Cyclotron Centre Bronowice, Henryk Niewodniczański Institute of Nuclear Physics Polish Academy of Sciences in Krakow, Poland.

Introduction

The effects of exposure to irradiation are of interest to patients considering radiotherapy as well as the space exploration community. Proton beam therapy has recently emerged as an alternative to γ -radiotherapy. Its therapeutic use is motivated by the fact that the proton stops at a specific tissue depth determined by its energy (Ricciotti, E. et al 2019). Proton radiation therapy offers a number of potential advantages over conventional γ -radiation therapy, but the pathophysiological effects following proton radiation exposure are less well characterized. It is already proven, that the type of irradiation and the dose are contributing factors to the irradiation results and side effects (Sanzari, J. K. et al. 2013). Primarily, the cellular response to irradiation was associated with alterations in the cell nucleus, with most of the deleterious effects of high (>0.5 Gy) and moderate (0.1–0.5 Gy) doses attributed to DNA damage (Lumniczky, K. et al. 2021). In addition, even low doses of irradiation induce cellular responses that are cell type-dependent. There are several reports already demonstrating that exposure to irradiation can affect epigenetic gene expression regulation (Sanders, J. T. et al. 2020; Beheshti, A. et al. 2021). DNA methylation is considered one of the main of such mechanisms that safeguard genome stability in cells, including regulating gene expression and chromatin structure (Merrifield, M. et al. 2013). It is known, that DNA methylation increases chromatin condensation, decreases overall DNA flexibility and the presence of DNA methylation around genes corresponds to expression levels. Hereby, DNA methylation intrinsically modulates chromatin structure and function, influencing the 3D structure (Buitrago, D. et al. 2021). However, the irradiation-induced modifications in 3D conformation and resulting changes in cellular response have not been studied.

Aim of the study

Characterization of the dose-dependent epigenetic effects of irradiation on peripheral blood mononuclear cells (PBMCs) and identification of epigenetic factors involved in the cell response to irradiation.

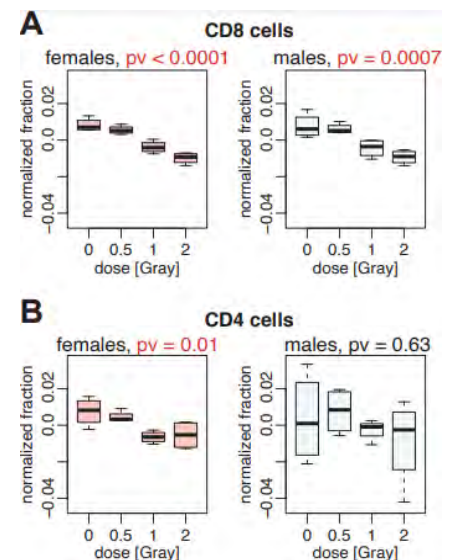
Methodology and research plan

1. Irradiation of PBMCs with proton irradiation in 3 doses in parallel (0.5 Gy, 1Gy, 2Gy.)
2. Fluorescence-activated Cell Sorting (FACS) of irradiated and control PBMCs into 4 subpopulations: CD4+ T cells, CD8+ T cells, CD19+ B cells, CD14+ monocytes.

3. Genome-wide epigenetic and transcriptomic profiling in the irradiated and control cells with Hi-C, ChIP-, ATAC-, and RNA-seq.
4. A systematic, computational analysis of the obtained profiles and identification of epigenetic characteristics associated with response to irradiation.

Figure 1:

Changes of fraction of T-cells after proton irradiation. (A) and (B) panels correspond to CD8+ and CD4+ cells respectively. Left and right plots correspond to cells collected from females and males respectively. The fractions were normalized to the levels in control (0 Gy).



Preliminary results

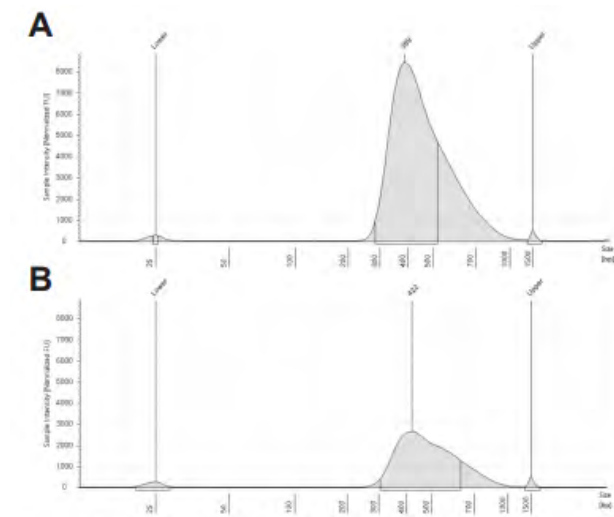
Proton irradiation influences fraction of mature leukocytes with regard to sex.

We have analyzed how different doses of proton irradiation (0.5, 1, and 2 Gy) affect immune cell composition in healthy patients with regard to sex. Among others, we have observed different behavior of the T-cells subpopulation. The fractions of CD8+ cells have decreased with the increase of proton irradiation doses (Figure 1A) in both sexes in a similar manner. However, the fraction of CD4+ cells has decreased only in the blood cells collected from females (Figure 1B). In the upcoming months, we are going to perform analysis of the chromatin structures corresponding to the presented results.

Sequencing-ready libraries for study 3D chromatin structure.

We already have tested the protocols needed for probing the 3D chromatin structure. Starting from only 1 million cells we have generated libraries for studying genome-wide interaction (Figure 2A) as well as libraries enriched for interactions with promoters of protein-coding genes (Figure 2B).

Figure 2: Fragment lengths of sequencing-ready libraries. (A) and (B) profiles correspond to Hi-C and promoter capture Hi-C respectively.



Conclusions

Coupling 3D chromatin conformation and chromatin accessibility data provide novel insights into chromatin regulation.

It has been reported that topologically associated domains (TADs, 0.5 – 1 Mb) are associated with chromatin landscape profiles (Sexton, T. et al 2012). We are planning to focus on smaller regions (5 kb) that are far apart on "linear" genomic distance, but get into gene proximity due to a particular spatial rearrangement. We observed that genomic regions with the strongest signal of chromatin accessibility were in each other's spatial, not genomic, vicinity.

Acknowledgments

The study was partially supported by the project POWR.03.05.00-00-z082/18 co-financed by the European Union through the European Social Fund under the Operational Programme Knowledge Education Development 2014–2020

References

- Ricciotti, E. et al. PLoS One 14, 1–20 (2019)
- Sanzari, J. K. et al. Gravitational Sp. Res. Publ. Am. Soc. Gravitational Sp. Res. 1, 79–94 (2013)
- Lumniczky, K. et al. Environ. Int. 149, (2021)
- Sanders, J. T. et al. Nat. Commun. 11, (2020)
- Beheshti, A. et al. Int. J. Mol. Sci. 22, (2021)
- Merrifield, M. et al. Front. Genet. 4, 1–16 (2013)
- Buitrago, D. et al. Nat. Commun. 12, (2021)
- Sexton, T. et al. Cell 148, 458–472 (2012)